

PATENT

IN THE UNITED STATES PATENT AND TRADEMARK OFFICE

In re Application of:
Eva KONTSEKOVA
Peter FILIPCIK

Serial No.: 10/521,049

Filed: November 1, 2005

For: TRANSGENIC ANIMAL EXPRESSING
ALZHEIMER'S TAU PROTEIN

Confirmation No.: 5434

Group Art Unit: 1633

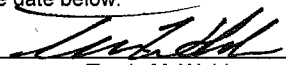
Examiner: Leavitt, Maria Gomez

Atty. Dkt. No.: SONN:066US

CERTIFICATE OF ELECTRONIC TRANSMISSION
37 C.F.R. § 1.8

I hereby certify that this Appeal Brief is being electronically
filed with the United States Patent and Trademark Office
via EFS-Web on the date below:

March 13, 2009
Date


Travis M. Wohlers

APPEAL BRIEF

Commissioner for Patents
P. O. Box 1450
Alexandria, VA 22313-1450

Dear Sir:

Appellant submits this Appeal Brief to the Board of Patent Appeals and Interferences in response to the Office Action dated November 13, 2008 and the Advisory Action dated January 27, 2009. Appellant filed a Notice of Appeal on February 13, 2009. Accordingly, the deadline for filing the Appeal Brief is April 13, 2009. The large entity filing fee for the Appeal Brief is included. Should any additional fees under 37 C.F.R. §§ 1.16 to 1.21 be required for any reason relating to the enclosed material, or should an overpayment be included herein, the Commissioner is authorized to deduct or credit said fees from or to Fulbright & Jaworski L.L.P. Deposit Account No.: 50-1212/SONN:066US/TMW.

TABLE OF CONTENTS

	Page
I. REAL PARTY IN INTEREST.....	1
II. RELATED APPEALS AND INTERFERENCES	1
III. STATUS OF THE CLAIMS	1
IV. STATUS OF AMENDMENTS.....	1
V. SUMMARY OF CLAIMED SUBJECT MATTER.....	1
VI. GROUNDS OF REJECTION TO BE REVIEWED ON APPEAL	3
VII. ARGUMENT.....	3
A. The Claims Are Enabled.....	3
1. The Transgenic Non-Human Animal	4
2. Promoters.....	13
3. Claims 19 and 37 Are Separately Patentable.....	16
4. Claim 34 Is Separately Patentable	17
5. Summary.....	18
VIII. APPENDIX A – APPEAL CLAIMS	19
IX. APPENDIX B - EVIDENCE APPENDIX.....	22
X. APPENDIX C - RELATED PROCEEDINGS.....	24

I. REAL PARTY IN INTEREST

The real party in interest is the assignee, Axon Neuroscience GmbH.

II. RELATED APPEALS AND INTERFERENCES

There are no related appeals or interferences.

III. STATUS OF THE CLAIMS

Claims 17-31 are pending and rejected. Claims 1-16 have been canceled. The rejection of claims 17-31 is being appealed.

IV. STATUS OF AMENDMENTS

No amendments are pending.

V. SUMMARY OF CLAIMED SUBJECT MATTER¹

Independent claim 17 is directed to a transgenic non-human animal having germ and/or somatic cells which comprise a DNA construct (para. [0023]²) comprising a cDNA molecule coding for N- and C-terminally truncated tau molecules, wherein: the cDNA molecule has truncated at least 30 nucleotides downstream of the start codon and truncated at least the 30 nucleotides upstream of the stop codon of the full length tau cDNA sequence coding for 4-repeat and 3-repeat tau protein (para: [0026]-[0027]); the cDNA molecule comprises SEQ ID No. 9 (para. [0028]); and the DNA construct encodes a protein, which has neurofibrillary (NF) pathology producing activity when expressed in brain cells of animals (para. [0029]).

Claim 19 depends from claim 17 and recites that the non-human animal is a rat (para. [0023]).

¹ Parentheticals citing to support in the specification for the claim language are exemplary and not meant to indicate that the specific citations are the only support in the specification for the claim language.

² Citations are to paragraphs as numbered in U.S. Publication No. 2006/0112437.

Claim 34 depends from claim 17 and recites that the non-human animal is a mouse (para. [0023]).

Independent claim 25 is directed to a screening assay system and validation system for a candidate for the treatment, prevention, and/or diagnosis of a tauopathy (para. [0088]) comprising: administering the candidate to a non-human transgenic animal of claim 17; evaluating the candidate by: detecting changes of neurofibrillar pathology in said animal (para. [0090]); measuring of neurobehavioral changes in said animal (para. [0091]); measuring of the cognitive score in said animal (para. [0092]); validating the candidate for the treatment and prevention of the tauopathy (para. [0094]); validating diagnostic markers and probes for the detection the tauopathy (para. [0095]); and validating the candidate for the treatment of hypertension, diabetes, dislipidaemia and/or hypercholesterolemia in combination with the tauopathy (para. [0096]).

Independent claim 37 is directed to a transgenic rat having germ and somatic cells which comprise a DNA construct (para. [0023]) comprising a cDNA molecule coding for N- and C-terminally truncated tau molecules operably linked to a promoter functional in mammalian cells (para. [0024]), wherein: the cDNA molecule has truncated at least 30 nucleotides downstream of the start codon and truncated at least the 30 nucleotides upstream of the stop codon of the full length tau cDNA sequence coding for 4-repeat and 3-repeat tau protein (para: [0026]-[0027]); the cDNA molecule comprises SEQ ID No. 9 (para. [0028]); and the DNA construct encodes a protein, which has neurofibrillary (NF) pathology producing activity when expressed in brain cells of rats (para. [0029]).

VI. GROUNDS OF REJECTION TO BE REVIEWED ON APPEAL

Claims 17-33 stand rejected under 35 U.S.C. § 112, first paragraph, as allegedly failing to comply with the enablement requirement.

VII. ARGUMENT

A. The Claims Are Enabled

The Examiner acknowledges that the specification is enabling for claims directed to a transgenic rat whose genome comprises a transgene comprising a DNA construct encoding a N- and C-terminally truncated human tau protein of SEQ ID NO: 9, said DNA operably linked to a promoter, wherein the promoter is a mouse Thy-1 promoter, wherein said truncated tau protein is expressed in the rat brain and neurofibrillary pathology occurs in the rat when compared to normal rats. The Examiner asserts, however, that there is insufficient description to enable the full scope of the current claims. Specifically, the Examiner alleges that the specification does not enable: (1) the scope of the transgenic non-human animal; and (2) the scope of promoters that could drive the expression of the cDNA molecule comprising SEQ ID NO: 9 (Action, p. 3). Contrary to the Examiner's assertions, the specification is enabling as discussed below.

As an initial point, Appellant would like to point out that the Examiner's concerns relating to variability of transgene expression in different animals or under the control of different promoters are misplaced with respect to independent claims 17 and 37 because these claims do not include or require any limitation on the amount of transgene expression. *See e.g., Ex parte Chen*, 61 U.S.P.Q.2D (BNA) 1025, 1028 (BPAI 2001) (non-precedential) ("The examiner's concerns relating to reproducibility of the exact carp, phenotypic characteristics, levels of expression, and reproducibility of identical fish are misplaced, because the claims do not include or require these limitations.")

1. The Transgenic Non-Human Animal

The Examiner asserts that the specification is not enabled for any transgenic animal other than rat because transgene expression in different species of transgenic animals is not predictable and varies according to the particular host species, specific promoter/gene combinations, random transgene insertion, and genetic imprinting. The Action cites publications by Williams (2000) (Exhibit 1), Moreadith (1997) (Exhibit 2), Keefer (2004) (Exhibit 3), and Sigmund (2000) (Exhibit 4) as allegedly supporting this rejection. As discussed below, the specification is enabling for the claimed transgenic animals.

a) The Specification Provides an Enabling Disclosure of How to Make and Use a Transgenic Non-Human Animal

The present specification teaches how to make and use non-human transgenic animals that exhibit pathology that is a useful model for tauopathies such as Alzheimer's disease. This is demonstrated through working examples (Examples 1-5) describing the generation and study of transgenic rat line #318, which expresses an N- and C- double truncated tau protein comprising SEQ ID NO: 9. SEQ ID NO: 9 encodes the minimally truncated tau protein, which corresponds to nucleotides 741-930 (Specification, FIG. 1). The presence of the minimally truncated tau core lacking the N- and C- termini leads to its conformational change, toxic gain of function, and the development of the tau-related neurofibrillary pathology.

The specification discloses that equivalent neurofibrillary pathological structures were observed when comparing the neurofibrillary pathology in the brains of patients suffering from Alzheimer's disease and those observed in the brain of transgenic rat line #318 (Specification, FIG. 10 and related text on pages 20-21 and 25; *see also* FIGs. 6-8 and related text on pages 19-20). Neurofibrillary pathology is the most important and earliest immunohistochemical finding in Alzheimer's disease (*see Braak et al., Acta Neuropathol (Berl)*, 112(4):389-404 (2006))

(Exhibit 5). Accordingly, the specification establishes that a transgenic animal encompassed by the current claims exhibits neurofibrillary pathology, which is the most important and earliest immunohistochemical finding in Alzheimer's disease.

Moreover, neurofibrillary pathology is not the only Alzheimer's disease related characteristic of the transgenic rat disclosed in the present specification. As described in the declaration of Dr. Filipcik provided with Appellant's response filed on January 10, 2007, the expression of truncated tau in rats is a net inducer of oxidative stress, which is another pronounced symptom in human Alzheimer's disease (*see* First Filipcik Declaration, para. 11) (Exhibit 6). This is further confirmed in a paper by Cente *et al.* (Eur J Neurosci., 24(4):1085-90 (2006)) (Exhibit 7), which discloses that truncated tau induces oxidative stress. Additionally, transgenic rat line #318 exhibits hypertension – up to 220 mm/Hg (First Filipcik Declaration, para. 11). It is also easy to induce diabetes in transgenic rat line #318 by using a specific diet formulation (First Filipcik Declaration, para. 11).

Thus, transgenic animals encompassed by the current claims are useful models of diseases exhibiting neurofibrillary pathology, including Alzheimer's disease, because they exhibit the most important and earliest immunohistochemical finding in Alzheimer's disease (*i.e.*, neurofibrillary pathology) and they exhibit other pathological features associated with Alzheimer's disease including cognitive impairment, oxidative stress, hypertension, and diabetes (Filipcik Declaration, para. 11).

b) Transgenic Rat Lines #24, #72, and SHR24/72

In addition to transgenic rat lines #318, other transgenic rats encompassed by the current claims have been created. These include transgenic rat lines #24, #72 (SHR and WKY genetic backgrounds), and SHR24/72. Transgenic rat line #24, which contains a cDNA coding for human tau protein that is shorter by 93 nucleotides (31 amino acids) than the cDNA coding for

human tau protein in transgenic rat line #318, was described in a second Filipcik Declaration filed on September 17, 2007. The DNA construct used in generating transgenic rat line #24 encodes a protein, which has neurofibrillary pathology producing activity when expressed in brain cells of animals, as evidenced by the fact that transgenic rat line #24 exhibits neurofibrillary pathology. In particular, transgenic rat line #24 developed neurofibrillary lesions in the brain stem, spinal cord, primary motor cortex, and hippocampus (Second Filipcik Declaration, para. 5) (Exhibit 8). Neurological examinations showed similar features in both the #24 and #318 transgenic rat lines. For example, the onset and progression of sensory-motor impairment of animals from transgenic line #318 and transgenic line #24 is almost identical (Second Filipcik Declaration, para. 8). Transgenic rats from line #24 were also shown to suffer from early cognitive impairment in an object recognition test (Second Filipcik Declaration, para. 8).

Transgenic rat line #72 was described in the third Filipcik Declaration. The same construct as used in the generation of transgenic rat line #318 also was used in the generation of transgenic rat line #72 (Third Filipcik Declaration, para. 5) (Exhibit 9). The onset and progression of neurodegeneration is the same in all three transgenic rat lines (*i.e.* Tg lines #24, #72, and #318) (Third Filipcik Declaration, para. 6). The only observed difference has been that the life span of those animals containing 4 repeat tau (*e.g.* Tg line #72) is much shorter when compared to those animals containing 3 repeat tau region (*e.g.* Tg line #24) of human tau protein (Third Filipcik Declaration, para. 6).

The phenotype produced by transgenic truncated tau expression was not dependent on genetic background (Third Filipcik Declaration, para. 12). The transgene was transferred from the genetic background of the hypertensive SHR strain (Tg line #72) into the normotensive

Wistar strain (WKY) (Third Filipcik Declaration, para. 12). In this new genetic environment, an almost identical phenotype at the level of biochemical examination and behavioral measurements was observed (Third Filipcik Declaration, para. 12 and Figures 6 and 7).

In addition, transgenic rats were created that contained both 4-repeat and 3-repeat human truncated tau. The resulting phenotype in transgenic line SHR24/72 (expressing both 3R and 4R truncated tau proteins) was synergistic (Third Filipcik Declaration, para. 13). For example, sensorimotor functions measured by beam walking test were significantly more impaired in transgenic line SHR24/72 (expressing both 3R and 4R truncated tau proteins) when compared with transgenic lines SHR24 (expressing 3R truncated tau) and SHR72 (expressing 4R truncated tau) (Third Filipcik Declaration, para. 13 and Figure 8). In addition, neuroscale evaluation showed that the complete neurobehavioral phenotype was significantly more impaired in transgenic line SHR24/72 (expressing both 3R and 4R truncated tau proteins) when compared with transgenic lines SHR24 (expressing 3R truncated tau) and SHR72 (expressing 4R truncated tau) (Third Filipcik Declaration, para. 13 and Figure 9).

Transgenic rat lines #318, #72 (SHR and WKY genetic backgrounds), and #24 are, therefore, evidence of a transgenic non-human animals having germ and/or somatic cells which comprise a DNA construct comprising a cDNA molecule coding for N- and C-terminally truncated tau molecules, wherein: the cDNA molecule is truncated at least 30 nucleotides downstream of the start codon and truncated at least the 30 nucleotides upstream of the stop codon of the full-length tau cDNA sequence coding for 4-repeat and 3-repeat tau protein; (2) the cDNA molecule comprises SEQ ID No. 9; and (3) the DNA construct encodes a protein, which has neurofibrillary (NF) pathology producing activity when expressed in brain cells. Moreover,

these transgenic animals show that a reproducible phenotype can be achieved from different insertional events and different animal strains.

c) **Many Animals Exhibit the Neurofibrillary Pathology Associated With Alzheimer's Disease**

In addition to rats, a variety of animal models would be suitable Alzheimer's disease (AD) models since AD associated neurofibrillary (NF) pathology, based on paired helical filaments (PHF), occurs in a number of animals. In fact, transgenic mouse models of neurofibrillary pathology based on the expression of mutant tau or the overexpression of tau were known at the time the present application was filed (*see* Specification, para. [0005] – [0007]). For example, Lewis *et al.*, (Nat Genet. 2000 Aug; 25(4):402-5)) (Exhibit 10), which is discussed in para. [0005] of the present specification, describes the formation of AD-related NF tangles through expression of mutant human tau in the JNPL3 mouse model. Lewis reported that *“[t]he phenotype of mice expressing P301L mutant tau mimics features of human tauopathies and provides a model for investigating the pathogenesis of diseases with NFT.”* (Lewis *et al.*, Abstract).

In addition to *rats* and *mice*, other animals have been shown to exhibit NF pathology, and therefore, someone of ordinary skill in the art also would expect these other animals to be suitable models for diseases involving NF pathology, such as Alzheimer's disease (AD). For example, Hartig *et al.* (European Journal of Neuroscience, Vol. 25, pp. 69–80, 2007) (Exhibit 11) shows that PHF-like tau occurs in *hamsters*, which parallels the situation in AD (abstract). Hartig also notes that PHF-like tau was observed in *ground squirrels* (p. 69, right col., para. 2).

Huang *et al.*, (Brain Research 771, 1997, 213–220) (Exhibit 12) describes neurofibrillary tangles based on abnormal tau in *rabbits*. The proteins have a molecular structure that closely

resembles that of primates, thus making such an animal system of relevance for human neurodegenerative disease like AD (abstract, p. 214, left col., para. 2, p. 219, left col., para. 2).

Gotz (Brain Research Reviews 35 (2001) 266–286) (Exhibit 13) is a review article that describes several transgenic animal models including the use of murine models expressing tau as system for the dysfunction of tau and neurodegeneration and dementia based on neurofibrillary lesions (abstract, p. 275, right col., item 4.3). Gotz also describes studies neurofibrillary pathology in *lampreys* expressing human tau protein (p. 274, right col., item 4.1).

These reference demonstrate that a variety of animals are capable of exhibiting NF pathology and, therefore, are suitable for the study of NF pathology and Alzheimer's disease. Moreover, the specification, the Lewis publication, and the Gotz publication demonstrate that a tau transgene can be successfully expressed in rat, mouse, and lamprey. In view of the above, the claims are enabled for non-human transgenic animals and the evidence demonstrates that such animals exhibit characteristics that make them suitable models for Alzheimer's disease.

d) The References Cited in the Action

It is well settled that in examining a patent application, the PTO is required to assume that the specification complies with the enablement provisions of 35 U.S.C. § 112 unless it has acceptable evidence or reasoning to suggest otherwise. MPEP § 2164.04. The Examiner's evidence and reasoning, however, fail to show that the specification is not in compliance with the enablement provisions of 35 U.S.C. § 112.

(1) Williams

First, the Action alleges that Williams (2000) (Exhibit 1) is evidence that transgene expression in different species of transgenic animals is not predictable (Action, p. 9-10). Williams points out some potential limitations of transgenic animal experiments (Williams, p. 1124, col. 1 to 1126, col. 1). These potential limitations include variability in transgene

expression level resulting from differences in gene dosage and the sequences surrounding the insertion site, genetic imprinting, and variability in phenotypes between strains. These limitations, however, were known to those in the art. For example, Williams states that the “**conventional practice** to deal with [variable expression] is to establish and analyze multiple lines of transgenic mice bearing any specific transgene, each of which represents a different chromosomal event. It is mandatory for most purposed to assess at least two independent lines.” (Williams, p. 1124, col. 2, 3rd paragraph) (emphasis added). Williams further teaches that “[i]t is a good practice to assess the effects of transgenes or knockouts in more than one mouse strain.” (Williams, p. 1125, col. 1, 3rd paragraph). Thus, it is routine in the art to take measures to account for potential variability in transgenic animals. Enablement is not precluded by the necessity for some experimentation such as routine screening. *In re Wands*, 858 F.2d 731, 737 (Fed. Cir. 1988).

(2) Moreadith

With regard to Moreadith (1997) (Exhibit 2), this publication discusses the history of the development of stem cell technology and methods employed to create knock-out mice. Moreadith does not teach that this technology is limited to mice, but merely states that this particular technology had not yet been applied to hamster, pig, sheep, cattle, rabbit, rat, mink, monkey, and humans (Summary, p. 214). Moreadith noted that as of 1997, putative pluripotential ES cell lines had been derived from each of these species and, therefore, concluded that it **seemed likely** that the technology would be advanced into these additional species over the next few years (Summary, p. 14).

Also in regard to Moreadith, it is important to note that this reference is discussing a particular stem cell technology, but the presently claimed invention is not limited to the use of stem cells. For instance, in Example 2 of the application, the employed technique was micro-

injecting DNA into fertilized oocytes (not ES cells), which were afterwards implanted to the foster mother in 1 or 2-cell stage and which develop normally into the whole animal. Accordingly, any argumentation that ES cells from different organisms may have different features and might in certain cases not continue developing during embryogenesis does not mean that one could not make and use the claimed invention because the claimed invention is not limited to transgenic animals created from ES cells. An applicant need only provide an enabling disclosure for *the claimed invention*. *In re Vaeck*, 947 F.2d 488, 496 (Fed. Cir. 1991).

Finally, Moreadith specifically states that “[t]he development of transgenic technology, whereby genes (or mutations) can be stably introduced into the germline of experimental mammals, *allows investigators to create mice of virtually any genotype* and to assess the consequences of these mutations in the context of a developing and intact mammal.” (Moreadith (1997), Abstract) (emphasis added). In light of (1) Meredith’s statement on the state of the art and (2) Lewis’ disclosure that transgenic mice expressing P301L mutant tau mimics features of human tauopathies and provides a model for investigating the pathogenesis of diseases with NFT (*see* Section VII.A.1.d., *infra*), it is unclear on what grounds the Examiner is basing the argument that the current claims are not enabled with respect to transgenic mice.

(3) Keefer

The Examiner cites Keefer (2004) (Exhibit 3) as teaching a lack of predictability in generating any transgenic animal (Action, p. 13). Keefer, however, discusses the *inefficiency* of pronuclear microinjection in generating transgenic animals. Inefficiency and unpredictability are not equivalent. Something can be inefficient *and* predictable. In fact, it is clear that while pronuclear transfer in cattle, sheep, and goats may be inefficient, Keefer finds it predictable to the point that Keefer teaches specific numbers of oocytes from each animal (1000, 300, and 200, respectively) that should be injected to produce 1 founder transgenic animal (Keefer, p. 6-7).

Thus, the state of pronuclear injection as described in Keefer is such that it is routine and reasonable to inject a few hundred to a thousand oocytes, depending on the animal, to produce a founder transgenic animal.

“The determination of what constitutes undue experimentation in a given case requires the application of a standard of reasonableness, having due regard for the nature of the invention and the state of the art.” *In re Wands*, 858 F.2d 731, 737 (Fed. Cir. 1988). For example, in *Ex parte Chen*, the Board found that a success rate of 1% (20 out of 1746 attempts) for the integration of a transgene into carp cells was not undue in view of disclosure in the specification. 61 U.S.P.Q.2D (BNA) 1025, 1028 (BPAI 2001) (non-precedential).

Keefer does not appear to show any concern as to whether the transgenic animal will express the desired protein, only a concern as to whether the animal will express high amounts of the protein (Keefer, p. 6-7). In this regard, it is important to note that Keefer is focused on the production of bioproducts in livestock, and not on creating an animal model of a disease. In addition, the primary concerns raised by Keefer with respect to the production of transgenic livestock appear to be the long generation intervals and the costs associated with maintaining livestock herds due to the larger size of the animals (Keefer, p. 6). This does not indicate that it will require undue experimentation to make transgenic livestock such as cattle, it only indicates that it will take longer and be more expensive when compared to smaller animals like mice because of the longer generation intervals and the increased cost of maintaining larger animals.

(4) Sigmund

The Examiner cites Sigmund (2000) (Exhibit 4) as corroborating the alleged lack of predictability of phenotypes in transgenic models by disclosing that the phenotype caused by a specific genetic modification is strongly influenced by genes unlinked to the targeted locus. While Sigmund describes that the phenotype caused by a specific genetic modification is

influenced by other genes, Sigmund's point is that researchers need to use an appropriate control animal when assessing the phenotype of the transgenic animal. In this regard, Sigmund states that it is "the responsibility of the investigator to use common sense and design the best possible control experiments that fit the individual situation, to assess whether the phenotype observed in their model is due specifically to the targeted modification or is affected by other loci." (Sigmund, p. 1428, col. 1, 3rd paragraph). Thus, as discussed above with regard to Williams, this variability is a potential limitation of transgenic animals that is known to those in the art. As discussed by both Williams and Sigmund, it is routine in the art to take measures to account for potential variability in transgenic animals. As discussed above, Applicants have confirmed the phenotype of the transgenic rats with multiple lines and in different rat strains. Also as discussed above, a variety of other animals exhibit AD-associated neurofibrillary (NF) pathology, and Lewis' transgenic mouse expressing P301L mutant tau was shown to mimic features of human tauopathies and thereby provide a model for investigating the pathogenesis of diseases with NFT.

2. Promoters

The Action acknowledges that the specification is enabling for a cDNA construct comprising a cDNA molecule comprising SEQ ID NO: 9, but only if the cDNA molecule is operably linked to the mouse Thy-1 promoter (Action, p. 3). In other words, the Examiner is asserting that it would require undue experimentation for a person of ordinary skill in the art to make and use a DNA construct with any promoter other than the mouse Thy-1 promoter, which was the promoter used in transgenic rat line #318.

The Examiner's arguments regarding promoters appear to focus on two issues. One being that it was well known at the time of filing that expression of a gene of interest in a transgenic animal requires operable linkage of the gene to a promoter, but current claim 17 does not expressly recite a promoter. The other being that it was also well known in the art that not all

promoters result in efficient expression in the appropriate target tissue to result in a useful phenotype. The Examiner's reasoning on both points is inconsistent with the legal standard for enablement.

Enablement must be evaluated from the position of a person of ordinary skill in the art. Moreover, ***"a patent need not teach, and preferably omits, what is well known in the art."*** *Hybridtech Inc. v. Monoclonal Antibodies, Inc.*, 802 F.2d 1367 (Fed. Cir. 1987). The Examiner admits that it was well known at the time of filing that expression of a gene of interest in a transgenic animal requires operable linkage of the gene to a promoter, and that it was also well known in the art that not all promoters result in efficient expression in the appropriate target tissue. Given that the Examiner finds that such things were so well known, why wouldn't a person of ordinary skill in the art be able to make and use them?

The Examiner's argument that DNA construct recited in claim 17 is lacking a promoter because the claim does not explicitly recite that cDNA molecule is operably linked to a promoter is unavailing. The specification teaches that a "construct" is a recombinant nucleic acid sequence, generally recombinant DNA sequences, operably linked to tissue specific or general promoter, that is generated for the purpose of the expression of a specific nucleotide sequence(s) in mammalian cells, or is to be used in the construction of other recombinant nucleotide sequences (Specification, p. 6). Thus, in light of the specification, a person of ordinary skill in the art would understand that a "DNA construct" as recited in claim 17 contains a promoter operably linked to the cDNA molecule coding for N- and C- terminally truncated tau molecules.

The Examiner's argument that not all promoters result in efficient expression in the appropriate target tissue is also unavailing. Numerous promoters were known and readily available to those in the art at the time of the filing of the present application. A person of

ordinary skill in the art would further understand that the promoter in the DNA construct is a promoter suitable for expression in mammalian cells. The specification teaches methods for the preparation and evaluation of DNA constructs that may be used in the presently claimed invention (Specification, p. 12, ln. 12-38). With regard to promoters for eukaryotic expression, this passage teaches the use of appropriate promoters for brain expression or ubiquitous expression.

Additional disclosure of cloning truncated tau coding by incorporating appropriate restriction sequences so that it can be cloned under general or tissue specific promoters in an eukaryotic expression vector is disclosed in the specification at page 21, lines 8-36. As noted in the specification, these methods are described in Sambrook *et al.*, *Molecular Cloning, A Laboratory Manual* (Cold Spring Harbor Laboratory Press, 1989) (Specification, p. 21, ln. 34-36).

As mentioned above, numerous promoters were known and readily available to those in the art at the time the application was filed. These include promoters that had been used to drive the expression of transgenic tau in mice. Lewis *et al.* showed the expression of human tau protein in mice using the mouse prior promoter (MoPrP). Table 1 in Gotz identifies four additional promoters that had been used to drive the expression of transgenic tau in mice. Examples of promoters that have been used to drive transgene expression in the central nervous system of various mammals are also provided in the review article by Fitzsimons *et al* (Methods 28:227-236 (2002); *see e.g.*, Tables 1 and 2) (Exhibit 14). The cytomegalovirus (CMV) promoter, for example, had been used to drive the expression of several different transgenes in the central nervous system of rat, mice, and monkeys (Fitzsimons, Table 1). Thus, someone of

ordinary skill in the art would have had a number of known, suitable promoters at his disposal at the time the application was filed.

It would require only routine cloning procedures, such as those described in the present specification or in Sambrook *et al.*, to place a cDNA molecule coding for N- and C-terminally truncated tau molecules under the control of an appropriate promoter. Such routine cloning does not constitute undue experimentation. *In re Wands*, 858 F.2d 731, 737 (Fed. Cir. 1988). Accordingly, the specification provides an enabling disclosure of promoters for the current claims.

3. Claims 19 and 37 Are Separately Patentable

In addition to the arguments presented above, Appellants separately argue the patentability of claims 19 and 37. Claims 19 and 37 are both directed to a transgenic rat. The Examiner acknowledges that the specification is enabling for a transgenic rat (Action, p. 3). Although, in the Advisory Action mailed January 27, 2009, the Examiner expresses concerns about germline transmission and the number of cells in the rat that contain the transgene (Advisory Action, p. 9). These concerns are misplaced, however, because claims 19 and 37 do not include or require germline transmission or a number of cells containing the construct. *See e.g., Ex parte Chen*, 61 U.S.P.Q.2D (BNA) 1025, 1028 (BPAI 2001) (non-precedential) (“The examiner’s concerns relating to reproducibility of the exact carp, phenotypic characteristics, levels of expression, and reproducibility of identical fish are misplaced, because the claims do not include or require these limitations.”)

The only other basis that the Examiner has presented for rejecting claims 19 and 37 is for lack of enablement of promoters that could drive the expression of the cDNA molecule comprising SEQ ID NO: 9. However, claims 19 and 37 do not contain a limitation on the amount of transgene expression. Moreover, for the reasons above in section VII.A.2., the

specification provides an enabling disclosure of promoters that could drive the expression of the cDNA molecule recited in the claims.

4. Claim 34 Is Separately Patentable

In addition to the arguments presented above, Appellants separately argue the patentability of claim 34. Claim 34 depends from claim 17 and recites that the non-human animal is a mouse. As discussed above, the working examples in the specification describe a transgenic rat encompassed by the current claims. The specification teaches that one could also make and use a transgenic mouse encompassed by the current claims. A person of ordinary skill in the art could make and use such a transgenic mouse based on the teachings in the specification and the knowledge in the art. The fact that (1) the methods in the specification successfully produced a transgenic rodent encompassed by the claims, and (2) transgenic mice expressing P301L mutant tau, which were shown to mimic features of human tauopathies, had been created (*see e.g., Lewis et al.*) establish that it would not have required undue experimentation to make and use a transgenic mouse as recited in claim 34.

5. Summary

To be enabling within the meaning of 35 U.S.C. § 112, the application must contain a description sufficient to enable one skilled in the art to make and use the claimed invention without unduly extensive experimentation. For the reasons set forth above, the present specification satisfies this requirement. Appellants, therefore, respectfully request that the Board overturn this rejection.

Respectfully submitted,



Travis M. Wohlers
Reg. No. 57,423
Attorney for Appellant

FULBRIGHT & JAWORSKI L.L.P.
600 Congress Avenue, Suite 2400
Austin, Texas 78701
(512) 536-5654 (telephone)
(512) 536-3035 (facsimile)

Date: March 13, 2009

VIII. APPENDIX A – APPEAL CLAIMS

17. A transgenic non-human animal having germ and/or somatic cells which comprise a DNA construct comprising a cDNA molecule coding for N- and C-terminally truncated tau molecules, wherein:

the cDNA molecule has truncated at least 30 nucleotides downstream of the start codon and truncated at least the 30 nucleotides upstream of the stop codon of the full length tau cDNA sequence coding for 4-repeat and 3-repeat tau protein;

the cDNA molecule comprises SEQ ID No. 9; and

the DNA construct encodes a protein, which has neurofibrillary (NF) pathology producing activity when expressed in brain cells of animals.

18. The transgenic non-human animal of claim 17, further defined as an animal with germ and somatic cells transiently or stably expressing said DNA construct and exhibiting NF pathology in the brain.

19. The transgenic non-human animal of claim 17, further defined as a rat.

20. The transgenic non-human animal of claim 17, wherein the protein encoded by said DNA molecules is expressed in the brain.

21. The transgenic non-human animal of claim 17, further defined as exhibiting NF pathology and having a genetic background allowing the induction of risk factors associated with Alzheimer's disease.

22. The transgenic non-human animal of claim 21, further defined as inducible to exhibit hypertension.

23. The transgenic non-human animal of claim 21, further defined as inducible to exhibit diabetes.

24. The transgenic non-human animal of claim 21, further defined as inducible to exhibit hypercholesterolemia.

25. A screening assay system and validation system for a candidate for the treatment, prevention, and/or diagnosis of a tauopathy comprising:
- administering the candidate to a non-human transgenic animal of claim 17;
 - evaluating the candidate by:
 - detecting changes of neurofibrillar pathology in said animal;
 - measuring of neurobehavioral changes in said animal;
 - measuring of the cognitive score in said animal;
 - validating the candidate for the treatment and prevention of the tauopathy;
 - validating diagnostic markers and probes for the detection the tauopathy; and
 - validating the candidate for the treatment of hypertension, diabetes, dislipidaemia and/or hypercholesterolemia in combination with the tauopathy.
26. The system of claim 25, wherein the tauopathy is Alzheimer's disease.
27. The system of claim 25, further defined as a system for identifying new drug targets in tauopathies and related neurodegeneration processes.
28. A method comprising assaying the efficacy of substances or therapies using an animal according to claim 17.
29. The method of claim 28, further defined as a method for assaying the efficacy of neurofibrillary pathology reducing therapies.
30. The method of claim 28, wherein said substances or therapies are for neurodegenerative diseases.
31. The method of claim 30, wherein said substances or therapies are for a tauopathy.
32. The method of claim 31, wherein said substances or therapies are for a neurodegenerative disease accompanied by neurofibrillary pathology.
33. The method of claim 32, wherein said substances or therapies are for Alzheimer's disease.
34. The transgenic non-human animal of claim 17, further defined as a mouse.

35. The transgenic non-human animal of claim 17, further defined as a rabbit.
36. The transgenic non-human animal of claim 17, further defined as a hamster.
37. A transgenic rat having germ and somatic cells which comprise a DNA construct comprising a cDNA molecule coding for N- and C-terminally truncated tau molecules operably linked to a promoter functional in mammalian cells, wherein:
- the cDNA molecule has truncated at least 30 nucleotides downstream of the start codon and truncated at least the 30 nucleotides upstream of the stop codon of the full length tau cDNA sequence coding for 4-repeat and 3-repeat tau protein;
 - the cDNA molecule comprises SEQ ID No. 9; and
 - the DNA construct encodes a protein, which has neurofibrillary (NF) pathology producing activity when expressed in brain cells of rats.

IX. APPENDIX B - EVIDENCE APPENDIX

Exhibit 1 - Williams *et al.*, J. Appl. Physiol., 88:1119-1126 (2000). First cited in the Office Action dated July 10, 2006.

Exhibit 2 – Moreadith *et al.*, J. Mol. Med., 75(3):208-216 (1997). First cited in the Office Action dated November 28, 2007.

Exhibit 3 – Keefer, Anim. Reprod. Sci, 82-83:5-12 (2004). First cited in the Office Action dated November 28, 2007.

Exhibit 4 – Sigmund, Arterioscler. Thromb. Biol., 20(6):1425-1429 (2000). First cited in the Office Action dated July 10, 2006.

Exhibit 5 - Braak *et al.*, Acta Neuropathol (Berl), 112(4):389-404 (2006). First made of record in the IDS filed on January 9, 2008.

Exhibit 6 - First Filipcik Declaration. Filed on January 10, 2007.

Exhibit 7 - Cente *et al.*, Eur J Neurosci., 24(4):1085-90 (2006). First made of record in the IDS filed on January 9, 2008.

Exhibit 8 - Second Filipcik Declaration. Filed on September 17, 2007.

Exhibit 9 - Third Filipcik Declaration. Filed August 14, 2008 (approved but unsigned) and January 13, 2009 (signed).

Exhibit 10 - Lewis *et al.*, Nat Genet. 2000 Aug; 25(4):402-5). First made of record in the IDS filed on January 9, 2008.

Exhibit 11 - Hartig *et al.*, European Journal of Neuroscience, Vol. 25, pp. 69–80, (2007).

First made of record in the IDS filed on January 9, 2008.

Exhibit 12 - Huang *et al.*, Brain Research 771, 1997, 213–220 (1997). First made of record in the IDS filed on January 9, 2008.

Exhibit 13 – Gotz, Brain Research Reviews 35 (2001) 266–286. First made of record in the IDS filed on January 9, 2008.

Exhibit 14 – Fitzsimons *et al.*, Methods 28:227–236 (2002). First made of record in the IDS filed on January 9, 2008.

X. APPENDIX C - RELATED PROCEEDINGS

None

EXHIBIT 1

invited review

Transgenic animals in integrative biology: approaches and interpretations of outcome

R. SANDERS WILLIAMS¹ AND PETER D. WAGNER²

¹University of Texas Southwestern Medical Center, Dallas, Texas 75390-8573; and

²University of California, San Diego, California 92093-0623

Williams, R. Sanders, and Peter D. Wagner. Transgenic animals in integrative biology: approaches and interpretations of outcome. *J. Appl. Physiol.* 88: 1119–1126, 2000.—Technological innovations in methods for genetic manipulation of laboratory animals and in techniques for assessment of cardiovascular, respiratory, behavioral, and metabolic physiology in mouse models afford unprecedented opportunities for research in integrative biology. We provide here an overview of basic and advanced techniques for generation of transgenic mice and a discussion of how transgenic technology can be most advantageously applied to important physiological questions that can be addressed only within the intact organism.

transgenic mice; homologous recombination; gene knockout; cardiovascular physiology; respiratory physiology; conditional gene knockout

THE COMBINED APPLICATION OF sophisticated methods for assessment of cardiovascular, respiratory, behavioral, and metabolic physiology in intact animals with techniques to generate defined genetic modifications in model organisms creates an almost unlimited horizon of opportunity for integrative biologists. Here, we review the methods used to generate transgenic animal models, the important advantages provided by this class of experimental approaches, and potential problems faced by those using them.

DESCRIPTIONS OF BASIC AND ADVANCED TRANSGENIC METHODS

At the present time, the mouse is the model organism most suitable for the application of transgenic methods to the study of problems in integrative biology. This is because of the well-developed state of techniques for manipulating the genome of this species, the rapid breeding time, the lower maintenance costs of mice compared with larger animals, and our general knowledge of mouse genetics. In addition, the mouse has been selected recently as a model organism in which every gene will be sequenced. Although the small size of these animals leads to challenges in the design and application of instrumentation for physiological measure-

ments, this disadvantage is usually counterbalanced by the many positive features of this species for transgenic experiments.

It is possible currently to introduce transgenes into rats and larger mammals, and physiological assessment of mutant strains of genetically modified zebrafish also holds promise for the future. Model experimental organisms larger than mice offer the obvious advantage that physiological assessments are easier and also provide alternatives when manipulation of the mouse genome does not produce the phenotype one wishes to investigate. Examples of this situation are provided by the hypertensive response of rats but not mice to forced expression of the *REN-2* gene (12) and the more severe spondyloarthropathy produced by *B27* and $\beta 2$ -microglobulin transgenes in rats (5). For most experimental questions that are addressed by transgenic methods, however, the mouse is likely to be the best choice, and this review will focus primarily on this species.

There are two basic approaches to manipulate the mouse genome: random chromosomal integration and homologous recombination of foreign DNA (Fig. 1). The first method is based on integration of DNA into unspecified locations of chromosomes following microinjection into one-cell embryos (fertilized oocytes). The microinjected oocytes are implanted into pseudopregnant females, and the resulting offspring are screened to identify those animals in which the transgene has

First in a series of invited mini-reviews on "Molecular and Cellular Basis of Exercise Adaptations."

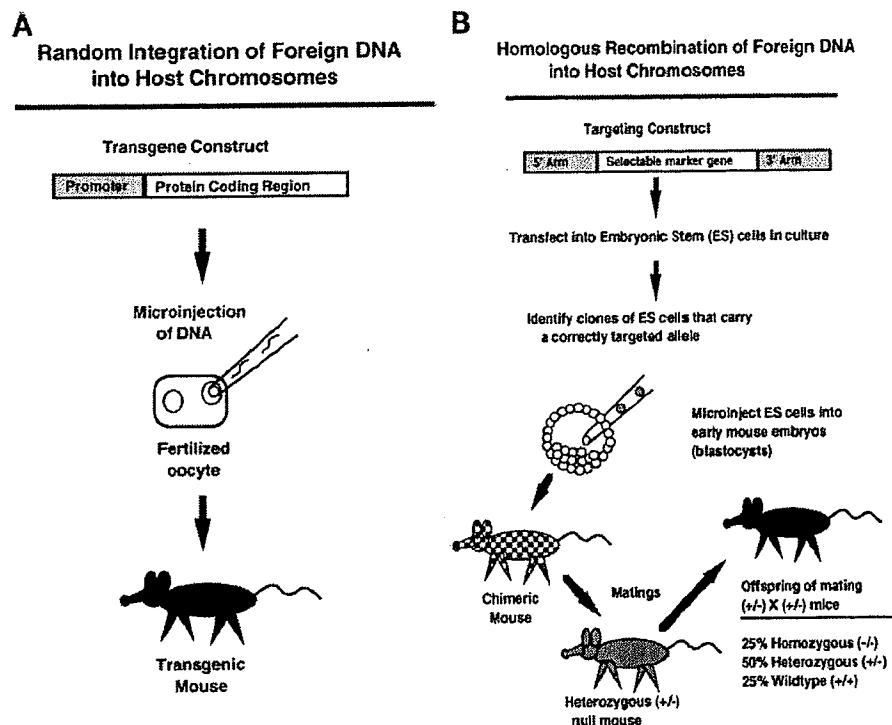


Fig. 1. Schematic illustration of basic transgenic procedures. *A*: generation of germ line transgenic mice by random integration of foreign DNA into host chromosomes following microinjection into one-cell embryos and implantation into pseudopregnant females. *B*: generation of mice bearing specific mutations in endogenous genes by homologous recombination of foreign DNA into specific chromosomal locations. Technique requires manipulation of embryonic stem (ES) cells in culture, followed by microinjection of cloned ES cells carrying the properly targeted allele into early mouse embryos at the blastocyst stage. Mice resulting from this procedure are chimeric, meaning that they include cells derived from the microinjected ES cells as well as the host embryo. If the targeted ES cells have contributed to the germ line (sperm and egg cells) of the chimera, then this animal can pass the targeted allele to its offspring. In the example shown here, the goal was a gene knockout, creating a null allele. Other applications of this procedure are discussed in the text. Initial offspring of a chimeric mouse carry only a single copy of the targeted allele (+/-), but animals homozygous for the null allele (-/-) are generated by mating of 2 heterozygotes. Unless the product of the targeted gene is essential for embryonic and fetal development, the frequency of each possible genotype in the progeny of matings between heterozygous males and females is predicted by Mendelian genetics.

inserted stably into a host chromosome. The second approach, targeted modification of a specific chromosomal locus by homologous recombination, is more complicated. This procedure requires introduction of the foreign DNA sequence into cultured embryonic stem (ES) cells, followed by identification of individual ES cell clones that have the correct mutation, and injection of these ES cells into early mouse embryos at the blastocyst stage. If all goes well, the genetically modified cells contribute to the germ line (sperm or egg cells) of mice that are born following this procedure, such that these animals can pass the modified allele to their offspring. Homologous recombination of foreign DNA, as opposed to random chromosomal integration, allows the investigator to create very precise changes in the genome.

Random integration of a transgene is employed most commonly for one of two purposes: the forced expression of a recombinant protein to alter the physiology and/or morphology of the animal or the analysis of transcriptional control mechanisms involved in regulatory pathways. For most applications, there is no intent to modify endogenous genes. To express a recombinant

protein in intact animals, the foreign DNA that is injected consists of at least two modules: a transcriptional regulatory region selected to direct expression of the foreign gene to a specific cell type or tissue and the region that encodes the foreign protein to be expressed.

To alter the phenotype of an intact animal, the transgene may encode a native protein, so that the experiment addresses the consequences of producing an abnormal quantity of this protein in a cell that normally expresses it ("overexpression"). In other experiments, the design is to express a protein in a cell type that normally does not produce that gene product ("ectopic expression"). Alternatively, the transgene is designed to encode a mutated protein that has been modified for a special purpose: to produce a constitutively active ("gain-of-function mutant") or dominant-negative ("loss-of-function mutant") form of a specific protein or to mimic a mutation observed in a human genetic disease.

Another common application of random chromosomal integration of transgenes is to identify transcriptional control elements (promoters, enhancers, and locus control regions) that respond to developmental

cues or physiological stimuli. In this application, the coding region of a so-called "reporter gene" is linked to the segment of DNA thought to contain the regulatory elements of interest (binding sites for transcription factors). Reporter genes, by definition, encode biologically innocuous proteins that are easily detected by convenient histological or biochemical assays. The goal is to avoid perturbation of the biology of cells in which the reporter gene is expressed while assessing the function of the transcriptional regulatory sequences that are attached to the reporter gene. Commonly used reporter genes encode β -galactosidase, which provides a brilliant blue stain in histological sections; green fluorescent protein, which lights up cells expressing it as green when examined by fluorescence microscopy; and chloramphenicol acetyltransferase or luciferase, which is reliably quantified in cell or tissue extracts using sensitive and simple biochemical assays.

The more complex procedure of homologous recombination of a transgene is used most commonly to produce a deficiency of a specific protein by disrupting transcribed regions (exons) of a specific endogenous gene. This application is called a "gene knockout." The mammalian genome includes two copies of each chromosome (except for the X and Y chromosomes in males), but only one copy of the gene of interest (the "targeted allele") is disrupted in the mice produced initially. This permits analysis of heterozygous animals bearing a single targeted (null) allele, which may or may not produce an abnormal phenotype. "Haploinsufficiency" is a term that is used when abnormalities result from mutation of only one of the two copies of a given gene. If heterozygous null animals are viable and fertile, they are mated. The mating of two heterozygote null animals generates litters in which, on average, 25% have two copies of the modified allele (homozygous null, $-/-$) and therefore are completely deficient in the protein encoded by this gene. On average, one-half of such litters will be heterozygous ($+/-$) for the null allele (like the parents) and the remaining 25% will be normal ($+/+$ or "wild type"). The actual percentages of genotypes represented in the offspring of such a mating will differ from those predicted by Mendelian genetics if the targeted gene has an essential function during embryonic or fetal life. Many different outcomes are possible, ranging from 100% survival of homozygous null animals to complete embryonic lethality of genetically modified animals. Prenatal or perinatal death of heterozygous or homozygous null animals may be an exciting result for the developmental biologist but a disappointing outcome for the integrative biologist interested in the function of the targeted gene in adult animals. For example, this problem has limited studies of homeostatic responses to hypoxia in adult animals mediated by the hypoxia-inducible transcription factor HIF-1 α (7) or the angiogenic growth factor VEGF (vascular endothelial growth factor) (3).

A solution to this problem can be provided by "conditional knockouts" (Fig. 2). A method successful for this purpose is based on the ability of an enzyme called Cre recombinase, a 30-kDa enzyme native to bacteriophage

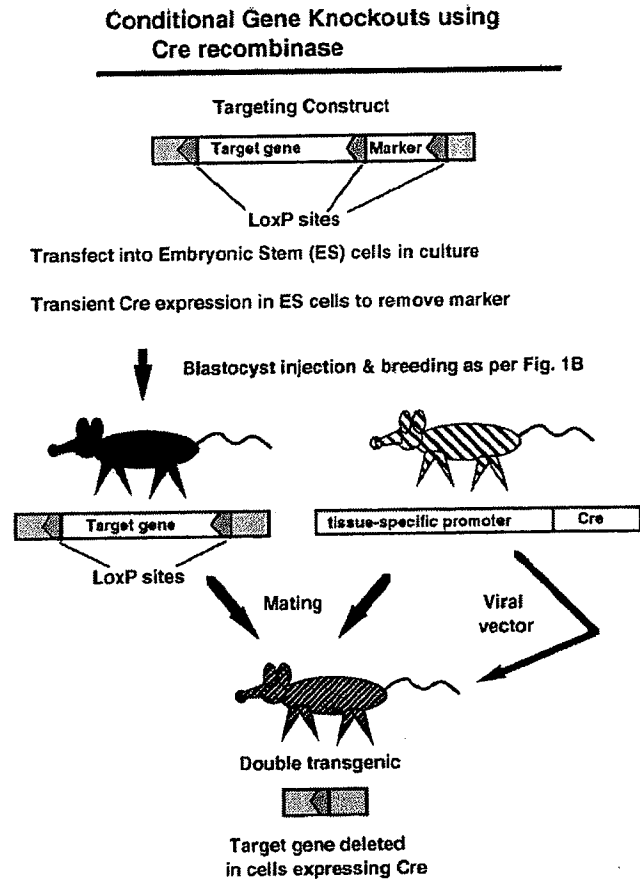


Fig. 2. A conditional gene knockout strategy using Cre recombinase. This sophisticated technique is based on the ability of Cre recombinase to recognize a unique nucleotide sequence (LoxP site), to remove the intervening DNA, and to recombine the ends. The usual procedure requires generation of 2 independent varieties of transgenic mice. The first is generated by homologous recombination (see Fig. 1B) to insert LoxP sites into the gene of interest in a manner in which function of the gene is not impaired (see text). A second line of transgenic mice is generated by random chromosomal insertion (see Fig. 1A) of a transgene expressing Cre recombinase under the control of a tissue-specific promoter. Double transgenic animals resulting from matings of these original transgenic lines will carry null alleles of the gene of interest only in those cells that have expressed Cre. It also is possible to introduce Cre by somatic cell gene transfer using viral vectors without a requirement for establishing germ line transmission of Cre.

P1, to remove segments of DNA that lie between two copies of a unique 34-bp sequence termed a LoxP site (9, 15). To apply this "Cre-Lox" strategy, the gene of interest is first modified by homologous recombination in ES cells in a manner analogous to a gene knockout but with the important difference that the targeted allele is modified by the insertion of two LoxP elements without disrupting the normal function of the gene. This usually means their insertion into introns at sites that do not influence RNA splicing but that flank coding regions (exons) essential to produce a functional gene product. After a number of technical steps we will not discuss here, transgenic mice are then produced that carry two copies of the targeted allele in all cells. These animals are phenotypically normal, since the function

of the targeted gene has not yet been altered. There are then two ways to create functionally null alleles at the targeted locus in the tissue of interest. One can introduce Cre recombinase via a viral vector, such that the targeted gene is knocked out only in infected cells. Alternatively, one can breed the mice carrying the LoxP-tagged gene to another line of transgenic mice in which Cre recombinase is expressed from a tissue-specific or drug-regulated promoter. By either method, Cre recognizes LoxP sequences, excises the segment of DNA between the LoxP sites, and recombines the remainder of the gene, thereby rendering it nonfunctional. Such a procedure will inactivate the gene but only in those cells in which Cre has been expressed. The alteration of the genome produced by Cre is permanent and will be passed to all daughter cells arising by mitosis of the cell originally expressing Cre, even if Cre is no longer present.

An example of how a conditional knockout strategy can be applied to a problem in cardiovascular physiology is provided by recent studies with respect to the role of endothelins in cardiac hypertrophy. A standard knockout of the endothelin-1 (ET-1) gene is lethal at birth in homozygous null animals because of craniofacial abnormalities that interfere with normal respiration (8). In contrast, animals bearing a conditional knockout of the ET-1 gene in cardiomyocytes (based on expression of Cre recombinase under the control of the cardiac-specific α -myosin heavy chain promoter) are viable and avoid the extra cardiac manifestations of ET-1 deficiency. When these animals are subjected to hypertrophic stimuli, however, their altered responses reveal autocrine or paracrine functions of ET-1 synthesized in cardiomyocytes in the control of hypertrophic growth of the heart (R. Shohet and M. Yanagisawa, personal communication).

These Cre-Lox strategies add additional layers of complexity and expense to the experiment. Nevertheless, these powerful techniques are likely to become a standard methodology used to approach problems in integrative biology, as applied to many genes of physiological importance. In principle, conditional knockouts permit the investigator to control the timing at which cells experience a deficiency in a given protein, thereby circumventing both embryonic lethality and confounding effects of complex adaptive responses that can occur when the physiological observations follow the gene knockout event by days or weeks.

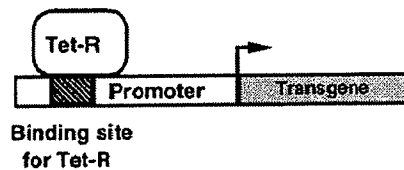
Another important variation on the theme of using homologous recombination to produce a null (knockout) allele is the related approach of introducing a new gene into the same locus (termed a "knock-in"). This strategy may be used to insert a reporter gene (e.g., green fluorescent protein), the expression of which is then subjected to the identical regulatory controls that were placed on the gene that was replaced. This is useful for tagging particular cell types or to facilitate studies of gene regulation. Alternatively, gene replacement may be used to assess the degree of functional redundancy among two related proteins or to examine the pheno-

type produced by replacing a normal protein with a mutated form.

The technique of drug-regulated transgene expression was mentioned previously with respect to controlling the timing at which Cre recombinase is expressed in a conditional knockout experiment. This strategy also can be applied productively to other types of experiments in which the investigator wishes to control the timing of transgene expression. Such control becomes important when acute rather than chronic responses to the transgene are the issue of greatest biological interest or when chronic transgene expression is lethal. A variety of systems have been developed for this purpose, the principles of which are illustrated in Fig. 3. The fundamental requirements include the expression of a transcription factor (either a repressor or an inducer of transcription) that becomes active in the presence of a drug that can be administered systemically to the animal. Methods based on binding of tetracycline to the inducible transcription factor have been most widely used (23). The transcriptional regulatory region of the transgene is designed to include a binding site for this drug-regulated transcription factor. Like conditional gene knockouts, this strategy requires two separate genetic modifications: the first to

Drug-Regulated Expression of Transgenes

Without drug: transgene is repressed



With drug: transgene is activated

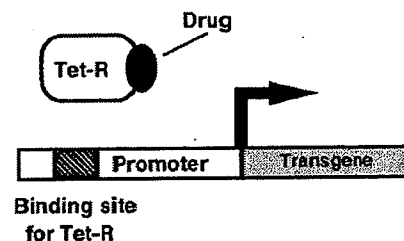


Fig. 3. A system for drug-regulated transgene expression. Investigators can control the expression of a transgene by engineering animals to express a transcription factor that is regulated by binding of small molecules. One such system is based on the ability of the bacterial Tet repressor (Tet-R) protein to inhibit transcription of genes that contain a unique nucleotide recognition sequence to which Tet-R binds (binding site for Tet-R). Transcriptional repression by Tet-R (small arrow) is relieved in the presence of tetracycline (drug) and the transgene becomes activated (large arrow).

express the drug-responsive transcription factor in the correct cell type and the second to insert the ultimate transgene of interest with its binding site for the drug-responsive transcription factor. This approach has great appeal, since an ability to regulate transgene expression effectively circumvents the difficulties posed by embryonic lethality or chronic adaptive responses. In practice, however, the current inducible systems appear often to suffer from either excessive transgene expression in the "off" state or insufficient transgene expression in the "on" state, and successful applications of drug-regulated transgene expression to questions of integrative biology have been uncommon. It is reasonable to anticipate that further technical improvements will bring this general approach into widespread use.

A number of other advanced transgenic technologies may be useful in special circumstances. It is possible, for example, to use homologous recombination to insert a single copy of a transgene construction into a specific chromosomal location that has been selected not to modify an endogenous gene but to provide a genomic site that is insulated from effects of flanking DNA that otherwise would modify transgene expression. This strategy markedly reduces the variations in transgene expression that plague experiments based on random integration of transgenes. Another maneuver that sometimes proves advantageous is the use of bicistronic transcriptional units in the transgene construction. This means placing cDNA segments encoding two different proteins downstream of a single promoter, separated by an internal ribosomal entry site element. The transgene is transcribed to generate a single mRNA species that is translated to make two different proteins at the same time. Finally, it is sometimes advantageous to study genetic chimeras, animals that include cells of two different genotypes. The generation of chimeric mice is a necessary step in the creation of gene knockout models, since genetically modified ES cells are admixed with wild-type cells at the blastula stage, and cells of both genotypes contribute to the adult animal produced by this procedure. In a typical knockout project, the chimeras are usually discarded after breeding. However, if one develops ES cells that are homozygous for a targeted allele and uses these to produce chimeric mice, it is then possible to compare the behavior of cells lacking the protein produced from the targeted gene with wild-type cells directly in the same animal.

ADVANTAGES OF TRANSGENIC ANIMAL EXPERIMENTS TO ADDRESS QUESTIONS IN INTEGRATIVE BIOLOGY

A properly designed transgenic experiment can be a thing of exquisite beauty in that the results support absolutely unambiguous conclusions regarding the function of a given gene or protein within the authentic biological context of an intact animal. A transgenic experiment may provide the most rigorous test possible of a mechanistic hypothesis that was generated by previous observational studies. A successful transgenic experiment can cut through layers of uncertainty that cloud the interpretation of the results produced by

other experimental designs. For example, drugs employed to inhibit the function of a given protein in an intact animal invariably produce effects other than the specific perturbation that is the focus of the investigation. Experiments that rely on gene transfer into tissues of intact animals (as opposed to the germ line transmission mode) suffer from the often inconsistent or transient nature of transgene expression and from artifacts relating to the gene transfer vector (e.g., immune responses to adenoviral proteins). However, genes may serve different functions during embryonic and fetal development as opposed to postnatal life, and unexpected consequences of genomic modifications are frequent. The initial results of a transgenic experiment not infrequently mark the beginning, and not the end, of a mechanistic journey.

Genomic interventions may reveal the biological importance of a gene product when other experimental strategies fail. A good example of this principle is that of HIF-1 α in the hypoxically challenged lung (22). The observation that normal mice exposed to 10% O₂ do not elevate HIF-1 α protein suggested that HIF-1 α is not involved in the pulmonary response to hypoxia. However, when HIF-1 α (+/-) animals were exposed to this level of hypoxia for 1-6 wk, there was substantial attenuation of the pulmonary vascular remodeling, pulmonary hypertension, and right ventricular hypertrophy seen in wild-type (HIF-1 α +/+) mice. Although these results cannot define the molecular mechanism(s) by which HIF-1 α is acting in this situation, they reveal unequivocally a functional involvement for this hypoxic response protein that could not be discerned by observational studies only. The explanation for how HIF-1 α is functioning without being detected by immunoblotting techniques may lie in the very rapid decay of this protein after hypoxia is relieved (19).

Genetically modified strains of mice also can provide convenient and authentic models of human diseases. Disease phenotypes produced by a given transgene are often highly penetrant within the inbred strains of mice that are commonly employed for such models, yielding reliable and consistent results. Such consistency of a disease phenotype contrasts favorably with disease models created by dietary, pharmacological, or surgical manipulations, and transgenic models can be generated quite rapidly when all goes well. For laboratories in which transgenic technology is well established, recombinant DNA is the only additional reagent that is required to produce transgenic mice by random chromosomal insertion, and the biochemical techniques required for assembly of the various components of the transgene construction are simple and rapid.

The application of transgenic technology to problems in integrative biology has several other advantageous features. Transgenic lines generated with one transgene can be crossed with other lines bearing a different transgene to create double mutants. It is particularly useful to identify measures capable of correcting ("rescuing") a disease phenotype that was modeled initially by a single transgenic approach. For example, two groups have recently described the genetic rescue of

cardiomyopathic mice that were generated initially by a knockout of the gene encoding muscle LIM protein (MLP). MLP-null ($-/-$) mice develop a dilated cardiomyopathy in the first few weeks of postnatal life. Rockman et al. (16) prevented cardiomyopathy in mice deficient in MLP by forced overexpression in the heart of a peptide inhibitor of the β -adrenergic receptor kinase. Minamisawa et al. (11) showed that mice deficient in expression of phospholamban because of disruption of this gene also are protected against the cardiomyopathy that otherwise would result from a deficiency of MLP. These studies have important implications both for our understanding of the pathobiology of heart failure and for the design of novel therapeutic approaches. These studies also demonstrate how genetically modified mice can provide a source of stably modified cells for experiments in tissue culture. In this manner, reductionist approaches in a more controlled environment can be used to complement analyses performed in intact animals.

Finally, the attractiveness of transgenic experiments in mice has been enhanced markedly by the ingenuity of integrative and systems biologists who have developed techniques for sophisticated physiological assessments of these tiny animals. For example, the heart of an adult mouse is smaller than a raisin, but a number of laboratories have achieved remarkable proficiency in the analysis of ventricular performance, contractile physiology, and myocardial metabolism within the intact animal or in isolated heart preparations. It also has been possible to assess respiratory control mechanisms in genetically modified mice, even at a relatively young age (1).

POTENTIAL PITFALLS AND LIMITATIONS OF TRANSGENIC ANIMAL EXPERIMENTS

All current transgenic procedures require specialized equipment and skilled operators. The best results are obtained in settings where the responsible individuals are dedicated to these activities. Even in settings where core labs provide this technology as a service to other investigators, the time and expense required to generate and analyze informative transgenic models should not be underestimated. Animal husbandry becomes a major component of the experiment, and it is easy to become mired down in the effort to produce and maintain a sufficient number of animals of the correct genotypes for the desired analyses. Even a modestly sized transgenic colony can consume \$5,000–10,000 a month or more in animal housing costs and occupy the efforts of several personnel.

Initially, positive and exciting results may be only a beginning. For example, Huang et al. (6) deleted the gene encoding endothelial nitric oxide synthase (eNOS) and found that mean arterial blood pressure was 20 mmHg higher than in wild-type controls. The appealingly simple explanation that peripheral vasodilation is impaired because of reduced synthesis of nitric oxide (NO) may not, however, be sufficient to account for this result. Perhaps eNOS-generated NO is important in regulating other molecules with vasoactive properties,

in controlling cardiac output as well as peripheral vasodilation as a determinant of blood pressure, or in modifying baroreceptor function or vasomotor controls in the central nervous system. Our point is to emphasize that a genomic manipulation followed by an initial description of a phenotype often opens up additional questions, and investigators should plan accordingly.

Negative results of an initial transgenic experiment, too, may represent only the beginning of an interesting and important scientific journey. If trivial or artifactual explanations for the lack of phenotype (i.e., no measurable structural or functional consequences) following a given genetic modification can be excluded, then a number of possible explanations should be considered, demanding additional experiments. A common trivial problem in gain-of-function or dominant-negative research designs is a failure to express the transgene to physiologically relevant levels in the temporal and spatial pattern expected. When the transgene integrates randomly into host chromosomes, several variables that can exert profound influences on expression of the transgene are uncontrolled, sometimes leading to negative or artifactual results. The foreign DNA usually integrates as linear arrays, comprising variable numbers of copies of the transgene construction. Although one might expect intuitively that a greater number of copies of the transgene would result in higher levels of expression, this is often not the case. In addition, the desired function of transcriptional regulatory elements included with the transgene (e.g., muscle-specific expression) can be influenced profoundly by the chromosomal location in which the transgene integrates. Random transgene insertion occasionally may alter endogenous genes (insertional mutagenesis), thereby confounding the interpretation of the phenotype. Finally, more exotic problems, such as genetic imprinting (transcriptional silencing of a gene based on transmission from parent to offspring of repressive nucleosomal structures), may arise and produce confusing results. Variability in transgene expression based on differences in gene dosage and in DNA sequences flanking the insertion site are a universal feature of all experiments using this approach, whereas the latter problems arise only occasionally.

The conventional practice to deal with this problem is to establish and analyze multiple lines of transgenic mice bearing any specific transgene, each of which represents a different chromosomal insertion event. It is mandatory for most purposes to assess at least two independent lines. Whenever possible, it is advantageous to assess dose-response relationships between transgene expression and a given phenotype by analyzing separate lines of transgenic mice that express the transgene product at each of several levels of abundance. For experiments designed to assess the function of transcriptional control elements contained within the transgene, it may be necessary to assess 5–10 independent transgenic lines to be confident of a correct interpretation.

Targeted modifications of endogenous genes by homologous recombination circumvents the uncertainties

associated with random chromosomal insertion of transgenes. However, surprises may occur even with this more sophisticated and demanding technology. For example, in creating a null allele in one gene, it is possible unwittingly to destroy transcriptional control elements that govern expression of a neighboring gene. Such events seem to explain occasions when two different labs knock out the same gene but observe different phenotypes based on subtle differences in the specific design of the targeting vector (13). It is advisable to have as much information as possible about the genomic organization of the targeted region to avoid or at least to be aware of potential difficulties of this nature.

We have already discussed how embryonic lethality may preclude testing of the original hypothesis, a disappointing initial result for some experiments. Transgenic experiments designed to test hypotheses that relate to physiological regulation or pathophysiology of adult animals become infeasible if the specific genetic modification impairs an essential developmental function and transgenic animals die in utero. An essential function for a given gene during development may be unrelated to its functions during adult life. For experiments in which overexpression or ectopic expression of a transgene or gene deletion is the goal, the problem of embryonic lethality can be avoided by the use of transcriptional control regions that are inactive (or nearly so) during embryonic and fetal life but highly active in the adult tissues of interest. The α -myosin heavy chain promoter has this property with respect to cardiac-specific expression (20) and has been widely and successfully employed to drive expression of transgenes in the adult or neonatal heart that would be likely to produce lethal effects in embryos. Unfortunately, correspondingly timed promoters are not available for transgene expression in many other cell types.

Investigators using transgenic animals also must be cognizant of potential differences in phenotypes observed when an apparently identical genetic modification is examined in different inbred strains of mice or in outbred animals. The same overexpressed transgene or gene knockout may produce a phenotype that is severe in one strain and mild in another. The hypoxia-responsive transcription factor EPAS-1 is essential for survival in certain strains of mice (21) but EPAS-1 $-/-$ animals survive when the null allele is crossed into different genetic backgrounds (R. Hammer, personal communication). The basis for such differences lies in so-called "modifier genes," allelic variations that influence the responses to a transgene. It is a good practice to assess the effects of transgenes or knockouts in more than one mouse strain.

Adaptive responses to a genetic modification may confound the interpretation of phenotypes. It is important to remember that the phenotype observed in any transgenic experiment is a function both of the planned genetic modification and of secondary responses of the organism to that perturbation. A dramatic example of this principle was provided recently by our own studies of mice in which the myoglobin gene was disrupted. Previous experiments using pharmacological inhibitors

of oxymyoglobin formation demonstrated that myoglobin was essential to maintain energy metabolism and contractile function of the myocardium. Surprisingly, however, we found that normal cardiac function could be maintained in mice completely devoid of myoglobin (4). Although this result could be interpreted to indicate that myoglobin is unimportant for oxygen transfer in the myocardium, this is probably not correct. We have subsequently determined that survival in the absence of myoglobin is possible only because of powerful adaptive responses that compensate for the absence of myoglobin. The examination of a large number of offspring from heterozygote crosses (i.e., mating of two myoglobin $+/-$ animals) revealed that more than half of embryos without myoglobin ($-/-$) die in utero between embryonic day 9.5 and 11.5, a period of rapid growth (and presumably increasing energetic demands) of the embryonic heart. The myoglobin $-/-$ animals that survive demonstrate increased expression of hypoxia-responsive genes, increased vascularity of the heart, increased coronary blood flow, increased Hb concentrations, and reprogramming of myocardial gene expression with respect to many other genes (D. Garry and R. S. Williams, unpublished observations). Apparently, myoglobin deficiency is fatal unless these pleiotropic adaptive responses are sufficiently robust to compensate for the defect in oxygen transfer. Further exploration of the molecular basis for survival in the absence of myoglobin using this transgenic model should extend our understanding of the repertoire of defense mechanisms used by mammalian organisms to maintain function when oxygen transport is limited.

The HIF-1 α gene deletion studies of Yu et al. (22) further illustrate the care that must be taken in studying the effects of a gene deletion. When HIF-1 α $+/-$ (heterozygous null) mice are exposed to 10% O₂ for 6 wk, two of the major physiological adaptations to hypoxia, polycythemia and right ventricular hypertrophy, are similar to those observed in wild-type (HIF-1 α $+/+$) littermates. If the animals had been examined at only this single time point, one would conclude that haploinsufficiency of HIF-1 α is unimportant for these adaptations. However, measurements made after 1, 2, 3, 4, and 5 wk of hypoxia showed a delay in both erythrocytosis and right ventricular hypertrophy in the early weeks, demonstrating a role for HIF-1 α in these processes.

Many mammalian proteins are present as multiple isoforms, closely related proteins derived from different genes. The planning and interpretation of gene knockout experiments, in particular, must take into account the potential for overlapping or redundant functions of such proteins. It often may be necessary to generate animals bearing null alleles in two or more proteins of multigene families to gain an understanding of their function. A prominent example of such functional redundancy among individual members of multigene families involves members of the MyoD family of basic helix-loop-helix proteins that we now know exert overlapping but distinctive functions during development of skeletal muscles and in muscle regeneration following injury.

Skeletal muscle development is nearly normal in mice that lack either MyoD or the closely related Myf5 protein (2, 17); however, the double knockout (MyoD^{-/-};Myf5^{-/-}) has a severe phenotype, and skeletal muscles fail to form (18). Although these two genes are not entirely redundant (14), each is capable of compensating for a deficiency of the other with respect to myogenic differentiation during embryonic life. Interestingly, however, the degree of functional redundancy of these two proteins is less complete during muscle repair following injury to adult muscles, and animals lacking only MyoD have a severe deficit in muscle regeneration (10).

Finally, it is important to use caution in interpreting the results of transgenic experiments that involve overexpression of a given protein in transgenic mice, as produced by linkage of a highly active promoter to the protein coding region of the gene of interest. It should be remembered that exaggerated physiological effects produced in such an experiment demonstrate only that the gene/protein in question is capable of the observed function. The results of an overexpression experiment cannot, in the absence of other data, establish the normal physiological role of that gene or protein.

SUMMARY AND CONCLUSIONS

This review has been intended as an introduction to transgenic technology for investigators skilled in physiological disciplines who are moving to incorporate transgenic technology into their research. The analysis of genetically modified animals can provide otherwise unattainable opportunities to advance our understanding of homeostatic mechanisms and pathophysiological principles. Integrative biologists have already leaped forward aggressively to embrace this technology, sometimes with dramatically pleasing results. Investigators who are just beginning to incorporate transgenic approaches into their experimental strategies are well advised to seek counsel from laboratories with long-standing experience in this methodology. Nuances of the design of transgenic experiments, in addition to those discussed here, may have an important influence on the outcome and interpretation of research. Overall, perhaps the best advice to investigators new to this mode of experimentation is "Expect the unexpected!"

Address for reprint requests and other correspondence: R. S. Williams, Univ. of Texas Southwestern Medical Center, 5323 Harry Hines Blvd., NB11.200, Dallas, TX 75390-8573 (E-mail: williams@ryburn.swmed.edu).

REFERENCES

- Bermingham, J. R., Jr., S. S. Scherer, S. O'Connell, E. Arroyo, K. A. Kalla, F. L. Powell, and M. G. Rosenfeld. Tst-1/Oct-6/SCIP regulates a unique step in peripheral myelination and is required for normal respiration. *Genes Dev.* 10: 1751-1762, 1996.
- Braun, T., M. A. Rudnicki, H. H. Arnold, and R. Jaenisch. Targeted inactivation of the muscle regulatory gene Myf-5 results in abnormal rib development and perinatal death. *Cell* 71: 369-382, 1992.
- Ferrara, N., K. Carver-Moore, H. Chen, M. Dowd, L. Lu, K. S. O'Shea, L. Powell-Braxton, K. J. Hillan, and M. W. Moore. Heterozygous embryonic lethality induced by targeted inactivation of the VEGF gene. *Nature* 380: 439-442, 1996.
- Garry, D. J., G. A. Ordway, J. N. Lorenz, N. B. Radford, E. R. Chin, R. W. Grange, R. Bassel-Duby, and R. S. Williams. Mice without myoglobin. *Nature* 395: 905-908, 1998.
- Hammer, R. E., S. D. Maika, J. A. Richardson, J. P. Tang, and J. D. Taurog. Spontaneous inflammatory disease in transgenic rats expressing HLA-B27 and human β 2m: an animal model of HLA-B27-associated human disorders. *Cell* 63: 1099-1112, 1990.
- Huang, P. L., Z. Huang, H. Mashimo, K. D. Bloch, M. A. Moskowitz, J. A. Bevan, and M. C. Fishman. Hypertension in mice lacking the gene for endothelial nitric oxide synthase. *Nature* 377: 239-242, 1995.
- Iyer, N. V., L. E. Kotch, F. Agani, S. W. Leung, E. Laughner, R. H. Wenger, M. Cassmann, J. D. Gearhart, A. M. Lawler, A. Y. Yu, and G. L. Semenza. Cellular and developmental control of O₂ homeostasis by hypoxia-inducible factor 1 α . *Genes Dev.* 12: 149-162, 1998.
- Kurihara, Y., H. Kurihara, H. Suzuki, T. Kodama, K. Mae-mura, R. Nagai, H. Oda, T. Kuwaki, W. H. Cao, N. Kamada, K. Jishage, Y. Ouchi, S. Azuma, Y. Toyoda, T. Ishikawa, M. Kumada, and Y. Yazaki. Elevated blood pressure and craniofacial abnormalities in mice deficient in endothelin-1. *Nature* 368: 703-710, 1994.
- Marth, J. D. Recent advances in gene mutagenesis by site-directed recombination. *J. Clin. Invest.* 97: 1999-2002, 1996.
- Megeney, L. A., B. Kablar, K. Garrett, J. E. Anderson, and M. A. Rudnicki. MyoD is required for myogenic stem cell function in adult skeletal muscle. *Genes Dev.* 10: 1173-1183, 1996.
- Minamisawa, S., M. Hoshijima, G. Chu, C. A. Ward, K. Frank, Y. Gu, M. E. Martone, U. A. Betz, W. Muller, J. Roes, K. Kranias, W. R. Giles, and K. R. Chien. Chronic phospholamban-sarcoplasmic reticulum calcium ATPase interaction is the critical calcium cycling defect in dilated cardiomyopathy. *Cell* 99: 313-322, 1999.
- Mullins, J. J., J. Peters, and D. Ganten. Fulminant hypertension in transgenic rats harbouring the mouse Ren-2 gene. *Nature* 344: 541-544, 1990.
- Olson, E. N., H. H. Arnold, P. W. Rigby, and B. J. Wold. Know your neighbors: three phenotypes in null mutants of the myogenic bHLH gene MRF4. *Cell* 85: 1-4, 1996.
- Ordahl, C. P., and B. A. Williams. Knowing chops from chuck: roasting myoD redundancy. *Bioessays* 20: 357-362, 1998.
- Rajewsky, K., H. Gu, R. Kuhn, U. A. Betz, W. Muller, J. Roes, and F. Schwenk. Conditional gene targeting. *J. Clin. Invest.* 98: 600-603, 1996.
- Rockman, H. A., K. R. Chien, D. J. Choi, G. Iaccarino, J. J. Hunter, J. Ross, Jr., R. J. Lefkowitz, and W. J. Koch. Expression of a β -adrenergic receptor kinase 1 inhibitor prevents the development of myocardial failure in gene-targeted mice. *Proc. Natl. Acad. Sci. USA* 95: 7000-7005, 1998.
- Rudnicki, M. A., T. Braun, S. Hinuma, and R. Jaenisch. Inactivation of MyoD in mice leads to up-regulation of the myogenic HLH gene Myf-5 and results in apparently normal muscle development. *Cell* 71: 383-390, 1992.
- Rudnicki, M. A., P. N. Schnegelsberg, R. H. Stead, T. Braun, H. H. Arnold, and R. Jaenisch. MyoD or Myf-5 is required for the formation of skeletal muscle. *Cell* 75: 1351-1359, 1993.
- Semenza, G. L., F. Agani, N. Iyer, B. H. Jiang, S. Leung, C. Wiener, and A. Yu. Hypoxia-inducible factor 1: from molecular biology to cardiopulmonary physiology. *Chest* 114: 40S-45S, 1998.
- Subramaniam, A., W. K. Jones, J. Gulick, S. Wert, J. Neumann, and J. Robbins. Tissue-specific regulation of the α -myosin heavy chain gene promoter in transgenic mice. *J. Biol. Chem.* 266: 24613-24620, 1991.
- Tian, H., R. E. Hammer, A. M. Matsumoto, D. W. Russell, and S. L. McKnight. The hypoxia-responsive transcription factor EPAS1 is essential for catecholamine homeostasis and protection against heart failure during embryonic development. *Genes Dev.* 12: 3320-3324, 1998.
- Yu, A. Y., L. A. Shimoda, N. V. Iyer, D. L. Huso, X. Sun, R. McWilliams, T. Beaty, J. S. Sham, C. M. Wiener, J. T. Sylvester, and G. L. Semenza. Impaired physiological responses to chronic hypoxia in mice partially deficient for hypoxia-inducible factor 1 α . *J. Clin. Invest.* 103: 691-696, 1999.
- Yu, Z., C. S. Redfern, and G. I. Fishman. Conditional transgene expression in the heart. *Circ. Res.* 79: 691-697, 1996.

EXHIBIT 2

REVIEW

Randall Wade Moreadith · Nina Butwell Radford

**Gene targeting in embryonic stem cells:
the new physiology and metabolism**

Received: 28 June 1996 / Accepted: 4 October 1996

Abstract The development of transgenic technology, whereby genes (or mutations) can be stably introduced into the germline of experimental mammals, now allows investigators to create mice of virtually any genotype and to assess the consequences of these mutations in the context of a developing and intact mammal. In contrast to traditional “gain-of-function” mutations, typically created by microinjection of the gene of interest into the one-celled zygote, gene targeting via homologous recombination in pluripotential embryonic stem cells allows one to modify *precisely* the gene of interest. The purpose of this review is to introduce the reader to the history of development of embryonic stem cell technology, the current methods employed to create “knock-out” mice, and the application of these methods to solve problems in biology. While the technology promises to provide enormous insight into mammalian development genetics, our desire is that this review will stimulate the application of gene targeting in embryonic stem cells to begin to unravel problems in complex regulatory pathways, specifically intermediary metabolism and physiology.

Key words Gene targeting · Transgenic animals · Molecular biology · Metabolism · Physiology

Abbreviations *EC cell* Embryonal carcinoma cell · *ES cell* Embryonic stem cell · *HPRT* Hypoxanthine phosphoribosyltransferase · *NMR* Nuclear magnetic resonance

Introduction

The development of techniques for introducing genes (or mutations) stably into the germline of experimental

mammals [1], referred to as “transgenic technology,” has provided unique insight into complex biologic phenomena. Although simplistic, this technology can now be broadly defined into two experimental categories: “gain-of-function” mutations, typically created by microinjection of the gene (transgene) of interest directly into the zygote stage of development (for example, to define the controlling elements for a muscle-specific gene), and “loss-of-function” mutations, which employ embryonic stem (ES) cells. The technique of DNA microinjection results in *random integration* of the transgene, giving rise to the founder animal(s). The founder animals are then bred individually to establish independent lines of transgenic animals that can undergo further characterization [e.g., pattern(s), levels and consequences of expression of the transgene]. However, many of these lines exhibit variable expression of the gene of interest since the transgene may integrate in a manner that alters its expression (for example, by integration near controlling elements that affect the pattern and level of expression), and this may confound the interpretation of results.

In contrast, the development of gene targeting via homologous recombination in pluripotential ES cells allows one to modify *precisely* the gene of interest. It is now possible to create mice of virtually any genotype, and to assess the consequences of these mutations in the context of a developing and intact mammal. This technology, which is typically used to create the null genotype (“knock-out” mice), has frequently provided the definitive experimental evidence regarding the functions of the encoded proteins. However, in many instances these mutations have changed the prevailing notions. For example, gene targeting at the endothelin loci subsequently led to the creation of mice with Hirschsprung’s disease (aganglionic megacolon [2]) instead of the anticipated phenotype (abnormal control of blood pressure). Indeed, if one had even predicted these mice would survive the absence of a cellular gene that is so widely expressed, one might have been in the minority!

The purpose of this review is to introduce the reader to the history of development of ES technology, the cur-

R.W. Moreadith (✉) · N.B. Radford
Molecular Cardiology Laboratories, 5323 Harry Hines Boulevard,
University of Texas Southwestern Medical Center, Dallas,
TX 75235-8573, USA

Present address:

¹ Quintiles, Inc., 1007 Slater Road, Morrisville, NC 27707, USA

rent methods employed to create "knock-out" mice, and the application of these methods to solve problems in biology. While the technology promises to provide enormous insight into mammalian development genetics, our desire is that this review will stimulate the application of gene targeting in ES cells to begin to unravel problems in complex regulatory pathways, specifically intermediary metabolism and physiology.

Historical development

Derivation and characterization of pluripotent stem cells

The development of gene-targeting technology in ES cells is an example of the convergence of classical cell biology with molecular biology. One of the seminal papers was published in 1975 by Mintz and colleagues at the Fox Chase Cancer Center [3]. It was well established that explantation of normal mouse embryos into extrauterine sites (typically the kidney capsule) subsequently led to the development of tumors known as teratocarcinomas. Cell lines could be derived from the tumors, passaged indefinitely in tissue culture, and when reintroduced into recipient mice gave rise to tumors with cell types representative of all germ layers (ectoderm, mesoderm, and endoderm). These properties suggested that these embryonal carcinoma (EC) cells were pluripotent, that is, capable of differentiating into a host of cell types under the appropriate conditions. In many instances these tumors contained cell types indistinguishable from the normal cellular counterpart in biochemical or ultrastructural detail. Thus, although these cells were considered to be "highly" malignant, it was quite clear that not all tissues derived from them displayed the malignant properties of the parental cells. Mintz and colleagues reasoned that these EC cells might in fact be totipotent – capable of contributing to the development of all normal tissues under the appropriate environmental cues. "For this to occur, the initially malignant cells would presumably have to be brought into association with early embryo cells so that the latter could provide an organizational framework appropriate for normal development [3]." This was an astounding leap of logic at the time. She and her colleagues subsequently demonstrated that malignant EC cells, grown as an ascites tumor for over 8 years, could give rise to apparently normal mosaic mice upon introduction into normal blastocysts. Furthermore, the mosaic mice were capable of transmitting the EC cell genotype through the germline, that is, mating of these mosaic mice with wild-type partners gave rise to mice that were genotypically derived from the EC cells! These results, and those from many other laboratories, established the experimental basis for subsequent developments in the field. Indeed, Mintz precisely predicted the emergence of stem cell technology. "Thus, EC cells ... offer new possibilities for studying mammalian regulatory systems: the carcinoma cells

could first be experimentally mutagenized and selected during a brief in vitro sojourn and then cycled through mice via blastocyst injections. Participation in differentiation of a mosaic individual would permit developmental and biochemical analyses of the mutations; conversion of some cells to gametes would enable genetic analysis and mapping of the mutated regions through recombination and segregation during meiosis [3]."

These observations, made prior to the large-scale development of classical molecular biology (note that the above experiments were published prior to the development of DNA sequencing!) were quickly verified by many laboratories. However, working with EC cells proved to be quite cumbersome due to their propensity for aneuploidy, and the attention turned to isolation of pluripotent cells from normal embryos. Early attempts failed until 1981, when Evans and Kaufman [4] and Martin [5] independently described the growth and maintenance of euploid cells, derived from normal mouse embryos explanted in culture, that displayed pluripotent properties (hereafter referred to as ES cells). This was quickly followed by the demonstration in 1984 these cells were capable of giving rise to germline chimeras upon introduction into normal blastocysts [6]. The stage was set – one could grow normal, diploid ES cells in culture for multiple passages without loss of the ability to contribute to normal development. Furthermore, the cells contributed to the development of gametes at a high frequency (germline competence), and the haploid genomes of these cells were transmitted to the next generation. Thus, introduction of mutations in these cells offered the possibility of producing mice with a predetermined genotype.

Homologous recombination: introduction of precise mutations into resident genes

In an elegant series of papers using mammalian cell lines [7–10], based primarily on prior work in *Saccharomyces cerevisiae*, it became clear that cloned DNA could be precisely altered in vitro, and when introduced into cells via a number of methods (infection, transfection) would homologously recombine with the resident gene and introduce the desired mutation at that site in the genome. In lower eukaryotes (yeast and *Neurospora*) recombination at the homologous locus is the favored reaction and can occur essentially without selection, but in higher eukaryotes (mouse and *Drosophila*) the frequency of homologous recombination is rare. This necessitates the use of positive selection; typically, these rare events are selected for by introduction of genes conveying resistance to otherwise toxic metabolites (hygromycin, neomycin). Note that the introduction of a positive selection marker gene is also frequently used to disrupt (mutate) the gene of interest. In addition, one can enhance the frequency of these events by employing the additional strategy of negative selection – most commonly performed by use of the thymidine kinase (TK) gene flanking the targeting vector. ES

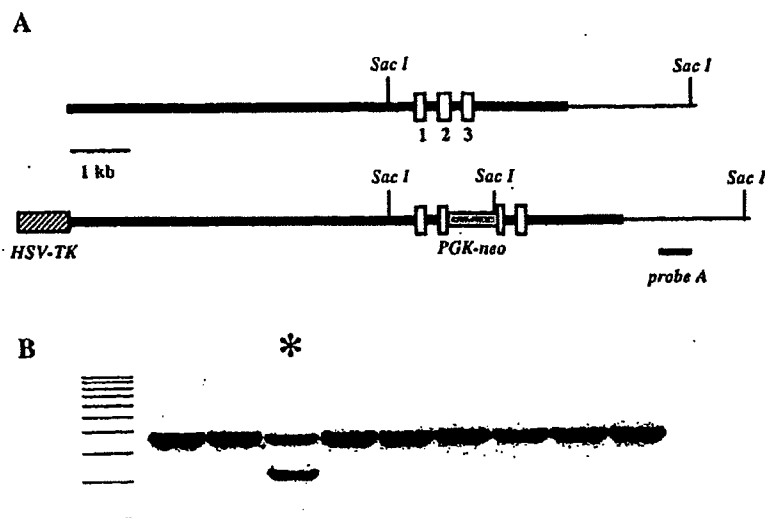


Fig. 1A, B Gene targeting at the murine cytochrome oxidase VIaH locus. A The structure of the gene, which has been reported elsewhere [12]. Briefly, the gene is comprised of three small exons (open rectangles). Exon 2 was disrupted with the expression cassette for neomycin phosphotransferase (*PGK-neo*), thus mutating the gene in its coding region and simultaneously providing positive selection. Heavy lines, the cloned vector used for transfection into J1 ES cells; note the targeting vector is flanked with the expression cassette for TK (*HSV-TK*) to allow for negative selection (see text). B Probe A was derived from a separate region of the gene (thin line) and was used to screen, by Southern analysis, DNA isolated from G418- and gancyclovir-resistant ES clones. Note the presence of the endogenous band at 5.7 kb in all clones, as well as the presence of the recombinant band at 4.2 kb (asterisk), in a *SacI* digest of genomic DNA. Clone 3 was then used for blastocyst injection as illustrated in Fig. 2 to generate germline chimeras. Bars (left), 1-kb-size markers

cell clones which retain the *TK* gene (nonhomologous recombination) do not survive the addition of gancyclovir (or homologues) to the media due to the accumulation of toxic nucleosides, whereas cell clones which have undergone an authentic recombination lose the *TK* gene. This combined strategy is known as *positive-negative* selection [11] and routinely increases the targeting frequency by an order of magnitude or more.

An example of gene targeting in ES cells is illustrated in Fig. 1. The gene of interest in this example is a muscle-specific subunit of cytochrome oxidase (VIaH). The structure and regulation of the gene have recently been defined in the author's laboratory [12], but the precise function of this subunit, postulated to regulate the steady-state activity of cytochrome oxidase, remains largely unknown in the context of an intact animal. It is anticipated that creation of mice which lack this subunit will provide more insight into the precise role this subunit may play in the bioenergetics of cardiac and skeletal muscle.

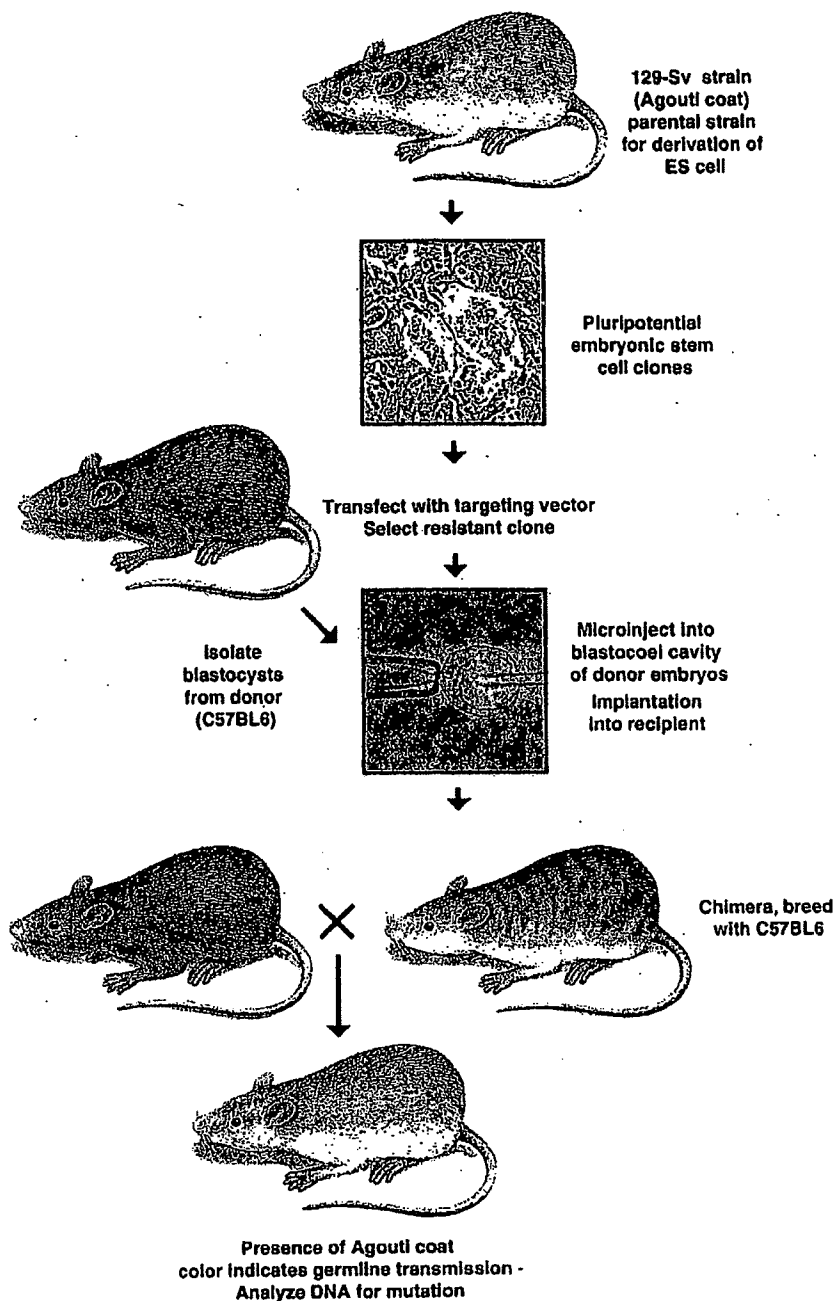
Once these mutated ES cells are isolated as a pure clone, they can be introduced into the blastocoele cavity of a normal embryo, where they participate in the devel-

opment of all tissues and result in the production of chimeras (usually assessed at birth by acquisition of the dominant coat color phenotype Agouti). In subsequent matings of these chimeric mice, if the ES cells have contributed to formation of germ cells, the mutant gene is transmitted to their progeny. By mating heterozygotes, each harboring a mutated copy of the gene of interest (detected by analysis of the isolated DNA), one can derive embryos and mice which are homozygous for the mutation. These techniques are illustrated schematically in Fig. 2.

"Knockout mice": the new genetics

The initial attempts at gene inactivation in murine ES cells took advantage of selection methods designed to reflect loss of an enzyme activity, hypoxanthine phosphoribosyltransferase (HPRT), following random integration of proviruses [13, 14]. Since the vast majority of ES cell lines used were male (male chimeric mice can be mated frequently, thus producing numerous offspring to assess germline competence), random integration of DNA (in this case retroviruses) would be expected to inactivate the single copy of the HPRT gene on the X chromosome at a low but detectable frequency and subsequently confer growth properties in a defined (hypoxanthine-aminopterin-thymidine) medium. These HPRT-minus cell lines were used to make mice deficient in HPRT, a potential mouse model of the human disorder Lesch-Nyhan syndrome [14, 15]. However, the absence of a neurologic phenotype in these mice was readily apparent, eventually precipitating a search for alternative explanations of why purine salvage might be different in the two species. This led to the elucidation that adenine phosphoribosyltransferase was the major enzyme involved in purine salvage in the mouse. Indeed, when HPRT-deficient mice were exposed to inhibitors of adenine phosphoribosyltransfer-

Fig. 2 General strategy for creating "knock-out" mice



ase, they developed neurologic phenotypes more representative of the human disorder [16]. The HPRT locus continued to be the subject of intense investigation, however, defining many of the parameters routinely employed now to target genes – for example, length and degree of homology to mediate highly efficient gene targeting [17, 18].

The first description of gene targeting via homologous recombination in murine ES cells was published in 1987 [19]. To date, several hundred novel mouse mutants – "knockout" mice – have been created, with dozens being reported monthly. A synopsis of these mutations is obviously beyond the scope of this review, but it is readily apparent from a perusal of these mutations that the

Table 1 Established methodologies for the study of murine physiology and metabolism

Methodology	Physiologic measure	References
Cardiovascular system		
Micromanometer catheter	LV hemodynamics	22-24
Indwelling arterial catheters	Blood pressure, heart rate	25-28
Reference microsphere and dilution	Cardiac output, regional blood flows, intravascular fluid volumes	26, 28
Echocardiography	LV mass, LV systolic function, wall motion abnormalities, heart rate	29-32
X-ray contrast microangiography	Ventricular volumes, ejection fraction	33
Swimming	Cardiac adaptations to chronic exercise	34
Langendorff perfusion	Intraventricular pressure, indices of LV contraction and relaxation, heart rate	35-37
Magnetic resonance imaging	Cardiac chamber sizes, coronary flow	38, 39
Magnetic resonance spectroscopy	pH, high energy phosphates	40
Tail-cuff sphygmomanometer	Blood pressure	27
Pulmonary system		
Plethysmography	Lung volumes, respiratory rate	41-44
Pulse oximetry	Arterial saturation	45
Pressure-volume curves	Elastic recoil	46
Forced oscillation	Pulmonary resistance	46
Methacholine challenge	Airway responsiveness	47
Skeletal muscle		
Skeletal muscle resection	Response to mechanical overload	48, 49
Magnetic resonance spectroscopy	pH, phosphocreatine, ATP, inorganic phosphate, creatine kinase flux	50, 51
	Ischemia/reperfusion injury	49, 52, 53
	Fatiguability	54
Microvascular flow		55
Programmable treadmill		
Miscellaneous		
Magnetic resonance imaging	Knee joint degeneration	56
	Polycystic kidneys	57
	Renal edema, hepatic iron deposition	58
	Hepatic ADP levels, creatine kinase flux	59
	Brain pH, free Mg, choline, N-acetylaspartate, creatine	60
	Phagocyte oxidase function	61
Pathogen inoculation	Spatial learning	62, 63
Morris Water maze task, visible or hidden-platform tasks		
Intruder test	Defensive aggression	64
Contextual and tone conditioning	Fear response	64
Swimming	Exercise-induced immunosuppression	65

technology has become one of the most powerful methods in the repertoire of approaches to gain insight into the functions of genes. To cite only a few applications, these include developmental biology, behavior and cognition, pharmaceutical research, and generation of models of human disease, such as cystic fibrosis and familial hypercholesterolemia [20, 21].

The new physiology and metabolism

Gene targeting in ES cells has only recently been applied to address problems in classical physiology and metabolism. Indeed, the creation of mutant animals, some of which have unpredictable and subtle phenotypes, has rekindled interest in developing techniques that allow one to characterize the animals precisely. This initiative, "molecular physiology," represents a new field of biology that addresses physiology and metabolism in the context of an intact animal harboring defined mutations in selected genes.

Established methodologies, such as light, immunofluorescence, and electron microscopy, are frequently used

in postmortem tissue to describe histologic and ultrastructural changes in organs of interest in particular transgenic models of disease. Functional studies in the isolated, intact organ have also been accomplished, but it is becoming increasingly clear that studies of physiology in the intact animal may yield the greatest insight. A summary of methodologies which have been adapted to study murine cardiovascular, respiratory, and skeletal muscle physiology in vitro and in vivo is presented in Table 1. The remainder of our discussion focuses on examples of methodologies which have been developed to interrogate primarily cardiovascular phenotypes. Although most of these examples represent gain-of-function mutations, it is clear the methods can be applied to loss-of-function mutations as well.

Cardiovascular "molecular physiology"

At the present time ES cell technology exists only in the mouse (although see discussion below); thus creation of animals with anticipated cardiac phenotypes requires that

techniques be developed to interrogate them (throughout development). Standard measures of cardiac function are well established in larger animals such as rabbits and dogs where invasive measurements can be made in anesthetized or chronically instrumented animals. Development of these same techniques in the mouse has only recently become available. In general this has necessitated the "miniaturization" of technology that allows investigators reproducibly to assess cardiovascular function, both in the isolated perfused heart and in the intact anesthetized mouse.

The isolated Langendorff preparation and the working heart model have been elegantly characterized in several native mouse strains under varied physiologic conditions [35]. Several laboratories, including our own, have used the Langendorff model to provide direct evidence linking overexpression of heat shock protein with enhanced myocardial recovery following global ischemia in transgenic mouse lines [36, 37, 40].

Our laboratory has combined isolated heart perfusions with nuclear magnetic resonance (NMR) to study the effect of overexpression of heat-shock proteins in the heart on changes in pH and high-energy phosphates at rest and following global ischemia [40]. We have found that NMR spectroscopy, which is routinely used to study perfused hearts from larger species such as the rat, rabbit, and guinea pig, can be adapted to suit a 100-mg mouse heart. Figure 3 shows ^{23}Na -, ^{31}P -, and ^{13}C -NMR spectra obtained from three different perfused mouse heart protocols.

In panel A the ^{23}Na -NMR spectra have been obtained in the presence of TmDOTP, a shift-reagent which shifts the extracellular sodium (Na) signal away from the intracellular Na signal [66]. Shown in the upper left is a single spectrum in which the extracellular Na and intracellular Na resonance peaks are labeled. Spectra, shown in a stacked plot format, were acquired every 3 min at baseline, during 15 min of ischemia, and during 24 min of recovery. In this heart there is sustained elevation of intracellular Na into recovery.

In panel B the ^{31}P -NMR spectra were acquired every 5 min at baseline, during 15 min of ischemia, and then at 15 and 30 min of recovery. Shown are spectra at baseline, after 15 min of ischemia, and after 30 min of recovery. The phosphocreatine (PCr), inorganic phosphate (P_i) and three P resonances of adenosine triphosphate (ATP) are labeled. Intracellular pH can be calculated from the chemical shift difference between the resonance peaks of phosphocreatine and inorganic phosphate [67]. These spectra show that there is incomplete recovery of adenosine triphosphate following this ischemic event.

In panel C there is a single ^{13}C -NMR spectrum of the C4 carbon of glutamate from a mouse heart extract. The extract was prepared after the isolated heart was subjected to 25 min of ischemia and then reperfused with ^{13}C -labeled acetate, octanoate (a short-chain fatty acid) and long-chain fatty acids. The resonance peaks marked with an asterisk arise from octanoate oxidation while the remainder arise from long-chain fatty acid oxidation. Analysis of this multiplet using ^{13}C -NMR isotopomer methods yields information about the relative contribution of octanoate and long-chain fatty acids to the acetyl coenzyme A pool from which glutamate is synthesized.

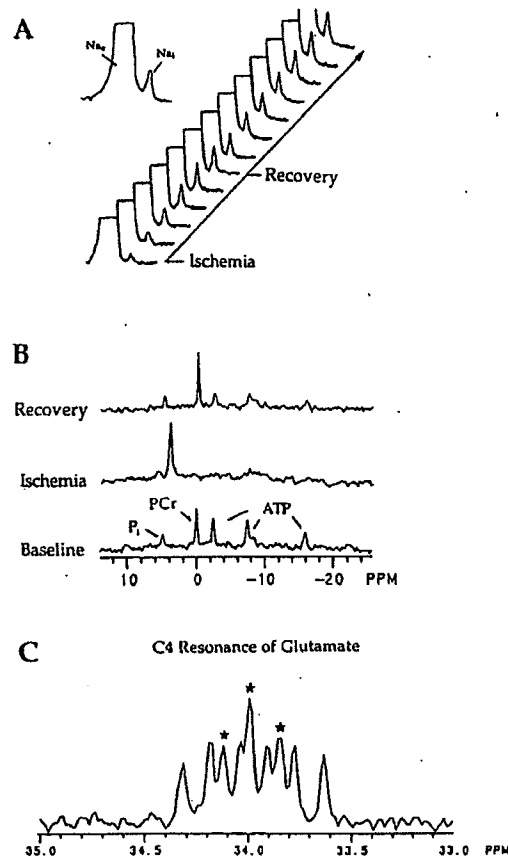


Fig. 3 A Upper left, a single ^{23}Na -NMR spectrum obtained in the presence of TmDOTP in which the extracellular Na and intracellular Na resonance peaks are labeled. Right, spectra, shown in a stacked plot format, were acquired at baseline, during 15 min of ischemia and during 24 min of recovery. B ^{31}P -NMR spectra acquired at baseline, after 15 min of ischemia and after 30 min of recovery. The phosphocreatine (PCr), inorganic phosphate (P_i) and three P resonances of adenosine triphosphate (ATP) are labeled. C ^{13}C -NMR spectrum of the C4 carbon of glutamate from a mouse heart extract which was prepared after the isolated heart was subjected to 25 min of ischemia and then reperfused with ^{13}C -labeled acetate, octanoate (a short-chain fatty acid), and long-chain fatty acids. The resonance peaks marked with an asterisk arise from octanoate oxidation while the remainder arise from long-chain fatty acid oxidation. Analysis of this multiplet using ^{13}C -NMR isotopomer methods yields information about the relative contribution of octanoate and long-chain fatty acids to the acetyl coenzyme A pool from which glutamate is synthesized.

ysis of this multiplet using ^{13}C -NMR isotopomer methods yields information about the relative contribution of octanoate and long-chain fatty acids to the acetyl coenzyme A pool from which glutamate is synthesized, in this case during reperfusion [68, 69]. This information may in turn provide insight into the postischemic activity of carnitine palmitoyl transferase (which is required for long-chain fatty acid metabolism).

Optimally of course cardiovascular phenotypes would be interrogated in the intact animal. A number of invasive, catheter-based methods have been successfully applied to the mouse to make hemodynamic measurements in both the conscious and unconscious animal. Exciting advances have also been made in the application of non-invasive techniques such as magnetic resonance imaging and echocardiography to interrogate murine cardiac function.

The importance of the application of these methodologies to murine models of disease cannot be understated. Using a number of techniques outlined in Table 1, investigators have been able to characterize the cardiovascular phenotypes of a number of transgenic mice including lines which overexpress atrial natriuretic factor [25, 28], heat-shock proteins [36, 37, 40], human tissue kallikrein [27], β -adrenergic receptors [24], β -adrenergic receptor kinase and β -adrenergic receptor kinase inhibitor [23] as well as phospholamban deficient lines [32].

Summary

The advent of techniques to generate gain-of-function and loss-of-function mutations in laboratory animals represents one of the major accomplishments in cell and molecular biology in mammals over the past two decades. Although the technology is generally limited only to the mouse at present, substantial effort is underway to develop these techniques, and to refine existing techniques, in other species. Putative pluripotent ES cell lines have been derived in a number of other species including hamster [70], pig [71–75], sheep [73], cattle [76], rabbit [77], rat [78], mink [79], monkey [80], and even humans [81]. Thus it seems likely the technology will be advanced into these additional species over the next few years, and each one of these may lend itself uniquely to problems ranging from development to tissue and organ physiology. Additionally, techniques such as those illustrated here and in Table 1 will need to be refined and applied to address each new mutation.

Acknowledgements The authors apologize to uncited investigators in many areas of developmental biology for not being able to cite all of the relevant literature in this field due to page constraints. R.W.M. is supported by grants from the National Institutes of Health (NHLBI, RO1-51568), National Aeronautics and Space Administration (NSCORT, NAGW 3582), the Leuven Research and Development Institute (Leuven, Belgium) and is an Established Investigator of the American Heart Association. N.B.R. is supported by grants from the American Heart Association (95004180 and 95009510) and from the National Institutes of Health (P41-RR02584).

References

- Gordon J, Scangos G, Plotkin D, Barbosa J, Ruddle F (1980) Genetic transformation of mouse embryos by microinjection of purified DNA. *Proc Natl Acad Sci USA* 77:7380–7384
- Hosoda K, Hammer R, Richardson J, Baynash A, Cheung J, Giaid A, Yanigasawa M (1994) Targeted and natural (piebald-lethal) mutations of endothelin-B receptor gene produce megacolon associated with spotted coat color in mice. *Cell* 79:1267–1276
- Mintz B, Illmensee K (1975) Normal genetically mosaic mice produced from malignant teratocarcinoma cells. *Proc Natl Acad Sci USA* 72:3585–3589
- Evans M, Kaufman M (1981) Establishment in culture of pluripotent cells from mouse embryos. *Nature* 292:154–156
- Martin G (1981) Isolation of a pluripotent cell line from early embryos cultured in medium conditioned by teratocarcinoma stem cells. *Proc Natl Acad Sci USA* 78:7634–7638
- Bradley A, Evans M, Kaufman M, Robertson E (1984) Formation of germ-line chimaeras from embryo-derived teratocarcinoma cell lines. *Nature* 309:255–256
- Lin F, Sperle K, Sternberg N (1985) Recombination in mouse L cells between DNA introduced into cells and homologous chromosomal sequences. *Proc Natl Acad Sci USA* 82:1391–1395
- Smithies O, Gregg R, Boggs S, Koralewski M, Kucherlapati R (1985) Insertion of DNA sequences into the human chromosomal beta-globin locus by homologous recombination. *Nature* 317:230–234
- Thomas K, Folger K, Capecchi M (1986) High frequency targeting of genes to specific sites in the mammalian genome. *Cell* 44:419–428
- Thomas K, Capecchi M (1986) Introduction of homologous DNA sequences into mammalian cells induces mutations in the cognate gene. *Nature* 324:34–38
- Mansour S, Thomas K, Capecchi M (1988) Disruption of the proto-oncogene int-2 in mouse embryo-derived stem cells: a general strategy for targeting mutations to non-selectable genes. *Nature* 336:348–352
- Wan B, Moreadith R (1995) Structural characterization and regulatory element analysis of the heart isoform of cytochrome c oxidase VIa. *J Biol Chem* 270:26433–26440
- Robertson E, Bradley A, Kuehn M, Evans M (1986) Germ-line transmission of genes introduced into cultured pluripotent cells by retroviral vector. *Nature* 323:445–448
- Hooper M, Hardy K, Handyside A, Hunter S, Monk M (1987) HPRT-deficient (Lesch-Nyhan) mouse embryos derived from germline colonization by cultured cells. *Nature* 326:292–295
- Kuehn M, Bradley A, Robertson E, Evans M (1987) A potential animal model for Lesch-Nyhan syndrome through introduction of HPRT mutations into mice. *Nature* 326:295–298
- Wu C, Melton D (1993) Production of a model for Lesch-Nyhan syndrome in HPRT-deficient mice. *Nat Genet* 3:235–240
- Hasty P, Rivera-Pérez J, Chang C and Bradley A (1991) Target frequency and integration pattern for insertion and replacement vectors in embryonic stem cells. *Mol Cell Biol* 11:4509–4517
- Hasty P, Rivera-Pérez J and Bradley A (1991) The length of homology required for gene targeting in embryonic stem cells. *Mol Cell Biol* 11:5586–5591
- Thomas K, Capecchi M (1987) Site-directed mutagenesis by gene targeting in mouse embryo-derived stem cells. *Cell* 51:503–512
- Snouwvaert J, Brigman K, Latour A, Malouf N, Boucher R, Smithies O, and Koller B (1992) An animal model for cystic fibrosis made by gene targeting. *Science* 257:1083–1088
- Ishibashi S, Brown MS, Goldstein JL, Gerard RD, Hammer RE and Herz J (1993) Hypercholesterolemia of low density lipoprotein receptor knockout mice and its reversal by adenovirus-mediated gene delivery. *Proc Natl Acad Sci USA* 89:7905–7909
- Hunter JJ, Tanaka N, Rockman HA, Ross J, Chien KR (1995) Ventricular expression of a MLC-2v-ras fusion gene induces cardiac hypertrophy and selective diastolic dysfunction in transgenic mice. *J Biol Chem* 270:23173–23178
- Koch WJ, Rockman HA, Samama P, Hamilton RA, Bond RA, Milano CA, Lefkowitz RJ (1995) Cardiac function in mice overexpressing the beta-adrenergic receptor kinase or a beta-ARK inhibitor. *Science* 268:1350–1353

24. Milano CA, Allen LF, Rockman HA, Dolber PC, McMin TR, Chien KR, Johnson TD, Bond RA, Lefkowitz RJ (1994) Enhanced myocardial function in transgenic mice overexpressing the beta 2-adrenergic receptor. *Science* 264:582-586
25. Steinhilber ME, Cochran KL, Field LJ (1990) Hypotension in transgenic mice expressing atrial natriuretic factor fusion genes. *Hypertension* 16:301-307
26. Barbee RW, Perry BD, Re RN, Murgu JP (1992) Microsphere and dilution techniques for the determination of blood flows and volumes in conscious mice. *Am J Physiol* 263:R728-R733
27. Wang J, Xiong W, Yang Z, Davis T, Dewey MJ, Chao J, Chao L (1994) Human tissue kallikrein induces hypotension in transgenic mice. *Hypertension* 23:236-243
28. Barbee RW, Perry BD, Re RN, Murgu JP, Field LJ (1994) Hemodynamics in transgenic mice with overexpression of atrial natriuretic factor. *Circ Res* 74:747-751
29. Manning MJ, Wei JY, Katz SE, Litwin SE, Douglas PS (1994) In vivo assessment of LV mass in mice using high-frequency cardiac ultrasound: necropsy validation. *Am J Physiol* 266:H1672-H1675
30. Gardin JM, Siri FM, Kitsis RN, Edwards JG, Leinwand LA (1995) Echocardiographic assessment of left ventricular mass and systolic function in mice. *Circ Res* 76:907-914
31. Manning WJ, Wei JY, Katz SE, Douglas PS, Gwathmey JK (1993) Echocardiographically detected myocardial infarction in the mouse. *Lab Animal Science* 43:583-585
32. Hoyt BD, Khoury SF, Kranias EG, Ball N, Walsh RA (1995) In vivo echocardiographic detection of enhanced left ventricular function in gene-targeted mice with phospholamban deficiency. *Circ Res* 77:632-637
33. Rockman HA, Ono S, Ross RS, Jones LR, Karimi M, Bhargava V, Ross J, Chien KR (1994) Molecular and physiological alterations in murine ventricular dysfunction. *Proc Natl Acad Sci USA* 91:2694-2698
34. Kaplan ML, Cheslow Y, Vikstrom K, Malhotra A, Geenen DL, Nakouzi A, Leinwand LA, Buttrick PM (1994) Cardiac adaptations to chronic exercise in mice. *Am J Physiol* 267:H1167-1173
35. Grupp IL, Subramaniam A, Hewett TE, Robbins J, Grupp G (1993) Comparison of normal, hypodynamic, and hyperdynamic mouse hearts using isolated work-performing heart preparations. *Am J Physiol* 265:H1401-1410
36. Marber MS, Mestral R, Chi SH, Sayen MR, Yellon DM, Dillmann WH (1995) Overexpression of the rat inducible 70-kD heat stress protein in a transgenic mouse increases the resistance of the heart to ischemic injury. *J Clin Invest* 95:1446-1456
37. Plumier JC, Ross BM, Currie RW, Angelidis CE, Kazlaris H, Kollias G, Pagoulatos GN (1995) Transgenic mice expressing the human heat shock protein 70 have improved post-ischemic myocardial recovery. *J Clin Invest* 95:1854-1860
38. Burstein D (1991) MR imaging of coronary artery flow in isolated and in vivo hearts. *J Magn Reson Imaging* 1:337-346
39. Rose SE, Wilson SJ, Zelaya FO, Crozier S, Doddrell DM (1994) High resolution high field rodent cardiac imaging with flow enhancement suppression. *Magn Reson Imaging* 12:1183-1190
40. Radford NB, Fina M, Benjamin IJ, Moreadith RW, Graves KH, Zhao PY, Gavva S, Wiethoff A, Sherry AD, Malloy CR, Williams RS (1996) Cardioprotective effects of 70-kDa heat shock protein in transgenic mice. *Proc Natl Acad Sci USA* 93:2339-2342
41. Lockhart SP, Hill D, King S, Down JD (1991) A semi-automated method of breathing rate measurement in the mouse. *Radiother Oncol* 22:68-70
42. Nielsen GD, Petersen SH, Vinggaard AM, Hansen LF, Wolkoff P (1993) Ventilation, CO₂ production, and CO₂ exposure effects in conscious, restrained CF-1 mice. *Pharm Toxicol* 72:163-168
43. Martin TR, Gerard NP, Galli SJ, Drazen JM (1988) Pulmonary responses to bronchoconstrictor agonists in the mouse. *J Appl Physiol* 64:2318-2323
44. Vijayaraghavan R, Schaper M, Thompson R, Stock MF, Boylstein LA, Luo JE, Alarie Y (1994) Computer assisted recognition and quantitation of the effects of airborne chemicals acting at different areas of the respiratory tract in mice. *Arch Toxicol* 68:490-499
45. Sidwell RW, Huffman JH, Gilbert J, Moscon B, Pedersen G, Burger R, Warren RP (1992) Utilization of pulse oximetry for the study of the inhibitory effects of antiviral agents on influenza virus in mice. *Antimicrobial Agents Chemother* 36:473-476
46. Kida K, Fujino Y (1993) Lung structure and elastic recoil properties in hereditary diabetes mellitus in KK-mice, C57 black mice, and F₁ hybrids. *J Lab Clin Med* 122:524-532
47. DiCosmo BF, Geba GP, Picarella D, Elias JA, Rankin JA, Stripp BR, Whitsett JA, Flavell RA (1994) Airway epithelial cell expression of interleukin-6 in transgenic mice. *J Clin Invest* 94:2028-2035
48. Roy RR, Edgerton VR (1995) Response of mouse plantaris muscle to functional overload: comparison with rat and cat. *Comp Biochem Physiol* 111A:569-575
49. Tsika RW, Hauschka SD, Gao L (1995) M-creatine kinase gene expression in mechanically overloaded skeletal muscle of transgenic mice. *Am J Physiol* 269:C665-C674
50. Dunn JF, Tracey I, Radda GK (1993) Exercise metabolism in duchenne muscular dystrophy: a biochemical and ³¹P-nuclear magnetic resonance study of *mdx* mice. *Proc R Soc Lond* 251:201-206
51. van Deursen J, Heerschap A, Oerlemans F, Ruitenbeek W, Jap P, Laak HT, Wieringa B (1993) Skeletal muscles of mice deficient in muscle creatine kinase lack burst activity. *Cell* 74:621-631
52. Brosnan MJ, Raman SP, Chen L, Koretsky AP (1993) Altering creatine kinase isoenzymes in transgenic mouse muscle by overexpression of the B subunit. *Am J Physiol* 264:C151-C160
53. Dunn JF, Tracey I, Radda GK (1992) A ³¹P-NMR study of muscle exercise metabolism in *mdx* mice: evidence for abnormal pH regulation. *J Neurol Sci* 113:108-113
54. Pemberton M, Anderson G, Barker J (1994) In vivo microscopy of microcirculatory injury in skeletal muscle following ischemia/reperfusion. *Microsurg* 15:374-382
55. Pachner AR, Itano A, Ricalton N, Choe S (1991) Chronic murine experimental myasthenia gravis: strength testing and serology. *Clin Immunol Immunopath* 59:398-406
56. Munasinghe JP, Tyler JA, Carpenter A, Hall LD (1995) High resolution MR imaging of joint degeneration in the knee of the STR/ORT mouse. *Magn Reson Imaging* 13:421-428
57. Townner RA, Yamaguchi T, Philbrick DJ, Holub BJ, Janzen EG, Takahashi H (1991) In vivo proton magnetic resonance imaging and localized spectroscopic analysis of polycystic kidney disease in DBA/2FG-psy mice. *Magn Reson Imaging* 9:429-434
58. Fabry ME, Costantini F, Pachnis A, Suzuka SM, Bank N, Ayyedjian HS, Factor SM, Nagel RL (1992) High expression of human β - and α -globins in transgenic mice: erythrocyte abnormalities, organ damage, and the effect of hypoxia. *Proc Natl Acad Sci USA* 89:12155-12159
59. Brosnan MJ, Chen L, Van Dyke TA, Koretsky AP (1990) Free ADP levels in transgenic mouse liver expressing creatine kinase. *J Biol Chem* 265:20849-20855
60. Kauppinen RA, Halmekyto M, Alhonen L, Janne J (1992) Nuclear magnetic resonance spectroscopy study on energy metabolism, intracellular pH, and free Mg²⁺ concentration in the brain of transgenic mice overexpressing human ornithine decarboxylase gene. *J Neurochem* 58:831-836
61. Pollock JD, Williams DA, Gifford MAC, Li LL, Du X, Fisherman J, Orkin SH, Doerschuk Dinuer MC (1995) Mouse model of X-linked chronic granulomatous disease, an inherited defect in phagocyte superoxide production. *Nat Genet* 9:202-209
62. Yamaguchi F, Richards SJ, Beyreuther K, Salbaum M, Carlson GA, Dunnett SB (1991) Transgenic mice for the amyloid precursor protein 695 isoform have impaired spatial memory. *Neuroreport* 2:781-784

63. Silva AJ, Paylor R, Wehner JM, Tonegawa S (1992) Impaired spatial learning in α -calcium-calmodulin kinase II mutant mice. *Science* 257:206-211
64. Mayford M, Abel T, Kandel ER (1995) Transgenic approaches to cognition. *Curr Opin Neurobiol* 5:141-148
65. Benquet C, Krzystyniak K, Savard R, Guertin F (1994) Modulation of exercise-induced immunosuppression by dietary polyunsaturated fatty acids in mice. *J Toxicol Env Health* 43:225-237
66. Malloy CR, Buster DC, Castro MC, Geraldles CF, Jeffrey FMH, Sherry AD (1990) Influence of global ischemia on Na⁺ in the perfused rat heart. *Magn Reson Med* 15:33-44
67. Kost GJ (1990) pH standardization for phosphorus-31 magnetic resonance heart spectroscopy at different temperatures. *Magn Reson Med* 14:496-506
68. Malloy CR, Thompson JR, Jeffrey FMH, Sherry AD (1990) Contribution of exogenous substrates to acetyl coenzyme A: measurement by ¹³C NMR under non-steady state conditions. *Biochem* 29:6756-6761
69. Malloy CR, Sherry AD, Jeffrey FMH (1990) Analysis of tricarboxylic acid cycle of the heart using ¹³C isotope isomers. *Am J Physiol* 259:H987-H995
70. Doetschman T, Williams P, Maeda N (1988) Establishment of hamster blastocyst-derived embryonic stem (ES) cells. *Dev Biol* 127:224-227
71. Evans MJ, Notarianni E, Laurie S, Moor RM (1990) Derivation and preliminary characterization of pluripotent cell lines from porcine and bovine blastocysts. *Theriogenology* 33:125-128
72. Notarianni E, Laurie S, Moor RM, Evans MG (1990) Maintenance and differentiation in culture of pluripotential embryonic cell lines from pig blastocysts. *J Reprod Fert* 40:51-56
73. Piedrahita JA, Anderson GB, BonDurant RH (1990) On the isolation of embryonic stem cells: comparative behavior of murine, porcine and ovine embryos. *Theriogenology* 34:879-891
74. Strojek M, Reed MA, Hoover JL, Wagner TE (1990) A method for cultivating morphologically undifferentiated embryonic stem cells from porcine blastocysts. *Theriogenology* 33:901-913
75. Talbot NC, Caird ER Jr, Vernon GP, Powell AM, Nel ND (1993) Culturing the pig epiblast cells of the pig blastocyst. *In Vitro Cell Dev Biol* 29A:543-554
76. Saito S, Strelchenko N, Niemann H (1992) Bovine embryonic stem cell-like cell lines cultured over several passages. *Roux Arch Dev Biol* 201:134-141
77. Graves KH, Moreadith RW (1993) Derivation and characterization of putative pluripotential embryonic stem cells from preimplantation rabbit embryos. *Mol Reprod Dev* 36:424-433
78. Iannaccone PM, Taborn GU, Garton RL, Caplice MD, Brenin DR (1994) Pluripotent embryonic stem cells from the rat are capable of producing chimeras. *Dev Biol* 163:288-292
79. Sukoyan MA, Golubitsa AN, Zhelezova AI, Shilov AG, Vatinin SY, Maximovsky LP, Andreeva LE, Mc Whir J, Pack SD, Bayborodin SI, Kerkis AY, Kizilova HI, Serov OL (1992) Isolation and cultivation of blastocyst-derived stem cell lines from American mink. *Mol Reprod Dev* 33:418-431
80. Thomson JA, Kalishman J, Golos TG, During M, Harris CP, Becker RA, Hearn JP (1995) Isolation of a primate embryonic stem cell line. *Proc Natl Acad Sci USA* 92:7844-7848
81. Bongso A, Fong C-Y, Ng S-C, Ratman S (1994) Isolation and culture of inner cell mass cells from human blastocyst. *Hum Reprod* 9:2110-2117

EXHIBIT 3



Production of bioproducts through the use of transgenic animal models

C.L. Keefer*

Department of Animal & Avian Sciences, University of Maryland, College Park, MD 20742, USA

Abstract

Transgenic livestock that produce recombinant proteins in their milk can provide an economic and safe system for production of valuable proteins, such as pharmaceutical proteins for treatment or prevention of human disease or biomaterials for medical use. This method of production is frequently referred to as biopharming. The promise of biopharming, that is the actual commercial production of pharmaceuticals and other bioproducts, is nearing fulfillment. Improvements in molecular and reproductive techniques and strong economic incentives have continued to drive the implementation of transgenic technology to domestic animals. Nuclear transfer using transgenic donor cells is rapidly becoming the predominant technique used in the production of transgenic livestock, replacing the direct injection of DNA into the zygotic pronuclei. Production of transgenic founder animals by nuclear transfer in combination with traditional reproductive technologies can result in the propagation of transgenic herds of sufficient size to meet market demands for commercially important proteins. While some of the companies that have established transgenic programs have run into setbacks owing to a combination of economic, scientific and regulatory difficulties, other companies are continuing to make significant advances. While further improvements are needed to increase efficiencies of production, economically viable production of recombinant proteins using livestock species is not only possible but should be a commercial reality in the very near future.

© 2004 Elsevier B.V. All rights reserved.

Keywords: Transgenic animals; Biopharming; Recombinant proteins

1. Introduction

Commercial production of bioproducts using such natural protein factories as the mammary glands of dairy animals has been a goal of animal scientists since the first report of a transgenic mouse (Gordon and Ruddle, 1981). Progress toward this goal has been steady, although perhaps not as fast as some may have hoped. A number of factors must come together

* Tel.: +1-301-405-3933; fax: +1-301-314-9059.

E-mail address: ckeef@umd.edu (C.L. Keefer).

in order to ensure the success of biopharming (Gavin, 2001; Goldman, 2003; Powell, 2003). These factors include improvements in reproductive and molecular techniques, identification of commercially viable products, efficient product purification processes, satisfaction of governmental regulations, and public acceptance.

2. Production of transgenic animals

A transgenic animal has a piece of foreign DNA stably integrated into its genome. This foreign DNA usually consists of a construct containing a specific promoter region, a gene coding for the protein of interest, insulators and other regulatory elements to protect or enhance gene expression. This foreign DNA is called a transgene. The protein coded by the transgene is known as a recombinant protein as it results from the recombination of the desired gene with the controlling elements. The transgene can be derived from another animal of the same species, from a different species, even from bacteria or plants. Transgenic production of domestic animals has been moving steadily from the research laboratory to commercial use. The pace may seem slow as researchers can visualize practical applications long before commercialization becomes feasible. The production of transgenic mice has become a common research tool to study gene function; however, application of transgenic technology to domestic animals has been limited owing to the high cost of livestock research. Long generation intervals, maintenance cost of recipient herds, and technical difficulties all combine to make the production of transgenic dairy animals a major undertaking. The estimated cost for producing one transgenic calf is over US\$ 500,000 (Seidel, 1993; Wall, 1996) and for setting-up a production herd could cost tens of millions (Powell, 2003). Programs using smaller dairy animals, such as goats and sheep, with their shorter generation interval are less costly, but still expensive. Even with the current low efficiencies and high cost of production of transgenic dairy animals, commercial interest in the production of pharmaceutical proteins in the milk of dairy animals is high (Rudolph, 1995; Velander et al., 1997; Rudolph, 1999; Powell, 2003). This is due in part to the high market value of pharmaceutical proteins and to the fact that current protein production methods using fermentation facilities are very expensive and methods using human donor material have significant health risks (Datar et al., 1992; Bremel, 1996; Powell, 2003).

Two techniques, pronuclear microinjection and nuclear transfer (cloning), have been the predominant techniques used to produce transgenic animals; however, nuclear transfer using pre-selected transgenic donor cells is rapidly superseding pronuclear microinjection as the method of choice. In pronuclear microinjection, many copies of the gene construct are injected directly into the pronuclei of a recently fertilized oocyte. If the transgene is incorporated at this pronuclear stage, then all cells of the resulting animal (the founder animal for a transgenic line) will contain the transgene. However, in reality, the transgene does not always incorporate at this stage but incorporates one or more cleavage divisions later. The result can be a mosaic animal with some cells containing the transgene and others not. Due to the inefficiencies in this technique, over 1000 bovine oocytes, 300 sheep and 200 goat pronuclear oocytes must be injected in order to produce one founder transgenic animal (Pursel and Rexroad, 1993; Seidel, 1993; Wall, 1996). Furthermore, there is no guarantee that the founder animal or its offspring will express high amounts of the desired protein because

of the random integration of the transgene into the genome. Somatic cell nuclear transfer using pre-selected transgenic donor cells overcomes many of the inefficiencies found in pronuclear microinjection and may help lower the costs of transgenic animal production by reducing the number of animals used during production (Baldassarre et al., 2002).

In somatic cell nuclear transfer, the DNA of an oocyte is removed and replaced by that of the donor cell. This process is also known as cloning as multiple, genetically identical individuals can be made from a donor cell source (an individual animal or fetus). During the process, the reconstructed oocyte is activated to initiate the embryonic developmental process. If transferred into a suitable recipient, the reconstructed or cloned embryo can result in a viable offspring, albeit at low efficiencies of 2–3%. The advantage to somatic cell nuclear transfer in the production of transgenic animals is that the donor cell can be screened *in vitro* prior to production of the animal. This pre-selection of the transgenic donor cell can help ensure that the resulting animal is transgenic (Keefer et al., 2002).

Cell lines derived from embryonic, fetal, and adult tissues can be transfected *in vitro* using standard techniques. This may include chemical (lipids, calcium phosphate), physical (electroporation, gene gun bombardment, direct injection) or retroviral transfection. Following transfection, these cells are selected for appropriate integration into the genome. In this manner, a cell line can be established which has a stably integrated transgene. Cell lines can also be derived from biopsied material taken from transgenic animals produced by other means (e.g. pronuclear microinjection). Transgenic animals have been produced in a number of different domestic species by nuclear transfer using somatic cell lines (Schnieke et al., 1997; Cibelli et al., 1998; Baguisi et al., 1999; Keefer et al., 2001). As nuclear transfer involves the replacement of the oocyte's DNA with that of the donor cell, the resulting offspring is derived from the single donor cell. All cells, including the germ cells, will be identical genetically and the problems associated with mosaic animals are avoided. Therefore, all offspring produced by nuclear transfer using transgenic cells should be transgenic. This represents a tremendous increase in efficiency over the low percentage (<10%) of transgenic offspring expected using pronuclear injection. Furthermore, with appropriate selection and screening of the cell lines, most of the transgenic animals produced should also appropriately express the transgene. This can significantly reduce the number of animals required to produce a transgenic offspring (Schnieke et al., 1997; Baldassarre et al., 2002). While time-lines for production of recombinant protein can be reduced using nuclear transfer (Brink et al., 2000), there remains a number of problems associated with production of animals by nuclear transfer, particularly in cattle and sheep. These include lower pregnancy rates following embryo transfer of nuclear transfer derived embryos, higher loss due to abortion, and higher loss due to postnatal mortality (Smith et al., 2000); however, differences have been noted between species in these losses. In goats, acceptable rates of pregnancy can be achieved without the high incidence of abortion that is seen in cattle (Baguisi et al., 1999; Keefer et al., 2001). Furthermore, there is some evidence in cattle and mice that the source of the donor cell, that is the tissue from which it was derived, its genetic background and its treatment *in vitro*, may affect the efficiencies of nuclear transfer and viability of the offspring (Wakayama and Yanagimachi, 1999; Kato et al., 2000; Wells et al., 2003). These results indicate that, with appropriate selection of donor cells and other technical improvements, the problems associated with nuclear transfer may be decreased or eliminated.

Once a founder animal that has a stably integrated transgene and correctly expresses the gene (e.g. foreign protein secreted into the milk) has been produced, then propagation of a transgenic herd may be initiated. The size of the transgenic herd depends on the market demands for that specific recombinant protein. Where demand requires few animals, then production of founder animals using a proven cell line could generate the needed animals. However, when large herds are needed to meet market demands, then more traditional techniques are needed. Embryos can be obtained from a transgenic female founder using either standard embryo transfer or by *in vitro* embryo production (Baldassarre et al., 2002). Embryos can then be screened by PCR analysis of embryonic biopsies for the presence of the transgene and for gender (Brink et al., 2000). Male founders can be readily propagated using standard artificial insemination techniques.

3. Selection of the recombinant protein

The transgene, which codes for the protein of interest, can be derived from another animal of the same species, from a different species, even from bacteria or plants. Selection of this gene should be based on economic, scientific and social realities. Is there a market niche for the recombinant protein or can one be created? If the recombinant protein will be used to treat a disease, can clear scientific endpoints (efficacy of treatment) be measured during clinical trials? Can sufficient amounts of the purified protein be produced to meet market requirements; if so, at what cost?

In addition to the gene coding for the protein of interest, promoter elements that confer tissue specificity, i.e. expression of the transgene protein in a specific tissue, must be utilized. Selection for milk specific expression takes advantage of the tremendous protein synthetic capabilities of dairy animals (Karatzas and Turner, 1997). For example, promoter elements derived from the casein and whey families have been used to direct expression and secretion of the recombinant proteins in the milk of sheep, cows and goats (Rudolph, 1999; Goldman, 2003). Other regulatory elements may be chosen to enhance or enable control of gene expression (Niemann and Kues, 2003).

One of the key issues in production of pharmaceutical proteins is whether the foreign protein will have any effect on physiology of the transgenic animal. Although many proteins of biomedical importance have been expressed successfully in the mammary glands of transgenic animals, a few have demonstrated adverse effects. Transgenic goats that express the long acting human tissue plasminogen activator in their milk experienced premature shut down of milk production, which has been attributed to the high levels and interactions of the newly expressed protein with its casein components (Ebert et al., 1994). In mice, expression of recombinant human protein C induced an abnormal lactation phenotype, although the authors thought this defect was due to secondary effects of the transgene, not to expression of the human protein C alone (Palmer et al., 2003). In another example, transgenic rabbits that expressed low levels of erythropoietin in their milk showed leakage of the protein into their blood. These animals were infertile and had abnormally viscous blood with a high haematocrit (Massoud et al., 1996). These problems may be avoided through careful selection of the transgene along with tighter control and tissue specific expression, which can be obtained with careful design of DNA constructs and prescreening of constructs

through cell lines and transgenic mice. Recombinant precursor proteins can also be designed which are not active until further processing during purification procedures. In addition to producing a transgenic line which secretes acceptable levels of the targeted protein in the milk without affecting the physiology of the animal, issues involving the purification of the protein are also extremely important as they will affect the final economics and commercialization of the product. Purification of the recombinant protein in commercially viable amounts is a critical but complicated step owing to the complexities of milk composition (Goldman, 2003). Furthermore, these processes must be completed in a highly controlled and documented manner in order to meet the regulatory demands (Gavin, 2001).

4. Production of bioproducts

Alteration of milk through transgenic techniques falls into four general categories: (1) value-added products, e.g. increased casein levels for cheese production, (2) improved nutritional value, e.g. humanized milk for infant formula, (3) production of proteins for treatment or prevention of human disease, and (4) biomaterials, e.g. collagen, spider silk proteins (Karatzas and Turner, 1997; Zuelke, 1998; Powell, 2003). The largest economic incentives are found in the third and fourth categories (production of proteins for treatment or prevention of human disease and biomaterials). Pharmaceutical proteins are products with much higher profit margins than those found in traditional agricultural products. Currently, human pharmaceutical proteins are either isolated from human fluids (e.g. blood-clotting factors) or produced as recombinant proteins in fermentation systems. The first method involves the risk of contamination (e.g. HIV, Creutzfeldt-Jakob disease (CJD)). The second, production of recombinant proteins through mammalian cell culture and bacterial fermentation systems, is very expensive (Datar et al., 1992; Powell, 2003). Production of these proteins in transgenic dairy animals provides significant advantages in areas of health risk and production costs. Transgenic livestock capable of secreting human proteins in their milk have been produced in research programs supported by commercial companies (Rudolph, 1999; Niemann and Kues, 2003; Powell, 2003). A survey by Rudolph published in 1999 indicated that over 17 different transgenic proteins had been produced in the milk of five livestock species (Rudolph, 1999). Since that report many more proteins have been added to the list. Several of these recombinant proteins are in the later stages of clinical trials. One has actually completed clinical trials. GTC Biotherapeutics filed for European-market authorization for its recombinant protein, anti-thrombin III in December of 2003. When this biopharmaceutical reaches the market, it will be the first recombinant protein produced in a transgenic animal to complete the regulatory process.

Until recently, application of transgenic technology to domestic animals has been limited to the research and development; with the GTC Biotherapeutics filing, actual commercial production should soon become a reality. Other products may soon follow (see Table 1). Two of the examples are particularly intriguing, one because of the product chosen and the other because of the unique technical approach taken. In the first, the company (Nexia Biotechnologies, Inc.) chose to produce a biomaterial, spider silk protein, rather than a biopharmaceutical. The unique features of this protein make it an exceptional flexible product, not only in its physical properties, but also in its ultimate uses. Modifications of the protein

EXHIBIT 4

Viewpoint: Are Studies in Genetically Altered Mice Out of Control?

Curt D. Sigmund

Abstract—Because the use of transgenic and gene-targeted models has increased in popularity, the number of reports describing unpredictable phenotypic effects caused by variation in the genetic background used to generate or propagate these models has steadily increased. There are now many examples in which animals containing the same exact genetic manipulation exhibit profoundly different phenotypes when present on diverse genetic backgrounds, demonstrating that genes unrelated, per se, to the ones being targeted can play a significant role in the observed phenotype. Herein, I will discuss (1) the source of genetic variability in mutant mouse models, (2) the appropriateness of using inbred mice as controls, and (3) strategies to help minimize genetic variation between experimental and control mice. (*Arterioscler Thromb Vasc Biol.* 2000;20:1425-1429.)

Key Words: transgenic mice ■ knockout mice ■ genetics ■ epigenetic

It is well documented that many physiological parameters in mammals are genetically determined. Therefore, it should not come as a surprise that many of the phenotypes examined in transgenic and knockout models are influenced by the genetic background in which they are studied. Genetic background is the collection of all genes present in an organism that influences a trait or traits. These genes may be part of the same biochemical or signaling pathway or of an opposing pathway or may appear unrelated to the gene being studied. Although all mouse strains contain the same collection of genes, it is allelic variation (sequence differences) and the interactions between allelic variants that influence a particular phenotype. These "epigenetic" effects can dramatically alter the observed phenotype and therefore can influence or alter the conclusions drawn from experiments.

Studies performed over the past few years have clearly illustrated that phenotypes caused by specific genetic modifications are strongly influenced by genes unlinked to the target locus. For example, whereas deletion of the p53 tumor suppressor gene causes a dramatic increase in the frequency of tumor formation in those mice compared with wild-type mice, the types of tumors formed, their numbers per animal, and age of tumor onset vary in different genetic backgrounds.¹⁻³ Other phenotypes observed in transgenic and gene-targeted animals influenced by genetic background include ethanol tolerance, sepsis, immunity, locomotor activity, behavior, organ structure, development, and cardiovascular physiology (Table). As examples of the latter, the incidence of stroke in mice deficient in tissue plasminogen activator and susceptibility to atherosclerosis in apoE-

deficient mice differ when the knockout loci are present on C57BL/6, 129/Sv, or FVB/N backgrounds.^{8,13}

On a positive note, phenotypic differences caused by allelic variation outside the target locus can provide a molecular genetic tool to identify and clone "modifier genes," which influence a phenotype.¹⁷ However, as stated above, these differences can cause significant problems when interpreting and comparing the results of transgenic and knockout studies between laboratories.

The Problem

At the heart of the problem is genetic heterogeneity among strains used to generate transgenic and knockout mice. It is generally acknowledged that it is easier and more efficient to generate transgenic mice by using hybrid strains derived from 2 different genetic backgrounds. Presumably, this is because hybrid strains exhibit superior reproductive performance, are easier to superovulate, and have higher quality embryos for microinjection, a phenomenon referred to as "hybrid vigor."^{18,19} Because of this, many transgenic laboratories use embryos derived from F₂ crosses of C57BL/6×SJL (B6SJL) or C57BL/6×DBA/2 (B6D2), among other combinations. When hybrid strains are used, each transgenic founder is genetically different from every other founder. This leaves the investigator with a choice of either continuing to breed their transgenic mice with hybrid strains to propagate the lines or, in cases in which genetic background issues are recognized and likely to be important, to generate congenic strains (defined below) by successive backcross breeding to 1 inbred strain, typically C57BL/6. Less frequently used are

Received January 6, 2000; revision accepted February 28, 2000.

From the Departments of Internal Medicine and Physiology & Biophysics, The University of Iowa College of Medicine, Iowa City.

Guest Editor for this article was Elizabeth Nabel, National Institutes of Health, Bethesda, Md.

Correspondence to Curt D. Sigmund, PhD, Chair, Molecular Biology Interdisciplinary Program, Director, Transgenic and Gene Targeting Facility, Department of Internal Medicine and Physiology & Biophysics, 2191 Medical Laboratory, The University of Iowa College of Medicine, Iowa City, IA 52242. E-mail: curt-sigmund@uiowa.edu

© 2000 American Heart Association, Inc.

Arterioscler Thromb Vasc Biol. is available at <http://www.atvbaha.org>

Phenotypes Exhibiting Genetic Background Effects in Knockout and Transgenic Mice

Phenotype	Genetic Alteration	Mouse Strains Tested	References
Tumor incidence	T antigen transgenic	C57BL/6, C57BL/6×NZW	4
	p53 knockout	129/Sv, C57BL/6×129/Sv	1, 2
	p53 knockout	VM, C57BL/6×129/Sv	3
	WAP-ras transgenic	FVB/N, SJL, C57BL/6, CD1	5
	Tsc2 knockout	Black Swiss, 129/SvJae	6
Ethanol tolerance	PKC-γ knockout	C57BL/6×129/Sv, C57BL/6	7
Atherosclerosis	ApoE knockout	FVB/N, C57BL/6	8
Sepsis	IL-4 knockout	129/Sv, C57BL/6	9
Locomotor activity	D2R knockout	129/SvEv×C57BL/6	10
		129/SvEv, C57BL/6	
	βAPP knockout	129/Sv, C57BL/6	11
Forebrain structure	βAPP knockout	129/SvEv	12
Stroke	tPA knockout	C57BL/6×129/Sv, C57BL/6	13
Renal development	AT1AR knockout	129/Sv, C57BL/6, 129Sv×C57BL/6	14
	AGT knockout	C57BL/6×CBA, C57BL/6	15
Development and pleiotropic effects	EGFR knockout	129/Sv, CD-1	16

PKC indicates protein kinase C; IL, interleukin; tPA, tissue plasminogen activator; and EGFR, epidermal growth factor receptor.

transgenic mice generated directly on inbred strains. The inbred FVB/N strain is used by some laboratories because it exhibits excellent reproductive performance, it has large litters, and the 1-cell fertilized embryos have prominent and easily injectable pronuclei.¹⁹ One limitation is that it is genetically distinct from the C57BL/6 strain, which is used by many investigators.

A second issue specifically related to transgenic mice (but not gene-targeted mice) is the position effect. Because of the random nature of the transgene insertion event after pronuclear injection, each resultant founder contains the transgene at a different site in the genome. These position effects can profoundly influence transgene expression and, therefore, the observed phenotype.^{20,21} This occurs because transcriptional regulatory elements present at or near the site of insertion (controlling the expression of a nearby gene or gene cluster) could impart new instructions on the transgene. Consequently, it is essential that several independent lines of mice, derived from founders with different insertion sites, are examined before a conclusion relating a phenotype to a specific pattern of transgene expression is made.

When performing gene targeting in embryonic stem (ES) cells, position effects are essentially eliminated but not the effects caused by genetic variability. As in the transgenic experiments, this results from the generation of hybrid strains. Most commonly used ES cell lines are derived from strain 129, and a number of 129 substrains are in existence (129/Sv, 129/SvEv, and 129/Ola), further complicating the scenario. As mentioned above, hybrid vigor has been reported for the viability of ES cell lines.²² Although many (but not all) ES cell lines are themselves inbred, most investigators report that the 129 strain exhibits poorer reproductive performance than other inbred strains and also exhibits other abnormalities, including development of teratocarcinoma. This has prompted most investigators to breed their chimeras to

C57BL/6, thus generating a hybrid mouse that is heterozygous (+/−) at the target locus and an F₁ between C57BL/6×129 at all other loci. The F₁ mice are all genetically identical because they inherit 1 chromosomal complement each from the 129 and C57BL/6 strains. However, when they are intercrossed to generate a mouse homozygous (−/−) for the target locus, the resultant offspring become an F₂ of the parent strains. Therefore, whether wild-type, heterozygous, or homozygous for the target locus, the offspring have a random mix of 129 or C57BL/6 chromosomal DNA throughout the genome. The maintenance of a strain homozygous at the target locus by continuous inbreeding of these F₂ mice can eventually select for phenotypic changes because loci causing deleterious effects are lost, and those providing a survival advantage are retained. Consequently, maintenance of the targeted locus in this manner is not recommended. Therefore, investigators are again left with the option to retain the mixed genetic background of the strains or to generate congenic strains.

Further complicating this problem has been the marked increase in the generation of double-knockout strains and the combinatorial use of knockout and transgenic rescue. In the latter, transgenes expressed either systemically or tissue-specifically are transferred into a knockout mouse to rescue some altered phenotype (often lethality).²³ Moreover, the development of inducible transgenes and methods using the cre-loxP recombinase system to generate cell-specific knockouts will necessitate the introduction of multiple transgenes into a single genetic background. Clearly, it will become important to avoid the creation of a mixed genetic background so complex as to preclude any reasonable use of controls and prevent replication by other investigators.

Effective Experimental Strategies

Clearly, when transgenic and gene-targeting experiments are designed, the ideal situation would have control mice that are

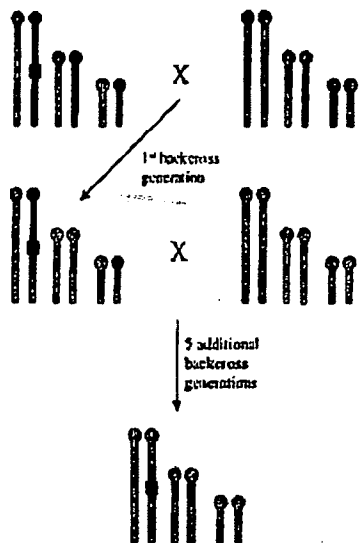


Figure 1. Generation of a congenic strain. A schematic representation of the chromosomal content in the generation of a congenic strain is shown. The 129 chromosomes are red, and the C57BL/6 chromosomes are blue. A targeted modification induced in ES cells is shown as a solid black box. Only 3 chromosomes are shown for simplicity. The top left illustrates a heterozygous knockout after germ-line transmission through a chimera. This mouse is heterozygous at the target locus, with an F₁ between 129 and C57BL/6 at all loci. To generate the congenic strain, the F₁ is successively backcrossed to a C57BL/6 mouse (all blue), and the targeted locus is selected in all offspring. The 129 genome is progressively diluted in each backcross because of the random assortment of chromosomes and homologous recombination. After 6 generations of backcross breeding, the resultant offspring are >99% C57BL/6 except for the region surrounding the targeted modification, which remains derived from the 129 strain.

genetically identical to the experimental mice. The use of isogenic strains differing only in the presence or absence of the target locus would be the "gold standard." However, this can only be achieved if inbred mice are used for the generation of experimental models. Therefore, whenever possible, inbred strains should be used as the choice of controls becomes obvious. As discussed above, when this is not a practical or feasible option, the next best alternative is to develop a program of continuous inbreeding to a common strain, thus generating congenic mice. A congenic strain is one that is genetically identical to a control strain except for a single region of 1 chromosome (Figure 1). In the context of this discussion, this refers either to the target locus or the inserted transgene. The generation of congenic strains also provides an opportunity to place the target locus on a number of different genetic backgrounds and thus directly test for strain-specific modifier loci.

Although the generation of congenic mice is simple, requiring only accurate record keeping, it can be time-consuming and expensive, especially when multiple lines must be developed. Six generations of backcross breeding (2 years) is required before the genetic backgrounds are statistically >99% homogeneous, and the return on additional generations of backcross breeding markedly diminishes thereafter. For example, it requires 4 additional generations to increase genetic homogeneity from 99.2% to 99.95%. The use of a speed-congenic approach or a combination of in vitro



Figure 2. Comparison between experimental and control strains. A schematic diagram of the chromosomal content between experimental (A) and control strains (B and C) is shown. The experimental mouse is homozygous for the targeted disruption (solid black box) and is a C57BL/6 (blue) congenic strain. A small amount of 129 genomic DNA (red) upstream and downstream from the target locus remains. A C57BL/6 inbred mouse (B) is blue at all loci, and although it lacks the targeted modification, it also lacks the 129 DNA linked to the disruption. The ideal control (C) would be a C57BL/6 congenic strain with a similar extent of 129 DNA as shown in panel A.

fertilization and prepubertal superovulation can be used to decrease the time needed to generate congenic strains.^{24,25} The speed-congenic approach makes use of the well-developed genetic map of the mouse, thus affording an opportunity to screen the DNA of each offspring generated along the route toward congenic production to select for mice containing markers from the appropriate genetic background at the target locus and elsewhere.^{26,27} Those mice that are "further" along in congenic development than expected, on the basis of random segregation alone, can be selected by this process for further breeding.

After a C57BL/6 congenic knockout strain is derived, either nontransgenic littermates or age-matched inbred C57BL/6 mice should serve as reasonable controls. However, it is important for the researcher to appreciate that even this scenario has weaknesses. Indeed, 1 limitation of using littermate or wild-type mice as controls for congenic transgenic (or knockout) strains is that some parental genomic DNA upstream and downstream from the target locus (129 DNA in the case of ES cell-derived gene targeting) remains. By use of the same example as described above, this occurs because as the targeted modification (made in 129 genomic DNA) is introgressed into the C57BL/6 strain, the targeted locus and therefore 129 DNA in the vicinity of (or linked to) the locus will be selected in each backcross generation (Figure 2A). The location of the breakpoint between C57BL/6 and 129 genomic DNA upstream and downstream from the target locus will depend on where the recombination between the 2 genomes occurred. Therefore, nontransgenic littermates and wild-type C57BL/6 mice will lack the targeted locus and also the closely linked 129 genomic DNA (Figure 2B). In some cases, this DNA may contain closely linked modifier genes. This may be especially critical when examining large gene families, which may have members closely clustered in the genome.

Therefore, the optimal control would be a congenic control strain containing a similar amount of foreign genomic information around the target locus but lacking the targeted modification itself (Figure 2C). Absolutely identical congenic strains cannot be generated. However, similarities between control and experimental strains can be maximized by taking advantage of the dense genetic map of the mouse and the thousands of polymorphic microsatellite markers distributed throughout the mouse genome.²⁸ For example, control mice can be selected that contain C57BL/6-specific markers throughout the genome except in the region of the target

locus, where 129-specific markers would be selected. These mice can then be propagated to generate a control congenic strain that is similar to the experimental mouse but lacks the targeted ES cell-induced modification.

Of course, we must recognize that from a practical standpoint, circumstances will often dictate assessing the phenotype of a knockout mouse long before a congenic strain can be generated. If these mice were derived from 129 ES cells and the chimera was bred to C57BL/6, it is predictable that each mouse, while containing the same targeted modification of the genome, will be genetically different at all other loci because of random segregation and recombination in the F_2 generation. In this case, it would be inappropriate to use either inbred C57BL/6 or 129 mice solely as controls. Instead, wild-type or heterozygous littermates from the same breedings should be included as well. The use of littermates would help minimize environmental variability in such experiments. Moreover, larger numbers of mice should be examined to ensure that the range of phenotypes possible due to epigenetic interactions with the genetic background is observed. Although not genetically identical, when examined as a population, the experimental and control groups could be considered "genetically similar." Once the phenotypes are assessed, it would be prudent to generate congenic strains and reexamine the phenotype in the resultant animals.

Guidelines

Until such time as a standardized mouse strain exists that facilitates easy generation of transgenic and knockout mice, the debate over the proper use of experimental and control mice will continue. There are no easy solutions to this problem. As illustrated above, in the absence of inbred strains, there is no optimal set of experimental and control conditions that normalizes the epigenetic effects of unlinked loci. Therefore, it becomes the responsibility of the investigator to use common sense and design the best possible control experiments that fit the individual situation, to assess whether the phenotype observed in their model is due specifically to the targeted modification or is affected by other loci, and to inform the scientific community if phenotypic alterations become evident. The geneticists at the Banbury Conference on Genetic Background in Mice²⁹ in 1996 established 3 general guiding principals for the use of transgenic and gene targeted mice in neuroscience. These principals should be applicable to all disciplines, and the reader is referred to that article for a detailed discussion of options for designing such experiments.²⁹ Their guidelines state the following: (1) Published reports must include a detailed description of the genetic background of the mice studied that is sufficient enough to allow replication of the study. (2) The genetic background chosen for the studies should not be so complex as to preclude replication. (3) Use of common or standardized genetic background would facilitate comparison of experimental results among laboratories.

Minimally, these guidelines provide a common-sense approach that provides the reader with sufficient information to understand and potentially replicate reported results and also provide a framework to identify the causes of phenotypic variation observed in different laboratories. It makes common

sense to recommend that these guidelines be adopted by all researchers using genetically modified mice as models of cardiovascular disease until such time as standardized strains are used universally.

References

1. Donehower LA, Harvey M, Vogel H, McArthur MJ, Montgomery CA Jr, Park SH, Thompson T, Ford RJ, Bradley A. Effects of genetic background on tumorigenesis in p53-deficient mice. *Mol Carcinog*. 1995;14:16-22.
2. Harvey M, McArthur MJ, Montgomery CA Jr, Bradley A, Donehower LA. Genetic background alters the spectrum of tumors that develop in p53-deficient mice. *FASEB J*. 1993;7:938-943.
3. van Meyel DJ, Sanchez-Sweetman OH, Kerkvliet N, Stitt L, Ramsay DA, Khokha R, Chambers AF, Cairncross JG. Genetic background influences timing, morphology and dissemination of lymphomas in p53-deficient mice. *Int J Oncol*. 1998;13:917-922.
4. Cho HJ, Seiberg M, Georgoff I, Teresky AK, Marks JR, Levine AJ. Impact of the genetic background of transgenic mice upon the formation and timing of choroid plexus papillomas. *J Neurosci Res*. 1989;24:115-122.
5. Nielsen LL, Gurnani M, Catino JJ, Tyler RD. In wip-ras transgenic mice, tumor phenotype but not cyclophosphamide-sensitivity is affected by genetic background. *Anticancer Res*. 1995;15:385-392.
6. Onda H, Lueck A, Marks PW, Warren HB, Kwiatkowski DJ. Tsc2(+/-) mice develop tumors in multiple sites that express gelatinase and are influenced by genetic background. *J Clin Invest*. 1999;104:687-695.
7. Bowers BJ, Owen EH, Collins AC, Abeliovich A, Tonogawa S, Wehner JM. Decreased ethanol sensitivity and tolerance development in gamma-protein kinase C null mutant mice is dependent on genetic background. *Alcohol Clin Exp Res*. 1999;23:387-397.
8. Dansky HM, Charlton SA, Sikes JL, Heath SC, Simantov R, Levin LF, Shu P, Moore KJ, Breslow JL, Smith JD. Genetic background determines the extent of atherosclerosis in apoE-deficient mice. *Arterioscler Thromb Vasc Biol*. 1999;19:1960-1968.
9. Hultgren O, Kopf M, Tarkowski A. Outcome of *Staphylococcus aureus*-triggered sepsis and arthritis in IL-4-deficient mice depends on the genetic background of the host. *Eur J Immunol*. 1999;29:2400-2405.
10. Kelly MA, Rubinstein M, Phillips TJ, Lessov CN, Burkhardt-Kasch S, Zhang G, Bunzow JR, Fang Y, Gerhardt GA, Grandy DK, Low MJ. Locomotor activity in D2 dopamine receptor-deficient mice is determined by gene dosage, genetic background, and developmental adaptations. *J Neurosci*. 1998;18:3470-3479.
11. Wolfer DP, Muller U, Staglar M, Lipp HP. Assessing the effects of the 129/Sv genetic background on swimming navigation learning in transgenic mutants: a study using mice with a modified beta-amyloid precursor protein gene. *Brain Res*. 1997;771:1-13.
12. Magara F, Muller U, Li ZW, Lipp HP, Weissmann C, Staglar M, Wolfer DP. Genetic background changes the pattern of forebrain commissure defects in transgenic mice underexpressing the beta-amyloid-precursor protein. *Proc Natl Acad Sci U S A*. 1999;96:4656-4661.
13. Tabrizi P, Wang L, Seeds N, McComb JG, Yamada S, Griffin JH, Carmeliet P, Weiss MH, Zlokovic BV. Tissue plasminogen activator (tPA) deficiency exacerbates cerebrovascular fibrin deposition and brain injury in a murine stroke model: studies in tPA-deficient mice and wild-type mice on a matched genetic background. *Arterioscler Thromb Vasc Biol*. 1999;19:2801-2806.
14. Le TH, Fogo A, Oliverio MI, Peterson AS, Smithies O, Coffman TM. Genetic modifiers in type 1A (AT1A) angiotensin II receptor deficiency. *J Am Soc Nephrol*. 1999;10:396A. Abstract.
15. Sugiyama F, Tanimoto Y, Kato H, Nomura T, Taniguchi K, Tanimoto K, Murakami K, Fukamizu A, Yagami K. Speedy backcrossing through in vitro fertilization, using pre-pubertal superovulation and neonatal death dependent on genetic background in angiotensinogen-deficient mice. *Lab Anim Sci*. 1997;47:545-548.
16. Threadgill DW, Dlugosz AA, Hansen LA, Tennenbaum T, Licht U, Yee D, LaMantia C, Mouton T, Herrup K, Harris RC. Targeted disruption of mouse EGF receptor: effect of genetic background on mutant phenotype. *Science*. 1995;269:230-234.
17. Takahashi JS, Pinto LH, Vitaterna MH. Forward and reverse genetic approaches to behavior in the mouse. *Science*. 1994;264:1724-1733.
18. Hogan E, Costantini F, Lacy E. *Manipulating the Mouse Embryo*. Cold Spring Harbor, NY: Cold Spring Harbor Laboratory; 1986.
19. Takeito M, Schroeder AC, Moberg LE, Gunning KB, Hantec G, Fox RR, Roderick TH, Stewart CL, Lilly F, Hansen CT. FVB/N: an inbred

- mouse strain preferable for transgenic analyses. *Proc Natl Acad Sci U S A*. 1991;88:2065-2069.
20. Clark AJ, Bissinger P, Bullock DW, Damak S, Wallace R, Whitelaw CBA, Yull F. Chromosomal position effects and the modulation of transgene expression. *Reprod Fertil Dev*. 1994;6:589-598.
 21. Sigmund CD. Manipulating genes to understand cardiovascular diseases: major approaches for introducing genes into cells. *Hypertension*. 1993; 22:599-607.
 22. Suzuki O, Matsuda J, Takano K, Yamamoto Y, Asano T, Naiki M, Kusanagi M. Effect of genetic background on establishment of mouse embryonic stem cells. *Exp Anim*. 1999;48:213-216.
 23. Davisson RL, Kim HS, Kregel JH, Lager DJ, Smithies O, Sigmund CD. Complementation of reduced survival, hypotension and renal abnormalities in angiotensinogen deficient mice by the human renin and human angiotensinogen genes. *J Clin Invest*. 1997;99:1258-1264.
 24. Lander ES, Schork NJ. Genetic dissection of complex traits. *Science*. 1994;265:2037-2048.
 25. Yokoyama M, Hasegawa T, Nomura T, Katsuki M. Conversion of the genetic background of transgenic mice by in vitro fertilization. *Exp Anim*. 1995;44:145-150.
 26. Morel L, Yu Y, Blenman KR, Caldwell RA, Wakeland EK. Production of congenic mouse strains carrying genomic intervals containing SLE-susceptibility genes derived from the SLE-prone NZM2410 strain. *Mamm Genome*. 1996;7:335-339.
 27. Yui MA, Muralidharan K, Moreno-Altamirano B, Perrin G, Chestnut K, Wakeland EK. Production of congenic mouse strains carrying NOD-derived diabetogenic genetic intervals: an approach for the genetic dissection of complex traits. *Mamm Genome*. 1996;7:331-334.
 28. Dietrich WF, Miller J, Sitten R, Merchant MA, Damron-Boles D, Husain Z, Dredge R, Daly MJ, Ingalls KA, O'Connor TJ. A comprehensive genetic map of the mouse genome. *Nature*. 1996;380:149-152.
 29. Mutant mice and neuroscience: recommendations concerning genetic background: Banbury Conference on genetic background in mice. *Neuron*. 1997;19:755-759.

EXHIBIT 5

METHODS REPORT

Staging of Alzheimer disease-associated neurofibrillary pathology using paraffin sections and immunocytochemistry

Heiko Braak · Irina Alafuzoff · Thomas Arzberger ·
 Hans Kretschmar · Kelly Del Tredici

Received: 8 June 2006 / Revised: 21 July 2006 / Accepted: 21 July 2006 / Published online: 12 August 2006
 © Springer-Verlag 2006

Abstract Assessment of Alzheimer's disease (AD)-related neurofibrillary pathology requires a procedure that permits a sufficient differentiation between initial, intermediate, and late stages. The gradual deposition of a hyperphosphorylated tau protein within select neuronal types in specific nuclei or areas is central to the disease process. The staging of AD-related neurofibrillary pathology originally described in 1991 was performed on unconventionally thick sections (100 μ m) using a modern silver technique and reflected the progress of the disease process based chiefly on the topographic expansion of the lesions. To better meet the demands of routine laboratories this procedure is

revised here by adapting tissue selection and processing to the needs of paraffin-embedded sections (5–15 μ m) and by introducing a robust immunoreaction (AT8) for hyperphosphorylated tau protein that can be processed on an automated basis. It is anticipated that this revised methodological protocol will enable a more uniform application of the staging procedure.

Keywords Alzheimer's disease · Neurofibrillary changes · Immunocytochemistry · Hyperphosphorylated tau protein · Neuropathologic staging · Pretangles

This study was made possible by funding from the German Research Council (Deutsche Forschungsgemeinschaft) and BrainNet Europe II (European Commission LSHM-CT-2004-503039). This publication reflects only the viewpoint of the authors, the European Community is not responsible for its use or contents.

H. Braak (✉) · K. Del Tredici
 Institute for Clinical Neuroanatomy,
 J.W. Goethe University Clinic, Theodor Stern Kai 7,
 60590 Frankfurt/Main, Germany
 e-mail: Braak@em.uni-frankfurt.de

I. Alafuzoff
 Institute of Clinical Medicine, Pathology,
 Kuopio University and University Hospital,
 Harjulantie 1, P.O. Box 1627, 70211 Kuopio, Finland

T. Arzberger · H. Kretschmar
 Institute of Neuropathology, Ludwig Maximilians University,
 81377 Munich, Germany

K. Del Tredici
 Clinic for Psychiatry and Neurology Winnenden,
 71364 Winnenden, Germany

Introduction

The development of intraneuronal lesions at selectively vulnerable brain sites is central to the pathological process in Alzheimer's disease (AD) [42, 46, 55, 56, 58, 94]. The lesions consist chiefly of hyperphosphorylated tau protein and include pretangle material, neurofibrillary tangles (NFTs) in cell bodies, neuropil threads (NTs) in neuronal processes, and material in dystrophic nerve cell processes of neuritic plaques (NPs) [7, 19, 30].

The AD-related pathological process spans decades and, during this time, the distribution pattern of the lesions develops according to a predictable sequence [8, 21, 89, 93, for a broader discussion of the histopathological diagnosis of AD, see 54, 69, 76]. A staging system for the intraneuronal lesions introduced in 1991 differentiated initial, intermediate, and late phases of the disease process in both non-symptomatic and symptomatic individuals [21, 24–28, 39, 40, 43, 44, 63, 71, 75, 79–82, 84, 85, 87]. In 1997, this staging system

was incorporated into the NIH-Reagan criteria for the neuropathological diagnosis of AD [64, 66, 83]. The Braak system was based upon assessment of two 100 μ m sections processed according to the silver-iodate technique proposed by Gallyas [49–51, 67, 68, 78]. The first section included the hippocampal formation at uncal level, the anterior parahippocampal gyrus, and portions of the adjoining occipito-temporal gyrus. The second section, taken from the occipital neocortex, encompassed portions of the striate area, parastriate area, and peristriate region (Fig. 1). Distinctive differences in the topographical distribution pattern of the neurofibrillary lesions enabled the observer to assign a given autopsy case to one of six stages [21, 22]. This simple system had the advantage of being reproducible without having to rely on quantitative assessments or knowledge of patient-related data (age, gender, cognitive status). Furthermore, the result of the silver reactions in unconventionally thick sections provided a means of “reading” a given stage with the unaided eye.

For routine diagnostic purposes, however, such a system is problematic because it calls for unusually thick sections cut from blocks embedded in an unconventional medium [polyethylene glycol (PEG)] [91]. In addition, the method requires that free floating sections be stained by experienced laboratory assistants using a non-automated silver technique. These features drastically limit the feasibility of the original staging protocol for routine diagnostic use in the majority of neuropathological laboratories [35]. At the same time, they account for the fact that the staging system has found broad acceptance in a research context while having been subjected to numerous modifications [9, 18, 36, 39, 40, 53, 59–62, 69–71, 75, 76, 83, 88]. Neuropathologists in routine diagnostic praxis as well as reference centers that maintain brain banks are interested in a uniform staging procedure so that the material submitted by various participating institutions can be used and evaluated according to the same criteria. Such a staging system must be reproducible, cost-effective, and easy.

In recent years, sensitive immunocytochemical methods have been developed, the application of which makes it possible to reliably detect not only incipient neurofibrillary pathology in mildly involved brain regions of non-symptomatic individuals but also, with disease progression, the full extent of the intraneuronal pathology in the end phase [19, 90]. Neurofibrillary changes of the Alzheimer type consist of stable proteins that are impervious to postmortal delay or suboptimal fixation conditions, and immunoreactions for demonstration of hyperphosphorylated tau protein

can be carried out even on tissue that has been stored for decades in formaldehyde [1, 72].

Immunoreactions against hyperphosphorylated tau, however, cannot fully replace the Gallyas silver staining method (see Technical addendum), inasmuch as both techniques identify partially different structures. At the beginning of the intraneuronal changes, a soluble and non-argyrophilic material develops, filling the somata of involved nerve cells as well as dendritic processes and axons. Thereafter, the distal dendritic segments become snarled and develop dilated appendages. The soluble “pretangle” material is identifiable in immunoreactions for hyperphosphorylated tau protein but remains Gallyas-negative. It is the harbinger of an argyrophilic, insoluble, and non-biodegradable fibrillary material that emerges after cross-linkage and aggregation of the soluble pretangle material [7, 19, 96]. The Gallyas-positive neurofibrillary aggregations gradually fill the cytoplasm, sometimes infiltrating the proximal dendrites to form a neurofibrillary tangle, and appear in dendritic segments as NTs without involving the axon [19, 45, 95]. Following neuronal death, the abnormal material remains visible in the tissue as extraneuronal ghost tangles or tombstone tangles. With time, ghost tangles are no longer immunoreactive for hyperphosphorylated tau protein and their argyrophilia gradually becomes less pronounced [17, 19, 34]. In summary, the pretangle material can only be detected by immunocytochemistry and this fact has been taken into account in the revised staging procedure presented here (Fig. 2).

In view of the progress that has been made in the demonstration of the neurofibrillary changes of the Alzheimer type, it seemed expedient to revise the 1991 staging procedure by introducing immunoreactions for visualization of hyperphosphorylated tau and by adapting the tissue selection and processing to the demands of the routine diagnostic laboratory. The goal remains the same, namely to stage the AD-related neurofibrillary pathology in six stages, as previously, with emphasis this time on the plexuses formed of both pretangle and tangle material, but using paraffin sections immunostained for hyperphosphorylated tau and processed on an automated basis. To illustrate the advantages and disadvantages of both methods, required brain regions with lesions representing AD stages I–VI have been digitally photographed both in silver- and immunostained 100 μ m PEG sections and in 7 μ m paraffin sections immunostained for hyperphosphorylated tau protein (AT8-antibody). The revised procedure is intended to facilitate the uniform application of the staging procedure, which now can be performed with greater efficiency than previously.

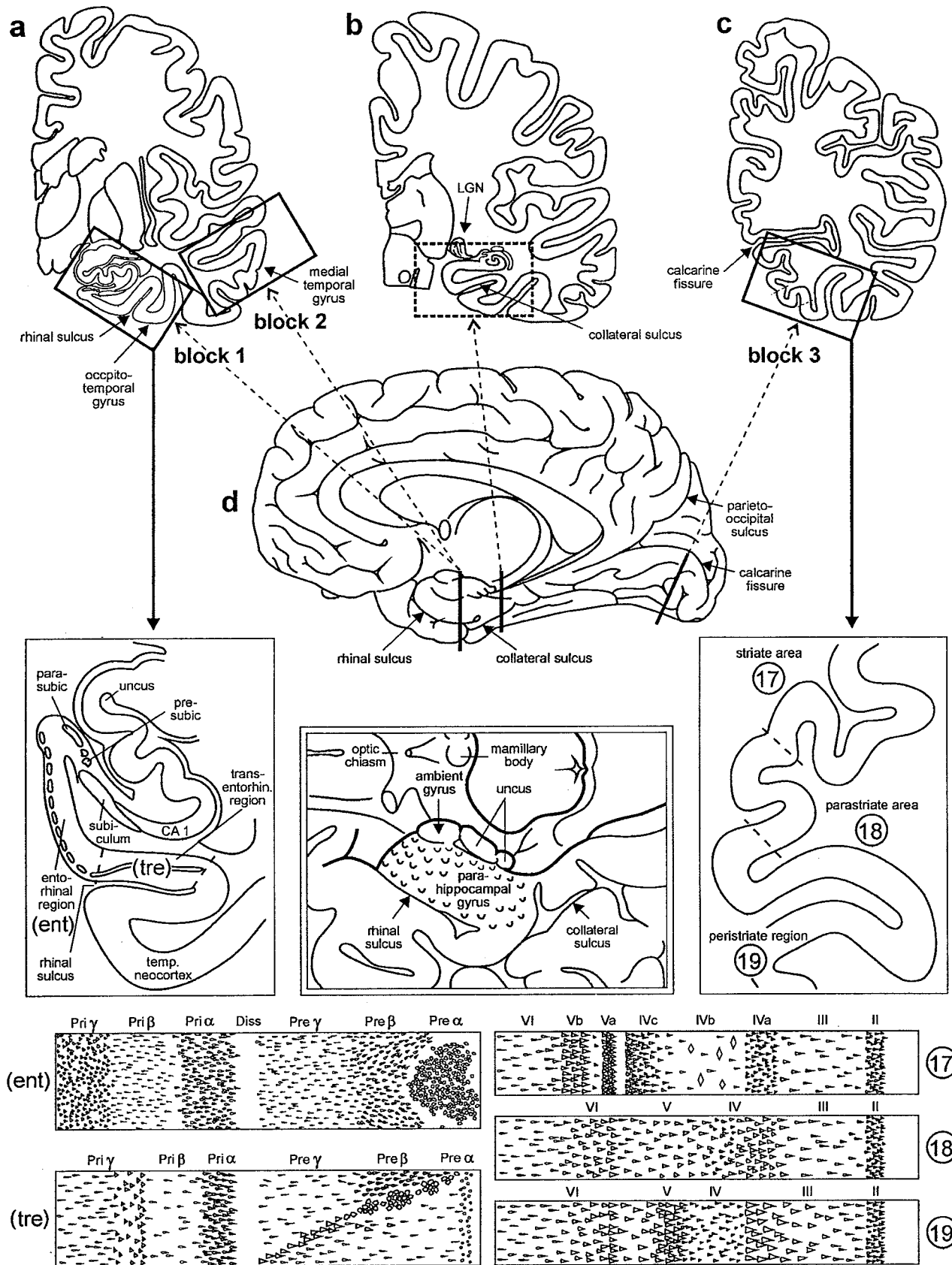


Fig. 1 Scheme showing the location of the three blocks of tissue required for staging of AD-related neurofibrillary changes. The *first block* at the far left (a) includes anteromedial portions of the temporal lobe. It is cut at the mid-uncal or amygdala level (frontal section at the level of the mamillary bodies) and includes the parahippocampal and adjoining occipito-temporal gyri (see *enlarged insert* below a). The *cutting line* runs through the rhinal sulcus. The *second block* comes from the same level and includes part of the medial and superior temporal gyri (a). The *third block* at the far right (c) is removed from basal portions of the occipital lobe. The cut is oriented perpendicular to the calcarine fissure. The block includes the neocortex covering the lower bank of the calcarine fissure and the adjoining basal occipital gyri. It thus shows portions of the peristriate region as well as of the parastriate and striate areas (see *enlarged insert* below c). (b) This block provides the classical view of the hippocampal formation and is removed at the level of the lateral geniculate nucleus. It is routinely dissected for diverse diagnostic purposes of the hippocampal formation. The *cutting line* runs through the collateral sulcus (d). The parahippocampal gyrus at this latitude abuts posteriorly on the lingual gyrus and contains either posterior portions of the entorhinal and transentorhinal regions or lingual neocortex. Insofar as the first temporal block at mid-uncal level is essential for the evaluation of the transentorhinal and entorhinal regions (diagnosis of AD stages I–III), the classical hippocampus section is not absolutely required for staging. The *middle drawing* in the second row indicated by a double frame shows the anatomical landmarks of the entorhinal region seen basally. Note the wart-like elevations in anterior portions of the parahippocampal gyrus roughly outlining the extent of the entorhinal allocortex. The lower schemata highlight the lamination pattern of the areas that need to be evaluated for staging purposes. The various allocortical and neocortical laminae are indicated across the upper margins. 17, 18, 19 striate area, parastriate area, peristriate region. Abbreviations: CA1 first sector of the Ammon's horn, *ent* entorhinal region, *parasubic* parasubiculum, *presubic* presubiculum, *temp. neocortex* temporal neocortex, *tre* transentorhinal region (mesocortex), *transentorhin.* transentorhinal

Processing

Fixation and macroscopic preparation

Brains obtained at autopsy should be fixed by immersion in 10% formalin (4% aqueous solution of HCHO) for one week or longer. Partially remove the meninges to uncover the rhinal sulcus, collateral sulcus, and calcarine fissure (Fig. 1a–d).

Whereas the original staging procedure requires evaluation of thick silver-stained sections from two relatively large blocks of cortical tissue, the revised version uses immunostained paraffin sections microtomed from three blocks of conventional size that fit routine tissue cassettes. Figure 1d shows the cutting lines for removal of the three blocks and, in addition, those for the classical view of the hippocampal formation. Alternatively, the tissue on one side of a cut can be used for conventional paraffin embedding (thin sections), and that on the other side for PEG embedding (thick sections).

The first block includes anteromedial portions of the temporal lobe cut at the mid-uncal or amygdala level (frontal section through the temporal lobe at the level of the mamillary bodies) encompassing anterior portions of both the parahippocampal gyrus and adjoining occipito-temporal gyrus. The cutting line runs through the rhinal sulcus (Fig. 1a, d). The sections from this block contain central portions of the entorhinal region and the adjoining transentorhinal region, the latter of which is concealed in the depths of the rhinal sulcus [23, 98]. This block is essential for assessment of neurofibrillary AD stages I–III.

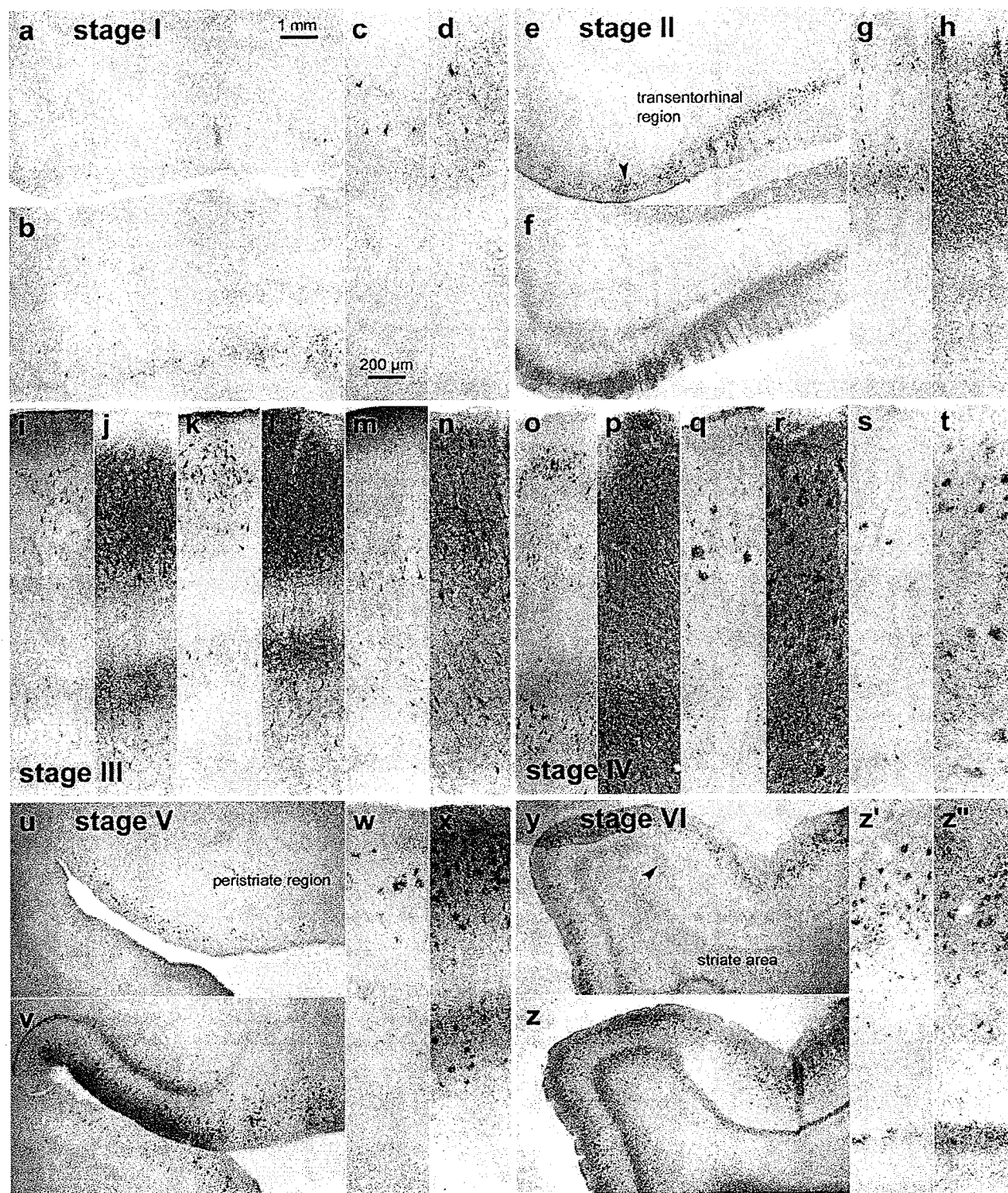
The second block simplifies assessment of stage IV. It is obtained from the same slice as the first block and includes portions of the medial and superior temporal gyri (Fig. 1a, d). As an alternative to the first two blocks, the entire slice through the temporal lobe can be used, provided slides of sufficient size are available. Reduction of this slice to two blocks is recommended to avoid exceeding the size of conventional tissue cassettes.

The third block is removed halfway between the occipital pole and the junction of the parieto-occipital sulcus with the calcarine fissure. The cut is oriented perpendicular to the calcarine fissure (Fig. 1c, d). Again, the size of the block has been reduced to fit standard tissue cassettes. Care has to be taken that the block includes part of the lower bank of the calcarine fissure and the adjoining basal occipital gyri encompassing portions of the neocortex, i.e., the peristriate region, parastriate field, and a clearly definable primary field, the striate area (Brodmann field 17 with the macroscopically identifiable line of Gennari). This block is indispensable for recognition of the neurofibrillary AD stages V and VI.

Immunocytochemistry

Mounted paraffin sections of 5–15 μ m thickness are de-waxed and re-hydrated.

The monoclonal antibody AT8 (Innogenetics, Belgium) is one of several commercially available specific antibodies that show robust immunoreactivity for hyperphosphorylated tau protein, and a recently published immunocytochemical trial using this antibody has yielded reproducible results [1]. AT8 does not cross-react with normal tau epitopes or require special pre-treatments, and it is exceptionally reliable in human autopsy material regardless of the length of the fixation time in formaldehyde and/or the condition of the preserved tissue [16, 19, 57, 77]. When performed on paraffin sections (5–15 μ m), AT8-immunoreactions permit counter-staining for other structures of interest,



provided that diaminobenzidine is used as a chromogen. Homogeneous immunoreactions can also be achieved using PEG sections (50–150 μm) (Fig. 2). The sections are incubated for 40 h at 4°C with the AT8 antibody (1:2,000) and thereafter processed for 2 h

with the second biotinylated antibody (anti-mouse IgG). Reactions are visualized with the ABC-complex (Vectastain) and 3,3-diaminobenzidine (Sigma).

Prolonged fixation of brain tissue in a formaldehyde solution may cause metachromatic precipitations

Fig. 2 Comparison of Gallyas silver- and AT8-immunostaining of cortical neurofibrillary pathology as seen in adjacent serial 100 μ m polyethylene glycol-embedded sections. The distribution pattern of the lesions throughout the various cortical fields that are necessary for staging purposes basically corresponds in both methods. It is possible with either technique to assess the progress of the neurofibrillary pathology. In the revised staging procedure, however, the greater emphasis on the presence of abnormal plexuses, which also include non-argyrophilic pretangle material in AT8-ir sections, facilitates rapid diagnostic assessment of the stages. **a–d stage I:** Mild involvement is confined to the transentorhinal region. Note that the plexus of AT8-ir nerve cell processes (**b** and **d**) is more conspicuous than that of argyrophilic neuropil threads (**a** and **c**). Sections originate from a non-demented 62-year-old male. **e–h stage II:** Lesional density increases and the pathology extends into the entorhinal region. Layer pre- α gradually sinks into a deeper position at the border between entorhinal and transentorhinal region (*arrowhead*). Note the greater breadth of the ir-plexus in comparison to silverstained nerve cell processes (compare **f** and **h** with **e** and **g**). Immunoreactions begin to show the deep entorhinal plexus (pri- α). The sections were obtained from a non-demented 78-year-old male. **i–n stage III:** The pathology in the outer and inner entorhinal (**i**, **j**) and transentorhinal (**k**, **l**) cellular layers worsens, and lesions extend into the adjoining neocortical association areas of the fusiform (occipito-temporal) gyrus (**m**, **n**). The sections originate from an 85-year-old female. **o–t stage IV:** The density of the lesions increases in both the entorhinal region (**o**, **p**) and fusiform gyrus (**q–r**) with a gradual decrease of the *pallid lines* (lamina dissecans in **p** and outer line of Baillarger in **r**). The neurofibrillary pathology now extends up to the medial temporal gyrus (**s**, **t**). Sections were taken from an 80-year-old female. **u–x stage V:** The lesions extend widely into the occipital lobe and appear in the peristriate region. Note the presence of a deep plexus in AT8-immunoreactions (**v**, **x**). Sections were obtained from a 66-year-old demented female. **y–z' stage VI:** Lesions are visible even in the parastriate and striate areas of the occipital neocortex. Note the clear-cut line in layer V of the striate area (**z'** and **z''**). The sections originate from a demented 75-year-old male. Scale bar in **a** applies to all overviews and that in **c** to all micrographs of cortical areas

(Buscaino bodies or mucocytes) [73]. Components of this material partially react with silver methods and also may interfere with immunoreactions. The precipitations can be removed with pyridine or a tenside solution [1 unit volume Tween 20 (Merck-Schuchardt 822184) and 9 unit volumes de-ionized water] at 80°C for 30 min or both. The sections are then rinsed thoroughly under running tap water and transferred to de-ionized water.

Comparison between Gallyas silver- and AT8-immunostained thick (100 μ m) sections

Figure 2 is designed to facilitate a direct comparison between selected cortical areas in 100 μ m thick PEG-embedded sections. The first section of each pair has been silverstained according to a modified version of the technique originally proposed by Gallyas [22, 31,

49–51, 67, 68, 78], whereas the second serial section (i.e., back-to-back sections from the identical tissue block) underwent staining with the antibody AT8.

Intraneuronal neurofibrillary tangles are visualized with equal clarity by both methods (Fig. 2). Further, the plexuses of argyrophilic NTs are visible not only in the Gallyas sections but also in the AT8-immunostained sections—in the latter, however, the plexuses can be seen to include additional pathologically altered neuronal components (dendrites, axons) that contain non-argyrophilic “pretangle” material (see Fig. 2f, h). Such immunostained plexuses appear much more compact than those depicted by the silver stain, and their obvious advantage is that they can be recognized immediately with the naked eye (see Fig. 3). This applies particularly to the AT8-immunoreactive plexuses located in the deep cortical layers (see Fig. 2v, x, z, z'), whereas in Gallyas sections such macroscopic recognition is not always possible (compare Fig. 2v with Fig. 2u).

Nonetheless, the distribution pattern of the immunoreactive cortical alterations throughout the various fields that are crucial for staging purposes corresponds to that of the argyrophilic lesions (Fig. 2) and, as such, it allows the observer to trace the progress of the neurofibrillary pathology in both silverstained (Fig. 2) and immunostained sections alike (Fig. 3). The greater emphasis on the abnormal plexuses in AT8-immunoreactive sections, however, facilitates the immediate diagnostic assessment of the stages, as, for instance, is readily evident even in the scaled down photographs of the hemisphere sections shown in Fig. 3. These immunopositive plexuses are still visible macroscopically in paraffin sections (5–15 μ m), and it is helpful, initially, without using the microscope, to view all three slides against a light background to assign them preliminarily to a given stage.

The final diagnosis is essentially based on recognition of the topographical distribution pattern of the neurofibrillary pathology and calls for a precise knowledge of which regions in the cerebral cortex, in which sequence, develop the AD-related neurofibrillary lesions. This decision can be made with almost the same degree of accuracy regardless of whether immunostained or silverstained sections are employed, although, based on experience, there is a slight tendency to assign a higher stage to the immunostained slides. The frequency of stage I cases, for example, is somewhat higher in AT8-immunostained sections because in the incipient phases of the disease process AT8-immunopositive nerve cells appear that still lack argyrophilic material. Thus, it is advisable to perform the staging procedure using either the Gallyas or AT8 technique but not both methods.

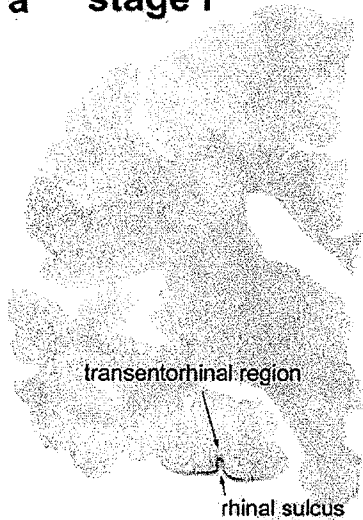
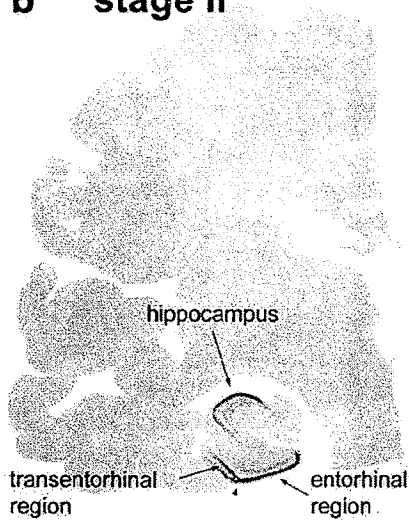
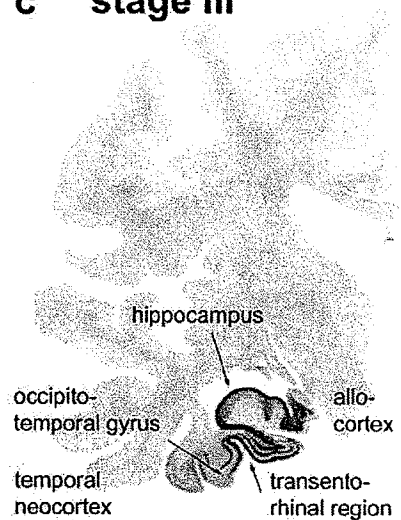
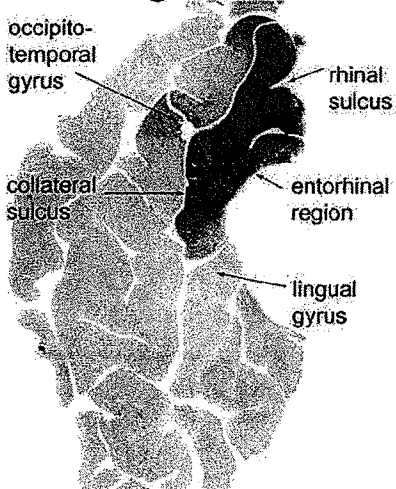
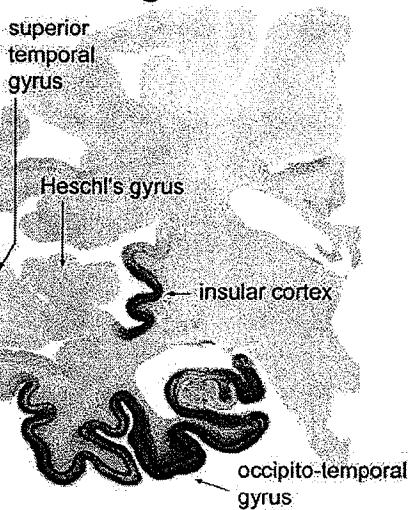
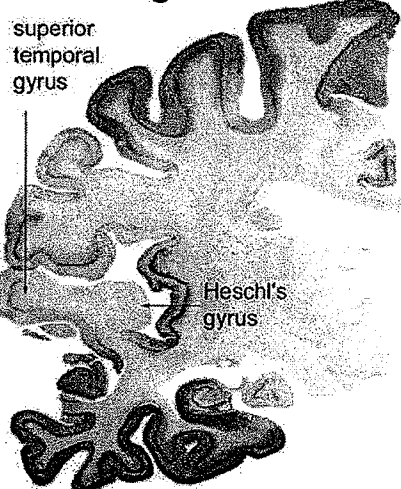
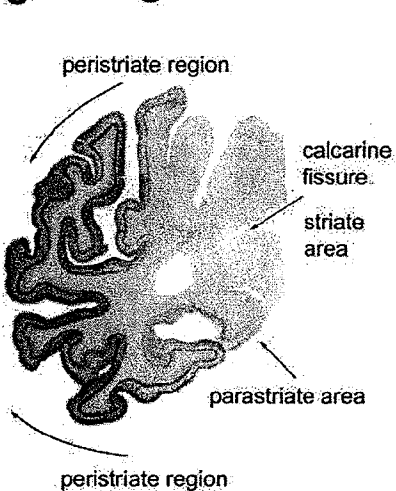
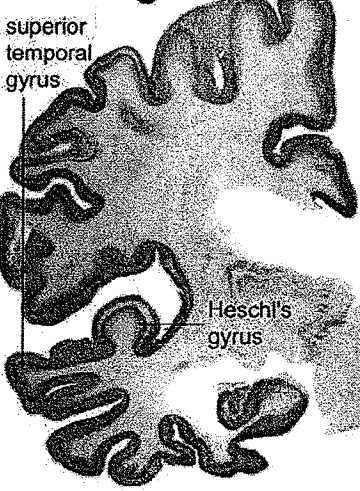
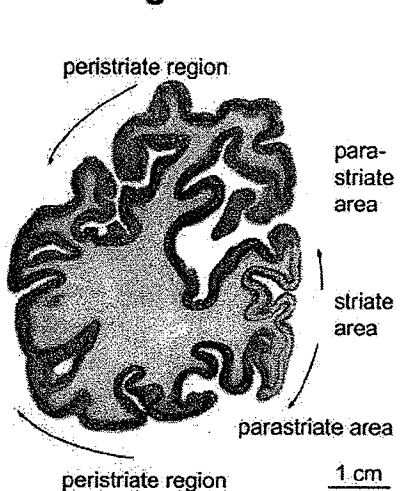
a stage I**b stage II****c stage III****d stage III****e stage IV****f stage V****g stage V****h stage VI****i stage VI**

Fig. 3 Stages I–VI of cortical neurofibrillary pathology in 100 μ m polyethylene glycol-embedded hemisphere sections immunostained for hyperphosphorylated tau (AT8, Innogenetics). **a stage I:** Involvement is slight and all but confined to the transentorhinal region (part of the temporal mesocortex), located on the medial surface of the rhinal sulcus. The section originates from a non-demented 80-year-old female. **b stage II:** Additional immunoreactivity occurs in layer pre- α or layer II of the entorhinal region. The layer gradually sinks into a deeper position in the transentorhinal region (arrow). The border between the entorhinal and transentorhinal regions is clearly recognizable in these early stages (arrowhead). Furthermore, the lesions make headway into the hippocampus (arrow). The section was obtained from a non-demented 80-year-old male. **c stage III:** The lesions in the hippocampal formation worsen. Entorhinal layers pre- α and, additionally, pri- α of the deep layers become strongly involved. Lesions extend through the transentorhinal region into the adjoining high order sensory association areas of the temporal neocortex. The lesions generally do not extend beyond the occipito-temporal gyrus laterally (arrow) and lingual gyrus posteriorly. The section originates from a 90-year-old female. **d stage III:** A flat section through the entire basal surface of the temporal lobe reveals the severe involvement of the entorhinal cortex (anterior portions of the parahippocampal gyrus) at stage III and shows the tendency of the pathology to extend from there into the adjacent neocortex, i.e., occipito-temporal gyrus laterally (arrow) and lingual gyrus posteriorly (arrow). **e stage IV:** The third and fourth sectors of the Ammon's horn and a large portion of the insular cortex (arrow) become affected. The involvement of the neocortical high order sensory association cortex of the temporal lobe now extends up to the medial temporal gyrus and stops short of the superior temporal gyrus (arrow). The primary fields of the neocortex (see transverse gyrus of Heschl) and, to a large extent, also the premotor and first order sensory association areas of the neocortex remain intact. This section was taken from an 82-year-old demented female. **f stage V:** In addition to the presence of AD-related lesions in all of the regions involved in stage IV, pathological changes appear in the superior temporal gyrus and even encroach to a mild degree upon the premotor and first order sensory association areas of the neocortex. **g stage V:** In the occipital lobe, the peristriate region shows varying degrees of affection, and lesions occasionally can even be seen in the parastriate area. Stage V sections were obtained from a 90-year-old female with dementia. **h–i stage VI:** Strong immunoreactivity can be detected even in the first order sensory association areas (e.g., the parastriate area) and the primary areas of the neocortex (e.g., the striate area) of the occipital neocortex. Compare the superior temporal gyrus and transverse gyrus of Heschl at stage V with the same structures at stage VI. Both stage VI sections originate from a severely demented 70-year-old female Alzheimer patient. Scale bar applies to all thick sections

The staging system

AD-related neurofibrillary changes occur at predisposed cortical and subcortical sites. The distribution pattern and developmental sequence of the lesions are predictable and permit identification of six stages, which can be subsumed under three more general units: I–II, III–IV, V–VI [4–6, 21, 28, 32, 37, 38, 47, 65, 66, 83]. Initial diagnosis as to whether the bulk of the abnormal tau protein is detectable in the transentorhi-

nal and entorhinal regions (stages I–II), in the limbic allocortex and adjoining neocortex (stages III–IV), or in the neocortex, including the secondary and primary fields (stages V–VI), simplifies the subsequent task of differentiation.

Cases without cortical AD-related neurofibrillary pathology The transentorhinal region as well as the entorhinal region and hippocampal formation remain devoid of AT8-immunoreactive nerve cells (Fig. 4a, b).

Major characteristics of stages I–II

Stage I: Lesions develop in the transentorhinal region (Figs. 2a–c, 3a, 4c, d) [23] Subcortical nuclei (i.e., locus coeruleus, magnocellular nuclei of the basal forebrain) occasionally show the earliest alterations in the absence of cortical involvement [29]. The transentorhinal region is the first site in the cerebral cortex to become involved. AT8-immunoreactive (ir) projection cells contain hyperphosphorylated tau in both the cell body and all of its neuronal processes (Fig. 4c, d). Late phases of the stage show abundant AT8-ir neurons that permit recognition of the descent of the superficial entorhinal cellular layer (pre- α , i.e., the outer layer- α of the external principal lamina) from its uppermost position at the entorhinal border to its deepest position at the transition towards the adjoining temporal neocortex (Figs. 1, 3a) [23]. The entorhinal region proper remains uninvolved or minimally involved.

Stage II: Lesions extend into the entorhinal region (Figs. 2e, f, 3b, 4e) From the transentorhinal region, the lesions encroach upon the entorhinal region, particularly its superficial cellular layer, pre- α (Figs. 1, 3b, 4e–g). The deep layer, pri- α , gradually becomes visible (Figs. 2f, 3b, 4e), shows sharply defined upper and lower boundaries, and is separated from pre- α by the broad, wedge-shaped lamina dissecans (myelinated fiber plexus) [23, 98]. AT8-ir pyramidal cells appear in sectors 1 and 2 of the hippocampal Ammon's horn (CA1/CA2) (Fig. 3b). Dilations develop transiently in apical dendrites that pass through the stratum lacunosum moleculare of CA1 [20]. Scattered NPs appear in CA1. Fine networks of AT8-ir neurites form in both the stratum radiatum and stratum oriens.

Major characteristics of stages III–IV

Stage III: Lesions extend into the neocortex of the fusiform and lingual gyri (Figs. 2i–n, 3c, d, 4h) The lesions in stage II sites become more severe. The outer entorhinal cellular layers (pre- α , pre- β , pre- γ) and most

of the molecular layer become filled with intermeshing AT8-ir neurites, whereas the pale lamina dissecans contains a few radially oriented neurites. The deep layer pri- α is heavily affected and gradually thins in the transentorhinal region as it approaches the temporal neocortex (Figs. 3c, 4h). CA1 appears band-like, and transient dendritic changes in CA1 reach their culmination point [20]. CA2 is filled with large and strongly AT8-ir pyramidal cells. A moderate number of mossy cells with characteristic dendritic excrescences appear in CA3 and CA4 [97]. The granule cells of the fascia dentata remain uninvolved. AT8-ir sections showing the classical view of the hippocampal formation (Figs. 1b, d) facilitate recognition of lesions in the fascia dentata and Ammon's horn [92].

From the transentorhinal region, the lesions encroach upon the neocortex of the fusiform and lingual gyri, and then diminish markedly beyond this point (Figs. 3d, 4j). An AT8-ir plexus fills the cellular layers of the temporal neocortex (Figs. 2n, 4l). The outer line of Baillarger is barely developed and gradually becomes recognizable only with increasing distance from the transentorhinal region. A few NPs develop in the outer layers II–IV.

Stage IV: The disease process progresses more widely into neocortical association areas (Figs. 2o–t, 3e, 5a) Lesional density increases in sites affected in stage III. A few AT8-ir pyramidal cells appear in the subiculum. The density of the neuritic plexuses of the entorhinal and transentorhinal regions increases and causes a corresponding blurring of the lamina dissecans. The deep plexus spans all of the deep layers: pri- α , pri- β , and pri- γ , and from there penetrates widely into the white substance. This aspect of maximum involvement undergoes little change until the end-phase of AD. Thus, the pathological features of the entorhinal and transentorhinal regions must not be taken into account for further differentiation of stages V and VI. CA1/CA2 are recognizable as dense bands. The varicose dendritic segments vanish from CA1 without leaving behind any remnants. Large numbers of mossy cells in CA3 and CA4 become AT8-ir. A few AT8-ir granule cells appear in the fascia dentata.

In stage IV, the pathology extends broadly into the mature neocortex. A slight decrease in the immunoreactivity of neocortical NPs can be recognized starting at the border facing the transentorhinal region. Dense neuritic plexuses develop up to the middle temporal convolution (Figs. 2s, t, 4a–c), and a rapid decrease in the severity of the lesions occurs at the transition to the

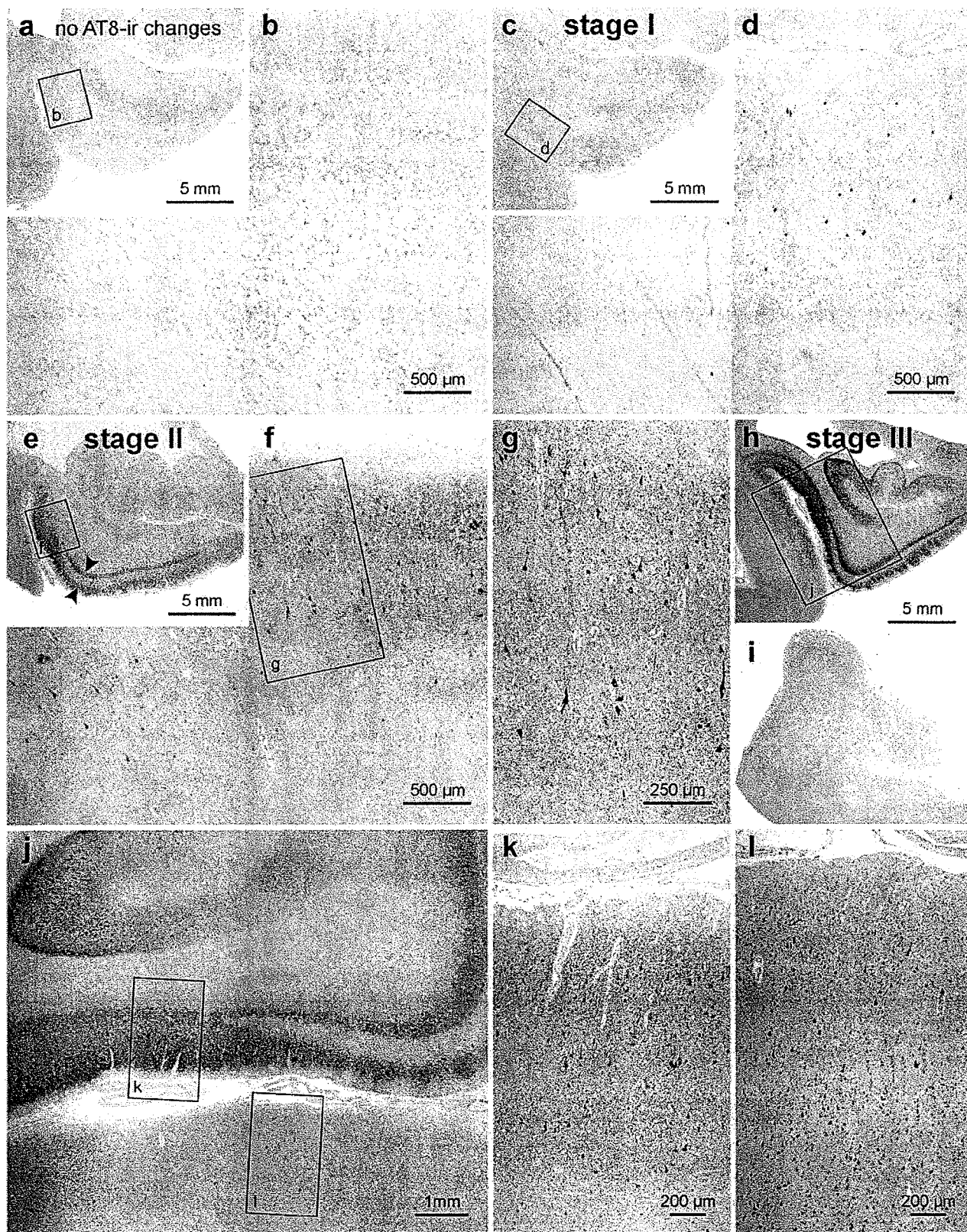
Fig. 4 Progress of cortical neurofibrillary pathology, as seen in paraffin sections immunostained for hyperphosphorylated tau (AT8, Innogenetics). **a, b** Control case displaying no AT8-ir intraneuronal changes. Note that even the transentorhinal region is devoid of immunoreactivity. **c, d** *stage I*: The first AT8-ir pyramidal cells often are more easily detected in thick sections than in paraffin material. Closer inspection of the predilection site (transentorhinal region in **d**, framed area in **c**), however, reveals the initial lesions. The meshwork of ir-neurites is as yet not well developed. **e–g** *stage II*: Many AT8-ir projection neurons are seen in the transentorhinal region accompanied by a well-developed plexus of ir-neurites (**f, g**). The pathology also extends into the entorhinal layers pre- α and pri- α (arrowheads in **e**). **h–j** *stage III*: The transentorhinal and entorhinal regions are more severely involved than in the preceding stage, and the pathology now extends into the adjoining temporal neocortex of the occipito-temporal and lingual gyri (**h, j**). The middle temporal gyrus remains uninvolved (**i**). Scale bar in **a, c, e, h** is also valid for **i** and Fig. 5 **a, e, f, j, k, o** below

superior temporal gyrus (Fig. 3e). The occipital neocortex is unaffected (Fig. 5e, d) or contains blotch-like local accumulations of AT8-ir pyramidal cells and/or NPs in the peristriate region (Brodmann area 19).

Major characteristics of stages V–VI:

Stage V: The neocortical pathology extends fanlike in frontal, superolateral, and occipital directions, and reaches the peristriate region (Figs. 2u–x, 3f, g, 5f, j) From sites involved at stage IV, the lesions appear in hitherto uninvolved areas and extend widely into the first temporal convolution (Fig. 3f) as well as into high order association areas of the frontal, parietal, and occipital neocortex (peristriate region, Figs. 2v–x, 3g). Initially, unevenly and loosely distributed NPs appear in layers II and III, followed by large numbers of AT8-ir pyramidal cells in layers IIIa, b and V. The lower border of the outer neuritic plexus in layers II–IIIab blurs at its transition to the uninvolved layers IIIC and IV (outer line of Baillarger, Fig. 5g). In stage V, the deep plexus of layer V is narrow and tends not to extend into layer VI and the white matter (Fig. 5g, h). The same pattern (only less pronounced) is seen in secondary areas of the neocortex, where uneven accumulations of NPs predominate. Affection of layer V is weak (Fig. 5j). The primary visual field (striate area) contains only isolated signs of the pathology consisting of NPs (Fig. 5i, j). Isolated AT8-ir neurons also can be seen in layer IIIab (Fig. 5i, j).

Stage VI: The pathology reaches the secondary and primary neocortical areas and, in the occipital lobe, extends into the striate area (Figs. 2y–z, 3h, i) Most areas of the neocortex show severe affection and nearly all layers are filled with AT8-ir neurites. As such, the outer line



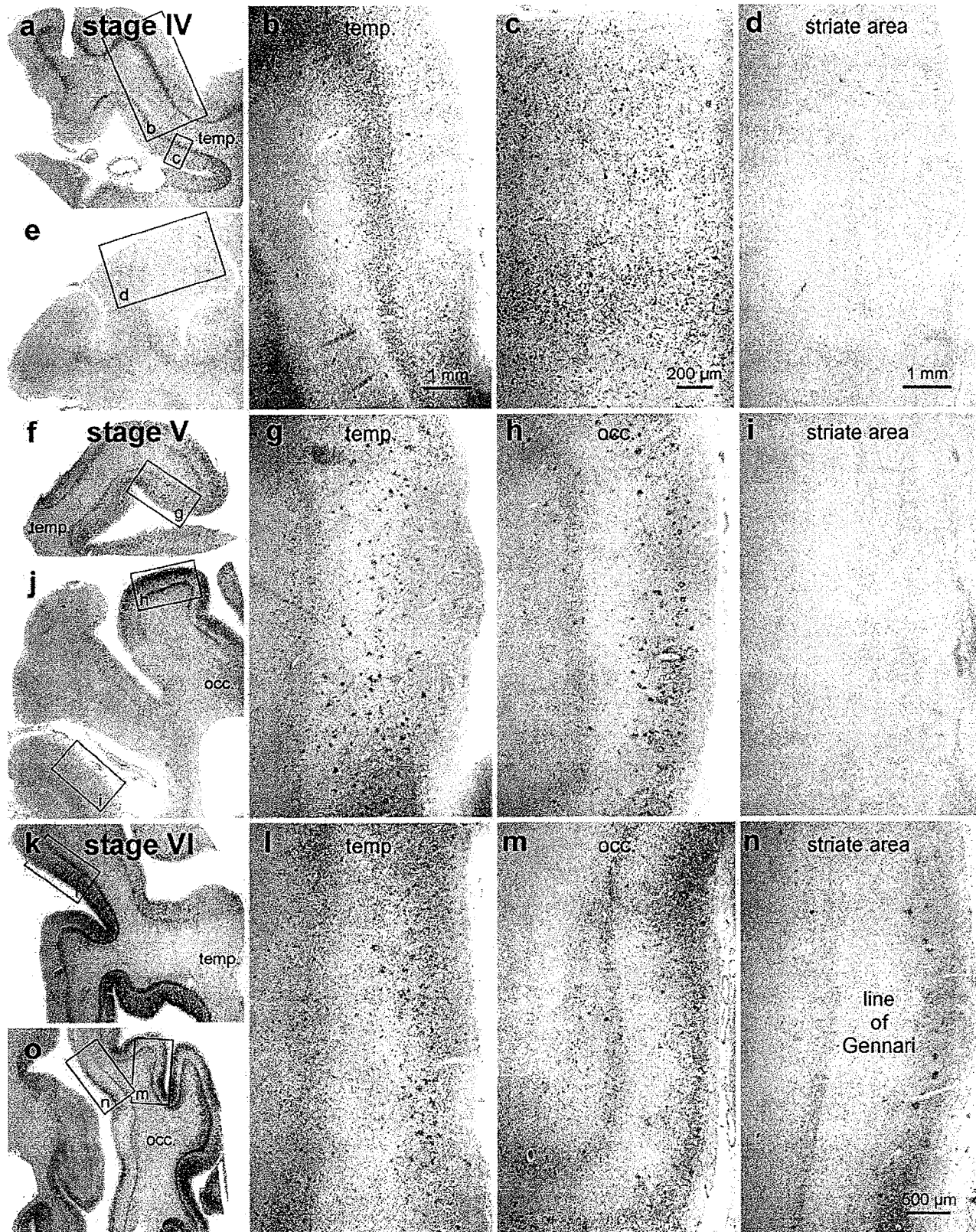


Fig. 5 Progress of cortical neurofibrillary pathology, as seen in paraffin sections immunostained for hyperphosphorylated tau (AT8, Innogenetics). **a–e stage IV:** The disease process extends into the high order sensory association neocortex of the temporal lobe (temp.) and includes the medial temporal gyrus (**a–c**). The peristriate region as well as the parastriate field and striate area of the occipital lobe (occ.) still lack the neurofibrillary pathology (**e, d**). **f–j stage V:** Large numbers of neuritic plaques appear in the neocortex (**g, h**). Pathological changes now encroach to a mild degree upon premotor areas and first order sensory association fields. In the occipital lobe (**j**), it is chiefly the peristriate region (**h**) that shows varying degrees of affection, and lesions occasionally even develop in the parastriate area. The striate area remains uninvolved (**i, j**). **k–o stage VI:** Drastic affection of the neocortex is seen at *stage VI* with involvement of almost all areas. Strong immunoreactivity can be recognized even in premotor areas and first order sensory association areas (e.g., the parastriate area **m**), as well as in primary neocortical areas (e.g., the striate area **n**). The borderline between the striate and the parastriate areas is drawn easily and—owing to the sudden cessation of the line of Gennari (plexus of myelinated fibers)—usually can be detected with the unaided eye. A key feature of *stage VI* is the involvement of the striate area (**n**), characterized by a dense neuritic mesh in layer V with sharply drawn upper and lower boundaries. Note that the myelin-rich line of Gennari (*layer IVb n*) is virtually devoid of neurofibrillary pathology. Scale bar in **n** also applies to **g, h, i, l, m**

of Baillarger—a pallid stripe in stage V—begins to blur (Fig. 5l). Layer V still appears as a recognizable band but continues into the neuritic plexus of layer VI. The underlying white substance contains AT8-ir axons. A decrease in immunoreactivity of NPs is seen in many neocortical areas and is most pronounced in the basal temporal fields. In the occipital lobe, the pathology breaches the parastriate and striate areas (Figs. 2y–z", 3i, 5m–o). Large numbers of NPs and AT8-ir nerve cells appear in layers II and IIIab. Baillarger's outer line or the line of Gennari maintains a light appearance, interrupted only by radially oriented AT8-ir neurites. A sharply drawn AT8-ir plexus follows in layer V (Figs. 2z, z", 5n, o).

Discussion

By applying the silver technique proposed by Bielschowsky [11–15] Alzheimer [2, 3] became the first to describe the NFTs that develop in the course of the disease that bears his name. This staining technique has been in use for decades but has been subjected to numerous modifications [10, 33, 36, 48, 52, 74, 99]. In systematic studies, Gallyas [49, 50] replaced the critical steps of the Bielschowsky technique by means of more manageable reactions and developed a reliable method for selectively demonstrating AD-related neurofibrillary changes. Following its adaptation for use on 100 µm thick sections, this method was standardized

for a procedure to stage the development of the cortical AD-related neurofibrillary pathology that gradually found international acceptance [64, 66, 83]. Nonetheless, one of the unavoidable pitfalls associated with using silverstaining techniques is that different laboratories produce results of widely varying quality [1]. Subsequently, the 1991 staging protocol, too, underwent a series of permutations, among them the application of various types of silver impregnations, the analysis of cortical sites that are fundamentally less well suited for the procedure, and the use of tissue sections, the thickness of which differed from that originally proposed [8, 9, 18, 21, 22, 36, 39–41, 53, 54, 59–61, 69–71, 75, 76, 78, 83]. A radical reduction of the different stages also has been suggested [62].

Since AD is an ongoing and not a static process, every staging procedure is, de facto, an artificial construct. It is the extent of brain involvement rather than qualitative changes in the neurofibrillary pathology that increases with disease progression and, as such, the concept of six neuropathological stages (and only six stages) is not entirely amenable to pathological states of a "transitional" nature that do not fulfill the criteria for one of the six neurofibrillary stages described above.

Here, a revised version of the 1991 staging procedure is presented that can be performed on paraffin sections of conventional thickness, which have been immunostained with the AT8 antibody and processed on an automated basis, thereby fulfilling the demands of the routine laboratory. The simplicity and uniformity of any staging system is the prerequisite for effective comparisons of results among laboratories and for reliable as well as reproducible classification of a disease process [35, 86].

Technical addendum

The previous staging protocol relied upon an advanced but inexpensive silver technique that exploits the physical development of the nucleation sites and in so doing permits careful control of the entire staining procedure [49–51]. Insoluble fibrillary AD-related material can be visualized virtually in the absence of distracting background staining [66, 67, 78]. The technique can be applied to routinely fixed autopsy material, even when the material has been stored for decades in formaldehyde solutions. It facilitates processing of large numbers and/or large sections (e.g., hemisphere sections). A homogeneous staining that permeates the entire thickness of a section is achieved even in 50–150 µm sections [22]. Thin paraffin sections (5–15 µm) can also be used

and counter-stained for easy identification of cytoarchitectonic units or specific nuclei [31]. Neurofibrillary changes of the Alzheimer type (NFTs, NTs, NPs) appear in black and, thus, contrast well against an almost unstained background. Connective tissue, glial filaments, normal components of the neuronal cytoskeleton, Pick bodies, Lewy bodies/neurites, and corpora amylacea remain unstained. Abnormal tau-protein in argyrophilic grain disease (AGD), in progressive supranuclear palsy (PSP), corticobasal degeneration (CBD), and Niemann Pick type C (NPC) can be visualized as well [46, 78].

The staging procedure originally required sectioning at a thickness of 100 μm . Silverstained or immunostained sections of such thickness are optimal for the demands of low power (stereo) microscopy and greatly facilitate recognition of the laminar and areal distribution pattern of the lesions (see hemisphere sections in Fig. 3). Sections of this thickness can be gained from non-embedded brain tissue with the aid of a vibratome or a freezing microtome. Alternatively, the tissue blocks can be embedded in PEG [91] and sectioned with a sliding microtome. Application of PEG (400 and 1,000; Merck-Schuchardt 807 485 and 807 488) is rapid, simple, and causes little shrinkage [22].

The blocks are transferred from 96% ethanol to PEG 400 and their surfaces covered with blotting paper. Blocks are placed on a rotating table and after having sunk to the bottom (this can take several days), they are transferred to fresh PEG 400 for an additional day. Then, transfer to PEG 1000 at 54°C for 1 day. Embed in fresh PEG 1000, mount, and section at 50–150 μm . Transfer sections to 70% ethanol to remove the embedding medium. Store sections in formaldehyde solutions. Prior to staining, transfer sections to de-ionized water. It is important to note that the Gallyas silver technique displays only highly aggregated fibrillary material, whereas the AT8-immunoreaction also visualizes the non-argyrophilic material that initially develops within involved neurons (pretangle material).

Acknowledgments The skillful assistance (tissue processing and staining) of Dr. R.A. Kauppinen (Kuopio), Mr. M. Bouzrou (Frankfurt/Main), and (illustrations) Ms. I. Szász (Frankfurt/Main) is gratefully acknowledged.

References

- Alafuzoff I, Pikkarainen M, Al-Sarraj S, Arzberger T, Bell J, Bodi I, Bogdanovic N, Budka H, Bugiani O, Ferrer I, Gelpi E, Gaicone G, Graeber MB, Hauw JJ, Kamphorst W, King A, Kopp N, Korkolopolou P, Kovacs GG, Meyronet D, Marchi P, Patsouris E, Preusser M, Ravid R, Roggendorf W, Seilhean D, Streichneberger N, Thal DR, BNE consortium, Kretzschmar H (2006) Inter-laboratory comparison of assessments of AD-related lesions. A study of the BrainNet Europe consortium. *J Neuropathol Exp Neurol* 65 (in press)
- Alzheimer A (1906) Über einen eigenartigen schweren Erkrankungsprozeß der Hirnrinde. *Neurolog Centralbl* 23:1129–1136
- Alzheimer A (1911) Über eigenartige Krankheitsfälle des späteren Alters. *Z ges Neurol Psychiatr* 4:356–385
- Arnold SE, Hyman BT, Flory J, Damasio AR, van Hoesen GW (1991) The topographical and neuroanatomical distribution of neurofibrillary tangles and neuritic plaques in the cerebral cortex of patients with Alzheimer's disease. *Cereb Cortex* 1:103–116
- Arriagada PV, Growdon J, Hedley-Whyte E, Hyman BT (1992a) Neurofibrillary tangles but not senile plaques parallel duration and severity of Alzheimer's disease. *Neurology* 42:631–639
- Arriagada PV, Marzloff K, Hyman BT (1992b) Distribution of Alzheimer-type pathologic changes in nondemented elderly individuals matches the pattern in Alzheimer's disease. *Neurology* 42:1681–1688
- Bancher C, Brunner C, Lassmann H, Budka H, Jellinger K, Wiche G, Seitelberger F, Grundke-Iqbal I, Wisniewski HM (1989) Accumulation of abnormally phosphorylated tau precedes the formation of neurofibrillary tangles in Alzheimer's disease. *Brain Res* 477:90–99
- Bancher C, Braak H, Fischer P, Jellinger KA (1993) Neuropathological staging of Alzheimer lesions and intellectual status in Alzheimer's and Parkinson's disease patients. *Neurosci Lett* 162:179–182
- Bancher C, Paulus W, Paukner K, Jellinger K (1997) Neuropathologic diagnosis of Alzheimer's disease: consensus between practicing neuropathologists? *Alzheimer Dis Assoc Disord* 11:207–219
- Beech RH, Davenport HA (1933) The Bielschowsky staining technique. A study of the factors influencing its specificity for nerve fibers. *Stain Technol* 8:11–30
- Bielschowsky M (1902) Die Silberimprägnation der Axenzylinder. *Neurol Centralbl* 13:579–584
- Bielschowsky M (1903) Die Silberimprägnation der Neurofibrillen. *Neurol Centralbl* 21:997–1006
- Bielschowsky M (1904) Die Silberimprägnation der Neurofibrillen. Einige Bemerkungen zu der von mir angegebenen Methode und den von ihr gelieferten Bildern. *J Psychol Neurol* 3:169–189
- Bielschowsky M (1905) Die Darstellung der Axenzylinder peripherischer Nervenfasern und der Axenzylinder zentraler markhaltiger Nervenfasern. Ein Nachtrag zu der von mir angegebenen Imprägnationsmethode der Neurofibrillen. *J Psychol Neurol* 4:228–231
- Bielschowsky M (1909) Eine Modifikation meines Silberimprägnationsverfahrens zur Darstellung der Neurofibrillen. *J Psychol Neurol* 12:135–137
- Biernat J, Mandelkow EM, Schröter E, Lichtenberg-Kraag B, Steiner B, Berling B, Meyer H, Mercken M, Vandermeeren A, Goedert M, Mandelkow E (1992) The switch of tau protein to an Alzheimer-like state includes the phosphorylation of two serin-proline motifs upstream of the microtubule binding region. *EMBO J* 11:1593–1597
- Bobinski M, Wegiel J, Tarnawski M, de Leon MJ, Reisberg B, Miller DC, Wisniewski HM (1998) Duration of neurofibrillary changes in the hippocampal pyramidal neurons. *Brain Res* 799:156–158

18. Bowler JV, Munoz DG, Merskey H, Haschinski V (1998) Falcies in the pathological confirmation of the diagnosis of Alzheimer's disease. *J Neurol Neurosurg Psychiatry* 64:18–24
19. Braak E, Braak H, Mandelkow EM (1994) A sequence of cytoskeleton changes related to the formation of neurofibrillary tangles and neuropil threads. *Acta Neuropathol* 87:554–567
20. Braak E, Braak H (1997a) Alzheimer's disease: transiently developing dendritic changes in pyramidal cells of sector CA1 of the Ammon's horn. *Acta Neuropathol* 93:323–325
21. Braak H, Braak E (1991a) Neuropathological staging of Alzheimer-related changes. *Acta Neuropathol* 82:239–259
22. Braak H, Braak E (1991b) Demonstration of amyloid deposits and neurofibrillary changes in whole brain sections. *Brain Pathol* 1:213–216
23. Braak H, Braak E (1992) The human entorhinal cortex. Normal morphology and lamina-specific pathology in various diseases. *Neurosci Res* 15:6–31
24. Braak H, Braak E (1994) Pathology of Alzheimer's disease. In: Calne DB (ed) *Neurodegenerative diseases*. Saunders, Philadelphia, pp 585–613
25. Braak H, Braak E (1995) Staging of Alzheimer's disease-related neurofibrillary changes. *Neurobiol Aging* 16:271–284
26. Braak H, Braak E (1997b) Frequency of stages of Alzheimer-related lesions in different age categories. *Neurobiol Aging* 18:351–357
27. Braak H, Braak E (1997c) Diagnostic criteria for neuropathologic assessment of Alzheimer's disease. *Neurobiol Aging* 18(Suppl 4):85–88
28. Braak H, Braak E (1999) Temporal sequence of Alzheimer's disease-related pathology. In: Peters A, Morrison JH (eds) *Cerebral cortex*, vol 14 Plenum Press, New York, pp 475–512
29. Braak H, Del Tredici K (2004) Alzheimer's disease: intraneuronal alterations precede insoluble amyloid- β formation. *Neurobiol Aging* 25:713–718
30. Braak H, Braak E, Grundke-Iqbal I, Iqbal K (1986) Occurrence of neuropil threads in the senile human brain and in Alzheimer's disease: a third location of paired helical filaments outside of neurofibrillary tangles and neuritic plaques. *Neurosci Lett* 65:351–355
31. Braak H, Braak E, Ohm TG, Bohl J (1988) Silver impregnation of Alzheimer's neurofibrillary changes counterstained for basophilic material and lipofuscin pigment. *Stain Technol* 63:197–200
32. Braak H, Del Tredici K, Schultz C, Braak E (2000) Vulnerability of select neuronal types to Alzheimer's disease. In: Khachaturian ZS, Mesulam MM (eds) *Alzheimer's disease. A compendium of current theories*. Ann NY Acad Sci 924:53–61
33. Churukian CJ, Kazee AM, Lapham LW, Eskin TA (1992) Microwave modification of Bielschowsky silver impregnation method for diagnosis of Alzheimer's disease. *J Histotechnol* 15:299–302
34. Cras P, Smith MA, Richey PL, Siedlak SL, Mulvihill P, Perry G (1995) Extracellular neurofibrillary tangles reflect neuronal loss and provide further evidence of extensive protein cross-linking in Alzheimer's disease. *Acta Neuropathol* 89:291–295
35. Coleman PD (1997) Research uses of neuropathological data. *Neurobiol Aging* 18(Suppl 4):97–98
36. Cullen KM, Halliday GM, Cartwright H, Kril JJ (1996) Improved selectivity and sensitivity in the visualization of neurofibrillary tangles, plaques and neuropil threads. *Neurodegeneration* 5:177–187
37. Delacourte A, David JP, Dergeant N, Buée L, Wattez A, Vermersch P, Ghosali F, Fallet-Bianco C, Pasquier F, Lebert F, Petit H, Di Menza C (1999) The biochemical pathway of neurofibrillary degeneration in aging and Alzheimer's disease. *Neurology* 52:1158–1165
38. Dickson DW (1997) The value of cross sectional neuroanatomical studies as a conceptual framework for prospective clinicopathological studies. *Neurobiol Aging* 18:382–386
39. Duyckaerts C, Hauw JJ (1997a) Diagnosis and staging of Alzheimer's disease. *Neurobiol Aging* 18(Suppl 4):33–42
40. Duyckaerts C, Hauw JJ (1997b) Prevalence, incidence and duration of Braak's stages in the general population: can we know? *Neurobiol Aging* 18(Suppl 4):362–369
41. Duyckaerts C, He Y, Seilhean D, Delaère P, Piette F, Braak H, Hauw JJ (1994) Diagnosis and staging of Alzheimer's disease in a prospective study involving aged individuals. *Neurobiol Aging* 15(Suppl 1):140–141
42. Duyckaerts C, Delaère P, He Y, Camilleri S, Braak H, Piette F, Hauw JJ (1995) The relative merits of tau- and amyloid markers in the neuropathology of Alzheimer's disease. In: Bergener M, Finkel SI (eds) *Treating Alzheimer's and other dementias*. Springer, Heidelberg Berlin New York, pp 81–89
43. Duyckaerts C, Bannecib M, Grignon Y, Piette F, Hauw JJ (1996) Is the topography of Alzheimer's disease lesions a clue to their pathogenesis? *Bull Acad Natl Med* 180:1703–1714
44. Duyckaerts C, Bannecib M, Grignon Y, Uchihara T, He Y, Piette F, Hauw JJ (1997) Modeling the relation between neurofibrillary tangles and intellectual status. *Neurobiol Aging* 18(Suppl. 4):267–273
45. Esiri MM, Hyman BT, Beyreuther K, Masters C (1997) Aging and dementia. In: Graham DL, Lantos PI (eds) *Greenfield's neuropathology*. Arnold, London, pp 153–234
46. Feany MB, Dickson DW (1996) Neurodegenerative disorders with extensive tau pathology: a comparative study and review. *Ann Neurol* 40:139–148
47. Fewster PH, Griffin-Brooks S, MacGregor J, Ojalvo-Rose E, Ball MJ (1991) A topographical pathway by which histopathological lesions disseminate through the brain of patients with Alzheimer's disease. *Dementia* 2:121–132
48. Flowers D, Harasty J, Halliday G, Kril J (1996) Microwave modification of the methenamine silver technique for the demonstration of Alzheimer-type pathology. *J Histotechnol* 19:33–38
49. Gallyas F (1971) Silver staining of Alzheimer's neurofibrillary changes by means of physical development. *Acta Morph Acad Sci Hung* 19:1–8
50. Gallyas F (1979) Light insensitive physical developers. *Stain Technol* 54:173–176
51. Gallyas F, Wolff JR (1986) Metal-catalyzed oxidation renders silver intensification selective. Application for the histochemistry of diaminobenzidine and neurofibrillary changes. *J Histochem Cytochem* 34:1667–1672
52. Garvey W, Fathi A, Bigelow F, Jimenez CL, Carpenter BF (1991) Rapid, reliable and economical silver stain for neurofibrillary tangles and senile plaques. *J Histotechnol* 14:39–42
53. Geddes JW, Tekirian TL, Soultanian NS, Ashford JW, Davis DG, Markesbery WR (1997) Comparison of neuropathologic criteria for the diagnosis of Alzheimer's disease. *Neurobiol Aging* 18(Suppl 4):99–105
54. Gertz HJ, Xuereb JH, Huppert FA, Brayne C, McGee MA, Paykel ES, Harrington C, Mukaetova-Ladinska E, Arendt T, Wischik CM (1998) Examination of the validity of the hierarchical model of neuropathological staging in normal aging and Alzheimer's disease. *Acta Neuropathol* 95:154–158
55. Goedert M (1993) Tau protein and the neurofibrillary pathology of Alzheimer's disease. *Trends Neurosci* 16:460–465
56. Goedert M (1999) Filamentous nerve cell inclusions in neurodegenerative diseases: tauopathies and α -synucleinopathies. *Phil Trans R Soc Lond B Biol Sci* 354:1101–1108

57. Goedert M, Jakes R, Vanmechelen E (1995) Monoclonal antibody AT8 recognises tau protein phosphorylated at both serine 202 and threonine 205. *Neurosci Lett* 189:167–169
58. Goedert M, Trojanowski JQ, Lee VMY (1997) The neurofibrillary pathology of Alzheimer's disease. In: Rosenberg RN (ed) *The molecular and genetic basis of neurological disease*. 2nd edn. Butterworth-Heinemann, Boston, pp 613–627
59. Gold G, Bouras C, Kövari E, Canuto A, González Glaría B, Malky A, Hof PR, Michel JP, Giannakopoulos P (2000) Clinical validity of Braak neuropathological staging in the oldest-old. *Acta Neuropathol* 99:579–582
60. Grober E, Dickson D, Sliwinski MJ, Buschke H, Katz M, Crystal H, Lipton RB (1999) Memory and mental status correlates of modified Braak staging. *Neurobiol Aging* 20:573–579
61. Halliday G, Ng T, Rodriguez M, Harding A, Blumbers P, Evans W, Fabian V, Fryer V, Gonzales M, Harper C, Kalnins R, Masters CL, McLean C, Milder DG, Pamphlett R, Scott G, Tannenberg A., Kril J (2002) Consensus neuropathological diagnosis of common dementia syndromes: testing and standardizing the use of multiple diagnostic criteria. *Acta Neuropathol* 104:72–78
62. Harding AJ, Kril JJ, Halliday GM (2000) Practical measures to simplify the Braak tangle staging method for routine pathological screening. *Acta Neuropathol* 99:199–208
63. Hyman BT (1997) The neuropathological diagnosis of Alzheimer's disease: clinical-pathological studies. *Neurobiol Aging* 18(Suppl. 4):27–32
64. Hyman BT (1998) New neuropathological criteria for Alzheimer's disease. *Arch Neurol* 55:1174–1176
65. Hyman BT, Gomez-Isla T (1994) Alzheimer's disease is a laminar, regional, and neural system specific disease, not a global brain disease. *Neurobiol Aging* 15:353–354
66. Hyman BT, Trojanowski JQ (1997) Editorial on consensus recommendations for the postmortem diagnosis of Alzheimer disease from the National Institute on Aging and the Reagan Institute working group on diagnostic criteria for the neuropathological assessment of Alzheimer disease. *J Neuropathol Exp Neurol* 56:1095–1097
67. Iqbal K, Braak E, Braak H, Zaidi T, Grundke-Iqbal I (1991) A silver impregnation method for labeling both Alzheimer paired helical filaments and their polypeptides separated by sodium dodecyl sulfate-polyacrylamide gel electrophoresis. *Neurobiol Aging* 12:357–361
68. Iqbal K, Braak H, Braak E, Grundke-Iqbal I (1993) Silver labeling of Alzheimer neurofibrillary changes and brain β amyloid. *J Histochemol* 16:335–342
69. Jellinger KA (1998) The neuropathological diagnosis of Alzheimer's disease. *J Neural Transm* 53(Suppl):97–118
70. Jellinger K (2000) Clinical validity of Braak staging in the oldest-old. *Acta Neuropathol* 99:583–584
71. Jellinger KA, Bancher C (1997) Proposals for re-evaluation of current autopsy criteria for the diagnosis of Alzheimer's disease. *Neurobiol Aging* 18(Suppl 4):55–65
72. Kauppinen T, Martikainen P, Alafuzoff I (2006) Human post-mortem brain tissue and 2 mm tissue microarrays. *Appl Immunohistochem Mol Morphol* (in press)
73. Kreutzberg GW, Blakemore WF, Graeber MB (1997) Cellular pathology of the central nervous system. In: Graham DI, Lantos PL (eds) *Greenfield's neuropathology*. Arnold, London, pp 85–156
74. Lamy C, Duyckaerts C, Delaère P, Payan C, Fermanian J, Poulain V, Hauw JJ (1989) Comparison of seven staining methods for senile plaques and neurofibrillary tangles in a prospective series of 15 elderly patients. *Neuropathol Appl Neurobiol* 15:563–578
75. Markesbery WR (1997) Neuropathological criteria for the diagnosis of Alzheimer's disease. *Neurobiol Aging* 18(Suppl 4):13–19
76. McKeel DW, Price JL, Miller JP, Grant EA, Xiong C, Berg L, Morris JC (2004) Neuropathologic criteria for diagnosing Alzheimer disease in persons with pure dementia of the Alzheimer type. *J Neuropathol Exp Neurol* 63:1028–1037
77. Mercken M, Vandermeeren M, Lübke U, Six J, Boons J, Van de Voorde A, Martin J-J, Gheuens J (1992) Monoclonal antibodies with selective specificity for Alzheimer tau are directed against phosphatase-sensitive epitopes. *Acta Neuropathol* 84:265–272
78. Munoz DG (1999) Stains for the differential diagnosis of degenerative diseases. *Biotechn Histochem* 74:311–320
79. Nagy Zs, Vatter-Bittner B, Braak H, Braak E, Yilmazer D, Schultz C, Hanke J (1997) Staging of Alzheimer-type pathology: an interrater-intrarater study. *Dementia* 8:248–251
80. Nagy S, Yilmazer-Hanke DM, Braak H, Braak E, Schultz C, Hanke J (1998) Assessment of the pathological stages of Alzheimer's disease in thin paraffin sections: a comparative study. *Dement Geriatr Cogn Disord* 9:140–144
81. Nagy S, Hindley NJ, Braak H, Braak E, Yilmazer-Hanke DM, Schultz C, Barnetson L, Jobst KA, Smith AD (1999a) Relationship between clinical and radiological diagnostic criteria for Alzheimer's disease and the extent of neuropathology as reflected by "stages": a prospective study. *Dement Geriatr Cogn Disord* 10:109–114
82. Nagy S, Hindley NJ, Braak H, Braak E, Yilmazer-Hanke DM, Schultz C, Barnetson L, King EMF, Jobst KA, Smith AD (1999b) The progression of Alzheimer's disease from limbic regions to the neocortex: clinical, radiological and pathological relationships. *Dement Geriatr Cogn Disord* 10:115–120
83. Newell KL, Hyman BT, Growdon JH, Hedley-Whyte ET (1999) Application of the National Institute on Aging (NIA)-Reagan Institute criteria for the neuropathological diagnosis of Alzheimer's disease. *J Neuropathol Exp Neurol* 58:1147–1155
84. Ohm TG, Müller H, Braak H, Bohl J (1995) Close-meshed prevalence rates of different stages as a tool to uncover the rate of Alzheimer's disease-related neurofibrillary changes. *Neuroscience* 64:209–217
85. Ohm TG, Glöckner F, Distl R, Treiber-Held S, Meske V, Schönheit B (2003) Plasticity and the spread of Alzheimer's disease-like changes. *Neurochem Res* 28:1715–1723
86. Paulus W, Bancher C, Jellinger K (1992) Interrater reliability in the neuropathologic diagnosis of Alzheimer's disease. *Neurology* 42:329–332
87. Petersen RC, Parisi JE, Dickson DW, Johnson KA, Knopman DS, Boeve BF, Jicha GA, Ivnik RJ, Smith GE, Tangalos EG, Braak H, Kokmen E (2006) Neuropathologic features of amnesic mild cognitive impairment. *Arch Neurol* 63:665–672
88. Price JL (1997) Diagnostic criteria for Alzheimer's disease. *Neurobiol Aging* 18(Suppl 4):67–70
89. Schönheit B, Zarski R, Ohm TG (2004) Spatial and temporal relationships between plaques and tangles in Alzheimer-pathology. *Neurobiol Aging* 25:697–711
90. Schmidt ML, Lee VMY, Trojanowski JQ (1991) Comparative epitope analysis of neuronal cytoskeletal proteins in Alzheimer's disease senile plaque neurites and neuropil threads. *Lab Invest* 64:352–357
91. Smithson KG, MacVicar BA, Hatton GI (1983) Polyethylene glycol embedding: a technique compatible with immunocytochemistry, enzyme histochemistry, histofluorescence and intracellular staining. *J Neurosci Methods* 7:27–41

92. Thal DR, Holzer M, Rüb U, Waldmann G, Günzel S, Zedlick D, Schober R (2000) Alzheimer-related τ -pathology in the perforant path target zone and in the hippocampal stratum oriens and radiatum correlates with onset and degree of dementia. *Exp Neurol* 163:98–110
93. Thal DR, Del Tredici K, Braak H (2004) Neurodegeneration in normal brain aging and disease. *SAGE* 23, p 26
94. Tolnay M, Probst A (1999) Review: tau protein pathology in Alzheimer's disease and related disorders. *Neuropathol Appl Neurobiol* 25:171–187
95. Trojanowski JQ, Shin RW, Schmidt ML, Lee VMY (1995) Relationship between plaques, tangles, and dystrophic processes in Alzheimer's disease. *Neurobiol Aging* 16:335–345
96. Uchihara T, Nakamura A, Yamazaki M, Moris O (2001) Evolution from pretangle neurons to neurofibrillary tangles monitored by thiazin red combined with Gallyas method and double immunofluorescence. *Acta Neuropathol* 101:535–539
97. van Hoesen GW, Hyman BT (1990) Hippocampal formation: anatomy and the patterns of pathology in Alzheimer's disease. *Prog Brain Res* 83:445–457
98. van Hoesen GW, Hyman BT, Damasio AR (1991) Entorhinal cortex pathology in Alzheimer's disease. *Hippocampus* 1:1–8
99. Yamamoto T, Hirano A (1986) A comparative study of modified Bielschowsky, Bodian, and thioflavin S stains on Alzheimer's neurofibrillary tangles. *Neuropathol Appl Neurobiol* 12:3–9

EXHIBIT 6

PATENT

IN THE UNITED STATES PATENT AND TRADEMARK OFFICE

In re Application of:
Eva KONTSEKOVA
Peter FILIPCIK

Serial No.: 10/521,049

Filed: November 1, 2005

For: TRANSGENIC ANIMAL EXPRESSING
ALZHEIMER'S TAU PROTEIN

Group Art Unit: 1633

Examiner: Leavitt, Maria Gomez

Atty. Dkt. No.: SONN:066US

CERTIFICATE OF ELECTRONIC SUBMISSION

DATE OF SUBMISSION: Jan. 10, 2007

FILIPCIK DECLARATION UNDER 37 C.F.R. § 1.132

Commissioner for Patents
P.O. Box 1450
Alexandria, VA 22313-1450

I, Peter Filipcik, declare that:

1. I am a co-inventor of the above-referenced patent application. I am also an employee of Axon Neuroscience, the assignee of the above-referenced application. A copy of my *Curriculum Vitae* is attached as Exhibit 1.
2. I am a co-author of the publication Zilka *et al.*, "Truncated tau from sporadic Alzheimer's disease suffices to drive neurofibrillary degeneration in vivo," *FEBS Letters* 580:3582-3588 (2006) (hereinafter, the "Zilka reference").
3. It is my understanding that the Examiner in charge of the above-captioned application has advanced an enablement rejection against claims 17-33. I am supplying this declaration to provide additional evidence of the enablement of the present claims. In particular, this

declaration provides additional data on transgenic rat line #318, which is the same transgenic rat line #318 described in the present patent application, demonstrating that a transgenic animal having a DNA construct coding for N- and C-terminally truncated tau molecules according to the present invention exhibits phenotypes that make it a suitable model for Alzheimer's disease.

4. Attached as Exhibit 2 is Zilka *et al.*, "Truncated tau from sporadic Alzheimer's disease suffices to drive neurofibrillary degeneration in vivo," *FEBS Letters* 580:3582-3588 (2006). The Zilka reference describes the generation of and studies on transgenic rat line #318. Transgenic rat line #318 is the same transgenic rat line #318 described in the specification of the present patent application. *See, e.g.*, Specification, p. 22, first full paragraph; p. 23, first full paragraph; and Fig. 3C.
5. According to the teachings in the present specification, the DNA constructs used for transgenic animal preparation in the Zilka reference are characterized by the following features: (1) the cDNA molecules are truncated at least 30 nucleotides downstream of the start codon and truncated at least the 30 nucleotides upstream of the stop codon of the full-length tau cDNA sequence coding for 4-repeat and 3-repeat tau protein; (2) the cDNA molecule comprises SEQ ID No. 9; (3) and the DNA construct encodes a protein, which has neurofibrillary (NF) pathology producing activity when expressed in brain cells.
6. The transgene construct used in the generation of transgenic rat lines #318 and #72 was prepared by ligation of a cDNA coding for human tau protein truncated at amino acid positions 151-391 into the mouse Thy-1 gene downstream of the brain promoter/enhancer sequence. *Zilka*, p. 3582, col. 2. Transgenic rat line #318 is the same rat line described

in the present patent application (*see e.g.*, Example 2). It should be noted that the numbering of the amino acids of the tau protein in the Zilka reference is based on tau isoform 40, whereas the numbering in the present patent application is based on tau isoform 43. Tau isoform 40 contains an extra insert of 58 amino acids (174 nucleotides) in the N-terminus of the protein. Thus, the truncated tau protein numbered amino acids 151-391 in the Zilka reference is the same as a truncated tau protein numbered amino acids 93-333 based on the numbering in the patent application. Using the numbering in the patent application, amino acids 93-333 correspond to nucleotides 279-999. Thus, the truncated tau cDNA molecule used to generate rat line #318 is truncated at least 30 nucleotides downstream of the start codon and truncated at least the 30 nucleotides upstream of the stop codon of the full-length tau cDNA sequence coding for 4-repeat and 3-repeat tau protein; and the truncated tau cDNA molecule comprises SEQ ID NO: 9 (nucleotides 741-930).

7. The transgenic DNA was linearized by cleavage with EcoRI, and the vector sequences were removed prior to microinjection. *Zilka*, p. 3582, col. 2. Transgenic rats were generated by pronuclear injection of one-day old SHR rat embryos. *Id.* Founders were screened by PCR using Thy-1-specific and human tau-specific primers. *Id.* Two independent transgenic founder lines, #318 and #72, that stably expressed human truncated tau were obtained. *Zilka*, p. 3582, col. 2 to p. 3583, col. 1.
8. The Zilka reference also describes the generation of transgenic rat line #72, which was created using the same transgene construct and the same SHR background as used in the generation of transgenic rat line #318. *See e.g.*, *Zilka*, paragraph spanning pp 3582-3583.

9. As described in the present specification transgenic rat line #318 exhibits neurofibrillary (NF) pathology producing activity when expressed. For example, Fig. 6 shows the detection of intracellular inclusions and neurofibrillary filaments using silver staining in the neurons of the central nervous system of transgenic rats, whereas wild-type rats did not show these structures in the homologous brain area. Figs. 7 and 8 show the detection of neurofibrillary tangles in the central nervous system of transgenic rats using the pan-tau monoclonal antibody DC 25 and the monoclonal antibody PHF-1, respectively. Additionally, Fig. 10 shows a comparison of neurofibrillary tangles detected by Gallyas silver technique (Fig. 10A and Fig. 10C) and also by immunohistochemistry (Fig. 10E) in AD diseased human brain, to the equivalent pathological structures observed in the transgenic rat of present invention. The observation of neurofibrillary pathology in transgenic rat line #318 described in the present specification was confirmed by the studies described in the Zilka reference in which transgenic rat lines #318 was shown to exhibit neurofibrillary pathology. *Zilka*, p. 3582-3583 and Fig. 3. Thus, the studies presented in the present patent application and in the Zilka reference demonstrate that the DNA construct used to make transgenic rat line #318 encodes a protein, which has neurofibrillary (NF) pathology producing activity when expressed in brain cells.
10. The evidence discussed above demonstrates that transgenic rat line #318 contains a DNA construct having a cDNA molecule coding for N- and C-terminally truncated tau molecules having the following features: (1) the cDNA molecule is truncated at least 30 nucleotides downstream of the start codon and truncated at least the 30 nucleotides upstream of the stop codon of the full-length tau cDNA sequence coding for 4-repeat and 3-repeat tau protein; (2) the cDNA molecule comprises SEQ ID No. 9; and (3) the DNA

construct encodes a protein, which has neurofibrillary (NF) pathology producing activity when expressed in brain cells.

11. In additional studies with transgenic rat line #318 performed at Axon Neuroscience, phenotypes including cognitive impairment, oxidative stress, metabolic (energy) stress, and phosphorylation have been observed. For example, a statistically significant cognitive deficit was measured in transgenic rat line #318 as compared to non-transgenic litter mates in a water maze test. Exhibit 3, Fig. 1. As shown in Fig. 2 of Exhibit 3, transgenic rat line #318 showed increased oxidative stress as a consequence of the pathological cascade initiated by transgene expression. As shown in Fig. 3 of Exhibit 3, the kinetic measurement of the creatine kinase reaction showed that the constant rate values of the brain specific creatine kinase was significantly reduced in transgenic rat line #318 indicating energy stress. In addition, western blot analysis showed strong AD-like phosphorylation pattern of tau protein in transgenic rat line #318. Exhibit 3, Fig. 5.
12. The observed phenotypes described above demonstrate that this transgenic animal is a suitable model for Alzheimer's disease.
13. Furthermore, in addition to the transgenic rat lines #318 and #72, which were generated in the SHR genetic background, the same DNA construct was introduced into the Wistar rat genetic background. The transgenic rat line in the Wistar background exhibited the same neurofibrillary pathology phenotype as the transgenic rat lines in the SHR background. This result indicates that the observed phenotype is associated with the expression of the truncated tau protein and not with the genetics of any particular rat line.
14. As noted in the specification (p. 12, first full paragraph) and in the Zilka reference (p. 3582, col. 2) the Thy-1 promoter was used for the expression of truncated tau. This

Thy-1 promoter is derived from mice and therefore, the constructs would be expected to work for a mouse model in addition to the rat models already tested. Furthermore, sequencing of the rat genome has revealed a high homology between genomes of the rat and the mouse. See Exhibit 4 (Rat Genome Sequencing Project Consortium, *Nature* 428:493-521 (2004), particularly Fig. 7), and tau protein exhibits high phylogenetic conservation across a variety of species. There are examples in neurobiology showing that the identical or very homologous gene constructs are responsible for very similar phenotypes in transgenic animals of different species. For example, expression of mutated SOD in rats and mice have produced a very similar phenotype (Gurney *et al.*, *Science*, 264:1772-1774 (1994) (Exhibit 5); Howland *et al.*, *PNAS*, 99(3):1604-1609 (2002) (Exhibit 6)). As a further example, similar results were obtained in modeling Huntington disease in mice and rats (von Horsten *et al.*, *Human Molecular Genetics*, 12(6):617-624 (2003) (Exhibit 7); Bates *et al.*, *Human Molecular Genetics*, 6(10):1633-1637 (1997) (Exhibit 8); Mangiarini *et al.*, *Cell*, 87(3):493-506 (1996) (Exhibit 9)). In view of these observations, it can be expected that the same phenotype as observed in the transgenic rat can also be observed in transgenic mice expressing the same gene construct.

15. I hereby declare that all statements made herein of my knowledge are true and that all statements made on information and belief are believed to be true; and further that these statements were made with the knowledge that willful false statements and the like so made are punishable by fine or imprisonment, or both, under Section 1001 of Title 18 of the United States Code and that such willful false statements may jeopardize the validity of the application or any patent issued thereon.

8. 1. 2007
Date

Peter Filipcik
Peter Filipcik

EXHIBIT 1

CURICULUM VITAE

NAME: RNDr. Peter Filipcik, PhD
BORN: June 26, 1962
CITIZENSHIP: Slovakia
ADDRESS: Podhaj 3, Lamac, 84103 Bratislava,
e-mail: peter.filipcik@savba.sk

EDUCATION:

June 1995 PhD Slovak Academy of Sciences, Bratislava, Slovakia
June 1986 RNDr. Comenius University, Faculty of Natural Sciences in Bratislava, Slovakia

EMPLOYMENT:

1996 – pres Senior scientist - Institute of Neuroimmunology, Slovak Academy of Sciences, Bratislava, Slovakia (part time)
2001 – pres Senior scientist - Axon Neuroscience GmbH, Vienna, Austria
1986 - 1996 Research assistant, Institute of Experimental Endocrinology, Slovak Academy of Sciences, Bratislava, Slovakia
2000 - 2001 University of Vienna, Vienna, Austria
1998 - 2000 Visiting scientist at the CCRI, St. Anna Children Hospital, Vienna, Austria
1995 - 1996 Research associate, Dept. of Pharmacol., University of Minnesota, Minneapolis, USA
1993 - 1994 Research assistant, Dept. of Chem. Pharmacol., University of Tokyo, Japan

INTERNATIONAL COURSES AND MEETINGS ATTENDED (selection):

1990 "3rd European Congress on Cell Biology", Florence, Italy
1993 "The Radioisotopes in Biological Research", The Univ. of Tokyo, Tokyo, Japan
1993 "5th Inter-Department Meeting on Chemical Pharmacol.", Seoul, South Korea
1998 "6th Int. Conf. on Alzheimer's Disease and Related Disorders, Amsterdam, Netherlands
2001 "Ageing and Dementia - Current and future concepts", Graz, Austria
2003 In Vitro Human Cell Systems Enabling Drug Discovery, London, UK
2004 "9th International Conference on Alzheimers Disease and Related Disorders", Philadelphia, Pennsylvania
2005 Molecular Medicine Triconference, CHI, San Francisco, California, USA
2006 "10th International Conference on Alzheimers Disease", Madrid, Spain

MEMBERSHIP OF LEARNED SOCIETIES:

1997 Slovak Immunological Society
1996 The Slovak Alzheimer Society
2005 The Slovak Neuroscience Society

PUBLICATION ACTIVITY:

Author and co-author of 21 scientific papers, 2 patents

Bratislava 6. 12. 2006

List of publications:

Filipcik P, Cente M, Ferencik M, Hulin I, Novak M. The role of oxidative stress in the pathogenesis of Alzheimer's disease. *Bratisl Lek Listy*. 2006; 107 (9-10), 384-394

Pevalova M, **Filipcik P**, Novak M, Avila J, Iqbal K. Post-translational modifications of tau protein *Bratisl Lek Listy* 2006; 107 (9-10), 346-353

*Cente M, ***Filipcik P**, Pevalova M, Novak M. Expression of a truncated tau protein induces oxidative stress in a rodent model of tauopathy. *Eur J Neurosci*. 2006 Aug;24(4):1085-90.

*Zilka N, ***Filipcik P**, Koson P, Fialova L, Skrabana R, Zilkova M, Rolkova G, Kontsekkova E, Novak M. Truncated tau from sporadic Alzheimer's disease suffices to drive neurofibrillary degeneration in vivo. *FEBS Lett*. 2006 Jun 26;580(15):3582-8.

Softys K, Rolkova G, Vechterova L, **Filipcik P**, Zilka N, Kontsekkova E, Novak M. First insert of tau protein is present in all stages of tau pathology in Alzheimer's disease. *Neuroreport*. 2005 Oct 17;16(15):1677-81.

Matuskova M, Csokova N, **Filipcik P**, Hanusovska E, Bires J, Cabadaj R, Kontsek P, Novak M. First confirmed sheep scrapie with A136R154Q171 genotype in Slovakia. *Acta Virol*. 2003;47(3):195-8.

Lion T, Daxberger H, Dubovsky J, **Filipcik P**, Fritsch G, Printz D, Peters C, Matthes-Martin S, Lawitschka A, Gadner H. Analysis of chimerism within specific leukocyte subsets for detection of residual or recurrent leukemia in pediatric patients after allogeneic stem cell transplantation. *Leukemia*. 2001 Feb;15(2):307-10. No abstract available.

Cattaneo A, Capsoni S, Margotti E, Righi M, Kontsekkova E, Pavlik P, **Filipcik P**, Novak M. Functional blockade of tyrosine kinase A in the rat basal forebrain by a novel antagonistic anti-receptor monoclonal antibody. *J Neurosci*. 1999 Nov 15;19(22):9687-97.

Brtko J, **Filipcik P**, Hudecova S, Brtkova A, Bransova J. Nuclear all-trans retinoic acid receptors: in vitro effects of selenium. *Biol Trace Elem Res*. 1998 Apr-May;62(1-2):43-50.

Filipcik P, Strbak V, Brtko J. Thyroid hormone receptor occupancy and biological effects of 3,5,3',5'-L-triiodothyronine (T3) in GH4C1 rat pituitary tumour cells. *Physiol Res*. 1998;47(1):41-6.

Wei LN, Lee CH, **Filipcik P**, Chang L. Regulation of the mouse cellular retinoic acid-binding protein-I gene by thyroid hormone and retinoids in transgenic mouse embryos and P19 cells. *J Endocrinol*. 1997 Oct;155(1):35-46.

Nikodemova M, Weismann P, **Filipcik P**, Mraz P, Greer MA, Strbak V. Both iso- and hyperosmotic ethanol stimulate release of hypothalamic thyrotropin-releasing hormone despite opposite effect on neuron volume. *Neuroscience*. 1997 Oct;80(4):1263-9.

Filipcik P, Brtko J. [The basis for the variable effects of thyroid hormones] *Cesk Fysiol*. 1996 Mar;45(1):13-20. Slovak.

Brtko J, **Filipcik P**, Hudecova S, Strbak V, Brtkova A. In vitro effects of sodium selenite on nuclear 3,5,3'-triiodothyronine (T3) receptor gene expression in rat pituitary GH4C1 cells. *Biol Trace Elem Res*. 1995 May;48(2):173-83.

Filipcik P, Saito H, Katsuki H. 3,5,3'-L-triiodothyronine promotes survival and axon elongation of embryonic rat septal neurons. *Brain Res*. 1994 May 30;647(1):148-52.

Brtko J, **Filipcik P**. Effect of selenite and selenate on rat liver nuclear 3,5,3'-triiodothyronine (T3) receptor. *Biol Trace Elem Res*. 1994 Apr-May;41(1-2):191-9.

Brtko J, Knopp J, **Filipcik P**, Baker ME. Effect of protease inhibitors and substrates on 3,5,3'-triiodothyronine binding to rat liver nuclear receptors. *Endocr Regul*. 1992 Sep;26(3):127-31.

Knopp J, Brtko J, **Filipcik P**. Effect of triiodothyronine on rat liver polysome profiles and translational activity of mRNA after partial hepatectomy. *Endocr Regul*. 1992 Jun;26(2):67-72.

Brtko J, **Filipcik P**, Knopp J, Sedlakova V, Rauova L. Thyroid hormone responsiveness of the L1210 murine leukemia cell line. *Acta Endocrinol (Copenh)*. 1992 Apr;126(4):374-7.

Filipcik P, Brtko J, Rauova L, Sedlakova V. Distribution of triiodothyronine nuclear receptors during the cell cycle in mouse leukemia cells. *Folia Biol (Praha)*. 1992;38(6):332-9.

Filipcik P, Brtko J, Knopp J. [Cell lines in experimental endocrinology] *Bratisl Lek Listy*. 1990 Apr;91(4):278-83. Slovak.

*Equal contribution.

NEUROBIOLOGY OF AGING supplement:

Filipcik, P; Pevalova, M; Smrzka, O; Novak, M. Neuronal assay based on developmentally inducible expression of Alzheimer's tau, designed for screening of AD therapeutics. *NEUROBIOLOGY OF AGING*, JUL 2004, 25, Suppl. 2, S265

Pevalova, M; **Filipcik, P**; Mederlyova, A; Cente, M; Smrzka, O; Novak, M Hyperphosphorylation and oxidative stress as early changes in axon's new AD rat model. *NEUROBIOLOGY OF AGING*, JUL 2004, 25, Suppl. 2, S264

Cente, M; **Filipcik, P**; Hanusovska, E; Zilka, N; Novak, M Onset and intensity of AD changes in transgenic rat expressing Alzheimer specific Tau protein correlates with gene dosage. *NEUROBIOLOGY OF AGING*, JUL 2004, 25 Suppl. 2, S239

Hrnkova, M; Zilka, N; **Filipcik, P**; Novak, M Cognitive deficit and progressive motor impairment in AD rat model, *NEUROBIOLOGY OF AGING*, JUL 2004, 25, Suppl. 2, S233

Koson, P; Zilka, N; **Filipcik, P**; Novak, M Neuronal loss in selected brain areas of a new transgenic AD rat model estimated with unbiased stereological methods, *NEUROBIOLOGY OF AGING*, JUL 2004, 25 Suppl. 2, S249, S250.

Zilka, N; Csokova, N; Vechterova, L; Skrabanova, M; Hrnkova, **M**; **Filipcik, P**; Novak, M. Staging of neuropathological changes in axon's novel transgenic AD rat model is linked to a lethal phenotype. *NEUROBIOLOGY OF AGING*, JUL 2004, 25. Suppl. 2, S255

EXHIBIT 2

FEBS Letters 580 (2006) 3582–3588

Truncated tau from sporadic Alzheimer's disease suffices to drive neurofibrillary degeneration in vivo

Norbert Zilka^{a,1}, Peter Filipcik^{a,1}, Peter Koson^a, Lubica Fialova^a, Rostislav Skrabana^a,
Monika Zilkova^a, Gabriela Rolkova^a, Eva Kontsejkova^a, Michal Novak^{a,b,*}

^a Axon Neuroscience GmbH, Rennweg 95b, 1030 Vienna, Austria

^b Institute of Neuroimmunology, Slovak Academy of Sciences, Dubravska 9, 845 10 Bratislava, Slovak Republic

Received 20 April 2006; revised 5 May 2006; accepted 8 May 2006

Available online 22 May 2006

Edited by Jesus Avila

Abstract Truncated tau protein is the characteristic feature of human sporadic Alzheimer's disease. We have identified truncated tau proteins conformationally different from normal healthy tau. Subpopulations of these structurally different tau species promoted abnormal microtubule assembly in vitro suggesting toxic gain of function. To validate pathological activity in vivo we expressed active form of human truncated tau protein as transgene, in the rat brain. Its neuronal expression led to the development of the neurofibrillary degeneration of Alzheimer's type. Furthermore, biochemical analysis of neurofibrillary changes revealed that massive sarcosyl insoluble tau complexes consisted of human Alzheimer's tau and endogenous rat tau in ratio 1:1 including characteristic Alzheimer's disease (AD)-specific proteins (A68). This work represents first insight into the possible causative role of truncated tau in AD neurofibrillary degeneration in vivo.

© 2006 Federation of European Biochemical Societies. Published by Elsevier B.V. All rights reserved.

Keywords: Alzheimer's disease; Truncated tau; Microtubule assembly; Neurofibrillary degeneration; Sarcosyl insoluble tau; Tau cascade

1. Introduction

Neurofibrillary structures in Alzheimer's disease are principally composed of hyperphosphorylated tau [1–4] and truncated forms of tau protein [2,5,6]. It has been shown that truncation is closely associated with Alzheimer's disease (AD)-typical conformational changes of the tau protein [5–10]. We have hypothesized that truncation could play major role in AD tau pathology [11]. This hypothesis originated from finding that AD-specific monoclonal antibody 423 (mAb 423) recognizes truncated tau species in the core of paired helical filaments (PHF) of Alzheimer's disease [5,6,12,13]. Furthermore, mAb DC11, raised against sporadic AD-brain derived tau extracts, recognized all and only those tau proteins that were truncated at the N-terminus or at both, the N- and C-termini [8]. Trun-

cated tau proteins from sporadic cases of human AD, recognized by mAb DC11 ("Tau DC11 state"), were further tested in vitro for their potency to promote microtubule assembly. The subpopulations of these truncated tau species induced abnormal microtubule assemblies, suggesting toxic gain of function. In order to elucidate the role of truncated tau in AD tau cascade we used truncated tau that was the most active in promotion of abnormal microtubule assembly, as a transgene in the rat brain. Rats displayed massive neurofibrillary structures induced by expressed human truncated tau. This is for the first time shown that truncated human tau could serve as a driving force in neurodegeneration of AD type in vivo.

2. Materials and methods

2.1. Preparation, expression and purification of tau proteins

The preparation of cDNA coding for human tau isoforms and truncated tau proteins was described elsewhere [6]. All DNA constructs were cloned in pET17 vector (Novagen) through *NdeI*–*EcoRI* restriction sites. Integrity of each construct was verified by DNA sequence analysis (ABI Prism 377DNA Sequencer, Perkin-Elmer). Tau proteins were expressed in *Escherichia coli* and purified from bacterial lysates by ion-exchange chromatography [14]. The protein concentration was determined by BCA kit (Pierce, USA).

2.2. Microtubule assembly

Tubulin for microtubule assembly assay was isolated from pig brains, using reversible assembly purification method [15]. Assay mixtures contained 1 mg/ml tubulin, 1 mM GTP, recombinant tau proteins (0.2 mg/ml) in assembly buffer (100 mM Pipes, pH 6.9; 1 mM MgSO₄ and 2 mM EGTA). After gentle and rapid mixing, the samples were pipetted into quartz microcuvettes and equilibrated at 37 °C in a thermostatically controlled spectrophotometer (Beckman Coulter). The turbidity was continuously monitored at 340 nm for a period of 5 min. For electron microscopy samples were fixed with 1% glutaraldehyde, put on the formvar/carbon coated 400 mesh copper grid (Agar Scientific, UK) and stained with 1% aqueous uranyl acetate.

2.3. Preparation of transgene construct and generation of transgenic rats

The transgene construct was prepared by ligation of a cDNA coding for human tau protein truncated at amino acid positions 151–391. Into the mouse Thy-1 gene downstream of the brain promoter/enhancer sequence. The original Thy-1 gene sequence coding for exons II–IV, together with thymus enhancer sequence was replaced by the cDNA. Transgenic DNA was linearized by cleavage with *HcoRI*. Vector sequences were removed prior to microinjection. Transgenic rats were generated by pronuclear injection of one-day old SHR rat embryos. Founders were double screened by PCR using Thy-1-specific and human tau-specific primers amplifying START and STOP codon flanking sequences. The rat endogenous tau sequence was used as an internal amplification control. Two independent transgenic founder

*Corresponding author. Fax: +421 2 54774276.

E-mail address: Michal.Novak@savba.sk (M. Novak).

¹ These authors contributed equally.

Abbreviations: AD, Alzheimer's disease; mAb, monoclonal antibody; NFT, neurofibrillary tangle; NT, neuropil threads; OD, optical density; PHF, paired helical filaments; SDS-PAGE, sodium dodecyl sulfate polyacrylamide gel electrophoresis

lines (#318 and #72) that stably expressed human truncated tau were engineered and displayed similar phenotype. The studies described below were performed using the line #318. The expression level of total human truncated tau in the transgenic rats was determined by Western blot analysis using protein extracts from different areas of brain and spinal cord.

2.4. Monoclonal antibodies

HT7 (Innogenetics, Belgium) recognizes residues 159–163 of human tau, AT8 (Innogenetics) recognizes phosphoserine 202 and 205, AT180 (Innogenetics) recognizes phosphothreonine 231. PHF 1 (a kind gift from Dr. Peter Davies) recognizes phosphoserine 396 and 404. As a control we have used pan tau antibody DC25 recognizing residues 347–354 (Axon Neuroscience, Austria).

2.5. Histology and immunohistochemistry

Animals were perfused transcardially with 4% paraformaldehyde in 0.1 M phosphate buffered saline, pH 7.2, and the tissues were post-fixed after perfusion and then cut on cryostat or embedded in paraffin and cut on microtome. Immunohistochemistry and histopathology were performed on 50 μ m free-floating and 8 μ m paraffin embedded sections. Tissue sections were immunostained using the standard avidin-biotin-peroxidase method. The modified Gallyas silver iodide, Congo red and Thioflavin S staining methods were utilized to demonstrate mature neurofibrillary pathology in neurons [16,17]. Sections were examined with an Olympus BX51 and Zeiss Axiovert 200 microscopes.

2.6. Stereological analysis

The quantified parameters were neuronal and neurofibrillary tangle (NFT) density. The left brain stems of 10 months old transgenic males were sectioned on cryostat in the frontal plane. The rostral part of the gigantocellular reticular nucleus was selected as a representative region of the reticular formation of the brain stem. NFTs were immunohistochemically visualized using mAb AT8 and thereafter the sections were counterstained with cresyl violet. The optical disector principle was applied [18], particles (neurons, NFTs) were counted and numerical densities per mm^3 were calculated. The obtained results were corrected to the number weighted final section thickness [19] to eliminate any possible bias in the data due to shrinkage of the sections during histological processing. The study was realized with the aid of a computer-based stereological system (StereoInvestigator, MicroBrightField, USA).

2.7. Extraction of sarcosyl insoluble tau

Sarcosyl insoluble tau was isolated from brain tissues of 3–12 months old rats based on the modified method of Greenberg and Davies [20]. Approximately 2 g of brain tissue was homogenized in 10 volumes of buffer (10 mM Tris, 0.8 M NaCl, 1 mM EGTA and 10% sucrose, pH 7.4) and centrifuged at $27200 \times g$ for 20 min. The supernatant was adjusted to 1% (w/v) *N*-lauroylsarcosine and incubated 1 h at RT. After the incubation supernatant was spun at $123000 \times g$ for 1 h at RT. Resulted pellet was resuspended in small volume of phosphate-buffered saline and analysed in Western blot and throughout the paper is designated as P2.

2.8. Western blotting

Sarcosyl insoluble tau proteins purified from brains were analyzed on 5–20% SDS-PAGE gradient gel and Western blot as described previously [14]. Enhanced chemiluminescence developed Western blot was digitized with LAS3000 CCD imaging system (Fujifilm, Japan). Densitometric data analysis and relative quantification of Western blot record were performed by AIDA Biopackage (Raytest, Germany) as described [14].

3. Results

3.1. Truncated tau protein (t151–391) induces abnormal assembly of microtubules in vitro

Monoclonal antibody DC11, raised using AD brain derived truncated forms of tau proteins, recognizes "Tau DC11 state"

that represents all and only those truncated tau proteins that are conformationally different from normal healthy tau proteins (Fig. 1A–C). The effect of these truncated tau proteins on the assembly of microtubules was analyzed. The physiological function of healthy tau is characterized mainly by promotion of microtubule assembly. The tau efficiency in promotion of microtubule assembly can be measured by increase in optical density at 340 nm. DC11 positive truncated tau species, except t99–441, displayed significantly higher microtubule assembly promotion activity than normal healthy tau. Short amino-terminal truncation (t99–441) produces no measurable difference from normal tau. Strikingly N- and C-terminally truncated tau species are promoting robust microtubule assembly, 3–4 times higher (OD_{340} : 1.2–1.6) than normal healthy tau (OD_{340} : 0.4) (Fig. 1D). For electron microscopy analysis of microtubule assembly was selected mAb DC11 positive double truncated tau species (t151–391) and normal healthy tau (t1–441). Electron micrographs show that normal tau induces formation of thin microtubular networks (Fig. 1E). However, interaction of truncated tau species (t151–391) with tubulin produces abnormally thick microtubular networks (bundles). (Fig. 1F), different in their appearance from normal microtubules under the same magnification (3600 \times).

3.2. AD-like neurofibrillary pathology induced by truncated tau (t151–391) in vivo

To validate suggested pathological function of truncated tau in vivo, we generated transgenic rat that overexpressed truncated tau (t151–391) in the brain and spinal cord (Fig. 2). The most prominent histopathological feature of transgenic rats was extensive argyrophilic NFT formation (Fig. 3A). No neurofibrillary pathology was found in wild type rats throughout their lifespan. The appearance of NFTs satisfied several histological criteria used to identify neurofibrillary degeneration in the human AD including argyrophilia (Fig. 3A), Congo red birefringence (Fig. 3B) and Thioflavin S reactivity (Fig. 3C).

The load of neurofibrillary pathology was stereologically quantified in the brain stem (gigantocellular reticular nucleus) where the mean NFT density was $690/\text{mm}^3$ with an observed coefficient of variation of 32.9% (Fig. 3D). The mean NFT: neuron ratio was 1:8 in transgenic animals. Furthermore, immunohistochemical analysis revealed that neurofibrillary tangle formation passed through the histologically well-defined maturation stages. The first stage was characterized by intraneuronal pre-tangles, immunoreactive for phosphorylated tau protein. The antibody AT8 detected the diffuse rod-like phospho-tau accumulations within the cytoplasm. The pre-tangle bearing neurons had detectable nuclei and normal appearance (Fig. 3E). The assembly of pre-tangles resulted in formation of intracellular NFTs in cell bodies (Fig. 3F) and in processes as neuropil threads (NTs). The late developmental stage represented extra-neuronal "ghost" tangles (eNFT) that were present as immunoreactive, densely packed tau fibrils or bundles outside the neurons (Fig. 3G). The cell soma revealed no stainable cytoplasm and nucleus.

3.3. The sarcosyl insoluble tau complexes consisted of human truncated tau and endogenous rat tau protein

To determine whether truncated tau (t151–391) was able to induce maturation of neurofibrillary pathology, manifested

3584

N. Zilka et al. / FEBS Letters 580 (2006) 3582–3588

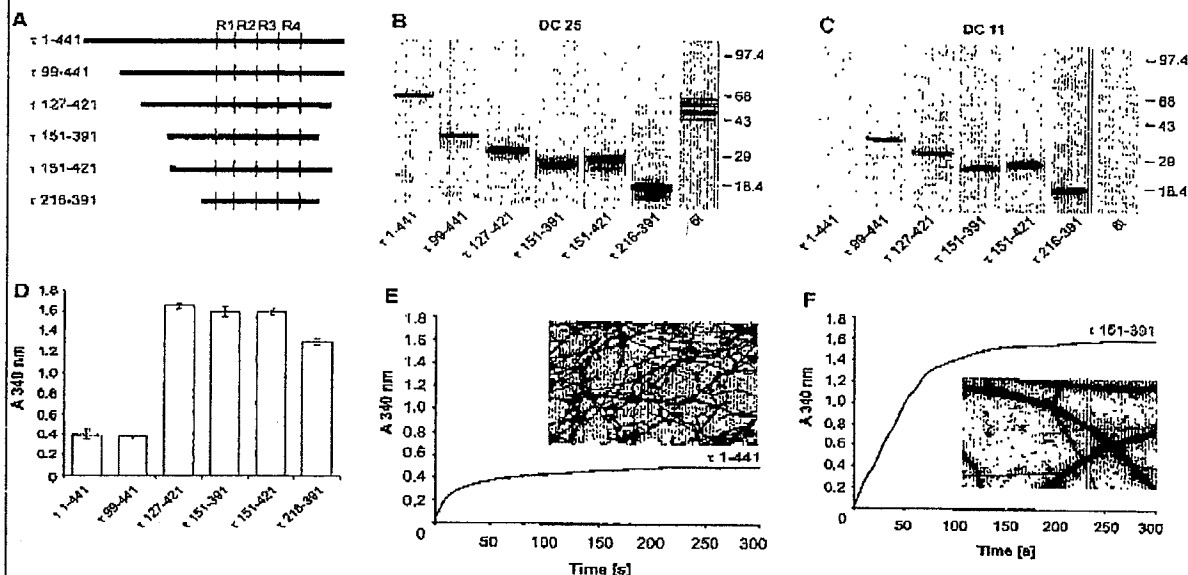


Fig. 1. Efficacy of truncated tau proteins in promotion of microtubule assembly. (A) Schematic diagram of tau species tested in vitro for their potency to promote microtubule assembly. The numbering of amino acids corresponds to that of the human tau 40 [30]. (B, C) Western blot analysis of tau proteins using pan tau mAb DC25 and tau conformation specific mAb DC11. Recombinant human tau six isoforms (6i) were used as a control. Monoclonal antibody DC25 (B) recognizes all tau proteins, however conformation-dependent mAb DC11 (C) stains only truncated forms of tau proteins and does not recognize any of six human tau isoforms. (D) Microtubule assembly induced by truncated tau proteins monitored by turbidimetry at OD 340 nm at 5 min. Individual bars reflect efficacy of tau species tested in promotion of microtubule assembly. (E, F) Electron microscopy images of microtubules induced by normal tau (E) and truncated tau (F). Samples were taken at steady state of polymerization (at 5 min). Both figures are at the same magnification (3600 \times).

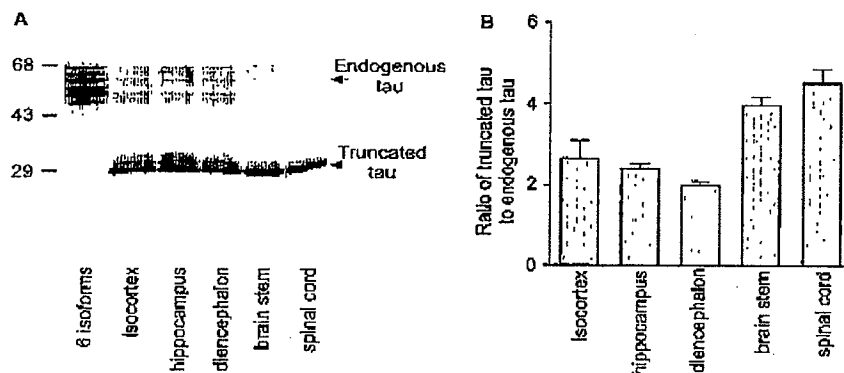


Fig. 2. Expression profile of human truncated tau in the brain and spinal cord of transgenic animals. (A) Pan tau monoclonal antibody DC25 was used for staining of rat endogenous and human truncated tau protein in different brain regions and spinal cord. (B) Transgenic protein expression levels were 2–5-fold over endogenous tau in the isocortex, hippocampus, diencephalon, brain stem and the spinal cord.

by the presence of sarcosyl insoluble tau complexes, we analysed sarcosyl insoluble protein extracts (P2) from 10 to 12 months old transgenic rats, age-matched control rats (wt) and from Alzheimer's diseased brain tissues. Western blot analysis of P2 fraction, from transgenic rat using pan tau mAb DC25, revealed similar staining pattern to that of human AD brain (Fig. 4, lanes 3 and 7). Age-matched control wild type rats had no tau in P2 fraction (Fig. 4, lane 2). To investigate whether human truncated tau (t151-391) co-

assembled with endogenous rat tau in transgenic rats, we analyzed the P2 fraction with antibodies reactive with both human and rat tau (DC25), with human tau only (H17) and with endogenous rat tau only (PHF1, human Alzheimer's truncated tau – transgene – does not contain the PHF1 epitope). Our results showed that sarcosyl insoluble P2 fractions from transgenic rats consisted of human tau (Fig. 4, lane 4) and rat endogenous tau (Fig. 4, lane 5). Phosphorylated tau immunoreactivities were detected in the same fraction

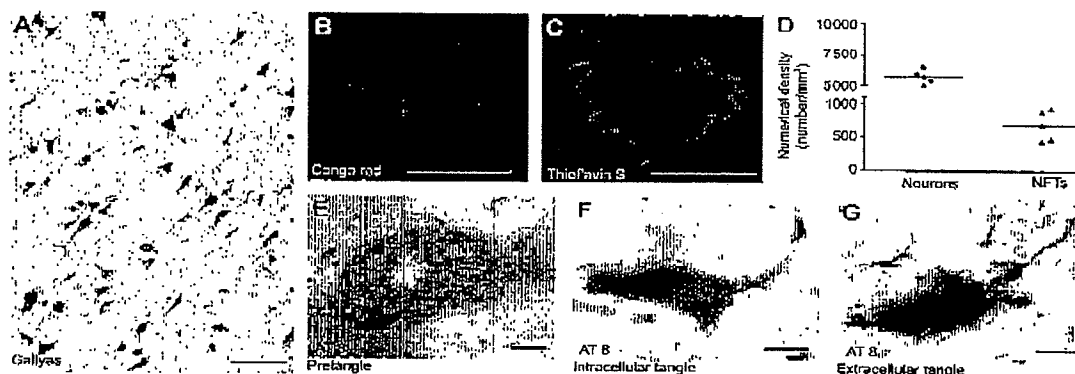


Fig. 3. Truncated tau induced AD-like neurofibrillary degeneration in vivo. (A) Development of extensive argyrophilic positive neurofibrillary tangles in 9 months old rats. High magnification of Congo red (B) and Thioflavin S positive (C) intraneuronal tangles showed similar appearance as in human AD. (D) Stereological analysis of rat brains expressing human truncated tau showed a mean neuronal density of 5703 neurons/mm³ (S.E.M. = 250.2) in brain stem. The estimated NFT density in this brain region was 690/mm³ (S.E.M. = 101.4). Ontogeny of the neurofibrillary degeneration in this rats is similar to that of human Alzheimer's disease: pre-tangles (E), intracellular tangles (F) and extracellular tangles (G). Tool bars 10 μ m.

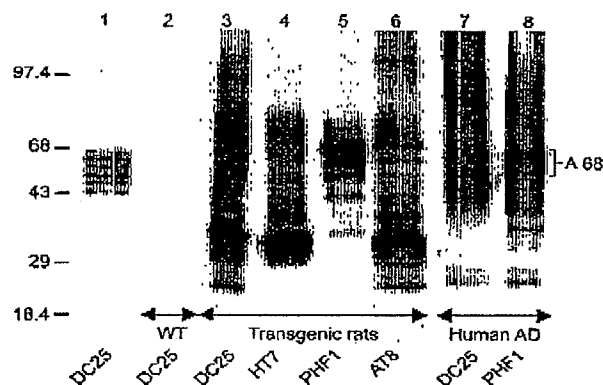


Fig. 4. Human truncated tau and endogenous rat tau are constituent parts of massive sarcosyl insoluble tau complexes. The series of ultracentrifugation and extraction steps was used to obtain sarcosyl insoluble fraction of tau (P2 fraction) from brain tissues of age-matched wild type (wt) rats, transgenic rats and human AD brain tissues. Recombinant human six tau isoforms (lane 1) were used as a control. Wild type rats did not show any sarcosyl insoluble tau (lane 2). Immunoblotting of P2 fraction from transgenic rats revealed sarcosyl insoluble complexes of tau (lane 3, mAb DC25) that were formed from human truncated tau (lane 4, HT7-human tau-specific mAb), endogenous phosphorylated rat tau (lane 5, mAb PHF1-endogenous rat tau specific, see Section 3), and human and rat phosphorylated tau (lane 6, mAb AT8). P2 fraction of human AD is shown as a positive control with characteristic A68 triplet (lane 7, mAb DC25, lane 8, mAb PHF1) seen in rats as well (lane 5).

(P2) with phosphorylation-dependent antibodies, AT8 and PHF1. AT8 phosphoserines 202 and 205 were present in both human and rat tau (Fig. 4, lane 6). Abnormal phosphorylation of rat endogenous tau was detected by PHF1 that does not recognize human truncated tau (Fig. 4, lane 5). Furthermore, it is noteworthy that the A68 triplet characteristic of human AD neurofibrillary degeneration (Fig. 4, lane 8) as revealed by PHF1 staining was found in transgenic animals as well (Fig. 4, lane 5).

3.4. Quantitative analyses of human transgenic and endogenous rat tau in sarcosyl insoluble fraction

We examined further the composition of mature sarcosyl insoluble tau complexes with respect to the ratio between the transgenic human truncated tau (t151-391) and endogenous rat tau. Insoluble P2 fractions from 12 months old rats were assayed on Western blot together with three respective sarcosyl soluble (S2) fractions. Both soluble and insoluble fractions were stained with pan-tau monoclonal antibody DC25 (Fig. 5A) and with human tau-specific monoclonal antibody HT7 (Fig. 5B). Data from immunoblotted transgenic human tau in S2 fractions were digitized and used as a standard for normalization of monoclonal antibodies staining. Both antibodies stained tau protein with similar intensities (Fig. 5E). Tau staining in P2 fraction was digitized as well (Fig. 5C and D) and the relative tau protein amount was calculated on the basis of correlation between amounts of proteins seen by both antibodies. The comparison of normalized peak areas revealed that mature sarcosyl insoluble tau complexes are composed of transgenic human truncated tau and endogenous rat tau at 1:1 ratio (Fig. 5F).

3.5. The level of sarcosyl insoluble formation correlates with lifespan of transgenic rats expressing truncated tau

Sarcosyl insolubility of tau is generally considered to be a definitive transformation point of physiological tau into pathological form. Therefore, we analysed development of sarcosyl insoluble tau complexes in the brain of transgenic rats expressing truncated tau (t151-391). The brain tissues were examined at 3, 6, 9 and 12 months old animals. The level of tau in the sarcosyl insoluble P2 fraction increased in an age-dependent manner and correlated positively with the development of neurofibrillary pathology. First sarcosyl insoluble tau consisting exclusively of transgene – human truncated tau – appeared in the brain of 3 months old transgenic rats and persisted until the late stages of neurodegeneration (Fig. 6A, lanes 1, 2). The first, phosphorylation induced electrophoretic mobility decrease (gel shift)

3586

N. Zilka et al. / FEBS Letters 580 (2006) 3582–3588

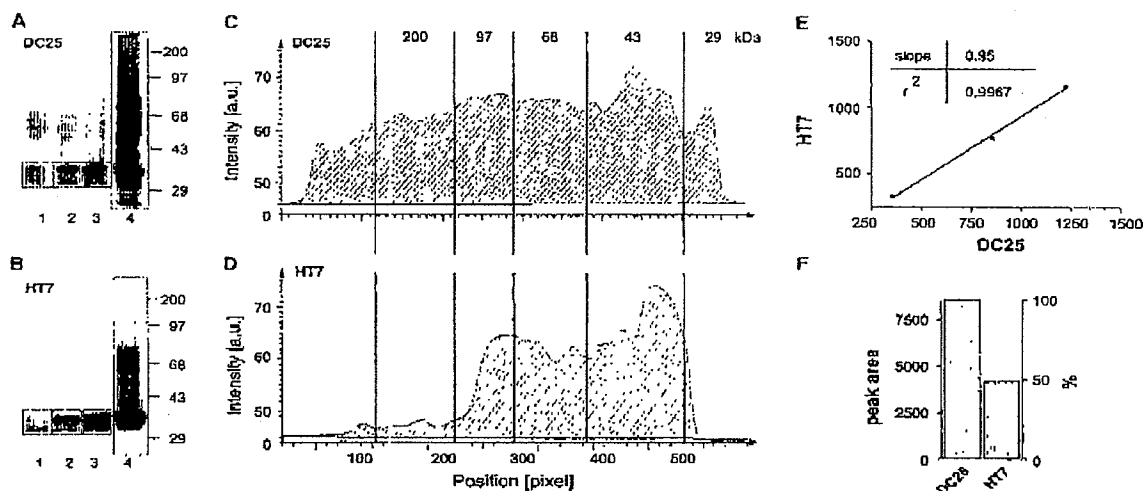


Fig. 5. Quantitative analyses of human transgenic and endogenous rat tau in sarcosyl insoluble fraction. The fractions containing sarcosyl insoluble tau (P2) were analyzed with pan tau monoclonal antibody DC25 and human tau-specific antibody HT7. Lanes 1–3 show sarcosyl soluble fraction (S2) from three independent transgenic animals; lane 4 shows sarcosyl insoluble fraction (P2) from transgenic animal (A, B). Boxed off are P2 fractions (A, B; lane 4) that were used for quantification (C, D). Integrated signals from S2 fractions (A, B; lanes 1–3) were used for construction of the correlation line (E). Ratio between human transgenic and endogenous rat tau in P2 fraction is 1:1 (F). The mAb DC25 staining reflects the total amount of tau present in sarcosyl insoluble P2 pellets, whereas HT7 detects human transgenic tau only.

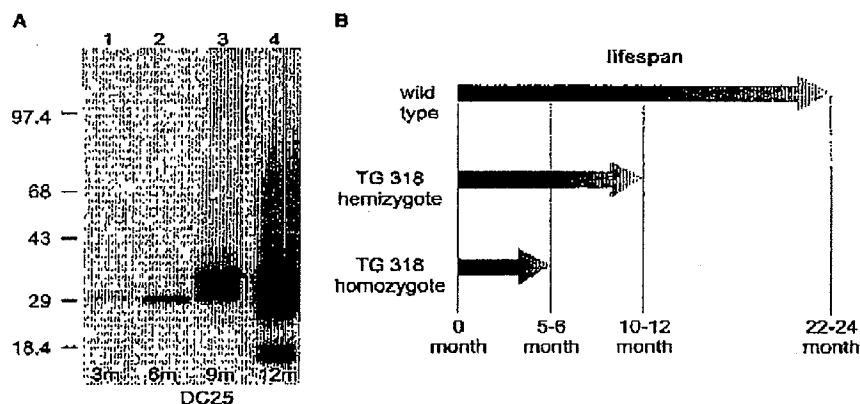


Fig. 6. Ontogenesis of sarcosyl insoluble tau complexes (P2) in the brain of 3, 6, 9 and 12 months old transgenic rats was monitored by Western blot analysis using pan tau mAb DC25. (B) Alzheimer's tau expression impact on lifespan of transgenic rats.

of sarcosyl insoluble tau monomer was observed in 9 months old animals (Fig. 6A, lane 3). Mature sarcosyl insoluble tau formations, characterized by the presence of tau species with high and low molecular weight, appeared in 12 months old animals (Fig. 6A, lane 4). It is noteworthy that the stage of "mature sarcosyl insoluble tau formation" correlated with death of animals expressing transgenic human truncated tau. The lifespan of hemizygous animals was 10–12 months and that of homozygotes was 5–6 months. Life expectation of wild type rats is 22–24 months. These results show that expression of human truncated tau shortens lifespan in hemizygotes by 50% and in homozygotes by 75% (Fig. 6B).

4. Discussion

During the work providing molecular proof that microtubule associated protein tau is a major (if not sole) constituent of paired helical filaments [2,21], it was noted that tau could be truncated. Molecular mapping of the epitope of monoclonal antibody 423, that recognizes tau protein derived from AD brains, revealed for the first time that tau is truncated at E³⁹¹ in Alzheimer's disease [6,12]. Since then, truncation of tau was suggested by many authors as a possible seminal event in the pathogenesis of Alzheimer's disease [22–24]. It is generally agreed that tau has to undergo significant conformational change(s) leading to the pathological polymerization process.

It has been shown that truncation could facilitate polymerization of tau in vitro [25–27]. Despite of these results, the role of truncation and truncated tau in AD cascade remains an open issue. Monoclonal antibody DC11, produced against AD brain derived truncated forms of tau protein, revealed the presence of conformationally distinct forms of tau protein in AD. Molecular analysis of these forms showed that DC11 recognizes all and only those N- and C-terminally truncated tau proteins that are conformationally different from normal healthy tau proteins [8]. The shift of tau into “DC11 state” in AD could represent a new pathogenic entity and important step in neurofibrillary degeneration itself. Therefore, we studied effect of N- and C-terminally truncated tau species, on their capacity to influence microtubule assembly. Strikingly, these double truncated tau species promoted robust microtubule assembly, that was 3–4 times higher ($OD_{340}:1.2–1.6$) than microtubule assembly induced by normal healthy tau ($OD_{340}:0.4$). Electron microscopy analysis of microtubules assembled by DC11 tau species revealed abnormally thick microtubular networks (bundles) that differed from normal microtubular networks. These results suggest that the truncated tau has large impact on microtubule assembly in vitro suggesting its possible gain of altered function that could lead to tau transformation into a pathological entity.

In order to explore the possible role of truncated tau in vivo, we expressed the most in vitro active DC11 tau species (t151-391) as a transgene in rat brains. Transgenic animals developed extensive neurofibrillary pathology satisfying several histopathological criteria used for identification of neurofibrillary degeneration in AD, including argyrophilia, Congo red birefringence and Thioflavin S reactivity. As in human AD, formation of NFT in transgenic animals passed through several histologically defined maturation stages. First stage was represented by pre-tangle formation (identified with mAb AT8) that is considered to be an early event in NFT development [28,29]. The second stage was characterized by formation of intracellular argyrophilic NFTs in neuronal cell bodies and NTs in their processes. The late developmental stage in these transgenic animals was represented by the presence of extra-neuronal “ghost” tangles (cNFT). The well-defined staging in transgenic rats expressing truncated tau offers an opportunity to study the neurodegenerative cascade of tau protein in vivo.

In human sporadic AD, mature neurofibrillary degeneration is characterized by extensive formation of sarcosyl insoluble tau protein complexes consisting of abnormally hyperphosphorylated full length and truncated tau forms [1–4]. The analysis of sarcosyl insoluble tau fractions derived from the brain of transgenic animals allowed drawing several important conclusions: First, sarcosyl insoluble tau complexes were composed of transgenic human truncated tau and endogenous rat tau at a 1:1 ratio. Second, both human and endogenous rat tau were phosphorylated (AT8) and third, tau A68 triplet pattern characteristic of human AD [3] was formed in transgenic animals. Furthermore, detailed time course experiments of neurofibrillary maturation revealed that first sarcosyl insoluble truncated tau monomer appeared already in very young transgenic animals (3 months old), well before the detection of intraneuronal tangles (9 months old). We suggest that sarcosyl insoluble monomer (“one band stage”) represents immature developmental stage of sarcosyl insoluble complex formations. Further “aging” of sarcosyl insoluble tau is represented by intensive phosphorylation (“stage of shifted mono-

mer”). Most probably the phosphorylated monomers led to the development of mature sarcosyl insoluble tau complexes (“stage of tau ladder”) encompassing both truncated and endogenous full-length tau (9–12 months old). It is intriguing that the stage of “mature sarcosyl insoluble tau formation” correlated with the death of animals expressing transgenic human truncated tau. The life span of hemizygous animals was 10–12 months and that of homozygotes was 5–6 months. Life expectancy of wild type rats is 22–24 months. Thus truncated tau expression shortens life span of hemizygotes by 50% and of homozygotes by 75%.

The present study provides experimental data introducing truncated tau protein as an important upstream factor in the pathogenesis of neurofibrillary degeneration of AD type. In addition, our data established that truncated tau is sufficient to drive neurofibrillary degeneration in the absence of tau mutation.

References

- [1] Grundke-Iqbal, I., Iqbal, K., Tung, Y.C., Quinlan, M., Wisniewski, H.M. and Binder, L.I. (1986) Abnormal phosphorylation of the microtubule-associated protein tau in Alzheimer cytoskeletal pathology. *Proc. Natl. Acad. Sci. USA* 83, 4913–4917.
- [2] Wischik, C.M., Novak, M., Thøgersen, H.C., Edwards, P.C., Runswick, M.J., Jakes, R., Walker, J.E., Milstein, C., Roth, M. and Klug, A. (1988) Isolation of a fragment of tau derived from the core of paired helical filament of Alzheimer's disease. *Proc. Natl. Acad. Sci. USA* 85, 4506–4510.
- [3] Lee, V.M., Balin, B.J., Orvos Jr., L. and Trojanowski, J.Q. (1991) A68: a major subunit of paired helical filaments and derivatized forms of normal Tau. *Science* 251, 675–678.
- [4] Goedert, M. and Klug, A. (1999) Tau protein and the paired helical filament of Alzheimer's disease. *Brain Res. Bull.* 50, 469–470.
- [5] Novak, M., Jakes, R., Edwards, P.C., Milstein, C. and Wischik, C.M. (1991) Difference between the tau protein of Alzheimer paired helical filament core and normal tau revealed by epitope analysis of monoclonal antibodies 423 and 7.51. *Proc. Natl. Acad. Sci. USA* 88, 5837–5841.
- [6] Novak, M., Kabat, J. and Wischik, C.M. (1993) Molecular characterization of the minimal protease resistant tau unit of the Alzheimer's disease paired helical filament. *EMBO J.* 12, 365–370.
- [7] Canu, N., Dus, L., Barbaro, C., Ciotti, M.T., Brancolini, C., Rinaldi, A.M., Novak, M., Cattaneo, A., Bradbury, A. and Calissano, P. (1998) Tau cleavage and dephosphorylation in cerebellar granule neurons undergoing apoptosis. *J. Neurosci.* 18, 7061–7074.
- [8] Vechterova, L., Kontsekova, E., Zilka, N., Ferencik, M., Ravid, R. and Novak, M. (2003) DC11: a novel monoclonal antibody revealing Alzheimer's disease specific tau epitope. *Neuroreport* 14, 87–91.
- [9] Horowitz, P.M., Patterson, K.R., Guillozet-Bongaarts, A.L., Reynolds, M.R., Carroll, C.A., Weintraub, S.T., Bennett, D.A., Cryns, V.L., Berry, R.W. and Binder, L.I. (2004) Early N-terminal changes and caspase-6 cleavage of tau in Alzheimer's disease. *J. Neurosci.* 24, 7895–7902.
- [10] Guillozet-Bongaarts, A.L., Garcia-Sierra, F., Reynolds, M.R., Horowitz, P.M., Fu, Y., Wang, T., Cahill, M.E., Bigio, E.H., Berry, R.W. and Binder, L.I. (2005) Tau truncation during neurofibrillary tangle evolution in Alzheimer's disease. *Neurobiol. Aging* 26, 1015–1022.
- [11] Novak, M. (1994) Truncated tau protein as a new marker for Alzheimer's disease. *Acta Virol.* 38, 173–189.
- [12] Novak, M., Wischik, C.M., Edwards, P., Pannell, R. and Milstein, C. (1989) Characterisation of the first monoclonal antibody against the pronase resistant core of the Alzheimer PHF. *Prog. Clin. Biol. Res.* 317, 755–761.
- [13] Skrabana, R., Kontsek, P., Mederlyova, A., Iqbal, K. and Novak, M. (2004) Folding of Alzheimer's core PHF subunit revealed by monoclonal antibody 423. *FEBS Lett.* 568, 178–182.

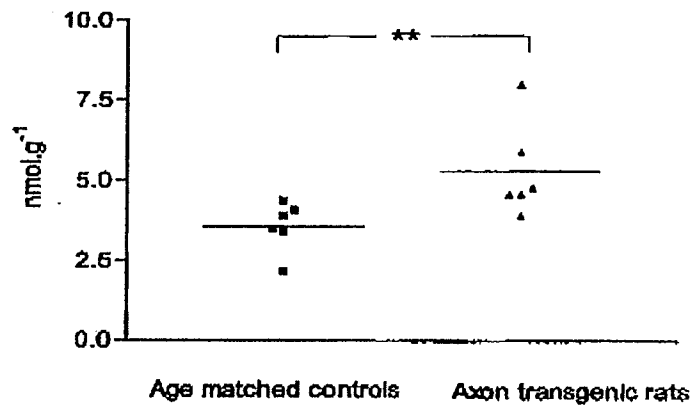
3588

N. Zilka et al. / *FEBS Letters* 580 (2006) 3582–3588

- [14] Csokova, N., Skrabana, R., Liebig, H.D., Mederlyova, A., Kontsek, P. and Novak, M. (2004) Rapid purification of truncated tau proteins: model approach to purification of functionally active fragments of disordered proteins. implication for neurodegenerative diseases. *Protein Expr. Purif.* 35, 366–372.
- [15] Vallee, R.B. (1986) Reversible assembly purification of microtubules without assembly-promoting agents and further purification of tubulin, microtubule-associated proteins, and MAP fragments. *Methods Enzymol.* 134, 89–104.
- [16] Gallyas, F. (1971) Silver staining of Alzheimer's neurofibrillary changes by means of physical development. *Acta Morphol. Acad. Sci. Hung.* 19, 1–8.
- [17] Sun, A., Nguyen, X.V. and Bing, G. (2002) Comparative analysis of an improved Thioflavin-S stain, Gallyas silver stain, and immunohistochemistry for neurofibrillary tangle demonstration on the same sections. *J. Histochem. Cytochem.* 50, 463–472.
- [18] Gundersen, H.J., Bagger, P., Bendtsen, T.F., Evans, S.M., Korbo, L., Marcussen, N., Møller, A., Nielsen, K., Nyengaard, J.R. and Pakkenberg, B. (1988) The new stereological tools: disector, fractionator, nucleator and point sampled intercepts and their use in pathological research and diagnosis. *Apmis* 96, 857–881.
- [19] Dorph-Petersen, K.A., Nyengaard, J.R. and Gundersen, H.J. (2001) Tissue shrinkage and unbiased stereological estimation of particle number and size. *J. Microsc.* 204, 232–246.
- [20] Greenberg, S.G. and Davies, P. (1990) A preparation of Alzheimer paired helical filaments that displays distinct τ proteins by polyacrylamide gel electrophoresis. *Proc. Natl. Acad. Sci. USA* 87, 5827–5831.
- [21] Wischik, C.M., Novak, M., Edwards, P.C., Klug, A., Tichelaar, W. and Crowther, R.A. (1988) Structural characterization of the core of the paired helical filament of Alzheimer disease. *Proc. Natl. Acad. Sci. USA* 85, 4884–4888.
- [22] Ghoshal, N., Garcia-Sierra, F., Fu, Y., Beckett, L.A., Mufson, E.J., Kuret, J., Berry, R.W. and Binder, L.I. (2001) Tau-66: evidence for a novel tau conformation in Alzheimer's disease. *J. Neurochem.* 77, 1372–1385.
- [23] Garcia-Sierra, F., Ghoshal, N., Quinn, B., Berry, R.W. and Binder, L.I. (2003) Conformational changes and truncation of tau protein during tangle evolution in Alzheimer's disease. *J. Alzheimer's Dis.* 5, 65–77.
- [24] Binder, L.I., Guillozet-Bonguarts, A.L., Garcia-Sierra, F. and Berry, R.W. (2005) Tau, tangles, and Alzheimer's disease. *Biochim. Biophys. Acta* 1739, 216–223.
- [25] Abrahams, A., Ghoshal, N., Gamblin, T.C., Cryns, V., Berry, R.W., Kuret, J. and Binder, L.I. (2000) C-terminal inhibition of tau assembly in vitro and in Alzheimer's disease. *J. Cell Sci.* 21, 3737–3745.
- [26] Iqbal, K., Alonso, C., Choa, S., Chohan, M.O., El-Akkad, E., Gong, C.X., Khatoon, S., Li, B., Liu, F., Rahman, A., Tanimukai, H. and Grundke-Iqbal, I. (2005) Tau pathology in Alzheimer disease and other tauopathies. *Biochim. Biophys. Acta* 1739, 198–210.
- [27] Avila, J. (2006) Tau phosphorylation and aggregation in Alzheimer's disease pathology. *FEBS Lett.* 580, 2922–2927.
- [28] Braak, E., Braak, H. and Mandelkow, E.M. (1994) A sequence of cytoskeleton changes related to the formation of neurofibrillary tangles and neuropil threads. *Acta Neuropathol.* 87, 554–567.
- [29] Augustinack, J.C., Schneider, A., Mandelkow, E.M. and Tyman, B.T. (2002) Specific tau phosphorylation sites correlate with severity of neuronal cytopathology in Alzheimer's disease. *Acta Neuropathol.* 103, 26–35.
- [30] Goedert, M., Spillantini, M.G., Jakes, R., Rutherford, D. and Crowther, R.A. (1989) Multiple isoforms of human microtubule-associated protein tau: sequences and localization in neurofibrillary tangles of Alzheimer's disease. *Neuron* 3, 519–526.

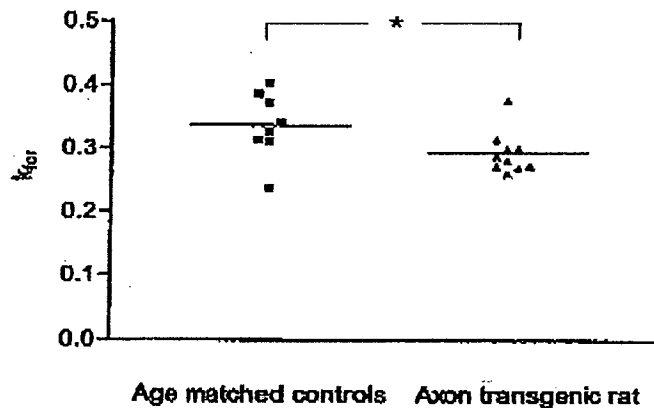
EXHIBIT 3

Figure 2



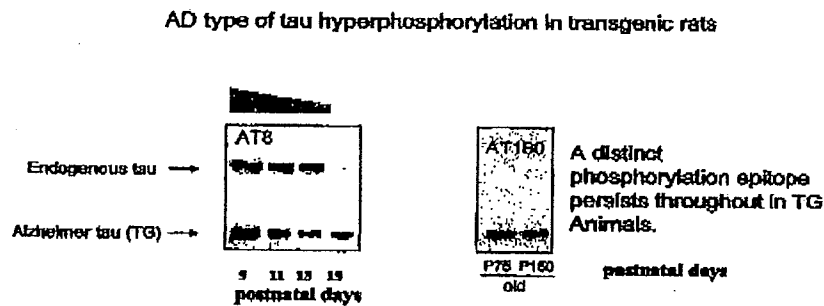
The ascorbate free radical electron paramagnetic resonance (EPR) signal show higher concentration of AFR in the homogenate obtained from brain stems of animals ($5.300 \text{ nmol.g}^{-1} \pm 0.6011$, $N=6$) than from age-matched control rats ($3.583 \text{ nmol.g}^{-1} \pm 0.3156$, $N=6$). Increased amount of AFR ($P < 0.01$) in the brain of transgenic rats at the terminal stage indicate, that oxidative stress is a consequence and not a cause of pathological cascade in the transgenic rats.

Figure 3



The kinetic measurement of CK reaction showed, that the rate constant values of the brain specific creatine kinase (CKBB) was significantly decreased in the brain of Axon transgenic rats. The kinetic measurement of CK reaction showed, that the rate constant values of the CKBB was significantly decreased ($P < 0.05$) in the brain of Axon transgenic rats ($k_{for} = 0.2942 \pm 0.01048$, $N=10$) in comparison with age-matched controls ($k_{for} = 0.3370 \pm 0.01862$, $N=8$).

Figure 4



Using mAB AT180 (Fig.4, right panel), strong AD-like phosphorylation persists in brain extracts from 75 and 150 day old animals. This type of phosphorylation (right panel) drives further development of neurofibrillary changes identical to human AD. None of these features is seen any previous tau transgenic animal using wild type or FTDP17 mutated tau transgene construct. The left panel of Fig. 4 shows the typical phosphorylation pattern of endogenous tau in embryos/early days p.n. which drops by day 19 p.n. In contrast, transgenic truncated tau remains phosphorylated thus reflecting distinct mechanisms of tau phosphorylation.

EXHIBIT 4

Genome sequence of the Brown Norway rat yields insights into mammalian evolution

Rat Genome Sequencing Project Consortium*

*Lists of participants and affiliations appear at the end of the paper

The laboratory rat (*Rattus norvegicus*) is an indispensable tool in experimental medicine and drug development, having made inestimable contributions to human health. We report here the genome sequence of the Brown Norway (BN) rat strain. The sequence represents a high-quality 'draft' covering over 90% of the genome. The BN rat sequence is the third complete mammalian genome to be deciphered, and three-way comparisons with the human and mouse genomes resolve details of mammalian evolution. This first comprehensive analysis includes genes and proteins and their relation to human disease, repeated sequences, comparative genome-wide studies of mammalian orthologous chromosomal regions and rearrangement breakpoints, reconstruction of ancestral karyotypes and the events leading to existing species, rates of variation, and lineage-specific and lineage-independent evolutionary events such as expansion of gene families, orthology relations and protein evolution.

Darwin believed that "natural selection will always act very slowly, often only at long intervals of time"¹. The consequences of evolution over timescales of approximately 1,000 millions of years (Myr) and 75 Myr were investigated in publications comparing the human with invertebrate and mouse genomes, respectively^{2,3}. Here we describe changes in mammalian genomes that occurred in a shorter time interval, approximately 12–24 Myr (refs 4, 5) since the common ancestor of rat and mouse.

The comparison of these genomes has produced a number of insights:

- The rat genome (2.75 gigabases, Gb) is smaller than the human (2.9 Gb) but appears larger than the mouse (initially 2.5 Gb (ref. 3) but given as 2.6 Gb in NCBI build 32, see <http://www.ncbi.nlm.nih.gov/genome/seq/NCBIContigInfo.html>).
- The rat, mouse and human genomes encode similar numbers of genes. The majority have persisted without deletion or duplication since the last common ancestor. Intronic structures are well conserved.
- Some genes found in rat, but not mouse, arose through expansion of gene families. These include genes producing pheromones, or involved in immunity, chemosensation, detoxification or proteolysis.
- Almost all human genes known to be associated with disease have orthologues in the rat genome but their rates of synonymous substitution are significantly different from the remaining genes.
- About 3% of the rat genome is in large segmental duplications, a fraction intermediate between mouse (1–2%) and human (5–6%). These occur predominantly in pericentromeric regions. Recent expansions of major gene families are due to these genomic duplications.
- The eutherian core of the rat genome—that is, bases that align orthologously to mouse and human—comprises a billion nucleotides (~40% of the euchromatic rat genome) and contains the vast majority of exons and known regulatory elements (1–2% of the genome). A portion of this core constituting 5–6% of the genome appears to be under selective constraint in rodents and primates, while the remainder appears to be evolving neutrally.
- Approximately 30% of the rat genome aligns only with mouse, a considerable portion of which is rodent-specific repeats. Of the non-aligning portion, at least half is rat-specific repeats.
- More genomic changes occurred in the rodent lineages than the

primate: (1) These rodent genomic changes include approximately 250 large rearrangements between a hypothetical murid ancestor and human, approximately 50 from the murid ancestor to rat, and about the same from the murid ancestor to mouse. (2) A threefold-higher rate of base substitution in neutral DNA is found along the rodent lineage when compared with the human lineage, with the rate on the rat branch 5–10% higher than along the mouse branch. (3) Microdeletions occur at an approximately twofold-higher rate than microinsertions in both rat and mouse branches.

- A strong correlation exists between local rates of microinsertions and microdeletions, transposable element insertion, and nucleotide substitutions since divergence of rat and mouse, even though these events occurred independently in the two lineages.

Background

History of the rat

The rat, hated and loved at once, is both scourge and servant to mankind. The "Devil's Lapdog" is the first sign in the Chinese zodiac and traditionally carries the Hindu god Ganesh⁴. Rats are a reservoir of pathogens, known to carry over 70 diseases. They are involved in the transmission of infectious diseases to man, including cholera, bubonic plague, typhus, leptospirosis, cowpox and hantavirus infections. The rat remains a major pest, contributing to famine with other rodents by eating around one-fifth of the world's food harvest.

Paradoxically, the rat's contribution to human health cannot be overestimated, from testing new drugs, to understanding essential nutrients, to increasing knowledge of the pathobiology of human disease. In many parts of the world the rat remains a source of meat.

The laboratory rat (*R. norvegicus*) originated in central Asia and its success at spreading throughout the world can be directly attributed to its relationship with humans⁷. J. Berkenhout, in his 1769 treatise *Outline of the Natural History of Great Britain*, mistakenly took it to be from Norway and used *R. norvegicus* Berkenhout in the first formal Linnaean description of the species. Whereas the black rat (*Rattus rattus*) was part of the European landscape from at least the third century AD and is the species associated with the spread of bubonic plague, *R. norvegicus* probably originated in northern China and migrated to Europe somewhere

around the eighteenth century⁸. They may have entered Europe after an earthquake in 1727 by swimming the Volga river.

The rat in research

R. norvegicus was the first mammalian species to be domesticated for scientific research, with work dating to before 1828 (ref. 9). The first recorded breeding colony for rats was established in 1856 (ref. 9). Rat genetics had a surprisingly early start. The first studies by Crampe from 1877 to 1885 focused on the inheritance of coat colour¹⁰. Following the rediscovery of Mendel's laws at the turn of the century, Bateson used these concepts in 1903 to demonstrate that rat coat colour is a mendelian trait¹⁰. The first inbred rat strain, PA, was established by King in 1909, the same year that systematic inbreeding began for the mouse¹⁰. Despite this, the mouse became the dominant model for mammalian geneticists, while the rat became the model of choice for physiologists, nutritionists and other biomedical researchers. Nevertheless, there are over 234 inbred strains of *R. norvegicus* developed by selective breeding, which 'fixes' natural disease alleles in particular strains or colonies¹¹.

Over the past century, the role of the rat in medicine has transformed from carrier of contagious diseases to indispensable tool in experimental medicine and drug development. Current examples of use of the rat in human medical research include surgery¹², transplantation^{13–15}, cancer^{16,17}, diabetes^{18,19}, psychiatric disorders²⁰ including behavioural intervention²¹ and addiction²², neural regeneration^{23,24}, wound^{25,26} and bone healing²⁷, space motion sickness²⁸, and cardiovascular disease^{29–31}. In drug development, the rat is routinely employed both to demonstrate therapeutic efficacy^{15,32,33} and to assess toxicity of novel therapeutic compounds before human clinical trials^{34–37}.

The Rat Genome Project

Over the past decade, investigators and funding agencies have participated in rat genomics to develop valuable resources. Before the launch of the Rat Genome Sequencing Project (RGSP), there was much debate about the overall value of the rat genome sequence and its contribution to the utility of the rat as a model organism. The debate was fuelled by the naive belief that the rat and mouse were so similar morphologically and evolutionarily that the rat sequence would be redundant. Nevertheless, an effort spearheaded by two NIH agencies (NHGRI and NHLBI) culminated in the formation of the RGSP Consortium (RGSPC).

The RGSP was to generate a draft sequence of the rat genome, and, unlike the comparable human and mouse projects, errors would not ultimately be corrected in a finished sequence³⁸. Consequently, the draft quality was critical. Although it was expected to have gaps and areas of inaccuracy, the overall sequence quality had to be high enough to support detailed analyses.

The BN rat was selected as a sequencing target by the research community. An inbred animal (BN/SsNHsd) was obtained by the Medical College of Wisconsin (MCW) from Harlan Sprague Dawley. Microsatellite studies indicated heterozygosity, so over 13 generations of additional inbreeding were performed at the MCW, resulting in BN/SsNHsd/Mcw animals. Most of the sequence data were from two females, with a small amount of whole genome shotgun (WGS) and flow-sorted Y chromosome sequencing from a male. The Y chromosome is not included in the current assembly.

A network of centres generated data and resources, led by the Baylor College of Medicine Human Genome Sequencing Center (BCM-HGSC) and including Celera Genomics, the Genome Therapeutics Corporation, the British Columbia Cancer Agency Genome Sciences Centre, The Institute for Genomic Research, the University of Utah, the Medical College of Wisconsin, The Children's Hospital of Oakland Research Institute, and the Max Delbrück Center for Molecular Medicine, Berlin. After assembly of the genome at the

BCM-HGSC, analysis was performed by an international team, representing over 20 groups in six countries and relying largely on gene and protein predictions produced by Ensembl.

Determination of the genome sequence

Atlas and the 'combined' sequencing strategy

Despite progress in assembling draft sequences^{2,3,39–44} the question of which method produces the highest-quality products is unresolved. A significant issue is the choice between logistically simpler WGS approaches versus more complex strategies employing bacterial artificial chromosome (BAC) clones^{45–48}. In the Public Human Genome Project² a BAC by BAC hierarchical approach was used and provided advantages in assembling difficult parts of the genome. The draft mouse sequence was a pure WGS approach using the ARACHNE assembler^{3,49,50} but underrepresented duplicated regions owing to 'collapses' in the assembly^{3,51–53}. This limitation of the mouse draft sequence was tolerable owing to the planned full use of BAC clones in constructing the final finished sequence.

The RGSPC opted to develop a 'combined' approach using both WGS and BAC sequencing (Fig. 1). In the combined approach, WGS data are progressively melded with light sequence coverage of individual BACs (BAC skims) to yield intermediate products called 'enriched BACs' (eBACs). eBACs covering the whole genome are then joined into longer structures (bactigs). Bactigs are joined to form larger structures: superbactigs, then ultrabactigs. During this process other data are introduced, including BAC end sequences, DNA fingerprints and other long-range information (genetic markers, syntenic information), but the process is constrained by eBAC structures.

To execute the combined strategy we developed the *Atlas* software package⁵⁴ (Fig. 1). The *Atlas* suite includes a 'BAC-Fisher' component that performs the functions needed to generate eBACs. WGS genome coverage was generated ahead of complete BAC coverage, so a BAC-Fisher web server was established at the BCM-HGSC to enable users to access the combined BAC and WGS reads as each BAC was processed (see Methods for data access). Each eBAC is assembled with high stringency to represent the local sequence accurately, and so provide a valuable intermediate product that assists all users of the genome data. Additional *Atlas* modules joined eBACs and linked bactigs to give the complete assembly (Fig. 1). Overall, the combined approach takes advantage of the strengths of both previous methods, with few of the disadvantages.

Sequence and genome data

Over 44 million DNA sequence reads were generated (Table 1; Methods). Following removal of low-quality reads and vector contaminants, 36 million reads were used for *Atlas* assembly, which retained 34 million reads. This was 7× sequence coverage with 60% provided by WGS and 40% from BACs. Slightly different estimates came from considering the entire 'trimmed' length of the sequence data (7.3×), or only the portion of Phred20 quality or higher (6.9×).

The sequence data were end-reads from clones either derived directly from the genome (insert sizes of <10 kb, 10 kb, 50 kb and >150 kb) or from small insert plasmids subcloned from BACs. Overall, these provided 42-fold clone coverage, with 32-fold coverage having both paired ends represented. Approximately equal contributions of clone coverage were from the different categories.

Over 21,000 BACs were used for BAC skims (1.6× coverage) with an average sequence depth of 1.8×, giving an overall 2.8× genomic sequence coverage from BACs. This was slightly more than the most efficient procedure would require (~1.2× each), because the genome size was not known at the project start.

Simultaneous with sequencing, 199,782 clones from the CHORI-230 BAC library⁵⁵ were fingerprinted by restriction enzyme

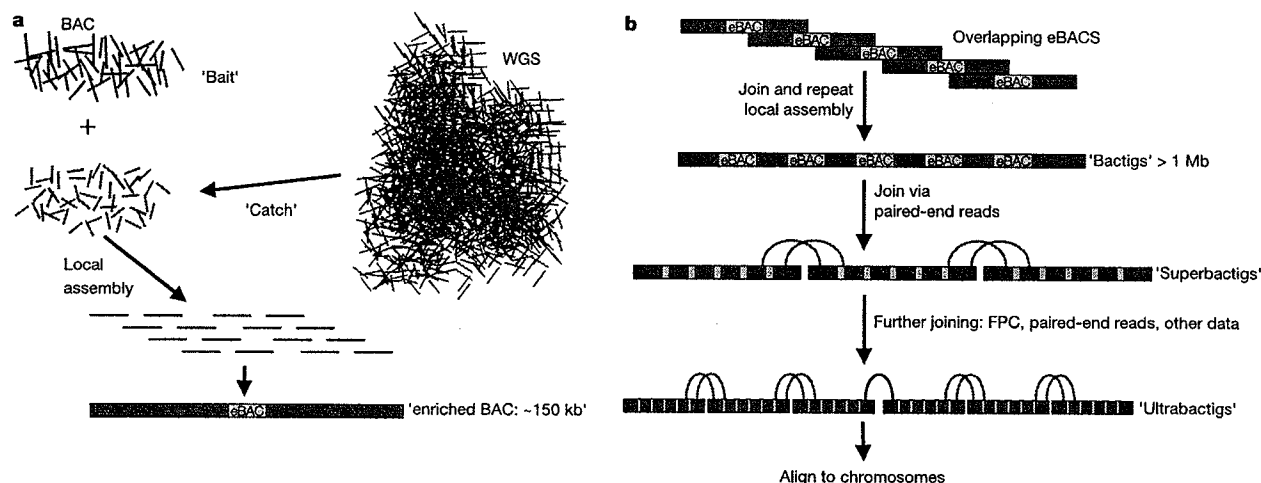


Figure 1 The new 'combined' sequence strategy and *Atlas* software. **a**, Formation of 'eBACs'. The RGSP strategy combined the advantages of both BAC and WGS sequence data⁶⁴. Modest sequence coverage (~1.8-fold) from a BAC is used as 'bait' to 'catch' WGS reads from the same region of the genome. These reads, and their mate pairs, are assembled using Phrap to form an eBAC. This stringent local assembly retains 95% of the 'catch'. **b**, Creation of higher-order structures. Multiple eBACs are assembled into bactigs

based on sequence overlaps. The bactigs are joined into superbactigs by large clone mate-pair information (at least two links), extended into ultrabactigs using additional information (single links, FPC contigs, synteny, markers), and ultimately aligned to genome mapping data (radiation hybrid and physical maps) to form the complete assembly.

digestion, representing 12-fold genomic coverage⁵⁶ (Methods). These were assembled into a 'fingerprint contig (FPC)' map (a contig is a set of overlapping segments of DNA) containing 11,274 FPCs. BAC selection for sequence skimming was based on overlaps between BACs using FPC mapping⁵⁶ (M.K. and C.F., unpublished work), ongoing BAC end sequencing (S.Z., unpublished work), and BAC sequence skimming⁵⁷. This strategy led to the sequence of a tiling path of BAC clones, covering the whole genome. In addition to the FPC map, a yeast artificial chromosome (YAC)-based physical map was constructed. 5,803 BAC and P1-derived artificial chromosome (PAC) clones from RPCI-32 and RPCI-31 libraries⁵⁵, respectively, were anchored to 51,323 YAC clones originating from two tenfold-coverage YAC libraries^{58,225} assembled into 605 contigs⁵⁶. This map was subsequently integrated with the FPC map and the sequence assembly, reducing the total number of map contigs to 376 (minimum length of contig containing the 'typical' nucleotide, $N_{50} = 172$ clones, 4.4 Mb; 358 anchored to the sequence assembly; Supplementary Information).

The combined strategy enabled development of resources such as the FPC map, BAC end sequences, and BAC skim sequences in parallel, rather than sequentially. In addition to allowing ongoing

quality checking, this permitted the data-gathering phase of the project to be completed in less than two years.

Atlas assembly

Statistics for the Rnor3.1 assembly are in Table 2. Contigs within eBACs were ordered and oriented using read-pair information. Read-pair information was also used to add WGS reads to eBACs, even when sequence overlaps could not be reliably detected owing to repeated sequences. BAC skim reads with repeats were included in the assembly of eBACs because they clearly originated within BAC insert sequences. Over 19,000 eBACs were eventually generated.

More than 98% of eBACs were successfully merged to form bactigs (Fig. 1). Bactigs were subsequently reassembled to process all reads from overlapping BACs simultaneously, and then ordered and oriented with respect to each other using FPC map and BAC end sequence read-pair information. These superbactig and ultrabactig structures (see below) were aligned with chromosomes using external information, such as positions of genetic markers. Ultrabactigs represented the largest sequence units used to build chromosomes.

The current release of the rat genome assembly, version Rnor3.1,

Table 1 Clones and reads used in the RGSP

Insert size* (kb)	Source or vector	Reads (millions)				Bases (billions)		Sequence coverage†		Clone coverage‡
		All§	Used	Paired	Assembled	Trimmed	≥Phred20	Trimmed	≥Phred20	
2–4	Plasmid	9.6	8.6	7.4	7.9	4.8	4.5	1.8	1.6	3.70
4.5–7.5	Plasmid	4.5	4.3	3.6	3.6	2.4	2.3	0.87	0.82	2.96
10	Plasmid	8.4	7.2	6.4	6.4	4.1	3.8	1.5	1.4	11.63
50	Plasmid	1.7	1.3	1.0	1.1	0.69	0.65	0.25	0.24	9.47
150–250	BAC	0.32	0.31	0.26	0.26	0.18	0.16	0.07	0.06	9.26
Total WGS		24.5	21.7	18.7	19.2	12.1	11.3	4.4	4.1	37.0
2–5	BAC skims	19.6	14.6	13.2	14.5	8.0	7.7	2.9	2.8	4.8
Total		44.1	36.3	31.9	33.7	20.2	19.0	7.3	6.9	41.8

*Grouped in ranges of sizes for individual libraries tracked to specific multiples of 0.5 kb.

†Total bases in used reads divided by sampled genome size including all cloned and sequenced euchromatic or heterochromatic regions.

‡Estimated as sum of insert sizes divided by sampled genome size.

§WGS reads available on the NCBI Trace Archive as of 21 March 2003; BAC skim reads attempted at BCM-HGSC as of 12 May 2003; BAC end reads obtained directly from TIGR.

||Refers to coverage from 2–5 kb subclones from BACs. The BACs that were skimmed amounted to 1.58 × clone coverage.

Table 2 Statistics of the RGSP draft sequence assembly

Features*	Number	N50 length (kb)	Bases (Gb)	Bases plus gaps† (Gb)	Percentage of genome‡			
					Sampled (2.78 Gb)		Assembled (2.75 Gb)	
					Bases	Bases + gaps	Bases	Bases + gaps
Anchored contigs	127,810	38	2.476	2.481	89.1	89.2	90.0	90.2
Anchored superbactig scaffolds	783	5,402	2.476	2.509	89.1	90.3	90.0	91.2
Anchored ultrabactigs	291	18,985	2.476	2.687	89.1	96.6	90.0	97.7
Unanchored superbactigs, main scaffolds	134	1,210	0.056	0.062	2.0	2.2	2.0	2.3
Unanchored ultrabactigs	128	1,529	0.056	0.069	2.0	2.5	2.0	2.5
All superbactigs, main scaffolds	917	5,301	2.533	2.571	91.1	92.5	92.1	93.5
Minor scaffolds	4,345	8	0.033	0.038	1.2	1.4	1.2	1.4

*Anchored sequences are those that can be placed on chromosomes because they contain known markers. The main scaffold for each superbactig is the largest set of contigs (in terms of total contig sequence) that can be ordered and oriented using mate-pair links and ordering of BACs. Scaffolds that cannot be ordered and oriented with respect to the main scaffold are termed minor scaffolds.

†Ambiguous bases (N) are counted in the gap sizes, and excluded in the base counts.

‡Computed as bases plus gaps divided by estimated genome size. Sampled genome size is based on oligonucleotide frequency statistics of unassembled WGS reads. Assembled genome size is based on cumulative contig sequence following assembly.

was generated using the data in Table 1. Earlier releases (Rnor2.0/2.1, Methods) were used for a substantial part of the annotation and analysis of genes and proteins, whereas the current release provided the genome description. Rnor3.1 has 128,000 contigs, with N_{50} length 38 kb—larger than the expected genomic extent of a mammalian gene. These sequence contigs were linked into 783 superbactigs that were anchored to the radiation hybrid map⁵⁹. These larger units had N_{50} length 5.4 Mb. Another 134 smaller superbactigs (N_{50} length 1.2 Mb) could not be anchored, presumably because they fell into gaps between markers or because they were in repeated regions that could not be unambiguously placed. From placement on the radiation hybrid map, adjacent superbactigs were further linked to maximize continuity of sequence if appropriate read-pair mates existed or FPC suggested links. This reduced linked superbactigs to 419 pieces with 71 singletons. 291 ultrabactigs with N_{50} length of nearly 19 Mb were placed on chromosomes. Orthology information with mouse and human sequences was also used to resolve conflicts and suggest placement of sequence units. Most of the 128 unplaced units were either singletons or small superbactigs that consisted of few clones. Thus, nearly the entire genome was represented in less than 300 large sequence units.

Quality assessment

Thirteen megabases of high-quality finished rat sequence from BACs were available for comparison with Rnor3.1 (Methods). This analysis showed that the majority of draft bases from within contigs were high quality (1.32 mismatches per 10 kb). This is essentially the accepted accuracy standard for finished sequence (1.0 errors per 10 kb)⁶⁰, so the overwhelming majority of contig bases are highly accurate. The highest frequency of mismatches occurred at the ends of contigs. We calculate the average size of these lower-accuracy regions to be 750 base pairs (bp) and they amount to less than 0.9% of the genome. These regions arise from misassembly of terminal reads due to repeated sequences.

Few mismatches were found within contigs. Six were found within contigs when compared with the 13 Mb of finished sequence, or one case per 2.2 Mb. All were insertions or deletions and may represent polymorphisms. Thus, at the fine structure level, the bulk of sequences that make up contigs is nearly the quality of finished sequence.

We judged accuracy of assembly at the chromosomal level by alignment with linkage maps⁶¹ and radiation hybrid map⁵⁹ (Fig. 2). Thirteen markers out of 3,824 from the SHRSP × BN genetic map were placed on different chromosomes in the assembly and in the genetic map. Similarly, of the 20,490 sequence tagged sites placed on both the assembly and radiation hybrid (v3.4) map, 96.9% had consistent chromosome placement⁵⁹. Initial alignments identified regions of misassembly, and these were corrected, so that in Rnor3.1 the maps are congruent except for possible mismapped markers. The distribution of assembled sequence among the chromo-

somes and chromosome sizes in Rnor3.1 are in Supplementary Table SI-2.

Landscape and evolution of the rat genome

Genome size

Genomic assemblies are usually smaller than the actual genome size owing to under-representation of sequences affected by cloning bias, and sequencing and assembly difficulties. Simply equating the assembled genome size with the euchromatic, cloneable portion does not take into account heterochromatin that may be included⁶². We therefore estimated both an assembled genome size, scaled by the inverse of the fraction of features (genetic markers, expressed sequence tags (ESTs), and so on) found in the Rnor3.1 assembly, and a cloneable (or sampled) genome size, which was the part of the genome present in the WGS reads before assembly, as measured by analysing the distribution of short oligomers⁶³. The former may be an underestimate because non-repetitive, easily assembled regions can be enriched for known features. The latter should be an overestimate because there are likely to be regions (such as repeats) that can be cloned and sequenced, but not assembled.

For the rat genome, the assembled and cloneable genome sizes are very close. Considering the fraction of the marker set successfully mapped to Rnor3.1 (92%), or the fraction of sequence finished outside the BCM-HGSC (to reduce bias) present in Rnor3.1 (91%), together with the assembled bases in main scaffolds (2.533 Gb, Table 2), we suggest a genome size of 2.75 Gb. Alternatively, analysis of the WGS oligomers of length 24 to 32 predicted a genome size of between 2.76 and 2.81 billion bases. We have used the more conservative value of 2.75 Gb for the rat genome size, but this is

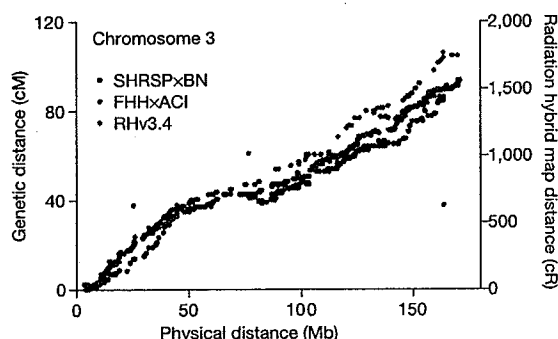


Figure 2 Map correspondence. Correspondence between positions of markers on two genetic maps of the rat (SHRSP × BN intercross and FHH × ACI intercross⁶¹), on the radiation hybrid map⁵⁹, and their position on the rat genome assembly (Rnor3.1).

still considerably higher (150 Mb) than the 2.6 Gb currently reported for the mouse draft genome sequence. A fraction of the size differences in these rodent genomes results from the different repeat content (see below); however, it is also recognized that segmental duplications may be under-represented in the mouse WGS draft sequence for technical reasons^{3,51}.

Telomeres, centromeres and mitochondrial sequence

The rat has both metacentric and telocentric chromosomes, in contrast to the wholly telocentric mouse chromosomes. As expected from previous draft sequences, the rat draft does not contain complete telomeres or centromeres. Their physical location relative to the rat draft sequence can however be approximated; the centromeres of the telocentric rat chromosomes (2, 4–10 and X) must be positioned before nucleotide 1 of these assemblies, and those for the remaining chromosomes are estimated as indicated in Fig. 3. Several of these putative centromere positions coincide with both segmental duplication blocks (see below) and classical satellite

clusters, consistent with enrichment of both of these sequence features in rat pericentromeric DNA. Human subtelomere regions are characterized by both an abundance of segmentally duplicated DNA and an enrichment of internal (TTAGGG)_n-like sequence islands⁶⁴. Approximately one-third of the euchromatic rat subtelomeric regions are similarly enriched, suggesting that Rnor3.1 might extend very close to the chromosome ends.

Fragments of the rat mitochondrial genome were also propagated within the WGS libraries and subsequently sequenced, allowing the assembly of the complete 16,313 bp mitochondrial genome (Supplementary Information). Comparison with existing mitochondrial sequences in the public databases revealed variable positions totalling 95 bp (0.6%) between this strain and the wild brown rat. Considerably more variation (2.2%) was found when compared with the Wistar strain: 357 bp differences over the whole genome, including 78 positions that are conserved in the other mammalian sequences. Such variation has also been reported in mouse mitochondrial sequences and attributed to errors in previously

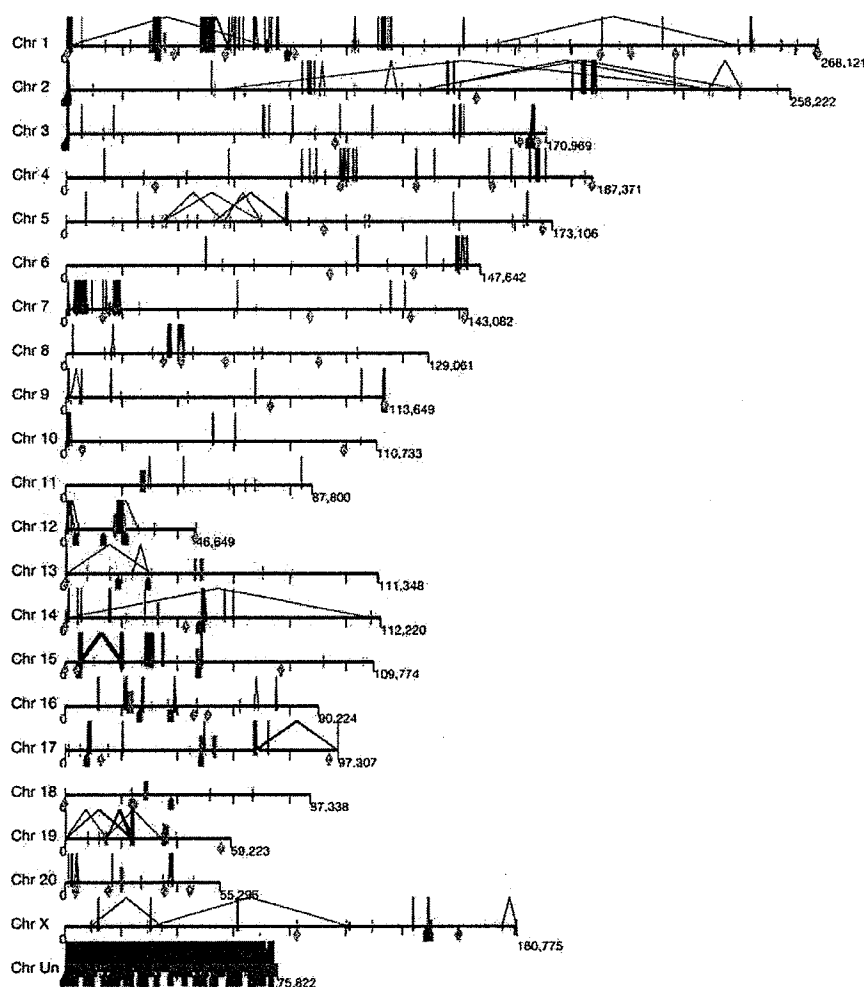


Figure 3 Distribution of segmental duplications in the rat genome. Interchromosomal duplications (red) and intrachromosomal duplications (blue) are depicted for all duplications with $\geq 90\%$ sequence identity and ≥ 20 kb length. The intrachromosomal duplications are drawn with connecting blue line segments; those with no apparent connectors are local duplications (spaced below the figure resolution limit). p arms are on the left and the q arms on the right. Chromosomes 2, 4–10, and X are telocentric; the assemblies begin with pericentric sequences of the q arms, and no centromeres are indicated. For the remaining chromosomes, the approximate centromere positions were

estimated from the most proximal STS/gene marker to the p and q arm as determined by fluorescent *in situ* hybridization (FISH) (cyan vertical lines; no chromosome 3 data). The 'Chr Un' sequence consists of contigs not incorporated into any chromosomes. Green arrows indicate 1 Mb intervals with more than tenfold enrichment of classic rat satellite repeats within the assembly. Orange diamonds indicate 1 Mb intervals with more than tenfold enrichment of internal (TTAGGG)_n-like sequences. For more detail see <http://ratparalogy.cwru.edu>.

sequenced genomes⁶⁵. The current sequence is very accurate, and we therefore favour the BN sequence as a reference for the rat mitochondrial genome.

Orthologous chromosomal segments and large-scale rearrangements

Multi-megabase segments of the chromosomes of the primate-rodent ancestor have been passed on to human and murid rodent descendants with minimal rearrangements of gene order^{66–68}. These intact regions, which are bounded by the breaks that occurred during ancient large-scale chromosomal rearrangements, are referred to as orthologous chromosomal segments. The same phenomenon has occurred in the descent of the rat and mouse from the genome of their common murid ancestor, and we were able to use the human genome, and in some cases other outgroup data, to tentatively reconstruct the sequence of many of these rearrangements in these lineages. To visualize the extent of orthologous chromosomal segments, each genome was 'painted' with the orthologous segments of the other two species (Fig. 4) using the Virtual Genome Painting method (M.L.G.-G. *et al.*, unpublished work; <http://www.genboree.org>). Inspection shows the interleaving of events that both preceded and occurred subsequently to the rat-mouse divergence.

Comparing the three species at 1 Mb resolution, BLASTZ⁶⁹, PatternHunter/Grimm-Synten^{70,71}, Pash⁷², and associated merging algorithms^{66,72,73} produce virtually indistinguishable sets of orthologous chromosomal segments. PatternHunter and the GRIMM-Synten algorithm⁷³ detect 278 orthologous segments between human and rat, and 280 between human and mouse. The mouse-rat comparison reveals a smaller number of segments (105) of larger average size. The larger number of breaks in orthologous segments between the human to the rodent pair is expected, because of the

latter's closer evolutionary relationship.

Understanding the number and timing of rearrangement events that have occurred in each of the three individual lineages (see tree in Fig. 5a) since the common primate-rodent ancestor required a more detailed analysis. We initially focused on the X chromosome, because rearrangements between the X and the autosomes are rare⁷⁴ and its history is somewhat easier to trace completely. The X chromosome consists of 16 human-mouse-rat orthologous segments of at least 300 kb in size⁷⁵ (Fig. 6a). In the most parsimonious scenario (found with MGR and GRIMM⁷⁵), these were created by 15 inversions in the descent from the primate-rodent ancestor (Fig. 6b). Outgroup data from cat, cow⁷⁶ and dog⁷⁷ resolved the timing of these rearrangements more precisely. Most of these events occurred in the rodent lineage: five (or four) before the divergence of rat and mouse, five in the rat lineage, and five in the mouse lineage. At most one rearrangement occurred in the human lineage since divergence from the common ancestor with rodents. The timing of this one event was ambiguous, owing to the limited resolution of the outgroup data. Even given this uncertainty, it is clear that the large-scale architecture of the X chromosome in humans is largely unchanged since the primate-rodent ancestor⁷³, whereas there has been considerable activity in the rodents. The assignment of the accelerated activity to the rodent branch, following the primate-rodent divergence, is consistent with previous studies at significantly lower resolution (these showed complete conservation of marker order between the X chromosomes of human and cat⁷⁸, human and dog⁷⁷, and human and lemur⁷⁹, as well as similar karyotypes of the X chromosomes in human, chimpanzees, gorillas and orangutans⁸⁰).

Large-scale reconstruction of the entire ancestral murid genome suggests that it retained many previously postulated chromosome associations of the placental ancestor^{81,82}. The most parsimonious scenario we found requires a total of 353 rearrangements: 247 between the murid ancestor and human, 50 from the murid ancestor to mouse and 56 from the murid ancestor to rat. A recent study⁸² implies that most of the 247 rearrangements between the murid ancestor and human occurred on the evolutionary subpath from the squirrel-mouse-rat ancestor to the murid ancestor. Our

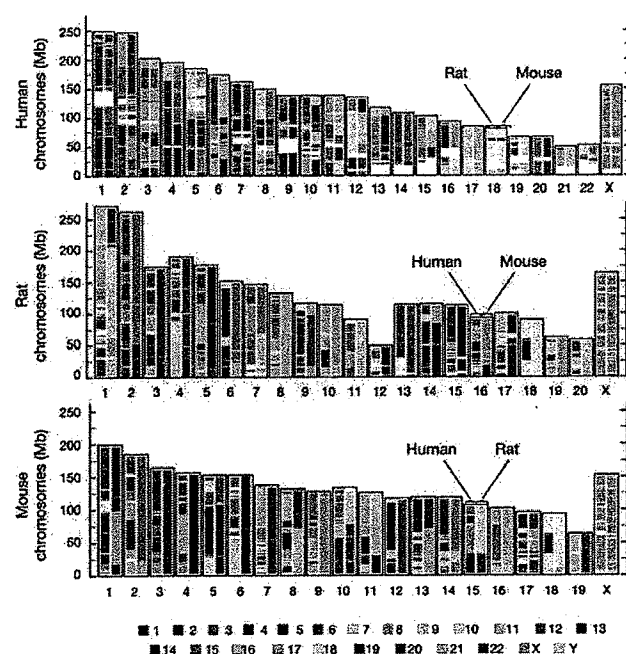
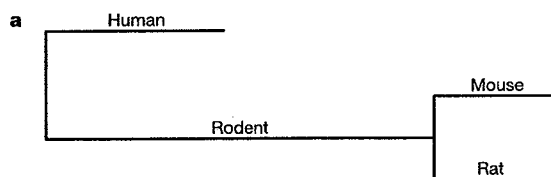


Figure 4 Map of conserved synteny between the human, mouse and rat genomes. For each species, each chromosome (x axis) is a two-column boxed pane (p arm at the bottom) coloured according to conserved synteny to chromosomes of the other two species. The same chromosome colour code is used for all species (indicated below). For example, the first 30 Mb of mouse chromosome 15 is shown to be similar to part of human chromosome 5 (by the red in left column) and part of rat chromosome 2 (by the olive in right column). An interactive version is accessible (<http://www.genboree.org>).



b	Substitutions, insertions and deletions			
	Human	Rodent	Mouse	Rat
Substitutions per site	0.11 ± 0.0012	0.24 ± 0.0012	0.073 ± 0.0014	0.077 ± 0.006
Substitutions in neutral sites only	0.13 ± 0.011	0.28 ± 0.033	0.083 ± 0.013	0.091 ± 0.011
Insertion events per kb	2.7 ± 0.94	4.74 ± 1.0	1.54 ± 0.84	1.43 ± 0.73
Deletion events per kb	5.3 ± 0.55	12 ± 1.2	3.8 ± 0.21	4.5 ± 0.13
Inserted bases per kb	6.4 ± 2.9	9.4 ± 1.6	3.6 ± 1.5	3.2 ± 1.3
Deleted bases per kb	18 ± 2.0	40 ± 4.9	11 ± 0.55	13 ± 0.05

Figure 5 Substitutions and microindels (1–10 bp) in the evolution of the human, mouse and rat genomes. **a**, The lengths of the labelled branches in the tree are proportional to the number of substitutions per site inferred using the REV model²²² from all sites with aligned bases in all three genomes. **b**, The table shows the midpoint and variation in these branch-length estimates when estimated from different sequence alignment programs and different neutral sites, including sites from ancestral repeats³, fourfold degenerate sites in codons, and rodent-specific sites ('in neutral sites only' row; Supplementary Information). Other rows give midpoints and variation for micro-indels on each branch of the tree in **a**.

analyses confirm that the rate of rearrangements in murid rodents is much higher than in the human lineage⁷³.

Segmental duplications

Segmental duplications are defined here as regions of the genome that are repeated over at least 5 kb of length and >90% identity. The rat has approximately 2.9% of its bases in these duplicated regions (Fig. 3), whereas the human genome has 5–6%⁸³. In contrast to the greater rate of large-scale rearrangement, the mouse genome shows substantially fewer of these events³, with only 1.0–2.0%⁵¹ of its sequenced bases in duplicated regions. These duplicated structures are particularly challenging to assemble, and we attribute at least some of the mouse–rat differences to the BAC-based approach we used for Rnor3.1, compared with the WGS mouse approach. The vast majority of these sequences (73 of 82 Mb) were regions with <99.5% identity and thus were not simply overlapping sequences that had not been joined by the assembly program Phrap. The ‘unplaced’ chromosome in Rnor3.1 showed a marked enrichment for blocks of segmental duplication (nearly 44% of the total), which indicates problems with anchoring these elements to the genome.

Intrachromosomal duplications are represented at a three-to-one excess when compared with interchromosomal duplications, and are significantly enriched near the telomeres and in centromeric regions (Fig. 3). The pericentromeric accumulation of segmental duplications in the rat is reminiscent of that observed in human and mouse^{83–86}, and seems to be a general property of mammalian chromosome architecture.

We observed considerable clustering of duplications⁸⁷, including 41 discrete genomic regions larger than 1 Mb in size in which duplications appear to be organized into groups with <100 kb

between duplicated segments. For many of these clusters, the underlying sequence alignments showed a wide range in the degree of sequence identity, suggesting that these areas have been subject to duplication events more or less continuously over millions of years. In contrast, an analysis of the evolutionary distance between all duplicated regions showed an unusual bimodal distribution, particularly for intrachromosomal segmental duplications. Two peaks were observed at 0.045 substitutions per site and 0.075 substitutions per site. Given that the rat genome has accumulated 8–10% substitutions (see below) since the speciation from mouse 12–24 Myr ago, this bimodal distribution may correspond to bursts of segmental duplication that occurred approximately 5 and 8 Myr ago, respectively.

The segmental duplications in the rat genome were of considerable interest because they represent an important mechanism for the generation of new genes. We found that 63 NCBI reference sequence⁸⁸ (RefSeq; see <http://www.ncbi.nih.gov/RefSeq/>) genes were located completely or partially within rat duplicated regions, out of a genome total of 4,532 rat RefSeq genes. As discussed below, many of these genes are present in multiple copies and belong to gene families that have been recently duplicated and contribute to distinctive elements of rat biology.

Gains and losses of DNA

In addition to large rearrangements and segmental duplications, genome architecture is strongly influenced by insertion and deletion events that add and remove DNA over evolutionary time. To characterize the origins and losses of sequence elements in the human, mouse and rat genomes, we categorized all the nucleotides in each of the three genomes, using our alignment data and

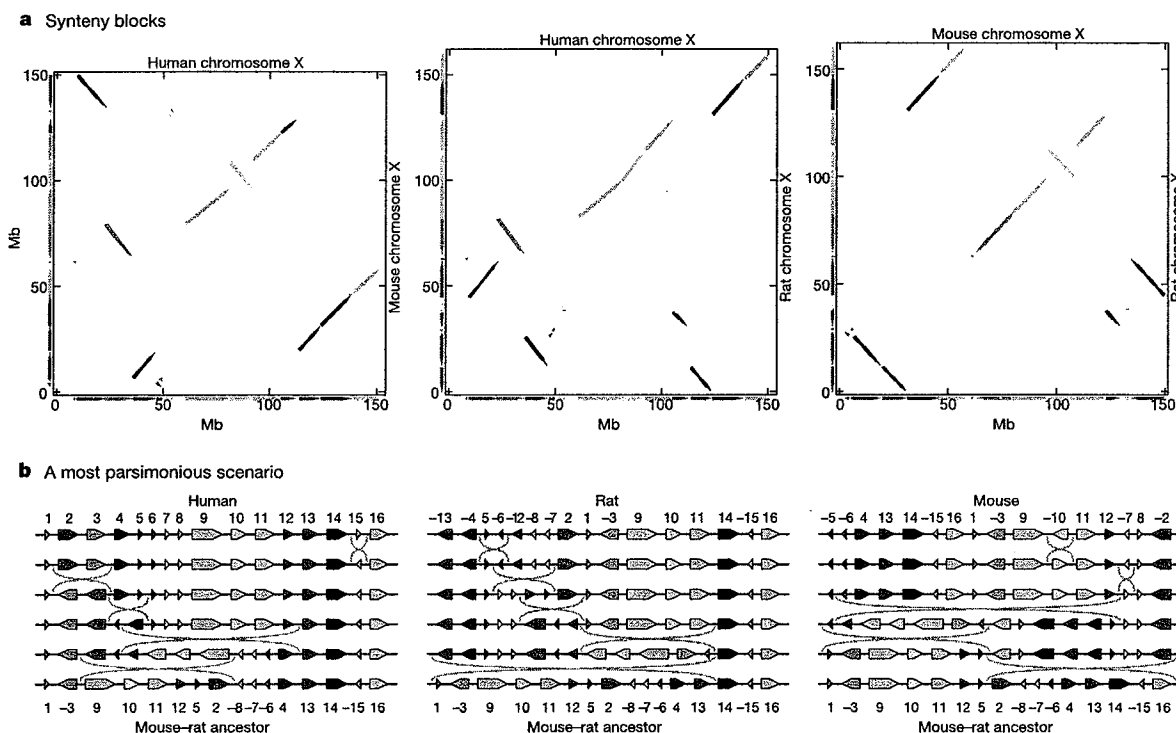


Figure 6 X chromosome in each pair of species. **a**, GRIMM-Synteny⁷¹ computes 16 three-way orthologous segments (≥ 300 kb) on the X chromosome of human, mouse and rat, shown for each pair of species, using consistent colours. **b**, The arrangement (order and orientation) of the 16 blocks implies that at least 15 rearrangement events occurred during X chromosome evolution of these species. The program MGR (<http://www.cs.ucsd.edu/groups/bioinformatics/MGR/>) determined that evolutionary scenarios

with 15 events are achievable and all have the same median ancestor (located at the last common mouse–rat ancestor). Shown is a possible (not unique) most parsimonious inversion scenario from each species to that ancestor. We note that the last common ancestor of human, mouse and rat should be on the evolutionary path between this median ancestor and human.

RepeatMasker annotations of the insertions of repetitive elements (Fig. 7). The rodent repeat database used by RepeatMasker was greatly expanded by analysing the rat and mouse genomes⁸⁹, but it is clear that not all repeats are being recognized, especially the older ones. Thus, these estimates of the amount of rodent repeats represent lower bounds.

About a billion nucleotides (39% of the euchromatic rat genome) align in all three species, constituting an 'ancestral core' that is retained in these genomes. This ancestral core contains 94–95% of the known coding exons and regulatory regions. Comparisons between the human and mouse genomes, using transposon relics retained in both species ('mammalian ancestral repeats') to model neutral evolution, have been used to estimate the fraction of the human genome that is accumulating substitutions more slowly than the neutral rate in both lineages since their divergence, and hence may be under some level of purifying selection³. Depending on details of methodology, such estimates have ranged between about 4% and 7%^{3,90,91}. The levels of three-way conservation observed here between the human, mouse and rat genomes in the ancestral core lend further support to these earlier estimates, giving values in the range of 5–6% when measured by two quite different methods (see Methods and ref. 92). In this constrained fraction, non-coding regions outnumber coding regions regardless of the strength of constraint⁹², an observation that supports recent comparative

analyses limited to subsets of the genome^{93,94}. The preponderance of non-coding elements in the most constrained fraction of the genome underscores the likelihood that they play critical roles in mammalian biology.

About 700 Mb (28%) of the rat euchromatic genome aligns only with the mouse. At least 40% of this comprises of rodent-specific repeats inserted on the branch from the primate–rodent ancestor to the murid ancestor, and some of the remainder can be recognized as mammalian ancestral repeats whose orthologues were deleted in the human lineage (Fig. 7). Another part is likely to consist of single-copy ancestral DNA deleted in the human lineage but retained in rodents. Although this 700 Mb of rodent-specific DNA is primarily neutral, it may also contain some functional elements lost in the human lineage in addition to sequences representing gains of rodent-specific functions, including some coding exons⁹⁵.

The remainder of the euchromatic rat genome (726 Mb, 29%) aligns with neither mouse nor human (Fig. 7). At least half of this (15% of the rat genome) consists of rat-specific repeats, and another large fraction (8% of the rat genome) consists of rodent-specific repeats whose orthologues are deleted in the mouse.

Substitution rates

The alignment data allow relatively precise estimates of the rates of neutral substitutions and microindel events (≤ 10 bp). Both synonymous fourfold degenerate ('4D') sites in protein-coding regions and sites in mammalian ancestral repeats were used in this analysis, as in previous studies comparing human and mouse^{3,96}. We additionally used a class of primarily neutral sites whose identification is made uniquely possible by the addition of the rat genome sequence: namely, the rodent-specific sites discussed above, identified by their failure to align to human sequence.

Our estimates for the neutral substitution level between the two rodents range from 0.15 to 0.20 substitutions per site, while estimates for the entire tree of human, mouse and rat range from 0.52 to 0.65 substitutions per site (Fig. 5). This difference was predictable because of the evolutionary closeness of the two rodents. For all classes of neutral sites analysed, however, the branch connecting the rat to the common rodent ancestor is 5–10% longer than the mouse branch (Fig. 5a). Thus, for as yet unknown reasons, the rat lineage has accumulated substantially more point substitutions than the mouse lineage since their last common ancestor.

We also analysed four-way alignments including sequence from orthologous ancestral repeats in human, mouse and rat, along with the repeat consensus sequences, which approximate the sequence of the progenitor of the corresponding repeat family (Methods). These alignments allow us to distinguish substitutions on the branch from the primate–rodent ancestor to the rodent ancestor from substitutions on the branch descending to human⁷⁷. This revealed an overall speed-up in rodent substitution rates relative to human of about three-to-one, larger than estimated previously³, but consistent with other more recent studies which also use multiple sequence alignments^{77,97,98}.

Estimates for rates of microdeletion events are, for all branches, approximately twofold higher than rates of microinsertion (Fig. 5b), suggesting a fundamental difference in the mechanisms that generate these mutations. Furthermore, there are substantial rate differences for each class of event between the various lineages. In particular, the rat lineage has accumulated microdeletions more rapidly than the mouse, while the opposite holds true for microinsertions. As with substitutions, both microinsertion and microdeletion rates are substantially slower in the human lineage. The size distribution of microindels (1–10 bp) on the rat branch was heavily weighted towards the smallest indels: 45% of indels are single bases, 18% are 2 bp, 10% are 3 bp, 8% are 4 bp, and so on, monotonically decreasing. Separate distributions for insertions and for deletions were similar, as were distributions of indel sizes on the mouse branch.

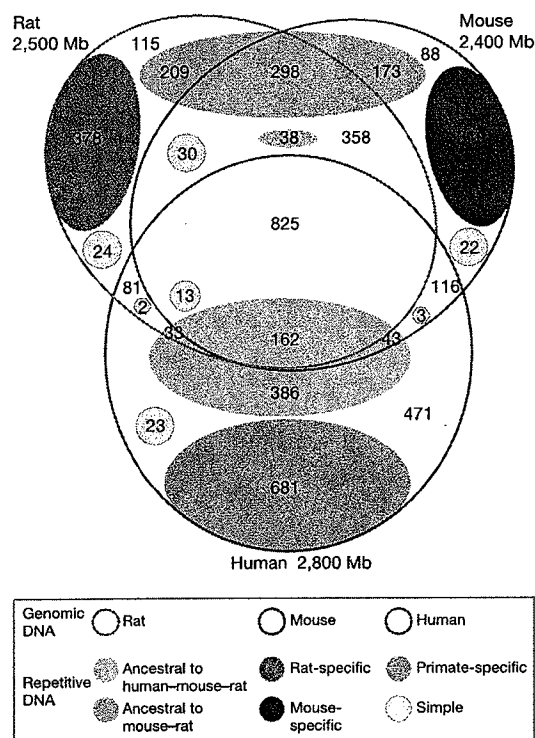


Figure 7 Aligning portions and origins of sequences in rat, mouse and human genomes. Each outlined ellipse is a genome, and the overlapping areas indicate the amount of sequence that aligns in all three species (rat, mouse and human) or in only two species. Non-overlapping regions represent sequence that does not align. Types of repeats classified by ancestry: those that predate the human–rodent divergence (grey), those that arose on the rodent lineage before the rat–mouse divergence (lavender), species-specific (orange for rat, green for mouse, blue for human) and simple (yellow), placed to illustrate the approximate amount of each type in each alignment category. Uncoloured areas are non-repetitive DNA—the bulk is assumed to be ancestral to the human–rodent divergence. Numbers of nucleotides (in Mb) are given for each sector (type of sequence and alignment category). Detailed results are tabulated (Supplementary Table S1-1).

Male mutation bias

As mouse and rat are similar in generation time and number of germline cell divisions^{99,100}, we investigated a potential sex bias in different types of observed genome changes. We compared substitution and indel rates between the X chromosome and autosomes in ancestral repeat sites (~5 Mb and ~100 Mb in total for X and autosomes, respectively¹⁰¹). We discovered that in rodents, small indels (<50 bp) are male-biased, with a male-to-female rate ratio of ~2.3. This is in contrast to a recent study in primates, based on a substantially smaller data set, that indicates no sex bias in small indels¹⁰². Our male-to-female nucleotide substitution rate ratio in rodents is ~1.9, confirming earlier reports^{103,104}. When substitution rates are compared for all sites aligned between mouse and rat (~78 Mb and ~1,691 Mb, respectively), we again observe an approximately twofold excess of small indels and nucleotide substitutions originating in males compared with females¹⁰¹. Interestingly, the ratio in the number of cell divisions between the male and female germlines is also about two^{99,100}, suggesting that these substitutions may arise from mutations that occur primarily during DNA replication.

G+C content and CpG islands

The G+C content of the rat varies significantly across the genome (Fig. 8a), and the distribution more closely resembles that of mouse than human. The variation in G+C content is coupled with differences in the distribution of CpG islands—short regions that are associated with the 5' ends of genes and gene regulation^{2,3,105}, and that escape the depletion of CpG dinucleotides that occurs from

deamination of methylated cytosine^{2,105}. The 2.6 Gb rat genome assembly (including unmapped sequences) contains 15,975 CpG islands in non-repetitive sequences of the genome. This is similar to the 15,500 CpG islands reported in the 2.5 Gb mouse genome³, but far fewer than the 27,000 reported in the human genome^{2,3,105}.

A summary of the CpG island distributions by chromosome is given in Fig. 8b. Chromosome X, with a low G+C content of 37.7%, has the fewest islands (362) and the lowest density of islands (2.6 per Mb). Chromosome 12 is at the other end of the range with a G+C content of 43.5% and the highest density of CpG islands (11.5 islands per Mb). This is similar to chromosome 10, with 11.3 islands per Mb. The average density of CpG islands is 5.7 islands per Mb over the whole genome and 5.9 CpG islands per Mb averaged by chromosome, which is similar to the distribution in mouse³. Neither rodent genome shows the extreme outliers in CpG island density that are seen for human chromosome 19 (ref. 2). The density of CpG islands in the rat genome correlates positively with the density of predicted genes (R of 0.96) (Fig. 8b).

These data show that the overall changes in CpG island content predate the rat–mouse split and are consistent with the accelerated loss of CpG dinucleotides in rodents compared with humans^{105,106}. It remains possible, however, that occurrences such as the greater number of human regions with extremely high G+C content are due to distributional changes mostly in the primate, rather than in the rodent lineage.

Shift in substitution spectra between mouse and rat

The non-repetitive fraction of the rat genome is enriched for G+C content relative to the mouse genome, by ~0.35% over 1.3 billion nucleotides. This is a subtle but substantial difference that may be explained, at least in part, by differences in the spectra of mutation events that have accumulated in the mouse and rat lineages. We analysed all alignment columns in which substitution events can be assigned to either the mouse or the rat lineage, by virtue of a nucleotide match between human and only one rodent⁹²; note that this is a small minority of substitutions. Of the ~117 million alignment columns meeting this criteria, ~60 million involve a change in the rat lineage versus ~57 million in the mouse, reflecting the increase in rates of point substitution in the rat lineage (Fig. 5b). While 50% of these changes in rat involve a substitution from an A/T to a G/C, these events constitute only 47% of all mouse changes. The complementary change, G/C to A/T, exhibits relative excess in the mouse versus the rat lineage (38% versus 35%, respectively). No substantial difference between changes that do not alter G+C content is observed. In addition, this bias is not confined to particular transition or transversion events, nor can it be explained simply as a result of divergent substitution rates of CpG dinucleotides (data not shown). Thus, this shift appears to be a general change that results in an increase in G+C content in the rat genome. Biochemical changes in repair or replication enzymes might be responsible, and the observation that recombination rates are slightly higher in rat than in mouse¹⁰⁷ may suggest a role for G+C-biased mismatch repair^{108,109}. However, population genetic factors, such as selection, cannot be ruled out.

Evolutionary hotspots

Comparison of the two rodent genomes, using human as outgroup, reveals regions that are conserved yet under different levels of constraint in mouse and rat. These regions may have distinct functional roles and contribute to species-specific differences. Analysis of the MAVID alignments¹¹⁰ revealed 5,055 regions ≥ 100 bp, in which there was at least a tenfold difference in the estimated number of substitutions per site on the mouse and rat branches. To avoid alignment problems and fast-evolving regions, the analysis was restricted to regions where the human branch had <0.25 substitutions per site¹¹¹. These regions are enriched twofold in transcribed regions: 39% of mouse hotspots were found in the

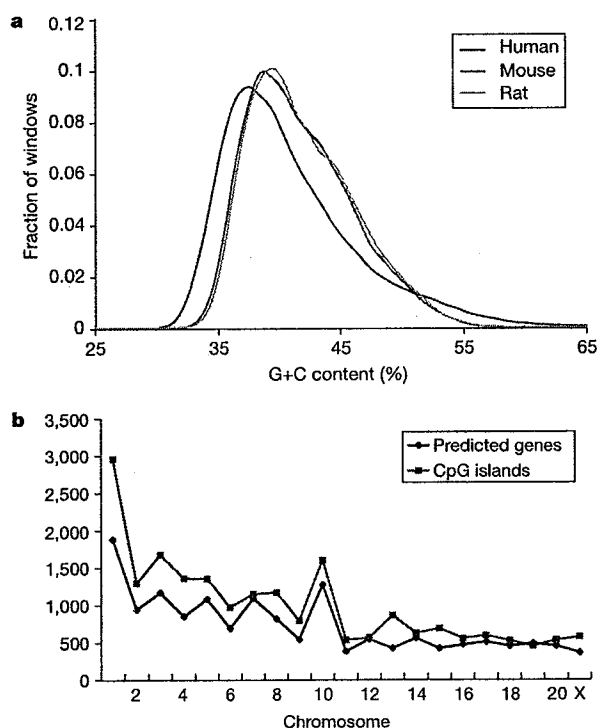


Figure 8 Base composition distribution analysis. **a**, The fraction of 20 kb non-overlapping windows³ with a given G+C content is shown for human, mouse and rat. **b**, The number of Ensembl-predicted genes per chromosome and the number of CpG islands per chromosome. The density of CpG islands averages 5.9 islands per Mb across chromosomes and 5.7 islands per Mb across the genome. Chromosome 1 has more CpG islands than other chromosomes, yet neither the island density nor ratio to predicted genes exceeds the normal distribution. The number of CpG islands per chromosome and the number of predicted genes are correlated ($R^2 = 0.96$).

18% of the mouse genome covered by RefSeq genes; and 17% of the rat hotspots were found in the 8% of the rat genome covered by RefSeq genes. Similar numbers are observed when examining coding exon and EST regions (not shown). Half of all hotspots in the mouse genome lie totally in non-coding regions. Many hotspots are several hundred bases long, with average length 190 ± 86 bp. Future work aimed at identifying the genomic differences that contribute to phenotypic evolution may benefit from analyses such as these, which will become more powerful as the repertoire of mammalian genome sequences expands.

Covariation of evolutionary and genomic features

To illustrate the genomic and evolutionary landscape of a single rat chromosome in depth, we characterized features for rat chromosome 10 at 1 Mb resolution (Fig. 9). This high-resolution analysis uncovered strong correlations between certain microevolutionary features^{89,92,98}. Particularly strongly correlated are the local rates of microdeletion ($R^2 = 0.71$; Fig. 9a), microinsertion ($R^2 = 0.56$; Fig. 9a), and point substitution ($R^2 = 0.86$; Fig. 9b) between the two independent lineages of mouse and rat. In addition, microinsertion rates are correlated with microdeletion rates ($R^2 = 0.55$; Fig. 9a). These strong correlations are also observed in an independent genome-wide analysis, both on the original data and after factoring out the effects of G+C content (not shown, see Supplementary Information).

Perhaps surprisingly, substantially less correlation is seen between microindel and point substitution rates (compare Fig. 9a and b). The amount of correlation varies among chromosomes (not

shown), but is generally weaker than the relationships mentioned above. Further studies will be required to determine whether local evolutionary pressures, which must have remained stable since the separation of the mouse and rat lineages, differentially drive microindel and point substitution rates.

We also find that the local point substitution rate in sites common to human, mouse and rat strongly correlates with that in rodent-specific sites ($R^2 = 0.57$; Fig. 9b, blue line versus red/green). These two classes of sites, while interdigitated at the level of tens to thousands of bases, constitute sites that are otherwise evolutionarily independent. This result confirms that local rate variation is not solely determined by stochastic effects and extends, at high resolution, the previously documented regional correlation in rate between 4D sites and ancestral repeat sites^{3,96}.

Evolution of genes

A substantial motivation for sequencing the rat genome was to study protein-coding genes. Besides being the first step in accurately defining the rat proteome, this fundamental data set yields insights into differences between the rat and other mammalian species with a complete genome sequence. Estimation of the rat gene content is possible because of relatively mature gene-prediction programs and rodent transcript data. Mouse and human genome sequences also allow characterization of mutational events in proteins such as amino acid repeats and codon insertions and deletions. The quality of the rat sequence also allows us to distinguish between functional genes and pseudogenes.

We estimate (on the basis of a subset) that 90% of rat genes

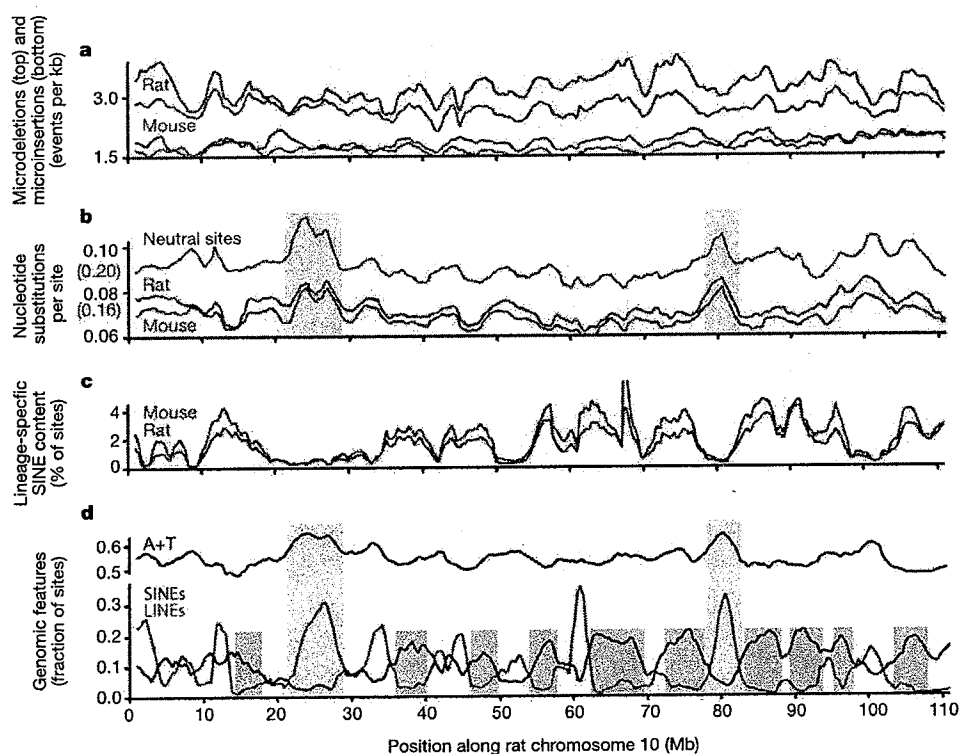


Figure 9 Variability of several evolutionary and genomic features along rat chromosome 10. **a**, Rates of microdeletion and microinsertion events (less than 11 bp) in the mouse and rat lineages since their last common ancestor, revealing regional correlations. **b**, Rates of point substitution in the mouse and rat lineages. Red and green lines represent rates of substitution within each lineage estimated from sites common to human, mouse and rat. Blue represents the neutral distance separating the rodents, as estimated from rodent-specific sites. Note the regional correlation among all three plots, despite being

estimated in different lineages (mouse and rat) and from different sites (mammalian versus rodent-specific). **c**, Density of SINEs inserted independently into the rat or mouse genomes after their last common ancestor. **d**, A+T content of the rat, and density in the rat genome of LINEs and SINEs that originated since the last common ancestor of human, mouse and rat. Pink boxes highlight regions of the chromosome in which substitution rates, A+T content and LINE density are correlated. Blue boxes highlight regions in which SINE density is high but LINE density is low.

possess strict orthologues in both mouse and human genomes. Our studies also identified genes arising from recent duplication events occurring only in rat, and not in mouse or human. These genes contribute characteristic features of rat-specific biology, including aspects of reproduction, immunity and toxin metabolism. By contrast, almost all human 'disease genes' have rat orthologues. This emphasizes the importance of the rat as a model organism in experimental science.

Construction of gene set and determination of orthology

The Ensembl gene prediction pipeline¹¹² predicted 20,973 genes with 28,516 transcripts and 205,623 exons (Methods). These genes contain an average of 9.7 exons, with a median exon number of 6.0. At least 20% of the genes are alternatively spliced, with an average of 1.3 transcripts predicted per gene. Of the 17% single exon transcripts, 1,355 contain frameshifts relative to the predicted protein and 1,176 are probably processed pseudogenes. Of the 28,516 transcripts, 48% have both 5' and 3' untranslated regions (UTRs) predicted and 60% have at least one UTR predicted.

These gene predictions considered homology to other sequences, including 26,949 rodent proteins, 4,861 non-rodent, vertebrate proteins, 7,121 rat complementary DNAs from RefSeq and EMBL, and 31,545 mouse cDNAs from Riken, RefSeq and EMBL. The majority (61%) of transcripts are supported by rodent transcript evidence. When combined with additional private EST data, the fraction of genes supported by transcript evidence could be increased to 72%¹¹³.

A number of other *ab initio* (GENSCAN¹¹⁴, GENEID¹¹⁵), similarity-based (FGENESH++; ref. 116) and comparative (SGP¹¹⁷, SLAM¹¹⁸, TWINSKAN^{119–121}) gene-prediction programs were used to analyse the rat genome. The number of genes predicted by these programs ranged from 24,500 to 47,000, suggesting coding densities ranging from 1.2% to 2.2%. The coding fraction of RefSeq genes covered by these predictions ranged from 82% to 98%. Such comparative *ab initio* programs using the rat genome were successfully used to identify and experimentally verify genes missed by other methods in rat¹²¹ and human¹²². The predictions of these programs can be accessed through the UCSC genome browser and Ensembl websites.

RefSeq genes (20,091 human, 11,342 mouse and 4,488 rat) mapped onto genome assemblies with BLAT¹²³ and the UCSC browser revealed that the number of coding exons per gene and average exon length were similar in the three species. Differences were observed in intron length, with an average of 5,338 bp in human, 4,212 bp in mouse and 5,002 bp in rat. These differences were also found in a smaller collection of 6,352 confidently mapped orthologous intron triads (see 'Conservation of intronic splice signals' section below): average intron lengths in this collection were 4,240 bp in human, 3,565 bp in mouse and 3,638 bp in rat.

Properties of orthologous genes

Orthology relationships were predicted on the basis of BLASTp reciprocal best-hits between proteins of genome pairs (human–rat, rat–mouse and mouse–human)³ (Supplementary Information). Using these methods and the ENSEMBL prediction sets, 12,440

rat genes showed clear, unambiguous 1:1 correspondence with a gene in the mouse genome. This is an underestimate, because random sampling of different classes of rat genes with less stringent criteria for comparison to mouse always identified additional gene pairs. Errors arose from pseudogene misclassification, sequence loss, duplication or fragmentation in assemblies; and missing or inappropriate gene predictions, including coding-gene predictions from non-coding RNAs. Taking these errors into account, we estimate the true proportion of 1:1 orthologues in rat and mouse genomes to lie between 86 and 94% (Methods). The remaining genes were associated with lineage-specific gene family expansions or contractions. These overall observations are consistent with a careful analysis of rat proteases showing that 93% of these genes have 1:1 orthologues in mouse^{124,125}.

Surprisingly, a similar proportion (89 to 90%) of rat genes possessed a single orthologue in the human genome. Because human represents an outgroup to the two rodents, it was expected that mouse and rat would share a higher fraction of orthologues. A close inspection of gene relationships indicates that these findings may suffer from incompleteness of rodent genome sequences, together with problems of misassembly and gene prediction within clusters of gene paralogues.

Further analysis of orthologous pairs considered the occurrence of nucleotide changes within protein-coding regions that reflected synonymous or non-synonymous substitutions. The majority of these studies measured evolutionary rates by determination of K_A (number of non-synonymous substitutions per non-synonymous site) and K_S (number of synonymous substitutions per synonymous site). K_A/K_S ratios of less than 0.25 indicate purifying selection, values of 1 suggest neutral evolution, and values greater than 1 indicate positive selection¹²⁶.

Evolutionary rates were first calculated from a reduced set of orthologue pairs that are embedded in orthologous genomic segments and are related by conservative values of K_S (Table 3) (Methods). A slight increase in median K_S values for rat–human as compared with mouse–human, was found, indicating that the rat lineage has more neutral substitutions in gene coding regions than the mouse lineage. Sequence conservation values were similar to those previously found using smaller data sets^{127,128}, and the overall trend is consistent with results of other evolutionary rate analyses discussed above (Fig. 5).

Next, we investigated examples of rat genes shared with mouse, but with no counterparts in human. Such genes might be rapidly evolving so that homologues are not discernible in human, or they might have arisen from non-coding DNA, or their orthologues in the human lineage might have formed pseudogenes. Thirty-one Ensembl rat genes were collected that have no non-rodent homologues in current databases (Methods). These are twofold over-represented among genes in paralogous gene clusters, and threefold over-represented among genes whose proteins are likely to be secreted. This is consistent with observations³ that clusters of paralogous genes, and secreted proteins, evolve relatively rapidly. Detailed examination of the 31 genes using PSI-BLAST determined that ten genes cannot be assigned homology relationships to experimentally described mammalian genes. These ten rodent-

Table 3 One-to-one orthologous genes in human, mouse and rat genomes

	Human–mouse	Human–rat	Mouse–rat
1:1 orthologue relationships	11,084	10,066	11,503
Median K_S values*	0.56 (0.39–0.80)	0.57 (0.40–0.82)	0.19 (0.13–0.26)
Median K_A/K_S values*	0.10 (0.03–0.24)	0.09 (0.03–0.21)	0.11 (0.03–0.28)
Median % amino acid identity*	88.0% (74.4–96.3%)	88.3% (75.9–96.4%)	95.0%† (88.0–98.7%)
Median % nucleotide identity*	85.1% (77.4–90.0%)	85.1% (77.8–89.9%)	93.4% (89.2–95.7%)

Data obtained from Ensembl, *Homo sapiens* version 11.31 (24,841 genes), *Mus musculus* version 10.3 (22,345 genes), *Rattus norvegicus* version 11.2 (21,022 genes).

*Numbers in parentheses represent the 16th and 83rd percentiles.

†This value is consistent with previous findings (93.9% in ref. 130).

specific genes may have evolved particularly rapidly, or have non-coding DNA homologues, or be erroneous predictions.

The paucity of rodent-specific genes indicates that *de novo* invention of complete genes in rodents is rare. This is not unexpected, because the majority of eukaryotic protein-coding genes are modular structures containing coding and non-coding exons, splicing signals and regulatory sequences, and the chances of independent evolution and successful assembly of these elements into a functional gene are small, given the relatively short evolutionary time available since the mouse–rat split. However, individual rodent-specific exons may arise more frequently, particularly if the exon is alternatively spliced¹²⁹. Applying a K_A/K_S ratio test^{130,131} to sequences that align only between rat and mouse, we identified 2,302 potential novel rodent-specific exons, with EST support, in BLASTZ alignments of rat and mouse sequences. None of these individual exons matched human transcripts, but approximately half (1,116) appear to be present in alternative splice forms found in rodents. We speculate that these exons contain the few successful lineage-specific survivors of the constant process of gene evolution, by birth and death of individual exons.

Indels and repeats in protein-coding sequences

In contrast to small indels occurring in the bulk of the genome (above), indels within protein-coding regions are probably lethal, or deleterious and so are rapidly removed from the population by purifying selection. Indel rates within rat coding sequences were 50-fold lower than in bulk genomic DNA¹³². The whole genome excess of deletions compared with insertions (Fig. 5b) was also evident in coding sequences. The magnitude was less, with a genome-wide deletion-to-insertion ratio of 3.1:1 reducing to 1.7:1 in the rat. In mouse this value reduced from 2.5:1 to 1.1:1 (ref. 132). These data suggest that deletions are ~16% more likely than insertions to be removed from coding sequences by selection.

Owing to the triplet nature of the genetic code, indels of multiples of three nucleotides in length (3_n indels) are less likely to be deleterious. Direct comparison of 3_n indel rates between bulk DNA (0.77 indels per kb for mouse, 0.83 indels per kb for rat) and coding sequence (0.087 indels per kb for mouse and 0.084 indel per kb for rat) showed that 3_n indels were ninefold under-represented in coding sequences. At least 44% of indels were duplicative insertion or deletion of a tandemly duplicated sequence, collectively termed sequence slippage¹³². Sequence slippage contributed approximately equally to observed insertions and deletions. The overall excess of deletions could be attributed specifically to an excess of non-slippage deletion over non-slippage insertion in both mouse and rat lineages¹³². Of the slippage indels, 13% were in the context of trinucleotide repeats ($n > 2$, excluding the inserted or deleted sequence) which are known to be particularly prone to sequence slippage and encode homopolymeric amino acid tracts^{133,134}.

To gain better understanding of dynamic changes in the length of homopolymeric amino acid tracts on gene evolution and disease susceptibility, we searched for other characteristics of amino acid repeat variation by analysing all size-five or longer amino acid repeats in a data set of 7,039 rat, mouse and human orthologous protein sequences¹³⁵. Most species-specific amino acid repeats (80–90%) were found in indel regions, and regions encoding species-specific repeats were more likely to contain tandem trinucleotide repeats than those encoding conserved repeats. This was consistent with the involvement of slippage in the generation of novel repeats in proteins and extended previous observations for glutamine repeats in a more limited human–mouse data set¹³⁶.

The percentage of proteins containing amino acid repeats was 13.7% in rat, 14.9% in mouse and 17.6% in human¹³⁵. The most frequently occurring tandem amino acid repeats were glutamic acid, proline, alanine, leucine, serine, glycine, glutamine and lysine. Using the same threshold size cut-off, tandem trinucleotide repeats

were significantly more abundant in human than in rodent coding sequences, in striking contrast to the frequencies observed in bulk genomic sequences (29 trinucleotide repeats per Mb in rat, 32 repeats per Mb in mouse and 13 repeats per Mb in human, see discussion of the general simple repeat structure below). The conservation of human repeats was higher in mouse (52%) than in rat (46.5%), suggesting a higher rate of repeat loss in the rat lineage than the mouse lineage.

Functional consequences of these in-frame changes in rat, mouse and human were investigated¹³² through clustering of proteins based on annotation of function and cellular localization¹¹², and mapping indels onto protein structural and sequence features. The rate that indels accumulated in secreted (3.9×10^{-4} indels per amino acid) and nuclear (4.0×10^{-4}) proteins is approximately twice that of cytoplasmic (2.4×10^{-4}) and mitochondrial (1.4×10^{-4}) proteins. Likewise, ligand-binding proteins acquire indels (3.1×10^{-4}) at a higher rate than enzymes (2.1×10^{-4})¹³². These trends exactly mirror those observed for amino acid substitution rates³, suggesting tight coupling of selective constraints between indels and substitutions. Transcription regulators showed the highest rate of indels (4.3×10^{-4}), a finding that may relate to the over-representation of homopolymorphic amino acid tracts in these proteins¹³⁵.

Known protein domains exhibited 3.3-fold fewer indels than expected by chance, again paralleling nucleotide substitution rate differences between domains and non-domain sequences³. Of the protein-sequence and structural categories considered (transmembrane, protein domain, signal peptide, coiled coil and low complexity), the transmembrane regions were the most refractory to accumulating indels, exhibiting a sixfold reduction compared with that expected by chance. Low-complexity regions were 3.1-fold enriched, reflecting their relatively unstructured nature and enrichment in indel-prone trinucleotide repeats. Mapping of indels onto groups of known structures revealed that indels are 21% more likely to be tolerated in loop regions than the structural core of the protein¹³².

We observed that indel frequency and amino acid repeat occurrence both correlated positively with the G + C coding sequence content of the local sequence environment^{132,135}. This may be explained in part by the correlation of polymerase slippage-prone trinucleotide repeat sequences and G + C content¹³⁵. There is also a positive correlation between CpG dinucleotide frequency and coding sequence insertions, but not deletions. This effect diminishes rapidly with increasing distance from the site of the insertion¹³².

Transcription-associated substitution strand asymmetry

A recent study reported a significant strand asymmetry for neutral substitutions in transcribed regions¹³³. Within introns of nine genes, the higher rate of A→G substitutions over that of T→C substitutions, together with a smaller excess of G→A over C→T substitutions, leads to an excess of G+T over C+A on the coding strand (also verified on human chromosome 22). The authors¹³³ hypothesized that the asymmetries are a byproduct of transcription-

Table 4 Strand asymmetry of substitutions in introns of rat genes

Base frequencies on coding strand* (G+T)/(C+A)	Rat genome 1.060	
Ratio of purine transitions to pyrimidine transitions† Rate(A→G)/Rate(C→T)	Rat–mouse 1.036	Rat–human 1.036
Rate of transitions‡ Rate(A→G)/Rate(T→C) Rate(G→A)/Rate(C→T)	Rat 1.058 1.017	Mouse 1.091 1.00

*Computed from the rat genome.

†Computed from pairwise alignments.

‡Computed from three-way alignments.

coupled repair in germline cells. Examining the three-way alignments of rat, mouse and human, we verified that the strand asymmetries for neutral substitutions exist in introns across the genome (Table 4).

Under the assumption of independence of sequence positions, large sample normal approximations to the binomial distribution allow us to test whether the fraction of G+T exceeds 0.5, and whether the rate at the numerator exceeds the rate at the denominator for each of the ratios in Table 4. With the large amount of data provided by pooling introns genome-wide, the tests are all highly significant (P values $< 10^{-4}$), except for the rate of G→A in mouse, which does not significantly exceed that of C→T (P value = 0.6369). These asymmetries are also seen if the study is limited to ancestral repeat sites, excludes ancestral repeat sites, excludes CpG dinucleotides, is limited to positions flanked by sites that are identical in the aligned sequences (in the case of observations 2 and 3 in Table 4), or considers introns of RefSeq genes for human or mouse. Thus it appears that strand asymmetry of substitution events within transcribed regions of the genome is a robust genome-wide phenomenon.

Conservation of intronic splice signals

Using 6,352 human–mouse–rat orthologous introns from 976 genes (Methods), we examined the dynamics of evolution of consensus splice signals in mammalian genes. We found that intron class¹³⁷ is extremely well conserved: we did not observe any U2 to U12 intron conversion, or vice versa, nor within U12 introns did we find any switching between the major AT–AC and GT–AG subtypes, although such events are documented at larger evolutionary distances¹³⁷. In contrast, conversions between canonical GT–AG and non-canonical GC–AG subtypes of U2 introns are not uncommon. Only ~70% of GC–AG introns are conserved between human and mouse/rat, and only 90% are conserved between mouse and rat. Using human as the outgroup, we detected nine GT to GC conversions after divergence of mouse and rat (from 6,282 introns that were likely to have been GT–AG before human and rodents split), and two GC to GT conversions (from 34 GC–AG introns that probably predated the human and rodent split). These results give some indication of the degree to which mutation from T to C is tolerated in donor sites. The GC donor site appears to be better tolerated in introns with very strong donor sites, because in these introns the proportion of GC donor sites is ~11%, much higher than the 0.7% overall frequency of GC donor sites in U2 introns. Although we found a variety of other non-canonical configurations in U2 introns, very few are conserved, which suggests that most correspond to transient, evolutionarily unstable states, pseudogenes, or mis-annotations.

Gene duplications

Duplication of genomic segments represents a frequent and robust mechanism for generating new genes¹³⁸. Because there were no compelling data showing rat-specific genes arising directly from non-coding sequences, we examined gene duplications to measure their potential contribution to rat-specific biology. A previous study showed that gene clusters in mouse without counterparts in human are subject to rapid, adaptive evolution^{3,139}. We used two methods to identify recent gene duplications: methods that directly identified paralogous clusters, and methods that analysed genomic segmental duplications (see above).

Using the first approach, we found 784 rat paralogue clusters containing 3,089 genes (Methods). This was lower than in mouse (910 clusters/3,784 genes), but the difference probably reflects the larger number of gene predictions from the mouse assembly.

To investigate the timing of expansion of these individual families, we measured rates of local gene duplication and retention within clusters. BLAST is not suited to this^{140,141} and so we instead calculated the number of synonymous substitutions per

synonymous site (K_S) between all pairs of homologous genes; constructed K_S -derived phylogenetic trees; and predicted orthology or paralogy gene duplication events automatically from their topologies (Supplementary Information). The results showed that the neutral substitution rate varies among orthologues by approximately twofold (Fig. 10). This is similar to chromosomal variation shown previously by a study of mouse and human ancestral repeats³. Rates of change among ancestral gene duplications (those that predate the mouse–rat split) were relatively constant. Mouse-specific and rat-specific duplications occurred at similar rates, except for those with $K_S < 0.04$, which are reduced in mouse-specific duplications (Fig. 10). More data are required to determine whether this reduction is a biological effect, as it might be accounted for by different protocols for assembling mouse and rat genomes, which differentially collapse areas of nearly identical sequence.

The rat paralogue pairs that probably arose after the rat–mouse split (12–24 Myr ago) have K_S values of ≤ 0.2 (Table 3). We found 649 $K_S < 0.2$ gene duplication events in rat, a lower number than is found in mouse (755). For both rodents, this represents a likelihood of a gene duplicating of between 1.3×10^{-3} and 2.6×10^{-3} every Myr. These are necessarily estimates, because gene deletions, conversions and pseudogene formation are not considered. Interestingly, the data are consistent with a previous estimate for *Drosophila* genes, but are an order of magnitude lower than an estimate for *Caenorhabditis elegans* genes¹⁴⁰.

A subset of clusters have at least three gene duplications with $K_S < 0.2$ (Table 5). These are expected to be enriched in genes whose duplications persist as a consequence of positive selection. The group is dominated by genes involved in adaptive immune response and chemosensation⁸⁷. Inspection of the K_S -derived trees allowed us to infer the gene numbers in these clusters for the common ancestor of rat and mouse (that is, at $K_S = 0.2$), assuming no gene deletions or pseudogene generation (Table 5). Immunoglobulin, T-cell receptor α -chain, and α_{2u} -globulin genes appear to be duplicating at the fastest rates in the rat genome (Table 5). Since divergence with mouse, these rat clusters have increased gene content several-fold. This recapitulates previous observations that rapidly evolving and duplicating genes are over-represented in olfaction and odorant detection, antigen recognition and reproduction¹⁴².

An examination of duplicated genomic segments showed this enrichment for most of the same genes and also elements involved in foreign compound detoxification (cytochrome P450 and carboxylesterase genes)⁸⁷. Together, these are exciting findings because each of these categories can easily be associated with a

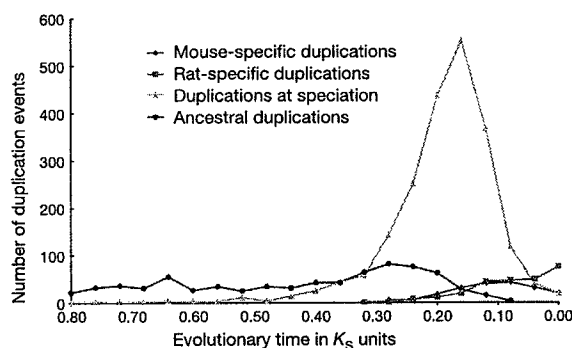


Figure 10 Variation in the frequency of gene duplications during the evolutionary histories of the rat and mouse. The sequence of gene duplication events was inferred from phylogenetic trees determined from pairwise estimates of genetic divergence under neutral selection (K_S , Methods). The median K_S value for mouse:rat 1:1 orthologues is 0.19. This value corresponds to the divergence time of mouse and rat lineages.

familiar feature of rat-specific biology, and further investigation could explain some differences between rats and their evolutionary neighbours.

Conservation of gene regulatory regions

As the third mammal to be fully sequenced, the rat can add significantly to the utility of nucleotide alignments for identifying conserved non-coding sequences^{143–147}. This power increases roughly as a function of the total amount of neutral substitution represented in the alignment^{97,98}, and rat adds about 15% to the human–mouse comparison (Fig. 5). Many conserved mammalian non-coding sequences are expected to have regulatory function, and can be predicted using further analyses based upon these alignments^{93,148–150}.

We applied such methods for detecting significantly conserved elements^{97,151} and scoring regulatory potential^{148,152} to the genome-wide human–mouse–rat alignments. Typical results show strong conservation for a coding exon, as well as for several non-coding regions (Fig. 11). For example, the intronic region in Fig. 11 contains 504 bp that are highly conserved in human, mouse and rat. The last 100 bp of this alignment block are identical in all three species. Peaks in regulatory potential score are correlated with conservation score, and in the highly conserved intronic segment, they are higher for the three-way regulatory potential score than for the two-way scores using human and just one rodent¹⁵². These data are illustrative, but form the foundation of ongoing efforts to identify genome sequences involved in gene regulation.

Requiring conservation among mammalian genomes greatly increases the specificity of predictions of transcription factor binding sites. Transcription factor databases such as TRANSFAC¹⁵³ contain known transcription factor binding sites and some knowledge of their distribution, but simply searching a sequence with these motifs provides little discriminatory power. For example, all of

the 85 known regulatory elements¹⁴⁸ and 151 functional promoters¹⁵⁴ have TRANSFAC matches, but so do 99% of the 2,049,195 mammalian ancestral repeats, most representing false-positive predictions. The introduction of conservation as a criterion for regulatory element identification greatly increases specificity, with only a modest cost in sensitivity. If we insist that the TRANSFAC matches be present and orthologously aligned in all three species—human, mouse and rat—then only 268 matches are recorded in ancestral repeats (0.01%), while 63 (74%) of the above matches in known regulatory elements and 121 (80%) in functional promoters are retained. Overall, using a set of 164 weight matrices for 109 transcription factors extracted from TRANSFAC¹⁵³, we find 186,792,933 matches in the April 2003 reference human genome sequence, but this was reduced to only 4,188,229 by demanding conservation in the human–mouse–rat three-way alignments. This is a 44-fold increase in specificity.

We examined one region in more detail: a complex *cis*-regulatory region consisting of a 4,000 bp segment containing two regulatory modules, hypersensitive sites 2 and 3 from the locus control region of the HBB complex^{155–157}. Considerable experimental work has identified six functional binding sites for the transcription factor GATA-1 in this segment. Requiring that matches to GATA-1 binding sites be conserved in all three species and occur within regions of strong regulatory potential is sufficient to find these six functional binding sites, and only these six, in the 4,000 bp segment. Thus, in this example we observed complete sensitivity and specificity by requiring this level of conservation.

Pseudogenes and gene loss

To complement the identification and analysis of protein-coding regions, we sought to examine rat pseudogenes. Using a previously described method^{158,159}, we found 18,755 pseudogenes in intergenic regions. Pseudogenes are normally not subjected to selective con-

Table 5 Recent gene duplications ($K_S < 0.2$) in the rat lineage

Cluster ID	Recent duplication events	Numbers of genes involved	Extant cluster size	Ancestral cluster size	Chromosome	Annotation	Process
249	38	53	60	22	4	Immunoglobulin κ -chain V	Immunity
640	38	47	53	15	15	TCR α -chain V	Immunity
346	25	35	44	15	6	Immunoglobulin heavy chain V	Immunity
190	22	42	168	146	3	Olfactory receptor	Chemosensation
578	16	28	59	43	13	Olfactory receptor	Chemosensation
400	15	26	82	67	8	Olfactory receptor	Chemosensation
743	15	21	37	22	20	Olfactory receptor	Chemosensation
72	12	22	102	90	1	Olfactory receptor	Chemosensation
500	12	18	32	20	10	Olfactory receptor	Chemosensation
51	6	7	16	10	1	Glandular kallikrein	Reproduction?
256	6	8	10	4	4	Vomerolateral receptor V1R	Chemosensation
488	6	10	11	5	10	Olfactory receptor	Chemosensation
644	6	10	14	8	15	Granzyme serine protease	Immunity
4	5	6	9	4	1	Trace amine receptor, GPCR	Neuropeptide receptors?
248	5	9	15	10	4	Vomerolateral receptor V1R	Chemosensation
393	5	10	31	26	8	Olfactory receptor	Chemosensation
522	5	8	19	14	10	Keratin-associated protein	Epithelial cell function
550	5	8	17	12	11	Olfactory receptor	Chemosensation
635	5	9	20	15	15	Olfactory receptor	Chemosensation
79	4	8	38	34	1	Olfactory receptor	Chemosensation
88	4	6	11	7	1	Olfactory receptor	Chemosensation
109	4	7	43	39	1	Olfactory receptor	Chemosensation
294	4	5	5	1	5	α_2 -globulin	Chemosensation
310	4	5	11	7	5	Olfactory receptor	Chemosensation
353	4	7	13	9	7	Olfactory receptor	Chemosensation
399	4	5	6	2	8	Ly6-like urinary protein	Chemosensation?
638	4	6	6	2	15	RNase A	Immunity
690	4	6	21	17	17	Prolactin paralogue	Reproduction
239	3	6	6	3	4	Prolactin-induced protein	Reproduction
253	3	4	5	2	4	Camello-like N-acetyltransferase	Developmental regulator
274	3	6	20	17	4	Ly-49 lectin natural killer cell protein	Immunity
297	3	4	5	2	5	Interferon- α	Immunity
523	3	4	6	3	10	Keratin-associated protein	Epithelial cell function
746	3	5	6	3	20	MHC class 1b (M10)	Chemosensation

Duplications involving retroviral genes, fragmented genes with internal repeats, and likely pseudogene clusters were removed from this list. Only gene clusters exhibiting at least three duplications are shown.

straint and therefore accumulate sequence modifications neutrally. Indeed, nearly all of our identified pseudogenes ($97 \pm 3\%$) evolved under neutrality according to a K_A/K_S test, and therefore are consistent with being pseudogenic.

We classified these pseudogenes according to whether they arose from retrotransposition, in which case they integrated into the genome randomly, or whether they arose from tandem duplication and neutral sequence substitution. Using human–rat synteny, we found that 80% of pseudogenes exhibited no significant similarity to the corresponding human orthologous region, and therefore were considered retrotransposed, processed pseudogenes. The total pseudogene count, and processed pseudogene proportion, are consistent with those found for human^{158,159}. These numbers are greater than those previously reported for mouse^{3,4}. However, reanalysis using the method employed here detects a similar pseudogene number (20,000) to that found for human and rat. This suggests that the rate of pseudogene creation is similar among these mammals.

As with the human genome^{159,160}, the largest group of rat pseudogenes (totalling 2,188), according to InterPro¹⁶¹, consists of ribosomal protein genes. Other large rat pseudogene families arose from olfactory receptors (552, see below), glyceraldehyde-3-phosphate dehydrogenase (GAPDH) (251), protein kinases (177), and RNA binding RNP-1 proteins (174). Pseudogenes homologous to a meiotic spindle-associated protein—spindlin¹⁶²—are particularly numerous in rat (at least 53 copies) compared with mouse (approximately three copies). This suggests that spindlin pseudogenes may have distributed rapidly by a recently active transposable element.

We investigated the much-studied metabolic enzyme GAPDH^{3,163}, and observed that: (1) the GAPDS gene arose from a duplication of the GAPDH gene; (2) biogenesis of the GAPDH pseudogenes has been occurring steadily over time both before and

after rodent–human and mouse–rat divergence; and (3) the GAPDS gene has undergone little retrotransposition in all three genomes compared with its relative, the GAPDH gene (consistent with respective gene-expression levels in the germ line).

In situ loss of rat genes

As an organism evolves, its need for certain genes may be reduced, or lost, owing to changes in its ecological niche. Loss of selective constraints leads to accumulation of nonsense and/or frameshift mutations without retrotransposition or duplication. These non-processed pseudogenes are interesting because they link environmental changes to genomic mutation events. However, predicted pseudogenes with disrupted reading frames might also be indicative of errors in genome sequence or assembly. By constraining the search to orthologous genomic regions, we identified 14 rat putative non-processed pseudogenes (Table 6) with apparently functional, single human and mouse orthologues. Half of these contain one in-frame stop or frameshift, whereas the remainder contain more. We expect this number of identified pseudogenic orthologues to be conservative because the methods employed required high fidelity of both gene prediction and orthologue identification in all three species (Methods).

Nevertheless, as only 14 recently evolved pseudogene candidates were identified, this indicates that the genome sequence and assembly (Rnor3.1) is of high quality. The improved quality of the most recent assembly is underscored by 11 additional candidate pseudogenes, predicted from rat assembly Rnor2.1, that are apparently functional, full-length genes in Rnor3.1. Consequently, some of the current 14 candidates, in particular those that are involved in fundamental processes of eukaryotic biology, may yet be ‘repaired’ by sequence changes in future assemblies, and thus be recognized as genic. However, genes associated with innate immunity (which is particularly susceptible to change via adaptive evolution), such as Forssman glycolipid synthetase and complement factor I, may yet be found to survive as true pseudogenes in the rat.

Non-coding RNA genes

We investigated the abundance and distribution of non-coding (nc)RNAs in rat. Cytoplasmic transfer (t)RNA gene identification in rodents is complicated by tRNA-derived identifier (ID) short interspersed nucleotide (SINEs) (B2 and ID). tRNAscan-SE predicted 175,943 tRNAs (genes and pseudogenes); however, the majority (175,285) were SINEs identified by RepeatMasker. This is far greater than the number found in mouse (24,402/25,078) or human (25/636). Of the remaining 666 predictions, 163 were annotated as tRNA pseudogenes and four were annotated as undetermined by tRNAscan-SE. An additional 68 predictions were removed because their best database match in either human, mouse or rat tRNA databases matched tRNAs with either a different amino acid or anticodon (violating the wobble rules that specify the distinct anticodons expected). The total of 431 tRNAs (including a single selenocysteine tRNA) identified in the rat genome is comparable to that for mouse—435 tRNAs (version mm2 from the UCSC genome browser)—and human—492 tRNAs (from the genomic tRNA database, <http://rna.wustl.edu/GtRDB/Hs/>). These three species share a core set of approximately 300 tRNAs, using a cutoff of $\geq 95\%$ sequence identity and $\geq 95\%$ sequence length.

A total of 454 ncRNAs (other than tRNAs) were identified by sequence comparison to known ncRNAs (Supplementary Information). These include 113 micro- (mi)RNAs, five ribosomal RNAs, 287 small nucleolar (sno)RNAs and small nuclear (sn)RNAs, 49 various other ncRNAs such as signal recognition particle (SRP) RNA, 7SK RNA, telomerase RNA, RNase P RNA, brain-specific repetitive (bsr)RNA, non-coding transcript abundantly expressed in brain (ntab)RNA, small cytoplasmic (sc)RNA and 626 pseudogenes. Complete 18S and 28S rRNA genes and more rRNAs were not identified, presumably owing to assembly issues.

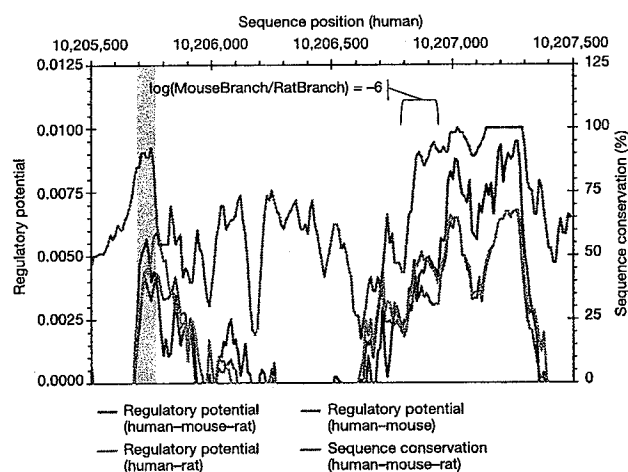


Figure 11 Close-up of PEX14 (peroxisomal membrane protein) locus on human chromosome 1 (with homologous mouse chromosome 4 and rat chromosome 5). Conservation score computed on three-way human–mouse–rat alignments (parsimony P values¹⁵¹) presents a clear coding exon peak (grey bar) and very high values in a 504 bp non-coding, intronic segment (right; last 100 bp of alignment are identical in all three organisms). The latter segment showed a striking difference between the inferred mouse and rat branch lengths^{110,111,222}; the grey bracket corresponds to a phylogenetic tree where the logarithm of mouse to rat branch-length ratio is -6 . Regulatory potential scores^{148,152} that discriminate between conserved regulatory elements and neutrally evolving DNA are calculated from three-way (human–mouse–rat) and two-way (human–rodent) alignments. Here the three-way regulatory potential scores are enhanced over the two-way scores.

Table 6 Candidate rat pseudogenes, orthologous to mouse and human functional genes

Mouse gene	Human gene	Strand	Rat genome coordinates*	Frameshifts/stops†	Annotation
ENSMUSG00000013611	ENSG00000174226	+	7:92752590-92807556	1/0	Sorting nexin
ENSMUSG00000024364	ENSG00000158402	+	18:62742414-62770427	2/0	Dual-specificity phosphatase CDC25c
ENSMUSG00000026293	ENSG00000077044	+	9:95634847-95692601	1/0	Diacylglycerol kinase δ
ENSMUSG00000026785	ENSG00000180447	+	3:9210762-9229984	5/0	Protein kinase PKN β
ENSMUSG00000026829	ENSG00000148288	+	3:7662414-7664521	2/2	Forssman glycolipid synthetase
ENSMUSG00000027426	ENSG00000125846	+	3:125918806-125924149	1/1	Zinc finger protein 133
ENSMUSG00000028000	ENSG00000138799	-	2:221272797-221304350	1/0	Complement factor I
ENSMUSG00000029203	ENSG00000078140	-	14:44385206-44441888	1/0	Ubiquitin-protein ligase E2 (HIP2)
ENSMUSG00000030270	ENSG00000144550	-	20:8332585-8362331	3/0	Copine (membrane trafficking)
ENSMUSG00000035449	ENSG00000167646	+	1:67374986-67381472	1/0	Cardiac troponin I
ENSMUSG00000037029	ENSG00000105261	-	1:82728049-82730272	1/0	Zinc finger protein 146
ENSMUSG00000037432	ENSG00000158142	+	9:42465695-42498651	1/1	Dysferlin-like protein
ENSMUSG00000039680	ENSG00000167137	-	3:9320401-9326997	4/0	Similar to yeast YMR310c RNA-binding protein
ENSMUSG00000042653	ENSG00000137634	+	8:49938446-49939091	1/0	Brush border 61.9 kDa-like protein

*Coordinates from rat v2.0.

†Mouse genes were used as templates for predicting rat pseudogenes.

Evolution of transposable elements

Most interspersed repeats are immobilized copies of transposable elements that have accrued substitutions in proportion to their time spent fixed in the genome (for introduction^{2,3,164-167}). About 40% of the rat genome draft is identified as interspersed repetitive DNA derived from transposable elements, similar to that for the mouse³ (Table 7) and lower than for the human (almost 50%²). The latter difference is mainly due to the lower substitution rate in the human lineage, which allows us to recognize much older (Mesozoic) sequences as interspersed repeats. Almost all repeats are derived from retrotransposons, elements that procreate via reverse transcription of their transcripts. As in mouse, there is no evidence for activity of DNA transposons since the rat-mouse split. Many aspects of the rat and the mouse genomes' repeat structure are shared; here we focus on the differences.

LINE-1 activity in the rat lineage

The long interspersed nucleotide element (LINE)-1 (L1) is an autonomous retroelement, containing an internal RNA polymerase II promoter and two open reading frames (ORFs). The ORF1 product is an RNA binding protein with chaperone-like activity, suggesting a role in mediating nucleic acid strand transfer steps

during L1 reverse transcription¹⁶⁸, whereas ORF2 encodes a protein with both reverse transcriptase and DNA endonuclease activity. LINEs are characteristically 5' truncated so that only a small subset extends to include the promoter region and can function as a source for more copies.

Many classes of LINE-like elements exist, but only L1 has been active in rodents. Over half a million copies, in variable stages of decay, comprise 22% of the rat genome. Although 10% of the human genome is comprised of L1 copies introduced before the rodent-primate split, owing to the fast substitution rate in the rodent lineage only 2% of the rat genome could be recognized as such. Thus, probably well over one-quarter of all rat DNA is derived directly from the L1 gene.

Following the mouse-rat split, L1 activity appears to have increased in rat. The 3' UTR sequences defined six rat-specific L1 subfamilies, represented by 150,000 copies that cover 12% of the rat genome. L1 copies accumulated over the same period in mouse cover only 10% of the genome (Table 7). This higher accumulation of L1 copies could explain some of the size difference of the rat and mouse genome.

In addition to the traditional L1 elements, there are 7,500 copies

Table 7 Composition of interspersed repeats in the rat genome

	Rat				Mouse	
	Copies ($\times 10^3$)	Total length (Mb)	Fraction of genome (%)	Lineage-specific (%)	Fraction of genome (%)	Lineage-specific (%)
LINEs	657	594.0	23.11	11.70	20.10	9.74
LINE-1	597	584.2	22.73	11.70	19.65	9.74
LINE-2	48	8.4	0.33	-	0.38	-
L3/CR1	11	1.4	0.06	-	0.06	-
SINEs	1,360	181.3	7.05	1.52	7.78	1.80
B1(A/u)	384	42.3	1.65	0.16	2.53	0.92
B4(ID_B1)	359	55.4	2.15	0.00	2.25	0.00
ID	225	19.6	0.76	0.54	0.20	0.00
B2	328	55.2	2.15	0.68	2.29	0.74
MIR	109	13.0	0.51	-	0.56	-
LTR elements	556	232.4	9.04	1.84	10.28	2.85
ERV_class I	40	24.9	0.97	0.56	0.79	0.36
ERV_class II	141	83.4	3.24	1.02	4.13	1.73
ERV_L (III)	74	21.6	0.84	0.04	1.08	0.23
MaLRs	302	102.5	3.99	0.22	4.27	0.53
DNA elements	108	20.9	0.81	-	0.86	-
Charlie(hAT)	80	14.8	0.58	-	0.60	-
Tigger(Tc1)	18	4.0	0.16	-	0.17	-
Unclassified	14	7.3	0.28	-	0.37	-
Total	2,690	1,036	40.31	14.90	39.45	14.26
Small RNAs	8	0.6	0.03	0.01	0.03	0.01
Satellites	14	6.4	0.25	?	0.31	?
Simple repeats	897	61.1	2.38	?	2.41	?

Data for Rnor3.1 and October 2003 mouse (MM4), excluding Y chromosome, using the 17 December 2003 version of RepeatMasker. To highlight the differences between rat and mouse repeat content, columns 5 and 7 show the fractions of the genomes comprising lineage-specific repeats. The LINE-1 numbers include all HAL1 copies, whereas all BC1 scRNA and >10% diverged tRNA-Ala matches, far more common than other small RNA pseudogenes and closely related to ID, have been counted as ID matches.

(10 Mb) of a non-autonomous element that is derived from L1 by deletion of most of its ORF2. A similar element, active in Mesozoic times, has been called HAL1 (for Half-a-LINE)¹⁶⁴. Given their low divergence, we conclude that the currently identified HAL1-like elements operated only a few million years ago in the mouse lineage (MusHAL1) and still propagate in the rat genome (RNHAL1). RNHAL1 contains only an ORF1, whereas MusHAL1 encoded an endonuclease as well, although no reverse transcriptase. The 5' 2,600 bases of RNHAL1 are 98% identical to the currently active L1 in rat (L1_Rn or L1mlv2¹⁶⁹). Unlike ancient HAL1 elements, which shared the 3' UTR with a contemporary L1, the 3' end of RNHAL1 is unrelated to other repeats. The repeated origin and high copy number of HAL1s suggest that the ORF1 product, which binds strongly to its messenger RNA¹⁶⁸, may render this transcript a superior target for L1-mediated reverse transcription. In this way HAL1 resembles the non-autonomous, endogenous retrovirus-derived MaLR elements (below), which, for over 100 million years, retained only the retroviral gag ORF that encodes an RNA binding protein. A potential advantage of HAL1 over L1 is its shorter length, which, considering the usual 5' truncation of copies, increases the chance that a copy may include the internal promoter elements and become a source gene.

Different activity of SINEs in the rat and mouse lineage

The most successful usurpers of the L1 retrotransposition machinery, however, are SINEs. These are small RNA-derived sequences with an internal RNA polymerase III promoter. Recently, the human Alu SINE has been experimentally proven to be transposed by L1¹⁷⁰. Most SINEs share the 3' end with their associated LINE elements, like the Mesozoic mammalian LINE-2 (L2) and MIR pair, increasing the efficiency with which a LINE reverse transcriptase recognizes the 3' end of a dependent SINE. However, L1 does not show sequence specificity and rodent and primate SINE sequences are unrelated to L1. Although any transcript can be retroposed, as can be seen from the numerous processed pseudogenes in mammalian genomes, L1-dependent SINEs probably have features that make them especially efficient targets of the L1 reverse transcriptase.

Although before the radiation of most mammalian orders L1 was at least as active as L2, the L2-dependent MIR was the only known (and very abundant) SINE of that time. All of the currently active SINEs in different mammalian orders appear to have arisen after the demise of L2 (and consequently MIR), as though an opportunity (or necessity) arose for the creation and expansion of other SINEs.

Four different SINEs are distinguished in rat and mouse. The B1 element seems to share its origin from a 7SL RNA gene with the primate Alu¹⁷¹. This probably happened just before the rodent-primate split and after the speciation from most other eutherians, where Alu/B1 elements are not known. The other SINEs are rodent-specific and have tRNA-like internal promoter regions. ID elements consist only of this tRNA-like region, which in older ID copies closely match an Ala-tRNA from which it may have been derived. B4 resembles a fusion of an ID and B1 SINE. Finally, B2 has a tRNA-like region of unknown affiliation followed by a unique 120 bp region.

The fortunes of these SINEs during mouse and rat evolution have been different (Fig. 12). B4 probably became extinct before the mouse-rat speciation, while B2 has remained productive in both lineages, scattering >100,000 copies in each genome after this time. Interestingly, the fate of the B1 and ID SINEs has been opposite in rat and mouse. While B1 is still active in mouse, having left over 200,000 mouse-specific copies in its trail, the youngest of the 40,000 rat-specific B1 copies are 6–7% diverged from their source, indicating a relatively early extinction in the rat lineage. On the other hand, after the mouse-rat split only a few hundred ID copies may have inserted in mouse, whereas this previously minor SINE (~60,000 copies predate the speciation) increased its activity in rat to produce 160,000 ID copies.

Co-localization of SINEs in rat and mouse

Despite the different fates of SINE families, the number of SINEs inserted after speciation in each lineage is remarkably similar: ~300,000 copies. Reminiscent of the replacement of MIR by L1 driven SINEs, it seems that the demise of B1 in rat allowed the expansion of IDs. Moreover, these independently inserted and unrelated SINEs (ID and B1 share only a mechanism of retro-position) accumulated at orthologous sites: the density of rat-specific SINEs in 14,243 ~100 kb windows in the rat genome is highly correlated ($R^2 = 0.83$) with the density of mouse-specific SINEs in orthologous regions in mouse. To avoid including elements fixed before the speciation, only SINEs labelled lineage-specific on the basis of subfamily assignment (Methods⁸⁹) were tallied with a divergence from the consensus that was well below the 9% average for neutral sites (Fig. 5). These data corroborate and refine the observation of a strong correlation between the location of primate- and rodent-specific SINEs in 1 Mb windows³. At 100 kb, no correlation is seen for interspersed repeats other than SINEs.

Insertions of SINEs at the same location in different species have been reported^{172–174}, and the correlation could reflect the existence of conserved hotspots for SINE insertions. However, only five of ~800 human specific Alu elements have an Alu inserted within 100–200 bp in any of six other primate lineages^{174–176}. Likewise, gene conversions of shared Alus into lineage-specific copies were observed five times in the same set, too low a level to contribute significantly to the observed correlation^{174–176}.

Figure 9c displays the lineage-specific SINE densities on rat chromosome 10 and in the mouse orthologous blocks, showing a stronger correlation than any other feature. The cause of the unusual distribution patterns of SINEs, accumulating in gene-rich regions where other interspersed repeats are scarce, is apparently a conserved feature, independent of the primary sequence of the SINE and effective over regions smaller than isochores.

In the human genome, the most recent (unfixed) Alus are distributed similarly to L1, whereas older copies gradually take on the opposite distribution of SINEs^{2,164}. This suggested that SINEs insert in the same places as LINEs, and that the typical SINE pattern is due to selection (or deletion bias) rather than a mechanistic insertion bias shared by all (unrelated) SINEs, but not by LINEs that use the same insertion process. This led to a proposal that SINEs are preferentially maintained in regions where they can easily be expressed^{2,164}; if so, this could be the local feature conserved between mammalian genomes that leads to the strong correlation of local SINE densities in different mammals. However, we did not observe this temporal shift in SINE distribution pattern in mouse, nor currently in the rat genome, despite a considerable effort to define the potentially unfixed SINEs in both species (see ref. 89 for details). The observations in human could reflect a recent change in Alu behaviour, which would necessitate another explanation for the contrary insertion-preference of older Alus and all other SINEs.

Some regions of high LINE content coincide with regions that exhibit both higher AT content and an increased rate of point substitution (Fig. 9, pink rectangles). In a genome-wide analysis, LINE content correlates strongly with substitution rates, and about 80% of this correlation is explained by higher rates in AT-rich regions⁸⁹. SINE density shows the opposite correlation both on chromosome 10 (Fig. 9) and genome-wide⁸⁹.

These phenomena, in conjunction with an overall trend in substitution rates towards AT-richness, suggest a model in which quickly evolving regions accumulate a higher-than-average AT content, which attracts LINE elements. Although distinct cause-effect relationships such as this remain largely speculative, these results reinforce the idea that local genomic context strongly shapes local genomic features and rates of evolution.

Endogenous retroviruses and derivatives

The other major contributors to interspersed repeats in the rodent

genome are retrovirus-like elements. These have several 100 bp long terminal repeats (LTRs) with transcriptional regulatory sequences that flank an internal sequence that, in autonomous elements, encodes all proteins necessary for retrotransposition. All mammalian LTR elements are endogenous retroviruses (ERVs) or their non-autonomous derivatives. They fall into three groups, of which representatives in mouse are: murine leukaemia virus (MuLV) (class I), intracisternal A-particle (IAP) and MMTV (class II), and MERV (class III).

The most productive retrovirus in mammals has been the class III element ERV-L, primarily through its ancient non-autonomous derivatives, called MaLRs, with 350,000 copies occupying ~5% of the rat genome (Table 7). Human ERV-L and MaLR copies are >6% diverged from their reconstructed source genes and must have died out around the time of human speciation from New World monkeys. In mouse, several thousand almost identical MaLR and ERV-L copies suggest sustained activity^{177–179}. In contrast, rat ERV-L activity must have been silenced a few million years ago, given that the least diverged MaLR and ERV-L (MTB_Rn and MT2_Rat1) copies differ by >4% from each other. Other class III ERVs were active earlier in rodent evolution, before the mouse–rat speciation.

In contrast to class III ERVs, class I and class II elements still thrive in rat. We reconstructed four rat-specific autonomous class I ERVs, of which two appear still active, and nine class II ERVs, of which four may still be active. The non-autonomous NICER and RAL elements represent over 60% of all rat-specific class I elements. The autonomous drivers of this group, RNNICER2 and 3, with several intact copies, are closely related to the mouse-specific MuLV. Among the potentially active autonomous class II ERVs are MYSERV_Rn, related to the Mys element in *Peromyscus*, and several IAP elements, one with a full-length envelope gene. The most prolific, still-active class II ERV, RNERVK3, is distantly related to the simian retroviruses and, like ERV-L and NICER, has spawned abundant non-autonomous elements characterized by closely related LTRs.

Simple repeats

Whereas the above interspersed repeats derive from transposed sequences, mammalian genomes also contain interspersed simple sequence repeats (SSRs), regions of tandemly repeated short (1–6 bp) units that probably arise from slippage during DNA replication and can expand and compress by unequal crossing

over. Remarkable differences were noted between the SSR contents of the human and mouse genomes³. Three times as many base pairs are contained in near (>90%) perfect SSRs in mouse than in human, and a 4–5-fold excess was revealed when excluding SSRs contained in or seeded by interspersed repeats (primarily SSRs derived from the poly A or simple repeat tails of SINEs and LINEs). SSRs are both more frequent and on average longer in mouse. Polypurine (or polypyrimidine) repeats are especially (tenfold) over-represented in the mouse genome. As discussed above, this contrasts sharply with the greater frequency of triplet repeats coding for amino acids in human than in the rodents.

Rat and mouse SSR contents show, perhaps not surprisingly, much smaller differences. They represent almost the same amount of the rat and mouse genomes (for >90% perfect elements, ~1.4% compared with 0.45% in human) and are of similar average length; for example, the average >90% perfect (CA)_n repeat, the most common SSR in mammals, is 42 bp long in mouse and 44 bp in rat. Some potentially significant differences are that polypurine SSRs are of similar average length but are 1.2-fold more common in mouse, whereas the rare SSRs containing CG dimers are 1.5-fold more frequently observed in rat.

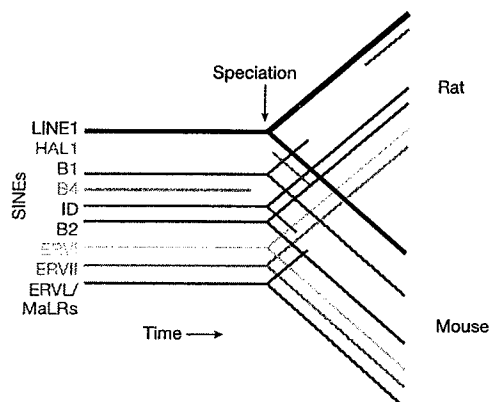


Figure 12 Historical view of rodent repeated sequences. Relationships of the major families of interspersed repeats (Table 7) are shown for the rat and mouse genomes, indicating losses and gains of repeat families after speciation. The lines indicate activity as a function of time. Note that HAL1-like elements appear to have arisen in both the mouse and rat lineages.

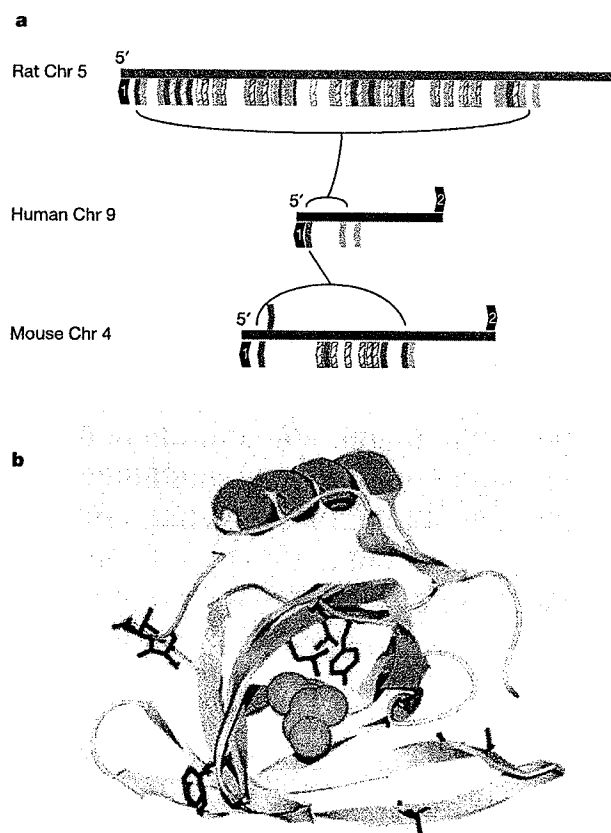


Figure 13 Adaptive remodelling of genomes and genes. **a**, Orthologous regions of rat, human and mouse genomes encoding pheromone-carrier proteins of the lipocalin family (α_{2u} -globulins in rat and major urinary proteins in mouse) shown in brown. Zfp37-like zinc finger genes are shown in blue. Filled arrows represent likely genes, whereas striped arrows represent likely pseudogenes. Gene expansions are bracketed. Arrowhead orientation represents transcriptional direction. Flanking genes 1 and 2 are *TSCOT* and *CTR1*, respectively. **b**, Site-specific K_a/K_s analysis of rat α_{2u} -globulins. Shown in red are side-chains from codons subject to positive selection. These have been mapped to a ribbon representation of the crystal structure of rat α_{2u} -globulin chain A.

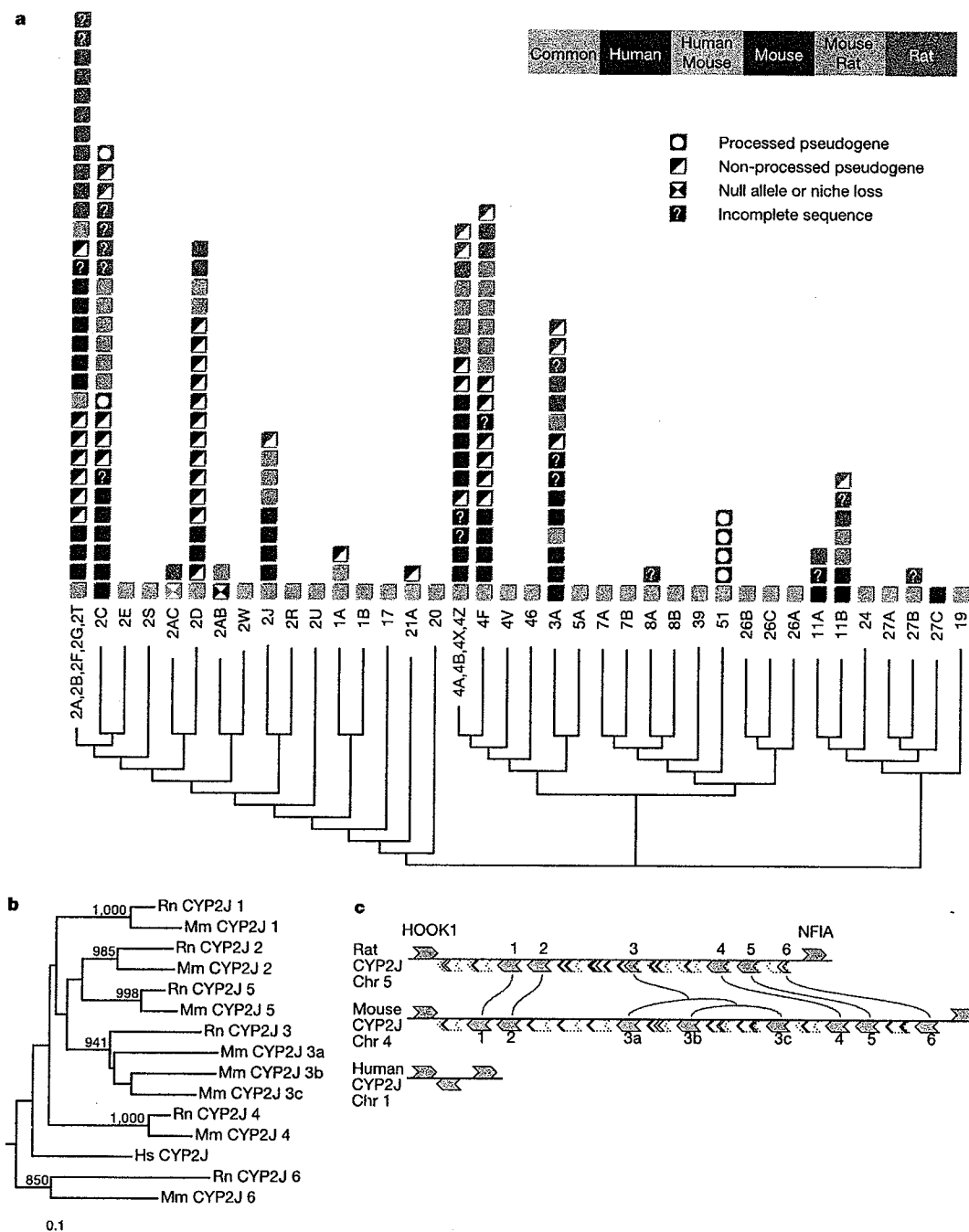


Figure 14 Evolution of cytochrome P450 (CYP) protein families in rat, mouse and human. **a**, Dendrogram topology from 234 full-length sequences. 279 sequences of ≥ 300 amino acids; subfamily names and chromosome numbers are shown. Black branches have $>70\%$ bootstrap support. Incomplete sequences (they contain Ns) are included in counts of functional genes (84 rat, 87 mouse and 57 human) and pseudogenes (including fragments not shown; 77 rat, 121 mouse and 52 human). 64 rat genes and 12 pseudogenes were in predicted gene sets. Human CYP4F is a null allele owing to an in-frame STOP codon in the genome, although a full-length translation exists (SwissProt P98187). Rat CYP27B, missing in the genome, is 'incomplete' because there is a RefSeq entry (NP_446215). Grouped subfamilies CYP2A, 2B, 2F, 2G, 2T and CYP4A, 4B, 4X, 4Z, occur in gene clusters; thus nine loci contain multiple functional genes in a species. One (CYP1A) has fewer rat genes than human, seven have more rodent than human, and all

nine differ in rodent copy numbers. CYP2AC is a rat-specific subfamily (orthologues are pseudogenes). CYP27C has no rodent counterpart. Rodent-specific expansion, rat CYP2J, is illustrated below. **b**, The neighbour-joining tree²²⁴, with the single human gene, contains clear mouse (Mm) and rat (Rn) orthologous pairs (bootstrap values $>700/1,000$ trials shown). Bar indicates 0.1 substitutions per site. **c**, All rat genes have a single mouse counterpart except for CYP2J 3, which has further expanded in mouse (mouse CYP2J 3a, 3b and 3c) by two consecutive single duplications. The genes flanking the CYP2J orthologous regions (rat chromosome 5, 126.9–127.3 Mb; mouse chromosome 4, 94.0–94.6 Mb; human chromosome 1, 54.7–54.8 Mb) are hook1 (HOOK1; pink) and nuclear factor I/A (NFIA; cyan). Genes (solid) and gene fragments (dashed boxes) are shown above (forward strand) and below (reverse strand) the horizontal line. No orthology relation could be concluded for most of these cases.

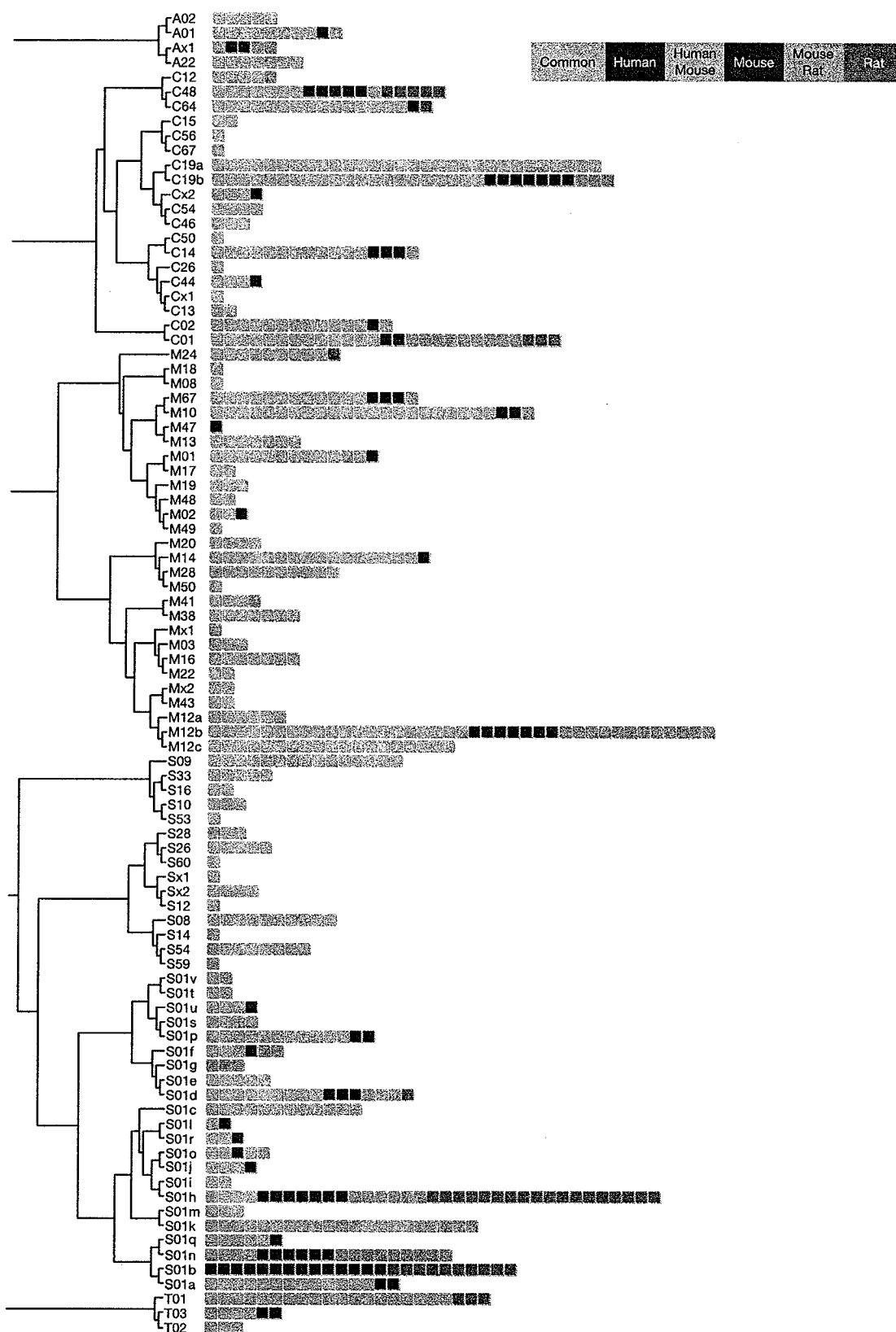


Figure 15 Comparative analysis of rat, mouse and human proteases. The complete non-redundant set of proteases and protease homologues from each species is distributed in five catalytic classes and 67 families. Each square represents a single protease, and is

coloured according to its presence or absence in rat, mouse and human as indicated in the inset.

Prevalent, medium-length duplications in rodents

In addition to the transpositionally derived interspersed repeats and simple repeats detected by RepeatMasker and Tandem Repeat Finder, the rat and mouse genomes contain a substantial amount of medium-length unclassified duplications (typically 100–5,000 bp). These are readily seen in self-comparisons and in intra-rodent comparisons after masking the known repeats, but they are substantially less prevalent in comparisons with the human genome (Supplementary Information). Clearly, a substantial fraction of the rodent genomes consists of currently unexplained repeats and a full characterization awaits further studies. The unclassified duplications may include: (1) novel families of low-copy rodent interspersed repeats; (2) extensions of known but not fully characterized rodent repeats; and (3) duplications generated by a mechanism different from transposition.

Rat-specific biology

A principal ambition of the RGSP was to reveal genetic differences between rats and mice that might specify their differences in physiology and behaviour. This view was well supported by the current draft sequence and predicted gene set. In particular, recently duplicated genes are enriched in elements involved in chemosensation and functional aspects of reproduction (Table 5). Here we illustrate the differences in the gene complements of rat and mouse by in-depth analyses of olfactory receptors (ORs), pheromones, cytochromes P450, proteases and protease inhibitors.

Chemosensation

The ability to emit and sense specific smells is a key feature of survival for most animals in the wild. Another paper¹⁸⁰ describes the evolution of rat and mouse pheromones, vomeronasal receptors, and ORs whose genes were duplicated frequently during the time since the common ancestor of rats and mice (Table 5). Their study yielded over 200 aligned codons predicted to have been subject to adaptive evolution. They attribute the rapid evolution of these genes to conspecific competition—in particular, sexual selection.

Using a homology-based identification procedure with manual curation¹⁸¹, we found 1,866 ORs in 113 locations in the rat genome: 69 multi-gene clusters and 44 single genes. After adjusting for missing sequences (the assembly covers 90.2% of the genome), we extrapolate that there are ~2,070 OR genes and pseudogenes. The rat therefore has ~37% more OR genes and pseudogenes than the ~1,510 ORs of the mouse^{181,182}, assuming similar representation of recently duplicated sequences in the two genome assemblies used. Of the 1,774 OR sequences that are not interrupted by assembly gaps, 1,227 (69%) encode intact proteins, while the remaining 547 (31%) sequences are probably pseudogenes with in-frame stop codons, frameshifts, and/or interspersed repeat elements. Fewer mouse OR homologues are pseudogenes (~20%)^{181,182}, but the larger family size in rat still leaves it with substantially more intact ORs than the mouse (~1,430 versus ~1,210). Striking rat-specific expansions of two ancestral clusters account for much of the difference in OR family size and pseudogene content between rat and mouse, although many other clusters exhibit more subtle changes (not shown). Significant differences between human and mouse OR families have also been reported^{181–183}, but the functional implications of OR repertoire size on the ability of different species to detect and discriminate odorants are not yet known.

α_{2u} -globulin pheromones

The α_{2u} -globulin genes are odorant-binding proteins that also contribute to essential survival functions in animals. α_{2u} -globulin homologues are likely to be highly heterogeneous among murid species. Several homologues (major urinary proteins) sequenced from the BALB/c mouse are distinct from their C57BL/6J mouse counterparts, and these also appear to be arranged differently along its genome¹⁸⁴. Moreover, two full-length genes from other mouse

strains¹⁸⁵ differ from their C57BL/6J orthologues—either lacking two of the bases or retaining 20 of the bases that render the C57BL/6J sequences likely to be pseudogenes (not shown).

The evolution of α_{2u} -globulin genes on rat chromosome 5 has clearly driven a significant 'remodelling' of this genomic region (Fig. 13a). The orthologous human genomic region contains a single homologue, suggesting that the common ancestor of rodents and human possessed one gene. The genome of C57BL/6J mice contains four homologous genes, and seven pseudogenes, whereas the rat genome contains ten α_{2u} -globulin genes and 12 pseudogenes in a single region (Fig. 13a).

Phylogenetic trees constructed using amino acid, and non-coding DNA, sequences show that, surprisingly, the rat α_{2u} -globulin gene clusters appear to have arisen recently via a rapid burst of gene duplication since the rat–mouse split (Table 5; data not shown). This is consistent with the Rfp37-like zinc-finger-like pseudogene having uniquely 'hitchhiked' for virtually all of the rat-specific α_{2u} -globulin gene duplications (Fig. 13a). The sequences of these genes are also evolving rapidly, with median K_A/K_S values of 0.77 and 1.06 for rat and mouse genes, respectively. Amino acid sites that appear to have been subject to adaptive evolution are situated both within the ligand-binding cavity, and on the solvent-exposed periphery of the α_{2u} -globulin structure¹³⁹ (Fig. 13b). This demonstrates how genome analysis can reveal the imprint of adaptive evolution from megabase to single-base levels.

The rapid evolution of these genes, and the remodelling of their genomic regions, can be attributed to the known roles of rat α_{2u} -globulins and mouse major urinary proteins in conspecific competition and sexual selection. These proteins are pheromones and pheromone carriers that are present in large quantities in rodent urine, and act as scent markers indicating dominance and subspecies identity^{186,187}.

Detoxification

Cytochrome P450 is a well-recognized participant in metabolic detoxification, and we also observe rapid evolution within this family. These enzymes metabolize a large number of toxic and endogenous compounds¹⁸⁸ and thus are particularly relevant to clinical and pharmacological studies in humans. As rodents are important model organisms for understanding human drug metabolism, it is important to identify 1:1 orthologues and species-specific expansions and losses¹⁸⁹. Compared with human genes, there are clear expansions of several rodent P450 subfamilies, but there are also significant differences between rat and mouse subfamilies (Fig. 14a). The fastest-evolving subfamily seems to be CYP2J, containing a single gene in human, but at least four in rat and eight in mouse (Fig. 14b, c). CYP2J enzymes catalyse the NADPH-dependent oxidation of arachidonic acid to various eicosanoids, which in turn possess numerous biological activities including modulation of ion transport, control of bronchial and vascular smooth muscle tone, and stimulation of peptide hormone secretion¹⁹⁰. The genomic ordering of genes and their phylogenetic tree indicate an ongoing expansion in the rodents (Fig. 14b, c). This suggests that adaptive evolution has been involved in diversifying their functions. Moreover, detailed study of the nuclear receptors, a highly conserved family of transcription factors, revealed that PXR and CAR, two nuclear receptors regulating CYP genes involved with detoxification¹⁹¹, have the two highest nucleotide substitution rates in their ligand binding domains, whereas SF-1, the nuclear receptor regulating CYP19 (ref. 192), which has not undergone expansion, is more conserved, like other nuclear receptors¹⁹³.

Proteolysis

Protease and protease inhibitor genes also represent an example of rapid evolution in the rat genome. Proteases are a structurally and functionally heterogeneous group of enzymes involved in multiple biological and pathological processes¹⁹⁴. The rat contains 626

protease genes, ~1.7% of the rat gene count¹²⁴, more than human (561) but similar to mouse (641)¹²⁵. Of the rat protease genes, 102 are absent from human, and 42 are absent from mouse (Fig. 15). Several rat gene families have expanded, including placental cathepsins, testases, kallikreins and haematopoietic serine proteases; others appear to have formed pseudogenes in humans (Table 8). These protease families are mainly involved in reproductive or immunological functions, and have evolved independently in the rat and mouse lineages.

The rat protease inhibitor complement contains 183 members, similar to mouse (199) but larger than human (156). As with the protease genes, the rapid evolution in protease inhibitors derives from differential expansions of specific families such as serpins and cystatins. The concomitant expansions in rat and mouse proteases and their inhibitors appear to reflect homeostasis of protein turnover.

These gene family expansions dramatically illustrate how large-scale genomic changes have accompanied species-specific innovation. Positive selection of duplicated genes has afforded the rat an enhanced repertoire of precisely those genes that allow reproductive success despite severe competition from both within its own, and with other, species. This serves as a general illustration of the importance of chemosensation, detoxification and proteolysis in innovation and adaptation.

Human disease gene orthologues in the rat genome

A further strong motivation for sequencing the rat genome was to enhance its utility in biomedical research. Although the rat is already recognized as the premier model for studying the physiological aspects of many human diseases, it has not had as prominent a role in the study of simple genetic disease traits. As more than 1,000 human mendelian disorders now have associated loci and alleles, there is now a tremendous opportunity to link the new knowledge of the rat genome with data from the human disease examples. The precise identification of the rat orthologues of human genes that are mutated in disease creates further opportunities to discover and develop rat models.

Predicted rat genes were compared with 1,112 well-characterized human disease genes¹⁹⁵ that were verified and classified on the basis of pathophysiology (H.H., E.E.W., H.W., K.G.W., H.X., L.G., P.D.S., D.N.C., D.S., M.M.A., C.P.P. and K.F., unpublished work). As predicted by Ensembl, 844 (76%) have 1:1 orthologues in the rat. These predictions are likely to be of high quality because 97.4% of

the 11,422 rat:human 1:1 orthologues predicted by Ensembl were found in orthologous genomic regions.

We asked if these 'disease orthologue' pairs were distinguishable from other rat-human orthologues. Ensembl automatically predicts that 11,522 human genes have rat 1:1 orthologues (corresponding to 46% of all Ensembl predicted human genes). By contrast, a much higher proportion (76%) of human disease genes have Ensembl-predicted rat 1:1 orthologues. Careful analysis of the remaining 268 human genes that were not predicted by Ensembl to show 1:1 orthology indicated that only six of the human disease genes lack likely rat orthologues among genome, cDNA, EST and protein sequences¹⁹⁶. Thus, it appears that, in general, genes involved in human disease are unlikely to have diverged, or to have become duplicated, deleted or lost as pseudogenes, between rat and human (conservation of orthologues discussed above).

We next compared K_S , K_A and the K_A/K_S ratio values of 'disease orthologues' with those of all remaining orthologue pairs. Only the K_S distributions differed significantly¹⁹⁶, suggesting that coding regions of human disease genes and their rat counterparts have mutated more rapidly than the non-disease genes. This might result from factors influencing the specific loci, or the disease genes may characteristically reside in genomic regions that exhibit higher mutation rates.

The disease gene set was next grouped into 16 disease-system categories and analysed using a non-parametric test for K_A/K_S (human/rat)¹⁹⁶ (Fig. 16). Only five disease systems exhibited significant K_A/K_S differences with respect to the remaining samples ($P < 0.05$). Neurological and malformation-syndrome disease categories manifested the lowest median K_A/K_S ratios that are consistent with purifying selection acting on these gene sets. With a comparison of the mean to the mean and standard deviation of the null hypothesis, [(Mean-Mean0)/Std0] of -4.63 ($P < 0.0001$), the neurological disease gene set revealed the most evidence for purifying selection of the disease gene categories examined. In contrast, the pulmonary, haematological and immune categories manifested the highest median K_A/K_S ratios, and the genes of the immune system disease category, with a value for (Mean-Mean0)/Std0 of 4.98 ($P < 0.0001$), show the highest K_A/K_S ratios. These results are consistent with a role for more positive selection, or reduced selective constraints, among these genes.

Where possible, we further considered conservation of these pathophysiology-based gene sets among orthologues of more diverse phyla, including mouse, fish, fly, nematode worm and

Table 8 Protease-expanded gene families and pseudogenes in rat, mouse and human genomes

Protease	Rat gene / locus	Human gene / locus	Mouse gene / locus	Function
Absent genes in assembly	13 from 626 (2.07%)	5 from 561 (0.89%)	5 from 641 (0.78%)	
Expanded families				
Placental cathepsins	10 genes / 17p14	Absent	8 genes / 13B3	Reproduction
Testins	3 genes / 17p14	Absent	3 genes / 13B3	Reproduction
Glandular kallikreins	10 genes / 1q21	Absent	15 genes / 7B2	Reproduction
Mast cell chymases/granzymes	28 genes / 15p13	4 genes / 14q11	17 genes / 14C1	Host defence
Human pseudogenes				
Chymosin	1 gene / 2q34	1 ps / 1p13	1 gene / 3F3	Digestion
Distal intestinal serine proteases	2 genes / 10q12	1 ps / 16p12	2 genes / 17A3	Digestion
Pancreatic elastase	1 gene / 7q35	1 ps / 12q13	1 gene / 15F3	Digestion
Fertilins and reproductive ADAMs	7 genes / various loci	6 ps / various loci	8 genes / various loci	Reproduction
Testases	4 genes / 16q12	3 ps / 8p22	9 genes / 8B1	Reproduction
Testis serine proteases	5 genes / various loci	5 ps / various loci	6 genes / various loci	Reproduction
Implantation serine proteases	2 genes / 10q12	1 ps / 16p13	2 genes / 17A3	Reproduction
Airway trypsin-like proteases	3 genes / 14p21	3 ps / 4q13	3 genes / 5E1	Host defence
Rat pseudogenes				
Calpain 13	1 ps / 6q12	1 gene / 2p23	1 gene / 17E2	Reproduction ?
Pyroglutamy-peptidase II	1 ps / 1q22	1 gene / 15q26	1 gene / 7C	Metabolism
Gln-fructose-6-P transamidase 3	1 ps / Xq14	1 gene / Xq21	1 ps / XC3	Metabolism
Aminopeptidase MAMS/L-RAP	1 ps / 1q12	1 gene / 5q15	1 ps / 17A3	Host defence
Carboxypeptidase O	1 ps / 9q31	1 gene / 2q33	1 ps / 1C2	Unknown
Procollagen III N-endopeptidase	1 ps / 19q12	1 gene / 16q24	1 ps / 8E2	Metabolism ?
Kallikrein-2 and -3	2 ps / 1q21	2 genes / 19q13	1 ps / 7B2	Reproduction
Testis-specific protein 50	1 ps / 8q32	1 gene / 3p21	1 gene / 9F2	Reproduction

yeast orthologues. Overall, we obtained results consistent with those reported here for these rat:human 1:1 orthologous gene disease categories¹⁹⁶. These results demonstrate that the individual genes that constitute various disease systems exhibit significantly different average evolutionary rates. The higher evolutionary rates noted for the immune system disease genes are consistent with a previous finding that lymphocyte-specific genes evolve relatively rapidly¹⁹⁷ and may indicate rapid diversification of the functions of the immune systems of rodents and humans. This is expected for genes involved in controlling species-restricted infectious agents if strong adaptive pressure acts during host-pathogen co-evolution. Thus, the results of studies of these rodent genes may be less directly relevant to our understanding of human immune system diseases than results obtained for other pathophysiology disease systems where conservation is greater and purifying selection is stronger.

We have also specifically examined a number of genes that harbour triplet nucleotide repeats, and are involved in human neurological disorders such as Huntington's disease, a condition known to be caused by CAG triplet repeat expansion producing abnormally long polyglutamine tracts in an otherwise normal protein¹⁹⁸. Analysis of the rat-human orthologues of these disease genes indicated that repeat-expansion disease genes exhibit a repeat length that is substantially shorter in the rat than that found in the normal human gene (Fig. 17). In all cases, human disease genes localize below the line demarcating 1:1 length correlation, showing that rat orthologues uniformly bear shorter repeats. At present, there are no naturally occurring rat strains described that exhibit neurological disease associated with repeat-expansion mechanisms. The shorter repeat length of these orthologues in the rat would be consistent with either the lack of repeat-expansion mutational mechanisms in the rat or the failure of these orthologues to achieve a 'critical repeat length' susceptible to such mutational mechanisms. Other human genes, not at present known to be associated with disease, also contain glutamine repeats that are much shorter in the rat orthologues, and thus, could be investigated as potential disease candidates¹⁹⁶. These triplet-repeat-bearing genes may be susceptible to mutations that arise through repeat-expansion mechanisms. In Fig. 17, it may also be observed that a relatively high proportion of repeats are significantly longer in the rat than in their corresponding human orthologue.

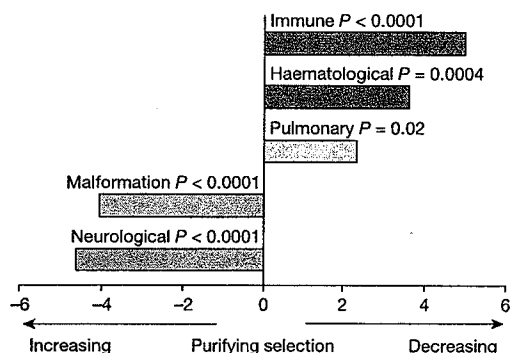


Figure 16 Selective constraints differ for human disease systems in the rat genome. Human disease system categories showing significant differences ($P < 0.05$) in a non-parametric test (Mann-Whitney-Wilcoxon) comparing K_A/K_S (human:rat) ratios. P values from two-level tests between genes from one disease system and the remaining genes. (Mean-Mean0)/Std0 values from multi-level tests from 16 categorized disease systems. Negative values (shown in yellow and orange) for neurological (-4.63) and malformation-syndrome (-4.04) categories were observed to be consistent with K_A/K_S ranges in which purifying selection predominates. Immune, haematological and pulmonary categories show positive values of 4.98, 3.59 and 2.34, respectively (for complete data set and details, see ref. 199).

In addition to enabling the direct comparison of rat-human disease orthologues, the rat genome sequence itself is an invaluable aid for the discovery of additional rat genes that can be studied as disease models. Two general modes can now be pursued. First, genes underlying disease phenotypes with simple inheritance that have been mapped to chromosomal regions can be more easily pursued in both species. Indeed, the rearrangements of conserved segments between the two species in this map were found to have significant value, because they tighten the boundaries of the mapped disease regions and thus reduce the number of genes that could potentially be associated with a given disease phenotype¹¹³. Second, the identification of multiple alleles contributing to quantitative and complex trait differences that are involved in disease processes can be pursued with more accuracy, both in the initial association phases, and in subsequent efforts to detect causative alleles.

Rat single nucleotide polymorphisms

The discovery and cataloguing of the natural DNA variation that persists between individual rat strains will allow further research using rat model systems. Although many rat microsatellites have been characterized and studied, single nucleotide polymorphisms (SNPs) are of more general interest because of their probable ubiquity, and the ease with which they can be assayed. SNP data have three broad applications: (1) the individual markers can be used in ongoing efforts to associate phenotypes that have complex underlying genetic components, with specific sites in the genome. (2) A panel of such markers can be used in conjunction with selective breeding and chromosome mechanics, to generate rat strains that are amenable to the kinds of manipulations that will hasten the discovery of important alleles. (3) A set of such markers can be used to detail the history of the different genomic events that have led to the structure of the genomes of contemporary rat strains. A detailed map of these events has a utility analogous to the current human haplotype (HapMap) mapping project¹⁹⁹ and will probably

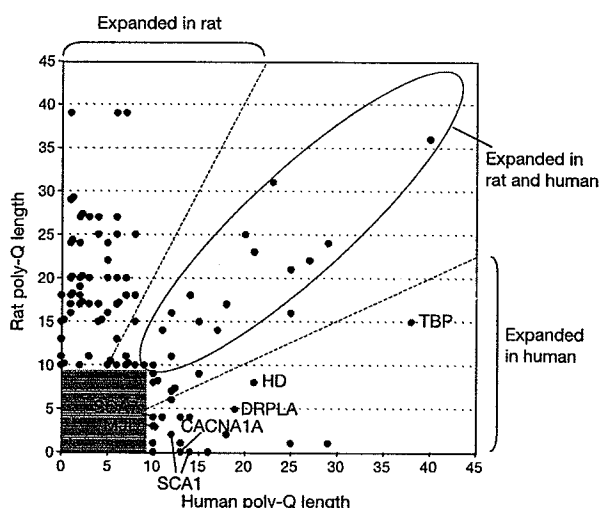


Figure 17 Polyglutamine repeat length comparison between human and rat. Points represent protein poly-Q length for rat and human. Red points correspond to repeats in genes associated with human disease: SCA1, spinocerebellar ataxia 1 protein, or ataxin1; SCA7, spinocerebellar ataxia 7 protein; MJD, Machado-Joseph disease protein; CACNA1A, spinocerebellar ataxia 6 protein, or calcium channel alpha 1A subunit isoform 1; DRPLA, dentatorubral pallidoluysian atrophy protein; HD, Huntington's disease protein, or huntingtin; TBP, TATA binding protein or spinocerebellar ataxia 17 protein. Repeat lengths over ten were examined; green shading delineates the range not included in our analysis. Also noted are a set that are expanded in rat and human (black circle) and a set where repeats are expanded in the rat.

aid disease gene identification, as recently suggested for the mouse²⁰⁰.

The Rnor3.1 draft sequence was generated primarily from DNA of a single inbred rat line. This maximized the likelihood of deriving an accurate sequence assembly, but reduced any likely discovery of natural variation in this phase of the project. As a consequence there has been no large-scale public SNP discovery from rat genomic sequencing. A pilot project based on coding (c)SNP discovery has been initiated, however²⁰¹, as these cSNPs represent a particularly important subset of variants that may have direct functional significance²⁰². These data have illustrated both immediate applications and the long-term potential for an effort aimed at comprehensive SNP discovery.

Conclusions

As the third mammalian genome to be sequenced, the rat genome has provided both predictable and surprising information about mammalian species. Although it was clear at the outset of this programme that ongoing rat research would benefit from the resource of a genome sequence, there was uncertainty about how many new insights would be found, especially considering the superficial similarities between the rat and the already sequenced mouse. Instead, the results of the sequencing and analysis have generated some deep insights into the evolutionary processes that have given rise to these different species. In addition, the project has been invaluable in further developing the methods for the generation and analysis of large genome sequence data sets.

The generation of the rat draft tested the new 'combined approach' for large genome sequencing. As the overall assembly is of high quality, there is no doubt that this overall strategy, and the supporting software we have developed, provides a suitable approach for this problem. Because we included a BAC 'skimming' component in the underlying data set, the assembly recovered a fraction of the genome that was expected, by analogy to the mouse project, to be difficult to assemble from pure WGS data. In addition, the BAC skimming component allowed progressive generation of high-quality local assemblies that were of use to the rat research community as the project developed. On the other hand, although the BAC component used here was far less expensive than the fully ordered and highly redundant set used in the hierarchical approach to sequencing the human genome, it nevertheless increased the overall cost of data production relative to a WGS approach.

The issue of efficacy of WGS versus other approaches to the sequencing of large genomes remains a matter of earnest scientific debate. In ongoing projects at different centres that participated in the RGSP consortium, different approaches are being used to tackle new genomes. These include pure WGS methods, the combined approach and variations on that methodology. The future application of the different procedures depends on the target genome sizes, the expected degree of heterogeneity (that is, polymorphism) in the organism to be sequenced, and the preferences of the individual centre. So far, all the genomes that have been analysed by RGSP consortium members have been of high quality and we anticipate that this will continue as the benefits and disadvantages of different approaches are further studied and analysed.

The rat genome data have improved the utility of the rat model enormously. Now that near-complete knowledge of the rat gene content is realizable, individual researchers have a data source for the rat 'parts list' that can be explored with the high degree of confidence and precision that is appropriate for biomedical research. A similar improvement has been made in the resources for physical and genetic mapping, because the relative position of individual markers is now known with high confidence and there are now computational resources to bridge the process of genetic association with gene modelling and experimental investigation. These advances have been reflected by measured increases in the use of all the rat-specific public genome data sets that can be accessed

online, as well as by the informally assessed increases in overall 'genomic' research of this model.

The expected benefit of a third mammalian sequence providing an outgroup by which to discriminate the timing of events that had already been noted between mouse and human was fully realized. Using the three sequences and other partial data sets from additional organisms, it was possible to measure some of the overall faster rate of evolutionary change in the rodent lineage shared by mice and rats, as well as the peculiar acceleration of some aspects of rat-specific evolution. The observation of specific expanded gene families in the rat should provide material for targeted studies for some time.

At this time there is no plan to further upgrade or finish the rat genome sequence. This programme decision is a consequence of the high cost of converting draft sequence to finished data, and the pressing need to analyse new genomes. However, as the distant objective of very-low-cost sequencing or other advances that can improve draft sequences inexpensively are realized, it might be envisioned that a rat sequence that approaches the quality of the current human data will be produced. A finished rat genome may answer many questions, as specific clues already show that areas of the genome that are most difficult to resolve in a random sequencing project are also those areas that are most dynamic, and therefore of high potential interest in an evolutionary context.

Despite the advances represented here, we are clearly still at the beginning of the full analysis of the mammalian genome and its complex evolutionary history. Much of the additional data that are required to complete this story will be from other genomes, distantly related to rat. Nevertheless, a considerable body of data remains to be developed from this species. In addition to the distant prospect of a finished rat genome, analysis of other rat strains may yield genome-wide polymorphism data, while targeted efforts to generate cDNA clone collections will provide rat-specific reagents for routine use in research. Together with the ongoing efforts to fully develop methods to genetically manipulate whole rats and provide effective 'gene knockouts', the current and future rat genome resources will ensure a place for this organism in genomic and biomedical research for some time. □

Methods

DNA sequencing and data access

Paired-end reads from BAC and WGS libraries were produced as previously described^{2,203}. Unprocessed sequence reads are available from the NCBI Trace Archive (ftp://ftp.ncbi.nih.gov/pub/TraceDB/rattus_norvegicus/); raw eBAC assembly data are available from the BCM-HGSC (<http://www.hgsc.bcm.tmc.edu/Rat/>); and the released Rnor3.1 assembly is available from the BCM-HGSC (<ftp://ftp.hgsc.bcm.tmc.edu/pub/analysis/rat/>), the NCBI (ftp://ftp.ncbi.nih.gov/genomes/R_norvegicus/), and the UCSC (<http://genome.ucsc.edu/downloads.html>).

Genome assembly

Assembly of the rat genome by the *Atlas* system is described in detail elsewhere²⁴. Earlier assemblies (Rnor2.0/2.1) of the initial data set were based on 40 million total reads and 19,000 BAC skims. These assemblies spanned 2.66 Gb and comprised over 900 ultrabac tags with N_{50} of over 5 Mb. They differed only in the removal of short artefactual duplications from Rnor2.0. Rnor3.1 includes another 1,100 BACs, selected to fill gaps in Rnor2.1. Because of the comprehensive coverage of the genome by Rnor2.0/2.1, it was used for the initial predictions of genes and proteins.

BAC fingerprints

An agarose-gel-based fingerprinting methodology^{204–207} was employed to generate *Hind*III fingerprints from 199,782 clones in the CHORI-230 BAC library. The contig assembly was subjected to manual review and editing to refine clone order within contigs and to make merges between contigs, using tools provided in the FPC software^{208–210}. Fingerprints for 5,250 RPCI-31 PACs²¹¹ and RPCI-32 BACs were subsequently added to allow correlation between the fingerprint map and a developing YAC map of the rat genome. BAC and PAC clones are available through BACPAC Resources at CHORI (bacpacorders@chori.org).

BAC, PAC and YAC maps

Markers generated from BAC and PAC clones were hybridized against YAC²⁸ (R.D., Pmatch, unpublished software) and radiation hybrid libraries^{21,22} to produce independent maps that were subsequently combined. Genetic markers from two rat

genetic maps⁶¹ and the radiation hybrid map⁵⁹ were aligned to the Rnor3.1 assembly using BLAT¹²³ (when sequence was available) or electronic polymerase chain reaction (EPCR)²¹³.

Finished sequence used for quality assessment of the assembly

To assess the accuracy of the *Atlas* assembly, the Rnor3.1 sequence was compared to 13 Mb of sequences that had been finished to high quality.

Large-scale rearrangements

We compared these assemblies: Human (April 2003, NCBI build 33); Mouse (February 2003, NCBI build 30); and Rat (June 2003, Rnor3.1). Repeats were masked using RepeatMasker (A.S. & P. Green, unpublished work; see <http://ftp.genome.washington.edu/RM/RepeatMasker.html>) and TandemRepeatFinder²¹⁴. Local alignments were produced using PatternHunter⁷⁰ (Supplementary Information). Repeat contamination was removed and the remaining similarities combined into two- and three-way anchors⁷³ and syntenic blocks produced at various resolutions using GRIMM-Synten⁷¹.

Genome-wide visualization of conserved synteny

Pairwise comparisons of the genomes of human, mouse and rat using MULTIZ^{69,215}, MLAGAN^{216,217}, MAVID¹¹⁰, PatternHunter⁷⁰ and Pash⁷² were merged into blocks of conserved synteny^{69,71,72}, and the 1-Mb-resolution images were displayed using the Virtual Genome Painting method (M.L.G.-G. *et al.*, unpublished work; <http://www.genboree.org>).

Rat segmental duplications

Segmental duplications >5 kb were identified, extracted and aligned as described²¹⁸, and paralogous sequence relationships were assessed using PARASIGHT visualization software (J.A.B., unpublished work; Supplementary Information).

Venn diagram

Pairwise and three-way alignments generated using BLASTZ²¹⁹ and MULTIZ²¹⁵ or HUMOR²¹⁵ were analysed to classify each nucleotide in the three genomes by the species with which it aligns: in all three species, aligning between human and rat (but not mouse), between human and mouse (but not rat), or between mouse and rat (but not human). Other nucleotides are species-specific; unassigned nucleotides occupying gaps in the genome assemblies were excluded. On the basis of output from RepeatMasker¹⁶⁴ and RepeatDater⁸⁹, nucleotides were assigned to categories (of non-repetitive, repetitive with a certain ancestry, or repetitive but unassigned) and counted. See Supplementary Table SI-1 for details.

Gene prediction

ENSEMBL transcript models were built from 28,478 rodent proteins that were aligned to the genome using a combination of Pmatch (R.D., unpublished software), BLAST²²⁰ and GeneWise²²¹. Models based on 5,083 vertebrate proteins were added in regions without rodent-protein-based models. UTRs were added using 11,170 transcripts built from 8,615 different rat cDNAs aligned to the genome using BLAT, with coverage ≥90% and identity ≥95%. This procedure (as described¹¹² but without GENSCAN predictions), gave rise to 18,241 genes and 20,373 transcripts. This is the protein-based gene set. Rat and mouse cDNA and rat EST-based gene sets were also built. See Supplementary Information for details.

Non-processed pseudogene identification

Human and mouse genes related by 1:1 orthology and lacking an apparent rat orthologue were considered. See Supplementary Information for details.

High-resolution analyses of chromosome 10

These were performed predominantly on the whole genome alignments²¹⁷. Plots in Fig. 9 were generated by sliding windows of width 2 Mb and a step size of 400 kb (total = 277 windows). See Supplementary Information for details.

Received 31 December 2003; accepted 20 February 2004; doi:10.1038/nature02426.

1. Darwin, C. *On The Origin of Species by Means of Natural Selection* 1st edn, Ch. 4, 108 (John Murray, London, 1859).
2. International Human Genome Sequencing Consortium. Initial sequencing and analysis of the human genome. *Nature* **409**, 860–921 (2001).
3. Mouse Genome Sequencing Consortium. Initial sequencing and comparative analysis of the mouse genome. *Nature* **420**, 520–562 (2002).
4. Adkins, R. M., Gelke, E. L., Rowe, D. & Honeycutt, R. L. Molecular phylogeny and divergence time estimates for major rodent groups: evidence from multiple genes. *Mol. Biol. Evol.* **18**, 777–791 (2001).
5. Springer, M. S., Murphy, W. J., Eizirik, E. & O'Brien, S. J. Placental mammal diversification and the Cretaceous-Tertiary boundary. *Proc. Natl Acad. Sci. USA* **100**, 1056–1061 (2003).
6. Canby, T. Y. The rat, lapdog of the devil. *Nat. Geogr.* July, 60–87 (1977).
7. Robinson, R. *Genetics of the Norway Rat* (Pergamon, Oxford, 1965).
8. Barnett, S. A. *The Story of Rats. Their Impact on Us, and Our Impact on Them* Ch. 2, 17–18 (Allen and Unwin, Crows Nest, Australia, 2002).
9. Hedrich, H. J. in *History, Strains, and Models in the Laboratory Rat* (ed. Krinke, G. J.) 3–16 (Academic, San Diego, 2000).
10. Lindsey, J. R. in *The Laboratory Rat* (eds Baker, H. J., Lindsey, J. R. & Weisbroth, S. H.) 1–36 (Academic, New York, 1979).
11. Greenhouse, D. D., Festing, M. F. W., Hasan, S. & Cohen, A. L. in *Genetic Monitoring of Inbred Strains of Rats* (ed. Hedrich, H. J.) 410–480 (Gustav Fischer, Stuttgart, 1990).

12. Kuntz, C. *et al.* Comparison of laparoscopic versus conventional technique in colonic and liver resection in a tumor-bearing small animal model. *Surg. Endosc.* **16**, 1175–1181 (2002).
13. Kitagawa, K., Hamada, Y., Nakai, K., Kato, Y. & Okumura, T. Comparison of one- and two-step procedures in a rat model of small bowel transplantation. *Transplant. Proc.* **34**, 1030–1032 (2002).
14. Sauve, Y., Girman, S. V., Wang, S., Keegan, D. J. & Lund, R. D. Preservation of visual responsiveness in the superior colliculus of RCS rats after retinal pigment epithelium cell transplantation. *Neuroscience* **114**, 389–401 (2002).
15. Wang, H. *et al.* Attenuation of acute xenograft rejection by short-term treatment with LF15–0195 and monoclonal antibody against CD45RB in a rat-to-mouse cardiac transplantation model. *Transplantation* **75**, 1475–1481 (2003).
16. Alves, A. *et al.* Total vascular exclusion of the liver enhances the efficacy of retroviral-mediated associated thymidine kinase and interleukin-2 genes transfer against multiple hepatic tumors in rats. *Surgery* **133**, 669–677 (2003).
17. Liu, M. Y., Poellinger, L. & Walker, C. L. Up-regulation of hypoxia-inducible factor 2α in renal cell carcinoma associated with loss of Tsc-2 tumor suppressor gene. *Cancer Res.* **63**, 2675–2680 (2003).
18. Jin, X. *et al.* Effects of leptin on endothelial function with OB-Rb gene transfer in Zucker fatty rats. *Atherosclerosis* **169**, 225–233 (2003).
19. Ravingerova, T., Neckar, J. & Kolar, F. Ischemic tolerance of rat hearts in acute and chronic phases of experimental diabetes. *Mol. Cell. Biochem.* **249**, 167–174 (2003).
20. Taylor, J. R. *et al.* An animal model of Tourette's syndrome. *Am. J. Psychiatry* **159**, 657–660 (2002).
21. Smyth, M. D., Barbaro, N. M. & Baraban, S. C. Effects of antiepileptic drugs on induced epileptiform activity in a rat model of dysplasia. *Epilepsy Res.* **50**, 251–264 (2002).
22. McBride, W. J. & Li, T. K. Animal models of alcoholism: neurobiology of high alcohol-drinking behavior in rodents. *Crit. Rev. Neurobiol.* **12**, 339–369 (1998).
23. Crisci, A. R. & Ferreira, A. L. Low-intensity pulsed ultrasound accelerates the regeneration of the sciatic nerve after neurotomy in rats. *Ultrasound Med. Biol.* **28**, 1335–1341 (2002).
24. Ozkan, O. *et al.* Reinnervation of denervated muscle in a split-nerve transfer model. *Ann. Plast. Surg.* **49**, 532–540 (2002).
25. Fray, M. J., Dickinson, R. P., Huggins, J. P. & Ocleston, N. L. A potent, selective inhibitor of matrix metalloproteinase-3 for the topical treatment of chronic dermal ulcers. *J. Med. Chem.* **46**, 3514–3525 (2003).
26. Petratos, P. B. *et al.* Full-thickness human foreskin transplantation onto nude rats as an *in vivo* model of acute human wound healing. *Plast. Reconstr. Surg.* **111**, 1988–1997 (2003).
27. Hussar, P. *et al.* Bone healing models in rat tibia after different injuries. *Ann. Chir. Gynaecol.* **90**, 271–279 (2001).
28. Yang, T. D., Pei, J. S., Yang, S. L., Liu, Z. Q. & Sun, R. L. Medical prevention of space motion sickness—animal model of therapeutic effect of a new medicine on motion sickness. *Adv. Space Res.* **30**, 751–755 (2002).
29. Forte, A. *et al.* Stenosis progression after surgical injury in Milan hypertensive rat carotid arteries. *Cardiovasc. Res.* **60**, 654–663 (2003).
30. Komamura, K. *et al.* Differential gene expression in the rat skeletal and heart muscle in glucocorticoid-induced myopathy: analysis by microarray. *Cardiovasc. Drugs Ther.* **17**, 303–310 (2003).
31. McBride, M. W. *et al.* Functional genomics in rodent models of hypertension. *J. Physiol. (Lond.)* **554**, 56–63 (2004).
32. Kasteleijn-Nolst Trenite, D. G. & Hirsch, E. Levitracetam: preliminary efficacy in generalized seizures. *Epileptic Disord.* **5**, S39–S44 (2003).
33. Malik, A. S. *et al.* A novel dehydroepiandrosterone analog improves functional recovery in a rat traumatic brain injury model. *J. Neurotrauma* **20**, 463–476 (2003).
34. Kostubsky, V. E. *et al.* Evaluation of hepatotoxic potential of drugs by inhibition of bile acid transport in cultured primary human hepatocytes and intact rats. *Toxicol. Sci.* **76**, 220–228 (2003).
35. Lindon, J. C. *et al.* Contemporary issues in toxicology: the role of metabolomics in toxicology and its evaluation by the COMET project. *Toxicol. Appl. Pharmacol.* **187**, 137–146 (2003).
36. Tam, R. C. *et al.* The ribavirin analog ICN 17261 demonstrates reduced toxicity and antiviral effects with retention of both immunomodulatory activity and reduction of hepatitis-induced serum alanine aminotransferase levels. *Antimicrob. Agents Chemother.* **44**, 1276–1283 (2000).
37. Yousef, A. F., Turck, P. & Fort, F. L. Safety and pharmacokinetics of oral lansoprazole in preadolescent rats exposed from weaning through sexual maturity. *Reprod. Toxicol.* **17**, 109–116 (2003).
38. National Institutes of Health. *Network for Large-Scale Sequencing of the Rat Genome* (<http://grants2.nih.gov/grants/guide/rfa-files/RFA-HG-00-002.html>) (2000).
39. Aparicio, S. *et al.* Whole-genome shotgun assembly and analysis of the genome of *Fugu rubripes*. *Science* **297**, 1301–1310 (2002).
40. Yu, J. *et al.* A draft sequence of the rice genome (*Oryza sativa* L. ssp. *indica*). *Science* **296**, 79–92 (2002).
41. Goff, S. A. *et al.* A draft sequence of the rice genome (*Oryza sativa* L. ssp. *japonica*). *Science* **296**, 92–100 (2002).
42. Adams, M. D. *et al.* The genome sequence of *Drosophila melanogaster*. *Science* **287**, 2185–2195 (2000).
43. Dehal, P. *et al.* The draft genome of *Ciona intestinalis*: insights into chordate and vertebrate origins. *Science* **298**, 2157–2167 (2002).
44. Myers, E. W. *et al.* A whole-genome assembly of *Drosophila*. *Science* **287**, 2196–2204 (2000).
45. Myers, E. W., Sutton, G. G., Smith, H. O., Adams, M. D. & Venter, J. C. On the sequencing and assembly of the human genome. *Proc. Natl Acad. Sci. USA* **99**, 4145–4146 (2002).
46. Waterston, R. H., Lander, E. S. & Sulston, J. E. On the sequencing of the human genome. *Proc. Natl Acad. Sci. USA* **99**, 3712–3716 (2002).
47. Waterston, R. H., Lander, E. S. & Sulston, J. E. More on the sequencing of the human genome. *Proc. Natl Acad. Sci. USA* **100**, 3022–3024 (2003); author reply (100), 3025–3026 (2003).
48. Green, P. Whole-genome disassembly. *Proc. Natl Acad. Sci. USA* **99**, 4143–4144 (2002).
49. Batzoglou, S. *et al.* ARACHNE: a whole-genome shotgun assembler. *Genome Res.* **12**, 177–189 (2002).

50. Jaffe, D. B. *et al.* Whole-genome sequence assembly for mammalian genomes: Arachne 2. *Genome Res.* 13, 91–96 (2003).
51. Cheung, J. *et al.* Recent segmental and gene duplications in the mouse genome. *Genome Biol.* 4, R47 [online] (2003).
52. Eichler, E. E. Masquerading repeats: Paralogous pitfalls of the human genome. *Genome Res.* 8, 758–762 (1998).
53. Eichler, E. E. Segmental duplications: what's missing, misassigned, and misassembled—and should we care? *Genome Res.* 11, 653–656 (2001).
54. Havlak, P. *et al.* The Atlas genome assembly system. *Genome Res.* 14, 721–732 (2004).
55. Osoegawa, K. *et al.* BAC Resources for the rat genome project. *Genome Res.* 14, 780–785 (2004).
56. Krzywinski, M. *et al.* Integrated and sequence-ordered BAC and YAC-based physical maps for the rat genome. *Genome Res.* 14, 766–779 (2004).
57. Chen, R., Sodergren, E., Gibbs, R. & Weinstock, G. M. Dynamic building of a BAC clone tiling path for genome sequencing project. *Genome Res.* 14, 679–684 (2004).
58. Cai, L. *et al.* Construction and characterization of a 10-genome equivalent yeast artificial chromosome library for the laboratory rat, *Rattus norvegicus*. *Genomics* 39, 385–392 (1997).
59. Kwitek, A. E. *et al.* High density rat radiation hybrid maps containing over 24,000 SSLPs, genes, and ESTs provide a direct link to the rat genome sequence. *Genome Res.* 14, 750–757 (2004).
60. Felsenfeld, A., Peterson, J., Schloss, J. & Guyer, M. Assessing the quality of the DNA sequence from the Human Genome Project. *Genome Res.* 9, 1–4 (1999).
61. Steen, R. G. *et al.* A high-density integrated genetic linkage and radiation hybrid map of the laboratory rat. *Genome Res.* 9 (insert), AP1–AP8 (1999).
62. Misra, S. *et al.* Annotation of the *Drosophila melanogaster* euchromatic genome: a systematic review. *Genome Biol.* 3, RESEARCH0083.1–0083.22 [online] (2002).
63. Li, X. & Waterman, M. S. Estimating the repeat structure and length of DNA sequences using L-tuples. *Genome Res.* 13, 1916–1922 (2003).
64. Riethman, H. *et al.* Mapping and initial analysis of human subtelomeric sequence assemblies. *Genome Res.* 14, 18–28 (2004).
65. Bayona-Bafaluy, M. P. *et al.* Revisiting the mouse mitochondrial DNA sequence. *Nucleic Acids Res.* 31, 5349–5355 (2003).
66. Kent, W. J., Baertsch, R., Hinrichs, A., Miller, W. & Haussler, D. Evolution's cauldron: duplication, deletion, and rearrangement in the mouse and human genomes. *Proc. Natl Acad. Sci. USA* 100, 11484–11489 (2003).
67. Pevzner, P. & Tesler, G. Human and mouse genomic sequences reveal extensive breakpoint reuse in mammalian evolution. *Proc. Natl Acad. Sci. USA* 100, 7672–7677 (2003).
68. Nadeau, J. H. & Taylor, B. A. Lengths of chromosomal segments conserved since divergence of man and mouse. *Proc. Natl Acad. Sci. USA* 81, 814–818 (1984).
69. Schwartz, S. *et al.* Human–mouse alignments with BLASTZ. *Genome Res.* 13, 103–107 (2003).
70. Ma, B., Tromp, J. & Li, M. PatternHunter: faster and more sensitive homology search. *Bioinformatics* 18, 440–445 (2002).
71. Pevzner, P. & Tesler, G. Genome rearrangements in mammalian evolution: lessons from human and mouse genomes. *Genome Res.* 13, 37–45 (2003).
72. Kalafatis, K. J., Jackson, A. R. & Milosavljevic, A. Pash: Efficient genome-scale sequence anchoring by positional hashing. *Genome Res.* 14, 672–678 (2004).
73. Bourque, G., Pevzner, P. A. & Tesler, G. Reconstructing the genomic architecture of ancestral mammals: lessons from human, mouse, and rat genomes. *Genome Res.* 14, 507–516 (2004).
74. Graves, J. A., Geetz, J. & Hamerster, H. Evolution of the human X—a smart and sexy chromosome that controls speciation and development. *Cytogenet. Genome Res.* 99, 141–145 (2002).
75. Bourque, G. & Pevzner, P. A. Genome-scale evolution: reconstructing gene orders in the ancestral species. *Genome Res.* 12, 26–36 (2002).
76. Murphy, W. J., Bourque, G., Tesler, G., Pevzner, P. & O'Brien, S. J. Reconstructing the genomic architecture of mammalian genomes using multispecies comparative maps. *Hum. Genom.* 1, 30–40 (2003).
77. Kirkness, E. F. *et al.* The dog genome: survey sequencing and comparative analysis. *Science* 301, 1898–1903 (2003).
78. Murphy, W. J., Sun, S., Chen, Z. Q., Pecon-Slatery, J. & O'Brien, S. J. Extensive conservation of sex chromosome organization between cat and human revealed by parallel radiation hybrid mapping. *Genome Res.* 9, 1223–1230 (1999).
79. Ventura, M., Archidiacono, N. & Rocchi, M. Centromere emergence in evolution. *Genome Res.* 11, 595–599 (2001).
80. Yunis, J. J. & Prakash, O. The origin of man: a chromosomal pictorial legacy. *Science* 215, 1525–1530 (1982).
81. Murphy, W. J., Fronick, L., O'Brien, S. J. & Stanyon, R. The origin of human chromosome 1 and its homologs in placental mammals. *Genome Res.* 13, 1880–1888 (2003).
82. Stanyon, R., Stone, G., Garcia, M. & Fronick, L. Reciprocal chromosome painting shows that squirrels, unlike murid rodents, have a highly conserved genome organization. *Genomics* 82, 245–249 (2003).
83. Bailey, J. A. *et al.* Recent segmental duplications in the human genome. *Science* 297, 1003–1007 (2002).
84. Thomas, J. W. *et al.* Pericentromeric duplications in the laboratory mouse. *Genome Res.* 13, 55–63 (2003).
85. Horvath, J. E. *et al.* Using a pericentromeric interspersed repeat to recapitulate the phylogeny and expansion of human centromeric segmental duplications. *Mol. Biol. Evol.* 20, 1463–1479 (2003).
86. Guy, J. *et al.* Genomic sequence and transcriptional profile of the boundary between pericentromeric satellites and genes on human chromosome arm 10p. *Genome Res.* 13, 159–172 (2003).
87. Tuzun, E., Bailey, J. A. & Eichler, E. E. Recent segmental duplications in the working draft assembly of the brown Norway rat. *Genome Res.* 14, 493–506 (2004).
88. Pruitt, K. D. & Maglott, D. R. RefSeq and LocusLink: NCBI gene-centered resources. *Nucleic Acids Res.* 29, 137–140 (2001).
89. Yang, S. *et al.* Patterns of insertions and their covariation with substitutions in the rat, mouse and human genomes. *Genome Res.* 14, 517–527 (2004).
90. Roskin, K. M., Diekhans, M. & Haussler, D. In *Proc. 7th Annu. Int. Conf. Res. Comput. Mol. Biol. (RECOMB 2003)* (eds Vingron, M., Istrail, S., Pevzner, P. & Waterman, M.) doi:10.1145/640075.640109, 257–266 (ACM Press, New York, 2003).
91. Chiaromonte, F. *et al.* The share of human genomic DNA under selection estimated from human–mouse genomic alignments. *Cold Spring Harbor Symp. Quant. Biol.* (in the press).
92. Cooper, G. M. *et al.* Characterization of evolutionary rates and constraints in three mammalian genomes. *Genome Res.* 14, 539–548 (2004).
93. Dermitzakis, E. T. *et al.* Numerous potentially functional but non-genic conserved sequences on human chromosome 21. *Nature* 420, 578–582 (2002).
94. Dermitzakis, E. T. *et al.* Evolutionary discrimination of mammalian conserved non-genic sequences (CNGs). *Science* 302, 1033–1035 (2003).
95. Nekrutenko, A. Rat–mouse comparisons to identify rodent-specific exons. *Genome Res.* (in the press).
96. Hardison, R. C. *et al.* Covariation in frequencies of substitution, deletion, transposition, and recombination during eutherian evolution. *Genome Res.* 13, 13–26 (2003).
97. Thomas, J. W. *et al.* Comparative analyses of multi-species sequences from targeted genomic regions. *Nature* 424, 788–793 (2003).
98. Cooper, G. M., Brudno, M., Green, E. D., Batzoglou, S. & Sidow, A. Quantitative estimates of sequence divergence for comparative analyses of mammalian genomes. *Genome Res.* 13, 813–820 (2003).
99. Huckins, C. The spermatogonial stem cell population in adult rats. I. Their morphology, proliferation and maturation. *Anat. Rec.* 169, 533–557 (1971).
100. Clermont, Y. Kinetics of spermatogenesis in mammals: seminiferous epithelium cycle and spermatogonial renewal. *Physiol. Rev.* 52, 198–236 (1972).
101. Makova, K. D., Yang, S. & Chiaromonte, F. Insertions and deletions are male biased too: A whole-genome analysis in rodents. *Genome Res.* 14, 567–573 (2004).
102. Sundstrom, H., Webster, M. T. & Ellegren, H. Is the rate of insertion and deletion mutation male biased? Molecular evolutionary analysis of avian and primate sex chromosome sequences. *Genetics* 164, 259–268 (2003).
103. Chang, B. H. & Li, W. H. Estimating the intensity of male-driven evolution in rodents by using X-linked and Y-linked Ube 1 genes and pseudogenes. *J. Mol. Evol.* 40, 70–77 (1995).
104. Chang, B. H., Shimmin, L. C., Shyue, S. K., Hewett-Emmett, D. & Li, W. H. Weak male-driven molecular evolution in rodents. *Proc. Natl Acad. Sci. USA* 91, 827–831 (1994).
105. Bird, A. P. DNA methylation and the frequency of CpG in animal DNA. *Nucleic Acids Res.* 8, 1499–1504 (1980).
106. Antequera, F. & Bird, A. Number of CpG islands and genes in human and mouse. *Proc. Natl Acad. Sci. USA* 90, 11995–11999 (1993).
107. Jensen-Seaman, M. I. *et al.* Comparative recombination rates in the rat, mouse, and human genomes. *Genome Res.* 14, 528–538 (2004).
108. Birdsall, J. A. Integrating genomics, bioinformatics, and classical genetics to study the effects of recombination on genome evolution. *Mol. Biol. Evol.* 19, 1181–1197 (2002).
109. Montoya-Burgos, J. I., Boursot, P. & Galtier, N. Recombination explains isochores in mammalian genomes. *Trends Genet.* 19, 128–130 (2003).
110. Bray, N. & Pachter, L. MAVID Constrained ancestral alignment of multiple sequence. *Genome Res.* 14, 693–699 (2004).
111. Yap, V. B. & Pachter, L. Identification of evolutionary hotspots in the rodent genomes. *Genome Res.* 14, 574–579 (2004).
112. Hubbard, T. *et al.* The Ensembl genome database project. *Nucleic Acids Res.* 30, 38–41 (2002).
113. Vitt, U. *et al.* Identification of candidate disease genes by EST alignments, synteny and expression and verification of Ensembl genes on rat chromosome 1q43–54. *Genome Res.* 14, 640–650 (2004).
114. Burge, C. & Karlin, S. Prediction of complete gene structures in human genomic DNA. *J. Mol. Biol.* 268, 78–94 (1997).
115. Guigo, R., Knudsen, S., Drake, N. & Smith, T. Prediction of gene structure. *J. Mol. Biol.* 226, 141–157 (1992).
116. Soloviyev, V. V., Salamov, A. A. & Lawrence, C. B. Identification of human gene structure using linear discriminant functions and dynamic programming. *Proc. Int. Conf. Intell. Syst. Mol. Biol.* 3, 367–375 (1995).
117. Parra, G. *et al.* Comparative gene prediction in human and mouse. *Genome Res.* 13, 108–117 (2003).
118. Alexandersson, M., Cawley, S. & Pachter, L. SLAM—Cross-species gene finding with a generalized pair hidden Markov model. *Genome Res.* 13, 496–502 (2003).
119. Flicek, P., Keibler, E., Hu, P., Korf, I. & Brent, M. R. Leveraging the mouse genome for gene prediction in human: from whole-genome shotgun reads to a global synteny map. *Genome Res.* 13, 46–54 (2003).
120. Korf, I., Flicek, P., Duan, D. & Brent, M. R. Integrating genomic homology into gene structure prediction. *Bioinformatics* 17 (suppl. 1), S140–S148 (2001).
121. Wu, J. Q., Shetye, D., Arumugam, M., Gibbs, R. A. & Brent, M. R. Identification of rat genes by TWINSCAN gene prediction, RT–PCR, and direct sequencing. *Genome Res.* 14, 655–671 (2004).
122. Dewey, C. *et al.* Accurate identification of novel human genes through simultaneous gene prediction in human, mouse and rat. *Genome Res.* 14, 661–664 (2004).
123. Kent, W. J. BLAT—the BLAST-like alignment tool. *Genome Res.* 12, 656–664 (2002).
124. Puente, X. S. & Lopez-Otin, C. A. A genomic analysis of rat proteases and protease inhibitors. *Genome Res.* 14, 609–622 (2004).
125. Puente, X. S., Sanchez, L. M., Overall, C. M. & Lopez-Otin, C. Human and mouse proteases: a comparative genomic approach. *Nature Rev. Genet.* 4, 544–558 (2003).
126. Hurst, L. D. The Ka/Ks ratio: diagnosing the form of sequence evolution. *Trends Genet.* 18, 486–487 (2002).
127. Makalowski, W. & Boguski, M. S. Evolutionary parameters of the transcribed mammalian genome: an analysis of 2,820 orthologous rodent and human sequences. *Proc. Natl Acad. Sci. USA* 95, 9407–9412 (1998).
128. Wolfe, K. H. & Sharp, P. M. Mammalian gene evolution: nucleotide sequence divergence between mouse and rat. *J. Mol. Evol.* 37, 441–456 (1993).
129. Modrek, B. & Lee, C. J. Alternative splicing in human, mouse and rat genomes is associated with an increased frequency of exon creation and/or loss. *Nature Genet.* 34, 177–180 (2003).
130. Nekrutenko, A., Makova, K. D. & Li, W. H. The K_A/K_S ratio test for assessing the protein-coding potential of genomic regions: an empirical and simulation study. *Genome Res.* 12, 198–202 (2002).

131. Nekrutenko, A., Chung, W. Y. & Li, W. H. An evolutionary approach reveals a high protein-coding capacity of the human genome. *Trends Genet.* 19, 306–310 (2003).
132. Taylor, M. S., Ponting, C. P. & Copley, R. R. Occurrence and consequences of coding sequence insertions and deletions in mammalian genomes. *Genome Res.* 14, 555–566 (2004).
133. Green, H. & Wang, N. Codon reiteration and the evolution of proteins. *Proc. Natl Acad. Sci. USA* 91, 4298–4302 (1994).
134. Levinson, G. & Gutman, G. A. Slipped-strand mispairing: a major mechanism for DNA sequence evolution. *Mol. Biol. Evol.* 4, 203–221 (1987).
135. Alba, M. M. & Guigo, R. Comparative analysis of amino acid repeats in rodents and humans. *Genome Res.* 14, 549–554 (2004).
136. Alba, M. M., Santibanez-Koref, M. F. & Hancock, J. M. Conservation of polyglutamine tract size between mice and humans depends on codon interruption. *Mol. Biol. Evol.* 16, 1641–1644 (1999).
137. Burge, C. B., Padgett, R. A. & Sharp, P. A. Evolutionary fates and origins of U12-type introns. *Mol. Cell* 2, 773–785 (1998).
138. Ohno, S. *Evolution by Gene Duplication* (Springer, Berlin, 1970).
139. Emes, R. D., Goodstadt, L., Winter, E. E. & Ponting, C. P. Comparison of the genomes of human and mouse lays the foundation of genome zoology. *Hum. Mol. Genet.* 12, 701–709 (2003).
140. Lynch, M. & Conery, J. S. The evolutionary fate and consequences of duplicate genes. *Science* 290, 1151–1155 (2000).
141. Prince, V. E. & Pickett, F. B. Splitting pairs: the diverging fates of duplicated genes. *Nature Rev. Genet.* 3, 827–837 (2002).
142. Hughes, A. L. *Adaptive Evolution of Genes and Genomes* Ch. 7, 143–179 (Oxford Univ. Press, New York, 1999).
143. Tagle, D. A. et al. Embryonic epsilon and gamma globin genes of a prosimian primate (*Galago crassicaudatus*). Nucleotide and amino acid sequences, developmental regulation and phylogenetic footprints. *J. Mol. Biol.* 203, 439–455 (1988).
144. Altschul, S. F. & Lipman, D. J. Protein database searches for multiple alignments. *Proc. Natl Acad. Sci. USA* 87, 5509–5513 (1990).
145. Gumucio, D. L. et al. Phylogenetic footprinting reveals a nuclear protein which binds to silencer sequences in the human gamma and epsilon globin genes. *Mol. Cell. Biol.* 12, 4919–4929 (1992).
146. Hardison, R. et al. Comparative analysis of the locus control region of the rabbit beta-like gene cluster: H3S increases transient expression of an embryonic epsilon-globin gene. *Nucleic Acids Res.* 21, 1265–1272 (1993).
147. Boffelli, D. et al. Phylogenetic shadowing of primate sequences to find functional regions of the human genome. *Science* 299, 1391–1394 (2003).
148. Elnitski, L. et al. Distinguishing regulatory DNA from neutral sites. *Genome Res.* 13, 64–72 (2003).
149. Loots, G. G., Ovcharenko, I., Pachter, L., Dubchak, I. & Rubin, E. M. rVista for comparative sequence-based discovery of functional transcription factor binding sites. *Genome Res.* 12, 832–839 (2002).
150. Pennacchio, L. A. & Rubin, E. M. Genomic strategies to identify mammalian regulatory sequences. *Nature Rev. Genet.* 2, 100–109 (2001).
151. Margulies, E. H., Blanchette, M., Haussler, D. & Green, E. Identification and characterization of multi-species conserved sequences. *Genome Res.* 13, 2507–2518 (2003).
152. Kolbe, D. et al. Regulatory potential scores from genome-wide 3-way alignments of human, mouse and rat. *Genome Res.* 14, 700–707 (2004).
153. Wingender, E. et al. The TRANSFAC system on gene expression regulation. *Nucleic Acids Res.* 29, 281–283 (2001).
154. Trinklein, N. D., Aldred, S. J., Saldanha, A. J. & Myers, R. M. Identification and functional analysis of human transcriptional promoters. *Genome Res.* 13, 308–312 (2003).
155. Philipsen, S., Pruzina, S. & Grossfeld, F. The minimal requirements for activity in transgenic mice of hypersensitive site 3 of the beta globin locus control region. *EMBO J.* 12, 1077–1085 (1993).
156. Reddy, P. M. & Shen, C. K. Protein-DNA interactions in vivo of an erythroid-specific, human beta-globin locus enhancer. *Proc. Natl Acad. Sci. USA* 88, 8676–8680 (1991).
157. Strauss, E. C. & Orkin, S. H. In vivo protein-DNA interactions at hypersensitive site 3 of the human beta-globin locus control region. *Proc. Natl Acad. Sci. USA* 89, 5809–5813 (1992).
158. Hillier, L. W. et al. The DNA sequence of human chromosome 7. *Nature* 424, 157–164 (2003).
159. Torrents, D., Suyama, M. & Bork, P. A genome-wide survey of human pseudogenes. *Genome Res.* 13, 2559–2567 (2003).
160. Zhang, Z., Harrison, P. & Gerstein, M. Identification and analysis of over 2000 ribosomal protein pseudogenes in the human genome. *Genome Res.* 12, 1466–1482 (2002).
161. Mulder, N. J. et al. The InterPro Database 2003 brings increased coverage and new features. *Nucleic Acids Res.* 31, 315–318 (2003).
162. Oh, B., Hwang, S. Y., Solter, D. & Knowles, B. B. Spindlin, a major maternal transcript expressed in the mouse during the transition from oocyte to embryo. *Development* 124, 493–503 (1997).
163. Garcia-Munier, P., Etienne-Julian, M., Fort, P., Piechaczyk, M. & Bonhomme, F. Concerted evolution in the GAPDH family of retrotransposed pseudogenes. *Mamm. Genome* 4, 695–703 (1993).
164. Smit, A. F. Interspersed repeats and other mementos of transposable elements in mammalian genomes. *Curr. Opin. Genet. Dev.* 9, 657–663 (1999).
165. Prak, E. T. & Kazazian, H. H. Jr Mobile elements and the human genome. *Nature Rev. Genet.* 1, 134–144 (2000).
166. Ostertag, E. M. & Kazazian, H. H. Jr Biology of mammalian L1 retrotransposons. *Annu. Rev. Genet.* 35, 501–538 (2001).
167. Weiner, A. M. SINEs and LINEs: the art of biting the hand that feeds you. *Curr. Opin. Cell Biol.* 14, 343–350 (2002).
168. Martin, S. L. & Bushman, F. D. Nucleic acid chaperone activity of the ORF1 protein from the mouse LINE-1 retrotransposon. *Mol. Cell. Biol.* 21, 467–475 (2001).
169. Hayward, B. E., Zavanelli, M. & Furano, A. V. Recombination creates novel L1 (LINE-1) elements in *Rattus norvegicus*. *Genetics* 146, 641–654 (1997).
170. Dewannieux, M., Esnault, C. & Heidmann, T. LINE-mediated retrotransposition of marked Alu sequences. *Nature Genet.* 35, 41–48 (2003).
171. Quentin, Y. A master sequence related to a free left Alu monomer (FLAM) at the origin of the B1 family in rodent genomes. *Nucleic Acids Res.* 22, 2222–2227 (1994).
172. Cantrell, M. A. et al. An ancient retrovirus-like element contains hot spots for SINE insertion. *Genetics* 158, 769–777 (2001).
173. Rothenburg, S., Eiben, M., Koch-Nolte, F. & Haag, F. Independent integration of rodent identifier (ID) elements into orthologous sites of some RT6 alleles of *Rattus norvegicus* and *Rattus rattus*. *J. Mol. Evol.* 55, 251–259 (2002).
174. Roy-Engel, A. M. et al. Non-traditional Alu evolution and primate genomic diversity. *J. Mol. Biol.* 316, 1033–1040 (2002).
175. Salem, A. H., Kilroy, G. E., Watkins, W. S., Jorde, L. B. & Batzer, M. A. Recently integrated Alu elements and human genomic diversity. *Mol. Biol. Evol.* 20, 1349–1361 (2003).
176. Salem, A. H. et al. Alu elements and hominid phylogenetics. *Proc. Natl Acad. Sci. USA* 100, 12787–12789 (2003).
177. Smit, A. F. Identification of a new, abundant superfamily of mammalian LTR-transposons. *Nucleic Acids Res.* 21, 1863–1872 (1993).
178. Benit, L. et al. Cloning of a new murine endogenous retrovirus, MuERV-L, with strong similarity to the human HERV-L element and with a gag coding sequence closely related to the Fv1 restriction gene. *J. Virol.* 71, 5652–5657 (1997).
179. Costas, J. Molecular characterization of the recent intragenomic spread of the murine endogenous retrovirus MuERV-L. *J. Mol. Evol.* 56, 181–186 (2003).
180. Emes, R. D., Beaton, S. A., Ponting, C. P. & Goodstadt, L. Evolution and comparative genomics of odorant- and pheromone-associated genes in rodents. *Genome Res.* 14, 591–602 (2004).
181. Young, J. M. et al. Different evolutionary processes shaped the mouse and human olfactory receptor gene families. *Hum. Mol. Genet.* 11, 535–546 (2002).
182. Zhang, X. & Firestein, S. The olfactory receptor gene superfamily of the mouse. *Nature Neurosci.* 5, 124–133 (2002).
183. Rouquier, S., Blancher, A. & Giorgi, D. The olfactory receptor gene repertoire in primates and mouse: evidence for reduction of the functional fraction in primates. *Proc. Natl Acad. Sci. USA* 97, 2870–2874 (2000).
184. Clark, A. J., Hickman, J. & Bishop, J. A 45-kb DNA domain with two divergently orientated genes is the unit of organisation of the murine major urinary protein genes. *EMBO J.* 3, 2055–2064 (1984).
185. Mural, R. J. et al. A comparison of whole-genome shotgun-derived mouse chromosome 16 and the human genome. *Science* 296, 1661–1671 (2002).
186. Cavagioni, A. & Mucignat-Caretta, C. Major urinary proteins, alpha₂-globulins and aphrodisin. *Biochim. Biophys. Acta* 1482, 218–228 (2000).
187. Hurst, J. L. et al. Individual recognition in mice mediated by major urinary proteins. *Nature* 414, 631–634 (2001).
188. Danielson, P. B. The cytochrome P450 superfamily: biochemistry, evolution and drug metabolism in humans. *Curr. Drug Metab.* 3, 561–597 (2002).
189. Nelson, D. R. Cytochrome P450 and the individuality of species. *Arch. Biochem. Biophys.* 369, 1–10 (1999).
190. Scarborough, P. E., Ma, J., Qu, W. & Zeldin, D. C. P450 subfamily CYP2J and their role in the bioactivation of arachidonic acid in extrahepatic tissues. *Drug Metab. Rev.* 31, 205–234 (1999).
191. Willson, T. M. & Kliever, S. A. PXR, CAR and drug metabolism. *Nature Rev. Drug Discov.* 1, 259–266 (2002).
192. Gurates, B. et al. WT1 and DAX-1 inhibit aromatase P450 expression in human endometrial and endometriotic stromal cells. *J. Clin. Endocrinol. Metab.* 87, 4369–4377 (2002).
193. Zhang, Z. et al. Genomic analysis of the nuclear receptor family: new insights into structure, regulation, and evolution from the rat genome. *Genome Res.* 14, 580–590 (2004).
194. Lopez-Otin, C. & Overall, C. M. Protease degradomics: a new challenge for proteomics. *Nature Rev. Mol. Cell Biol.* 3, 509–519 (2002).
195. Stenson, P. D. et al. Human Gene Mutation Database (HGMD): 2003 update. *Hum. Mutat.* 21, 577–581 (2003).
196. Huang, H. et al. Evolutionary conservation of human disease gene orthologs in the rat and mouse genomes. *Genome Biol.* (submitted).
197. Duret, L. & Mouchiroud, D. Determinants of substitution rates in mammalian genes: expression pattern affects selection intensity but not mutation rate. *Mol. Biol. Evol.* 17, 68–74 (2000).
198. Reddy, P. S. & Housman, D. E. The complex pathology of trinucleotide repeats. *Curr. Opin. Cell Biol.* 9, 364–372 (1997).
199. The International HapMap Consortium. The International HapMap Project. *Nature* 426, 789–796 (2003).
200. Wade, C. M. et al. The mosaic structure of variation in the laboratory mouse genome. *Nature* 420, 574–578 (2002).
201. Zimdahl, H. et al. A SNP map of the rat genome generated from cDNA sequences. *Science* 303, 807 (2004).
202. Mendell, J. T. & Dietz, H. C. When the message goes awry: disease-producing mutations that influence mRNA content and performance. *Cell* 107, 411–414 (2001).
203. Venter, J. C. et al. The sequence of the human genome. *Science* 291, 1304–1351 (2001).
204. Marra, M. et al. A map for sequence analysis of the *Arabidopsis thaliana* genome. *Nature Genet.* 22, 265–270 (1999).
205. Marra, M. A. et al. High throughput fingerprint analysis of large-insert clones. *Genome Res.* 7, 1072–1084 (1997).
206. The International Human Genome Mapping Consortium. A physical map of the human genome. *Nature* 409, 934–941 (2001).
207. Schein, J. E. A. in *Bacterial Artificial Chromosomes: Methods and Protocols* (eds Zhao, S. & Stodolsky, M.) 143–156 (Humana, Totowa, New Jersey, 2004).
208. Soderlund, C. I. et al. FPC: a system for building contigs from restriction fingerprinted clones. *Comput. Appl. Biosci.* 13, 523–535 (1997).
209. Soderlund, C. S. et al. Contigs built with fingerprints, markers, and FPC V4.7. *Genome Res.* 10, 1772–1787 (2000).
210. Ness, S. R. et al. Assembly of fingerprint contigs: parallelized FPC. *Bioinformatics* 18, 484–485 (2002).
211. Woon, P. Y. et al. Construction and characterization of a 10-fold genome equivalent rat P1-derived artificial chromosome library. *Genomics* 50, 306–316 (1998).
212. Watanabe, T. K. et al. A radiation hybrid map of the rat genome containing 5,255 markers. *Nature Genet.* 22, 27–36 (1999).

213. Schuler, G. D. Sequence mapping by electronic PCR. *Genome Res.* 7, 541–550 (1997).
214. Benson, G. Tandem repeats finder: a program to analyze DNA sequences. *Nucleic Acids Res.* 27, 573–580 (1999).
215. Blanchette, M. *et al.* Aligning multiple genomic sequences with the threaded blockset aligner. *Genome Res.* 14, 708–715 (2004).
216. Brudno, M. *et al.* LAGAN and Multi-LAGAN: efficient tools for large-scale multiple alignment of genomic DNA. *Genome Res.* 13, 721–731 (2003).
217. Brudno, M. *et al.* Automated whole-genome multiple alignment of rat, mouse, and human. *Genome Res.* 14, 685–692 (2004).
218. Bailey, J. A., Yavor, A. M., Massa, H. F., Trask, B. J. & Eichler, E. E. Segmental duplications: organization and impact within the current human genome project assembly. *Genome Res.* 11, 1005–1017 (2001).
219. Schwartz, S. *et al.* MultiPipMaker and supporting tools: Alignments and analysis of multiple genomic DNA sequences. *Nucleic Acids Res.* 31, 3518–3524 (2003).
220. Altschul, S. F. *et al.* Gapped BLAST and PSI-BLAST: a new generation of protein database search programs. *Nucleic Acids Res.* 25, 3389–3402 (1997).
221. Birney, E. & Durbin, R. Using GeneWise in the *Drosophila* annotation experiment. *Genome Res.* 10, 547–548 (2000).
222. Yang, Z., Goldman, N. & Friday, A. Comparison of models for nucleotide substitution used in maximum-likelihood phylogenetic estimation. *Mol. Biol. Evol.* 11, 316–324 (1994).
223. Chakrabarti, K. & Pachter, L. Visualization of multiple genome annotations and alignments with the K-BROWSER. *Genome Res.* 14, 716–720 (2004).
224. Saitou, N. & Nei, M. The neighbor-joining method: a new method for reconstructing phylogenetic trees. *Mol. Biol. Evol.* 4, 406–425 (1987).
225. Haldi, M. L. *et al.* Construction of a large-insert yeast artificial chromosome library of the rat genome. *Mamm. Genome* 8, 284 (1997).

Supplementary Information accompanies the paper on www.nature.com/nature.

Acknowledgements Work at Baylor College of Medicine was supported by a grant from the NHGRI and NHLBI to R.A.G. Work at Genome Therapeutics was supported by grants from the NHGRI to D.S. A.S. acknowledges support from the NIGMS. M.B. acknowledges support from the NIH. N.H. was supported by the NGFN/BMBF (German Ministry for Research and Education). B.J.T. and J.M.Y. are supported by an NIH grant from the NIDCD. K.M.R. and G.M.C. are Howard Hughes Medical Institute Predoctoral Fellows. L.M.D'S., K.M. and K.J.K. are supported by training fellowships from the W. M. Keck Foundation to the Gulf Coast Consortia through the Keck Center for Computational and Structural Biology. Work at Case Western Reserve was supported in part by NIH grants to E.E.E. Work at IMIM was supported by a grant from Plan Nacional de I + D (Spain). M.M.A. acknowledges support from programme Ramón y Cajal and a grant from the Spanish Ministry of Science and Technology. Work at Universidad de Oviedo was supported by grants from the European Union, Obra Social Cajastur and Gobierno del Principado de Asturias. Work at Penn State University was supported by NHGRI grants. Work at the University of California Berkeley was supported by a grant from the NIH. Work at the Washington University School of Medicine Genome Sequencing Center and the British Columbia Cancer Agency Genome Sciences Centre was supported by an NIH grant. Work at UCSC and CHORI was supported by the NHGRI.

Competing interests statement The authors declare that they have no competing financial interests.

Correspondence and requests for materials should be addressed to R.A.G. (agibbs@bcm.tmc.edu). The genomic sequence is available under accession numbers AABR03000000 to AABR03137910 in the international sequence databases (GenBank, DDBJ and EMBL).

Rat Genome Sequencing Project Consortium (Participants are arranged under area of contribution, and then by institution.)

DNA sequencing: Baylor College of Medicine Richard A. Gibbs (Principal Investigator)¹, George M. Weinstock (Co-principal Investigator)¹, Michael L. Metzker¹, Donna M. Muzny¹, Erica J. Sodergren¹, Steven Scherer¹, Graham Scott¹, David Steffen¹, Kim C. Worley¹, Paula E. Burch¹, Geoffrey Okwuonu¹, Sandra Hines¹, Lora Lewis¹, Christine DeRamo¹, Oliver Delgado¹, Shannon Dugan-Rocha¹, George Miner¹, Margaret Morgan¹, Alicia Hawes¹, Rachel Gill¹; Celera Robert A. Holt (Principal Investigator)^{2,3}, Mark D. Adams^{3,4}, Peter G. Amanatides^{3,5}, Holly Baden-Tillson^{3,6}, Mary Barnstead^{3,7}, Soo Chin³, Cheryl A. Evans³, Steve Ferreira^{3,8}, Carl Foster³, Anna Glodek^{3,9}, Zhiping Gu³, Don Jennings³, Cheryl L. Kraft^{3,10}, Trixie Nguyen³, Cynthia M. Pfannkoch^{3,6}, Cynthia Sitter^{3,11}, Granger G. Sutton³, J. Craig Venter^{3,8}, Trevor Woodage³; Genome Therapeutics Douglas Smith (Principal Investigator)^{12,13}, Hong-Mei Lee¹², Erik Gustafson^{12,13}, Patrick Cahill¹², Arnold Kana¹², Lynn Doucette-Stamm^{12,13}, Keith Weinstock¹², Kim Fechtel¹²; University of Utah Robert B. Weiss (Principal Investigator)¹⁴, Diane M. Dunn¹⁴; NISC Comparative Sequencing Program, NHGRI Eric D. Green¹⁵, Robert W. Blakesley¹⁵, Gerard G. Bouffard¹⁵

BAC library production: Children's Hospital Oakland Research Institute Pieter J. de Jong (Principal Investigator)¹⁶, Kazutoyo Osoegawa¹⁶, Baoli Zhu¹⁶

BAC fingerprinting: British Columbia Cancer Agency, Canada's Michael Smith Genome Sciences Centre Marco Marra (Principal Investigator)², Jacqueline Schein (Principal Investigator)², Ian Bosdet², Chris Fjell², Steven Jones², Martin Krzywinski², Carrie Mathewson², Asim Siddiqui², Natasja Wye²; Genome Sequencing Center, Washington University School of Medicine John McPherson^{1,17}

BAC end sequencing: TIGR Shaying Zhao (Principal Investigator)¹⁸, Claire M. Fraser¹⁸, Jyoti Shetty¹⁸, Sofiya Shatsman¹⁸, Keita Geer¹⁸, Yixin Chen¹⁸, Sofiya Abramzon¹⁸, William C. Nierman¹⁸

Sequence assembly: Baylor College of Medicine Richard A. Gibbs (Principal Investigator)¹, George M. Weinstock (Principal Investigator)¹, Paul H. Havlak¹, Rui Chen¹, K. James Durbin¹, Amy Egan¹, Yanru Ren¹, Xing-Zhi Song¹, Bingshan Li¹, Yue Liu¹, Xiang Qin¹

Analysis and annotation: Affymetrix Simon Cawley¹⁹; Baylor College of Medicine George M. Weinstock (Coordinator)¹, Kim C. Worley (Overall Coordinator)¹, A. J. Cooney²⁰, Richard A. Gibbs¹, Lisa M. D'Souza¹, Kirt Martin¹, Jia Qian Wu¹, Manuel L. Gonzalez-Garay¹, Andrew R. Jackson¹, Kenneth J. Kalafus^{1,58}, Michael P. McLeod¹, Aleksandar Milosavljevic¹, Davinder Virk¹, Andrei Volkov¹, David A. Wheeler¹, Zhengdong Zhang¹; Case Western Reserve University Jeffrey A. Bailey⁴, Evan E. Eichler⁴, Eray Tuzun⁴; EBI, Wellcome Trust Genome Campus Ewan Birney²¹, Emmanuel Mongin²¹, Abel Ureta-Vidal²¹, Cara Woodmark²¹; EMBL, Heidelberg Evgeny Zdobnov²², Peer Bork^{22,23}, Mikita Suyama²², David Torrents²²; Fraunhofer-Chalmers Research Centre for Industrial Mathematics, Gothenburg Marina Alexandersson²⁴; Fred Hutchinson Cancer Research Center Barbara J. Trask²⁵, Janet M. Young²⁵; Genome Therapeutics Douglas Smith (Principal Investigator)^{12,13}, Hui Huang¹², Kim Fechtel¹², Huajun Wang¹², Heming Xing¹², Keith Weinstock¹²; Incyte Corporation Sue Daniels²⁶, Darryl Gietzen²⁶, Jeanette Schmidt²⁶, Kristian Stevens²⁶, Ursula Vitt²⁶, Jim Wingrove²⁶; Institut Municipal d'Investigació Mèdica, Barcelona Francisco Camara²⁷, M. Mar Albà²⁷, Josep F. Abril²⁷, Roderic Guigo²⁷; The Institute for Systems Biology Arian Smit²⁸; Lawrence Berkeley National Laboratory Inna Dubchak^{29,30}, Edward M. Rubin^{29,30}, Olivier Couronne^{29,30}, Alexander Poliakov²⁹; Max Delbrück Center for Molecular Medicine Norbert Hübner²³, Detlev Ganten²³, Claudia Goesele^{23,31}, Oliver Hummel^{23,31}, Thomas Kreitler^{23,31}, Young-Ae Lee²³, Jan Monti²³, Herbert Schulz²³, Heike Zimdahl²³;

Max Planck Institute for Molecular Genetics, Berlin Heinz Himmelbauer³¹, Hans Lehrach³¹; **Medical College of Wisconsin** Howard J. Jacob (Principal Investigator)³², Susan Bromberg³³, Jo Gullings-Handley³², Michael I. Jensen-Seaman³², Anne E. Kwikite³², Jozef Lazar³², Dean Pasko³³, Peter J. Tonellato³², Simon Twigger³²; **MRC Functional Genetics Unit, University of Oxford** Chris P. Ponting (Leader, Genes and Proteins Analysis Group)³⁴, Jose M. Duarte³⁴, Stephen Rice³⁴, Leo Goodstadt³⁴, Scott A. Beatson³⁴, Richard D. Emes³⁴, Eitan E. Winter³⁴, Caleb Webber³⁴; **MWG-Biotech Petra Brandt**³⁵, Gerald Nyakatura³⁵; **Pennsylvania State University** Margaret Adetobi³⁶, Francesca Chiaromonte³⁶, Laura Elinitzki³⁶, Pallavi Eswara³⁶, Ross C. Hardison³⁶, Minmei Hou³⁶, Diana Kolbe³⁶, Katerina Makova³⁶, Webb Miller³⁶, Anton Nekrutenko³⁶, Cathy Riemer³⁶, Scott Schwartz³⁶, James Taylor³⁶, Shan Yang³⁶, Yi Zhang³⁶; **Roche Genetics and Roche Center for Medical Genomics** Klaus Lindpaintner³⁷; **Sanger Institute** T. Dan Andrews³⁸, Mario Caccamo³⁸, Michele Clamp³⁸, Laura Clarke³⁸, Valerie Curwen³⁸, Richard Durbin³⁸, Eduardo Eyras³⁸, Stephen M. Searle³⁸; **Stanford University** Gregory M. Cooper (Co-Leader, Evolutionary Analysis Group)³⁹, Serafim Batzoglou⁴⁰, Michael Brudno⁴⁰, Arend Sidow³⁹, Eric A. Stone³⁹; **The Center for the Advancement of Genomics** J. Craig Venter^{3,8}; **University of Arizona** Bret A. Payseur⁴¹; **Université de Montréal** Guillaume Bourque⁴²; **Universidad de Oviedo** Carlos López-Otin⁴³, Xose S. Puente⁴³; **University of California, Berkeley** Kushal Chakrabarti⁴⁴, Sourav Chatterji⁴⁴, Colin Dewey⁴⁴, Lior Pachter⁴⁵, Nicolas Bray⁴⁵, Von Bing Yap⁴⁵, Anat Caspi⁴⁶; **University of California, San Diego** Glenn Tesler⁴⁷, Pavel A. Pevzner⁴⁸; **University of California, Santa Cruz** David Haussler (Co-Leader, Evolutionary Analysis Group)⁴⁹, Krishna M. Roskin⁵⁰, Robert Baertsch⁵⁰, Hiram Clawson⁵⁰, Terrence S. Furey⁵⁰, Angie S. Hinrichs⁵⁰, Donna Karolchik⁵⁰, William J. Kent⁵⁰, Kate R. Rosenbloom⁵⁰, Heather Trumbower⁵⁰, Matt Weirauch^{50,51}; **University of Wales College of Medicine** David N. Cooper⁵¹, Peter D. Stenson⁵¹; **University of Western Ontario** Bin Ma⁵²; **Washington University** Michael Brent⁵³, Manimozhiyan Arumugam⁵³, David Shteynberg⁵³; **Wellcome Trust Centre for Human Genetics, University of Oxford** Richard R. Copley⁵⁴, Martin S. Taylor⁵⁴; **The Wistar Institute** Harold Riethman⁵⁵, Uma Mudunuri⁵⁵

Scientific management: Jane Peterson⁵⁶, Mark Guyer⁵⁶, Adam Felsenfeld⁵⁶, Susan Old⁵⁷, Stephen Mockrin⁵⁷ & Francis Collins⁵⁶

Affiliations for participants: 1, Human Genome Sequencing Center, Department of Molecular and Human Genetics, Baylor College of Medicine, MS BCM226, One Baylor Plaza, Houston, Texas 77030, USA (<http://www.hgsc.bcm.tmc.edu>); 2, British Columbia Cancer Agency, Canada's Michael Smith Genome Sciences Centre, 600 W 10th Avenue, Vancouver, British Columbia V5Z 4E6, Canada (<http://www.bccsc.ca>); 3, Celera, 45 West Gude Drive, Rockville, Maryland 20850, USA; 4, Department of Genetics and the Center for Computational Genomics, Case Western Reserve University, School of Medicine, 10900 Euclid Avenue, Cleveland, Ohio 44106, USA; 5, DSM Pharmaceuticals Inc., 5900 NW Greenville Blvd, Greenville, North Carolina 27834, USA; 6, The Institute for Biological Energy Alternatives (IBEA), 1901 Research Blvd, Rockville, Maryland 20850, USA; 7, Intron, Inc., 910 Clopper Road, South Building, Gaithersburg, Maryland 20878, USA; 8, The Center for the Advancement of Genomics (TCAG), 1901 Research Blvd, Suite 600, Rockville, Maryland 20850, USA; 9, Avalon Pharmaceuticals, 20358 Seneca Meadows Parkway, Germantown, Maryland 20876, USA; 10, Basic Immunology Branch, Division of Allergy, Immunology and Transplantation, National Institutes of Health and Infectious Diseases (NIAID), NIH, DHHS, 6610 Rockledge Blvd, Room 3005, Bethesda, Maryland 20892-7612, USA; 11, DynPort Vaccine Company, LLC, 64 Thomas Jefferson Drive, Frederick, Maryland 21702, USA; 12, Genome Therapeutics Corporation, 100 Beaver Street, Waltham, Massachusetts 02453, USA; 13, Agencourt Bioscience Corporation, 100 Cummings Center, Beverly, Massachusetts 01915, USA; 14, Department of Human Genetics, University of Utah, Salt Lake City, Utah 84112, USA; 15, NIH Intramural Sequencing Center (NISC) and Genome Technology Branch, National Human Genome Research Institute (NHGRI), National Institutes of Health, Bethesda, Maryland 20892, USA; 16, BACPAC Resources, Children's Hospital Oakland Research Institute, 747 52nd Street, Oakland, California 94609, USA (<http://bacpac.chori.org>); 17, Genome Sequencing Centre, Washington University School of Medicine, 4444 Forest Park Blvd, St Louis, Missouri 63108, USA (<http://genome.wustl.edu>); 18, The Institute for Genomic Research, 9712 Medical Center Dr., Rockville, Maryland 20850, USA (<http://www.tigr.org>); 19, Affymetrix, 6550 Vallejo St, Suite 100, Emeryville, California 94608, USA; 20, Department of Cell Biology, Baylor College of Medicine, One Baylor Plaza, Houston, Texas 77030, USA; 21, EBI, Wellcome Trust Genome Campus, Hinxton, Cambridgeshire CB10 1SD, UK; 22, EMBL, Meyerhofstrasse 1, Heidelberg 69117, Germany; 23, Max Delbrück Center for Molecular Medicine (MDC), Experimental Genetics of Cardiovascular Disease, Robert-Rössle-Strasse 10, Berlin 13125, Germany (<http://www.mdc-berlin.de/ratgenome/>); 24, Fraunhofer-Chalmers Research Centre for Industrial Mathematics, Chalmers Science Park, S-412 88 Gothenburg, Sweden; 25, Division of Human Biology, Fred Hutchinson Cancer Research Center, 1100 Fairview Avenue N., C3-168, Seattle, Washington 98109, USA (<http://www.fhcrc.org/labs/trask/>); 26, Incyte Corporation, 3160 Porter Drive, Palo Alto, California 94304, USA (<http://www.incyte.com>); 27, Grup de Recerca en Informàtica Biomèdica, Institut Municipal d'Investigació Mèdica, Universitat Pompeu Fabra, and Programa de Bioinformàtica i Genòmica, Centre de Regulació Genòmica, C/ Dr. Aiguader 80, 08003 Barcelona, Catalonia, Spain; 28, Computational Biology Group, The Institute for Systems Biology, 1441 North 34th Street, Seattle, Washington 98103, USA; 29, Genomics Division, Lawrence Berkeley National Laboratory, 1 Cyclotron Rd., Berkeley, California 94720, USA (<http://www.lbl.gov>); 30, US Department of Energy Joint Genome Institute, 2800 Mitchell Drive, Walnut Creek, California 94598, USA (<http://jgi.doe.gov>); 31, Max Planck Institute for Molecular Genetics, Ihnestrasse 73, Berlin 14195, Germany; 32, Human and Molecular Genetics Center, Bioinformatics Research Center, and Department of Physiology, Medical College of Wisconsin, Milwaukee, Wisconsin 53226, USA; 33, Rat Genome Database, Bioinformatics Research Center, Medical College of Wisconsin, Milwaukee, Wisconsin 53226, USA; 34, MRC Functional Genetics Unit, University of Oxford, Department of Human Anatomy and Genetics, South Parks Road, Oxford OX1 3QX, UK; 35, MWG-Biotech, Anzinger Strasse 7a, Ebersberg 85560, Germany; 36, Center for Comparative Genomics and Bioinformatics, Huck Institutes of Life Sciences, Departments of Biology, Statistics, Biochemistry and Molecular Biology, Computer Science and Engineering, and Health Evaluation Sciences, The Pennsylvania State University, University Park, Pennsylvania 16802, USA; 37, Roche Genetics and Roche Center for Medical Genomics, F. Hoffmann-La Roche Ltd, 4070 Basel, Switzerland; 38, Sanger Institute, The Wellcome Trust Genome Campus, Hinxton, Cambridgeshire CB10 1SA, UK; 39, Departments of Pathology and Genetics, Stanford University, Stanford, California 94305, USA; 40, S256 James H. Clark Center, Department of Computer Science, Stanford University, Stanford, California 94305, USA; 41, Department of Ecology and Evolutionary Biology, University of Arizona, Tucson, Arizona 85721, USA; 42, Centre de Recherches Mathématiques, Université de Montréal, 2920 Chemin de la tour, Montréal, Québec H3T 1J8, Canada (<http://www.crm.umontreal.ca>); 43, Departamento de Bioquímica y Biología Molecular, Instituto Universitario de Oncología, Universidad de Oviedo, 33006 Oviedo, Spain (<http://web.uniovi.es/degradome>); 44, Department of Electrical Engineering and Computer Science, University of California Berkeley, Berkeley, California 94720, USA; 45, Department of Mathematics, University of California Berkeley, Berkeley, California 94720, USA; 46, Bioengineering Graduate Group, University of California Berkeley, Berkeley, California 94720, USA; 47, University of California, San Diego, Department of Mathematics, 9500 Gilman Drive, San Diego, California 92093-0112, USA (<http://www-cse.ucsd.edu/groups/bioinformatics>); 48, University of California, San Diego, Department of Computer Science and Engineering, 9500 Gilman Drive, San Diego, California 92093-0114, USA (<http://www-cse.ucsd.edu/groups/bioinformatics>); 49, Howard Hughes Medical Institute, Center for Biomolecular Science & Engineering, Mailstop SOE, Baskin School of Engineering, University of California, Santa Cruz, 1156 High Street, Santa Cruz, California 95064, USA; 50, UCSC Genome Bioinformatics Group, Center for Biomolecular Science and Engineering, Mailstop SOE, Baskin School of Engineering, University of California, Santa Cruz, 1156 High Street, Santa Cruz, California 95064, USA; 51, Institute of Medical Genetics, University of Wales College of Medicine, Heath Park, Cardiff, CF14 4XN, UK; 52, Department of Computer Science, University of Western Ontario, London, Ontario N6A 5B7, Canada; 53, Laboratory for Computational Genomics, Campus Box 1045, Washington University, St Louis, Missouri 63130, USA (<http://genes.cse.wustl.edu>); 54, Wellcome Trust Centre for Human Genetics, University of Oxford, Roosevelt Drive, Oxford OX3 7BN, UK; 55, The Wistar Institute, 3601 Spruce Street, Philadelphia, Pennsylvania 19104, USA; 56, US National Institutes of Health, National Human Genome Research Institute, 31 Center Drive, Bethesda, Maryland 20892, USA; 57, US National Institutes of Health, National Heart, Lung, and Blood Institute, Bethesda, Maryland 20892, USA; 58, Program in Structural and Computational Biology and Molecular Biophysics, Baylor College of Medicine, One Baylor Plaza, Houston, Texas 77030, USA

EXHIBIT 5

Motor Neuron Degeneration in Mice That Express a Human Cu,Zn Superoxide Dismutase Mutation

Mark E. Gurney,* Haifeng Pu, Arlene Y. Chiu, Mauro C. Dal Canto, Cynthia Y. Polchow, Denise D. Alexander, Jan Caliando, Afif Hentati, Young W. Kwon, Han-Xiang Deng, Wenje Chen, Ping Zhai, Robert L. Sufit, Teepu Siddique

Mutations of human Cu,Zn superoxide dismutase (SOD) are found in about 20 percent of patients with familial amyotrophic lateral sclerosis (ALS). Expression of high levels of human SOD containing a substitution of glycine to alanine at position 93—a change that has little effect on enzyme activity—caused motor neuron disease in transgenic mice. The mice became paralyzed in one or more limbs as a result of motor neuron loss from the spinal cord and died by 5 to 6 months of age. The results show that dominant, gain-of-function mutations in SOD contribute to the pathogenesis of familial ALS.

Amyotrophic lateral sclerosis occurs in both sporadic and familial forms and results from the degeneration of motor neurons in the cortex, brainstem, and spinal cord. The disease typically begins in adults as an asymmetric weakness in two or more limbs and then progresses to complete paralysis (1). Familial ALS is inherited as an autosomal dominant trait (2). About 10% of ALS cases are familial and, of these, ~20% have mutations in Cu,Zn superoxide dismutase (SOD) (3–5). SOD catalyzes the dismutation of superoxide radical ($O_2^{\cdot-}$) into hydrogen peroxide and molecular oxygen. Familial ALS patients heterozygous for SOD mutations have 50 to 60% of the normal level of SOD activity in their red blood cells and brains (4, 6).

To explore how mutations in SOD might selectively cause motor neuron degeneration, we produced transgenic mice that express wild-type or mutant forms of human SOD (7, 8). Two mutations were analyzed: an Ala⁴ → Val substitution (A4V) and a Gly⁹³ → Ala substitution (G93A) (3, 4). Previously described mice that express wild-type human SOD (NSOD) show no signs of overt motor neuron disease but do have mild pathologic

changes in the innervation of muscle that are suggestive of premature aging (8, 9).

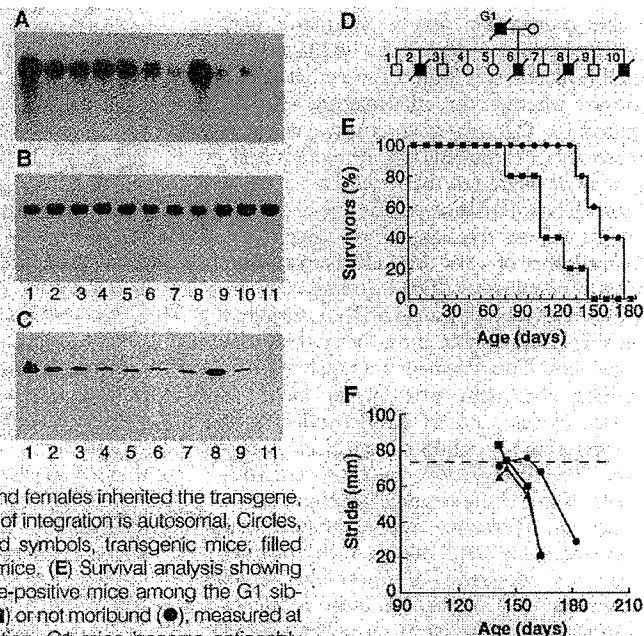
Transgenic founder mice were produced by DNX (Princeton, New Jersey) or through the National Transgenic Development Facility (National Institutes of Health). Fertilized eggs for injection were obtained from crosses of (C57BL/6 × SJL) F₁ hybrid mice. Founder mice were bred with C57BL/6 mice, and their progeny were used for subsequent analysis (10). Transgenic mice were identified by polymerase chain reaction amplification of tail DNA (11) and were screened for expression of human SOD in red blood cells by an antigen capture enzyme immunoassay (EIA)

that used a polyclonal antibody to human SOD and the mouse monoclonal antibody SD-G6 (12). The EIA detected human SOD in G93A and NSOD mice, but not in A4V mice. However, Northern (RNA) analysis (13) and immunoblots (14) developed with a different mouse monoclonal antibody (CZSODF2) demonstrated expression of human SOD1 mRNA and protein in the brains of G93A, NSOD, and A4V mice (Fig. 1, A to C). Thus, the A4V mutation altered an epitope needed for recognition in the EIA.

The mutations of SOD found in familial ALS alter the stability of human SOD as shown by DNA transfection of cultured cells (15). Consistent with those results, we found that the mutant transgenic lines expressed only one-half as much human SOD as did NSOD mice expressing comparable amounts of mRNA (Table 1). In addition, we found that the G93A mutation had little discernible effect on human SOD activity, whereas the A4V mutation greatly reduced enzymatic activity (15, 16). Although we detected enzymatically active mouse-human dimers in NSOD and G93A transgenic mice on SOD activity gels (17), we did not detect any active mouse-human A4V dimers. These results are compatible with the finding that recombinant human SOD bearing an Ala⁴ → Gln substitution is enzymatically inactive (18).

Mice from one of the G93A transgenic lines (G1) (Table 1) that expressed the largest amounts of mutant SOD in the brain

Fig. 1. (A) Northern analysis of human SOD1 mRNA expression in transgenic mouse brain. (B) The same membrane hybridized with a probe for G3PDH. (C) Expression of human SOD in transgenic brain by immunoblotting. Lanes contain samples from the following mice: 1, G1; 2, G5; 3, G12; 4, G20; 5, A1073; 6, A1074; 7, N1026; 8, N1029; 9, N1030; 10, G12.15; and 11, non-transgenic littermate. (D) Partial pedigree of the G1 transgenic line. In the F₂ generation, both males and females inherited the transgene, which indicates that the site of integration is autosomal. Circles, female; squares, male; filled symbols, transgenic mice; filled symbols with bar, affected mice. (E) Survival analysis showing the percentage of transgene-positive mice among the G1 siblings that are not impaired (■) or not moribund (●), measured at 10-day intervals of observation. G1 mice became noticeably impaired by 121 ± 23 days of age (mean ± SD, n = 5) and moribund by 169 ± 16 days. (F) The condition of G1 transgenic mice deteriorated rapidly over the 2-week period before their death, as shown by the shortening of their stride (■, G1.2; ●, G1.6; ▲, G1.8; and dotted line, average stride of normal male mice).



M. E. Gurney, H. Pu, D. D. Alexander, Y. W. Kwon, P. Zhai, Department of Cell and Molecular Biology and Northwestern University Institute of Neuroscience, Northwestern University Medical School, 303 East Chicago Avenue, Chicago, IL 60611, USA.
A. Y. Chiu, Division of Neurosciences, Beckman Research Institute of the City of Hope Medical Center, 1450 East Duarte Road, Duarte, CA 91010, USA.
M. C. Dal Canto, Department of Pathology, Northwestern University Medical School, Chicago, IL 60611, USA.
C. Y. Polchow, Department of Physiology, Northwestern University Medical School, Chicago, IL 60611, USA.
J. Caliando, A. Hentati, H.-X. Deng, W. Chen, R. L. Sufit, T. Siddique, Department of Neurology and Northwestern University Institute of Neuroscience, Northwestern University Medical School, Chicago, IL 60611, USA.

*To whom correspondence should be addressed.

developed a stereotyped syndrome suggestive of motor neuron disease. The disease has not been observed in any line of NSOD mice expressing wild-type human SOD, nor have symptoms developed in any A4V mouse at comparable ages. At 3 to 4

months of age, G1 mice began to show signs of hind limb weakness (Fig. 1E). They extended their hind legs less than normal when lifted by the base of the tail, their coats developed a coarse appearance suggestive of impaired grooming, and they ap-

peared thin along their flanks. Normal mice have a fairly constant stride of 74 ± 1.6 mm (95% confidence interval, $n = 50$ mice) when using an alternating gait (19). G1 mice had a normal stride at 3 to 4 months of age, but by 5 months of age it deteriorated rapidly (Fig. 1F). Over a span of 2 weeks, the mice became paralyzed in one or more limbs. The founder mouse and four of five transgenic F_1 progeny developed paralysis of one or more hind limbs. A fifth transgenic F_1 mouse (G1.6) retained use of his hind limbs but developed complete paralysis of his right forelimb. The six nontransgenic littermates of these mice showed no signs of disease. All affected mice developed a tremor of the hind limbs when suspended in the air. They had a normal posture when quiet with the hind limbs held in flexion, but after initiating movement, their hind limbs and toes frequently locked in a hyperextended position. Affected mice became moribund by 5 months of age and were killed when they were no longer able to forage for food or water.

The founder of the G1 line, all of his transgenic F_1 progeny, and at least one male F_2 mouse developed the same stereotyped syndrome suggestive of motor neuron disease affecting both upper and lower motor neurons. The other lines of G93A transgenic mice (Table 1) expressed smaller amounts of the mutant protein and so far have had normal motor behavior. In G1 mice as well as in humans with ALS (2), the onset of the disease is dependent on age, so it is conceivable that the other lines of G93A mice may develop the disease at a later age. However, because the disease is expressed in only one line of mice, we cannot exclude the possibility that the site of integration of the transgene caused the disease syndrome in these mice. Disease is not due simply to overexpression of SOD in the brains of G1 mice, because NSOD mice that express comparable or greater amounts of total brain SOD do not develop the disease (10) (Table 1).

Pathological analysis of G1 mice demonstrated a severe loss of choline acetyltransferase (ChAT)-containing spinal motor neurons (Fig. 2, A to D). A few motor neurons appeared normal, but most of the remaining neurons were filled with a neurofibrillar material (Fig. 3) that appeared to be phosphorylated neurofilaments (20). The most pronounced changes were observed in the ventral spinal cord, whereas the dorsal spinal cord, especially the substantia gelatinosa, was better preserved. Immunohistochemical staining revealed large amounts of human SOD in ventral horn motor neurons, best shown in NSOD mice (Fig. 2, E and F). In G1 mice, there was severe loss of large, myelinated axons from the ventral motor roots (Fig. 2, H and

Fig. 2. Loss of spinal motor neurons in affected G1 transgenic mice. Spinal cords from a normal littermate (A) and a G1 transgenic mouse (B) show loss in the latter of lateral motor columns in the L4 spinal segment (cresylecht-violet stain). (C and D) Spinal cords from a normal littermate (C) and a G1 transgenic mouse (D), showing loss in the latter of ChAT-positive ventral horn motor neurons in the L3 spinal segment (27). Lumbar spinal cords from an N1026 mouse (E) and a normal littermate (F) show staining of ventral horn motor neurons with an antibody to human SOD (CZ-SODF2). (G through J) Normal littermate dorsal (G) and ventral (H) lumbar spinal roots and G1 transgenic dorsal (I) and ventral (J) lumbar roots (stained with toluidine blue). The dorsal sensory roots were relatively spared (I), whereas severe loss of myelinated axons, myelin debris, and infiltrating phagocytic cells were apparent in the ventral motor roots (J).

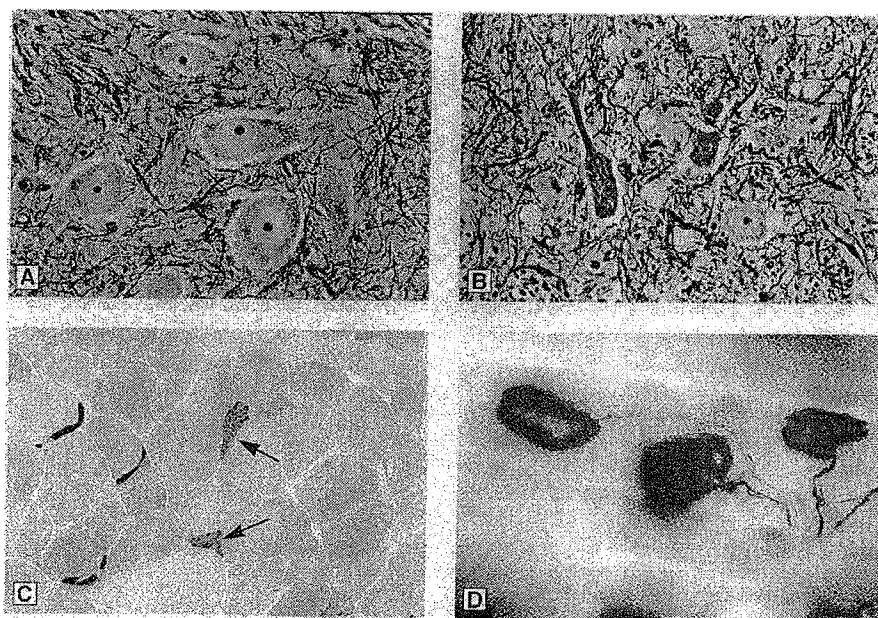
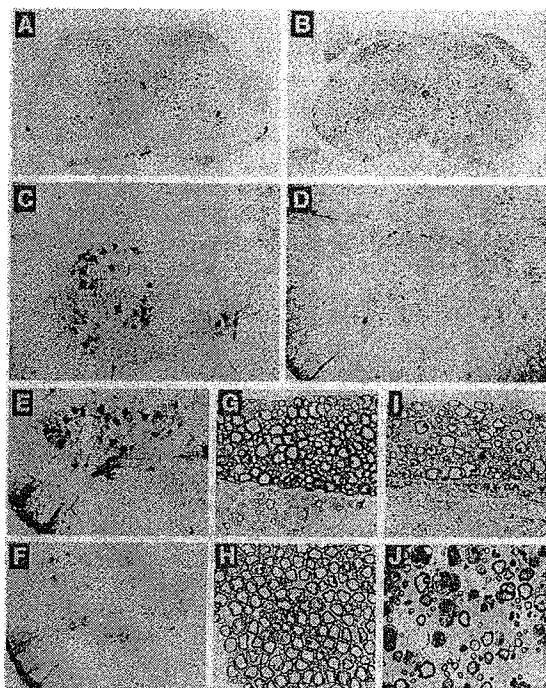


Fig. 3. Pathology in spinal cord and muscle of transgenic G1 mice. (A and B) Lumbar spinal segments from a normal littermate (A) and a G1 transgenic mouse (B), stained by the Bielschowski technique to reveal neurofibrils. (C) Nonspecific esterase stain of gastrocnemius, showing the low frequency of denervated, angulated muscle fibers (arrows) in G1 mice. (D) Sprouting and reinnervation of three denervated endplates in the gluteus muscle of a G1 mouse, revealed by a combined silver and cholinesterase stain (28).

Table 1. Expression in brain of human *SOD1* mRNA, human SOD protein, and total SOD enzymatic activity in different transgenic mouse lines. All values are the mean \pm SEM ($n = 3$), except where indicated.

Line	Mutation	Gene copy number*	<i>SOD1</i> mRNA (ng)/10 μ g of total RNA	Human SOD (ng)/total protein (μ g)†	SOD (U)/total protein (μ g)
G1	Gly ⁹³ \rightarrow Ala	18.0 \pm 2.6	2.5 \pm 0.5	4.1 \pm 0.54	42.6 \pm 2.1
G5		4.0 \pm 0.6	0.8 \pm 0.1	1.3 \pm 0.21	27.0 \pm 2.9
G12		2.2 \pm 0.8	0.8 \pm 0.1	1.1 \pm 0.22	19.5 \pm 0.8
G20		1.7 \pm 0.6	0.8 \pm 0.1	0.7 \pm 0.06	16.9 \pm 0.4
A1073	Ala ⁴ \rightarrow Val	4.7 \pm 0.4	1.1 \pm 0.1	1.0 \pm 0.21‡	14.6 \pm 0.4
A1074		3.2 \pm 0.2	0.7 \pm 0.1	0.9 \pm 0.21‡	9.1 \pm 0.4
N1029	Wild-type	7.2 \pm 2.4	1.5 \pm 0.1	6.7 \pm 0.76	37.3 \pm 1.9
N1026		3.3 \pm 1.0	0.4 \pm 0.1	0.9 \pm 0.11	18.6 \pm 0.9
N1030		1.7 \pm 0.7	0.3 \pm 0.1	0.6 \pm 0.16	11.8 \pm 0.3
Nontransgenic		—	—	—	10.4 \pm 0.5

*Per diploid genome. †The amount of human SOD was determined by EIA. ‡Determined by immunoblotting (mean \pm SEM of regression).

J). The dorsal sensory roots appeared relatively spared when compared to the ventral roots; however, scattered swollen axons with dense axoplasm and occasional myelin-laden macrophages were observed at all levels of the spinal cord (Fig. 2, G and I). These changes extended into the central component of the afferent sensory fibers within the dorsal columns of the spinal cord, a pathology also seen in familial ALS (21). Severe loss of myelinated axons occurred in intramuscular nerves, but less than 10% of muscle fibers had the characteristics of denervated fibers—that is, a small, angular profile and an esterase-positive phenotype (Fig. 3C).

To investigate whether sprouting and reinnervation compensated for the destruction of motor units caused by the disease, we examined whole mounts of the gluteus muscle of a G1 mouse (Fig. 3D). The muscles showed severe loss of myelinated axons from the intramuscular nerves and consequent reinnervation of muscle fibers by primarily nodal sprouts. Ongoing reinnervation and remodeling of muscle innervation were indicated by the frequency of multiply innervated endplates and by the scarcity of denervated endplates. In one gluteus muscle, two surviving axons in the inferior gluteal nerve appeared sufficient to innervate more than 90% of the myofibers in the muscle. These data suggest that sprouting probably compensates for the loss of motor neurons until late in the course of the disease.

Toxicity by a free-radical mechanism is one plausible explanation for motor neuron death in the G1 transgenic mice and, by implication, in humans with familial ALS. This mechanism could involve the formation of the strong oxidant peroxynitrite (ONOO⁻) from O₂⁻ and nitric oxide (NO⁻) free radicals (22, 23). The formation of peroxynitrite and its decomposition into

toxic chemical species have been linked to neurotoxicity in cell culture (24) and in brain ischemia (25). SOD mutations may facilitate this pathway of oxidative damage (26). Because formation of peroxynitrite is a second-order reaction that depends on the concentration of O₂⁻ and NO⁻, decreased SOD activity in familial ALS may also contribute to pathogenesis if the amount of O₂⁻ in tissues is increased (4). Our results indicate that dominant, gain-of-function mutations in SOD play a key role in the pathogenesis of familial ALS.

REFERENCES AND NOTES

1. D. W. Mulder, in *Human Motor Neuron Diseases*, L. P. Rowland, Ed. (Raven, New York, 1982), pp. 15–22.
2. T. Siddique, *Adv. Neurol.* **56**, 227 (1991).
3. D. R. Rosen et al., *Nature* **362**, 59 (1993).
4. H.-X. Deng et al., *Science* **261**, 1047 (1993).
5. T. Siddique, unpublished observations.
6. A. C. Bowling, J. B. Schulz, R. H. Brown Jr., M. F. Beal, *J. Neurochem.* **61**, 2322 (1993).
7. The A4V mutation was introduced into exon 1 of the human *SOD1* gene by two-primer mutagenesis with the polymerase chain reaction (PCR); the template for mutagenesis was a Sty I–Stu I fragment encompassing exon 1. The G93A mutation was cloned in a Hind III and Nsi I fragment encompassing exon 4 that was amplified from the genomic DNA of family 3-192 (3). These fragments were used to reassemble a complete 14.5-kb Eco RI–Bam HI fragment of the *SOD1* gene [R. A. Hawell, J. P. Puma, G. T. Mullenbach, R. C. Najarian, in *Superoxide and Superoxide Dismutase in Chemistry, Biology and Medicine*, G. Rotilio, Ed. (Elsevier, New York, 1986), pp. 249–256] in two more steps. Exons 1 and 4 of the transgenes were sequenced to verify that they contained only the desired mutation. The 14.5-kb Eco RI–Bam HI *SOD1* transgene directs tissue-specific expression of human SOD in mice under control of the endogenous human promoter (8).
8. C. J. Epstein et al., *Proc. Natl. Acad. Sci. U.S.A.* **84**, 8044 (1987).
9. I. Ceballos-Picot et al., *Brain Res.* **552**, 198 (1991); K. B. Avraham et al., *Cell* **54**, 823 (1988); K. B. Avraham, H. Sugarman, S. Rotshenker, Y. Groner, *J. Neurocytol.* **20**, 208 (1991).
10. Mice were housed in microisolator cages within a barrier facility. Frequent monitoring revealed no evidence for infection by viral or bacterial pathogens.
11. The primers described (3) were used for identification of transgenic mice by PCR. Transgene copy number was estimated by Southern (DNA) DNA hybridization. Denatured DNA (10 μ g) isolated from mouse tails or human placenta was transferred to a nitrocellulose membrane together with a dilution series of the cloned *SOD1* gene. The membrane was hybridized with a random-primed, ³²P-labeled probe to sequences within the 3' untranslated region of the 0.9-kb human *SOD1* complementary DNA (cDNA); these sequences are specific to the human transgene. Bound radioactivity was quantitated by phosphor image analysis, and linear regression was used to calculate transgene copy number.
12. The EIA was constructed with a goat immunoglobulin G (IgG) antibody to human SOD (Chiron, Emeryville, CA) and a mouse monoclonal antibody designated SD-G6 (Sigma, St. Louis, MO). Recombinant human SOD (Chiron) was used as a standard. Samples were diluted to within the log-linear range of the assay (0.1 to 1.5 ng of human SOD per well). There was no cross-reactivity with mouse SOD.
13. Northern RNA hybridization was performed with 10 μ g of total brain RNA. The membrane was hybridized with a random-primed, ³²P-labeled probe specific for the 3' untranslated region of the human *SOD1* cDNA. Quantitation standards (a 0.9-kb sense human *SOD1* cDNA) were loaded on the gel with 10 μ g of yeast RNA as a carrier, and the hybridization signal was analyzed by phosphor image analysis. To control for RNA loading variations, we rehybridized the blot with a glyceraldehyde 3-phosphate dehydrogenase (G3PDH) cDNA probe.
14. Samples containing 2 μ g of soluble brain protein were subjected to electrophoresis through 10% SDS-polyacrylamide gels, transferred to a nitrocellulose membrane, and probed with antibody CZSODF2. Bound antibody was detected with a biotinylated horse antibody to mouse IgG and a Vector ABC kit. The membrane was developed with an enhanced chemiluminescence kit (Amersham, Arlington Heights, IL), and the chemiluminescence was quantitated by film densitometry. The amount of human SOD in brain extracts of A4V transgenic mice was determined by comparison to recombinant SOD standards in adjacent lanes.
15. D. R. Borchelt et al., *Proc. Natl. Acad. Sci. U.S.A.*, in press.
16. Mouse brains were homogenized in cold 10 mM Tris HCl (pH 7.5) and 10 mM β -mercaptoethanol. After centrifugation at 50,000g for 15 min at 4°C, the protein content of the supernatant was measured by a bicinchoninic acid assay (Pierce, Rockford, IL). We assayed total SOD activity within brain extracts in microwells by measuring the inhibition of nitroblue tetrazolium reduction [D. R. Spitz and L. W. Oberley, *Anal. Biochem.* **179**, 8 (1989)]. Wells were monitored kinetically, and a (V_{max}/V) – 1 transform (where V is velocity) [K. Asada, M. Takahashi, M. Nagate, *Agric. Biol. Chem.* **38**, 471 (1974)] was used to linearize the data. Recombinant human SOD had an activity of 6 U per nanogram. The contribution of Mn SOD in the sample was determined in the presence of 5 mM sodium cyanide and was ~2% of the total SOD activity in the brain extract.
17. O. Elroy-Stein, Y. Bernstein, Y. Groner, *EMBO J.* **5**, 615 (1986).
18. R. A. Hawell et al., *Nucleic Acids Res.* **13**, 2017 (1985).
19. Mice were trained to walk up a 75-cm, U-shaped ramp that was inclined at one end against the wire lid of their cage. Testing was performed in a horizontal, laminar flow hood to maintain barrier conditions. A bright lamp was placed at the base of the ramp, and the cage lid was left in semidarkness. The ramp obscured each mouse's view of the laminar flow hood and surrounding room. Testing was initiated by allowing the mice 1 to 2 min to explore the cage lid and the top of the

- ramp. The hind feet of the mice were painted with children's poster paints of contrasting colors. The tracks left by the mice as they ran up the ramp were recorded on paper tape.
20. Degenerating neurons were positive for immunohistochemical staining with SMI-31 monoclonal antibody (Sternberger Monoclonal Antibodies, Baltimore, MD) to phosphorylated neurofilaments, although the small number of motor neurons remaining in affected spinal cords and their marked pathology require confirmation of this result.
 21. W. K. Engel, L. T. Kurland, I. Klatzo, *Brain* 82, 203 (1959); A. Hirano, L. T. Kurland, G. P. Sayre, *Arch. Neurol.* 16, 232 (1967).
 22. J. S. Beckman *et al.*, *Proc. Natl. Acad. Sci. U.S.A.* 87, 1624 (1990).
 23. H. Ischiropoulos *et al.*, *Arch. Biochem. Biophys.* 298, 431 (1992).
 24. S. A. Lipton *et al.*, *Nature* 364, 626 (1993).
 25. J. P. Nowicki, D. Duvall, H. Poignet, B. Scatton, *Eur. J. Pharmacol.* 204, 339 (1991).
 26. J. S. Beckman, M. Carson, C. D. Smith, W. Koppenol, *Nature* 364, 584 (1993).
 27. A. Y. Chiu, E. W. Chen, S. Loera, *J. Comp. Neurol.* 328, 351 (1993).
 28. M. E. Gurney, H. Yamamoto, Y. Kwon, *J. Neurosci.* 12, 3241 (1992).
 29. We thank R. Huntress, S. Potter, and R. Hallowell for research materials and F. Cutting, B. Lom, and R. Mihalik for technical assistance. Supported by the National Institutes of Neurological Disorders and Stroke, the Muscular Dystrophy Association, the Les Turner ALS Foundation, the Searle Family Center for Neurological Disorders, the Vena E. Schaaf ALS Research Fund, and the Herbert and Florence C. Wenske Foundation.

24 March 1994; accepted 20 May 1994

Molecular Genetic Analyses of the Tyrolean Ice Man

Oliva Handt, Martin Richards, Marion Trommsdorff, Christian Kilger, Jaana Simanainen, Oleg Georgiev, Karin Bauer, Anne Stone, Robert Hedges, Walter Schaffner, Gerd Utermann, Bryan Sykes, Svante Pääbo*

An approximately 5000-year-old mummified human body was recently found in the Tyrolean Alps. The DNA from tissue samples of this Late Neolithic individual, the so-called "Ice Man," has been extracted and analyzed. The number of DNA molecules surviving in the tissue was on the order of 10 genome equivalents per gram of tissue, which meant that only multi-copy sequences could be analyzed. The degradation of the DNA made the enzymatic amplification of mitochondrial DNA fragments of more than 100 to 200 base pairs difficult. One DNA sequence of a hypervariable segment of the mitochondrial control region was determined independently in two different laboratories from internal samples of the body. This sequence showed that the mitochondrial type of the Ice Man fits into the genetic variation of contemporary Europeans and that it was most closely related to mitochondrial types determined from central and northern European populations.

In September 1991, the frozen mummy of a man was found in the Tyrolean Alps. Radiocarbon dates of skin and bone samples indicated an age between 5100 and 5300 years (1). Because no comparable archaeological discovery exists, this find has attracted considerable scientific and public interest. It has also been the subject of various rumors and even allegations of fraud (2). Molecular genetic investigations of the Ice Man could address some of the questions surrounding the find. Comparisons of

DNA sequences from the body with contemporary populations may reveal aspects of his ethnic affiliation. Molecular studies of other organisms such as viruses or bacteria associated with the body may furthermore illuminate the evolution of these organisms. As a first step toward such investigations, we have analyzed the state of preservation of the DNA in the Ice Man and determined the sequence of a hypervariable segment of the mitochondrial control region from numerous samples removed from the body.

Ancient DNA has been retrieved from a variety of plant, animal, and human remains (3, 4) that go back a few tens of thousands of years as well as from some fossils that are millions of years old (5-7), although the latter results are partially controversial (8). In most cases, work on archaeological DNA has been limited to mitochondrial DNA because its high copy number increases the chance of survival of a few molecules in the face of molecular damage that accumulates post mortem. Be-

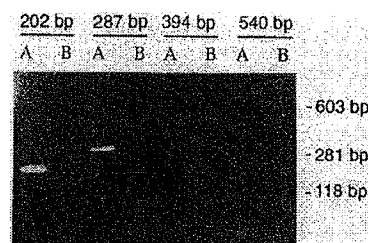


Fig. 1. Agarose gel electrophoresis of mitochondrial DNA amplification of different lengths from the Ice Man. For every primer pair, amplifications from (A) an extract of the Ice Man and (B) an extraction control are shown. The primer pairs used are as follows: L16055/H16218 (202 bp), L16055/H16303 (287 bp), L16055/H16410 (394 bp), and L15997/H16498 (540 bp), where L and H refer to the light and heavy strand, respectively, followed by the number to the nucleotide position (14) at the 3' end of the primer. Migration positions of molecular size markers are given in numbers of base pairs.

cause the body of the Ice Man has been frozen with the exception of a short period after its discovery, its DNA may be preserved better than that of other finds. This unusual condition might allow nuclear markers such as microsatellites to be studied in addition to mitochondrial DNA and thus open several additional avenues of study.

A total of eight samples of muscle, connective tissue, and bone were removed under sterile conditions from the left hip region of the body, which had been damaged during salvage of the mummy. Additionally, parts of one sample that has been radiocarbon dated (1) were analyzed. Extracts of DNA were made from 10 to 200 mg of each sample by a silica-based method that is highly efficient in the retrieval of ancient DNA (9). Enzymatic amplifications from the mitochondrial control region were attempted. Because this region encodes no structural gene products and evolves faster than other parts of the mitochondrial genome, it is particularly suited for the reconstruction of the history of human popula-

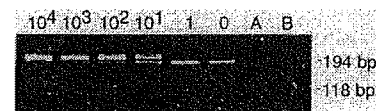


Fig. 2. Quantitation of mitochondrial DNA in an extract from the Ice Man. A dilution series of a competitor template, containing a 20-bp insertion in a mitochondrial fragment, was added to a constant amount of extract, and a PCR that used primers L16068/H16218 was performed as described in (10). The numbers above the lanes indicate the numbers of competition molecules added to the amplifications. (A) An extraction control and (B) a control where no template was added. Migration positions of molecular size markers are given in numbers of base pairs.

O. Handt, C. Kilger, K. Bauer, A. Stone, S. Pääbo, Institute of Zoology, University of Munich, Postfach 202136, D-80021 München, Germany.
M. Richards and B. Sykes, Institute of Molecular Medicine, University of Oxford, Oxford OX3 9DU, UK.
M. Trommsdorff and G. Utermann, Institute of Medical Biology and Genetics, University of Innsbruck, Schöpfstrasse 41, A-6020 Innsbruck, Austria.
J. Simanainen, O. Georgiev, W. Schaffner, Institut für Molekularbiologie II, Universität Zürich, Winterthurerstrasse 190, CH-8057 Zürich, Switzerland.
R. Hedges, Research Laboratory for Archaeology, University of Oxford, 6 Keble Road, Oxford OX1 3QJ, UK.

*To whom correspondence should be addressed.

EXHIBIT 6

Focal loss of the glutamate transporter EAAT2 in a transgenic rat model of SOD1 mutant-mediated amyotrophic lateral sclerosis (ALS)

David S. Howland^{*,†}, Jian Liu[†], Yijin She[†], Beth Goad[†], Nicholas J. Maragakis[‡], Benjamin Kim[‡], Jamle Erickson^{*}, John Kulik^{*}, Lisa DeVito^{*}, George Psaltis^{*}, Louis J. DeGennaro[†], Don W. Cleveland[‡], and Jeffrey D. Rothstein^{*}

^{*}Department of Molecular Genetics, Wyeth Research, CN8000, Princeton, NJ 08543; [†]Ludwig Institute for Cancer Research, University of California at San Diego, La Jolla, CA 92093; and [‡]Department of Neurology, Johns Hopkins University School of Medicine, Baltimore, MD 21287

Edited by Thomas Maniatis, Harvard University, Cambridge, MA, and approved December 5, 2001 (received for review October 11, 2001)

Transgenic overexpression of Cu²⁺/Zn²⁺ superoxide dismutase 1 (SOD1) harboring an amyotrophic lateral sclerosis (ALS)-linked familial genetic mutation (SOD1^{G93A}) in a Sprague-Dawley rat results in ALS-like motor neuron disease. Motor neuron disease in these rats depended on high levels of mutant SOD1 expression, increasing from 8-fold over endogenous SOD1 in the spinal cord of young presymptomatic rats to 16-fold in end-stage animals. Disease onset in these rats was early, ~115 days, and disease progression was very rapid thereafter with affected rats reaching end stage on average within 11 days. Pathological abnormalities included vacuoles initially in the lumbar spinal cord and subsequently in more cervical areas, along with inclusion bodies that stained for SOD1, Hsp70, neurofilaments, and ubiquitin. Vacuolization and gliosis were evident before clinical onset of disease and before motor neuron death in the spinal cord and brainstem. Focal loss of the EAAT2 glutamate transporter in the ventral horn of the spinal cord coincided with gliosis, but appeared before motor neuron/axon degeneration. At end-stage disease, gliosis increased and EAAT2 loss in the ventral horn exceeded 90%, suggesting a role for this protein in the events leading to cell death in ALS. These transgenic rats provide a valuable resource to pursue experimentation and therapeutic development, currently difficult or impossible to perform with existing ALS transgenic mice.

Amyotrophic lateral sclerosis (ALS) is a late-onset neuromuscular disorder characterized by progressive motor dysfunction that leads to paralysis and eventually death. The pathology of the disease results from the death of large motor neurons in the spinal cord and brainstem (1, 2). ALS occurs in both sporadic and familial forms (3). Familial ALS accounts for ~5–10% of all reported cases. Approximately 15–20% of familial ALS cases has been linked to inheritance in an autosomal dominant fashion of a mutant form of Cu²⁺/Zn²⁺ superoxide dismutase 1 (SOD1) (4, 5). SOD1 normally functions in the regulation of oxidative stress by conversion of free radical superoxide anions to hydrogen peroxide and molecular oxygen. Over 90 distinct familial SOD1 mutations have been found to date. SOD1 mutations that have been tested in transgenic mice result in ALS-like motor neuron disease (6–8), but SOD1-null mice do not develop motor neuron disease (9). Furthermore, crossing SOD1-null mice with transgenic ALS mice does not alter disease onset or progression (10). Taken together, these results indicate that familial ALS does not result from loss of SOD1 function but rather an unidentified gain of function. There is no consensus as to the mechanism, and theories include alterations in SOD1 folding, oxidative stress from aberrant catalysis (11), or cytoplasmic aggregates (12). New studies also suggest that the disease is not cell autonomous—that nonneuronal cells are necessary for motor neuron degeneration (13, 14, 15).

Transgenic mouse models expressing mutant forms of SOD1 (15–21) develop neuromuscular disease very similar to human ALS. Age of onset of disease varies as a function of both the type of mutant expressed in mouse and the relative expression levels attained. High expressing SOD1^{G93A} (13-fold above endogenous

SOD1) and G37R SOD1 (7–14-fold above endogenous SOD1) transgenic mice contain membrane-bound vacuoles in cell bodies (15, 22) and dendrites (15, 16, 22), which most likely result from degenerating mitochondria. Lower expressing SOD1^{G93A} mice (7-fold above endogenous SOD1) also contain Lewy-body-like cytoplasmic inclusions in the cell bodies of motor neurons (21) containing SOD1, ubiquitin, and phosphorylated neurofilament (23). SOD1^{G85R} transgenic mice expressing mutant SOD1 as little as 20% of endogenous levels also develop neuromuscular disease characterized by loss of large motor neurons in brainstem and in spinal cord (10, 17). No vacuolization has been reported in G85R mice or in similar mice expressing the murine counterpart mutation G86R (18, 24). However, these mice also develop cytoplasmic inclusions that appear in astrocytes and neurons before clinical signs of disease and dramatically increase in abundance with disease progression (10). SOD1^{G85R} mice have also shown to be deficient in the spinal cord astroglial glutamate transporter EAAT2 (GLT-1), similar to observations in sporadic ALS (25), suggesting that astroglial dysfunction in ALS may contribute to motor neuron degeneration.

We sought to create a transgenic rat model for ALS by using mutant SOD1 to pursue experimental paradigms currently difficult or impossible to achieve in the smaller transgenic mouse models. Rats provide an advantage in pursuit of therapeutic strategies such as stem cell replacement and are the preferred laboratory animal species for pharmacological manipulations.

Materials and Methods

Generation and Characterization of Transgenic Rats Expressing Human SOD1^{G93A}. A 12-kb *EcoRI*/*Bam*HI restriction fragment of the human SOD1 gene harboring the G93A mutation was microinjected into Sprague-Dawley rat embryos. Transgenic rats were produced as described (26). Embryos were allowed to develop to term and were analyzed for the presence of the transgene. Tail biopsies from 8-day-old rats were digested in proteinase K and then diluted 1:20 in dH₂O followed by heating at 95°C for 15 min. Two microliters were subjected to PCR by using primers SOD-13f (5'-GTGGCATCAGCCCTAATCCA-3') and SOD-E4r (5'-CACCAGTGTGCGGCCAATGA-3') specific to human SOD1 to determine the genotypes of founders and offspring.

Taqman quantitative DNA PCR was performed to determine DNA copy number of transgene loci segregating from the multiintegrant founders 26, 46, and 51 to their respective F1

This paper was submitted directly (Track II) to the PNAS office.

Abbreviations: SOD1, superoxide dismutase 1; ALS, amyotrophic lateral sclerosis; EMG, electromyography.

To whom reprint requests should be addressed. E-mail: howland@war.wyeth.com.

^{*}Clement, A. M., Roberts, E. A., Goldstein, L. S., & Cleveland, D. W. (2001) *Soc. Neurosci. Abstr.* 27, no. 580.4.

The publication costs of this article were defrayed in part by page charge payment. This article must therefore be hereby marked "advertisement" in accordance with 18 U.S.C. 5173a solely to indicate this fact.

Table 1. Multiple transgene integrations in SOD1^{G93A} founders were resolved into individual lines

Line	Subline	dCt	Copy no.	Spinal cord hSOD1/rSOD1	Blood hSOD1/rSOD1	Pathology
26	26L	-3	8	nd	0.4	None
	26H	-6	64	8.6	0.8	~115 days
	26HL	-7	72	10.4	1.1	~102 days
46	46L	-0.5	1-2	0.4	<0.1	None
	46H	-2.5	5-6	2.6	0.2	None
51	51L	-2	4	2.2	0.5	None
	51H	-4	16	5.8	1.2	None
61	—	-2.3	4-5	2.4	0.1	None

ND, not determined; H, high copy; L, low copy; h, human; r, rat; dCt, delta cycle threshold.

generation progeny. Primer-probe sets specific for human *SOD1* and an internal normalizer gene, *Thy1.2*, were used in multiplex PCR on a Taqman 770 PCR thermocycler (PE Biosystems) following the manufacturer's recommended conditions. Data were represented as delta cycle threshold (dCt) and were converted to relative transgene DNA copy number by the equation $2^{-(dCt)}$ (Table 1).

Quantitation of SOD1 in Blood and SOD1 and EAAT2 in Spinal Cord. Blood samples from tail vein bleeds were solubilized in 10 vol of 50 mM Tris-HCl, pH 7.5/150 mM NaCl/5 mM EDTA/1% Nonidet P-40/1% SDS. For SOD1 detection, 25 μ g was electrophoresed on 12% SDS/polyacrylamide gel and transferred to nitrocellulose. Cervical spinal cord was homogenized in 2 ml of 50 mM Tris-HCl, pH 7.5/150 mM NaCl/5 mM Na₂EDTA/1% Nonidet P-40/1% SDS, and 5 μ g was electrophoresed as described above. For detection of EAAT2, ventral horn of cervical spinal cord was dissected by using 0.5-mm micropunches (Zivic-Miller) and homogenized as described above, and 25 μ g of total protein was electrophoresed on 7.5% SDS/polyacrylamide gels. Western blots were probed with either anti-SOD1 (27) (1:5,000), anti-GLT-1 (EAAT2; 1:1,000; Chemicon), or anti-actin (C4; 1:10,000; Roche Molecular Biochemicals) Abs.

Immunohistochemical Analyses. Animals were killed by using approved animal welfare protocols and perfused by cardiac puncture with 4% paraformaldehyde/PBS. Muscle, brain, and spinal cord were removed followed by regional dissection of spinal cord and spinal nerve roots. Tissue blocks were embedded in paraffin or araldite for sectioning (7 and 1 μ m, respectively). Immunostains and semithin plastic sections were processed as described (16, 17, 28). Hematoxylin and eosin stains of muscle and spinal cord were performed on paraffin sections, whereas semithin sections of spinal roots were stained with toluidine blue. Immunostaining was performed with Abs to neurofilament with SMI-32 (1:8,000; Sternberger-Mayer, Jarrettsville, MD), glutamate transporter GLT-1 (1:1,000), SOD1 (1:10,000), heat shock protein (HSP70; 1:100; StressGen Biotechnologies, Victoria, BC, Canada); ubiquitin (1:1,500; Dako), and glial fibrillary acidic protein (1:50; Dako).

Electrophysiological Recording. Electromyography (EMG) and nerve conduction were performed by using an ADI (Greenwich, CT) Powerlab/8SP stimulator and BioAMP amplifier followed by computer assisted data analysis (CHART 4.0 and scope 3.5.6; ADI). Compound muscle action potentials were recorded by stimulating the sciatic nerve at the sciatic notch and recording from the foot. EMG was performed by using a bipolar needle and sampling at 200 Hz.

Results

Multiple Transgenic Rat Lines Express Mutant SOD1^{G93A}. We identified three SOD1^{G93A} founders that expressed mutant human SOD1 in blood (Fig. 1A). A fourth (founder 46) showed no detectable SOD1^{G93A} expression; however, subsequent immunoblots of whole blood from the F1 animals of this line did indeed show low-level SOD1^{G93A} (not shown). These four founders were bred to the F1 generation to establish transgenic lines.

Transgene transmission frequency to the F1 generation was greater than the expected 50% in lines 26, 46, and 51 and was determined to be the result of multiple transgene integration sites in each of these founders. Distinct transgene integrations can be resolved by using quantitative Taqman PCR if the number of transgene copies differs at each chromosomal site. This was indeed the case for lines 26, 46, and 51. Taqman PCR data were used to track inheritance of distinct low- or high-copy transgene loci by F1 generation animals thereby allowing us to establish separate sublineages for each of these lines (Table 1).

Development of Motor Neuron Disease in SOD1^{G93A} Transgenic Rats. SOD1^{G93A} founder 26 developed motor neuron disease at 93 days of age, whereas all other founders did not develop disease. Because of the multiple integration of the transgene, the F1 generation animals derived from founder 26 inherited either the high- or low-copy transgene locus or both (see Table 1). F1 animals containing only the low-copy locus (L26L) did not develop motor neuron disease. F1 animals that inherited both loci from founder 26 (L26HL) developed motor neuron disease by 93 days of age, the same age as disease onset in the founder. F1 animals that inherited only the high-copy locus (L26H) developed motor neuron disease between 104–121 days of age. The apparent earlier onset in L26HL vs. L26H animals most likely was the result of slightly higher mutant SOD1 expression (Table 1). Because the single high-copy locus (L26H) in rats was sufficient to elicit motor neuron disease, we chose to breed this subline to the F2 and subsequent generations for further analysis.

Mutant SOD1 Expression in SOD1^{G93A} Transgenic Rats. SOD1^{G93A} expression in the spinal cord of L26H transgenic rats was determined to be ~8-fold above endogenous SOD1 as assessed by immunoblot analysis of young presymptomatic animals (Fig. 1C; Table 1). As expected, these levels exceeded other transgenic rat lines that did not go on to develop motor neuron disease (Table 1). SOD1^{G93A} expression in L26H rats was also evident across many brain regions as well as peripheral tissues (Fig. 1B), similar to that seen in described SOD1 transgenic mice (16). By end stage, mutant SOD1 levels accumulated ~16-fold over endogenous, representing a further 2-fold increase in SOD1^{G93A} compared with levels in young presymptomatic rats (6 weeks old) (Fig. 1C). Spinal cord SOD1^{G93A} levels were directly compared

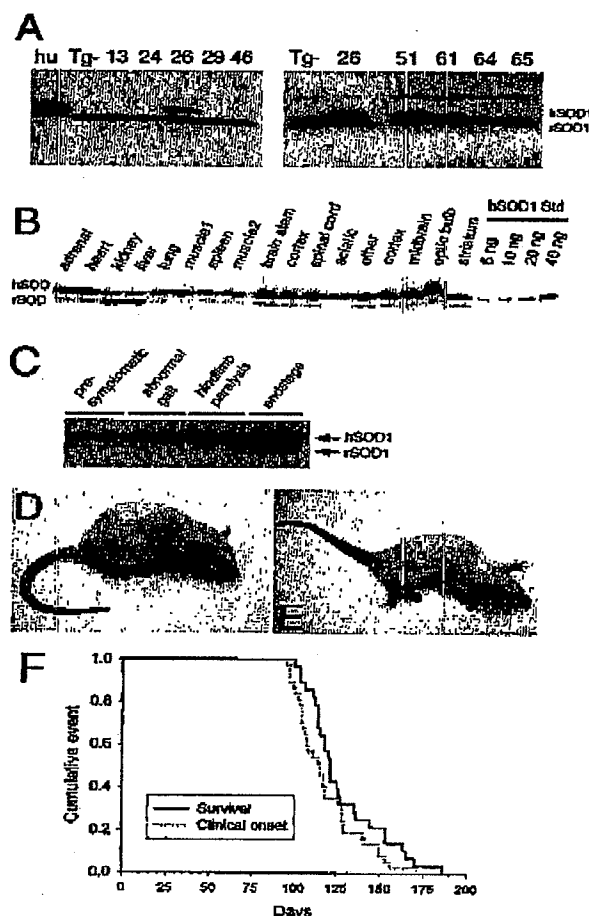


Fig. 1. Mutant SOD1 expression and disease in SOD1^{G93A} transgenic rats. SOD1 expression in blood from transgenic founders (A) is highest in founder number 26. L26H F1 generation rats exhibit SOD1^{G93A} expression throughout the nervous system and peripheral tissues (B). SOD1^{G93A} expressed at ~8-fold over endogenous in young (6 weeks) presymptomatic transgenic rat spinal cord increases to ~16-fold by end-stage disease (16 weeks) (C). Normal age-matched littermate control animal (D) at ~120 days compared with an end-stage transgenic rat showing signs of muscle wasting, paralysis of both hindlimbs and one forelimb (E). Kaplan-Meier survival curve (n = 25) generated from F2 generation L26H transgenic rats depicting disease onset and survival.

in end-stage L26H transgenic rats and the previously described G1H and G1L transgenic mice, which also express SOD1^{G93A}. We found that SOD1^{G93A} levels in end-stage G1H and G1L (15, 21, 22) transgenic mice were 3- and 1.5-fold, respectively, higher than levels attained in end-stage L26H transgenic rats (data not shown).

Characterization of Motor Neuron Disease in SOD1^{G93A} L26H Transgenic Rats. A subset (n = 25) of F2 generation animals for L26H were observed closely for onset of disease symptoms, as well as progression to death. Onset of motor neuron disease was scored as the first observation of an abnormal gait or evidence of

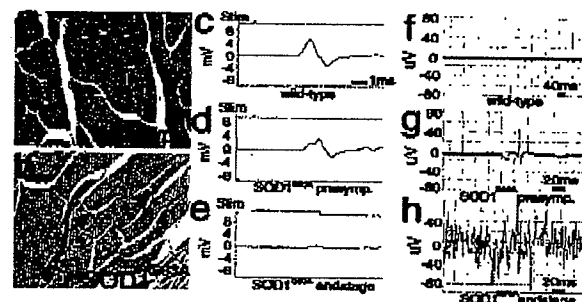


Fig. 2. Muscle atrophy and denervation in SOD1^{G93A} rats. Leg muscle myofibers from end-stage (age >120 days) SOD1^{G93A} rats were often seen as groups of atrophic angular fibers (b, arrows), compared with aged-matched control rats (a). Compound muscle action potential in nontransgenic control foot muscle (c; 5.48 mV) was reduced in the foot (d; 4.3 mV) in presymptomatic rats and was almost unobtainable in end-stage foot (e; 0.71 mV) after supra-maximal stimulation (1 ms per division). Needle EMG of presymptomatic SOD1^{G93A} rat (g) demonstrates a rare fibrillation potential recorded in the lumbar paraspinal muscles compared with age-matched wild-type control rat (f). EMG of end-stage (>125 days age) SOD1^{G93A} rat (h) revealed continuous fibrillation potentials and positive sharp waves (20 ms per division).

hindlimb weakness. Affected animals were tested daily for the ability to right themselves after being turned on either side for a maximum of 30 sec; failure at this task was seen in end-stage animals and scored as "death" (see Fig. 1E). All end-stage animals were killed. Righting reflex failure was coincident with complete paralysis of both hindlimbs and at least 1 forelimb. F2 L26H transgenic rats had an average age of onset of motor neuron disease of 115 days. Onset typically appeared as hindlimb abnormal gait and progressed very quickly (1–2 days) to overt hindlimb paralysis, typically affecting one limb first. Within 1–2 days, the second hindlimb was involved, although animals could still ambulate through the use of forepaws. Affected rats showed signs of weight loss, poor grooming, and porphyrin staining around the eyes. L26H transgenic rats typically reached end-stage disease very quickly, an average of 11 days after onset of symptoms. All F2 generation L26H transgenic rats monitored for this study reached end-stage disease within 173 days after birth.

Muscle Pathology and Impaired Function in SOD1^{G93A} L26H Rats. Leg muscles (distal and proximal) from end-stage rats revealed obvious and frequent angular atrophic myofibers, most often in discrete clumps typical of neurogenic atrophy (Fig. 2b), whereas muscles from wild-type littermate controls were normal (Fig. 2a). In parallel, electrophysiologic recordings from end-stage SOD1^{G93A} rats (n = 5) exhibiting obvious hindlimb paralysis or paresis revealed markedly reduced amplitude of compound motor action potentials (CMAP) in the intrinsic foot muscles (Fig. 2e), indicating motor neuron loss (compare 5.48 mV in wild-type animals to 0.71 mV in end-stage SOD1^{G93A} rats). CMAP in presymptomatic animals was diminished only partially (Fig. 2d; n = 5) compared with littermate controls (Fig. 2c). Needle EMG of age-matched wild-type rats demonstrated absence of any spontaneous activity, compared with rare fibrillation potentials in paraspinal muscles from presymptomatic rats (Fig. 2f and g). Continuous fibrillation potentials and positive sharp waves were evident in leg muscles from end-stage L26H rats (Fig. 2h).

Immunohistochemical Characterization of SOD1^{G93A} L26H Transgenic Rats. Analysis of hematoxylin/eosin-stained sections of lumbar spinal cord from end-stage SOD1^{G93A} rats (n = 10) revealed a

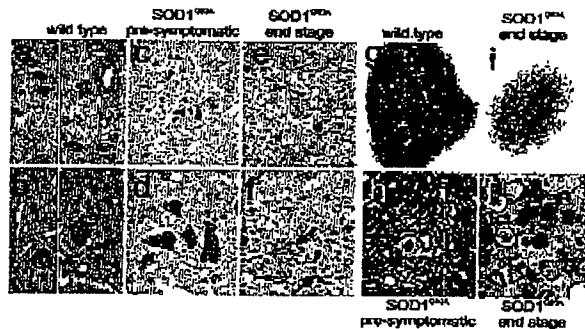


Fig. 3. Motor neuron and axon loss in $SOD1^{G93A}$ rats. Ventral spinal cord gray matter reveals vacuolar degeneration in the neuropil of presymptomatic $SOD1^{G93A}$ rats (c and d) and astrogliosis and loss of motor neurons in end-stage rats (e and f) compared with age-matched wild-type rats (a and b). Glial nodules, around remnants of degenerating motor neurons, were evident throughout the ventral gray matter (f, arrows). Ventral motor roots from an end-stage rat (i) were atrophic compared with aged-matched control roots (g). Closer inspection revealed active ongoing degeneration in end-stage $SOD1^{G93A}$ ventral roots (j), whereas roots from presymptomatic rats showed little degeneration (h). Magnification: $\times 4$, g and i; $\times 10$, a, c, and e; $\times 40$, b, d, and f; $\times 100$, h and j.

dense gliosis with a complete loss of ventral large motor neurons (alpha-motor neurons) as shown in Fig. 3e and f compared with similarly aged wild-type rats (Fig. 3a and b). Closer inspection demonstrated frequent "glial nodules" (Fig. 3f, arrows), representing active degeneration and engulfment of neurons. Inspection of ventral horn gray matter from lumbar spinal cord from presymptomatic rats (~ 90 – 100 days of age) revealed a normal population of motor neurons but a profound vacuolar degeneration of the neuropil (Fig. 3c and d), similar to that seen in end-stage $SOD1^{G93A}$ mice (15, 22). However, in the rat these vacuoles were transient, appearing at the time of active motor neuron loss but were nearly absent in the lumbar cord by end-stage disease (Fig. 3e and f). Brainstem and cervical spinal cord of end-stage rats also revealed vacuolar and glial nodule changes in motor neurons (not shown), albeit these appeared later in these regions, again consistent with vacuolar presence preceding neuronal loss. In concert with the changes in gray matter, ventral roots from end-stage $SOD1^{G93A}$ rats were atrophic (Fig. 3i). On closer inspection (Fig. 3j) active degeneration of most axons was observed with macrophage infiltration and myelin ovoids. In contrast, analysis from presymptomatic $SOD1^{G93A}$ rat ventral roots ($n = 5$) showed almost normal-appearing axons (Fig. 3h), compared with age-matched controls (Fig. 3g), with rare (1–2 axons per root) undergoing degeneration (Fig. 3h arrow).

As was reported in earlier examples of $SOD1$ mutant-mediated disease in mice (10), onset of clinical disease was accompanied by aggregates of $SOD1$ throughout the rat ventral horn (Fig. 4b) and brain (not shown) especially in prominent focal deposits in which mutant $SOD1$ immunoreactivity was frequently most robust at the perimeter. Similar pathology was not found in nontransgenic controls (Fig. 4a). These aggregates could be found in a few surviving motor neuron perikarya, axons, and surrounding glia. Aggregates were intensely stained with Abs to ubiquitin (Fig. 4g), consistent with disruption in protein clearance by the proteasome. Aggregates also contained endogenous Hsc70 especially within surviving motor neuron cell bodies (Fig. 4c), suggesting mutant-dependent depletion of the intracellular protein folding chaperone pool. Aberrant accumulations of neurofilaments, reported in $SOD1^{G93A}$ -expressing

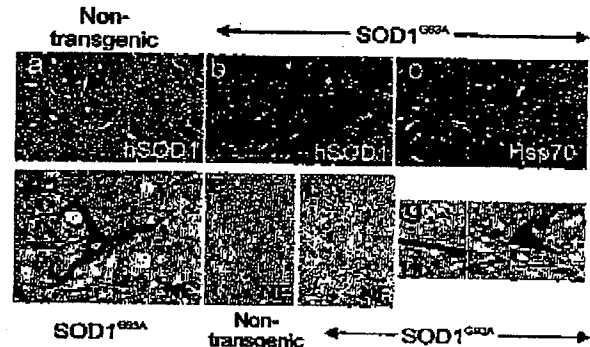


Fig. 4. Aberrant accumulations of proteins in $SOD1^{G93A}$ rats. Accumulation in the neuropil of $SOD1^{G93A}$ rats (b) compared with age-matched wild-type rats (a). Hsc70 (c) and ubiquitin (Ub) (d) were abnormally accumulated in the neuropil and cytoplasm of ventral gray neurons. Similarly, neurofilament (NF) aggregates were found in the soma of large motor neurons (d) and their axons, often in spheroid structures in the neuropil and especially in the ventral root zone white matter (f) compared with dorsal white tracts (e).

transgenic mice (29), were prominent abnormalities after disease onset, both in perikarya (Fig. 4d) and in distended axonal swellings [compare the neurofilament staining in transgenic axons (Fig. 4f) with that of the wild-type littermate controls (Fig. 4e)]. These accumulations were selective for axons within the ventral root exit zone and were not found in the dorsal ascending columns (not shown).

EAAT2 Deficits in the Ventral Horn Spinal Cord of $SOD1^{G93A}$ L26H Rats. EAAT2 is the predominant glutamate transporter in the central nervous system, normally expressed widely throughout the spinal gray matter (Fig. 5a) in astrocytes but not in motor neurons (arrows, Fig. 5b). Previous studies have documented a profound loss of the protein in sporadic and familial ALS (25, 28, 30). In presymptomatic $SOD1^{G93A}$ rats, just before disease onset, motor neurons are still present (Fig. 5c, arrows) and ventral horns have not started to degenerate (Fig. 5h). At this time point, there is an obvious patchy loss of EAAT2 immunoreactivity in the ventral horn (Fig. 5c). By end stage, there is a profound focal loss of EAAT2 immunoreactivity despite a striking increase in the number of astrocytes (Fig. 5d and e). These changes were mirrored by a quantitative loss of EAAT2 immunoreactivity measured from immunoblots of extracts from spinal cord, especially in the ventral gray regions (Fig. 5f). Assays of glutamate transport also confirmed a nearly 50% loss of functional transport (data not shown). Astroglial reactivity, as revealed by glial fibrillary acidic protein immunostaining, also showed activation before motor neuron degeneration, in presymptomatic spinal cord ventral gray (Fig. 5h) compared with nontransgenic controls (Fig. 5g), followed by a more dramatic activation (Fig. 5i and j) in end-stage tissue.

Discussion

We have generated transgenic Sprague–Dawley rats that express human mutant $SOD1^{G93A}$ at levels ~ 8 -fold over endogenous $SOD1$ in the spinal cord of young presymptomatic rats. This level of expression was sufficient to cause an ALS-like motor neuron disease in rats by 3–4 months of age. Additional transgenic lines expressing mutant $SOD1$ between 0.1- to ~ 6 -fold over endogenous levels of $SOD1$ have not developed any signs of motor neuron disease by 1 year of age. Recapitulation of an ALS-like motor neuron disease in the transgenic rat using the G93A

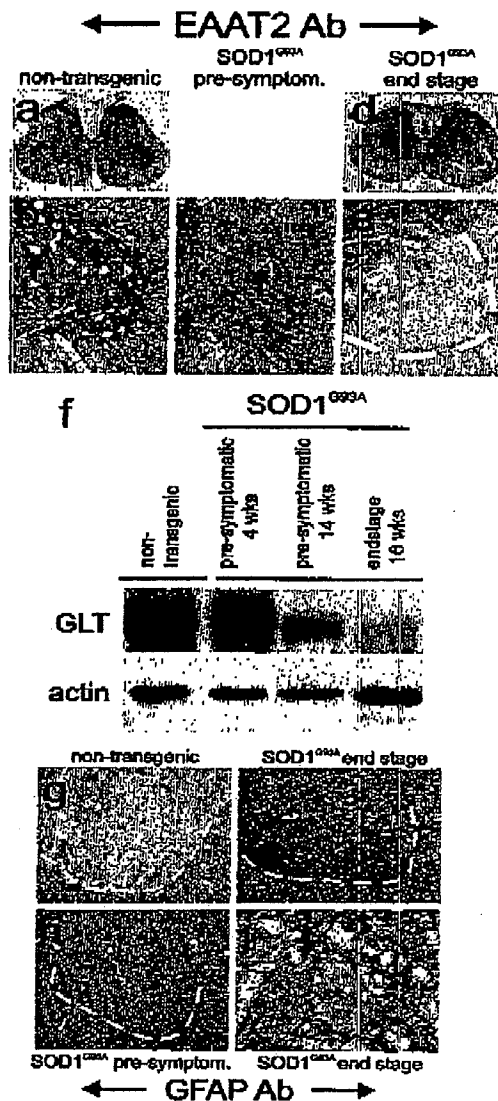


Fig. 5. Astroglial alterations in $SOD1^{G93A}$ rats. The usual ubiquitous astroglial expression of the glutamate transporter EAAT2 (a and b), surrounding motor neurons (arrows), was markedly altered in $SOD1^{G93A}$ rats with a patchy loss in the ventral horn in presymptomatic rats (d) and almost a complete loss of protein in end-stage ventral gray from $SOD1^{G93A}$ rats (d and e). This loss of EAAT2 (GLT) was paralleled in immunoblots from ventral gray of presymptomatic and end-stage rats (f). In parallel, astroglial expression of glial fibrillary acidic protein (GFAP) increased somewhat in presymptomatic ventral gray (h), compared with age-matched wild-type control (g), and was markedly increased in end-stage rats (i), especially around rare motor neuron profiles (j).

mutant $SOD1$ clearly depended on the ability to obtain high-level transgene expression in the spinal cord as reported for the $SOD1^{G93A}$ (15) and $SOD1^{G37R}$ (16) transgenic mice.

No overt motor neuron loss was evident in presymptomatic $SOD1^{G93A}$ transgenic rats between 3–4 months of age as determined by both histological and electrophysiological observations. However, we noted the appearance of vacuoles in motor neurons as well as gliosis preceding both motor neuron loss and clinical signs of disease in rats. The presence of vacuoles was transient, correlating with the time of active motor neuron loss. In the most affected regions vacuoles were nearly absent by end-stage disease. Progression to end-stage paralysis was rapid, with an average of 11 days after first observation of symptoms. This finding is in contrast to the slower progression of disease observed in $SOD1^{G93A}$ transgenic mice (G1H and G1L) where disease duration approached 60–70 days (15, 21, 22) but instead was more similar to that reported for $SOD1^{G85R}$ mice (17) whose disease duration was only 7–14 days. Mutant $SOD1$ levels in end-stage G1L and G1H transgenic mouse spinal cord (15, 21, 22) were higher than in $SOD1^{G93A}$ L26H transgenic rats, and therefore the rapid progression of disease in the $SOD1^{G93A}$ transgenic rats seems not to be a function of expression levels but rather may be characteristic of a species difference in the presentation of clinical phenotype. The rapid decline of the $SOD1^{G93A}$ rats coincided with substantial loss of spinal cord motor neurons as well as marked increases in gliosis and degeneration of muscle integrity and function.

The astroglial glutamate transporter EAAT2 is the primary means of maintaining low extracellular glutamate levels. Loss of this protein induced by either pharmacological or molecular methods *in vitro* and *in vivo* results in increased extracellular glutamate, as measured by microdialysis and excitotoxic neuronal degeneration, including degeneration of motor neurons. Elevations of extracellular glutamate and loss of EAAT2 are characteristic of at least 40% of sporadic patients with ALS, and similar changes have been observed in the mutant mouse models of the disease (17, 25, 31–33). Interestingly, a recent study of a similar transgenic rat model, however, did not observe changes in cerebrospinal fluid (CSF) glutamate (34). The reason for the difference between that rat model, the work in the current study, and previous human observations is not clear. However, a focal loss of EAAT2 would be expected to increase glutamate only locally and therefore might not be detectable in the CSF. In addition, CSF glutamate measurements are fraught with technical problems.

The cause of EAAT2 loss is not known, but multiple studies demonstrate that astroglial changes can occur early, before actual motor neuron degeneration (13, 17). However, loss of neurons can lead to glial responses that include transient down-regulation of EAAT2 expression (35, 36). Yet, there is no loss of EAAT2 in another motor neuron disease, spinal muscular atrophy (33, 37). Previous reports have documented a loss of EAAT2 to ~50% its normal level in $SOD1^{G85R}$ transgenic mice (17) by using whole spinal cord at end-stage disease. The current study provides a thorough evaluation of EAAT2 at a time point when motor neurons are intact histologically and physiologically, as revealed by EMG/nerve conduction studies. At these “early” time points, there was a patchy loss of EAAT2 expression around motor neurons in the ventral gray areas of the spinal cord, suggesting that the loss of EAAT2 may contribute to motor neuron degeneration. Concomitant with decreased EAAT2 expression was a marked increase in gliosis, and by end stage, where motor neuron loss is severe, EAAT2 was present at only 5–10% of normal levels in the ventral horn. Importantly, the contribution of altered EAAT2 expression to neuronal death/injury was demonstrated by a recent study where EAAT2 overexpression offered protection in $SOD1^{G93A}$ mice.¹¹

¹¹Eutherland, M. L., Martinovich, K. & Rothstein, J. D. (2001) *Soc. Neurosci. Abstr.* 27, no. 607.6.

We describe a transgenic rat model for ALS based on the *SOD1^{G93A}* mutation. The clinical and pathological changes displayed resemble the "high expressing" *SOD1^{G93A}* mice first described by Gurney *et al.* (15) including a characteristic vacuolar degeneration of the neuropil, which seems to occur just before motor neuron degeneration and aggregates staining with SOD1 and neurofilament. Proteins, Hsc70 and ubiquitin, involved in protein folding as well as degradation are also present in these aggregates in these transgenic rats. Notable differences between the rat and mouse models, however, include a more rapid progression of disease and the transient appearance of vacuoles in the transgenic rat. The rapid decline of the *SOD1^{G93A}* rats to end stage could account for the disappearance of vacuoles in sections of the spinal cord that display severe motor neuron loss.

We have also demonstrated, using the *SOD1^{G93A}* rats, that BAAT2 levels decrease in the spinal cord before clinical onset of symptoms and that decrease becomes more severe by end-stage sickness, suggesting a role for glutamate toxicity and astroglial dysfunction in disease pathogenesis.

D.S.H. thanks Drs. Lucie Bruijn, John Moyer, Seung Kwak, and Erika Holzbaur for critical comments and advice. D.W.C. and J.D.R. gratefully acknowledge support from National Institutes of Health Grants NS 27036, NS33958, and AG 12992, and the Center for ALS Research. J.L. is the recipient of a fellowship from the Spinal Cord Disease Foundation. D.W.C. receives salary support from the Ludwig Institute for Cancer Research. This work was initiated by the ALS Association as part of its Lou Gehrig Challenge Initiative.

- Dollals, M. B. & Carpenter, S. (1984) *J. Neurol. Sci.* 63, 241-250.
- Banker, B. Q. (1986) In *Myology*, eds. Engel, A. G. & Banker, B. Q. (McGraw-Hill, New York), pp. 2031-2066.
- Horton, W. A., Eldredge, R. & Brady, J. A. (1976) *Neurology* 26, 460-465.
- Rosen, D. R., Siddique, T., Patterson, D., Figlewicz, D. A., Sapp, P., Hentati, A., Donaldson, D., Goto, J., O'Regan, J. P., Deng, H. X., *et al.* (1993) *Nature (London)* 362, 59-62.
- Deng, H. X., Hentati, A., Turner, J. A., Iqbal, Z., Cayabyab, A., Hung, W. Y., Genotoff, E. D., Hu, P., Herzfeldt, B., Roos, R. P., *et al.* (1993) *Science* 261, 1047-1051.
- Morrison, B. M., Morrison, J. H. & Gordon, J. W. (1998) *J. Exp. Zool.* 282, 32-47.
- Wong, P. C., Rothstein, J. D. & Price, D. L. (1998) *Curr. Opin. Neurobiol.* 8, 791-799.
- Shibata, N. (2001) *Neuropathology* 21, 82-92.
- Reaume, A. G., Elliot, J. L., Hofman, E. K., Kowall, N. W., Ferrante, R. J., Siwick, D. F., Wilcox, H. M., Flood, D. G., Beal, M. F., Brown, R. H., *et al.* (1996) *Nat. Genet.* 13, 43-47.
- Bruijn, L. L., Houseweart, M. K., Kato, S., Anderson, K. L., Anderson, S. D., Ohnaka, E., Reaume, A. G., Scott, R. W. & Cleveland, D. W. (1998) *Science* 281, 1851-1854.
- Beckman, J. S., Carson, M., Smith, C. D. & Koppenol, W. H. (1993) *Nature (London)* 364, 584.
- Johnston, J. A., Dalton, M. J., Gurney, M. E. & Kopito, R. R. (2000) *Proc. Natl. Acad. Sci. USA* 97, 12571-12576.
- Gong, Y. H., Parsadanian, A. S., Andreeva, A., Snider, W. D. & Elliott, J. L. (2000) *J. Neurosci.* 20, 660-665.
- Framatarova, A., Laganier, J., Roussel, J., Brisebois, K. & Rouleau, G. A. (2001) *J. Neurosci.* 21, 3369-3374.
- Gurney, M. E., Fu, H., Chiu, A. Y., Dal Canto, M. C., Polchow, C. Y., Alexander, D. D., Caliendo, J., Hentati, A., Kwon, Y. W. & Deng, H. X. (1994) *Science* 264, 1772-1775.
- Wong, P. C., Pardo, C. A., Borchelt, D. R., Lee, M. K., Copeland, N. G., Jenkins, N. A., Sisodia, S. S., Cleveland, D. W. & Price, D. L. (1995) *Neuron* 14, 1105-1116.
- Bruijn, L. L., Becher, M. W., Lee, M. K., Anderson, K. L., Jenkins, N. A., Copeland, N. G., Sisodia, S. S., Rothstein, J. D., Borchelt, D. R., Price, D. L. & Cleveland, D. W. (1997) *Neuron* 18, 327-338.
- Ripps, M. E., Huxley, G. W., Hof, P. R., Morrison, J. H. & Gordon, J. W. (1995) *Proc. Natl. Acad. Sci. USA* 92, 689-693.
- Brannstrom, T., Ernhill, K., Jonsson, A., Nilsson, A. & Marklund, S. (2000) *Brain Pathol.* 10, 775.
- Friedlander, R., Brown, R., Gagliardini, V., Wang, J. & Yuan, J. (1997) *Nature (London)* 388, 31.
- Dal Canto, M. & Gurney, M. (1997) *Acta Neuropathol.* 93, 537-550.
- Dal Canto, M. & Gurney, M. E. (1995) *Brain Res.* 676, 25-40.
- Shibata, N., Hirano, A., Kobayashi, M., Dal Canto, M. C., Gurney, M. E., Komori, T., Umahara, T. & Asayama, K. (1998) *Acta Neuropathol.* 95, 136-142.
- Morrison, B. M., Janssen, W. G., Gordon, J. W. & Morrison, J. H. (1996) *J. Comp. Neurol.* 373, 619-631.
- Rothstein, J. D., Van Karumen, M., Levey, A. I., Martin, L. J. & Kuncel, R. W. (1995) *Ann. Neurol.* 38, 73-84.
- Hogan, B. (1983) *Nature (London)* 306, 313-314.
- Pardo, C. A., Xu, Z., Borchelt, D. R., Price, D. L., Sisodia, S. S. & Cleveland, D. W. (1995) *Proc. Natl. Acad. Sci. USA* 92, 954-958.
- Rothstein, J. D., Martin, L., Levey, A. I., Dykes-Hoberg, M., Jin, L., Wu, D., Nash, N. & Kuncel, R. W. (1994) *Neuron* 13, 713-725.
- Tu, P. H., Raju, P., Robinson, K. A., Gurney, M. E., Trojanowski, J. Q. & Lee, V. M. (1996) *Proc. Natl. Acad. Sci. USA* 93, 3155-3160.
- Rothstein, J. D., Martin, L. J. & Kuncel, R. W. (1992) *N. Engl. J. Med.* 326, 1464-1468.
- Guo, Z., Kindy, M. S., Kruman, I. & Mattson, M. P. (2000) *J. Cereb. Blood Flow Metab.* 20, 463-468.
- Pedersen, W. A., Fu, W., Keller, J. N., Markesbery, W. R., Appel, S., Smith, R. G., Karsanik, E. & Mattson, M. P. (1998) *Ann. Neurol.* 44, 819-824.
- Shaw, P. J., Chimery, R. M. & Ince, P. G. (1994) *Brain Res.* 659, 195-201.
- Nagai, M., Aoki, M., Miyoshi, I., Kato, M., Pasinelli, P., Kasai, N., Brown, R. H. & Itoyama, Y. (2001) *J. Neurosci.* 21, 9246-9254.
- Ginsberg, S. D., Martin, L. J. & Rothstein, J. D. (1995) *J. Neurochem.* 65, 2800-2803.
- Ginsberg, S. D., Rothstein, J. D., Price, D. L. & Martin, L. J. (1996) *J. Neurochem.* 67, 1208-1216.
- Lin, C. L., Erlend, L. A., Jin, L., Dykes-Hoberg, M., Crawford, T., Clawson, L. & Rothstein, J. D. (1998) *Neuron* 20, 589-602.

EXHIBIT 7

Transgenic rat model of Huntington's disease

Stephan von Hörsten^{1,*}, Ina Schmitt^{2,†}, Huu Phuc Nguyen¹, Carsten Holzmann³, Thorsten Schmidt⁴, Thomas Walther⁵, Michael Bader⁶, Reinhard Pabst¹, Philipp Kobbe¹, Jana Krotova¹, Detlef Stiller⁷, Ants Kask⁸, Annika Vaarmann⁸, Silvia Rathke-Hartlieb⁹, Jörg B. Schulz⁹, Ute Grasshoff⁴, Ingrid Bauer³, Ana Maria Menezes Vieira-Saecker^{2,†}, Martin Paul¹⁰, Lesley Jones¹¹, Katrin S. Lindenberg¹², Bernhard Landwehrmeyer¹², Andreas Bauer¹³, Xiao-Jiang Li¹⁴ and Olaf Riess⁴

¹Department of Functional and Applied Anatomy, Hannover Medical School, Hannover, Germany, ²Department of Molecular Human Genetics, University of Bochum, Bochum, Germany, ³Department of Medical Genetics, Children's Hospital, University of Rostock, Rostock, Germany, ⁴Department of Medical Genetics, University of Tübingen, Tübingen, Germany, ⁵Department of Cardiology, University Hospital Benjamin Franklin, Free University of Berlin, Berlin, Germany, ⁶Max Delbrück Center for Molecular Medicine, Berlin-Buch, Germany, ⁷Department of Non-invasive Imaging, Leibniz Institute for Neurobiology, Magdeburg, Germany, ⁸Department of Pharmacology, University of Tartu, Tartu, Estonia, ⁹Department of Neurology, University of Tübingen, Tübingen, Germany, ¹⁰Institute of Pharmacology and Toxicology, University Hospital Benjamin Franklin, Free University of Berlin, Berlin, Germany, ¹¹Institute of Medical Genetics, University of Wales, College of Medicine, Cardiff, UK, ¹²Department of Neurology, University of Ulm, Ulm, Germany, ¹³Institute of Medicine, Research Center, Jülich, Germany and ¹⁴Department of Human Genetics, Emory University School of Medicine, Atlanta, CA, USA

Received October 24, 2002; Revised and Accepted January 4, 2003

Huntington's disease (HD) is a late manifesting neurodegenerative disorder in humans caused by an expansion of a CAG trinucleotide repeat of more than 39 units in a gene of unknown function. Several mouse models have been reported which show rapid progression of a phenotype leading to death within 3–5 months (transgenic models) resembling the rare juvenile course of HD (Westphal variant) or which do not present with any symptoms (knock-in mice). Owing to the small size of the brain, mice are not suitable for repetitive *in vivo* imaging studies. Also, rapid progression of the disease in the transgenic models limits their usefulness for neurotransplantation. We therefore generated a rat model transgenic of HD, which carries a truncated huntingtin cDNA fragment with 51 CAG repeats under control of the native rat huntingtin promoter. This is the first transgenic rat model of a neurodegenerative disorder of the brain. These rats exhibit adult-onset neurological phenotypes with reduced anxiety, cognitive impairments, and slowly progressive motor dysfunction as well as typical histopathological alterations in the form of neuronal nuclear inclusions in the brain. As in HD patients, *in vivo* imaging demonstrates striatal shrinkage in magnetic resonance images and a reduced brain glucose metabolism in high-resolution fluor-deoxy-glucose positron emission tomography studies. This model allows longitudinal *in vivo* imaging studies and is therefore ideally suited for the evaluation of novel therapeutic approaches such as neurotransplantation.

INTRODUCTION

Huntington's disease (HD) is an autosomal dominant disorder caused by an expanded and unstable CAG trinucleotide repeat

within the coding region of the HD gene (IT15) (1). The mutation leads to a progressive degeneration of neurons primarily in striatum and cerebral cortex. Clinically, HD is characterized by movement abnormalities, cognitive impairments, and emotional

*To whom correspondence should be addressed at: Department of Functional and Applied Anatomy, OE 4120, Hannover Medical School, Carl Neuberg Str. 1, 30625 Hannover, Germany. Tel: +49 5115322868; Fax: +49 5115328868; Email: hoersten.stephan.von@mh-hannover.de

†Present address: Department of Neurology, University of Bonn, Bonn, Germany.

disturbances (2). In general, movement disturbances begin with chorea. Depressed mood and more subtle deficits apparent in neuropsychological tests may precede motor symptoms by years. The disease progresses relentlessly until death within 15–20 years. No effective treatment to influence the onset or the progression is presently available.

Many attempts have been made to generate animal models of HD. Excitotoxin models replicate many of the histological and neurochemical features as well as some of the motor and cognitive signs of HD (3–5), but neurodegeneration is not truly progressive. Therefore, their usefulness for the evaluation of treatment effects is limited.

Transgenic animal models of HD (6–11) provide new ways of studying the neuropathological mechanisms underlying HD. In particular the R6/2 transgenic mouse line, which expresses the first exon of the human HD gene carrying 141–157 CAG repeat expansions (6), develops a number of key features of HD, including progressive motor deterioration (12,13), appearance of neuronal intranuclear inclusions (14), discriminative learning impairments (15), and altered emotionality (16). However, R6/2 mice express very large numbers of CAG repeats that are only found in the juvenile type of HD. A rapid disease progression associated with diabetes in R6/2 mice (13) is not typical for the adult-type HD and may complicate the assessment of potential therapeutic approaches. Although HD transgenic mice provide important insights into the molecular basis of HD, there is still a need for animal models which resemble the common adult type of disease and which are more suitable for repetitive *in vivo* imaging. These rapidly emerging techniques offer the opportunity to compare directly the pathological alterations of the human condition with the corresponding animal model in longitudinal studies (17).

In this report, we describe the first transgenic rat model bearing a human HD mutation with a high-end adult onset allele of 51 CAG repeats that exhibits progressive neurological, neuropathological and neurochemical phenotypes closely resembling the common late manifesting and slowly progressing type of disease. We demonstrate that HD transgenic rats are well suited for complex behavioral studies and the evaluation of *in vivo* progression markers using high-resolution PET and MRI.

RESULTS

Generation of the HD transgenic rat model

A 1962 bp rat HD cDNA fragment (18) carrying expansions of 51 CAG repeats under the control of 885 bp of the endogenous rat HD promoter (19) was used for microinjection (Fig. 1A). Two founders were obtained and transgenic lines established. Of these, we followed up line 2762 for more than 2 years and found the CAG repeat length remaining stable in more than 147 meioses (data not shown). The mutant amino terminal portion of huntingtin is expressed in the brain as shown by western blot analysis (Fig. 1B), in particular in the frontal and temporal cortex, the hippocampus, the basal ganglia, and the mesencephalon, but at a much lower level in the cerebellum or the spinal cord (Fig. 1C).

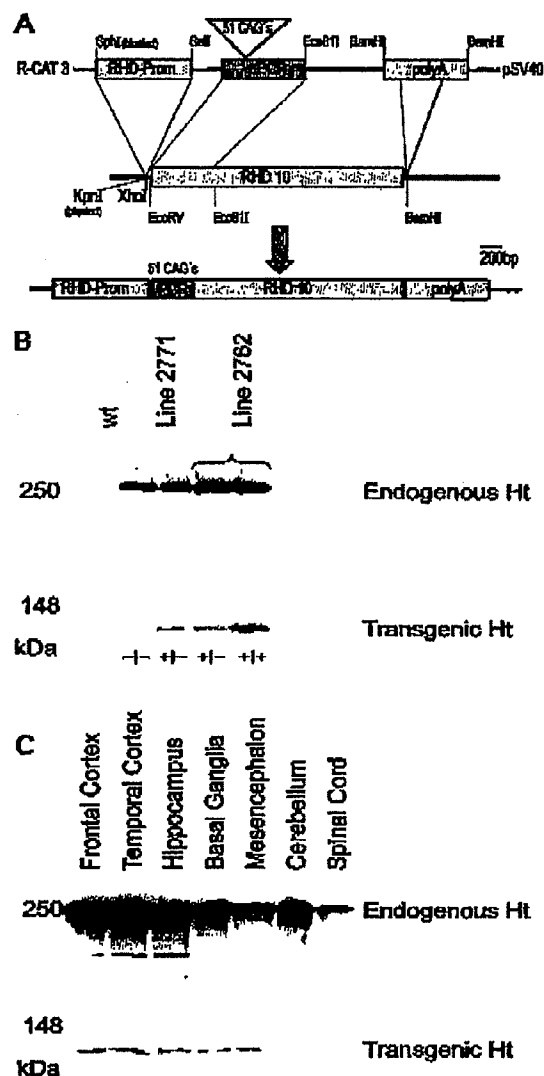


Figure 1. Transgenic construct and huntingtin expression in transgenic rats. (A) The first 154 bp of a partial huntingtin cDNA spanning 1962 bp of the N-terminal rat sequence (RHD10) (18) were replaced by a PCR product from the affected allele of a HD patient. The cDNA is driven by a 885 bp fragment of the rat HD promoter (position -900 to -15 bp) (19). A 200 bp fragment containing the SV40 polyadenylation signal was finally added downstream of the cDNA resulting in RHD/Prom31A. (B) Western blot analysis of brain tissue of transgenic rat line 2771 and 2762 using polyclonal anti-huntingtin antibody 675 demonstrates a 75 kDa product representing the expression of the transgene although at a lower level than the endogenous protein. Homozygotic rats (+/+) express about double the amount of the transgene protein as hemizygotic lines (+/-). (C) Western blot analysis of tissue from different brain areas of transgenic rat line 2762 at the age of 6 months, demonstrating a 75 kDa product representing the expression of the transgene in the frontal cortex, the temporal cortex, hippocampus, basal ganglia and mesencephalon, but not in the cerebellum or the spinal cord. However, overexposure of the same western blot clearly demonstrates that the transgene is also expressed in the cerebellum and the spinal cord though at a much lower level (data not shown).

Slow progressive phenotypes with emotional, cognitive and motor dysfunction

At birth we found transgenic rats and wild-type littermates phenotypically indistinguishable. Transgenic rats of both sexes are fertile without any sign of atrophy of the sexual organs. We observed a lower body weight gain in transgenic rats that was slowly progressive with the animals being about 20% lighter at the age of 24 months (Fig. 2A). At this age, transgenic rats commonly died after a 2 week period of rapid weight loss, which is associated with emaciation and muscular atrophy (Fig. 2B). Plasma glucose levels were always normal in routine screening (data not shown).

Transgenic animals often showed opisthotonus-like movements of the head. No resting tremor, ataxia, claspings, vocalizations, dyskinesia or seizures were observed. Except for occasional dyskinetic movements of the head, overt behavioral abnormalities were only found on dedicated behavioral testing.

At the age of 2 months transgenic rats developed a reduction of anxiety-like behavior in the elevated plus maze test (Fig. 2C), which is similar to the findings in R6/2 transgenic mice (16). At the age of 10 months transgenic rats showed cognitive decline in a spatial learning task for testing working memory in the radial maze (Fig. 2D and E). At the age of 5 months we had no indication of motor dysfunction in the animals (Fig. 2F), while at the age of 10 and 15 months progressive impairments of hind- and forelimb coordination and balance in the accelerated test were found (Fig. 2G and H). Thus, as in HD patients, emotional and cognitive impairments preceded progressive motor deterioration.

Accumulation of huntingtin aggregates and nuclear inclusions in striatal neurons

We examined whether mutant huntingtin forms aggregates and inclusions in the brain of 18-month-old rats using EM48, a rabbit antibody selective for mutant huntingtin (20,21). Most of the EM48 immunoreactive products appeared as punctuate labeling in the striatum, especially in the ventral region near the lateral ventricles and in the caudal part (Fig. 3B). Occasionally EM48 labeled aggregates were observed in the cortex. Other regions including hippocampus and cerebellum showed very weak or no EM48 label. In wild-type animals no EM48 labeled aggregates or puncta were found (Fig. 3A).

Two types of EM48 labeling, neuropil aggregates and nuclear inclusions were observed. As in other HD animal models (11,22) and in HD patient brains (20) some neuropil aggregates were arranged in linear arrays and most of them were scattered (Fig. 3C). Single nuclear inclusions were mainly observed in the striatum (Fig. 3D), resembling other HD mouse models (14,21). Since the striatal projection neurons terminate their axons in the lateral globus pallidus (LGP), we also examined the caudal region of the striatum. Nuclear staining and neuropil aggregates were common in the striatum. In the LGP, however, most EM48 labeling existed as neuropil aggregates.

To examine at what age mutant huntingtin forms aggregates and inclusions in the ventral region of the striatum, we additionally screened brains of 1-, 6-, 12- and 24-month-old rats for EM48 immunoreactive products (Fig. 3E-H). At the

ages of 12 (Fig. 3G), 18 (Fig. 3A-D), and 24 months punctuate labeling was evident, which was most pronounced at the age of 24 months. No aggregates or inclusions were found in the brain of 1- and 6-month-old rats.

Postmortem concentrations of tryptophan and biogenic amines

Since altered tryptophan and dopamine metabolism is linked to HD, we examined neurochemical alterations in the transgenic HD rats using a highly sensitive HPLC method (23). Striatal dopamine levels were decreased only about 20% in heterozygotic rats whereas in homozygotic rats a reduction of nearly 80% was found (Fig. 4A). The levels of dopamine and DOPAC in the parietal cortex of homozygotic animals were not significantly changed (Fig. 4B, D and E). Tryptophan concentrations were decreased 2-fold in striatum (Fig. 4E), but not significantly different in parietal cortex (Fig. 4F). Interestingly, the levels of xanthurenic acid were nearly depleted in the striatum of homozygotic transgenic rats (Fig. 4G) and undetectable in the parietal cortex (Fig. 4H). In contrast, in heterozygotes levels of xanthurenic acid were elevated in the parietal cortex (Fig. 4H), but unchanged in the striatum (Fig. 4G). No significant changes in other neurotransmitter levels were found.

Focal lesions in the striatum, enlarged lateral ventricles, and reduced brain glucose metabolism

To examine whether transgenic animals display neuropathological signs detectable by magnetic resonance (MR) imaging, we performed MR investigations on 8-month-old homozygotic HD rats. MR scans revealed enlarged lateral ventricles (Fig. 5C and D) and focal lesions in the striatum (Fig. 5F).

Since clinical studies have consistently revealed reductions in striatal glucose metabolism, we studied the local cerebral metabolic rate of glucose (ICMR_{Glc}) in transgenic rats using [¹⁸F]FDG (fluor-deoxy-glucose) and a high-resolution small-animal PET (positron emission tomography). PET studies were accompanied by *ex vivo* [¹⁸F]FDG measurements in order to test their reliability.

Harderian glands and different parts of the brain, such as olfactory bulb and caudato-putamen, were clearly distinguishable (Fig. 6). Individually co-registered MR images allowed a precise delineation of the whole brain as region of interest (ROI), as indicated by the red line (Fig. 6A and E). The defined ROI was measured in the co-registered PET image (Fig. 6B-D, F-H). Mean ICMR_{Glc} values, as calculated from animal PET data of control animals, were 54.98 ± 15.53 [$\mu\text{mol}/(100\text{ g} \times \text{min})$] for the whole brain. Mean ICMR_{Glc} values of hetero- and homozygotic animals were lower than control values (see legend of Fig. 6). Metabolic abnormalities of homozygotic animals were significantly different from controls ($P < 0.05$).

After completion of the PET scanning, we subsequently acquired ICMR_{Glc} values *ex vivo* using [¹⁸F]FDG autoradiography (Fig. 6J and K). Similar to the *in vivo* situation determined by [¹⁸F]FDG-PET, mean *ex vivo* ICMR_{Glc} values of homozygotic animals were significantly lower than control values ($P < 0.05$). A statistical comparison of autoradiographic

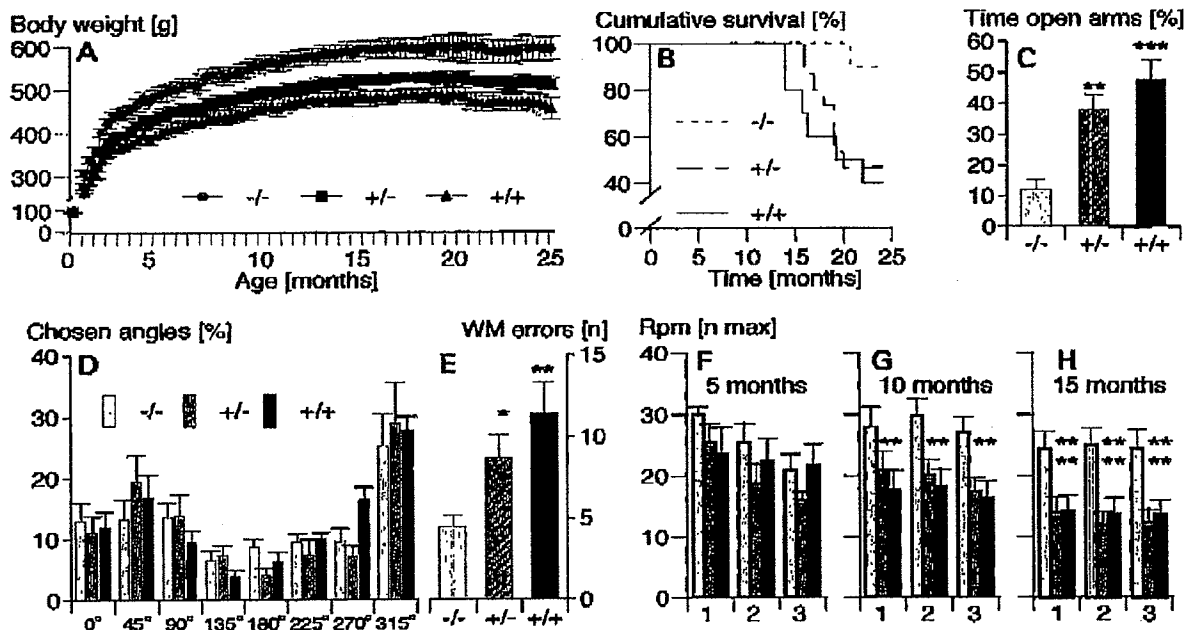


Figure 2. Growth, survival, and behavioral phenotyping. Growth chart representing absolute body weight measured once a week of male wild-type (—/—; gray round symbols) and HD transgenic (+/-, dark squares and +/+, black triangles) rats from 1 to 24 months of age (A). Symbols indicate means \pm SEM. A significant effect of genotype ($P < 0.001$) and a significant genotype \times weight-gain interaction ($P < 0.0001$) indicate a progressive decline in body weight gain in HD transgenics. (B) Cumulative survival of male wild-type (—/—; dotted line) and HD transgenic (+/-, mixed dots/lines and +/+, line) rats from 1 to 24 months of age (end of study) using Kaplan-Meier estimator. Log-rank test revealed a $P < 0.05$. (C) Percentage of time spent on the open arms of the elevated plus maze. Transgenic rats (+/-, hatched columns and +/+, black columns) spent more time (** $P < 0.001$; *** $P < 0.0001$) on the open arms. (D, E) Radial maze behavior. During exploration of the radial maze, transgenic rats showed no major differences in preference for certain angles when choosing arms (D) suggesting that the animals have general motor, cognitive and sensory abilities sufficient to master this task. Activity (total of arm visits and total of time in arms) was not significantly changed (data not shown). Radial maze reinforced alternation demonstrated an increased number of arm visits required to collect all food pellets. The increased number of working memory (WM) errors (E) indicates that the transgene affected the ability to retain and manipulate mnemonic information to guide ongoing behavior (* $P < 0.01$; ** $P < 0.001$). Bars indicate means \pm SEM of each measurement across the trials. (F-H) Balance and motor coordination on the accelerating rod. The means \pm SEM of the maximal speed (rpm) and the duration of balance (data not shown) were recorded. At the age of 5 months HD transgenic rats were not significantly impaired in their ability to stay on the rotating rod (F). At the age of 10 and 15 months HD transgenic rats exhibit difficulty and a progressive decline in performance on the accelerated (G-H). Asterisks indicate significant differences between wild-type (—/—) control and homo- as well as heterozygotic HD transgenic rats (* $P < 0.01$; ** $P < 0.001$).

and animal PET data indicated that ICMR_{Glc} values were significantly similar ($P < 0.05$).

DISCUSSION

In this report we describe the first transgenic rat model for Huntington's disease, which displays symptoms similar to the most frequent late-onset form of HD. It should be emphasized that these transgenic rats represent the first animal model of a human neurodegenerative disorder of the brain *per se* and that these animals express a high-end adult-onset HD allele, which is associated with a slow disease progression and pathology restricted to the striatum. Other symptomatic transgenic mice, however, express very large repeats that are only found in juvenile HD patients. Thus, these HDtg rats are especially useful for studying pathological changes that may be commonly present in the majority of adult HD patients,

making this rat model more valuable than other mouse models in evaluating novel therapeutics on HD.

Transgenic rats develop slowly progressive phenotypes with emotional, cognitive, and motor deteriorations. The emotional disturbance is characterized by a reduction of anxiety, which resembles similar observations in R6/2 HD transgenic mice (16). Cognitive decline is also a feature of HD (24). Early in the course of HD, patients frequently show impairments of spatial working memory (25), and comparable deficits are also found in R6/2 mice (15,26) as well as in our HD transgenic rats. These data suggest a common underlying neuropathological mechanism in HD and corresponding animal models.

Neuropathological examination revealed nuclear inclusions and neuropil aggregates. EM48 labeled aggregates are mainly found in the striatum of transgenic rats at the age of one year and older. EM48 labeling shows a distribution pattern similar to that in the human condition (20). Similar results were previously reported in HD knock-in mice expressing full-length

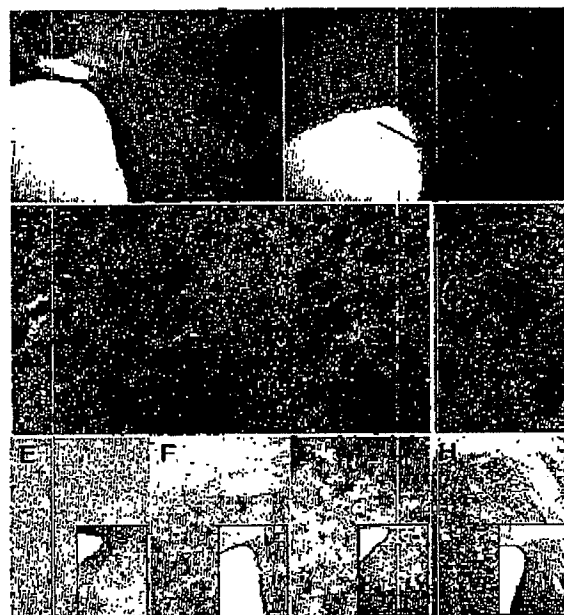


Figure 3. EM48 immunostaining of brains of wild-type and HD transgenic rats. (A, B) Low magnification of micrographs of wild-type (A) and HD (B) rat brains. Note that EM48 immunoreactive product is particularly enriched in the ventral part of striatum (Str) near the ventricle (arrow) in HD rat brain. Ctx, cortex. Scale bar, 50 μ m. (C) In the caudate part of the striatum of HD rats, many nuclear aggregates and small neuropil aggregates are evident. Neuropil aggregates (arrows) are also present in the lateral globus pallidus (LGP). Scale bar, 25 μ m. (D) High magnification of micrograph showing that both EM48 labeled nuclear inclusion (arrowheads) and small neuropil aggregates (arrows) are present in the striatum of HD rat brain. (E-H) Corresponding micrographs of coronal sections at the level of the bregma of 1-month (E), 6-month (F), 12-month (G), 24-month old transgenic rats. Scale bar, 10 μ m.

mutant huntingtin under the endogenous mouse HD promoter (21,27). A remarkable observation in neurochemistry was that xanturenic acid was nearly completely depleted in the striatum and the parietal cortex. The levels of xanturenic acid were higher in the less afflicted heterozygotes, perhaps reflecting a neurochemical defense mechanism against the excitotoxicity of the overactive indoleamine (2,3)-dioxygenase pathway (28). Similar to HD patients, the levels of tryptophan were decreased in the striatum of homozygotes. Decreased DA and normal DOPAC levels are indicative of increased DA turnover. Decreased levels of tryptophan may be related to an increased formation of quinolinic acid, a neuroexcitant molecule with neurotoxic properties (5). These findings support the hypothesis that both increased formation of quinolinic acid (28) and decreased production of neuroprotective metabolites from tryptophan (29) may be relevant to the pathogenesis of HD.

An important feature of the presented HD rat model is its suitability for *in vivo* metabolic and structural imaging, which cannot yet be achieved with transgenic mice. MR scanning demonstrated an enlargement of the lateral ventricles and focal signal abnormalities in the striatum of HD transgenic animals,

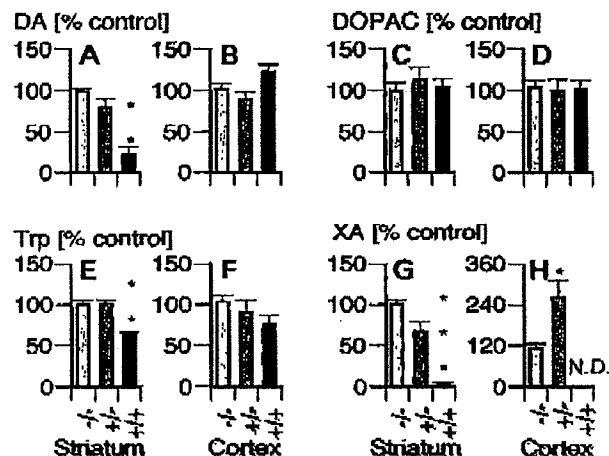


Figure 4. Regional alterations in tryptophan metabolism in HD transgenic rats. The levels of dopamine (A, B), DOPAC (C, D), tryptophan (E, F) and xanturenic acid (G, H) in striatum (A, C, E, G) or parietal cortex (B, D, F, H) in wild-type (-/-) or homozygous (+/+) and heterozygous (+/-) transgenic rats expressing human HD mutation at the age of 18 months. Asterisks indicate significant differences from control rats (* P < 0.05, ** P < 0.001, *** P < 0.0001).

although quantitative assessment of striatal neurons revealed no significant cell loss. This indicates that striatal atrophy depicted by MR imaging is rather a consequence of shrinkage than neuronal death. In high-resolution animal PET we found a significant reduction of brain glucose metabolism in 2-year-old homozygous HD rats. In late stages of human HD, clinical PET studies consistently revealed reduced ICMR_{glc} in the striatum (30,31). Thus, this report provides evidence that the novel HD transgenic rat model does closely resemble the human pathological condition. It is suited for non-invasive *in vivo* investigations of brain metabolism and most probably of further *in vivo* parameters (e.g. receptor density, enzyme activity). Brain atrophy and extracranial tracer accumulation, however, necessitate the application of high-resolution tomographs and a careful evaluation of partial volume and spill over effects.

We report the successful development of a transgenic rat model of HD, which expresses a high-end adult onset HD allele with 51 CAG repeats and which exhibits a high degree of similarity to the most frequent adult type of the disease, thereby permitting *in vivo* monitoring of individual disease progression by high-resolution imaging (PET and MRI). For the first time it is now possible to follow up disease progression in longitudinal *in vivo* studies and to monitor the effects of long-term treatments, microsurgery, neuronal cell transplantation, or antisense approaches on discourse of experimental HD.

MATERIALS AND METHODS

Generation of transgenic rats

To generate the transgene construct, PCR was performed using DNA from a HD patient (19/51 CAGs) with Primer Hu 4

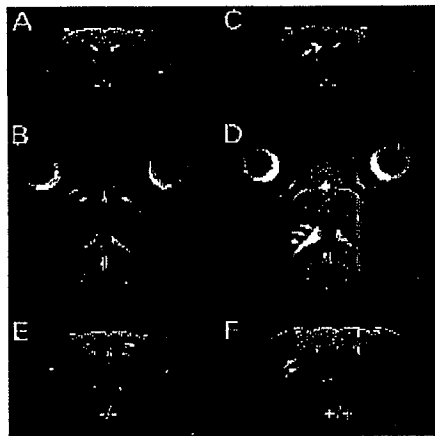


Figure 5. MR scanning of brains of wild-type and HD transgenic rats. (A–D) MR scans of lateral ventricles in coronal (A, C) and horizontal (B, D) projection of wild-type (A, B) and HD (C, D) rat brain at the age of 8 months. MR scans of the striatum of a wild-type (E) and an HD transgenic (F) rat brain. Note the enlargement of the lateral ventricles (arrows) and the focal lesions in the striatum (arrows).

(ATGGCGACCCTGGAAAAGCTGATGAA) and Hu3-510 (GGGCGCCTGAGGCTGAGGCAGC). This PCR product was subsequently digested with *EcoRI*. The first 154 nucleotides of the cDNA RHD10 containing nt 1–1962 of the rat HD-gene (18) were removed by restriction of the clone with *EcoRV* and *EcoRI*. This fragment was replaced by the PCR product. Subsequently, a 885 bp rat HD promoter fragment from position –900 to –15 (19) was ligated upstream of the cDNA and a 200 bp fragment containing the SV40 polyadenylation signal was added downstream of the cDNA resulting in RHD/Prom51A. The insert was excised with *XbaI* and *SspI* out of the cloning vector and microinjected into oocyte donors of Sprague–Dawley (SD) rats (32,33). Tail DNA was extracted from each of the offspring and Southern blots of *EcoRI* digested DNA were performed to screen for founders.

For western blot analysis, frozen brain halves and dissected brain areas were homogenized and protein extracted. Protein extracts were subjected to SDS–PAGE and blotted electrophoretically onto Immobilon-P membranes. Detection of huntingtin protein was performed basically as described (34) using the polyclonal anti-huntingtin antibody 675.

Behavioral phenotyping of the HD transgenic rat line

The considerations for behavioral phenotyping of transgenic and knockout mice (35) were adapted with specific modifications for testing rats. All procedures were approved by the Government of Lower Saxony in Hannover, Germany, and performed in compliance with international animal welfare standards. The elevated plus maze (TSE-Systems, Bad Homburg, Germany) was equipped with light beam sensors and had two open arms (50 × 10 cm) and two enclosed arms of the same size. The experiment was conducted with 2-month-old rats as previously described (36). An increase of the time

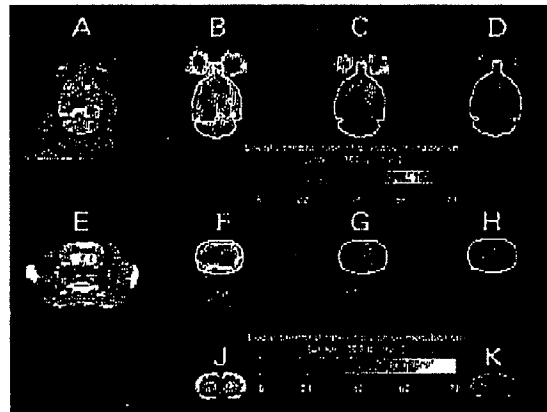


Figure 6. Studies with [^{18}F]FDG and high-resolution small-animal PET. Representative images with [^{18}F]FDG and high-resolution small-animal PET in horizontal (B–D) and coronal (A–C) planes along with individual MR images (A, E) and ex vivo autoradiographs (J, K). Individual MR images (A, E) of a control animal are co-registered with respective [^{18}F]FDG-PET images (B, F). Planes are cutting the caudate-putamen level of the brain. Representative sections of ex vivo autoradiography (J, K) are taken from identical animals as in [^{18}F]FDG-PET (B, F; D, H). The rat brain is defined within the [^{18}F]FDG-PET on the basis of individually co-registered MR images, as indicated by the red line. Local cerebral rates of glucose metabolism (ICMR_{Glu}) are absolutely quantified (see color and black/white bars). The high accumulation of activity in caudate-putamen is clearly visible in [^{18}F]FDG-PET (F, G, H) and ex vivo autoradiography (J, K). Homozygous animals exhibit significantly ($P < 0.05$) lower ICMR_{Glu} values compared with controls, both in [^{18}F]FDG-PET [$34.54 \pm 18.52 \mu\text{mol}/(100 \text{ g} \times \text{min})$ versus $54.98 \pm 15.53 \mu\text{mol}/(100 \text{ g} \times \text{min})$] and in ex vivo autoradiography [$43.54 \pm 6.77 \mu\text{mol}/(100 \text{ g} \times \text{min})$ versus $63.02 \pm 8.24 \mu\text{mol}/(100 \text{ g} \times \text{min})$].

spent in the open arms is interpreted as an anxiolytic-like response. An automated sensor-equipped eight-arm radial maze (TSE) was used to measure learning and memory in an experimental design testing exploring behavior and working memory (WM) errors in allocentric orientation (37). An accelerating rotarod for rats (TSE) was used to measure fore- and hind-limb motor coordination and balance. Training consisted of three trials per day on four consecutive days. The duration of each trial was 5 min on accelerating mode of the apparatus. The maximal speed level and the mean latency to fall off the rotarod were recorded on three consecutive tests. Data were subjected to one- or two-way ANOVA with one between-subject factor (genotype) and with repeated measurements on one or more factors depending on the test used. The PLSD test was used for *post hoc* comparisons. Cumulative survival was calculated by means of Kaplan–Meier analysis. A critical value for significance of $P < 0.05$ was used throughout the study.

Immunohistology and light microscopic examination

Brains of HD transgenic rats and controls at the age of 1, 6, 12, 18 and 24 months were perfused intracardially with PBS followed by paraformaldehyde and postfixed. Free-floating sections were pre-blocked in normal goat serum, Triton-X and

avidin, and incubated with EM48 antibody (1:400 dilution) at 4°C for 24 h (20,21). The EM48 immunoreactive product was visualized with the avidin-biotin complex kit (Vector ABC Elite, Burlingame, CA, USA).

Analysis of neurotransmitters from post-mortem tissue samples

Tryptophan and its kynurenine, catechol- and indoleamine metabolites were measured by electrochemical HPLC, as described previously (23). Briefly, striatum and parietal cortex of 18-month-old transgenic HD rats were dissected, weighed and sonicated in perchloric acid. The homogenate was centrifuged and 20 µl of supernatant was injected into a HPLC system (ESA model 5600 CoulArray module, Chelmsford, MA, USA) with two coulometric arraycell modules, each with four working electrodes. The chromatographic separation was achieved on an ESA MD-150 reversed-phase C₁₈ analytical column with a Hypersil pre-column.

MR scanning

Rats were anesthetized with 2% isoflurane and fixed in a stereotaxic frame. MRI was performed on a 4.7 T Bruker Biospec scanner with a free-bore of 20 cm equipped with an actively RF-decoupled coil system. A whole-body birdcage resonator enabled homogeneous excitation, and a 3 cm surface coil was used as receiver. T₂-weighted spin echo images were acquired using a rapid acquisition relaxation enhanced (RARE) sequence (38). Eleven axial and seven coronal slices were measured (slice thickness: 1.5 mm axial; 1.3 mm coronal; field of view, 3.2 × 3.2 cm; matrix, 256 × 256; TR/TE 3000/19 ms; six averages).

PET studies

PET imaging was performed on a dedicated high-resolution small-animal PET scanner ('TierPET') as previously described (39) on 24-month-old homozygotic (+/+; n=6) and heterozygotic animals (+/-; n=7), as well as age-matched controls (-/-; n=6). Reconstructed image resolution was 2.1 mm, which is homogeneously maintained throughout the entire field of view. A precise anatomical identification of rat brain regions was achieved by co-registration of magnetic resonance (MRI; Siemens Magnetom, 1.5 T, equipped with a dedicated small limb coil) and PET images. Animals received an injection of 0.3 ml [¹⁸F]FDG (1 mCi/ml, solved in NaCl 0.9%) under isoflurane sedation. After 30 min animals were anesthetized with ketamine/xylazine and glucose concentrations and input function were detected by serial blood samples. After a 60 min PET scan brains were removed and immediately frozen. Cryostat sections (20 µm) were exposed to a phosphor imaging plate (BAS-SR 2025, Fuji, Germany) together with calibrated fluorine-18 brain paste standards. Imaging plates were scanned with a high-performance imaging plate reader (BAS5000 BioImageAnalyzer, Fuji, Germany; spatial resolution, 50 µm). Local cerebral metabolic rate of glucose (ICMR_{Glc}) was calculated on the basis of the operational equation used in 2DG autoradiography studies (40) with modified rate and lumped constants to account for the difference in kinetic

characteristics between FDG and 2DG. The following constants (41) were used: $k_1=0.30$; $k_2=0.40$; $k_3=0.068$; lumped constant, $LC=0.60$. Similarity of ICMR_{Glc} as determined by FDG-PET and *ex vivo* autoradiography was analyzed by linear regression analysis.

ACKNOWLEDGEMENTS

We thank R. Barnow for excellent technical assistance and S. Fryk for the correction of the English. We gratefully acknowledge S. Weber, M. Cremer, U. Pietrzyk, and T. Rustige for their technical assistance with the TierPET and N.J. Shah for his help with high-resolution MRI (all Research Center Jülich). [¹⁸F]FDG was provided in clinical purity by the Institute of Nuclear Chemistry (Research Center Jülich). This work was supported by a Volkswagen Foundation grant to R.P. and S.v.H. (U75169), by NIH grants NS41669 and AG19206 to X.J.L., by HGF strategy funds to A.B. (project 2000/09: 'Primate PET'), and by a BMBF grant to O.R. (01KV9523/6).

REFERENCES

1. The Huntington's Disease Collaborative Research Group (1993) A novel gene containing a trinucleotide repeat that is expanded and unstable on Huntington's disease chromosomes. *Cell*, **72**, 971-983.
2. Harper, P.S. (1996) *Huntington's Disease*. W.B. Saunders, London.
3. Borlongan, C.V., Koutouzie, T.K., Frocman, T.B., Cahill, D.W. and Seuberg, P.R. (1995) Behavioral pathology induced by repeated systemic injections of 3-nitropropionic acid mimics the motoric symptoms of Huntington's disease. *Brain Res.*, **697**, 254-257.
4. Bronillet, E., Hantraye, P., Ferrante, R.J., Dolan, R., Leroy-Willig, A., Kowall, N.W. and Beal, M.F. (1995) Chronic mitochondrial energy impairment produces selective striatal degeneration and abnormal choreiform movements in primates. *Proc. Natl. Acad. Sci. USA*, **92**, 7105-7109.
5. Miranda, A.R., Boegman, R.J., Beninger, R.J. and Jhamandas, K. (1997) Protection against quinolinic acid-mediated excitotoxicity in nigrostriatal dopaminergic neurons by endogenous kynurenine acid. *Neuroscience*, **78**, 967-975.
6. Mangiarini, L., Sathasivam, K., Siller, M., Cozens, B., Harper, A., Hetherington, C., Lawton, M., Trotter, Y., Leach, H., Davies, S.W. *et al.* (1996) Exon 1 of the HD gene with an expanded CAG repeat is sufficient to cause a progressive neurological phenotype in transgenic mice. *Cell*, **87**, 493-506.
7. Reddy, P.H., Williams, M., Charles, V., Garrett, L., Pike-Buchanan, L., Whetsell, W.O., Jr., Miller, G. and Tagle, D.A. (1998) Behavioural abnormalities and selective neuronal loss in HD transgenic mice expressing mutated full-length HD cDNA. *Nat. Genet.*, **20**, 198-202.
8. Hodgson, J.G., Agopyan, N., Gutekunst, C.A., Leavitt, B.R., LePiane, F., Singaraja, R., Smith, D.J., Bissada, N., McCutcheon, K., Nasir, J. *et al.* (1999) A YAC mouse model for Huntington's disease with full-length mutant huntingtin, cytoplasmic toxicity, and selective striatal neurodegeneration. *Neuron*, **23**, 181-192.
9. Schilling, G., Becher, M.W., Sharp, A.H., Jinnah, H.A., Duan, K., Kotzke, J.A., Slunt, H.H., Ratovinski, T., Cooper, J.K., Jenkins, N.A. *et al.* (1999) Intracellular inclusions and neuritic aggregates in transgenic mice expressing a mutant N-terminal fragment of huntingtin. *Hum. Mol. Genet.*, **8**, 397-407.
10. Shelbourne, P.F., Killeen, N., Hevner, R.F., Johnston, H.M., Tocco, L., Levandoski, M., Ennis, M., Ramirez, L., Li, Z., Immitola, C. *et al.* (1999) A Huntington's disease CAG expansion at the murine Hdh locus is unstable and associated with behavioural abnormalities in mice. *Hum. Mol. Genet.*, **8**, 763-774.
11. Yamamoto, A., Lucas, J.J. and Hen, R. (2000) Reversal of neuropathology and motor dysfunction in a conditional model of Huntington's disease. *Cell*, **101**, 57-66.

12. Dunnett, S.B., Carter, R.J., Wans, C., Torres, E.M., Mahal, A., Mangiarini, L., Bates, G. and Morton, A.J. (1998) Striatal transplantation in a transgenic mouse model of Huntington's disease. *Exp. Neurol.*, **154**, 31–40.
13. Carter, R.J., Lione, L.A., Humby, T., Mangiarini, L., Mahal, A., Bates, G.P., Dunnett, S.B. and Morton, A.J. (1999) Characterization of progressive motor deficits in mice transgenic for the human Huntington's disease mutation. *J. Neurosci.*, **19**, 3248–3257.
14. Davies, S.W., Turmaine, M., Cozens, B.A., DiFiglia, M., Sharp, A.H., Ross, C.A., Scherzinger, E., Wanker, E.E., Mangiarini, L. and Bates, G.P. (1997) Formation of neuronal intranuclear inclusions underlies the neurological dysfunction in mice transgenic for the HD mutation. *Cell*, **90**, 537–548.
15. Lione, L.A., Carter, R.J., Hunt, M.J., Bates, G.P., Morton, A.J. and Dunnett, S.B. (1999) Selective discrimination learning impairments in mice expressing the human Huntington's disease mutation. *J. Neurosci.*, **19**, 10428–10437.
16. File, S.E., Mahal, A., Mangiarini, L. and Bates, G.P. (1998) Striking changes in anxiety in Huntington's disease transgenic mice. *Brain Res.*, **805**, 234–240.
17. Jacobs, R.E. and Cherry, S.R. (2001) Complementary emerging techniques: high-resolution PET and MRI. *Curr. Opin. Neurobiol.*, **11**, 621–629.
18. Schmitz, I., Bachner, D., Mogow, D., Heuklein, P., Hameister, H., Epplen, J.T. and Riess, O. (1995) Expression of the Huntington disease gene in rodents: cloning the rat homologue and evidence for downregulation in non-neuronal tissues during development. *Hum. Mol. Genet.*, **4**, 1173–1182.
19. Holzmann, C., Maucier, W., Petersohn, D., Schmidt, T., Thiel, G., Epplen, J.T. and Riess, O. (1998) Isolation and characterization of the rat huntingtin promoter. *Biochem. J.*, **336**, 227–234.
20. Gutekunst, C.A., Li, S.H., Yi, H., Mulroy, J.S., Kuemmerle, S., Jones, R., Rye, D., Ferrante, R.J., Hersch, S.M. and Li, X.J. (1999) Nuclear and neuropil aggregates in Huntington's disease: relationship to neuropathology. *J. Neurosci.*, **19**, 2522–2534.
21. Li, H., Li, S.H., Johnston, H., Shelbourne, P.F. and Li, X.J. (2000) Amino-terminal fragments of mutant huntingtin show selective accumulation in striatal neurons and synaptic toxicity. *Nat. Genet.*, **25**, 385–389.
22. Li, H., Li, S.H., Cheng, A.L., Mangiarini, L., Bates, G.P. and Li, X.J. (1999) Ultrastructural localization and progressive formation of neuropil aggregates in Huntington's disease transgenic mice. *Hum. Mol. Genet.*, **8**, 1227–1236.
23. Vaarmaa, A., Kask, A. and Maeorg, U. (2002) Novel and sensitive high-performance liquid chromatographic method based on electrochemical coulometric array detection for simultaneous determination of catecholamines, kynurenine and indole derivatives of tryptophan. *J. Chromatogr. B Analyt. Technol. Biomed. Life Sci.*, **769**, 145–153.
24. Mohr, E., Brouwers, P., Claus, J.J., Mann, U.M., Fedio, P. and Chase, T.N. (1991) Visuospatial cognition in Huntington's disease. *Mov. Disord.*, **6**, 127–132.
25. Lawrence, A.D., Sahakian, B.J., Hodges, J.R., Rossor, A.E., Lange, K.W. and Robbins, T.W. (1996) Executive and mnemonic functions in early Huntington's disease. *Brain*, **119**, 1633–1645.
26. Murphy, K.P., Carter, R.J., Lione, L.A., Mangiarini, L., Mahal, A., Bates, G.P., Dunnett, S.B. and Morton, A.J. (2000) Abnormal synaptic plasticity and impaired spatial cognition in mice transgenic for exon 1 of the human Huntington's disease mutation. *J. Neurosci.*, **20**, 5115–5123.
27. Wheeler, V.C., White, I.K., Gutekunst, C.A., Vrbancic, V., Weaver, M., Li, X.J., Li, S.H., Yi, H., Vonsattel, J.P., Gusella, J.F. et al. (2000) Long glutamine tracts cause nuclear localization of a novel form of huntingtin in medium spiny striatal neurons in HdhQ92 and HdhQ111 knock-in mice. *Hum. Mol. Genet.*, **9**, 503–513.
28. Bruyn, R.P. and Stoof, J.C. (1990) The quinolinic acid hypothesis in Huntington's chorea. *J. Neurol. Sci.*, **95**, 29–38.
29. Stone, T.W. (2001) Kynurenic acid in the CNS: from endogenous obscurity to therapeutic importance. *Prog. Neurobiol.*, **64**, 185–218.
30. Kuwert, T., Lange, H.W., Langen, K.J., Herzog, H., Aulich, A. and Feineisen, L.E. (1990) Cortical and subcortical glucose consumption measured by PET in patients with Huntington's disease. *Brain*, **113**, 1405–1423.
31. Young, A.B., Penney, J.B., Starosta-Rubinstein, S., Markel, D.S., Berent, S., Giordani, B., Ehrenkrofer, R., Jewett, D. and Hichwa, R. (1986) PET scan investigations of Huntington's disease: cerebral metabolic correlates of neurological features and functional decline. *Ann. Neurol.*, **20**, 296–303.
32. Mullins, J.J., Peters, J. and Ganten, D. (1990) Fulminant hypertension in transgenic rats harbouring the mouse Ren-2 gene. *Nature*, **344**, 541–544.
33. Schinke, M., Baltatu, O., Bohm, M., Peters, J., Rascher, W., Bricca, G., Lippoldt, A., Ganon, D. and Bader, M. (1999) Blood pressure reduction and diabetes insipidus in transgenic rats deficient in brain angiotensinogen. *Proc. Natl. Acad. Sci. USA*, **96**, 3975–3980.
34. Schmidt, T., Landwehrmeyer, G.B., Schmitz, I., Trotter, Y., Anburger, G., Lacomme, F., Klockgether, T., Volpel, M., Epplen, J.T., Schols, L. et al. (1998) An isoform of ataxin-3 accumulates in the nucleus of neuronal cells in affected brain regions of SCA3 patients. *Brain Pathol.*, **8**, 669–679.
35. Crawley, J.N. (1999) Behavioral phenotyping of transgenic and knockout mice: experimental design and evaluation of general health, sensory functions, motor abilities, and specific behavioral tests. *Brain Res.*, **835**, 18–26.
36. Breivik, T., Stephan, M., Brabant, G.E., Straub, R.H., Pabst, R. and von Horsten, S. (2002) Postnatal lipopolysaccharide-induced illness predisposes to periodontal disease in adulthood. *Brain Behav. Immun.*, **16**, 421–438.
37. Holscher, C. and Schmidt, W.J. (1994) Quinolinic acid lesion of the rat entorhinal cortex pars medialis produces selective amnesia in allocentric working memory (WM), but not in egocentric WM. *Behav. Brain Res.*, **63**, 187–194.
38. Hennig, J., Nawroth, A. and Friedburg, H. (1986) RARE imaging: a fast imaging method for clinical MR. *Magn. Reson. Med.*, **3**, 823–833.
39. Weber, S., Bauer, A., Herzog, F., Kehlen, H., Mühlensiepen, J., Vogelbruch, H., Coenen, H., Zilles, K. and Halling, H. (2000) Recent results of the TierPET scanner. *IEEE Trans. Nucl. Sci.*, **47**, 1665–1669.
40. Sokoloff, L., Reivich, M., Kennedy, C., Des Rosiers, M.H., Patlak, C.S., Pettigrew, K.D., Sakurada, O. and Shinohara, M. (1977) The [¹⁴C]deoxyglucose method for the measurement of local cerebral glucose utilization: theory, procedure, and normal values in the conscious and anesthetized albino rat. *J. Neurochem.*, **28**, 897–916.
41. Ackermann, R.F. and Lear, J.L. (1989) Glycolysis-induced discordance between glucose metabolic rates measured with radiolabeled fluorodeoxyglucose and glucose. *J. Cereb. Blood Flow. Metab.*, **9**, 774–785.

EXHIBIT 8

Transgenic models of Huntington's disease

Gillian P. Bates*, Laura Mangiarini, Amarbirpal Mahal and Stephen W. Davies¹

Medical and Molecular Genetics, UMDS, Guy's Hospital, London SE1 9RT, UK and ¹Department of Anatomy and Developmental Biology, University College London, Gower Street, London WC1E 6BT, UK

Received May 7, 1997

CAG/polyglutamine expansion has been shown to form the molecular basis of an increasing number of inherited neurodegenerative diseases. The mutation is likely to act by a dominant gain of function but the mechanism by which it leads to neuronal dysfunction and cell death is unknown. The proteins harbouring these polyglutamine tracts are unrelated and without exception are widely expressed with extensively overlapping expression patterns. The factors governing the cell specific nature of the neurodegeneration have yet to be understood. Upon a certain size threshold, expanded CAG repeats become unstable on transmission and a modest degree of somatic mosaicism is apparent. Similarly, the molecular basis of the instability and its tissue specificity has yet to be unravelled. Recent reports describing the first mouse models of CAG/polyglutamine disorders indicate that it will be possible to model both the pathogenic mechanism and the CAG repeat instability in the mouse. This has great potential and promise for uncovering the molecular basis of these diseases and developing therapeutic interventions.

INTRODUCTION

Huntington's disease (HD) (1) is one of an increasing number of neurodegenerative disorders caused by a CAG/polyglutamine (polyglu) repeat expansion, including spinal and bulbar muscular atrophy (SBMA) (2), dentatorubral pallidoluysian atrophy (DRPLA) (3,4) and spinocerebellar ataxia (SCA) types 1 (5), 2 (6-8), 3 (9) and 6 (10). The inheritance patterns are autosomal dominant (with the exception of X-linked SBMA) and in each case, the proteins can tolerate a large variation in the size of the polyglu tracts in the normal range but upon a certain size (~37-40 glutamines) these tracts become pathogenic. It is likely that the novel molecular pathways initiated by this mutation have a common basis (except possibly in the case of SCA6 in which the pathogenic threshold is smaller). The proteins harbouring the polyglu stretches are mostly novel and otherwise unrelated. In all cases the proteins are widely or ubiquitously expressed, but despite extensively overlapping expression patterns, the neuronal cell death is relatively specific and can differ markedly (reviewed in 11).

The molecular events by which a polyglu expansion causes cell death remain to be unravelled (reviewed in 12). These mutations are likely to act by a dominant gain of function, this mechanism being supported by the identification of the 1C2 antibody which specifically detects polyglu expansions, suggestive of a conformational change at a certain size threshold (13). In addition, the factors which convey the specific and differing patterns of cell death between these diseases are not understood. Possible mechanisms include differences in expression levels, subcellular localisation of the mutated protein or cell specific subcellular interactions. A number of proteins have now been reported to interact with huntingtin which include HAP 1 (14), HIP-1 (15), a specific ubiquitin-conjugating enzyme (16) and GAPDH (17). It is yet to be established whether any of these proteins play a role in the pathogenic mechanism. Huntingtin has also been shown to be specifically cleaved by apopain, a cysteine

protease with a key role in the proteolytic events leading to apoptosis (18). Similarly, it is not clear if this participates in the chain of events leading to neurodegeneration.

Expanded triplet repeats are invariably unstable when inherited from one generation to the next and they generally show varying degrees of somatic mosaicism. The intergenerational instability forms the molecular basis of anticipation: the observation that the age of onset of a disease decreases and/or the severity increases as the gene is passed from one generation to the next. Repeat instability on transmission has been described in all of the CAG repeat diseases and, in general, repeats tend to be more unstable on paternal transmission. This may present as larger increases on paternal inheritance as in HD (19) (reflected in the paternal sex bias to the anticipation) or as a tendency to increase on male and decrease on female transmission as in SCA1 (20). A relatively modest degree of somatic repeat instability has been identified in HD, DRPLA, SCA1 and MID. In general, expansions have been identified in regions of the CNS, with the exception of the cerebellum which presents a smaller repeat relative to the other brain regions tested (21-26). Of non-CNS tissues, instability has consistently been reported in liver and kidney (21,24-26) and also in muscle, lung, testis (21), leukocytes (23) and colon (24,26). Studies of DRPLA patients also identified a significant correlation between the range of the expanded allele and the age at death of the patient rather than with the onset of disease (25). The molecular events governing triplet repeat instability are not understood and possible mechanisms must address both a CAG repeat size threshold and cell specificity.

TRANSGENIC MODELLING OF HUNTINGTON'S DISEASE

It has been proposed for many years that the HD mutation most probably acts through a dominant gain of function. Analysis of mice arising from the first transgenic models of HD, SCA1 and

*To whom correspondence should be addressed. Tel: +44 171 955 4485; Fax: +44 171 95 4444; Email: g.bates@umds.ac.uk

MJD in addition to gene targeted knockouts of the mouse HD gene (*Hdh*) supports this hypothesis.

Knockouts of the mouse *Hdh* gene

Three research groups have independently generated knockouts of the mouse HD gene (*Hdh*) (27–29). In all cases the nullizygous phenotype was embryonic lethal, clearly demonstrating that the HD gene plays an important role in development. In two of these studies, heterozygous mice expressing only one copy of *Hdh* were phenotypically normal (28,29). In contrast, Nasir *et al.* (27) reported that heterozygotes showed increased motor activity and cognitive deficits with a significant neuronal loss in the subthalamic nucleus. To explain this discrepancy, it has been suggested that the targeted allele (targeted to replace exon 5) may allow the production of a truncated protein which could conceivably cause a dominant effect in the heterozygous mice, generating a phenotype. Together, these studies demonstrate that HD is not caused by haplo-insufficiency (loss of function of one copy of the gene) or a simple dominant-negative mechanism. In the first case, loss of one allele and in the second case, loss of both alleles, would be expected to generate a model of HD.

Transgenic models of HD

A dominant gain of function mechanism would predict that a mouse model of a polyglutamine neurodegenerative disorder could be generated by the introduction into the mouse germ line of a mutant copy of the gene in question, irrespective of the presence of two copies of the endogenous mouse homologue. The first description of HD transgenic mice used a full length cDNA construct under the control of a CMV promoter carrying (CAG)₄₄ (30). Of the HD transgenes, 2/6 founders expressed high levels of transgene mRNA but a transgene protein was not detected. Whilst these results could be interpreted as providing evidence that translation of the CAG repeat into a polyglutamine expansion is necessary for pathogenesis, the repeat expansion in this experiment is comparatively modest and it is possible that larger expansions are necessary to generate a phenotype with an age of onset that falls within the lifetime of a mouse.

Genomic clones are frequently more successful at generating transgenic models than cDNAs as they often direct an expression profile that mimics the endogenous gene. The large size of the HD gene (170 kb) necessitates that genomic constructs are prepared and manipulated in the form of yeast artificial chromosomes (YACs). Using YAC technology, Hodgson *et al.* (31) have successfully generated mice that are transgenic for the normal human HD gene. They have crossed the human HD transgene onto an *Hdh* nullizygous background and shown that the human YAC can rescue the embryonic lethal phenotype. This indicates that the transgene is expressed appropriately and predicts that the introduction of a mutant version of the human YAC would be successful in generating a model of HD.

Mice transgenic for a mutant version of exon 1 of the HD gene

We have described four lines of mice that are transgenic for exon 1 of the HD gene carrying CAG expansions of 115–156 (R6/1, R6/2, R6/5 and R6/0) and a further two lines transgenic for the same construct carrying 18 repeats (HDex6 and HDex27) (32). The transgene is ubiquitously expressed at both the RNA and

protein levels in all lines except R6/0, in which no evidence of expression has been detected (32,33). The transgene protein contains the first 69 amino acids of huntingtin in addition to the number of residues encoded by the CAG repeat (i.e. ~3% of huntingtin).

A progressive neurological phenotype has been observed in three lines: R6/1, (CAG)₁₁₅; R6/2, (CAG)₁₄₅; and R6/5, (CAG)_{130–155}. Line R6/2 has an onset of ~2 months, line R6/1 at ~5 months and R6/5 hemizygotes do not show symptoms after >1 year. Lines R6/1 and R6/5 show an earlier age of onset and more rapid progression of the disease when bred to homozygosity. The phenotype includes an irregular gait, resting tremor, stereotypic and abrupt, irregularly timed movements and epileptic seizures. Coincident with the onset of the motor disorder there is a progressive reduction in body weight in the transgenes as compared with their littermate controls. The absence of a phenotype in lines R6/0, HDex6 and HDex27 suggests that expression of the polyglutamine expansion forms the molecular basis of the phenotype rather than the expression of a novel peptide. It is notable that the R6 phenotype does not include an overt cerebellar ataxia as described for the spinocerebellar ataxia lines (34,35) (see below). Extensive neuropathological analysis has been performed on the brains of R6/2 mice. At 12 weeks, the only difference that could be identified between the transgene and control brains was that the R6/2 brains were ~20% smaller, and that this reduction in brain size occurred across all structures with an apparently normal neuronal density. This is consistent with early changes that occur in the brains of HD patients. More recently, immunocytochemistry with huntingtin N-terminal antibodies has identified the presence of neuronal intranuclear inclusions (NII) in the brains of symptomatic transgenic mice (33).

COMPARISON WITH OTHER CAG/POLYGLUTAMINE MOUSE MODELS

Mice transgenic for both SCA1 (34) and MJD (35) constructs have also been reported to develop a phenotype. A summary of the main features of these and the R6 transgenes is presented in Table 1. The SCA1 transgenes were the first demonstration that modelling a polyglutamine repeat disorder would be possible in the mouse. They included mice transgenic for the SCA1 cDNA carrying either a normal interrupted allele of (CAG)₁₂CATCAGCAT(CAG)₁₅ (PS-30) or an expanded uninterrupted allele of (CAG)₈₂ (PS-82) under the control of the *pcp2* promoter (Purkinje cell-specific) (34). Five of six PS-82 lines showed RNA expression between 10- and 100-fold of endogenous levels. In the original report, transgene protein could not be detected but this has since been shown to be present by immunocytochemistry (H.Orr and H.Zoghbi, personal communication). Mice from all five lines developed ataxia. Onset varied from 12 to 26 weeks and a dosage effect was apparent: in two lines studied, homozygotes were more severely affected than hemizygotes. Neuropathological analysis showed significant loss of the Purkinje cell population, with Bergmann glial proliferation, and shrinkage and gliosis of the molecular layer. Ectopic Purkinje cells were present in the molecular layer and occasionally the granular layer and the dendritic arrays also appeared to be abnormal.

Ikeda *et al.* (35) used expression constructs containing the MJD cDNA carrying 79 CAG repeats (MJD79), the CAG repeat followed by only the C-terminus of the MJD gene with both 79 and 35 CAG repeats (Q₇₉C and Q₃₅C) and a 79 CAG repeat in

isolation (Q79) under the control of a Purkinje cell-specific promoter. Ataxia was observed in 3/3 Q79C and 2/6 Q79 transgenic mice, occurring as early as 1 month of age after full activation of the promoter. In contrast, a phenotype was not observed in any of the ten Q35C or four MJD79 transgenic mice as of 7 and 5 months, respectively. Neuropathological analysis of a 2 month old ataxic Q79C mouse showed a very atrophic cerebellum, in which all three layers were affected. The authors suggest that comparison of their data with that of Burright *et al.* (34) indicates that the polyglutamine tracts are more toxic when present in isolation or in the context of a truncated protein. In the absence of any data relating to expression levels it is difficult to come to strong conclusions with regard to the comparative toxicity of the full length and truncated constructs. However, these conclusions were strongly supported by a series of transient transfections of COS cells described in the same paper (35).

MOUSE MODELS OF CAG/CTG REPEAT STABILITY

Repeat stability studies carried out on the first mice transgenic for CAG repeat expansions showed no evidence of instability and suggested that the molecular mechanism underlying triplet repeat instability in humans may not exist in the mouse. These initial studies included (CAG)₄₅ in the androgen receptor cDNA (36), (CAG)₄₄ in the HD cDNA (30), (CAG)₈₂ in the SCA1 cDNA (34) and (CAG)₇₉ in constructs based on the MJD/SCA3 cDNA (35).

Triplet repeat instability in lines transgenic for the HD mutation (R6)

The R6 lines transgenic for exon 1 of the HD gene carrying (CAG)₁₁₅–(CAG)₁₅₅ expansions showed both intergenerational and somatic repeat instability (32,37). The repeats were clearly unstable on transmission in lines R6/1, R6/2 and R6/5, although this was less clear in line R6/0 as the changes observed in this line could be accounted for by errors in sizing. In line R6/2, the degree of instability increases with the age of the transmitting male (as R6/2 females are sterile it was not possible to look for an age effect on female transmission). R6/5 was the only line in which an extensive comparison of instability on both male and female transmission was conducted and the repeats had a tendency to increase on male transmission and decrease on female transmission

(37). This trend was supported by the intergenerational instability observed in the other lines. The CAG expansions introduced into these mice are considerably larger than are normally seen in HD patients. The change in size of the repeat on transmission in the mice is smaller than would be expected from comparison with size changes associated with highly expanded CAG repeats seen in humans. The discrepancy in the degree of instability between humans and mice may reflect the difference in their life span, a model supported by the observation that the size of the intergenerational expansion increased with the age of the transmitting male.

Somatic instability was detected in lines R6/1, R6/2 and R6/5 but not in line R6/0 (Fig. 1). In all three lines, onset of instability was at ~6 weeks and the CAG repeat range increased with the age of the mouse. This argues against a pathogenic role for repeat instability as the age of onset of symptoms in these lines differs markedly. The pattern of instability was more widespread in some lines than others although on the whole it was first present and most prominent in brain regions. Peripheral tissues that consistently showed instability included liver and kidney. Overall the somatic instability was comparable with that described in individuals carrying CAG expansions (21–26). The major difference between line R6/0, in which instability was not apparent, and the other lines was the absence of transgene expression. This is probably due to gene silencing by a position effect as the R6/0 transgene has clearly integrated into a region of unusual genomic structure (32).

Other mouse models of triplet repeat instability

Triplet repeat instability has also been reported in two series of lines transgenic for the myotonic dystrophy (DM) mutation (CTG on the sense strand) (38,39). The integration fragments used in these lines were a genomic fragment (*Dmf162*) from the myotonic dystrophy (DM) locus containing a small portion of the coding region and the 3'UTR with (CTG)₁₆₂ (39) and a cosmid (DM55-5) containing the myotonic dystrophy protein kinase gene (DMPK) with (CTG)₅₅ and the flanking DMR-N9 and DMAHP genes (38). Intergenerational instability was observed in both of these cases. The DM55-5 transgenes showed intergenerational instability in 6.8% of transmissions, the changes generally being expansions of one repeat unit. A higher frequency of unstable transmissions was observed in the *Dmf* lines (as in the R6 lines), most likely as a consequence of the larger size of the repeat tracts.

Table 1. Summary of CAG/polyglutamine transgenic mouse lines in which a progressive neurological phenotype has been observed

Disease	Construct	Promoter	(CAG) _n	Expression		Phenotype	Freq. of lines showing phenotype
				RNA	Protein		
HD	exon 1 (genomic)	HD	18	+	+	none	0/2
HD	exon 1 (genomic)	HD	142	–	–	none	0/1
HD	exon 1 (genomic)	HD	115–156	+	+	+	3/3
SCA1	cDNA (full length)	pcp2 ^a	30 ^b	+	+	none	0/7
SCA1	cDNA (full length)	pcp2 ^a	82	+	+	+	3/6
MJD	cDNA (full length)	L7 ^a	79	NR	NR	none	0/4
MJD	cDNA (C-terminus)	L7 ^a	35	NR	NR	none	0/10
MJD	cDNA (C-terminus)	L7 ^a	79	NR	NR	+	3/3
MJD	polyglutamine tract	L7 ^a	79	NR	NR	+	2/6

NR, not reported.

^aPurkinje cell-specific promoter.

^bInterrupted repeat: (CAG)₁₂CATCAGCAT(CAG)₁₅.

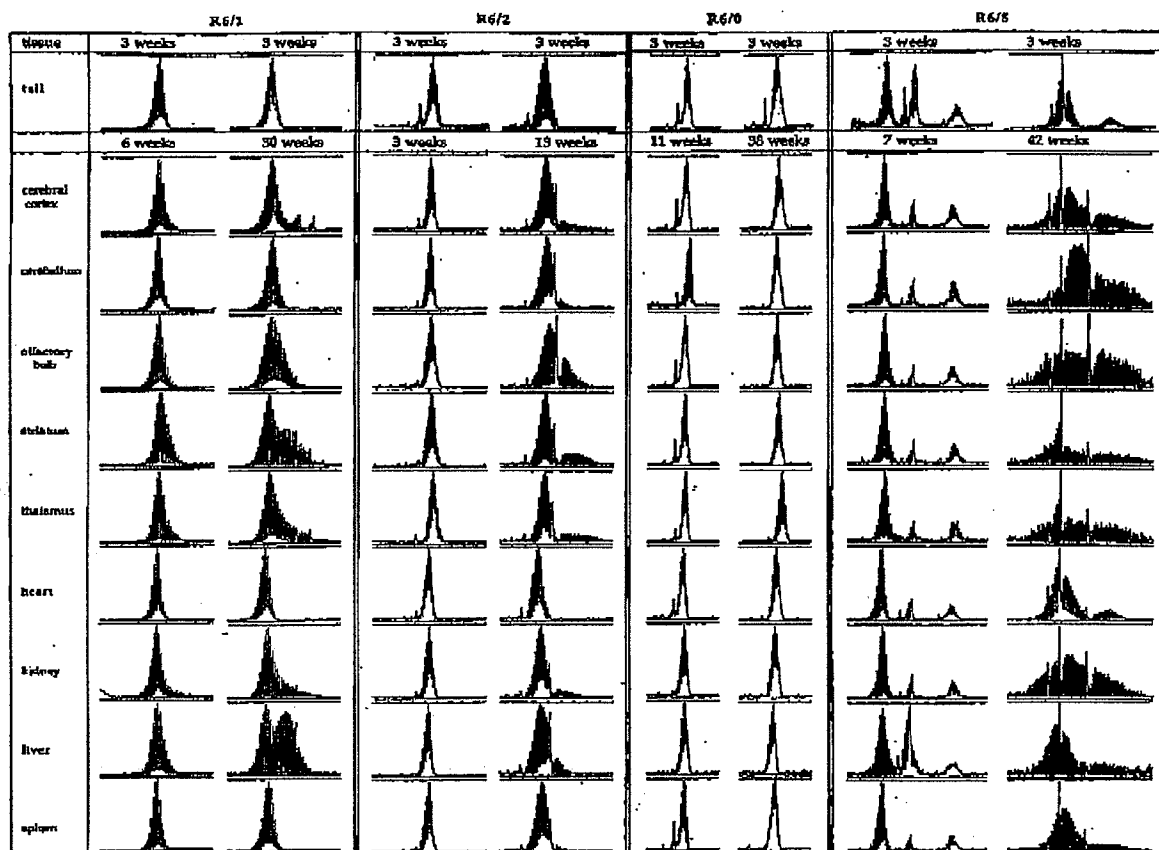


Figure 1. Illustration of the CAG repeat somatic instability seen in the R6 lines. The repeats were amplified by PCR using a fluorescent primer and sized on an ABI sequencer using the Genescan and Genotyper software packages (37). In each case the genescan trace arising from a range of tissues at the age at which the mouse was culled is compared with the trace obtained from tail DNA taken at 3 weeks (top row). The size of the major peaks in the tail traces are: R6/1, 115; R6/2, 145; R6/0, 142; R6/5, range from 123 to 156. The R6/5 line contains four copies of the CAG repeat and the difference in the tail trace between the two R6/5 mice has arisen from germ line instability. It is clear that even after 38 weeks there is no evidence for somatic instability in line R6/0.

The *Dmt* lines [(CTG)₁₄₃₋₁₆₂], like the R6 lines [(CAG)₁₁₅₋₁₅₅], showed a tendency to repeat expansion on male, and contraction on female, transmission. It would appear that the instability seen in the *Dmt* lines parallels that seen in the R6 lines and represents more closely instability seen in some of the CAG/polyglutamine neurodegenerative disorders rather than that seen in DM. Myotonic dystrophy is caused by a CTG expansion which expands to between (CTG)₂₀₀ and (CTG)₄₀₀₀ in the adult and congenital forms of the disease with a maternal bias to the anticipation (40). Somatic instability was described in one of the DM55-5 transgenes which had additional repeat bands in brain, liver, kidney and eye. A similar pattern of instability was also seen in one of the progeny of this mouse, with most instability apparent in sperm (38).

Comparison of the R6, *Dmt* and DM55-5 lines with the transgenic lines that do not exhibit CAG/CTG repeat instability does not lead to an understanding of the molecular basis of instability. The absence of instability observed in the first four reports could not simply be due to a size threshold effect. It is not clear whether the size threshold in the mouse is larger than that seen in humans; however, it must be below 55 repeats as a moderate amount of instability was seen in the DM55-5 transgenes. Similarly, the absence of instability in the first four lines cannot be due to differences in *trans*-acting factors which are likely to be invariant. If *cis*-acting sequences are important, the analysis of four series of lines (30,34-36) which do not show instability and three series (37-39) which fairly consistently do would suggest that these sequences are likely to be present on the

transgenes themselves rather than at the integration sites. The absence of instability in the R6/O line as compared with the other R6 lines could have mechanistic implications. The R6/O line only differs from the other three at the site of integration which is probably acting to silence the expression of the transgene. This argues against a model in which contractions and expansions of the repeat occur through a mechanism linked to DNA replication. It raises the possibility that the instability is linked to expression which may be a consequence of the open configuration of chromatin leading to DNA damage rather than being directly linked to transcription.

CONCLUSION

It is clear that a polyglutamine expansion can give rise to a progressive neurological phenotype in the mouse. The analysis of existing and further transgenic models of CAG/polyglutamine repeat disease will be informative with respect to uncovering the molecular basis of these disorders. Comparison of transgenes arising from full length and truncated constructs may resolve the speculation that the toxic agent is a truncated version of the proteins in question. The models will be useful in allowing the study of the early disease stages for which patient material is rarely available. Comparison of future models in which the transgenes are under the control of endogenous or ubiquitous promoters may shed light on the factors which determine the differing patterns of neurodegeneration.

REFERENCES

1. HD-CRG (1993) A novel gene containing a trinucleotide repeat that is unstable on Huntington's disease chromosomes. *Cell* 72, 971-983.
2. La Spada, A.R. *et al.* (1991) Androgen receptor gene mutations in X-linked spinal and bulbar muscular atrophy. *Nature* 352, 77-79.
3. Koide, R. *et al.* (1994) Unstable expansion of CAG repeat in hereditary dentatorubral-pallidoluysian atrophy (DRPLA). *Nature Genet.* 6, 9-13.
4. Nagafuchi, S. *et al.* (1994) Dentatorubral and pallidoluysian atrophy expansion of an unstable CAG trinucleotide on chromosome 12p. *Nature Genet.* 6, 14-18.
5. Orr, H.T. *et al.* (1993) Expansion of an unstable trinucleotide CAG repeat in spinocerebellar ataxia type 1. *Nature Genet.* 4, 221-226.
6. Lubert, G. *et al.* (1996) Cloning of the gene for spinocerebellar ataxia 2 reveals a locus with high sensitivity to expanded CAG/glutamine repeats. *Nature Genet.* 14, 285-291.
7. Sampet, K. *et al.* (1996) Identification of the spinocerebellar ataxia type 2 gene using a direct identification of repeat expansion and cloning technique, DIRECT. *Nature Genet.* 14, 277-284.
8. Pulst, S.M. *et al.* (1996) Moderate expansion of a normally biallelic trinucleotide repeat in spinocerebellar ataxia type 2. *Nature Genet.* 14, 269-276.
9. Kawaguchi, Y. *et al.* (1994) CAG expansions in a novel gene for Machado-Joseph disease at chromosome 14q32.1. *Nature Genet.* 8, 221-228.
10. Zhuchenko, O. *et al.* (1997) Autosomal dominant cerebellar ataxia (SCA6) associated with small polyglutamine expansions in the alpha 1A-voltage dependent calcium channel. *Nature Genet.* 15, 62-69.
11. Ross, C.A. (1995) When more is less: pathogenesis of glutamine repeat neurodegenerative diseases. *Neuron* 15, 493-496.
12. Perutz, M.E. (1996) Glutamine repeats and inherited neurodegenerative diseases: molecular aspects. *Curr. Opin. Struct. Biol.* 6, 848-858.
13. Trotter, Y. *et al.* (1995) Polyglutamine expansion as a pathological epitope in Huntington's disease and four dominant cerebellar ataxias. *Nature* 378, 403-406.
14. Li, X.-J. *et al.* (1995) A huntingtin-associated protein enriched in brain with implications for pathology. *Nature* 378, 398-402.
15. Wanker, E.E. *et al.* (1997) HIP-1: A huntingtin interacting protein isolated by the yeast two-hybrid system. *Hum. Mol. Genet.* 6, 487-495.
16. Kalchauer, M.A. *et al.* (1996) Huntingtin is ubiquitinated and interacts with a specific ubiquitin-conjugating enzyme. *J. Biol. Chem.* 271, 19385-19394.
17. Burke, J.R. *et al.* (1996) Huntingtin and DRPLA proteins selectively interact with the enzyme GAPDH. *Nature Med.* 2, 347-350.
18. Goldberg, Y.P. *et al.* (1996) Cleavage of huntingtin by apolipoprotein A, a proapoptotic cysteine protease, is modulated by the polyglutamine tract. *Nature Genet.* 13, 442-449.
19. Duyao, M. *et al.* (1993) Trinucleotide repeat length instability and age of onset in Huntington's disease. *Nature Genet.* 4, 387-392.
20. Chung, M. *et al.* (1993) Evidence for a mechanism predisposing to intergenerational CAG repeat instability in spinocerebellar ataxia type 1. *Nature Genet.* 5, 254-258.
21. Telenius, H. *et al.* (1994) Somatic and gonadal mosaicism of the Huntington disease gene CAG repeat in brain and sperm. *Nature Genet.* 6, 409-413.
22. Aronin, N. *et al.* (1995) CAG expansion affects the expression of mutant huntingtin in the Huntington's disease brain. *Neuron* 15, 1193-1201.
23. Chong, S.S. *et al.* (1995) Gametic and somatic tissue-specific heterogeneity of the expanded SCA1 CAG repeat in spinocerebellar ataxia type 1. *Nature Genet.* 10, 344-350.
24. Ueno, S. *et al.* (1995) Somatic mosaicism of CAG repeat in dentatorubral-pallidoluysian atrophy (DRPLA). *Hum. Mol. Genet.* 4, 663-666.
25. Takano, H. *et al.* (1996) Somatic mosaicism of expanded CAG repeats in brains of patients with dentatorubral-pallidoluysian atrophy: cellular population-dependent dynamics of mitotic instability. *Am. J. Hum. Genet.* 58, 1212-1222.
26. Tanaka, F. *et al.* (1996) Differential pattern of tissue-specific somatic mosaicism of expanded CAG trinucleotide repeat in dentatorubral-pallidoluysian atrophy, Machado-Joseph disease, and X-linked recessive spinal and bulbar muscular atrophy. *J. Neurol. Sci.* 135, 43-50.
27. Nasir, J. *et al.* (1995) Targeted disruption of the Huntington's disease gene results in embryonic lethality and behavioral and morphological changes in heterozygotes. *Cell* 81, 811-823.
28. Duyao, M.P. *et al.* (1995) Inactivation of the mouse Huntington's disease gene homolog *Hdh*. *Science* 269, 407-410.
29. Zeldin, S. *et al.* (1995) Increased apoptosis and early embryonic lethality in mice nullizygous for the Huntington's disease gene homologue. *Nature Genet.* 11, 155-163.
30. Goldberg, Y.P. *et al.* (1996) Absence of the disease phenotype and intergenerational stability of the CAG repeat in transgenic mice expressing the human Huntington's disease transcript. *Hum. Mol. Genet.* 5, 177-185.
31. Hodgson, J.G. *et al.* (1996) Human huntingtin derived from YAC transgenes compensates for loss of murine huntingtin by rescue of the embryonic lethal phenotype. *Hum. Mol. Genet.* 5, 1875-1885.
32. Mangiarini, L. *et al.* (1996) Exon 1 of the Huntington's disease gene containing a highly expanded CAG repeat is sufficient to cause a progressive neurological phenotype in transgenic mice. *Cell* 87, 493-506.
33. Davies, S.W. *et al.* (1997) Formation of neuronal intranuclear inclusions (NII) underlies the neurological dysfunction in mice transgenic for the HD mutation. *Cell*, in press.
34. Burright, E.N. *et al.* (1995) SCA1 transgenic mice: a model for neurodegeneration caused by an expanded CAG trinucleotide repeat. *Cell* 82, 937-948.
35. Ikeda, H. *et al.* (1996) Expanded polyglutamine in the Machado-Joseph disease protein induces cell death *in vitro* and *in vivo*. *Nature Genet.* 13, 196-202.
36. Bingham, P.M. *et al.* (1995) Stability of an expanded trinucleotide repeat in the androgen receptor gene in transgenic mice. *Nature Genet.* 9, 191-196.
37. Mangiarini, L. *et al.* (1997) Instability of highly expanded CAG repeats in transgenic mice is related to expression of the transgene. *Nature Genet.* 15, 197-200.
38. Gourdon, G. *et al.* (1997) Moderate intergenerational and somatic instability of a 55-CTG repeat in transgenic mice. *Nature Genet.* 15, 190-192.
39. Monkton, D.G. *et al.* (1997) Hypermutable myotonic dystrophy CTG repeats in transgenic mice. *Nature Genet.* 15, 193-196.
40. Wieringa, B. (1994) Commentary: Myotonic dystrophy reviewed: back to the future? *Hum. Mol. Genet.* 3, 1-7.

EXHIBIT 9

Exon 1 of the *HD* Gene with an Expanded CAG Repeat Is Sufficient to Cause a Progressive Neurological Phenotype in Transgenic Mice

Laura Mangiarini,¹ Kirupa Sathasivam,¹ Mary Seller,¹ Barbara Cozens,⁷ Alex Harper,² Colin Hetherington,³ Martin Lawton,⁴ Yvon Trottier,⁵ Hans Lehrach,⁶ Stephen W. Davies,⁷ and Gillian P. Bates¹

¹Division of Medical and Molecular Genetics
UMDS

Guy's Hospital
London SE1 9RT

United Kingdom

²UMDS Transgenic Unit

The Rayne Institute
St. Thomas's Hospital
London SE1 7EH

United Kingdom

³Biomedical Services
John Radcliffe Hospital

University of Oxford
Oxford OX3 9DU

United Kingdom

⁴Biological Services Division

UMDS

Guy's Hospital
London SE1 9RT

United Kingdom

⁵Institut de Genetique et Biologie Moleculaire
et Cellulaire

CNRS/INSERM/ULP

Illkirch

CU Strasbourg 67404

France

⁶Max Planck Institut für Molekulare Genetik

Dahlem, Berlin D14195

Germany

⁷Department of Anatomy and Developmental Biology

University College

London WC1E 6BT

United Kingdom

Summary

Huntington's disease (HD) is one of an increasing number of neurodegenerative disorders caused by a CAG/polyglutamine repeat expansion. Mice have been generated that are transgenic for the 5' end of the human *HD* gene carrying (CAG)₁₁₅–(CAG)₁₅₀ repeat expansions. In three lines, the transgene is ubiquitously expressed at both mRNA and protein level. Transgenic mice exhibit a progressive neurological phenotype that exhibits many of the features of HD, including choreiform-like movements, involuntary stereotypic movements, tremor, and epileptic seizures, as well as nonmovement disorder components. This transgenic model will greatly assist in an eventual understanding of the molecular pathology of HD and may open the way to the testing of intervention strategies.

Introduction

Huntington's disease (HD) is an autosomal dominant progressive neurodegenerative disorder (Harper, 1991).

The onset of symptoms is generally in midlife although it can range from early childhood to >70 years. Anticipation is observed, predominantly when the disease is inherited through the male line, with the result that 70% of juvenile cases inherit the disease from their father. The symptoms have an emotional, motor, and cognitive component. A detailed description of all aspects of HD can be found in Harper (1991). Chorea is a characteristic feature of the motor disorder and is defined as excessive spontaneous movement, irregularly timed, randomly distributed, and abrupt. It can vary from being barely perceptible to extremely severe. It involves all parts of the body, can have repetitive and stereotypic elements, and may have a pseudopurposive appearance (Harper, 1991). Other frequently observed motor abnormalities include dystonia (sustained muscle contraction), rigidity, bradykinesia (abnormally slow movements), oculomotor dysfunction, and tremor. Cerebellar dysfunction, upper motor neuron abnormalities, epilepsy, and myoclonus (brief shock-like muscle jerks) are rare except in the juvenile form of the disease, which commonly presents with a "Parkinsonlike rigidity." Voluntary movement disorders include fine motor incoordination, dysarthria (impairment of articulation), and dysphagia (difficulty in swallowing). The emotional disorder is commonly depression and irritability, and the cognitive component comprises a subcortical dementia. The biochemical basis of this disease is not understood, and there is no effective therapy.

The HD mutation results in the expansion of a polyglutamine (polyglu) tract in a large 350 kDa protein of unknown function (Huntington's Disease Collaborative Research Group, 1993). The normal and expanded *HD* allele sizes have been defined as CAG_{6–37} and CAG_{35–121} repeats, respectively. An inverse correlation between age of onset and repeat length is most pronounced for juvenile HD for which the longest repeats have been observed (Huntington's Disease Collaborative Research Group, 1993; Telenius et al., 1993). Despite the selective cell death, the *HD* transcript is ubiquitously expressed (Strong et al., 1993). The polyglutamines are successfully translated and the huntingtin protein (htt) products arising from expanded alleles have been identified in protein extracts from HD patients (Jou and Myers, 1995; Trottier et al., 1995a).

CAG/gln expansion has been found to be the causative mutation in five neurodegenerative diseases for which the gene has been cloned. In addition to HD, these include spinal and bulbar muscular atrophy (SBMA) (La Spada et al., 1991), spinocerebellar ataxia type 1 (SCA1) (Orr et al., 1993), dentatorubral-pallidoluysian atrophy (DRPLA) (Koide et al., 1994), and Machado Joseph disease (MJD or SCA3) (Kawaguchi et al., 1994). Many aspects of the genetics and molecular biology are common to these diseases. They are autosomal dominant (with the exception of X-linked SBMA) and show varying degrees of anticipation on paternal transmission. The size of the normal and expanded CAG repeat ranges are comparable, and available data indicate that age of onset correlations and patterns of repeat stability are

reproduced. A similar ubiquitous expression pattern is also characteristic, and the presence of the expanded forms of ataxin-1 (SCA1 protein) and atrophin-1 (DRPLA protein) in lysates from patient tissues have been observed (Servadio et al., 1995; Yazawa et al., 1995).

Despite the otherwise apparent universality of this mutation, the patterns of cell death differ between these diseases. In HD, the most striking atrophy occurs in the caudate nucleus, which is often reduced to a rim of tissue. The putamen and globus pallidus also undergo atrophy, and there are subtle changes in the cerebral cortex (Vonsattel et al., 1985). SBMA is a form of motor neuron disease with both spinal and bulbar motor neuron involvement (Kennedy et al., 1968). The SCA1 and SCA3 spinocerebellar ataxias are clearly distinguished by major neuropathological features: Purkinje cell, pontine nuclei, and inferior olivary nuclei degeneration in SCA1 (Zoghbi et al., 1993) and pontine nuclei and the molecular layer of the cerebellum in SCA3 (Durr et al., 1996). In DRPLA, neuropathology includes the cerebellar dentate nucleus, globus pallidus, red and subthalamic nuclei, Purkinje cells, brain stem tegmentum, and the lateral corticospinal tract (Takahashi et al., 1988). The proteins containing the polyglutamine repeats are otherwise unrelated. In SBMA, the repeat lies within the androgen receptor (La Spada et al., 1991), while the others are in novel genes of unknown function. Subcellular localization suggests differing roles for these proteins (DiFiglia et al., 1995; Servadio et al., 1995; Trotter et al., 1995a; Yazawa et al., 1995).

It is essential that transgenic models of these diseases are developed. There have been two previous reports of a neurological phenotype observed in mice transgenic for a protein carrying a polyglutamine repeat expansion. The first used a SCA1 cDNA construct with (CAG)₈₂ under the control of a Purkinje cell specific promoter (Burrage et al., 1995). Three heterozygous lines overexpressing the SCA1 transcript by 10- to 100-fold and two homozygous lines showed a progressive ataxic phenotype between 12 and 26 weeks of age. The mice became clearly ataxic when walking and routinely fell when attempting to stand on their hind legs. Pathologic examination showed significant loss of the Purkinje cell population with Bergmann glial proliferation and shrinkage and gliosis of the molecular layer. More recently, transgenic mice have been reported with a (CAG)₇₀ version of the SCA3 gene and also the (CAG)₇₀ polyglutamine tract in isolation, both under the control of the Purkinje cell specific promoter (Ikeda et al., 1996). Affected mice transgenic for the isolated polyglutamine tract were severely ataxic, they exhibit a wide-based hind limb stance, frequently fall when moving, and are unable to rear. Overt Purkinje cell death was observed with secondary effects to the molecular and granular cell layers. No phenotype was observed in the mice transgenic for the entire mutated SCA3 gene. The authors suggested that the polyglutamine tracts are more toxic in isolation than in the context of a protein, although in the absence of any information concerning transgene copy number, genomic structure of the integration sites, or expression levels, this interpretation should be treated with caution. These reports have shown that Purkinje cell specific overexpression of an expanded polyglutamine tract, both in the context of the SCA1

gene or in isolation, is toxic to Purkinje cells and causes a corresponding ataxic phenotype.

In our initial attempt to generate a murine model of HD, we have focused on the construction of a mutant yeast artificial chromosome (YAC) for introduction by pronuclear injection. Progress was severely hampered by both instability of YAC intermediates and the severe instability of highly expanded CAG repeats in yeast. Consequently, to address the question of CAG repeat stability in the mouse, transgenic lines were established with a 1.9 kb human genomic fragment containing promoter sequences and exon 1 carrying expansions of approximately (CAG)₁₃₀. Unexpectedly, this fragment has been sufficient to generate a progressive neurological phenotype that displays many of the characteristics of HD. This is the first time that a model of one of these diseases has been generated by a transgene driven from an endogenous promoter. The availability of a mouse model of the disease is extremely informative with regard to the size of the polyglutamine expansion and level of expression required to produce a phenotype with a given age of onset in the mouse. This work suggests that the polyglutamine-containing domain of the htt protein may be sufficient to generate a mouse model of HD.

Results and Discussion

Fragment Used for Transgenesis

The microinjection fragment was a 1.9 kb *SacI*-*EcoRI* fragment from the 5' end of the human HD gene isolated from a phage genomic clone derived from an HD patient (Figure 1a). It is composed of ~1 kb of 5' UTR sequences, exon 1 carrying expanded CAG repeats of ~130 units and the first 262 bp of intron 1. As the CAG repeats are unstable when propagated in *E. coli*, the DNA preparation used for microinjection contained a heterogeneous set of repeats of varying size but of the order of 130 units. In the event that an unspliced mRNA should be transcribed from this fragment, an "in-frame" stop codon immediately at the beginning of intron 1 would result in a truncated protein corresponding to the first 90 amino acids of the published htt protein (repeat size of (CAG)₂₁).

Genomic Organization of the Integration Events

Transgenic mice were generated by microinjection of single cell CBAXC57BL/6 embryos. Of 29 newborn mice, seven died neonatally, and of the remaining 22 pups, one male was transgenic. This founder (R6) was initially backcrossed to both C57BL/6 and to CBAXC57BL/6 females. However, a subsequent need to optimize litter size has resulted in the maintenance of the transgene on the CBAXC57BL/6 hybrid background. F1 mice were genotyped both by Southern analysis and by PCR to determine the CAG repeat size. Figure 1b shows a Southern blot of *Bam*HI digested DNA from a number of F1 progeny. It was possible to deduce that the microinjection fragment had integrated into five different regions of the founders' genome. The predicted genomic organization of the integration events is illustrated in Figure 1c. In lines R6/1 and R6/0, the fragment has integrated as an intact single copy, and in line R6/T as

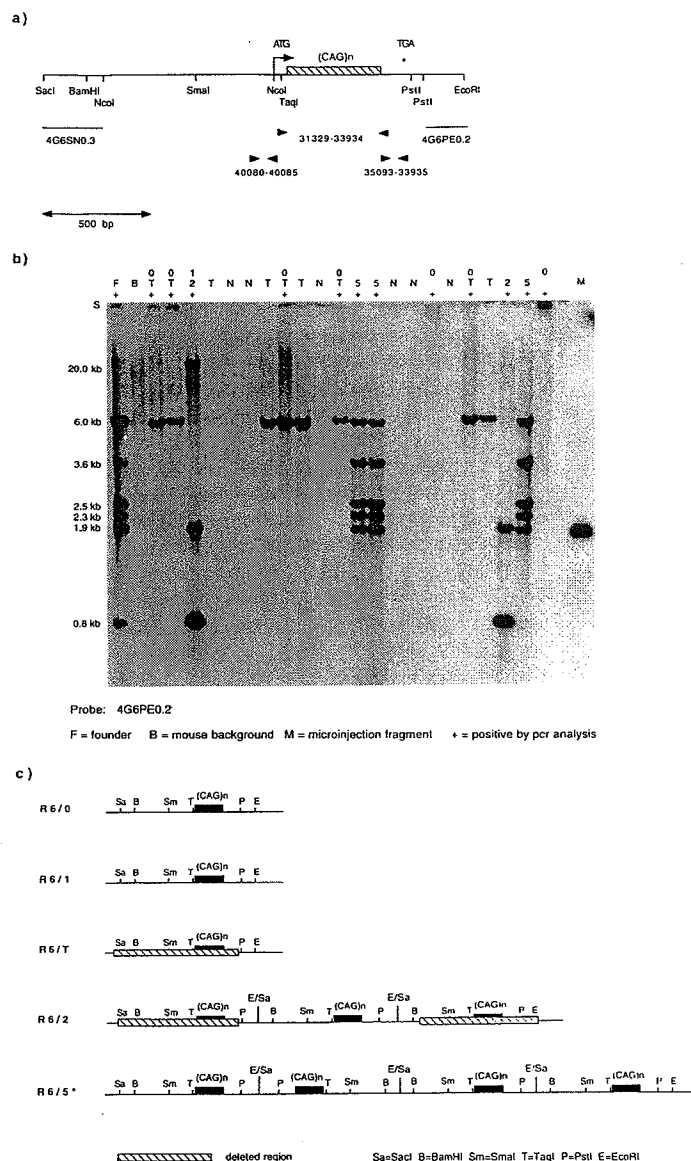


Figure 1. Microinjection Fragment and Identification of the Integration Events

(a) Restriction map of the human genomic fragment used for microinjection. An arrow denotes the transcription start site and asterisk indicates the position of an in-frame stop codon at the beginning of intron 1. 4G6SN0.3 and 4G6PE0.2 are fragments used as hybridization probes, and solid triangles indicate the location of PCR assays used for genotyping and RNA analysis.

(b) Southern blot of genomic DNA from the R6 founder and a number of F1 progeny. DNA was digested with BamHI and probed with 4G6PE0.2. The genotypes are indicated above the lanes (1, 2, 0, T, or 5). A plus sign indicates that the mouse also scored as transgenic when typed with the CAG repeat PCR assay. BamHI fragment sizes are as follows: R6/1, 20.0 kb; R6/2, 1.9 and 0.8 kb; R6/5, 6.0, 3.6, 2.5, 2.3, and 1.9 kb; R6/0, band migrates close to slot (S); R6/T, 6.0 kb. The R6/T genotype is negative with the CAG repeat PCR assay.

(c) Genomic organization of the integration sites of the transgenes. R6/0, R6/1, and R6/T are single copy integrants although R6/T is highly deleted. R6/2 probably originated as a three copy integrant, the flanking fragments having undergone deletions. (asterisk) It has not been possible to completely resolve the structure of the R6/5 integration event. Three of the five BamHI fragments can be accounted for by the structure as drawn.

a highly truncated fragment. In line R6/0, the fragment has most probably inserted adjacent to a repetitive genomic structure. When the probe 4G6PE0.2 is hybridized to Southern blots of transgene genomic DNA digested with BamHI, SmaI, PstI, or NcoI, in each case a band is detected that has barely migrated into the gel. If the same blots are probed with 4G6SN0.3, the 5'UTR probe, bands of a more expected size range are seen. Line R6/2 most probably originated as a three copy integration event, the flanking fragments having been subject to deletions, with the result that this transgene functions essentially as a single copy integrant. Finally line R6/5 is represented by five bands on a BamHI Southern blot. It is clear that four fragments have integrated as illustrated in Figure 1c. This includes both a tail-to-tail and head-to-head arrangement. However, other hybridization bands could not be explained by a straightforward

configuration, as in those illustrated, or by simple deletions. It seems likely, therefore, that a complicated rearrangement must have occurred for which it has not been possible to completely unravel the genomic structure.

Size of the CAG Expansion in Each of the Transgenic Lines

Four of the transgenic lines: R6/0, R6/1, R6/2, and R6/5 carry expanded CAG repeats. The size of the expansion was determined by PCR amplification of the repeat using a fluorescently labeled primer and subsequent size determination using an ABI sequencer (Figure 2). The peak sizes are as follows: R6/1, 116 repeat units; R6/0, 142 repeat units; R6/2, 144 repeat units. Line R6/5 is more complicated with peaks at 128, 132, 135, 137,

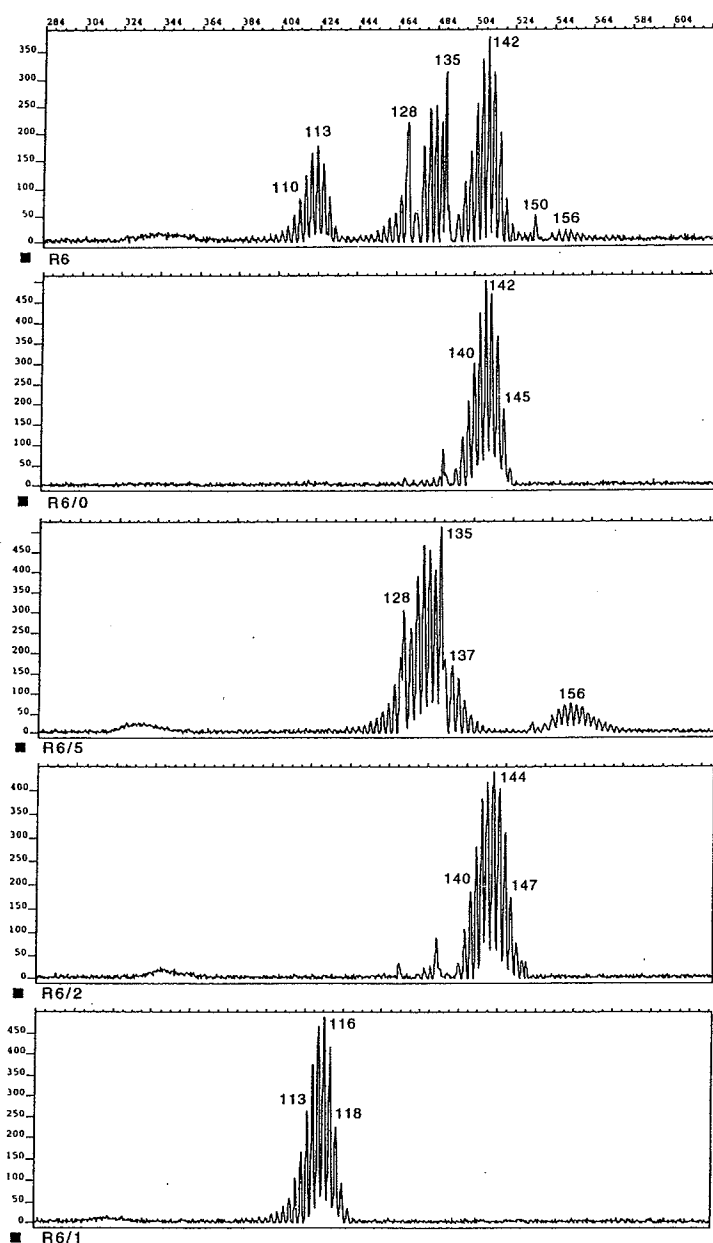


Figure 2. Measurement of the Size of the CAG Expansion in the R6 Transgenic Lines

The CAG repeats were amplified with a FAM-labeled primer as described. The top panel shows the trace specific to the founder (R6) and the four lower panels, the traces obtained in F1 mice with the R6/0, R6/5, R6/2, and R6/1 genotypes.

and 156 repeat units. These repeat sizes are considerably larger than those that have generally been reported to cause the juvenile form of HD in humans. Both gametic and somatic repeat instability have been observed (manuscript submitted).

Segregation of the Integration Events

The specific genotype frequencies found in 321 F1 mice derived from the R6 founder are summarized in Table 1. The integration events appear to segregate independently but are only seen in certain combinations. The founder is therefore a germ line chimera with one set of germ cells containing the R6/0 and R6/T transgenes and

the other containing the R6/1, R6/2 and R6/5 transgenes.

Phenotype Observed in the R6/2 Transgenic Line

The age of onset in line R6/2 has been observed as early as four weeks (one mouse) but most frequently occurs between nine and eleven weeks. Age at death has generally been between 10 and 13 weeks although the mouse with the age of onset at four weeks died at six and a half weeks. The mice display a progressive neurological phenotype. As far as can be ascertained, the mice remain alert, exploratory and inquisitive, and responsive

Table 1. Frequency of Genotypes Arising in 321 F1 Progeny

Genotype	N
R6/0	56
R6/T	61
R6/0 + R6/T	62
Negative ^a	(56/71)
R6/1	8
R6/2	16
R6/5	15
R6/1 + R6/2	9
R6/1 + R6/5	8
R6/2 + R6/5	11
R6/1 + R6/2 + R6/5	4
Negative ^a	(15/71)

^a The total number of nontransgenic mice are divided between the two genotype clusters in a proportion consistent with the genotype frequencies.

to sensory stimuli. The phenotype is complex. There are a number of components to the motor disorder including a resting tremor, movements described as resembling chorea, stereotypic involuntary movements, and in some cases a mild ataxia manifesting as dysmetria. One of the first symptoms is a dyskinesia of the limbs when held by the tail. This progresses to an alternating clasp ing together and releasing of the feet until the mice clasp their feet together immediately after they are picked up, (Figure 3a), and can no longer release this posture. The mice develop a constant tremor that becomes progressively worse. The tremor tends to be less noticeable when they are quiet or asleep, but worsens under stress (for example, the removal of the cage lid) or if they reach for food or to climb out of the cage. As the disorder progresses, stereotypic involuntary movements are apparent, which include repetitive stroking of the nose and face, and a hind limb kicking/scratching motion. Sudden movements that involve the whole body and may resemble chorea are observed. These are rapid, abrupt, irregular, and manifest as a shaking/shudder of the trunk. The mice do not develop a wide-based gait, can stand on their hind limbs and climb out of the cage without falling. They only consistently lose balance when sitting on their hind limbs, turning, and reaching round to groom their backs, which results in a somersault. The mice exhibit severe handling-induced epileptic seizures that can last for several minutes.

At weaning, the R6/2 transgenes are indistinguishable from their normal litter mates. Coincident with the onset of motor symptoms, their weight plateaus and then progressively decreases. In the end stages, mice have been observed to weigh as little as 60%–70% of their normal sibs. As the disease becomes more severe, they are very frequently observed to be eating but do not gain weight. It appears that the mice are eating rather than just breaking off food. Their food comprises an expanded chow, which does not crumble easily, and excess food crumbs are not observed in the bedding. On autopsy, the mice are often emaciated with an overall loss of muscle bulk although food is observed in the stomach and fecal pellets in the gut. Histological analysis of muscle samples showed no evidence of a myopathy.

Characteristic vocalizations have been observed. These include a sound similar to that made by a new born litter, which resembles teeth chattering from cold, but is likely to have a respiratory basis (since it occurs before the young mice have teeth). A second sound, a type of chirping noise, is more reminiscent of a bird than of a mouse. The mice are more likely to make these sounds when they are under stress (for example, away from the home cage).

The mice appear to urinate more frequently. The bedding at the front of the cage becomes excessively wet as compared to that in cages housing normal mice. They are unlikely to be suffering from spastic bladders as the wetting of the bedding is not uniform. Urine tests in 18 transgenic mice (11 male and 7 female) showed no abnormality in glucose or protein levels. Similarly, blood tests in two mice showed glucose and protein levels to be within the normal range.

R6/2 females are sterile and, of ten R6/2 males that have been placed with females from a time just prior to expected sexual maturity, five have mated. Of these, one mouse produced one litter, two mice produced two litters and two produced four litters. On autopsy, the reproductive organs consistently appear vestigial or atrophied. Females often have miniscule ovaries and a hair-like uterus. Males have small testes, seminal ducts, and coagulation glands. On histology, one male that had failed to mate was found to have testicular atrophy with an absence of spermatazoa, an atrophy of the epididymus with aspermia, and no secretion present in the coagulation gland.

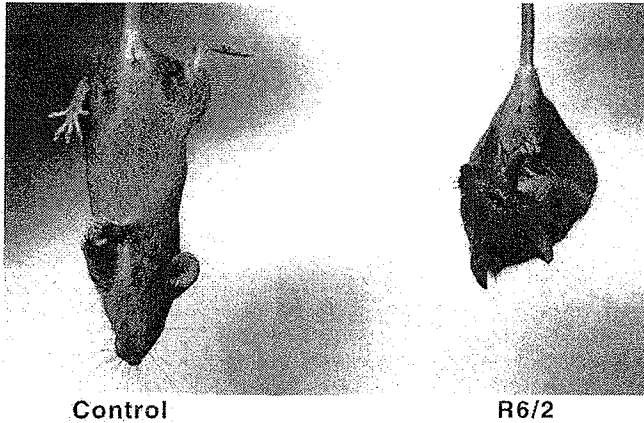
The mice die suddenly and the cause of death is generally unknown although one mouse was observed to die during an epileptic seizure.

Dosage Effect on Age of Onset and Phenotype Severity in Complex Genotypes

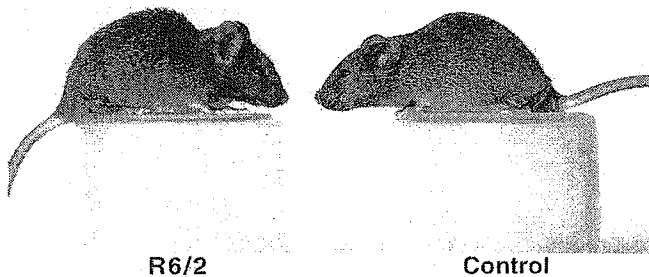
Lines R6/1, R6/2, and R6/5 have been established from the founder. In the F1 generation, mice with all possible combinations of these transgenes were identified. Each aspect of the phenotype, as described for line R6/2, has been observed for the genotypes listed in Table 2. In the end stages of the disease, the transgenes are always considerably smaller than their normal littermates. The age of onset varies from <3 weeks (R6/1+R6/2+R6/5 genotype) to ~4 or 5 months (R6/1 line).

The (R6/1+R6/2+R6/5) genotype is the most severe. Only four such mice were recovered in the F1 generation. The overall genotype frequency (Table 1) would have predicted more than this, and it is possible that some mice with this genotype died neonatally or in utero. All aspects of the phenotype are more severe and have a more rapid progression. The (R6/1+R6/2+R6/5) mice are considerably smaller than their litter mates at weaning. For example, one weighed 5.2 g at 23 days of age as compared to a mean of 9.2 g for her female sibs. She reached a maximum weight of 7.5 g but was only 6.0 g at death at 51 days as compared to a mean of 16.3 g for her sibs. In contrast, line R6/1 has the latest age of onset and the slowest progression. The mice begin to exhibit the feet-clasping posture when suspended by the tail at ~4–5 months. At between 6 and 7 months,

a)



b)



c)

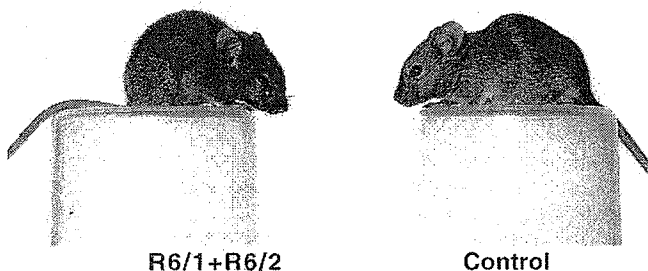


Figure 3. Comparison of R6 Transgenic Mice and Littermate Controls

(a) An R6/2 transgenic mouse demonstrating the feet-clasping posture adopted when suspended by the tail. The normal mouse holds its hind limbs outward in order to steady itself.

(b) The R6/2 mouse (17.7 g) and normal littermate (21.3 g) at 12 weeks of age. The transgenic mouse is thinner.

(c) An R6/1 + R6/2 (10.1 g) transgenic mouse and normal littermate (19.6 g) at seven weeks, three days. There is a considerable size difference.

some show a mild tremor and intermittently exhibit all aspects of the involuntary movement disorder as described for the R6/2 line. Epileptic seizures have also been observed. The effect of transgene dosage on the size of the mice is illustrated in Figure 3.

On autopsy, atrophy or gross atrophy of the primary and secondary reproductive organs is routinely observed. Otherwise, hepatic changes in the form of polyploid hepatic nuclei and a loss of cytoplasmic mass with

no obvious cell death was the only consistent observation resulting from a routine histopathological examination (two R6/2 and six R6/1 + R6/5 mice in the end stages of the disease and displaying all aspects of the phenotype). Thymic atrophy is sometimes present, more frequently in the more severely affected lines, but this does not correlate with the presence or absence of phenotypic features. In a few mice there is a slight deformation to the cranial vault resulting in a boney ridge over the

Table 2. Comparison of the Onset and Duration of the Phenotype Associated with the R6 Genotypes

	Age of Onset	Age at Last Litter	Age at Death
R6/1 + R6/2 + R6/5	< 3 weeks	N/A	4–7 weeks
R6/1 + R6/2	3–4 weeks	N/A	6–8 weeks
R6/2 + R6/5	6–7 weeks	N/A	8–12 weeks
R6/2	9–11 weeks	6–9 weeks ^a (5 males)	10–13 weeks
R6/1 + R6/5	12–16 weeks	12 weeks ^a (1 male)	24–36 weeks
R6/1	15–21 weeks	14 weeks ^b (1 male)	32–40 weeks ^c

^a Mice bred continuously.

^b Mouse failed to breed when cross set up at 19 weeks.

^c Oldest R6/1 mouse is alive at 40 weeks.

cerebellum. This has been seen more frequently in the lines with the more severe phenotype but has also been observed in line R6/1 + R6/5.

A phenotype has not been observed in the heterozygous (R6/5)/+ or (R6/0)/+ lines, the oldest mice now being ~14 months. R6/5 homozygotes are developing symptoms at ~9 months, and the R6/5 transgene clearly contributes to the onset and progression of the disorder when in combination with R6/1 or R6/2 transgenes.

Expression of the Transgene

PCR primers specific to exon 1 of the human *HD* gene were used to examine the expression and tissue distribution of the transgenes. RT-PCR showed the transgene to be expressed in every tissue examined for lines R6/2 (Figure 4a), R6/1, and R6/5, but was not expressed in line R6/0. This ubiquitous pattern of expression for three of the lines suggests that the transgene is most likely expressed from promoter sequences present on the microinjection fragment. The absence of expression in line R6/0 is probably due to a position effect as Southern analysis of this line predicts that the R6/0 transgene has integrated adjacent to a genomic region of unusual structure. Northern analysis revealed transcripts of 2.5 and 2.3 kb in lines R6/1 and R6/2, respectively (Figure 4b) and the suggestion of a larger R6/5 transcript. The 4G6PE0.2 probe is derived from intron 1 of the human gene, and the presence of this sequence in the transcripts indicates that the human exon 1 has not spliced to mouse exonic sequences potentially occurring close to the integration sites.

The level of expression of the transgene with respect to the endogenous mouse *hd* gene was assessed in total RNA from six tissues for each of the lines R6/1, R6/2, R6/5, and R6/0. The PCR primers had identical recognition sequences in exon 1 of both the mouse and human genes and amplified mouse and human products of 121 and 114 bp, respectively. No expression was detected in the R6/0 transgene. While the comparative expression level varies between tissues, the average expression of the R6/2, R6/1, and R6/5 transgenes was 75%, 31%, and 77% of the endogenous level (data not shown). The tissue variability made absolute quantitation difficult, but this analysis nevertheless places the level of expression of the transgene within the range of the murine gene.

The monoclonal antibody, 1C2, binds specifically and in a size-dependent manner to pathogenic polygl

expansions (Trottier et al., 1995b). This antibody was used to immunoprobe Western blots of cell lysates derived from a complete set of tissues from lines R6/1, R6/2, and R6/5. A transgene-specific product was detected in lines R6/2 and R6/5 in all tissues tested. Figure 5 shows the Western blots obtained for a subset of tissues from lines R6/2 and R6/5. The predicted size of the R6/2 protein would be ~23 kDa. The migration of the R6/2 and R6/5 products, at a size larger than this with respect to the markers, is consistent with the aberrant migration observed for the expanded polygl containing htt, ataxin-1, and atrophin-1 products when compared to their normal counterparts. A constant band detected in all transgene and control tissues was found to be due to cross-reactivity of the antimouse secondary antibody. Comparison of the intensity of the the constant band between the R6/2 and R6/5 tissues suggests that the transgene protein is present at similar levels in these lines. A protein product has not been detected in line R6/1 despite testing ranges of polyacrylamide concentration and antibody dilution. It would be extremely unlikely that a protein product were not present in this line. One possible explanation is that the length of polygl tract in the R6/1 protein does not present an epitope to the 1C2 antibody. It is not clear from expression analysis why the R6/5 phenotype should be so much milder than that observed in lines R6/2 and R6/1.

Neuropathology

Nine R6/2 transgenic mice, exhibiting a broad spectrum of severe symptoms of 2–3 weeks duration, and nine nontransgenic littermates were used for neuropathological investigation. Brains from the transgenic animals were consistently smaller than controls (controls 490 ± 9.8 mg, transgenes 395 ± 8.0 mg). Serial 40 μ m sections in either the coronal (12 mice) or horizontal (6 mice) planes were processed for either Nissl staining (Figures 6 and 7) or the immunocytochemical localization of glial fibrillary acidic protein (GFAP) or the mouse macrophage and microglial marker F4/80. The morphology of the central nervous system (CNS) in the transgenic mice appeared normal with no focal areas of malformation or neurodegeneration; however, sections of the brains of these animals were consistently smaller than those of their litter mates ($19\% \pm 1.6\%$). This reduction in size appeared to be uniform throughout all CNS structures. Analysis of thionin-stained sections showed no evidence of neuronal cell loss, oligodendrocyte loss, reac-

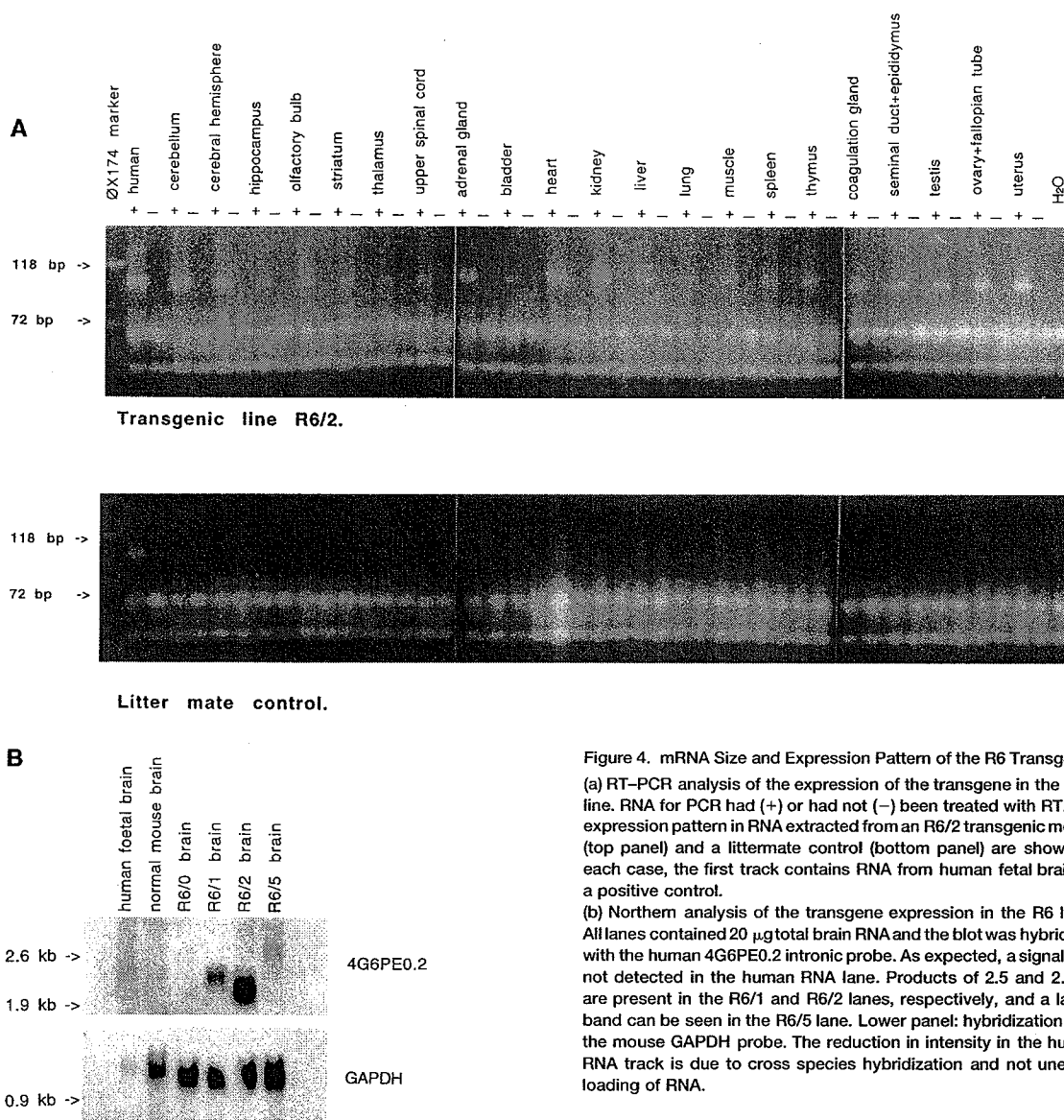


Figure 4. mRNA Size and Expression Pattern of the R6 Transgenes
(a) RT-PCR analysis of the expression of the transgene in the R6/2 line. RNA for PCR had (+) or had not (-) been treated with RT. The expression pattern in RNA extracted from an R6/2 transgenic mouse (top panel) and a littermate control (bottom panel) are shown. In each case, the first track contains RNA from human fetal brain as a positive control.

(b) Northern analysis of the transgene expression in the R6 lines. All lanes contained 20 µg total brain RNA and the blot was hybridized with the human 4G6PE0.2 intronic probe. As expected, a signal was not detected in the human RNA lane. Products of 2.5 and 2.3 kb are present in the R6/1 and R6/2 lanes, respectively, and a larger band can be seen in the R6/5 lane. Lower panel: hybridization with the mouse GAPDH probe. The reduction in intensity in the human RNA track is due to cross species hybridization and not unequal loading of RNA.

tive gliosis, or inflammatory change. These latter two observations were corroborated by the GFAP and F4/80 stained sections, where the normal distribution of astrocytes and ramified microglia cells was observed in the absence of any indication of increased reactivity of astrocyte staining or the presence of rounded microglia or infiltrating macrophages.

Cerebral Cortex and Hippocampus

The cytoarchitectonic structure of the cerebral cortex was maintained in the frontal, temporal, occipital and parietal lobes, although all regions were noticeably thinner when measured between the pia and subcortical white matter. The large pyramidal cells of the motor regions of the frontal cortex were present in normal number and morphological appearance. Similarly the pyramidal cells of hippocampus, subiculum and para-

hippocampal gyrus, the stellate cells of layer II of the entorhinal cortex, and the granule cells of the dentate gyrus were of normal size and distribution.

Basal Ganglia

A detailed analysis of the striatum, nucleus accumbens, globus pallidus, entopeduncular nucleus, subthalamic nucleus, and substantia nigra demonstrated normal neuronal density and patterns of morphological diversity. The striatum is composed of a normal complement of medium-sized striatal neurons interspersed with fewer large and small neurons, together with satellite glia. The white matter of the corpus callosum and the fascicles of fibers forming the internal capsule contain as many oligodendrocytes as similar sections from control mice. The striatum is again consistently smaller in the transgenic animals.

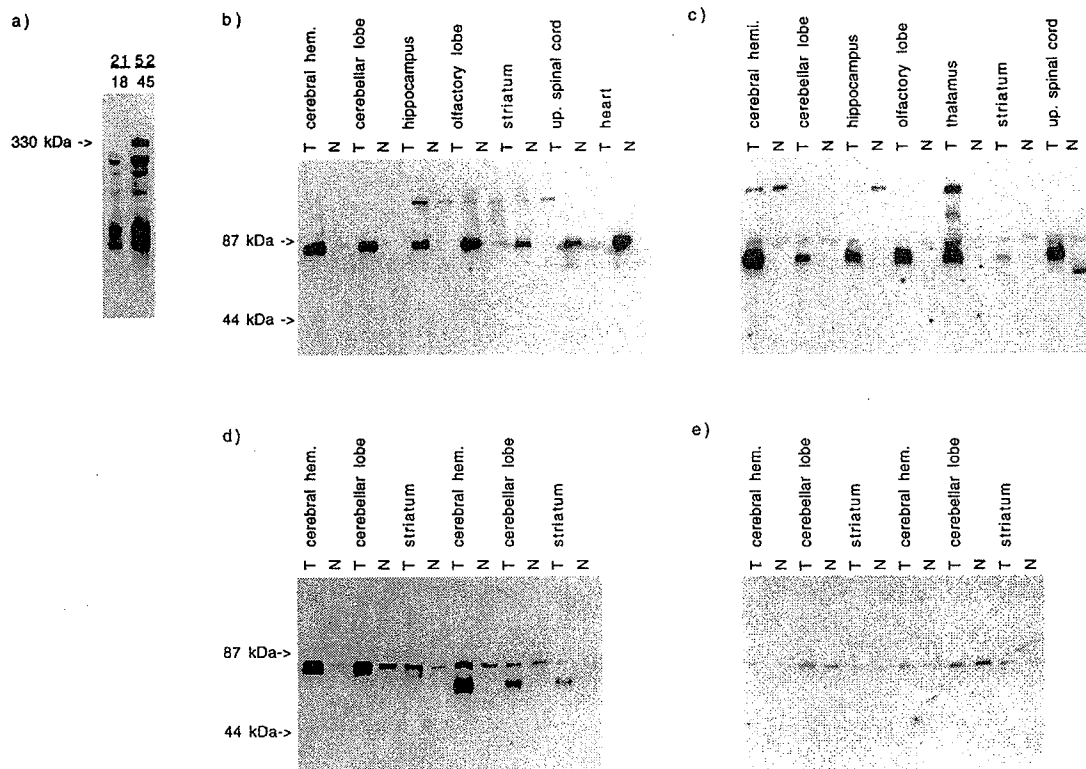


Figure 5. Expression Profile of the Transgene Protein Products

Identification of the transgene protein product in the R6/2 and R6/5 lines using a monoclonal antibody (1C2) that specifically detects polyglutamine expansions.

(a) Identification of htt in lysates prepared from lymphoblastoid cell lines from a normal individual and an HD homozygote and fractionated on a 6% SDS-PAGE gel. The size of the respective CAG expansions are indicated above the tracts. The position at which the fibrinogen marker (330 kDa) migrates is indicated.

(b) Lysates from an R6/2 transgene (T) and littermate control (N) were fractionated on a 10% SDS-PAGE gel.

(c) Lysates from an R6/5 transgene (T) and a littermate control were fractionated on a 10% gel.

(d) Lysates from the R6/2 and R6/5 lines fractionated on a 10% SDS-PAGE gel.

(e) The filter in (d) stripped and re-probed with the secondary antiserum, which detects the constant band seen in (b)-(d).

Cerebellum and Spinal Cord

The granule cells, Purkinje cells, and the neurons of the molecular layer of the cerebellum show no differences from the control mice. Similarly, the large motor neurons of the anterior horn of the cervical and lumbar enlargements of the spinal cord and the dorsal horns are again of normal appearance.

Examination of all other areas of the CNS revealed no gross or microscopic abnormalities.

Discussion

Transgenic mice that develop a progressive neurological phenotype have been generated by the introduction of a genomic fragment containing exon 1 of the human HD gene. Four lines have been established, with CAG repeat expansions ranging from ~115 to 150 repeat units. In the three lines that exhibit a phenotype, R6/1, R6/2, and R6/5, the transgene has a ubiquitous mRNA and protein expression pattern. The transgene mRNA is most likely transcribed from human promoter elements and extends into the flanking mouse sequences.

The presence of human intron 1 sequences in the mRNA rules out the possibility that the human exon splices to mouse exonic sequences and therefore predicts that the corresponding transgene protein products contain 69 amino acids in addition to the number of polyglutamine residues encoded by the repeat expansion.

The polyglutamine expansions in the R6 transgenic mice are of a size considerably greater than is generally associated with the juvenile form of HD. Even so, it is not possible to predict the phenotypic expression of such a mutation in the mouse. In HD, the major focus of neuropathological change is in the striatum (part of the basal ganglia) and the cerebral cortex. The motor disorder observed in the R6 lines is strongly suggestive of a basal ganglia lesion. The mice exhibit involuntary jerky shudders that have been described as resembling chorea and likened to the choreic movements observed in the neurological disease arising from canine distemper (Lauder et al., 1954). As far as we can ascertain, chorea has not previously been described in mice (Lyon and Searle, 1990). The neuropathological correlate of chorea is accepted as a basal ganglia lesion. The pronounced

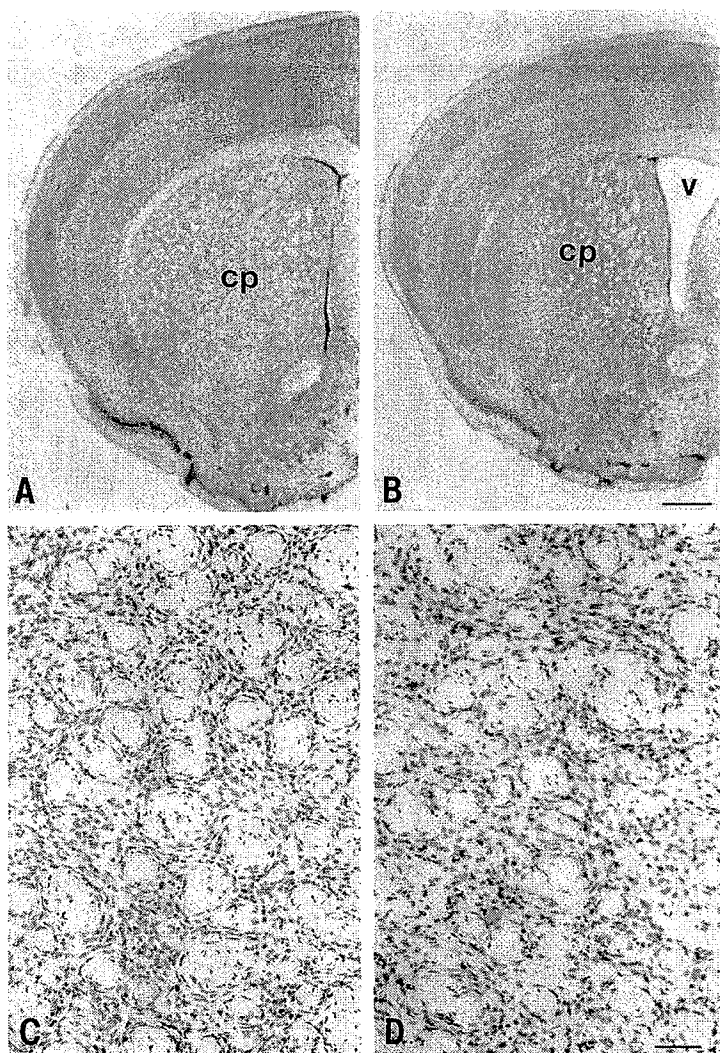


Figure 6. Nissl Sections Through the Mouse Forebrain

Frontal section through the caudate/putamen (cp) at the level of the lateral ventricle (v) of a normal littermate control (A) and R6/2 transgenic mouse (B). The caudate putamen is shown in higher power in C (control) and D (R6/2 transgene). Scale bars, 500 μ m in (A) and (B), 80 μ m in (C) and (D).

progressive resting tremor that occurs in all limbs, trunk, and head of affected mice also points to a basal ganglia abnormality. The observation of epileptic seizures is compatible with juvenile HD; however, while seizures have a cerebral focus, they could result from many imbalances that are both intracranial or extracranial.

The R6 mice also suffer from a progressive decrease in body weight and an overall loss of muscle bulk. Similarly, loss of body weight and a generalized lack of muscle bulk is a progressive and characteristic symptom of HD, despite increased calorific intake (Sanberg et al., 1981). The weight loss appears to be independent of the hyperkinesia and its molecular basis is not understood (Harper, 1991). In addition, the R6 mice appear to urinate more frequently as judged by wetting of the bedding. Urinary incontinence has also been noted in HD with symptoms including frequency, urgency, nocturia, and incontinence (Wheeler et al., 1985). Finally, chorea affecting face, jaw, and pharyngeal muscles affects both speech and swallowing and can also cause grunting and clicking sounds that may reflect respiratory movements

(Harper, 1991). It is possible that the unusual vocalizations made by the R6 transgenes arise by a similar mechanism.

A landmark study of the neuropathology of HD has classified the neuropathological changes into five grades that progress from grade 0, in which HD brains show no gross or microscopic abnormalities consistent with HD despite premortem symptomatology and positive family history, to grade 4, in which the most extreme atrophy is observed (Vonsattel et al., 1985). The brains from the R6/2 transgenic mice were found to be on average 19% smaller than those of their normal littermates, a reduction in size that was maintained through all CNS structures. This finding is consistent with neuropathological changes occurring in HD in which it has been noted that a 30% reduction in brain weight in HD is associated with 20%–30% areal reductions in cerebral cortex, white matter, hippocampus, amygdala, and thalamus (de la Monte et al., 1988). This atrophy was similar for all grades of HD, suggesting that the shrinkage of these structures occurs early in the

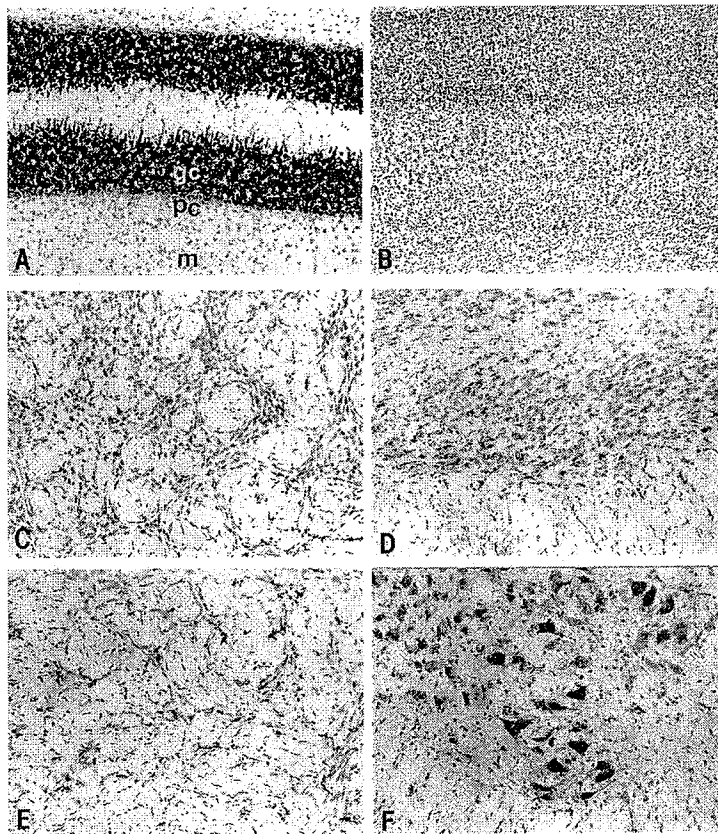


Figure 7. Nissl Sections throughout the CNS. Coronal sections through the cerebellum (A), cerebral cortex (B), globus pallidus (C), subthalamic nucleus (D), entopeduncular nucleus (E) and ventral horn of the lumbar spinal cord (F) of an R6/2 transgenic mouse. Within the cerebellum, note the normal density of the granule cell layer (gc), the monocellular layer of pyramidal cells (pc) and the normal structure of the molecular layer (m).

disease process, is not progressive, and reflects cell loss of both neurons as well as fibers. Interestingly, gliosis was not readily apparent in these structures, and the neuronal density was assessed to be normal (de la Monte et al., 1988). In contrast, a 60% reduction in the cross-sectional area of the caudate, putamen, and globus pallidus increases with the higher grades of HD brains, indicating that these structures progressively degenerate with prolonged survival. It is this specific progressive atrophy, associated with reactive astrocytosis, that was not apparent in the R6/2 transgenes and is also absent from grade 0 HD brains (Myers et al., 1991; Vonsattel et al., 1985). The grade 0 brains came from patients that had had HD symptomatology for between 2 and 13 years (Vonsattel et al., 1985; Myers et al., 1988; Hedreen and Folstein et al., 1995), thereby providing no pathological correlate for chorea and other early signs (Hedreen and Folstein et al., 1995). It seems likely that the brains of the R6/2 transgenes have neuropathology consistent with that found in the early stages of HD and that the progression of the phenotype in these mice is so rapid that there is insufficient time for the progressive atrophy to take place. A detailed morphometric analysis did uncover a neuronal loss in the caudate of grade 0 brains (Myers et al., 1991), and the absence of reactive astrocytosis was taken as evidence that the neuronal cell loss was not a recent event and may support the hypothesis that the HD striatum is compromised from early in development (Myers et al., 1991). A detailed

morphometric analysis of the R6/2 transgene brains is merited. The neuropathological analysis of the transgenes was also focused on the additional regions that undergo neurodegeneration in the polyglutamine expansion diseases as a whole, and no evidence of localized neurodegeneration was identified.

To date, five neurodegenerative diseases have been described that are caused by polyglutamine expansions in ubiquitously expressed unrelated proteins. It is most probable that in each case the polyglutamine expansion confers a gain of function to the proteins and that this may operate by a common molecular mechanism. It has been proposed that the specific selective cell death is directed by the remainder of the respective proteins. The R6 transgene protein products contain polyglutamine tracts in a domain consisting of only 69 other amino acids amounting to ~3% of the htt protein. Therefore, the R6 transgenic mice might be expected to represent a generic CAG/glutamine disease model rather than a specific model of HD. However, the R6 mice do not develop a pronounced ataxia as described by Burright et al. (1995) and Ikeda et al. (1996). They do not develop a wide-based gait or fall while moving, are able to rear, and do not lose their righting response when turned onto their backs. This would suggest that there is no major cerebellar lesion and that the R6 lines do not display the major movement disorder of SCA1, SCA3, and late onset DRPLA. Similarly, they do not show a pronounced motor neuron disease, although the SBMA symptoms in

humans are mild with a very slow progression and it would probably be difficult to identify this component as part of the complex R6 phenotype. The diagnosis of HD and DRPLA was not infrequently confused before the advent of mutation analysis afforded an unequivocal test. Both disorders present with complex and variable symptoms that can include chorea, myoclonus, dystonia, dysarthria, and seizures. Some features are more or less associated with the juvenile or adult forms but the boundaries are not absolute. It would therefore be difficult to express any strong claims as to the specificity of a mouse model with respect to these two diseases.

The R6 mice are the first transgenic model of a polyglutamine expansion disease in which the transgenes are ubiquitously expressed (as are the mutant human genes). The two previous reports of a neurological phenotype observed in mice transgenic for a protein carrying a polyglutamine repeat expansion used a Purkinje cell specific promoter to drive either a SCA1 cDNA construct with (CAG)₈₂ (Burright et al., 1995) or a (CAG)₇₉ polyglutamine tract in isolation (Ikeda et al., 1996). Purkinje cell death was identified with a corresponding ataxic phenotype. It is possible that comparable overexpression of these constructs in any other cell would also demonstrate toxicity. The dramatic dosage effect on the phenotype observed with the R6 transgenes expressing at less than endogenous levels suggest that ubiquitous overexpression of the R6 transgene could be lethal.

The apparent absence of specific neurodegeneration in the R6 mice supports the possibility that localized atrophy may be secondary to a primary imbalance that is directly responsible for the clinical symptoms that arise in HD. Indeed, replication of the patterns of cell death observed in HD by intrastriatal injections of quinolinic acid does not cause chorea in rats (Harper, 1991). It remains remarkable that the introduction of the expanded version of the polyglutamine-containing domain of htt protein into transgenic mice has succeeded in reproducing not only features of the movement disorder, but also other aspects of the complex HD phenotype.

Two further lines of transgenic mice are required to determine the extent to which the R6 mice represent a model of HD. First, mice transgenic for the entire HD gene carrying repeat expansions of a comparable size must be generated. The large size of the HD gene necessitates that the construct be introduced in the form of a YAC clone (experiments in progress). An identical phenotype would indicate that the remainder of the htt protein is superfluous to the course of the disease, and any differences would aid in the dissection of the protein into functional domains. Second, mice transgenic for the nonexpanded CAG repeat version of the R6 lines have not been described in this paper. The original purpose of the R6 transgenes was to study repeat stability and, consequently, the nonexpanded controls were not generated in parallel. However, it is important to characterize such mice, to rule out the unlikely scenario that the phenotype observed is the result of a novel peptide. Three founders have now been established that contain the SacI-EcoRI fragment with a (CAG)₁₈ tract: Hdex/6, Hdex/27, and Hdex/28. F1 mice derived from the Hdex/6 founder are currently 20 weeks, and the mice show no signs of a neurological phenotype or weight loss. These

mice are twice as old as the R6/2 mice at the onset of the phenotype. Quantitative RNA analysis shows the Hdex/6 transgene to be expressed at levels comparable to that in the R6/2 and R6/5 lines; however, it is not possible to use the 1C2 antibody to detect the Hdex/6 transgene protein as this is specific to polyglutamine expansions. The Hdex lines will be bred to homozygosity and the mice observed over the course of at least one year.

This work raises the intriguing possibility that exon 1 of the HD gene carrying highly expanded repeats is sufficient to generate a transgenic model of HD. The mutation is predicted to operate by conferring a gain of function to the mutated protein to which some cells are particularly sensitive. The cell-selective toxicity may be afforded by differing compartmentalization of the polyglutamine-carrying proteins or by the specificity of their intermolecular interactions. In order that the small R6 transgene could initiate a chain of molecular events comparable to those involving the entire htt protein, it would be necessary to predict that the transgene occupies the same subcellular localization. It has not been possible to make this comparison as our attempts at immunohistochemistry with the 1C2 antibody have been consistently unsuccessful, and in addition, the subcellular localization of htt remains to some extent controversial. If the selectivity of the cell death arises through the interacting proteins, the polyglutamine-containing domain of the htt protein must be sufficient to convey this specificity. There may be some evidence to suggest that this could be the case, arising from the isolation of HAP1 (huntingtin associated protein 1) (Li et al., 1995). HAP1 binds to htt containing a polyglutamine of 21 residues, and the association is enhanced by increasing lengths of the glutamine repeat. There was no binding to atrophin-1 (the mutant protein in DRPLA) also containing 21 glutamines.

It is impossible to predict the accuracy with which transgenic mouse lines will model a corresponding human disease. The R6 transgenes display many characteristics of HD, and had this phenotype arisen in mice transgenic for the entire mutant protein, the model would have needed little justification. It is clearly possible that the polyglutamine-containing domain may be the only part of the htt protein involved in the disease process. The R6 transgenic mice already provide a valuable resource for uncovering the molecular pathology of HD and may present a target for the testing of potential therapeutic interventions.

Experimental Procedures

Genotyping

DNA was prepared from tail biopsy and Southern blots and hybridizations were as described (Monaco et al., 1985). CAG repeats were sized by PCR using FAM-labeled primer 31329 (ATGAAGGCCTTC GAGTCCCTCAAGTCCTTC) and primer 33934 (GGCGGCTGAG GAAGCTGAGGA) in AM buffer (67 mM Tris-HCl [pH 8.8], 16.6 mM NH₄SO₄, 2.0 mM MgCl₂, 0.17 mg/ml BSA, 10 mM 2-mercaptoethanol), 10% DMSO, 200 μM dNTPs, 8 ng/μl primers with 0.5 U/μl Taq polymerase (Cetus). Cycling conditions were 90" @ 94°C, 25 × (30" @ 94°C, 30" @ 65°C, 90" @ 72°C), 10" @ 72°C. PCR products were sized using an ABI sequencer and the Genescan and Genotyper software packages. The size of the CAG repeat was 85 bp less than the size of the PCR product.

RNA Analysis

Northern blots were prepared by standard methods and hybridized as described (Monaco et al., 1985). RNA was reverse transcribed (14 U/μl MMTV RTase, BRL) in 50 mM KCl, 10 mM Tris-HCl (pH 9.0), 0.1% Triton X-100, 6.5 mM MgCl₂, 10 mM DTT, 1 mM dNTPs, 10 ng/μl random hexamers with 0.35 U/μl RNasin (Promega) at 10' @ 23°C and then 40' @ 37°C. Primers for specific transgene RNA detection were 33935 (CGGCTGAGGCAGCAGCGGCTGT) and 35093 (GCAGCAGCAGCAGCAACAGCCGCCACCGCC). PCR was in AM buffer, 10% DMSO, 200 μM dNTPs, 10 ng/μl primer with 0.5 U/μl Taq polymerase (Cetus). Cycling conditions were 90" @ 94°C, 34 × (30" @ 94°C, 30" @ 68°C, 90" @ 72°C), 10' @ 72°C.

Protein Analysis

Frozen tissue was homogenized in 50–100 μl 50 mM Tris (pH 8.0), 150 mM NaCl, 1% NP-40, 0.5% Deoxycholate, 0.1% SDS, and 1 mM 2-mercaptoethanol with 1 mM PMSF, 0.5 mM DTT, 25 mM benzamide and leupeptin, pepstatin and chymostatin each at 200 ng/ml. Homogenates were sonicated on ice 10–20 s, spun at high speed at 4°C, and the supernatant transferred to a fresh tube. Protein was quantified by the Bradford assay when in sufficient quantity. Approximately 50 μg of protein was loaded per track onto 6% or 10% SDS-PAGE gels. Kaleidoscope prestained standards were used as size markers (Biorad). Fibrinogen (Sigma) was added as a size marker of 330 kDa (Jou and Myers, 1995). Proteins were transferred to PVDF membranes (Biorad) that were blocked at 4°C overnight in PBS with 5% nonfat dry milk and 2% fetal calf serum. Immunoprobings with antibody 1C2 was at a 1:2000 dilution in PBS with 0.5% nonfat dry milk for 1 hr at RT. Washes were in PBS containing 1% NP-40 and 1% fetal calf serum. Secondary antibody probing and detection was by use of the ECL kit (Amersham).

Histopathology

Brains from nine R6/2 transgenes and nine nontransgenic littermates were analyzed for neuropathological change. A 1:3 series of sections was stained for Nissl substance with thionin, or processed free floating for the immunocytochemical localization of the glial marker, glial fibrillary acidic protein (GFAP), or the macrophage/microglial marker F4/80. Nuclear cells groups within the mouse brain were verified by reference to Sidman, Angevine, and Taber-Pierce (Sidman et al., 1971).

Acknowledgments

This paper is dedicated to the memory of Dennis Shea. The authors wish to thank Nancy Wexler and Anne Young for helpful discussions regarding the symptoms and progression of HD. We also thank Carl Hobbs for preliminary histopathology and Yuh-Shan Jou and Rick Myers for making their αHD1 antibody available. This work was supported by grants from the Medical Research Council, the Hereditary Disease Foundation (in the form of an award donated by Harry Liebermann), and the Special Trustees of Guy's Hospital.

Received July 25, 1996; revised September 10, 1996.

References

- Burright, E.N., Clark, H.B., Servadio, A., Matilla, T., Feddersen, R.M., Yunis, W.S., Duvick, L.A., Zoghbi, H.Y., and Orr, H.T. (1995). SCA1 transgenic mice: a model for neurodegeneration caused by an expanded CAG trinucleotide repeat. *Cell* 82, 937–948.
- de la Monte, S.M., Vonsattel, J.-P., and Richardson, E.P. (1988). Morphometric demonstration of atrophic changes in the cerebral cortex, white matter and neostriatum in Huntington's disease. *J. Neuropath. Exp. Neurol.* 47, 516–525.
- DiFiglia, M., Sapp, E., Chase, K., Schwarz, C., Meloni, A., Young, C., Martin, E., Vonsattel, J.-P., Carraway, R., Reeves, S.A., Boyce, F.M., and Aronin, N. (1995). Huntingtin is a cytoplasmic protein associated with vesicles in human and rat brain neurons. *Neuron* 14, 1075–1081.
- Durr, A., Stevanin, G., Cancel, G., Duyckaerts, C., Abbas, N., Didierjean, O., Chneiweiss, H., Benomar, A., Lyon-Caen, O., Julien, J., et al. (1996). Spinocerebellar ataxia 3 and Machado-Joseph disease: clinical, molecular and neuropathological features. *Ann. Neurol.* 39, 490–499.
- Harper, P.S. (1991). Huntington's Disease (London: W.B. Saunders).
- Hedreen, J.C., and Folstein, S.E. (1995). Early loss of early neostriatal neurons in Huntington's disease. *J. Neuropath. Exp. Neurol.* 54, 105–120.
- Huntington's Disease Collaborative Research Group (1993). A novel gene containing a trinucleotide repeat that is unstable on Huntington's disease chromosomes. *Cell* 72, 971–983.
- Ikeda, H., Yamaguchi, M., Sugai, S., Aze, Y., Narumiya, S., and Kakizuka, A. (1996). Expanded polyglutamine in the Machado-Joseph disease protein induces cell death in vitro and in vivo. *Nature Genet.* 13, 196–202.
- Jou, Y.-S., and Myers, R.M. (1995). Evidence from antibody studies that the CAG repeat in the Huntington disease gene is expressed in the protein. *Hum. Mol. Genet.* 4, 465–469.
- Kawaguchi, Y., Okamoto, T., Taniwaki, M., Aizawa, M., Inoue, M., Katayama, S., Kawakami, H., Nakamura, S., Nishimura, M., Akiguchi, I., Kimura, J., Narumiya, S., and Kakizuka, A. (1994). CAG expansions in a novel gene for Machado-Joseph disease at chromosome 14q32.1. *Nature Genet.* 8, 221–228.
- Kennedy, W.R., Alter, M., and Sung, J.H. (1968). Progressive proximal spinal and bulbar atrophy of late onset. A sex linked recessive trait. *Neurology* 18, 671–680.
- Koide, R., Ikeuchi, T., Onodera, O., Tanaka, H., Igarashi, S., Endo, K., Takahashi, H., Kondo, R., Ishikawa, A., Hayashi, T., et al. (1994). Unstable expansion of CAG repeat in hereditary dentatorubral-pallidolysian atrophy (DRPLA). *Nature Genet.* 6, 9–13.
- La Spada, A.R., Wilson, E.M., Lubahn, D.B., Harding, A.E., and Fischbeck, K.H. (1991). Androgen receptor gene mutations in X-linked spinal and bulbar muscular atrophy. *Nature* 352, 77–79.
- Lauder, I.M., Martin, W.B., Gordon, E.D., Lawson, D.D., Campbell, R.S.F., and Watrach, A.M. (1954). A survey of canine distemper. *Veterinary Record* 66, 607–611.
- Li, X.-J., Li, S.-H., Sharp, A.H., Nucifora, F.C., Schilling, G., Lanahan, A., Worley, P., Snyder, S.H., and Ross, C.A. (1995). A huntingtin-associated protein enriched in brain with implications for pathology. *Nature* 378, 398–402.
- Lyon, M.F., and Searle, A.G. (1990). Genetic Variants and Strains of the Laboratory Mouse (Oxford: Oxford University Press).
- Monaco, A.P., Bertelson, C.J., Middlesworth, W., Colletti, C.-A., Aldridge, J., Fischbeck, K.H., Bartlett, R., Pericak-Vance, M.A., Roses, A.D., and Kunkel, L.M. (1985). Detection of deletions spanning the Duchenne muscular dystrophy locus using a tightly linked DNA probe. *Nature* 316, 842–845.
- Myers, R.H., Vonsattel, J.P., Stevens, T.J., Cupples, L.A., Richardson, E.P., Martin, J.B., and Bird, E.D. (1988). Clinical and neuropathological assessment of severity in Huntington's disease. *Neurology* 38, 341–347.
- Myers, R.H., Vonsattel, J.P., Paskevich, P.A., Kiely, D.K., Stevens, T.J., Cupples, L.A., Richardson, E.P., and Bird, E.D. (1991). Decreased neuronal and increased oligodendroglial densities in Huntington's disease caudate nucleus. *J. Neuropath. Exp. Neurol.* 50, 729–742.
- Orr, H.T., Chung, M., Banfi, S., Kwiatkowski, T.J., Jr., Servadio, A., Beaudet, A.L., McCall, A.E., Duvick, L.A., Ranum, L.P.W., and Zoghbi, H.Y. (1993). Expansion of an unstable trinucleotide CAG repeat in spinocerebellar ataxia type 1. *Nature Genet.* 4, 221–226.
- Sanberg, P.R., Fibiger, H.C., and Mark, R.F. (1981). Body weight and dietary factors on Huntington's disease patients compared with matched controls. *Med. J. Aust.* 1, 407–409.
- Servadio, A., Koshy, B., Armstrong, D., Antalffy, B., Orr, H.T., and Zoghbi, H.Y. (1995). Expression analysis of the ataxin-1 protein in tissues from normal and spinocerebellar ataxia type 1 individuals. *Nature Genet.* 10, 94–98.
- Sidman, R.L., Angevine, J.B.J., and Taber-Pierce, E. (1971). Atlas of the Mouse Brain and Spinal Cord (Cambridge, Massachusetts: Harvard University Press).

- Strong, T.V., Tagle, D.A., Valdes, J.M., Elmer, L.W., Boehm, K., Swaroop, M., Kaatz, K.W., Collins, F.S., and Albin, R.L. (1993). Widespread expression of the human and rat Huntington's disease gene in brain and nonneuronal tissues. *Nature Genet.* 5, 259-263.
- Takahashi, H., Ohama, E., Naito, H., Takeda, S., Nakashima, S., Makifuchi, T., and Ikuta, F. (1988). Hereditary dentatorubral-pallidoluysian atrophy: clinical and pathological variants in a family. *Neurology* 38, 1065-1070.
- Telenius, H., Kremer, H.P.H., Theilmann, J., Andrew, S.E., Almquist, E., Anvret, M., Greenberg, C., Greenberg, J., Lucotte, G., Squitieri, F., Starr, E., Goldberg, Y.P., and Hayden, M.R. (1993). Molecular analysis of juvenile Huntington disease: the major influence on (CAG)*n* repeat length is the sex of the affected parent. *Hum. Mol. Genet.* 2, 1535-1540.
- Trottier, Y., Devys, D., Imbert, G., Sandou, F., An, I., Lutz, Y., Weber, C., Agid, Y., Hirsch, E.C., and Mandel, J.-L. (1995a). Cellular localisation of the Huntington's disease protein and discrimination of the normal and mutated forms. *Nature Genet.* 10, 104-110.
- Trottier, Y., Lutz, Y., Stevanin, G., Imbert, G., Devys, D., Cancel, G., Sandou, F., Weber, C., David, G., Tora, L., et al. (1995b). Polyglutamine expansion as a pathological epitope in Huntington's disease and four dominant cerebellar ataxias. *Nature* 378, 403-406.
- Vonsattel, J.-P., Myers, R.H., Stevens, T.J., Ferrante, R.J., Bird, E.D., and Richardson, E.P. (1985). Neuropathological classification of Huntington's disease. *J. Neuropath. Exp. Neurol.* 44, 559-577.
- Wheeler, J.S., Sax, D.S., Krane, R.J., and Siroky, M.B. (1985). Vesico-urethral function in Huntington's chorea. *Brit. J. Urol.* 57, 63-66.
- Yazawa, I., Nukina, N., Hashida, H., Goto, J., Yamada, M., and Kanazawa, I. (1995). Abnormal gene product identified in hereditary dentatorubral-pallidoluysian atrophy (DRPLA) brain. *Nature Genet.* 10, 99-103.
- Zoghbi, H.Y. (1993). In *Current Neurology*, S.H. Appel, ed. (St. Louis, MO: Mosby-Year Book), pp. 87-110.

EXHIBIT 7

Expression of a truncated tau protein induces oxidative stress in a rodent model of tauopathy

Martin Cente,^{1,2,*} Peter Filipcik,^{1,2,*} Miroslava Pevalova,^{1,2} and Michal Novak¹

¹Institute of Neuroimmunology, Slovak Academy of Sciences, Centre of Excellence, Dubravská cesta 9, 845 10 Bratislava, Slovakia

²Axon Neuroscience GmbH, Rennweg 95b, A-1030 Vienna, Austria

Keywords: Alzheimer's disease, neurodegeneration, oxidative stress, transgenic rat

Abstract

Truncation of tau protein and oxidative stress have been implicated as important pathogenetic events in tauopathies including Alzheimer's disease (AD). We have generated a transgenic rat model that expresses a human truncated tau protein analogous to a variant form derived from sporadic AD. We employed this model to investigate the relationship between tau protein truncation and oxidative stress. We have found that rat cortical neurons (derived from transgenic animals) that had been cultured *in vitro* for 16 days showed an increased accumulation of reactive oxygen species (up to 1.4-fold increase; $P < 0.01$) when compared to neurons derived from nontransgenic control animals. Transgene-expressing neurons treated with inducers of oxidative stress, such as glucose oxidase (GO) and buthionine sulfoximine (BSO), displayed dramatically reduced survival (31.4 ± 3.3 and $24.9 \pm 3.6\%$, respectively; both $P < 0.001$) compared to neurons from control animals ($79.9 \pm 7.1\%$, survival following treatment with GO and to $98.2 \pm 3.8\%$, survival following treatment with BSO). The number of mitochondria in processes of neurons from transgenic animals was decreased by about one-third from that present in neurons from control animals. The results reveal that expression of a human truncated variant form of tau protein leads to the accumulation of reactive oxygen species and sensitizes rat cortical neurons to cell death induced by oxidative stress. This indicates that truncation of tau may precede oxidative stress in the pathogenesis of neurodegenerative diseases such as AD and other tauopathies. These findings may have implications for therapeutic strategies aiming at prevention of neurofibrillary degeneration and cognitive decline, and identify potential new targets for drug development.

Introduction

Neurodegenerative tauopathies including Alzheimer's disease (AD) are major causes of memory impairment and cognitive decline in adulthood. Despite the consistent presence of senile plaques and neurofibrillary tangles in the brain of AD patients, only paired helical filaments are known to correlate with disease progression (Braak & Braak, 1991). Therefore, tau protein and its post-translationally modified forms, which represent the main component of paired helical filaments, have drawn intense investigation. The post-translational modifications of tau protein such as phosphorylation (Grundke-Iqbal *et al.*, 1986; Iqbal *et al.*, 2005), glycation (Yan *et al.*, 1994), glycosylation (Wang *et al.*, 1996), ubiquitination (Bondareff *et al.*, 1990) and truncation (Novak *et al.*, 1993; Garcia-Sierra *et al.*, 2003) have been implicated in the pathogenesis of AD and related tauopathies for many years.

The sporadic form of AD is defined as a multifactorial disease influenced by risk factors such as hypertension, diabetes and hypercholesterolemia but also environmental stressors including oxidative stress. There is strong evidence in the recent literature that oxidative stress may be a major cause of neurodegeneration (Perry *et al.*, 2002; Aliev *et al.*, 2004; Moreira *et al.*, 2005). According to several epidemiological studies, a high dietary intake of vitamin C and vitamin E may lower the risk of AD (Engelhart *et al.*, 2002; Morris *et al.*, 2002). However, other studies have failed to detect any beneficial effects of antioxidant

therapies, and have instead concluded that the intake of carotenes, vitamin C and vitamin E was not associated with reduced incidence of AD (Luchsinger *et al.*, 2003; Laurin *et al.*, 2004). Moreover, vitamin E has no benefit in patients with mild cognitive impairment (Petersen *et al.*, 2005). Furthermore, oxidative stress is also associated with many different diseases, such as cancer (Toyokuni, 1998), autoimmune disorders (Gilgun-Sherki *et al.*, 2004), diabetes (Matteucci *et al.*, 2004), atherosclerosis and stroke (Madamanchi *et al.*, 2005), supporting the hypothesis that oxidative stress is a normal by-product of ageing rather than the principal cause of neurodegeneration associated with AD.

As truncation of tau protein has emerged as one of the critical post-translational modifications in AD (Novak *et al.*, 1993), we examined the effect of expressing a truncated tau protein on the susceptibility of rat cortical neurons to oxidative stress. The data presented below demonstrate that expression of a truncated tau protein leads to elevated steady-state levels of reactive oxygen species in cultured rat neurons *in vitro*. Cells expressing the truncated tau protein also display an elevated susceptibility to oxidative stress-induced cell death. Taken together, these results suggest that it may be necessary to reassess the sequence of events in AD pathogenesis, especially to consider whether expression of truncated variants of tau protein in the brains of AD patients may lead to a higher susceptibility of neurons to oxidative stress and consequently increase their vulnerability to external stress.

Materials and methods

Dulbecco's modified Eagle medium, fetal bovine serum, neurobasal medium, B27 and N2 supplements were purchased from Gibco

Correspondence: Dr Michal Novak, as above.
E-mail: Michal.Novak@savba.sk

*P.F. and M.C. contributed equally to this study.

Received 11 May 2006, accepted 6 June 2006

(Paisley, Scotland, UK). Papain, sodium pyruvate, poly D-lysine, boric acid, L-glutamine, gentamicin, glucose oxidase (GO) and buthionine sulfoximine (BSO) were purchased from Sigma-Aldrich Chemie (Steinheim, Germany). Accutase and L-15 medium were purchased from PAA Laboratory (Pasching, Austria) and basic fibroblast growth factor (bFGF) from Serva (Heidelberg, Germany). Neurons were cultured in plastic 96-well plates (Becton-Dickinson Biosciences, UK). Culture media consisted of B27-supplemented neurobasal medium containing 0.5 mM L-glutamine and gentamicin (50 µg/mL). HT-7 and anti-βIII tubulin antibodies were purchased from Pierce (Rockford, IL, USA). For determination of free radicals 2',7'-dichlorodifluorofluorescein diacetate (DCF-DA) was purchased from Molecular Probes Inc. (Eugene, OR, USA). Sodium chloride, calcium chloride, magnesium chloride and HEPES were purchased from Sigma-Aldrich. Cell viability was measured using CellTiter-Glo assay from Promega Co. (Madison, WI, USA) and ToxiLight nondestructive cytotoxicity assay from Cambrex (Rockland, ME, USA).

Generation of transgenic (TG) rats expressing human truncated tau protein

The transgenic construct encoding the truncated tau protein was designed according to the sequence of tau protein expressed in paired helical filaments of human AD brain (Novak *et al.*, 1993). The transgenic rat expressing truncated human tau protein has been described elsewhere (Zilka *et al.*, 2006). Briefly, the transgene was prepared by ligation of a human cDNA encoding truncated tau protein into the mouse *Thy-1* gene immediately downstream of the brain-specific promoter and enhancer sequence. The ATG codon follows immediately after the BanI site at the end of the brain-specific enhancer. The original *Thy-1* gene sequence encoding exons II–IV, including the thymus enhancer sequence, was thereby replaced with the tau cDNA. A stop codon was included immediately before the internal Xho I site of the *Thy-1* gene. The cloned construct was amplified in bacteria, and plasmid DNA was extracted using EndoFree Plasmid Maxi Kit (Qiagen, Hilden, Germany). Transgenic DNA was linearized with EcoRI and subjected to electrophoresis in SeaPlaque GTG agarose gel (Cambrex, Rockland, ME, USA). The fragment encoding the recombinant human tau protein was excised from the gel and purified using QIAquick Gel Extraction Kit (Qiagen), and dissolved in microinjection buffer (10 mM Tris-HCl with 0.1 mM EDTA; pH 7.5). Transgenic rats were generated by pronuclear injection of 1-day-old rat embryos [spontaneously hypertensive rat strain (SHR)], which were reimplanted into pseudopregnant females (Wistar strain). Founder rats were double screened by PCR using *Thy-1* specific and tau-specific primers amplifying start and stop codon flanking sequences. The experiments were approved by "State Veterinary and Food Committee of Slovak Republic" (No. Ro-2064/05-221/3b), and by Ethic Committee of Institute of Neuroimmunology, Slovak Academy of Sciences. The animals were anaesthetized and killed according to ethical guidelines. The ether anaesthesia for postnatal animals and hypothermia for embryos were chosen with the effort to minimize pain and any suffering to the experimental animals.

Preparation of primary cortical neurons from transgenic and wild type (WT) rats

Cell cultures of cortical neurons were prepared under sterile conditions according to the modified method of Eide & McMurray (2005). Briefly, brains of anaesthetized rats (either 18-day-old embryos for

biochemical analysis or 10-day-old postnatal animals for immunocytochemistry) were dissected in L-15 medium. After removal of meninges, cortical tissue was isolated, minced into small pieces and treated with accutase or papain (2.5 U/mL) for 10 min at 37 °C. The enzymatic treatment was stopped with horse serum and suspension was gently centrifuged at 17 g for 3 min. The supernatant was aspirated and replaced with 5 mL of culture medium. The cells were plated onto poly D-lysine-coated 96-well plates at densities of 90 000, 70 000 and 25 000 cells/cm² for determination of cell survival, biochemical analysis and immunofluorescence, respectively. The medium for postnatal cultures (NBA) was supplemented with B27 (2%) and bFGF (2.5 ng/mL). The cells were maintained in a humidified atmosphere of 5% CO₂ and 95% air at 37 °C and medium was replaced every 3–4 days.

Western blot analysis

Neurons were lysed with Hunt buffer (20 mM Tris, 100 mM NaCl, 1 mM EDTA, 0.5% NP-40; pH 8.0), containing 1 mM DTT and a mix of protease inhibitors (Complete; Roche, Mannheim, Germany). Proteins in cell lysates were separated by 10% sodium dodecyl sulphate-polyacrylamide gel electrophoresis and transferred to nitrocellulose membranes. The membranes were incubated with pan-tau primary antibody DC25, which detects all endogenous and human truncated isoforms of tau proteins, then with goat antimouse HRP-conjugated secondary antibody. Labelled second antibody was visualized with a chemiluminescence detection system (ECL, Amersham). Quantification and analysis of chemiluminescence was performed with a computer-linked LAS-3000 Bio-Imaging Analyser System (Fuji film) using the software program Aida-Image Analyser (Raytest, Isotopenmessgeräte GmbH, Staubenhard, Germany) according to a previously published method (Csokova *et al.*, 2004).

Vital mitochondrial staining and immunofluorescence

Neurons cultured on glass cover slips were incubated with 125 nM MitoTracker Red 580 for 30 min (Invitrogen, Karlsruhe, Germany), washed with phosphate-buffered saline and fixed in microtubule-stabilizing PHEM buffer (60 mM PIPES, 25 mM HEPES, 10 mM EGTA, 2 mM MgCl₂; pH 6.9) including 3% paraformaldehyde for 10 min at 37 °C. Subsequently, neurons were permeabilized with 0.1% Triton X-100 in phosphate-buffered saline for 2 min. The indirect immunofluorescent staining with antihuman tau-specific monoclonal antibody HT-7 was carried out in order to visualize neurons expressing truncated tau protein. Non-transgenic neurons were stained with anti-βIII tubulin. The incubation with primary antibodies was followed by incubation with secondary, FITC-labelled, antimouse polyclonal antibody. Photomicrographs were taken using a cooled CCD camera (Visitron) and the number of mitochondria present per unit length of neuronal process was determined using the public domain NIH Image program (developed at the US National Institutes of Health and available on the Internet at <http://rsb.info.nih.gov/nih-image>).

Determination of free radical levels and survival of primary cortical neurons

Quantification of cellular radical levels was performed using a fluorescent microplate reader according to the modified method of Wang & Joseph (1999). Primary neurons were cultured on 96-well plates in B27-supplemented neurobasal medium. One day before each

experiment, the culture medium was replaced with antioxidant-free N2-supplemented neurobasal medium. After 24 h, the cells were incubated with 50 μ M DCF-DA in 5% CO₂–95% air at 37 °C for 30 min. Subsequently, medium containing fluorescent dye was removed and the cells were washed and incubated in Ringer–HEPES buffer (in mM: NaCl, 150; KCl, 5.2; CaCl₂, 2.2; MgCl₂, 0.2; NaHCO₃, 6; glucose, 2.8; and HEPES, 5; pH 7.4) for 30 min. Fluorescence was measured and recorded using a Fluoroskan Ascent FL reader (Labsystems, Helsinki, Finland) at excitation and emission wavelengths of 485 and 538 nm, respectively.

Neuron survival was determined using CellTiter-Glo assay, which quantifies ATP levels in viable cells. The assay was designed for quantitative analysis of viability of rat primary cerebrocortical neurons and was used according to manufacturer's protocol (<http://www.promega.com/tbs/>). Treatment with oxidative stressors was initiated before and after elevation of truncated tau protein expression. The culture medium was replaced with N2-supplemented neurobasal medium 24 h before addition of stressors. GO and BSO were used at indicated concentrations for 24 and 60 h, respectively.

Each experimental group was represented by reactive oxygen species and ATP data from at least six wells ($n = 6$). The experiments with GO and BSO were repeated at least three times. Statistical differences were evaluated with analysis of variance (two-way ANOVA; $P < 0.05$ considered significant).

Results

The expression of truncated human tau protein and endogenous rat tau protein in transgenic rat cortical neurons was detected by immunoblotting using antitau monoclonal antibody DC25, which recognizes both the human and rat isoforms. Expression of truncated human recombinant tau protein is directed by the *Thy-1* promoter, which is active in postmitotic neurons. We therefore anticipated that expression levels of this protein would gradually increase during neuronal maturation *in vitro*. Consistent with this prediction, recombinant tau protein was detected in primary cultures of differentiated neurons after 10 days *in vitro* (DIV). Expression levels gradually increased until maximal levels were reached at 14–16 DIV, as shown in Fig. 1. Densitometric quantification revealed that the recombinant tau protein

was expressed at levels ~20–50% of that of endogenous rat tau protein at 14 DIV. Subsequent experiments were therefore performed using neuronal cultures older than 14 days.

Next we performed immunocytochemical analysis of transgenic and control rat cortical neurons using the human tau-specific monoclonal antibody HT-7 and a monoclonal antibody against β III tubulin. The HT-7 antibody selectively recognizes human tau protein, and therefore no immunofluorescence signal is observed in wild-type neurons (not shown). Anti- β III tubulin antibody was therefore used to stain neural processes in nontransgenic neurons. Cultures were also counterstained with MitoTracker, which selectively visualizes mitochondria. As the results in Fig. 2 reveal, there was a remarkable reduction in the number of mitochondria present in the processes of neurons expressing the truncated recombinant tau protein (Fig. 2B) compared to those present in identical cultures derived from control neurons (Fig. 2A). The number of mitochondria observed per unit length (100 μ m) of neuronal process in wild-type neurons (Fig. 2A) was 1.5-fold greater than that found per unit length of neuronal process in neurons expressing the truncated recombinant tau (Fig. 2B). The results in Fig. 2 led us to investigate whether the differences in mitochondrial distribution associated with expression of the truncated recombinant tau protein were also associated with impaired oxidative status in transgenic neurons, which could be related to enhanced susceptibility to stress-induced cell death. The survival of neurons was determined by measurement of intracellular ATP levels and adenylate kinase activity in culture medium. We did not observe any significant differences in viability between transgenic and wild-type neurons before or after the onset of transgene expression (data not shown). However, analysis revealed that 16-day-old cultures derived from rats expressing the recombinant tau protein harboured significantly elevated levels of free radicals compared to identical neuronal cultures from control rats. Our results indicated that the free radical levels in the transgene-expressing cultures were $127.2 \pm 2.5\%$ of those detected in control cell cultures ($P < 0.001$). The data were generated from five independent experiments, each performed in octuplicate ($n = 8$).

As increased production of reactive oxygen species is an important underlying cause of neuronal injury leading to neuronal death we tested the hypothesis that transgene-expressing neurons are hypersusceptible to stress-induced cell death. Neuronal cultures from control

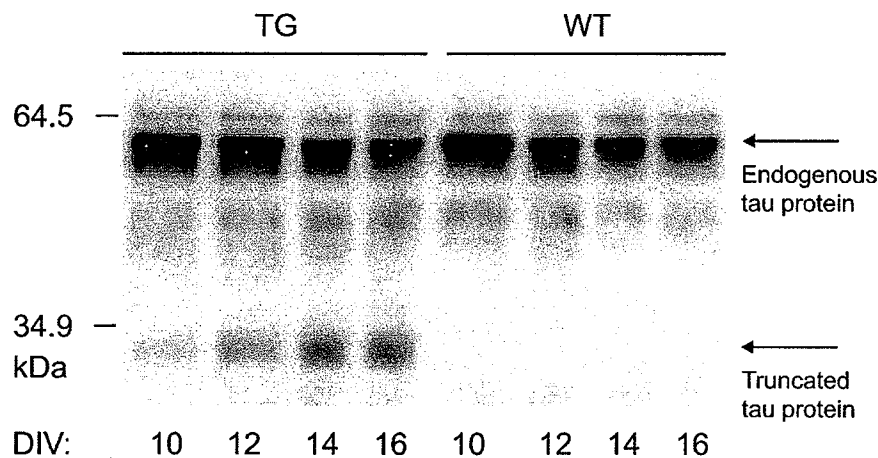


FIG. 1. The expression of truncated tau protein in neurons derived from 18-day-old rat embryos. Western blot analysis was performed on neuronal cultures from rat embryos expressing truncated human recombinant tau (TG) and from control nontransgenic rat embryos (WT), cultured *in vitro* for the indicated number of DIV as described in the Materials and Methods section, using DC25 pan-tau antibody. The arrows reveal the electrophoretic mobility of the endogenous and transgene-encoded tau proteins. The mobility and size (in kDa) of molecular weight standards is also indicated. Protein samples from control WT neurons were collected at the same time points in culture 10–16 DIV and analysed simultaneously.

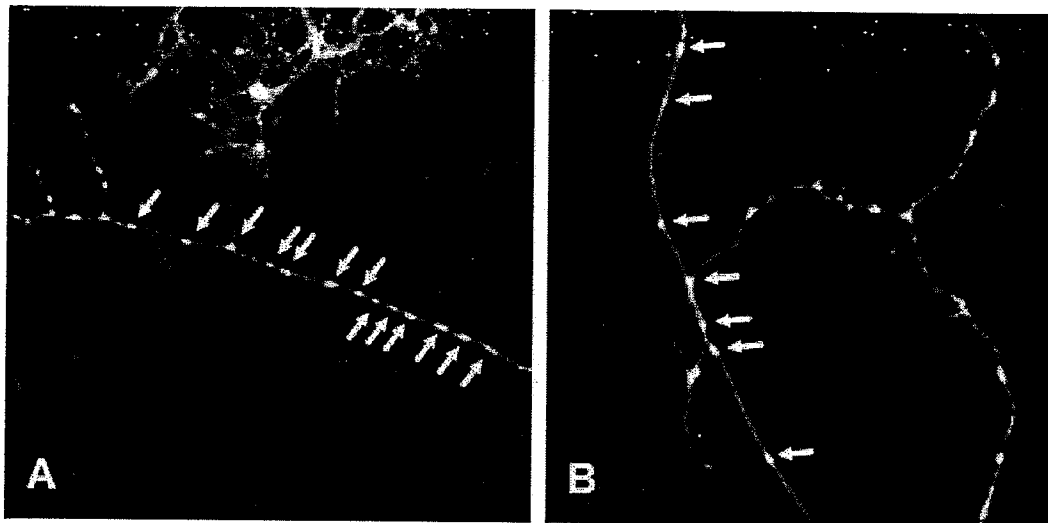


Fig. 2. Distribution of mitochondria in the processes of rat cortical neurons expressing human truncated tau protein. Mitochondria were visualized with vital staining using MitoTracker Red (see arrows). Counterstaining was performed with (A, control neurons) anti- β III tubulin antibody and with (B, transgenic neurons) HT-7, human tau-specific antibody. The number of mitochondria per unit length (100 μ m) of neural process was determined. More than thirty neurites of transgenic and control neurons were randomly selected and analysed at a magnification of 1000 \times .

and transgenic rats were briefly incubated with GO for induction of extracellular stress and BSO in order to block synthesis of glutathione, the main antioxidant of the cells. These treatments were followed by determinations of cell viability monitored by adenylate kinase activity in culture media and measurement of ATP levels in cell lysates. Because these two parameters inversely correlated (data not shown), we subsequently evaluated ATP levels to determine cell viability. We found that neurons expressing human truncated tau protein were significantly more susceptible to oxidative stress-induced death than were control neurons. At all concentrations tested, neurons expressing recombinant truncated tau protein were significantly more susceptible to GO-induced cell death (survival reduction to $31.4 \pm 3.3\%$) than were identical cultures of neurons from WT rats (survival $79.9 \pm 7.1\%$; Fig. 3A). Similarly, we observed that neurons expressing the recombinant tau protein were more susceptible to BSO-induced cell death ($24.9 \pm 3.6\%$) than were WT neurons ($98.2 \pm 3.8\%$; Fig. 3B). Additional experiments revealed that transgene-expressing neurons were also hypersusceptible to cell death induced by exposure to the stress inducers Sin-1 and glutamic acid (data not shown). The enhanced susceptibility to stress-induced cell death observed in transgenic neurons was very consistent and independent of the type of stressor used. These data revealed a strong sensitizing effect of human truncated tau protein on cortical neurons. This finding may have implications for the pathogenesis of AD in relation to the role of oxidative stress, which can accelerate the toxic effect of tau protein gained via truncation, a frequent post-translational modification observed in sporadic cases of AD.

Discussion

Despite extensive investigation of AD pathogenesis, the initial molecular events associated with this disorder remain incompletely understood. Truncation of tau protein was described as an early event in AD, and is believed to occur prior to formation of neurofibrillary tangles (Novak *et al.*, 1993, 1999; Novak, 1994). Furthermore, it is well documented that activation of specific proteases (Horowitz *et al.*, 2004) or specific chemical modifications (Watanabe *et al.*, 2004) may

give rise to truncated tau species. Conversely, environmental factors such as oxidative stress have been frequently implicated in the pathogenesis of AD. They have often been seen as critical for induction of neurodegeneration (Aliev *et al.*, 2004; Moreira *et al.*, 2005). However, the important question of the chronological primacy of oxidative stress in the context of truncated tau protein has not been addressed experimentally to date. In order to address this issue we examined the effect of expression of a truncated recombinant human tau protein on the susceptibility of primary rat neurons to oxidative stress-induced cell death.

As neuronal loss is considered an important feature of neurodegeneration, we have tested the influence of truncated tau expression on the viability of cortical neurons. No difference in neuron survival of truncated tau-expressing neurons was observed compared to wild-type controls (data not shown). However, this is not surprising when we take into consideration that the loss of neuronal connectivity is more important in the early stage of neurodegeneration than is cell death (Selkoe, 2002). The incidence and accumulation of neurofibrillary tangles correlates with disease progression; however, according to published data, neuronal loss does not correlate with tangle formation (Morsch *et al.*, 1999; Kril *et al.*, 2002).

Over the past years, experimental evidence on interaction between oxidative stress and tau pathology has arisen, surprisingly suggesting a protective function of neurofibrillary tangles (Nunomura *et al.*, 2002). According to these authors neurons bearing neurofibrillary tangles showed reduced oxidative damage compared with neurons free of tau pathologic structures. However, this phenomenon is most probably related to the deep functional and metabolic impairment of disconnected tangle-bearing neurons (Callahan & Coleman, 1995; Hatanpaa *et al.*, 1996; Chow *et al.*, 1998).

In our model, we found reduced numbers of mitochondria in transgenic neurons. This finding is in agreement with previously published data showing that tau protein can cause an inhibition of kinesin-dependent transport of peroxisomes, neurofilaments and Golgi-derived vesicles into neurites (Stamer *et al.*, 2002). Additionally, disturbed transport of mitochondria and endoplasmic reticulum to the cell periphery was also reported in transiently transfected neurons with

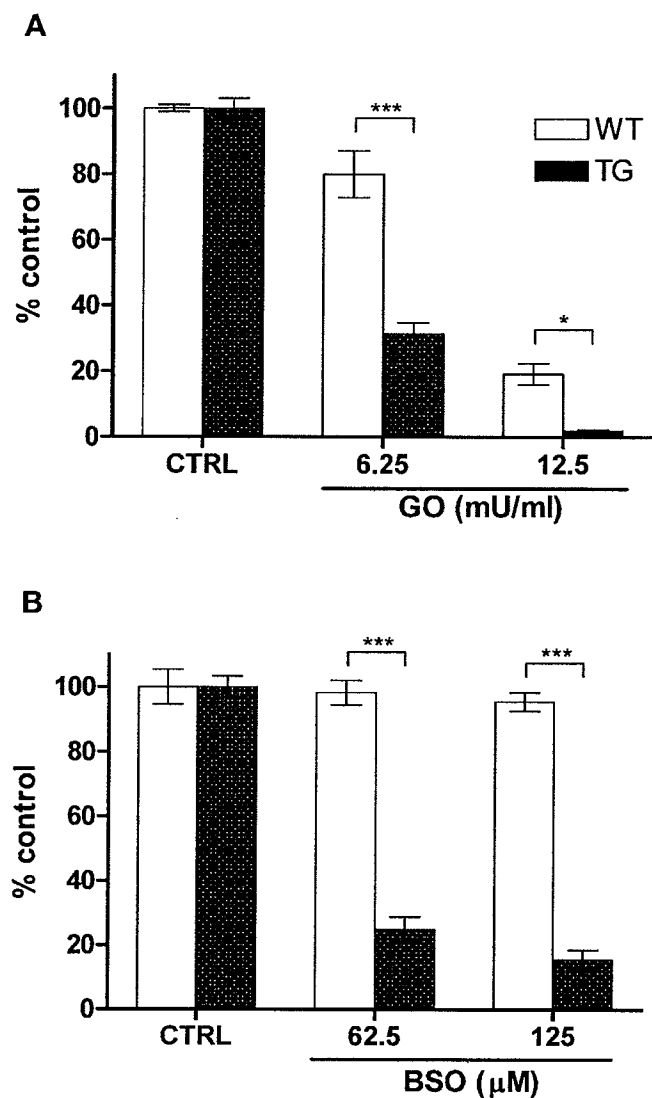


FIG. 3. The effect of oxidative stress on viability of control and transgenic rat cortical neurons. Embryonic neurons were cultured for 14 DIV and subsequently exposed to the indicated concentrations of BSO (B) or GO (A). Cell viability of treated neurons was determined (as described in the text) and is expressed as a percentage of the viability observed in nontreated neurons. Enhanced susceptibility of transgene-expressing neurons to stress was statistically significant ($P < 0.001$) at 62.5 μM of BSO and at 6.25 and 12.5 mU/mL of GO. Empty columns represent wild-type and filled columns transgenic neurons. Error bars show \pm SD; $n = 6$, $*P < 0.05$, $***P < 0.001$.

full length tau (Ebner *et al.*, 1998). The tau overexpression decreased the number of functional mitochondria in presynaptic terminals, leading to synaptic dysfunction of motor neurons (Chee *et al.*, 2005).

We have shown that expression of truncated human recombinant tau protein is associated with significantly increased levels of free radicals in cortical neurons *in vitro*. Such neurons are therefore more prone to additional external or internal insult, which can be followed by cell death. According to our observations, the truncated tau proteins strongly perturb mitochondrial distribution and increase accumulation of free radicals in transgenic neurons. We hypothesize that this mitochondrial interference is the underlying cause of the increased susceptibility to oxidative stress observed in neurons expressing the truncated recombinant tau protein. These results support the hypothesis that oxidative stress is a consequence or accompanying phenom-

enon rather than an inducer of the AD tau cascade. Furthermore, these findings suggest that the tau truncation cascade may represent a viable target for novel drugs with which to treat AD.

Acknowledgements

This work was partially supported by research grants: VEGA, No. 2/4126/26 and ESF project No. 13120200026.

Abbreviations

AD, Alzheimer's disease; bFGF, and basic fibroblast growth factor; BSO, buthionine sulfoximine; DCF-DA, 2',7'-dichlorodifluorofluorescein diacetate; DIV, days *in vitro*; GO, glucose oxidase; NFT, neurofibrillary tangles.

References

- Aliev, G., Smith, M.A., de la Torre, J.C. & Perry, G. (2004) Mitochondria as a primary target for vascular hypoperfusion and oxidative stress in Alzheimer's disease. *Mitochondrion*, **4**, 649–663.
- Bondareff, W., Wischik, C.M., Novak, M., Amos, W.B., Klug, A. & Roth, M. (1990) Molecular analysis of neurofibrillary degeneration in Alzheimer's disease. An immunohistochemical study. *Am. J. Pathol.*, **137**, 711–723.
- Braak, H. & Braak, E. (1991) Neuropathological staging of Alzheimer-related changes. *Acta Neuropathologica*, **82**, 239–259.
- Callahan, L.M. & Coleman, P.D. (1995) Neurons bearing neurofibrillary tangles are responsible for selected synaptic deficits in Alzheimer's disease. *Neurobiol. Aging*, **16**, 311–314.
- Chee, F.C., Mudher, A., Cuttle, M.F., Newman, T.A., MacKay, D., Lovestone, S. & Shepherd, D. (2005) Over-expression of tau results in defective synaptic transmission in *Drosophila* neuromuscular junctions. *Neurobiol. Dis.*, **20**, 918–928.
- Chow, N., Cox, C., Callahan, L.M., Weimer, J.M., Guo, L. & Coleman, P.D. (1998) Expression profiles of multiple genes in single neurons of Alzheimer's disease. *Proc. Natl Acad. Sci. USA*, **95**, 9620–9625.
- Csokova, N., Skrabana, R., Liebig, H.D., Mederlyova, A., Kontsek, P. & Novak, M. (2004) Rapid purification of truncated tau proteins: model approach to purification of functionally active fragments of disordered proteins, implication for neurodegenerative diseases. *Protein Expr. Purif.*, **35**, 366–372.
- Ebner, A., Godemann, R., Stamer, K., Illenberger, S., Trinczek, B. & Mandelkow, E. (1998) Overexpression of tau protein inhibits kinesin-dependent trafficking of vesicles, mitochondria, and endoplasmic reticulum: implications for Alzheimer's disease. *J. Cell. Biol.*, **143**, 777–794.
- Eide, L. & McMurray, C.T. (2005) Culture of adult mouse neurons. *Biotechniques*, **38**, 99–104.
- Engelhart, M.J., Geerlings, M.I., Ruitenber, A., van Swieten, J.C., Hofman, A., Witteman, J.C. & Breteler, M.M. (2002) Dietary intake of antioxidants and risk of Alzheimer disease. *JAMA*, **287**, 3223–3229.
- Garcia-Sierra, F., Ghoshal, N., Quinn, B., Berry, R.W. & Binder, L.I. (2003) Conformational changes and truncation of tau protein during tangle evolution in Alzheimer's disease. *J. Alzheimers Dis.*, **5**, 65–77.
- Gilgun-Sherki, Y., Melamed, E. & Offen, D. (2004) The role of oxidative stress in the pathogenesis of multiple sclerosis: the need for effective antioxidant therapy. *J. Neurol.*, **251**, 261–268.
- Grundke-Iqbal, I., Iqbal, K., Tung, Y.C., Quinlan, M., Wisniewski, H.M. & Binder, L.I. (1986) Abnormal phosphorylation of the microtubule-associated protein tau (tau) in Alzheimer cytoskeletal pathology. *Proc. Natl Acad. Sci. USA*, **83**, 4913–4917.
- Hatanpaa, K., Brady, D.R., Stoll, J., Rapoport, S.I. & Chandrasekaran, K. (1996) Neuronal activity and early neurofibrillary tangles in Alzheimer's disease. *Ann. Neurol.*, **40**, 411–420.
- Horowitz, P.M., Patterson, K.R., Guillozet-Bongaarts, A.L., Reynolds, M.R., Carroll, C.A., Weintraub, S.T., Bennett, D.A., Cryns, V.L., Berry, R.W. & Binder, L.I. (2004) Early N-terminal changes and caspase-6 cleavage of tau in Alzheimer's disease. *J. Neurosci.*, **24**, 7895–7902.
- Iqbal, K., Alonso Adel, C., Chen, S., Chohan, M.O., El-Akkad, E., Gong, C.X., Khatoon, S., Li, B., Liu, F., Rahman, A., Tanimukai, H. & Grundke-Iqbal, I. (2005) Tau pathology in Alzheimer disease and other tauopathies. *Biochim. Biophys. Acta*, **1739**, 198–210.

- Kril, J.J., Patel, S., Harding, A.J. & Halliday, G.M. (2002) Neuron loss from the hippocampus of Alzheimer's disease exceeds extracellular neurofibrillary tangle formation. *Acta Neuropathol.*, **103**, 370–376.
- Laurin, D., Masaki, K.H., Foley, D.J., White, L.R. & Launer, J.J. (2004) Midlife dietary intake of antioxidants and risk of late-life incident dementia: the Honolulu-Asia Aging Study. *Am. J. Epidemiol.*, **159**, 959–967.
- Luchsinger, J.A., Tang, M.X., Shea, S. & Mayeux, R. (2003) Antioxidant vitamin intake and risk of Alzheimer disease. *Arch. Neurol.*, **60**, 203–208.
- Madamanchi, N.R., Vendrov, A. & Runge, M.S. (2005) Oxidative stress and vascular disease. *Arterioscler. Thromb. Vasc. Biol.*, **25**, 29–38.
- Matteucci, E., Mavaldi, G., Fagnani, F., Evangelista, I. & Giampietro, O. (2004) Redox status and immune function in type I diabetes families. *Clin. Exp. Immunol.*, **136**, 549–554.
- Moreira, P.I., Smith, M.A., Zhu, X., Honda, K., Lee, H.G., Aliev, G. & Perry, G. (2005) Oxidative damage and Alzheimer's disease: are antioxidant therapies useful? *Drug News Perspect.*, **18**, 13–19.
- Morris, M.C., Evans, D.A., Bienias, J.L., Tangney, C.C., Bennett, D.A., Aggarwal, N., Wilson, R.S. & Scherr, P.A. (2002) Dietary intake of antioxidant nutrients and the risk of incident Alzheimer disease in a biracial community study. *JAMA*, **287**, 3230–3237.
- Morsch, R., Simon, W. & Coleman, P.D. (1999) Neurons may live for decades with neurofibrillary tangles. *J. Neuropathol. Exp. Neurol.*, **58**, 188–197.
- Novak, M. (1994) Truncated tau protein as a new marker for Alzheimer's disease. *Acta Virol.*, **38**, 173–189.
- Novak, M., Kabat, J. & Wischik, C.M. (1993) Molecular characterization of the minimal protease resistant tau unit of the Alzheimer's disease paired helical filament. *EMBO J.*, **12**, 365–370.
- Novak, M., Ugolini, G., Fasulo, L., Visintin, M., Ovecka, M. & Cattaneo, A. (1999) Truncation of tau and neurodegeneration. In Iqbal, K., Swaab, D.F., Winblad, B. & Wisniewski, H.M. (eds), *Alzheimer's Disease and Related Disorders. Etiology, Pathogenesis and Therapeutics*. John Wiley & Sons Ltd, New York, pp. 281–291.
- Nunomura, A., Perry, G., Aliev, G., Hirai, K., Takeda, A., Balraj, E.K., Jones, P.K., Ghanbari, H., Wataya, T., Shimohama, S., Chiba, S., Atwood, C.S., Petersen, R.B. & Smith, M.A. (2002) Oxidative damage is the earliest event in Alzheimer disease. *J. Neuropathol. Exp. Neurol.*, **60**, 759–767.
- Perry, G., Nunomura, A., Hirai, K., Zhu, X., Perez, M., Avila, J., Castellani, R.J., Atwood, C.S., Aliev, G., Sayre, L.M., Takeda, A. & Smith, M.A. (2002) Is oxidative damage the fundamental pathogenic mechanism of Alzheimer's and other neurodegenerative diseases? *Free Radic. Biol. Med.*, **33**, 1475–1479.
- Petersen, R.C., Thomas, R.G., Grundman, M., Bennett, D., Doody, R., Ferris, S., Galasko, D., Jin, S., Kaye, J., Levey, A., Pfeiffer, E., Sano, M., van Dyck, C.H. & Thal, L.J. (2005) Vitamin E and donepezil for the treatment of mild cognitive impairment. *N. Engl. J. Med.*, **352**, 2379–2388.
- Selkoe, D.J. (2002) Alzheimer's disease is a synaptic failure. *Science*, **298**, 789–791.
- Stamer, K., Vogel, R., Thies, E., Mandelkow, E. & Mandelkow, E.M. (2002) Tau blocks traffic of organelles, neurofilaments, and APP vesicles in neurons and enhances oxidative stress. *J. Cell. Biol.*, **156**, 1051–1063.
- Toyokuni, S. (1998) Oxidative stress and cancer: The role of redox regulation. *Biotherapy*, **11**, 147–154.
- Wang, J.Z., Grundke-Iqbal, I. & Iqbal, K. (1996) Glycosylation of microtubule-associated protein tau: an abnormal posttranslational modification in Alzheimer's disease. *Nat. Med.*, **2**, 871–875.
- Wang, H. & Joseph, J.A. (1999) Quantifying cellular oxidative stress by dichlorofluorescein assay using microplate reader. *Free Radic. Biol. Med.*, **27**, 612–616.
- Watanabe, A., Hong, W.K., Dohmae, N., Takio, K., Morishima-Kawashima, M. & Ihara, Y. (2004) Molecular aging of tau: disulfide-independent aggregation and non-enzymatic degradation in vitro and in vivo. *J. Neurochem.*, **90**, 1302–1311.
- Yan, S.D., Chen, X., Schmidt, A.M., Brett, J., Godman, G., Zou, Y.S., Scott, C.W., Caputo, C., Frappier, T., Smith, M.A., Yen, S.H. & Stern, D. (1994) Glycated tau protein in Alzheimer disease: a mechanism for induction of oxidant stress. *Proc. Natl Acad. Sci. USA*, **91**, 7787–7791.
- Zilka, N., Filipcik, P., Koson, P., Vechterova, L., Skrabana, R., Zilkova, M., Rolkova, G., Kontseikova, E. & Novak, M. (2006) Truncated tau from sporadic Alzheimer's disease suffices to drive neurofibrillary degeneration in vivo. *FEBS Lett.*, **580**, 3582–3588.

EXHIBIT 8

PATENT

IN THE UNITED STATES PATENT AND TRADEMARK OFFICE

In re Application of:

Eva KONTSEKOVA

Peter FILIPCIK

Serial No.: 10/521,049

Filed: November 1, 2005

For: TRANSGENIC ANIMAL EXPRESSING
ALZHEIMER'S TAU PROTEIN

Group Art Unit: 1633

Examiner: Leavitt, Maria Gomez

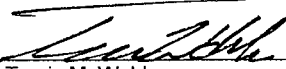
Atty. Dkt. No.: SONN:066US

Confirmation No.: 5434

CERTIFICATE OF ELECTRONIC TRANSMISSION
37 C.F.R. § 1.8

I hereby certify that this declaration is being electronically
filed with the United States Patent and Trademark Office
via EFS-Web on the date below:

September 17, 2007
Date


Travis M. Wohlers

FILIPCIK DECLARATION UNDER 37 C.F.R. § 1.132

Commissioner for Patents
P.O. Box 1450
Alexandria, VA 22313-1450

I, Peter Filipcik, declare that:

1. I am a co-inventor of the above-referenced patent application. I am also an employee of Axon Neuroscience, the assignee of the above-referenced application. A copy of my *Curriculum Vitae* is attached as Exhibit 1.
2. It is my understanding that the Examiner in charge of the above-captioned application has advanced an enablement rejection against claims 17-33. I am supplying this declaration to provide additional evidence of the enablement of the present claims.
3. This declaration describes the generation of and studies on transgenic rat line #24. According to the teachings in the present specification, the DNA construct used for the

preparation of transgenic rat line #24 is characterized by the following features: (1) the cDNA molecule is truncated at least 30 nucleotides downstream of the start codon and truncated at least the 30 nucleotides upstream of the stop codon of the full-length tau cDNA sequence coding for 4-repeat and 3-repeat tau protein; (2) the cDNA molecule comprises SEQ ID NO:9; and (3) the DNA construct encodes a protein, which has neurofibrillary (NF) pathology producing activity when expressed in brain cells.

4. The transgene construct used in the generation of transgenic rat line #24 was prepared by ligation of a cDNA coding for human tau protein truncated at amino acid positions 93-302 into the mouse Thy-1 gene downstream of the brain promoter/enhancer sequence. This numbering is based on isoform 44 (3-repeat tau) as it is in the application. Amino acids 93-302 correspond to nucleotides 277-906, SEQ ID NO: 12 in the application. Thus, the truncated tau cDNA molecule used to generate rat line #24 is truncated at least 30 nucleotides downstream of the start codon and truncated at least the 30 nucleotides upstream of the stop codon of the full-length tau cDNA sequence coding for 4-repeat and 3-repeat tau protein; and the truncated tau cDNA molecule comprises SEQ ID NO: 9 (nucleotides 741-930). The truncated tau cDNA molecule also comprises SEQ ID NO: 12.
5. The cDNA coding for human tau protein in transgenic rat line #24 is shorter by 93 nucleotides (31 amino acids) than the cDNA coding for human tau protein in transgenic rat line #318.
6. The transgenic DNA was linearized by cleavage with EcoRI, and the vector sequences were removed prior to microinjection. Transgenic rats were generated by pronuclear injection of one-day old SHR rat embryos. Founders were screened by PCR using Thy-

1-specific and human tau-specific primers. Transgenic founder line #24, which stably expressed human truncated tau, was obtained.

7. Like transgenic rat line #318 described in the specification, transgenic rat line #24 exhibits neurofibrillary (NF) pathology. Transgenic rat line #24 developed neurofibrillary lesions in the brain stem, spinal cord, primary motor cortex, and hippocampus. Attached Figure 1 shows the staining of neurofibrillary lesions in the hippocampus and cortex of transgenic rat line #24 in the late stage of the disease.
8. Neurological examinations showed similar features in both the #24 and #318 transgenic rat lines. Sensory-motor impairment was measured by the "NeuroScale" method. NeuroScale represents a multi-test battery intended for the quantitative neurobehavioural evaluation of transgenic rats suffering from progressive sensorimotor neurodegeneration. Testing protocol enables complex sensorimotor, neuromuscular and neurological assessment of rats at different age periods. Complex neurobehavioural characterization of rats involves basic observational assessment, examination of neurological functions and evaluation of rat neuromuscular functions by prehensile traction test, assessing forelimb muscle strength and assessment of sensorimotor coordination abilities using beam walking test. This experimental strategy can reveal the impairment, which could otherwise be hidden and permits observation of changes caused by chronic neurodegenerative process. As shown in attached Figure 2, the progress of sensory-motor impairment of animals from transgenic line #318 and transgenic line #24 is almost identical. The onset and progression of neurodegeneration is the same in both transgenic rat lines. The transgene is transmitted to subsequent offspring generations and the phenotype stays unchanged even in the 4th generation of offspring.

9. Another measure of cognitive impairment is the object recognition test (ORT). ORT is used to measure object recognition memory, which is the ability to discriminate between objects that have been previously encountered and those that have not been. A spontaneous exploratory activity can be used for measurement of memory function in rats. ORT in animals is based on natural preference of investigating rather a novel than a familiar object. The intensity of memory storage can be tested using various types of delays between the first (presentation) and second (challenge) trial, in which the new object replaces a familiar object. As shown in attached Figure 3, transgenic rats from line #24 suffer from early cognitive impairment in the object recognition test.
10. The evidence discussed above demonstrates that transgenic rat line #24 contains a DNA construct having a cDNA molecule coding for N- and C-terminally truncated tau molecules having the following features: (1) the cDNA molecule is truncated at least 30 nucleotides downstream of the start codon and truncated at least the 30 nucleotides upstream of the stop codon of the full-length tau cDNA sequence coding for 4-repeat and 3-repeat tau protein; (2) the cDNA molecule comprises SEQ ID No. 9; and (3) the DNA construct encodes a protein, which has neurofibrillary (NF) pathology producing activity when expressed in brain cells.
11. I understand that the Examiner of this application asserts that there is no correlation between expression of any truncated tau protein in rat with any relevant characteristics or useful phenotype other than neurofibrillary pathology. This assertion is incorrect. First, neurofibrillary pathology is the most important and earliest immunohistochemical finding in Alzheimer's disease. Thus, an animal model that exhibits neurofibrillary pathology is a useful model of Alzheimer's disease. The transgenic rats described in the present

specification also exhibit other pathological features associated with Alzheimer's disease including cognitive impairment, oxidative stress, hypertension, and diabetes. As described in my declaration filed on January 10, 2007, transgenic rat line #318 exhibits cognitive impairment and oxidative stress (*see* para. 11). Additional studies conducted in my laboratory have also shown that transgenic rat line #318 exhibits hypertension – up to 220 mm/Hg compared to control rats at 121mm/Hg. Furthermore, diabetes can be induced in transgenic rat line #318 by using a specific high-carbohydrate diet. The spontaneous hypertensive rat strain is a genetic model for the study of obesity and diabetes. Obese rats exhibit both metabolic and histopathologic characteristics associated with non-insulin-dependent diabetes mellitus (type II) in humans. Obese male rats, when fed a high-carbohydrate diet, exhibit some of the metabolic alterations associated with human non-insulin-dependent diabetes mellitus, including hyperinsulinemia, hyperlipidemia, glucose intolerance, and glycosuria. Thus, the transgenic animals encompassed by the current claims are useful models of Alzheimer's disease because they exhibit the most important and earliest immunohistochemical finding in Alzheimer's disease (*i.e.*, neurofibrillary pathology) and they exhibit other pathological features associated with Alzheimer's disease including cognitive impairment, oxidative stress, hypertension, and diabetes.

12. I hereby declare that all statements made herein of my knowledge are true and that all statements made on information and belief are believed to be true; and further that these statements were made with the knowledge that willful false statements and the like so made are punishable by fine or imprisonment, or both, under Section 1001 of Title 18 of the United States Code and that such willful false statements may jeopardize the validity of the application or any patent issued thereon.

12.9.2007
Date

Peter Filipcik
Peter Filipcik

Figure 1

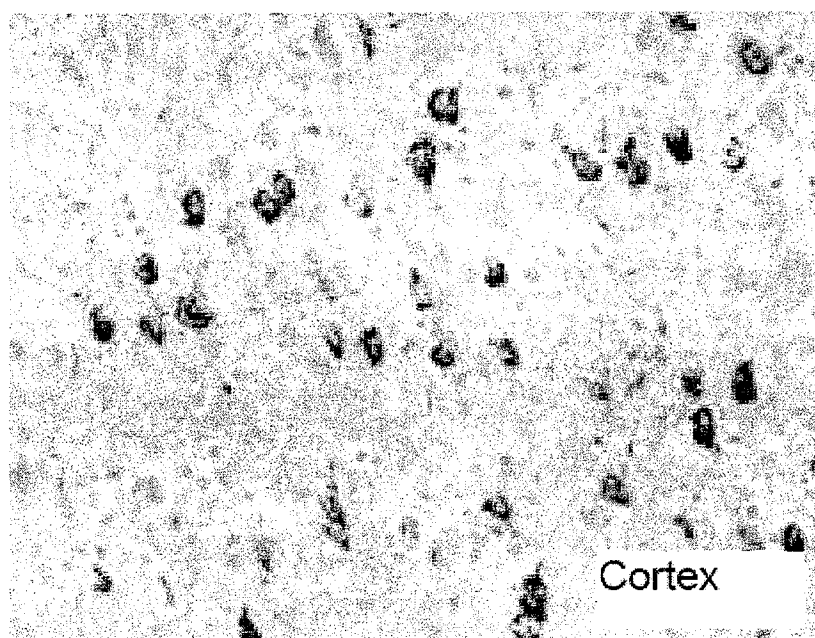
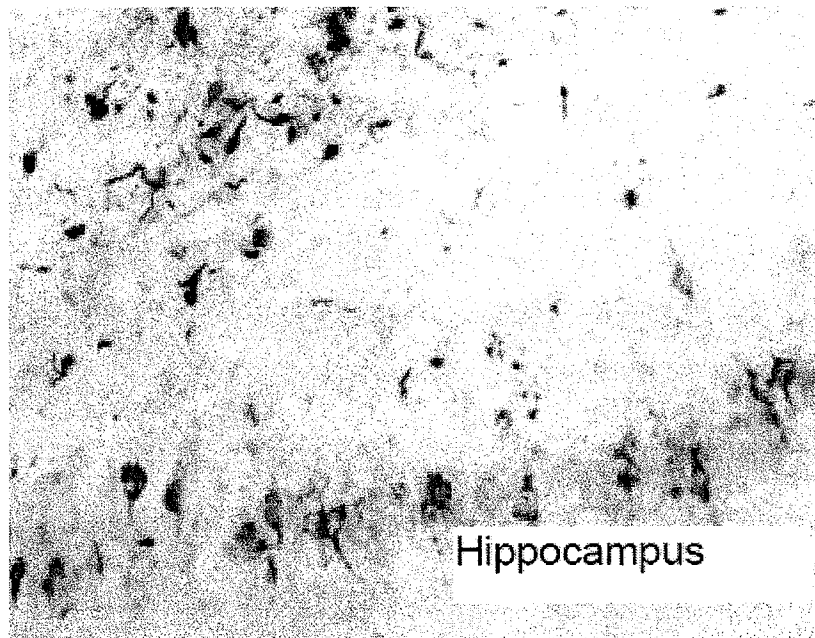


Figure 2

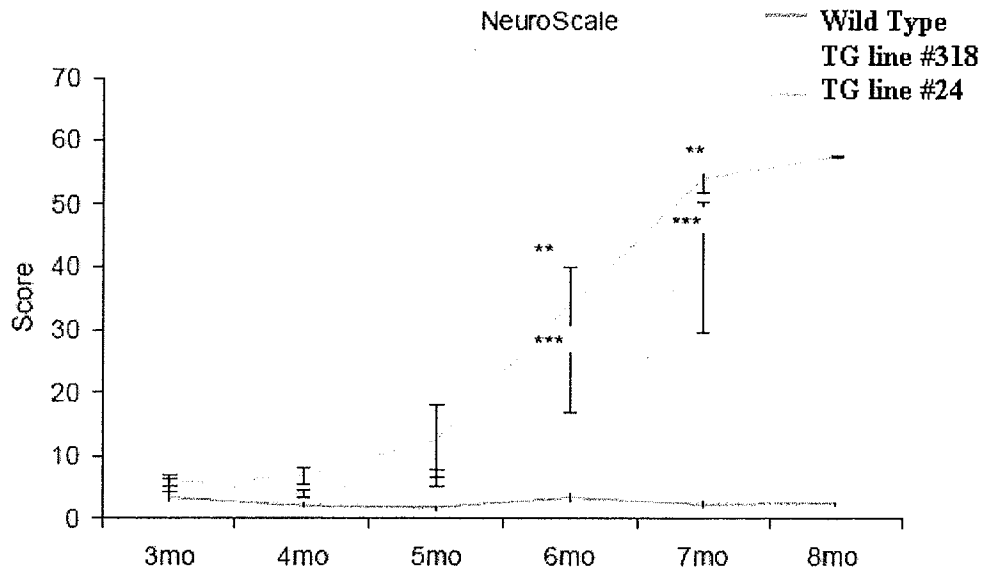
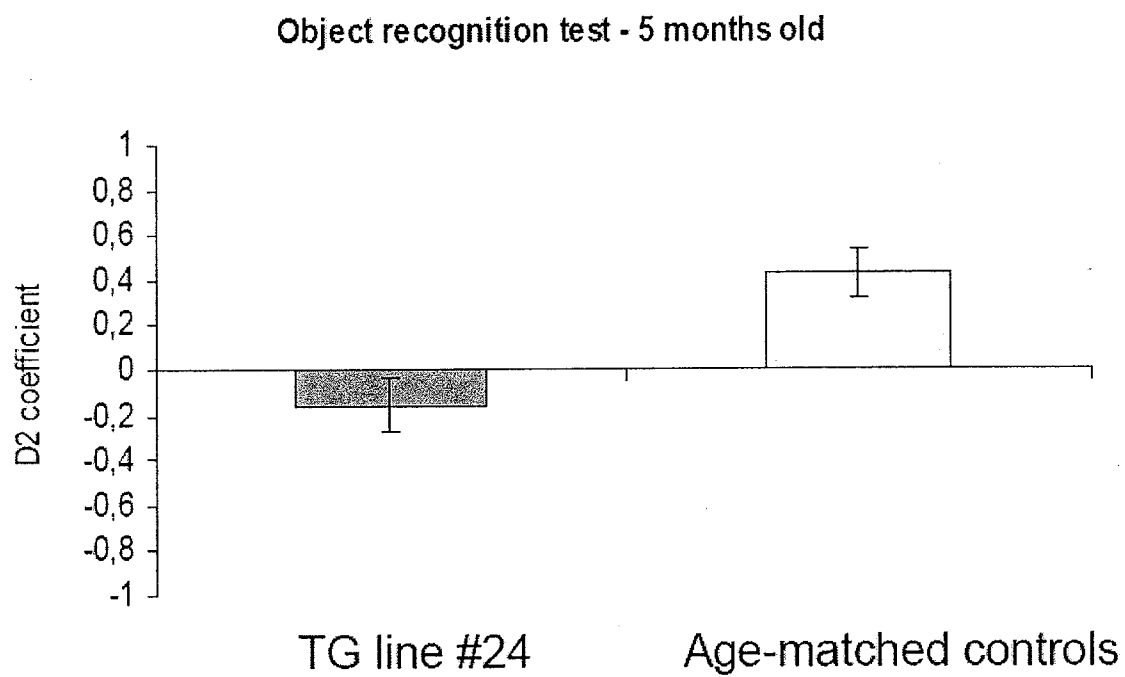


Figure 3



CURRICULUM VITAE

NAME: RNDr. Peter Filipcik, PhD
BORN: June 26, 1962
CITIZENSHIP: Slovakia
ADDRESS: Podhaj 3, Lamac, 84103 Bratislava,
e-mail: peter.filipcik@savba.sk

EDUCATION:

June 1995 PhD Slovak Academy of Sciences, Bratislava, Slovakia
June 1986 RNDr. Comenius University, Faculty of Natural Sciences in Bratislava, Slovakia

EMPLOYMENT:

1996 – pres Senior scientist - Institute of Neuroimmunology, Slovak Academy of Sciences, Bratislava, Slovakia (part time)
2001 – pres Senior scientist - Axon Neuroscience GmbH, Vienna, Austria
1986 - 1996 Research assistant, Institute of Experimental Endocrinology, Slovak Academy of Sciences, Bratislava, Slovakia
2000 - 2001 University of Vienna, Vienna, Austria
1998 - 2000 Visiting scientist at the CCRI, St. Anna Children Hospital, Vienna, Austria
1995 - 1996 Research associate, Dept. of Pharmacol., University of Minnesota, Minneapolis, USA
1993 - 1994 Research assistant, Dept. of Chem. Pharmacol., University of Tokyo, Japan

INTERNATIONAL COURSES AND MEETINGS ATTENDED (selection):

1990 "3rd European Congress on Cell Biology", Florence, Italy
1993 "The Radioisotopes in Biological Research", The Univ. of Tokyo, Tokyo, Japan
1993 "5th Inter-Department Meeting on Chemical Pharmacol.", Seoul, South Korea
1998 "6th Int. Conf. on Alzheimer's Disease and Related Disorders, Amsterdam, Netherlands
2001 "Ageing and Dementia - Current and future concepts", Graz, Austria
2003 In Vitro Human Cell Systems Enabling Drug Discovery, London, UK
2004 "9th International Conference on Alzheimers Disease and Related Disorders", Philadelphia, Pennsylvania
2005 Molecular Medicine Triconference, CHI, San Francisco, California, USA
2006 "10th International Conference on Alzheimers Disease", Madrid, Spain

MEMBERSHIP OF LEARNED SOCIETIES:

1997 Slovak Immunological Society
1996 The Slovak Alzheimer Society
2005 The Slovak Neuroscience Society

PUBLICATION ACTIVITY:

Author and co-author of 21 scientific papers, 2 patents

Bratislava 6. 12. 2006

List of publications:

Filipcik P, Cente M, Ferencik M, Hulin I, Novak M. The role of oxidative stress in the pathogenesis of Alzheimer's disease. Bratisl Lek Listy. 2006; 107 (9-10), 384-394

Pevalova M, **Filipcik P**, Novak M, Avila J, Iqbal K. Post-translational modifications of tau protein Bratisl Lek Listy 2006; 107 (9-10), 346-353

*Cente M, ***Filipcik P**, Pevalova M, Novak M. Expression of a truncated tau protein induces oxidative stress in a rodent model of tauopathy. Eur J Neurosci. 2006 Aug;24(4):1085-90.

*Zilka N, ***Filipcik P**, Koson P, Fialova L, Skrabana R, Zilkova M, Rolkova G, Kontsekkova E, Novak M. Truncated tau from sporadic Alzheimer's disease suffices to drive neurofibrillary degeneration in vivo. FEBS Lett. 2006 Jun 26;580(15):3582-8.

Soltys K, Rolkova G, Vechterova L, **Filipcik P**, Zilka N, Kontsekkova E, Novak M. First insert of tau protein is present in all stages of tau pathology in Alzheimer's disease. Neuroreport. 2005 Oct 17;16(15):1677-81.

Matuskova M, Csokova N, **Filipcik P**, Hanusovska E, Bires J, Cabadaj R, Kontsek P, Novak M. First confirmed sheep scrapie with A136R154Q171 genotype in Slovakia. Acta Virol. 2003;47(3):195-8.

Lion T, Daxberger H, Dubovsky J, **Filipcik P**, Fritsch G, Printz D, Peters C, Matthes-Martin S, Lawitschka A, Gadner H. Analysis of chimerism within specific leukocyte subsets for detection of residual or recurrent leukemia in pediatric patients after allogeneic stem cell transplantation. Leukemia. 2001 Feb;15(2):307-10. No abstract available.

Cattaneo A, Capsoni S, Margotti E, Righi M, Kontsekkova E, Pavlik P, **Filipcik P**, Novak M. Functional blockade of tyrosine kinase A in the rat basal forebrain by a novel antagonistic anti-receptor monoclonal antibody. J Neurosci. 1999 Nov 15;19(22):9687-97.

Brtko J, **Filipcik P**, Hudecova S, Brtkova A, Bransova J. Nuclear all-trans retinoic acid receptors: in vitro effects of selenium. Biol Trace Elem Res. 1998 Apr-May;62(1-2):43-50.

Filipcik P, Strbak V, Brtko J. Thyroid hormone receptor occupancy and biological effects of 3,5,3',5'-L-triiodothyronine (T3) in GH4C1 rat pituitary tumour cells. Physiol Res. 1998;47(1):41-6.

Wei LN, Lee CH, **Filipcik P**, Chang L. Regulation of the mouse cellular retinoic acid-binding protein-I gene by thyroid hormone and retinoids in transgenic mouse embryos and P19 cells. J Endocrinol. 1997 Oct;155(1):35-46.

Nikodemova M, Weismann P, **Filipcik P**, Mraz P, Greer MA, Strbak V. Both iso- and hyperosmotic ethanol stimulate release of hypothalamic thyrotropin-releasing hormone despite opposite effect on neuron volume. Neuroscience. 1997 Oct;80(4):1263-9.

Filipcik P, Brtko J. [The basis for the variable effects of thyroid hormones] Cesk Fysiol. 1996 Mar;45(1):13-20. Slovak.

Brtko J, **Filipcik P**, Hudecova S, Strbak V, Brtkova A. In vitro effects of sodium selenite on nuclear 3,5,3'-triiodothyronine (T3) receptor gene expression in rat pituitary GH4C1 cells. Biol Trace Elem Res. 1995 May;48(2):173-83.

Filipcik P, Saito H, Katsuki H. 3,5,3'-L-triiodothyronine promotes survival and axon elongation of embryonic rat septal neurons. Brain Res. 1994 May 30;647(1):148-52.

Brtko J, **Filipcik P**. Effect of selenite and selenate on rat liver nuclear 3,5,3'-triiodothyronine (T3) receptor. Biol Trace Elem Res. 1994 Apr-May;41(1-2):191-9.

Brtko J, Knopp J, **Filipcik P**, Baker ME. Effect of protease inhibitors and substrates on 3,5,3'-triiodothyronine binding to rat liver nuclear receptors. *Endocr Regul*. 1992 Sep;26(3):127-31.

Knopp J, Brtko J, **Filipcik P**. Effect of triiodothyronine on rat liver polysome profiles and translational activity of mRNA after partial hepatectomy. *Endocr Regul*. 1992 Jun;26(2):67-72.

Brtko J, **Filipcik P**, Knopp J, Sedlakova V, Rauova L. Thyroid hormone responsiveness of the L1210 murine leukemia cell line. *Acta Endocrinol (Copenh)*. 1992 Apr;126(4):374-7.

Filipcik P, Brtko J, Rauova L, Sedlakova V. Distribution of triiodothyronine nuclear receptors during the cell cycle in mouse leukemia cells. *Folia Biol (Praha)*. 1992;38(6):332-9.

Filipcik P, Brtko J, Knopp J. [Cell lines in experimental endocrinology] *Bratisl Lek Listy*. 1990 Apr;91(4):278-83. Slovak.

*Equal contribution.

NEUROBIOLOGY OF AGING supplement:

Filipcik, P; Pevalova, M; Smrzka, O; Novak, M. Neuronal assay based on developmentally inducible expression of Alzheimer's tau, designed for screening of AD therapeutics. *NEUROBIOLOGY OF AGING*, JUL 2004, 25. Suppl. 2, S265

Pevalova, M; **Filipcik, P**; Mederlyova, A; Cente, M; Smrzka, O; Novak, M Hyperphosphorylation and oxidative stress as early changes in axon's new AD rat model. *NEUROBIOLOGY OF AGING*, JUL 2004, 25, Suppl. 2, S264

Cente, M; **Filipcik, P**; Hanusovska, E; Zilka, N; Novak, M Onset and intensity of AD changes in transgenic rat expressing Alzheimer specific Tau protein correlates with gene dosage. *NEUROBIOLOGY OF AGING*, JUL 2004, 25 Suppl. 2, S239

Hrnkova, M; Zilka, N; **Filipcik, P**; Novak, M Cognitive deficit and progressive motor impairment in AD rat model, *NEUROBIOLOGY OF AGING*, JUL 2004, 25, Suppl. 2, S233

Koson, P; Zilka, N; **Filipcik, P**; Novak, M Neuronal loss in selected brain areas of a new transgenic AD rat model estimated with unbiased stereological methods, *NEUROBIOLOGY OF AGING*, JUL 2004, 25 Suppl. 2, S249, S250.

Zilka, N; Csokova, N; Vechterova, L; Skrabanova, M; Hrnkova, **M**; **Filipcik, P**; Novak, M. Staging of neuropathological changes in axon's novel transgenic AD rat model is linked to a lethal phenotype. *NEUROBIOLOGY OF AGING*, JUL 2004, 25. Suppl. 2, S255

EXHIBIT 9

PATENT

IN THE UNITED STATES PATENT AND TRADEMARK OFFICE

In re Application of:
Eva KONTSEKOVA
Peter FILIPCIK

Serial No.: 10/521,049

Filed: November 1, 2005

For: TRANSGENIC ANIMAL EXPRESSING
ALZHEIMER'S TAU PROTEIN

Confirmation No.: 5434

Examiner: Leavitt, Maria Gomez

Group Art Unit: 1633

Atty. Dkt. No.: SONN:066US

THIRD FILIPCIK DECLARATION UNDER 37 C.F.R. § 1.132

I, PETER FILIPCIK, declare that:

1. I am a named inventor on the above-referenced patent application and I am an employee of Axon Neuroscience, the assignee of the above-referenced patent application. A copy of my Curriculum Vitae is attached.
2. It is my understanding that the Examiner in charge of this application has advanced an enablement rejection against claims 17-36. I am supplying this declaration to provide additional evidence of the enablement of the present claims.
3. This declaration provides evidence that we are able to produce transgenic animals with a predictable phenotype using gene constructs described in the present application. In our studies we have clearly shown that the phenotype induced by the transgenes, which are truncated tau, is robust, highly reproducible and predictable.

4. So far we have generated several independent transgenic lines (Tg line #318, Tg line #72 and Tg line #24) using DNA gene constructs encoding proteins, which have shown neurofibrillary (NF) pathology producing activity when expressed in brain cells.

5. Tg line #318 is described in the specification of the present patent application. The transgene construct used in the generation of transgenic rat line #318 encodes a truncated tau protein of amino acids 93-333 based on the numbering for the four-repeat containing tau 43 isoform. Amino acids 93-333 correspond to nucleotides 279-999 (SEQ ID NO: 3). The normal tau 43 protein is 383 amino acids. Thus, the truncated tau cDNA molecule used to generate rat line #318 is truncated at least 30 nucleotides upstream of the stop codon of the full-length tau cDNA sequence coding for 4-repeat and 3-repeat tau protein; and the truncated tau cDNA molecule comprises SEQ ID NO: 9 (nucleotides 741-930). The same construct as used in the generation of transgenic rat line #318 also was used in the generation of transgenic rat line #72. The transgene construct used in the generation of transgenic rat line #24 encodes amino acids 93-302, which correspond to nucleotides 277-906 (SEQ ID NO: 12), based on the numbering used for isoform 44 (3-repeat tau). The normal tau 44 protein is 352 amino acids. Thus, the truncated tau cDNA molecule used to generate rat line #24 is truncated at least 30 nucleotides upstream of the stop codon of the full-length tau cDNA sequence coding for 4-repeat and 3-repeat tau protein; and the truncated tau cDNA molecule comprises SEQ ID NO: 9 (nucleotides 741-930). The generation and studies of Tg line #24 were described in my previous declaration, which I signed on 12 September 2007.

6. The phenotype of these independent transgenic animals is very similar. The progress of sensory-motor impairment of animals from transgenic line #318 and transgenic line #24 is almost

identical. The onset and progression of neurodegeneration is the same in all three transgenic rat lines. The only difference we have observed is in the strength of the resulting phenotype when comparing Tg line #72 and Tg line #24. While behavioral features are almost the same, the life span of those animals containing 4 repeat tau (e.g. Tg line #72) is much shorter when compared to those animals containing 3 repeat tau region (e.g. Tg line #24) of human tau protein. However we are aware that the aggressiveness of neurodegeneration in human tauopathies including Alzheimer's disease may also be different in different patients.

7. Transgenic rat lines #318 and #24 exhibit neurofibrillary (NF) pathology. Transgenic rat line #24 developed neurofibrillary lesions in the brain stem, spinal cord, primary motor cortex, and hippocampus. Attached Figure 1 shows the staining of neurofibrillary lesions in the hippocampus and cortex of transgenic rat line #24 in the late stage of the disease.

8. Neurological examinations showed similar features in both the #24 and #318 transgenic rat lines. Sensory-motor impairment was measured by the "NeuroScale" method. NeuroScale represents a multi-test battery intended for the quantitative neurobehavioral evaluation of transgenic rats suffering from progressive sensorimotor neurodegeneration. Testing protocol enables complex sensorimotor, neuromuscular, and neurological assessment of rats at different age periods. Complex neurobehavioral characterization of rats involves basic observational assessment, examination of neurological functions and evaluation of rat neuromuscular functions by prehensile traction test, assessing forelimb muscle strength and assessment of sensorimotor coordination abilities using a beam walking test. This experimental strategy can reveal impairment, which could otherwise be hidden, and permits observation of changes caused by chronic neurodegenerative process. As shown in attached Figure 2, the progress of sensory-

motor impairment of animals from transgenic line #318 and transgenic line #24 was almost identical. The onset and progression of neurodegeneration was the same in both transgenic rat lines. The transgene was transmitted to subsequent offspring generations and the phenotype remained unchanged even in the 4th generation of offspring.

9. Another measure of cognitive impairment is the object recognition test (ORT). ORT is used to measure object recognition memory, which is the ability to discriminate between objects that have been previously encountered and those that have not been. A spontaneous exploratory activity can be used for measurement of memory function in rats. ORT in animals is based on the natural preference of investigating a novel object rather than a familiar object. The intensity of memory storage can be tested using various types of delays between the first (presentation) and second (challenge) trial, in which the new object replaces a familiar object. As shown in attached Figure 3, transgenic rats from line #24 suffer from early cognitive impairment in the object recognition test.

10. According to our latest data we have concluded that the final neurofibrillary tangle (NFT) load in the terminal stage of life of transgenic animal lines, which were produced using different truncated tau gene constructs, is independent of human tau expression levels as shown in Figure 4. We have quantified those mAb AT8-immunoreactive tangle bearing neurons that display characteristic fibrillary structures in the neuronal cytoplasm. (A) Representative pathological structures present in the reticular formation of the brain stems of transgenic rats stained by mAb AT8 are depicted: perinuclear tangles, intracellular tangles that fill the neuronal soma and neurofibrillary tangles distributed in the somatodendritic compartment (Scale bar = 10 μ m). (B) Total number of neurons and neurofibrillary tangles were determined in male rats from the

SHR72 (7.5 months old) and SHR318 (10.5 months old) transgenic lines. (C) The final NFT loads in SHR72 and SHR318 male rats showed no significant difference ($P = 0.71$). Bars represent mean values for each group \pm SEM.

11. Figure 5 shows that truncated tau transgenic expression in two different lines does not cause neuronal loss in the brainstem and hippocampus of transgenic animals. (A) Stereological analysis of neuronal loss in GRN in 7.5-month old transgenic SHR72 males and 10.5-month-old SHR318 males did not reveal any difference in total neuron numbers in comparison with age-matched wild-type rats (t-test: SHR72 vs wt, $P > 0.05$; SHR318 vs wt, $P > 0.05$). (B) Age related neuronal loss was present in GRN in the SHR rat strain. 7.5-month-old wild type SHR rat males display on average 25.4% fewer Nissl-stained neurons (Bonferroni's post hoc test, $P < 0.01$) and 10.5-month-old animals on average 39.7% fewer Nissl-stained neurons (Bonferroni's post hoc test, $P < 0.001$) than 5-month-old animals. Bars represent mean values for each group \pm SEM. (C) Cresyl violet staining of hippocampal pyramidal neurons (CA 1 area) in the transgenic and control rats did not show any visible differences (Scale bar = 50 μ m). (D) Stereological analysis of the total number of pyramidal cells in the hippocampal area CA 1-3 revealed no statistically significant differences between transgenic and wild type rat males in either of the investigated groups (t-test: SHR72 vs wt, $P > 0.05$; SHR318 vs wt, $P > 0.05$).

12. Another striking feature of animals produced by transgenic truncated tau expression is that the observed phenotype is not dependent on genetic background. After the transfer of the transgene from the genetic background of the hypertensive SHR strain into the normotensive Wistar strain (WKY) we have observed, in this new genetic environment, almost the identical phenotype at the level of biochemical examination as well as in behavioral measurements.

Although we expected less aggressive neurodegeneration in WKY animals, this was not the case. To illustrate this phenomenon see data included in Figure 6, showing that neurobehavioral impairment of the WKY transgene #72 goes in parallel with that of SHR transgene #72 as demonstrated by an almost identical increase in the neuroscale score. Figure 7 shows no significant influence of the strain differences on phospho-tau level in CSF at the biochemical level.

13. The resulting phenotype was synergistic in those animals that we have generated by crossing animals encompassing human truncated tau with 4 and 3 repeat. As shown in Figure 8, sensorimotor functions measured by beam walking test were significantly more impaired in transgenic line SHR24/72 (expressing both 3R and 4R truncated tau proteins) when compared with transgenic lines SHR24 (expressing 3R truncated tau) and SHR72 (expressing 4R truncated tau). To further demonstrate the synergistic effect of 3R and 4R truncated tau we performed neuroscale evaluation and we found that the complete neurobehavioral phenotype was significantly more impaired in transgenic line SHR24/72 (expressing both 3R and 4R truncated tau proteins) when compared with transgenic lines SHR24 (expressing 3R truncated tau) and SHR72 (expressing 4R truncated tau) as shown in Figure 9.

14. Neurofibrillary pathology is the most important and earliest immunohistochemical finding in Alzheimer's disease. Thus, an animal model that exhibits neurofibrillary pathology is a useful model of Alzheimer's disease. Among the published animal models our transgenic model belongs to those with the most aggressive neurodegenerative phenotype moreover resembling fundamental neuropathological features of brain typical for Alzheimer's disease sufferers.

Furthermore, all the transgenic lines we have generated exert stable phenotype even after several years of continual breeding.

15. I hereby declare that all statements made herein of my knowledge are true and that all statements made on information and belief are believed to be true; and further that these statements were made with the knowledge that willful false statements and the like so made are punishable by fine or imprisonment, or both, under Section 1001 of Title 18 of the United States Code and that such willful false statements may jeopardize the validity of the application or any patent issued thereon.

Date:

20.11.2008



PETER FILIPCIK

Figure 1

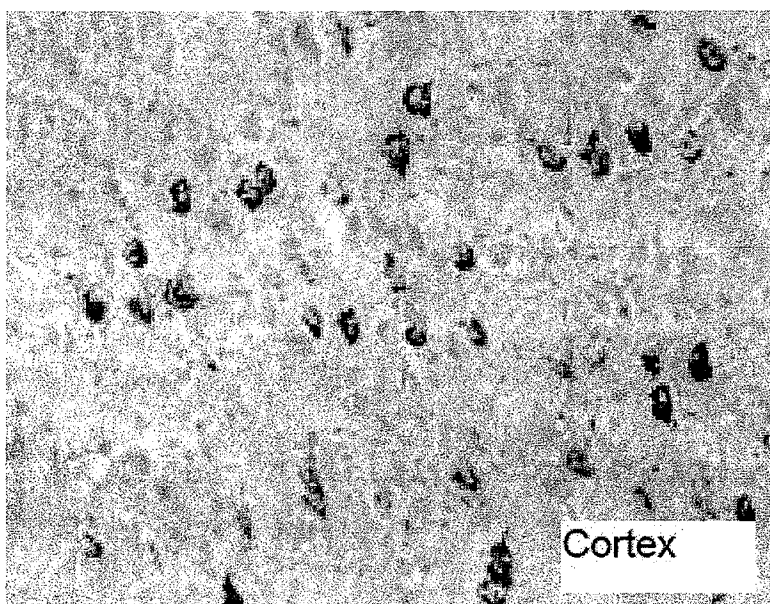
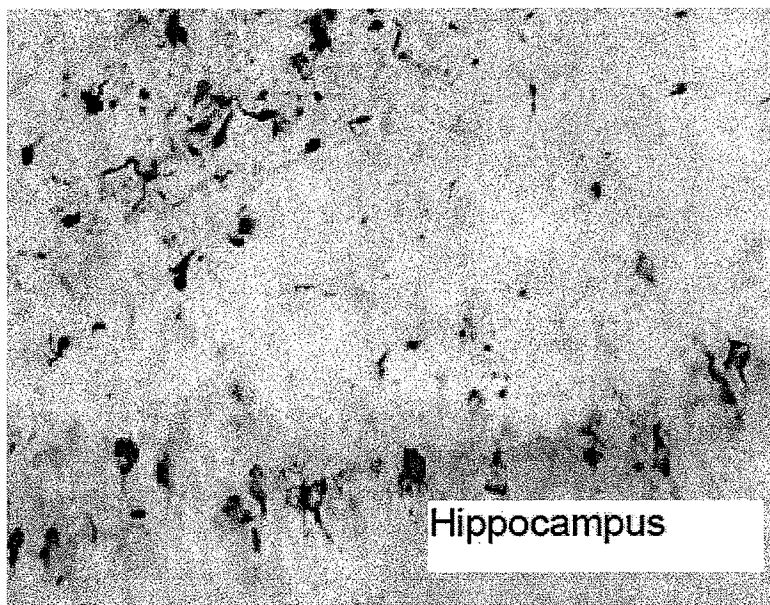


Figure 2

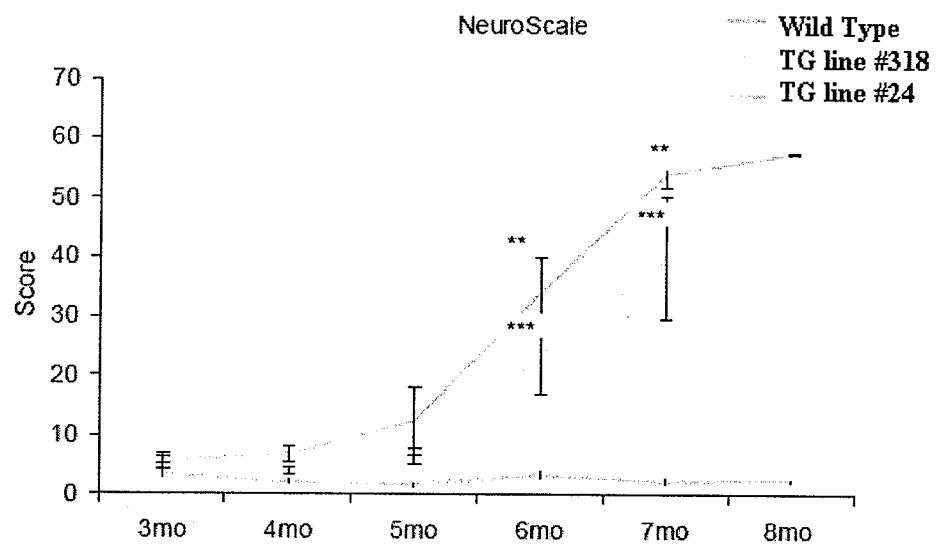


Figure 3

Object recognition test - 5 months old

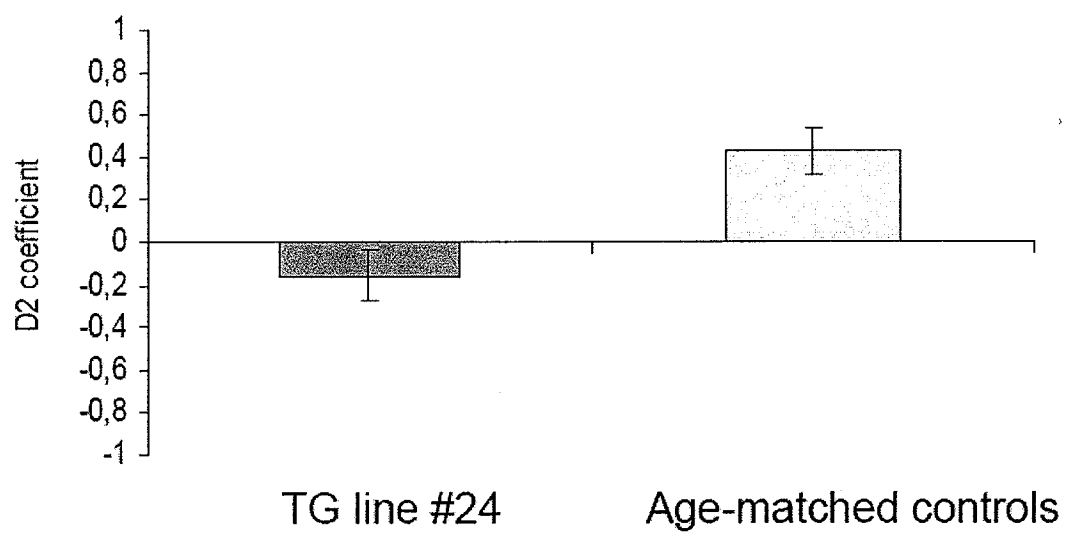


Fig.4

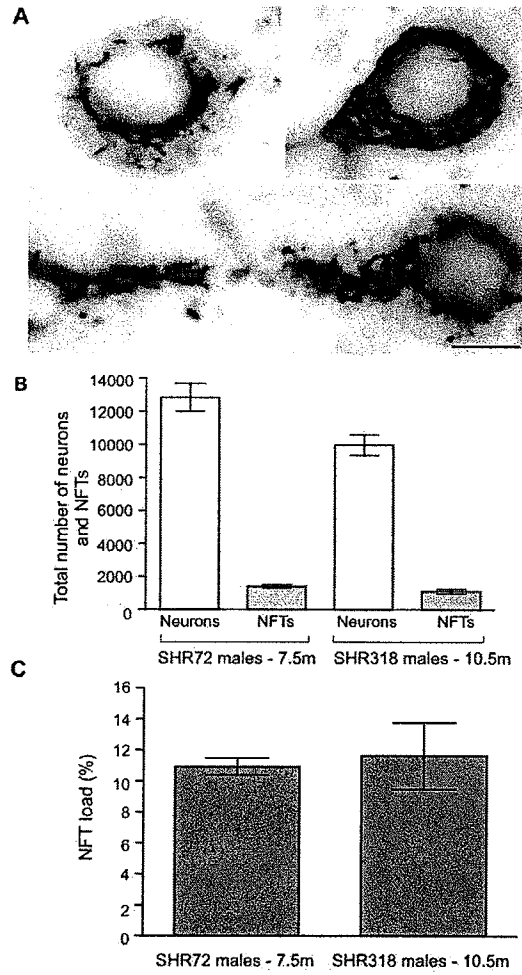


Fig. 5

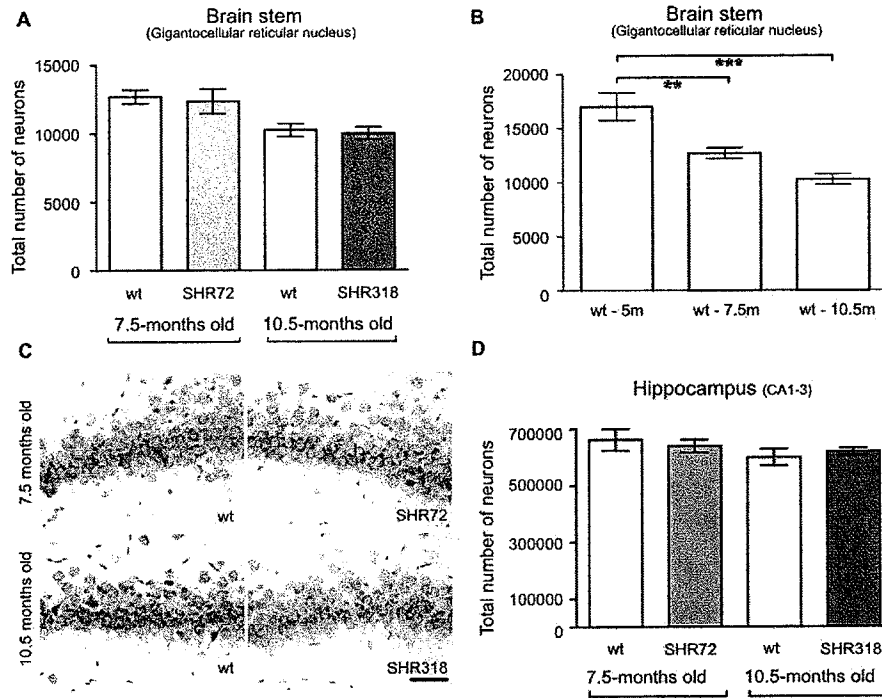


Fig. 6

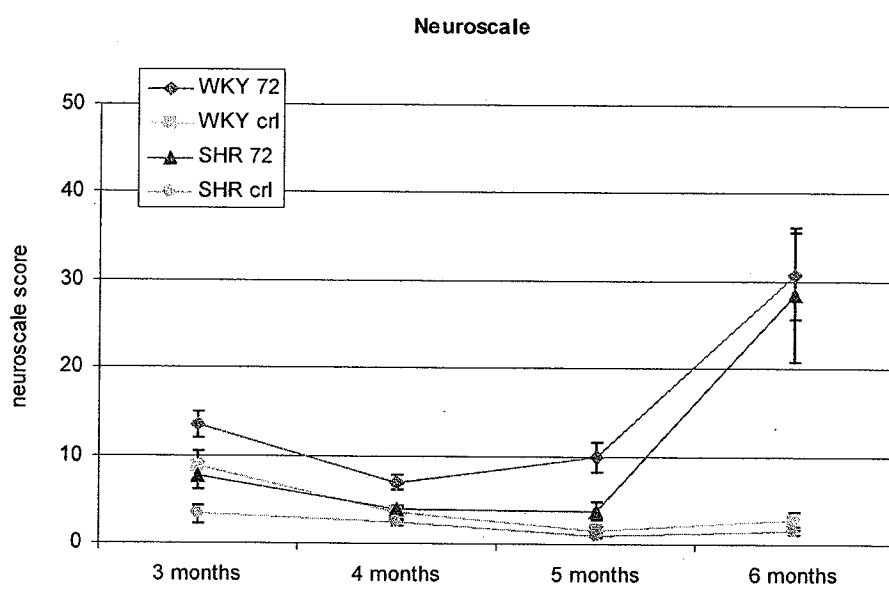


Fig. 7

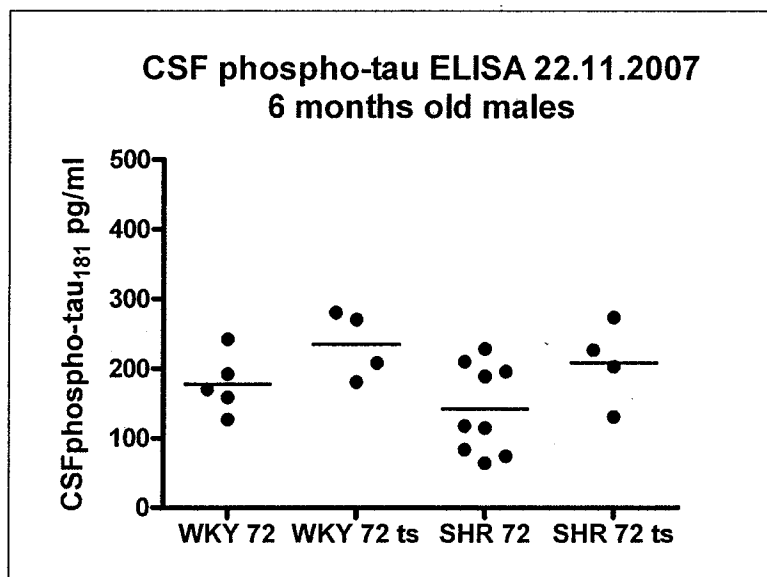


Fig. 8.

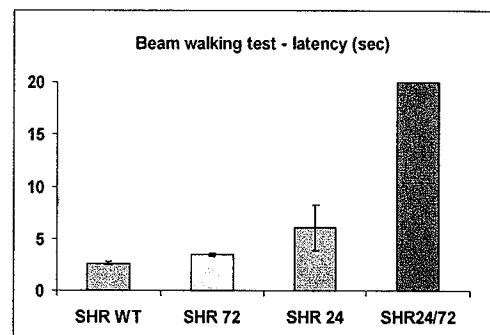
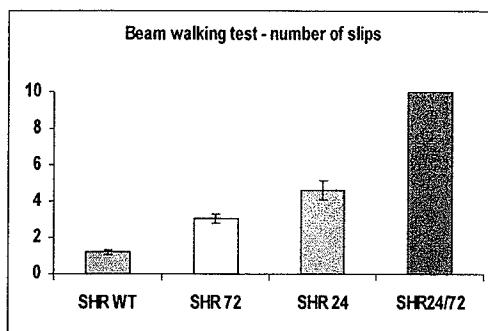


Fig. 9.

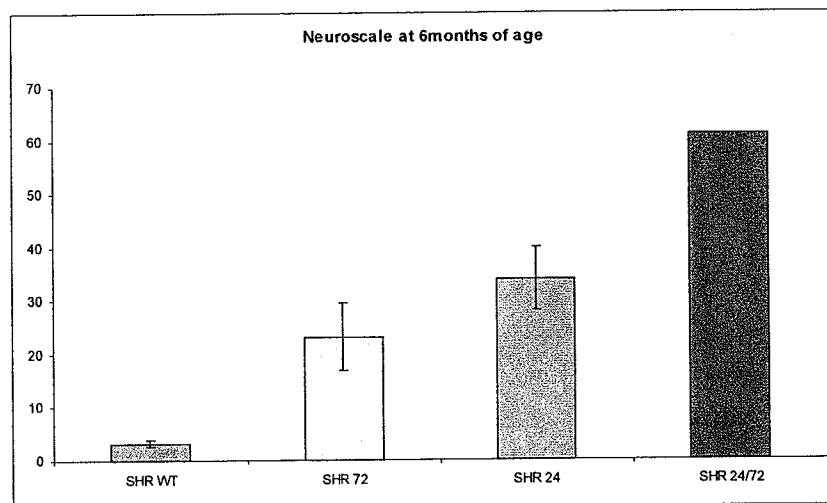


EXHIBIT 10

Neurofibrillary tangles, amyotrophy and progressive motor disturbance in mice expressing mutant (P301L) tau protein

Jada Lewis¹, Eileen McGowan¹, Julia Rockwood², Heather Melrose¹, Parimala Nacharaju¹, Marjon Van Slegtenhorst¹, Katrina Gwinn-Hardy¹, M. Paul Murphy¹, Matt Baker¹, Xin Yu¹, Karen Duff¹, John Hardy¹, Anthony Corral¹, Wen-Lang Lin¹, Shu-Hui Yen¹, Dennis W. Dickson¹, Peter Davies² & Mike Hutton¹

Neurofibrillary tangles (NFT) composed of the microtubule-associated protein tau are prominent in Alzheimer disease (AD), Pick disease, progressive supranuclear palsy (PSP) and corticobasal degeneration¹ (CBD). Mutations in the gene (*Mtapt*) encoding tau protein cause frontotemporal dementia and parkinsonism linked to chromosome 17 (FTDP-17), thereby proving that tau dysfunction can directly result in neurodegeneration². Expression of human tau containing the most common³⁻⁵ FTDP-17 mutation (P301L) results in motor and behavioural deficits in transgenic mice, with age- and gene-dose-dependent development of NFT. This phenotype occurred as early as 6.5 months in hemizygous and 4.5 months in homozygous animals. NFT and Pick-body-like neuronal lesions occurred in the amygdala, septal nuclei, pre-optic nuclei, hypothalamus, midbrain, pons, medulla, deep cerebellar nuclei and spinal cord, with tau-immunoreactive pre-tangles in the cortex, hippocampus and basal ganglia. Areas with the most NFT had reactive gliosis. Spinal cord had axonal spheroids, anterior horn cell loss and axonal degeneration in anterior spinal roots. We also saw peripheral neuropathy and skeletal muscle with neurogenic atrophy. Brain and spinal cord contained insoluble tau that co-migrated with insoluble tau from AD and FTDP-17 brains. The phenotype of mice expressing P301L mutant tau mimics features of human tauopathies and provides a model for investigating the pathogenesis of diseases with NFT.

To examine the effects of the P301L mutation, we expressed, under the mouse prion promoter⁶ (MoPrP), either human P301L or wild-type *Mtapt* cDNA containing exon 10 and lacking exons 2 and 3. These encode four-repeat tau without amino-terminal inserts (4R0N; see ref. 7 for tau isoform nomenclature). Mice normally have 4R0N, 4R1N and 4R2N tau isoforms⁸. On the basis of ELISA, western- and northern-blot analyses, we expanded a P301L founder line (JNPL3) and two WT4R lines (JN4 and JN25) with the highest transgene expression. Hemizygous JNPL3 and JN25 mice expressed the transgenic tau at levels roughly equivalent to that of endogenous tau (that is, approximately 50% of total tau). JN4 mice expressed the transgene at a level below that of endogenous tau (approximately 25% of total tau). As expected, homozygous JNPL3 mice expressed human P301L tau at about twice the level observed in hemizygous mice. A largely neuronal transgene expression pattern was demonstrated by *in situ* hybridization, with strongest signals in the cerebellum and hippocampus followed by the thalamus, hypothalamus, spinal cord, brainstem and cortex.

We detected the absence of escape extension during tail elevation and spontaneous back paw clenching while standing (Fig. 1a,c) in F1 JNPL3 hemizygotes as early as 6.5 months (21 animals) and in F2 JNPL3 homozygotes at 4.5 months (4 animals). By 10 months, approximately 90% of JNPL3 mice developed motor and behavioural disturbances. JNPL3 mice showed a delayed righting response and eventually became unable to right (Fig. 1e). In hang

tests, JNPL3 mice fell after grasping the rope briefly, whereas JN4, JN25 and non-transgenic mice held with three limbs and tail without falling. Within two weeks of phenotype onset, JNPL3 animals could not ambulate. Weakness spread to all limbs and dystonic posturing (Fig. 1d) developed. Affected animals showed a reduction in weight, grooming and vocalization, and an increase in docility. JNPL3 mice (19/21 examined) developed eye irritations and had difficulty in opening their eyes (Fig. 1b). Within 3–4 weeks of initial signs, mice became moribund. JN4, JN25 (WT4R) and non-transgenic animals appeared normal.

We examined JNPL3 (P301L) mice with motor and behavioural disturbances for neuropathological changes. Spinal cords of affected P301L mice showed fibrillary gliosis in the anterior horns, axonal degeneration in the anterior roots and axonal spheroids (Fig. 4a–f, h–i). Motor neuron counts of P301L mice showed a reduction of approximately 48% in the spinal cord (Fig. 4j). Gliosis (GFAP immunoreactivity) also occurred in the brainstem, diencephalon and basal telencephalon. We identified NFT in the diencephalon, brainstem, cerebellar nuclei and spinal cord by tau immunostaining, which we confirmed by Congo red, thioflavin-S fluorescent microscopy, Gallyas⁹, Bielschowsky and Bodian silver stains (Fig. 2a–k). Apparent extracellular tangles in the spinal cord were consistent with motor neuron loss. Granular somatodendritic tau immunoreactivity consistent with 'pre-tangles' and tau-positive processes occurred with a wider distribution in the brain than NFT, including neurons in the cortex (especially piriform and entorhinal cortices), hippocampus and basal ganglia.

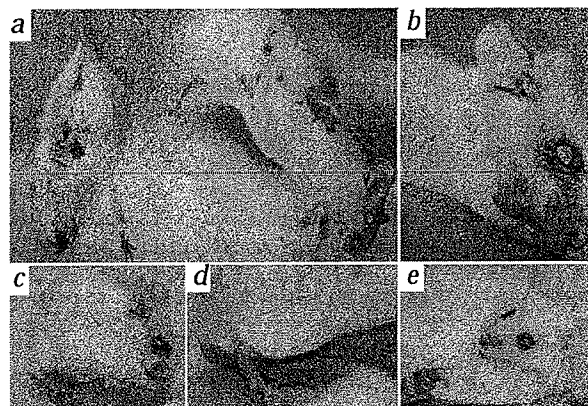


Fig. 1 Motor deficits in P301L transgenic mice. **a**, P301L (JNPL3) mice (left) held their legs in a crossed position close to their bodies upon tail elevation. Control littermates (right) showed normal escape response with their hindlimbs. Reduction in both weight and grooming were also observed in P301L mice. P301L animals developed eye irritations (**b**) and hunched postures with clenched paws while sitting (**c**). As the disease progressed, the hindlimbs of the P301L animals became dystonic (**d**). P301L animals with hindlimb dysfunction had delayed or absent righting reflexes (**e**).

¹Mayo Clinic Jacksonville, Jacksonville, Florida, USA. ²Department of Pathology, Albert Einstein College of Medicine, Bronx, New York, USA. Correspondence should be addressed to M.H. (e-mail: hutton.michael@mayo.edu).

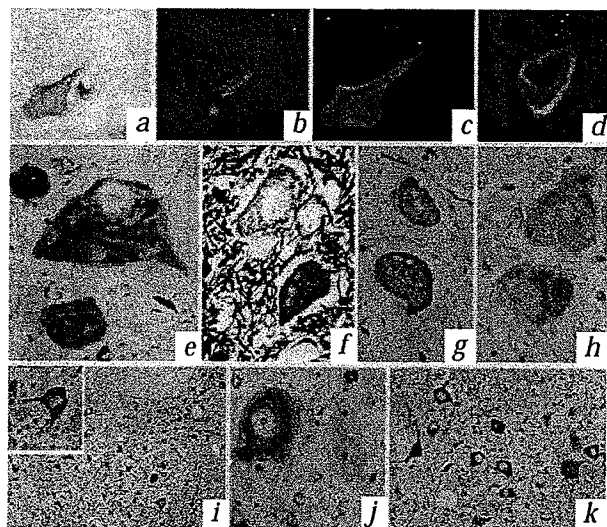


Fig. 2 Characterization of NFT from P301L (JNPL3) mice. NFT stained with Congo red under light microscopy (**a**), with polarization (**b**), and under confocal microscopy (**c**). Thioflavin-S (**d**) also stained NFT. NFT were positive with Gallyas (**e**), Bielschowsky (**f**) and Bodian (**g**) silver stains. Ubiquitin immunostaining was identified in most NFT (**h**). Tau hyperphosphorylation was evident from staining with numerous tau antibodies that recognize specific phospho-epitopes including AT8 (**i** and inset), AT180 (**j**) and CP13 (**k**). All sections are from spinal cord except (**k**), which is from cerebellar dentate nucleus.

The tau-positive NFT appeared to be morphologically heterogeneous, including flame- or globose-shaped NFT, as well as Pick bodies and smaller, more irregular, dense cytoplasmic inclusions similar to those found in FTDP-17 and CBD (refs 1,10). Neuronal lesions were immunoreactive, with tau antibodies recognizing conformational (Ab39, Ab69, Alz50, MC1), phosphorylated (AT8, AT180, CP3, CP9, CP13, PG5, PHF-1, TG3) and nonphosphorylated (E1) epitopes (Fig. 2*i-k*), and were intensely immunoreactive for ubiquitin (UH19; Fig. 2*h*). NFT were not immunoreactive for α -B crystallin or phosphorylated neurofilament (SMI-31).

Ultrastructurally, brainstem and spinal cord neurons with NFT had filamentous aggregates in the perikarya and proximal dendrites. Filaments were randomly oriented, were not membrane-bound and were immunoreactive for phosphorylated and nonphosphorylated tau. Most filaments were straight (10–30-nm diameter), but others had a twisted ribbon appearance (Fig. 3*a-d*). Affected neurons also showed chromatin dispersal, nuclear membrane infolding, Nissl body reduction and increased polysomes. Reactive astrocytes with abundant glial filaments, but not tau inclusions, occurred near NFT.

Skeletal muscle showed groups of small, acutely angulated fibres consistent with neurogenic atrophy (Fig. 4*g*). Ultrastructurally, the atrophic fibres had disorganized sarcomeres, increased glycogen and lipofuscin, and redundant basement membranes, but myopathic changes were absent. Peripheral nerves had extensive axonal degeneration with segmental swelling of axon fibres and advanced myelin degeneration (Fig. 4*j,k*).

Non-transgenic littermates, JN4 or JN25 (WT4R) mice up to 10 months of age lacked these pathological changes; however, we found MC-1 (refs 11–13)-positive cell bodies in the cortex, hippocampal pyramidal layer, hippocampal dentate gyrus and cerebellar dentate nucleus in the highest expressing WT4R line (JN25).

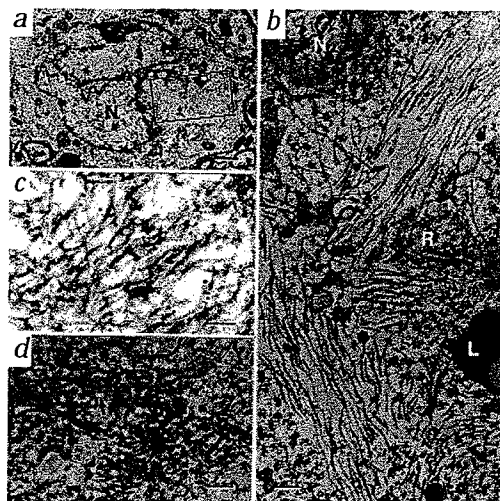
The spinal cord pathology observed in the JNPL3 mice correlates with motor dysfunction. The appendicular weakness is consistent with loss of anterior horn cells and degeneration and skeletal muscle denervation atrophy. Determining the exact cause of the behavioural abnormalities, which may result from

the motor deficits, will require extended analysis; however, the severe neurofibrillary pathology in the basal forebrain and the reticular system throughout the brainstem of P301L mice is consistent with the docility observed. The hypothalamic involvement may contribute to the cachexia of end-stage animals. Finally, degeneration of cranial nerve nuclei, including the motor nucleus of the trigeminal nerve and the hypoglossal nucleus, may explain the lack of vocalization in P301L animals.

Tau-filament aggregation in JNPL3 mice accompanied decreased tau solubility. We analysed sarkosyl-insoluble tau from brains and spinal cords of JNPL3 mice at progressive ages, littermate controls, JN4 and JN25 (WT4R) mice by western blot using human tau-specific antibody (E1; Fig. 5*a*). Human tau with normal mobility was present in soluble fractions only in transgenic mice. Only the JNPL3 (P301L) mice had sarkosyl-insoluble tau. A prominent insoluble tau band migrating more slowly (~64 kD) than the normal expressed human 4R tau was observed along with a diffuse protein smear at the top of the gel, consistent with aggregated tau. The amount of higher molecular weight forms of insoluble tau increased (Fig. 5*a*) and soluble human tau decreased with age (data not shown), suggesting a shift of tau to the insoluble pool as NFT form. Comparison of insoluble tau from JNPL3 mice with that from human FTDP-17 (P301L; Fig. 5*b*) and AD brains revealed similarities including co-migration of a prominent 64-kD band¹⁴. Dephosphorylation of the sarkosyl-insoluble tau eliminated the slower migrating tau bands (including the 64-kD band), demonstrating that these represented hyperphosphorylated species and that insoluble tau in JNPL3 mice consisted almost entirely of human tau (Fig. 5*b*). The 64-kD tau band observed in FTDP-17 and AD pathologic tau contains hyperphosphorylated 4R tau¹⁵, the isoform expressed in JNPL3 mice. This indicates that similar tau hyperphosphorylation occurs in both human tauopathies and in JNPL3 mice.

Given the relatively low transgene expression in the JNPL3 mice, the severe phenotype was surprising, as NFT pathology was absent from previous wild-type tau transgenic mice with higher tau levels^{16–19}. This presumably reflects the inclusion of the P301L

Fig. 3 Electron microscopy of NFT in P301L (JNPL3) mice. **a**, A neuron with a NFT shows deep nuclear infolding (N) and filamentous cytoplasmic aggregates (boxed area; bar, 1 μ m). **b**, Magnification of boxed area in (**a**) shows filaments in longitudinal and cross sections. L, lipofuscin granule; N, nucleus; R, polyribosomes. Bar, 0.2 μ m. **c**, Immunogold labelling (CP13) of neuronal filaments (bar, 0.1 μ m). **d**, Immunolabelling of filaments (CP13) with arrows indicating heavy peroxidase reaction product association (bar, 0.2 μ m).



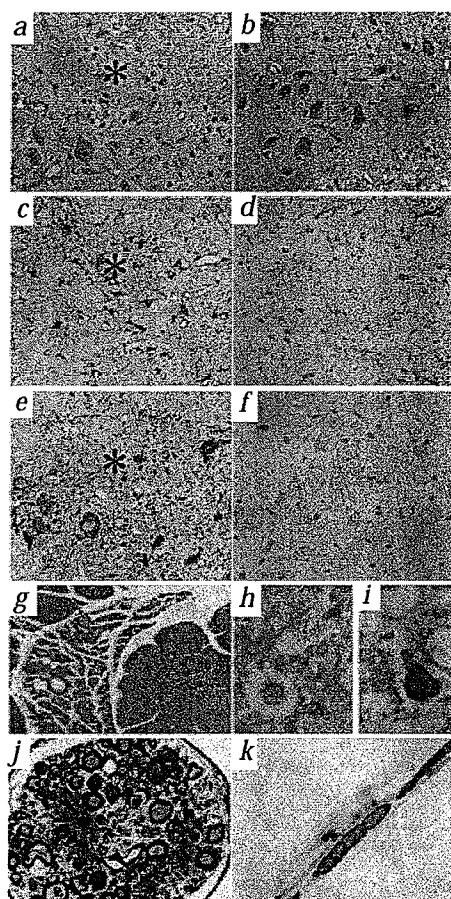


Fig. 4 Anterior horn and neuromuscular pathology in P301L (JNPL3) mice. **a**, Identical area of anterior horn. Haematoxylin and eosin staining shows patchy neuronal loss and gliosis in a P301L mouse (**a**) compared with a non-transgenic (NT) littermate (**b**). Prominent gliosis (GFAP immunoreactivity) was present in P301L mice (**c**) compared with NT mice (**d**), which showed minimal staining in perivascular astrocytes. Tau (CP13)-immunoreactive neurons were present in P301L mice (**e**), but not in NT mice (**f**). **g**, Large group atrophy and focal fatty metaplasia in skeletal muscle. **h**, Spinal cord white matter had scattered eosinophilic and granular axonal spheroids. **i**, Ubiquitin immunostained many spinal cord axonal spheroids. **j**, Extensive axonal degeneration in peripheral nerve (toluidine blue staining), with many myelin digestion chambers (arrows). **k**, Teased peripheral nerve fibre shows segmental swelling, extensive axonal degeneration and advanced myelin degeneration with many myelin ovoids. Graph (**k**) shows ~48% ($P < 1 \times 10^{-9}$ lumbar; $P < 1 \times 10^{-12}$ cervical) motor neuronal loss in P301L compared with non-transgenic spinal cords.

mutation that is associated with FTDP-17. The development of NFT and similar motor dysfunction in an additional mouse line (JNPL+23) expressing P301L tau (4R2N) at twofold higher levels than JNPL3 hemizygotes further demonstrates the impact of the P301L mutation on the development of tau pathology.

We have reported a transgenic mouse line, JNPL3, expressing human tau with the P301L mutation that develops NFT with neuronal loss. The distribution of the lesions is similar to some forms

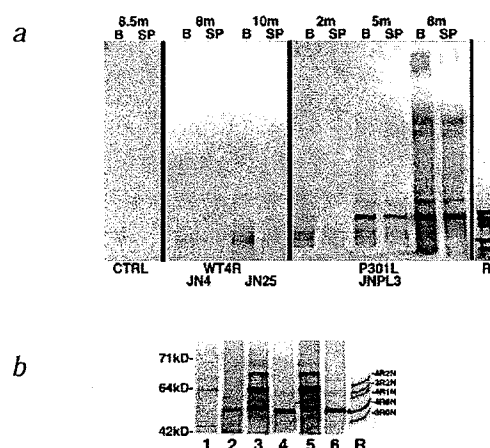


Fig. 5 Age-dependent increase in insoluble tau in P301L (JNPL3) mouse brains. We examined sarkosyl-insoluble material with human specific tau antibody E1 from the brain (B) and spinal cord (SP) of non-transgenic mice (control), WT4R (JN4, JN25) and P301L (JNPL3) transgenic mice (**a**). Significant insoluble tau was absent from the brain and spinal cord of control, JN4 and JN25 (WT4R) aged mice. Sarkosyl-insoluble tau accumulated with age and onset of phenotype in the JNPL3 mice. The 8-month P301L mouse showed end-stage motor and behavioural dysfunction. The ages of the animals are given in months (m). **b**, Comparison of insoluble tau extracted from the brain of a human FTDP-17 P301L patient (lane 1), hemizygous P301L (JNPL3) mice showing mid-stage motor and behavioural phenotype (lane 3), and a homozygous P301L mouse (JNPL3) with end-stage phenotype (lane 5) demonstrated co-migration of a prominent 64-kD band. Analysis of dephosphorylated insoluble tau from the human (P301L) patient (lane 2), mid-stage P301L hemizygous mice (lane 4), and an end-stage homozygous P301L mouse (lane 6) yielded a tau band that co-migrated with the 4R0N tau isoform. Using WKS46 tau antibody for total tau, no mouse tau isoforms were evident in the accumulated insoluble tau. An additional tau band representing the 4R1N isoform was seen in the insoluble tau (hyperphosphorylated and dephosphorylated) extracted from the human P301L sample, but was absent from the transgenic mice, which express only 4R0N human tau. Recombinant tau isoforms (R) were run in parallel. Migration of the human isoform expressed in the transgenic mice (4R0N) is indicated by an asterisk.

of FTDP-17 and other human tauopathies¹⁴ especially PSP, a four-repeat tau disorder²⁰. Human tauopathies, however, occur in the context of six tau isoforms and the P301L transgenic mouse pathology results from expression of one (human) isoform using a heterologous promoter; thus, differences in selective neuronal vulnerability are not surprising. The importance of these observations is threefold: first, they link neurofibrillary pathology to neuronal loss in the mice and allow key events in tau-induced neurodegeneration to be examined; second, they offer a system in which the relationship of neurofibrillary degeneration to other pathologies, specifically A β production, can be examined; and third, they provide a model in which therapies can be assessed.

Methods

Transgenic constructs and animals. The *Mtapt* cDNAs (exons 1, 4–5, 7, 9–13, intron 13 and exon 14) were provided by A. Andreadis. We carried out mutagenesis using Promega Gene Editor site-directed mutagenesis kit according to the manufacturer's recommendations using P301L (5'-dAA CACGTCCTGGGAGGCG-3') and selection (5'-p-dCCGCGAGACCCAC CCTTGAGGCTCCAGATTATC-3') primers. We sequenced using the BigDye Terminator Sequencing kit (Perkin Elmer) on an ABI377 automated sequencer with Sequence Navigator software (Perkin Elmer).

Transgenic constructs were generated by ligating a *Sall* fragment of each *Mtapt* construct into the *XhoI* linearized MoPrP vector⁶. Constructs were linearized (*NotI*), gel purified and digested with β -agarase according to the manufacturer's conditions (New England Biolabs). DNA was filtered, concentrated and diluted to 3 ng/ μ l (WT4R), 7 ng/ μ l (P301L) in microinjection buffer (5 mM Tris-HCl, pH 7.4, 10 mM NaCl, 0.1 mM EDTA).

Transgenes were microinjected into fertilized mouse (C57BL/DBA/2

SW) eggs and reimplanted into pseudopregnant females. We screened founders by PCR between exons 1 and 5 of the human *Mtapt* cDNA against an internal PS-2 control PCR.

In situ hybridization. We sectioned (at a thickness of 15 μ m) frozen mouse brains. Human-specific synthetic oligomers to exons 1 (5'-CTTTCAGGC CAGCGTCCGTGTCACCCCTCTGGTC-3') and 5 (5'-TTGTGTCATCGC TTCCAGTCCCGTCTTTGCTTTTAC-3') of human *Mtapt* cDNA were 3'-end labelled with α [³⁵S]dATP (NEN DuPont). Slides were fixed, dehydrated and hybridized overnight at 37 °C with labelled oligonucleotide. Control sections were hybridized in the presence of a 50-fold molar excess of unlabeled oligonucleotide. After hybridization, slides were stringently washed, dehydrated and exposed to Hyperfilm β -Max (Amersham) for 1–2 weeks.

Western-blot analysis. We carried out insoluble tau extraction²¹ and dephosphorylation²² as described on frozen brains. Soluble and insoluble tau was run on 7.5% SDS-PAGE gels, transferred to nitrocellulose and stained with a human tau-specific polyclonal antibody (E1, aa 19–33) and with antibodies (WKS45, Tau46) that recognize both human and mouse tau. Antibodies AT100 and AT180 that recognize tau phosphoepitopes were also used. Brains and spinal cords were prepared in the same volume; therefore, the amount of insoluble tau loaded from the spinal cord was 80% less than that loaded from the brains.

Tau ELISAs. Mouse hemibrains were homogenized at a w/v ratio of 100 mg/ml in TBS containing protease and phosphatase inhibitors, serially diluted and used to coat Maxi-sorb ELISA plates. Samples were evaporated to dryness at 37 °C and blocked in TBS containing 5% non-fat, dry milk. We added anti-tau monoclonal antibodies, human (CP27) and total (MN37 and Tg5) tau at 1:20 dilutions. Following incubation overnight at 4 °C, plates were washed in TBS containing 0.5% Tween 20 and incubated with goat anti-mouse antibodies coupled to HRP. Plates were washed and bound antibodies were quantified using ABTS peroxidase substrate (Bio-rad). Ratio of human to total tau was then assessed.

Immunohistochemistry. Perfused (0.9% saline followed by 4% paraformaldehyde) or immersion fixed (4% paraformaldehyde) brain sections were immunostained²³ with tau antibodies using standard avidin or streptavidin biotin peroxidase methods: MC-1 (Davies, 1:25–1:50; refs 11–13), AT8 (1:5,000) and AT180 (1:100; Endogen); CP3 (Davies, 1:100); CP9 (Davies, 1:100); CP13 (Davies, 1:100), PHF-1 (Davies, 1:100), Alz50 (Davies, 1:10), E-1 (Yen, 1:1,000) and α B crystallin (Novacastra, 1:1,000);

ubiquitin, UH19 (Ksiezak-Reding, 1:500); NFT antibody, Ab39 (Yen, 1:20); Ab69 (Yen, 1:20); TG3 (1:10); GFAP (Biogenex, 1:100); and phosphorylated neurofilament (Sternberger-Meyer, SMI-31; 1:5,000). Double immunostaining was performed on free-floating vibratome sections of brainstem incubated with rabbit GFAP and CP13 or Alz50 and SMI-31, followed 16 h later with isotype-specific second antibodies conjugated to fluorescein or rhodamine. MC-1 (refs 11–13) recognizes a unique conformation of human tau similar to that seen in AD brains. We used paraffin-embedded sections for histochemical stains (haematoxylin and eosin), thioflavin-S, Congo red and silver stains.

Electron microscopy. The brainstem, spinal cord and skeletal muscle from perfused mice (4% paraformaldehyde) were dissected and immersion fixed in paraformaldehyde. For pre-embedding, we performed immuno-EM as described above. The immunolabelled areas were dissected, fixed in OsO₄, dehydrated and embedded in Epon. For post-embedding immuno-EM, small pieces of fixed tissue from brainstem and spinal cord were embedded in LR White resin. Primary tau antibodies (CP13) were used to stain ultrathin sections on nickel grids, followed by gold-conjugated secondary antibodies. For routine ultrastructural studies, mice were perfused with 2% glutaraldehyde/2% paraformaldehyde/0.1 M cacodylate buffer, pH 7.4, and the tissues were immersion fixed in the same fixative for another 4 h, followed by OsO₄ and uranyl acetate and then dehydrated and embedded in Epon.

Neuronal cell counts. We performed cell counts on matching lumbosacral and cervical enlargement paraffin sections (of 5 μ m) of P301L (JNPL3) and non-transgenic mice stained with haematoxylin and eosin. Neuronal counts were from every fifth section from images captured by CCD camera. We counted 30 sections from each animal.

Acknowledgements

We thank S. Munger for oocyte injections; C. Zehr, L. Skipper, A. Grover and J. Adamson for genotyping; L. Rousseau and V. Phillips for brain sectioning; M. McKinney for spinal cord dissections; F. Conkle, C. Ortega and D. Forste for mouse maintenance; and D. Borchelt for the MoPrP vector. This work was supported by the NIA (RO1 and PO1 grants to M.H., D.W.D., S.-H.Y., J.H., P.D.), The Mayo Foundation, The Society for Progressive Supranuclear Palsy (to D.W.D.) and The Smith Scholar Program (to M.H.).

Received 24 April; accepted 27 June 2000.

- Dickson, D.W. Neurodegenerative diseases with cytoskeletal pathology: a biochemical classification. *Ann. Neurol.* **42**, 541–544 (1997).
- Hutton, M. Missense and splicing mutations in tau associated with FTDP-17: multiple pathogenic mechanisms. *Neurosci. News* **2**, 73–82 (1999).
- Hutton, M. et al. Association of missense and 5'-splice-site mutations in tau with the inherited dementia FTDP-17. *Nature* **393**, 702–705 (1998).
- Dumanchin, C. et al. Segregation of a missense mutation in the microtubule-associated protein tau gene with familial frontotemporal dementia and parkinsonism. *Hum. Mol. Genet.* **7**, 1825–1829 (1998).
- Rizzu, P. et al. High prevalence of mutations in the microtubule-associated protein tau in a population study of frontotemporal dementia in the Netherlands. *Am. J. Hum. Genet.* **64**, 414–421 (1999).
- Borchelt, D.R. et al. A vector for expressing foreign genes in the brains and hearts of transgenic mice. *Genet. Anal.* **13**, 159–163 (1996).
- Trojanowski, J.Q. & Lee, V.M. Transgenic models of tauopathies and synucleinopathies. *Brain Pathol.* **9**, 733–739 (1999).
- Kosik, K.S., Orecchio, L.D., Bakalis, S. & Neve, R.L. Developmentally regulated expression of specific tau sequences. *Neuron* **2**, 1389–1397 (1989).
- Iqbal, K., Braak, E., Braak, H., Zaidi, T. & Grundke-Iqbal, I. A silver impregnation method for labeling both Alzheimer paired helical filaments and their polypeptides separated by sodium dodecyl sulfate-polyacrylamide gel electrophoresis. *Neurobiol. Aging* **12**, 357–361 (1991).
- Mirra, S.S. et al. Tau pathology in a family with dementia and a P301L mutation in tau. *J. Neuropathol. Exp. Neurol.* **58**, 335–345 (1999).
- Ikonomic, M.D. et al. The loss of GluR2(3) immunoreactivity precedes neurofibrillary tangle formation in the entorhinal cortex and hippocampus of Alzheimer brains. *J. Neuropathol. Exp. Neurol.* **56**, 1018–1027 (1997).
- Jicha, G.A., Bowser, R., Kazam, I.G. & Davies, P. Alz-50 and MC-1, a new monoclonal antibody raised to paired helical filaments, recognize conformational epitopes on recombinant tau. *J. Neurosci. Res.* **48**, 128–132 (1997).
- Jicha, G.A., Berenfeld, B. & Davies, P. Sequence requirements for formation of conformational variants of tau similar to those found in Alzheimer's disease. *J. Neurosci. Res.* **55**, 713–723 (1999).
- Spillantini, M.G., Bird, T.D. & Ghetti, B. Frontotemporal dementia and Parkinsonism linked to chromosome 17: a new group of tauopathies. *Brain Pathol.* **8**, 387–402 (1998).
- Spillantini, M.G. & Goedert, M. Tau protein pathology in neurodegenerative diseases. *Trends Neurosci.* **21**, 428–433 (1998).
- Götz, J. et al. Somatodendritic localization and hyperphosphorylation of tau protein in transgenic mice expressing the longest human brain tau isoform. *EMBO J.* **14**, 1304–1313 (1995).
- Ishihara, T. et al. Age-dependent emergence and progression of a tauopathy in transgenic mice overexpressing the shortest human tau isoform. *Neuron* **24**, 751–762 (1999).
- Spittaels, K. et al. Prominent axonopathy in the brain and spinal cord of transgenic mice overexpressing four-repeat human tau protein. *Am. J. Pathol.* **155**, 2153–2165 (1999).
- Probst, A. et al. Axonopathy and amyotrophy in mice transgenic for human four-repeat tau protein. *Acta Neuropathol.* **99**, 469–481 (2000).
- Sergeant, N., Watzek, A. & Delacourte, A. Neurofibrillary degeneration in progressive supranuclear palsy and corticobasal degeneration: tau pathologies with exclusively "exon 10" isoforms. *J. Neurochem.* **72**, 1243–1249 (1999).
- Greenberg, S.G. & Davies, P. A preparation of Alzheimer paired helical filaments that displays distinct tau proteins by polyacrylamide gel electrophoresis. *Proc. Natl. Acad. Sci. USA* **87**, 5827–5831 (1990).
- Greenberg, S.G., Davies, P., Schein, J.D. & Binder, L.I. Hydrofluoric acid-treated tau PHF proteins display the same biochemical properties as normal tau. *J. Biol. Chem.* **267**, 564–569 (1992).
- Feany, M.B. & Dickson, D.W. Widespread cytoskeletal pathology characterizes corticobasal degeneration. *Am. J. Pathol.* **146**, 1388–1396 (1995).

EXHIBIT 11

Hibernation model of tau phosphorylation in hamsters: selective vulnerability of cholinergic basal forebrain neurons – implications for Alzheimer's disease

Wolfgang Härtig,¹ Jens Stieler,¹ Ate S. Boerema,² Jennifer Wolf,¹ Udo Schmidt,¹ Jana Weißfuß,¹ Torsten Bullmann,¹ Arjen M. Strijkstra² and Thomas Arendt

¹Departments of Neurochemistry and Neuroanatomy, Paul Flechsig Institute for Brain Research, University of Leipzig, Jahnallee 59, 04109 Leipzig, Germany

²Department of Chronobiology, University of Groningen, Kerklaan 30, 9751 NN Haren, the Netherlands

Keywords: animal model, AT8, septo-hippocampal projection, Syrian hamster, torpor

Abstract

Neurofibrillar tangles made up of 'paired helical filaments' (PHFs) consisting of hyperphosphorylated microtubule-associated protein tau are major hallmarks of Alzheimer's disease (AD). Tangle formation selectively affects certain neuronal types and systematically progresses throughout numerous brain areas, which reflects a hierarchy of neuronal vulnerability and provides the basis for the neuropathological staging of disease severity. Mechanisms underlying this selective neuronal vulnerability are unknown. We showed previously that reversible PHF-like phosphorylation of tau occurs during obligate hibernation. Here we extend these findings to facultative hibernators such as Syrian hamsters (*Mesocricetus auratus*) forced into hibernation. In this model, we showed in the basal forebrain projection system that cholinergic neurons are selectively affected by PHF-like phosphorylated tau, while γ -aminobutyric acid (GABA)ergic neurons are largely spared, which shows strong parallels to the situation in AD. Formation of PHF-tau in these neurons apparently does not affect their function as pacemaker for terminating hibernation. We conclude that although formation of PHF-like phosphorylated tau in the mammalian brain follows a certain hierarchy, affecting some neurons more frequently than others, it is not necessarily associated with impaired neuronal function and viability. This indicates a more general link between PHF-like phosphorylation of tau and the adaptation of neurons under conditions of a 'vita minima'.

Introduction

Alzheimer's disease (AD) is a dementia neurodegenerative disorder characterized by extracellular neuritic plaques, composed of β -amyloid peptides (Selkoe, 2001) and intracellular neurofibrillar tangles made up of 'paired helical filaments' (PHFs) consisting of hyperphosphorylated microtubule-associated protein tau (Goedert *et al.*, 1989; Lee *et al.*, 2001). Neurofibrillar degeneration, i.e. neuronal death associated with PHF-tau pathology, typically affects long-axon projection neurons of cortical input systems arising in the basal forebrain and intracortical circuitry, which are both involved in the cortical processing of memory function (Morrison & Hof, 1997). Degeneration at very early and even pre-symptomatic stages of AD starts at circumscribed sites and progresses in an orderly fashion throughout numerous cortical and subcortical brain areas. This systematic progression of neurofibrillar pathology reflecting a hierarchy of neuronal vulnerability provides the basis for the commonly accepted neuropathological staging of disease severity (Braak & Braak, 1991).

The cholinergic basal forebrain projection neurons giving rise to the cholinergic innervation of the entire cortical mantle (Wenk *et al.*, 1980; Bigl *et al.*, 1982; Butcher & Woolf, 2004; Semba, 2004) is one of those areas where neurofibrillar degeneration occurs very early on

in AD (Morrison & Hof, 1997; Arendt *et al.*, 1983). Cholinergic projection neurons in the basal forebrain were classified according to their mainly cortical projection targets as Ch1–Ch4 regions in the rat (Mesulam *et al.*, 1983). The medial septum/diagonal band (MSDB) complex (also termed Ch1–Ch2) projects to the hippocampus and contains a cholinergic and a γ -aminobutyric acid (GABA)ergic component (Köhler *et al.*, 1984; Freund & Antal, 1988; Záborszky *et al.*, 1999; Sarter & Bruno, 2002), as well as numerous glutamatergic neurons (Gritti *et al.*, 2003; Colom, 2006). Loss of cholinergic basal forebrain neurons causes cholinergic deafferentation of both the hippocampus and neocortex, and is considered as an early pathological event in AD (Davies & Maloney, 1976; Whitehouse *et al.*, 1981; Arendt *et al.*, 1983; McGeer *et al.*, 1984; Geula *et al.*, 1998; Härtig *et al.*, 2002), which very likely contributes to cognitive dysfunction (Kása *et al.*, 1997; Geula & Mesulam, 1999). Both neuronal loss and tangle load in the basal forebrain inversely correlate with antemortem neuropsychological assessments of cognitive function in patients with AD (Samuel *et al.*, 1994; Iraizoz *et al.*, 1999). Other components of basal forebrain corticopetal projections, with GABAergic neurons being the most prominent (Fisher *et al.*, 1988), are largely spared in AD (Sarter & Bruno, 2002), indicating a selective neuronal vulnerability of cholinergic basal forebrain projection neurons.

In a previous study, we have described the reversible formation of PHF-like phosphorylated tau during hibernation in the European ground squirrel (Arendt *et al.*, 2003). As hibernation in mammals is associated with a high degree of structural neuronal plasticity

Correspondence: Dr W. Härtig, as above.

E-mail: hartig@medizin.uni-leipzig.de

Received 8 June 2006, revised 14 September 2006, accepted 25 October 2006

(Popov & Bocharova, 1992; Popov *et al.*, 1992; Arendt *et al.*, 2003) it might be a model suitable to analyse cellular aspects of selective neuronal vulnerability potentially linked to plastic neuronal mechanisms. Therefore, the present study was focused on the tau phosphorylation in cholinergic and other neuronal subpopulations in the basal forebrain of hibernating Syrian hamsters.

Materials and methods

Hibernating animals

This study was performed with 53 wild-type Syrian hamsters (*Mesocricetus auratus*). Forty animals were derived from the breeding colony in Haren, University of Groningen, and 13 hamsters were from the colony in the Paul Flechsig Institute, University of Leipzig. Twelve animals were maintained at a constant temperature of 21 °C and a daily photoperiod of 14 h light and 10 h darkness. Forty-one animals were subjected to hibernation conditions according to Oklejewicz *et al.* (2001). Torpor was induced by exposing the animals to several weeks of short photoperiod as follows: 4 weeks of 'short day' (8 h light and 16 h darkness) at room temperature (20–25 °C) were followed by continuous dim red light conditions (< 0.5 Lux, 25 W red light bulb) and a reduction of the ambient temperature to 5–7 °C. General locomotor activity was monitored with passive infrared detectors allowing the discrimination between torpor (periods with >24 h of inactivity) and euthermic phases (Oklejewicz *et al.*, 2001). Upon death the state of the animals was confirmed by measurements of rectal body and mouth temperatures, ranging between ~7 °C for torpid animals and ~34 °C for euthermic hamsters. According to their hibernation state the following animal groups were distinguished: euthermic (EU), torpor early (TE), torpor late (TL), arousal early (AE) and arousal late (AL). Depending on their time of inactivity after an euthermic episode hamsters were designated as TE (24 h of inactivity) or TL (4 days of inactivity), while animals that were sampled 2.5 h and 8.5 h after arousal induction represented the groups AE and AL, respectively. All animals were about 11 months old when they were killed by means of an intraperitoneal injection of 60 mg/kg pentobarbital, preceding perfusion or decapitation. The experiments were approved by the Animal Experiments Committee of the University of Groningen (license number DEC-2954), and the Animal Care and Use Committee of the University of Leipzig (T74/05). They conformed to the European Communities Council Directive (86/609/EEC).

Tissue preparation

For immunohistochemistry, six animals each of all experimental groups were perfused with 4% paraformaldehyde in 0.1 M phosphate-buffered saline, pH 7.4 (PBS) followed by post-fixation overnight at 6 °C. After equilibration and cryoprotection with 30% sucrose in PBS,

30-µm-thick coronal sections from forebrains were cut using a freezing microtome. Sections were collected in 0.1 M Tris-buffered saline, pH 7.4 (TBS) containing sodium azide. For Western blot analysis, 23 animals of all experimental groups were decapitated. The brains were removed from the skulls, dissected and frozen on dry-ice within less than 2 min and then stored until further processing at –80 °C.

Western blotting

For the detection of PHF-like phosphorylated tau, samples containing the MSDB, the neostriatum, the neocortex or the hippocampus were dissected according to the atlas of Morin & Wood (2001). They were homogenized in ninefold volumes of cold protein extraction buffer [in mM: Tris, 20, pH 7.2; NaCl, 150; MgCl₂, 2; 1% nonylphenyl-polyethylenglycol, 40; dithiothreitol, 1; Na₃VO₄, 1; NaF, 5; phenylmethylsulphonylfluoride, 1; 1 µg/mL leupeptin and complete proteinase inhibitor (Roche Diagnostics GmbH, Mannheim, Germany)] using an Ultra Turrax T8 (IKA Labortechnik, Staufen, Germany). Homogenates were centrifuged for 30 min at 40 000 g and 4 °C. Clear supernatants were removed and their protein concentration was determined by Bradford assay. Samples were adjusted to an equal protein concentration and applied to sodium dodecyl sulphate-polyacrylamide gel electrophoresis (SDS-PAGE) using 10% gels.

Following SDS-PAGE, separated proteins were transferred to polyvinylidene fluoride (PVDF) membranes (Polyscreen, Perkin-Elmer Life Sciences, Boston, MA, USA). Blots were then treated with blocking buffer (TBS containing 2% bovine serum albumin and 0.05% Tween 20) and probed overnight with the primary antibody AT8 (1 : 1000; Perbio, Bonn, Germany) recognizing phosphorylated serine 202 and threonine 205 from tau (Goedert *et al.*, 1995), affinity-purified goat anti-choline acetyltransferase (ChAT) (1 : 500) or rabbit anti-vesicular acetylcholine transporter (VACHT) (1 : 1000, see also Table 1), which were all diluted in blocking buffer. Following several rinses with PBS, the blots were processed with peroxidase-conjugates of goat anti-mouse IgG (1 : 10 000 in blocking buffer; Pierce, Rockford, IL, USA), donkey anti-goat IgG (1 : 5000; Dianova, Hamburg, Germany, supplier for Jackson ImmunoResearch, West Grove, PA, USA) or swine anti-rabbit IgG (1 : 5000, Dakocytomation, Hamburg, Germany) and rinsed again with PBS. Immunoreactivities were then detected by enhanced chemiluminescence (0.23 mg/mL Luminol, 0.1 mg/mL p-coumaric acid and 0.27 µL/mL H₂O₂ in 0.1 M Tris solution, pH 8.6) and visualized applying a KODAK Image Station 2000R (Tokyo, Japan).

Immunohistochemistry

Free-floating sections were applied to immunoperoxidase staining of phospho-tau with AT8 (1 : 2000) and a streptavidin/biotinyl-peroxidase

TABLE 1. Applied antibodies for immunofluorescence labelling of neuronal subpopulations

Antigen	Host	Source	Designation	Dilution for Cy2/Cy5 labelling
VACHT	Rabbit	Synaptic Systems, Göttingen, Germany	139003	1 : 50
ChAT	Goat	Chemicon, Temecula, CA, USA	AB144P	1 : 25
p75 ^{NTR}	Rabbit	Advanced Targeting Systems, San Diego, CA, USA	AB-01AP	1 : 300
VGLUT2	Rabbit	Synaptic Systems	135102	1 : 250
VGAT	Rabbit	Synaptic Systems	131002	1 : 250
Parvalbumin	Rabbit	Swant, Bellinzona, Switzerland	PV28	1 : 200
Calbindin	Rabbit	Chemicon	AB 1778	1 : 200
Calretinin	Rabbit	Swant	7699/4	1 : 300

method using nickel-enhanced diaminobenzidine as chromogen, as previously described (Härtig *et al.*, 1995, 2005).

Double- and triple-fluorescence labelling with AT8 in combination with various markers was started by blocking of sections with 5% normal donkey serum in TBS containing 0.3% Triton X-100 for 1 h. Subsequently, AT8 was used at a dilution of 1 : 300 in the blocking solution at room temperature combined with neuronal markers as listed in Table 1.

For double-immunofluorescence labelling, AT8 was concomitantly used with primary rabbit antibodies directed against the neuronal markers VACHT, low-affinity neurotrophin receptor p75 (p75^{NTR}), vesicular glutamate transporter 2 (VGLUT2), vesicular GABA transporter (VGAT), parvalbumin, calbindin and calretinin. Immunoreactivities were revealed with a cocktail of carbocyanine (Cy)3-tagged donkey anti-mouse IgG and donkey anti-rabbit IgG conjugated to Cy2. Both fluorochromated antibodies were obtained as all other secondary immunoreagents from Dianova and applied at 20 µg/mL in TBS containing 2% bovine serum albumin for 1 h. Combined immunofluorescence staining of phospho-tau and ChAT was achieved by applying mixtures of AT8 and goat anti-ChAT, which were visualized by Cy3-tagged donkey anti-mouse IgG and donkey anti-goat IgG coupled to Cy2. In parallel, this double-labelling was combined with the application of rabbit anti-parvalbumin and Cy5-conjugated donkey anti-rabbit IgG. For the triple-immunofluorescence labelling of phospho-tau, p75^{NTR} and ChAT, the latter was visualized by Cy5-donkey anti-goat IgG, whereas the other markers were stained as described above.

Controls were performed by omitting primary antibodies. In additional control experiments, the fluorophores related to the relevant markers were switched.

After fluorescence labelling, all sections were treated with Sudan Black B to quench their autofluorescence, as described by Schnell *et al.* (1999). Finally, the sections were mounted onto fluorescence-free glass slides and coverslipped with glycerol/gelatin (Sigma, Taufkirchen, Germany).

Microscopy

The analysis of immunolabelling was based on an atlas for the hamster brain (Morin & Wood, 2001) and the previous detailed description of cholinergic neurons in the hamster basal forebrain by Brauer and co-workers (Schober *et al.*, 1989). Tissue sections were inspected with a Zeiss Axioplan microscope equipped with the filters no. 9 and 15 for the visualization of Cy2 and Cy3, respectively. For the concomitant detection of both carbocyanines, the 'double' filters 24 and 25 were used.

In addition, sections were examined with a confocal laser-scanning microscope (LSM 510 Meta, Zeiss) equipped with an argon laser exciting Cy2 (at 488 nm) and two helium-neon lasers (543 nm for Cy3 and 633 nm for Cy5). Possibly interfering red fluorescence within the green spectrum in sections stained both for Cy2 and Cy3 was prevented by applying a band-pass filter (530–550 nm). In triple-stained sections, Cy5-labelled structures were colour-coded in blue.

In general, original pictures were slightly altered in brightness, contrast and sharpness using Adobe Photoshop 7.0 software (Adobe Systems, Mountain View, CA, USA).

Results

Western blot analysis of forebrain regions of hibernating hamsters revealed reversible tau phosphorylation. PHF-like phosphorylated

tau, detected by AT8 in the MSDB complex, the striatum, the hippocampus and the neocortex was strongly elevated in samples from torpid compared with euthermic animals, and after arousal returned to pre-torpid levels (Fig. 1). In euthermic and arousing animals, it was completely absent in striatal, hippocampal and neocortical samples, while it could be detected at a low level in the MSDB. Electrophoretically separated double-bands in torpor displayed the expected molecular weights between 50 and 70 kDa (Janke *et al.*, 1999).

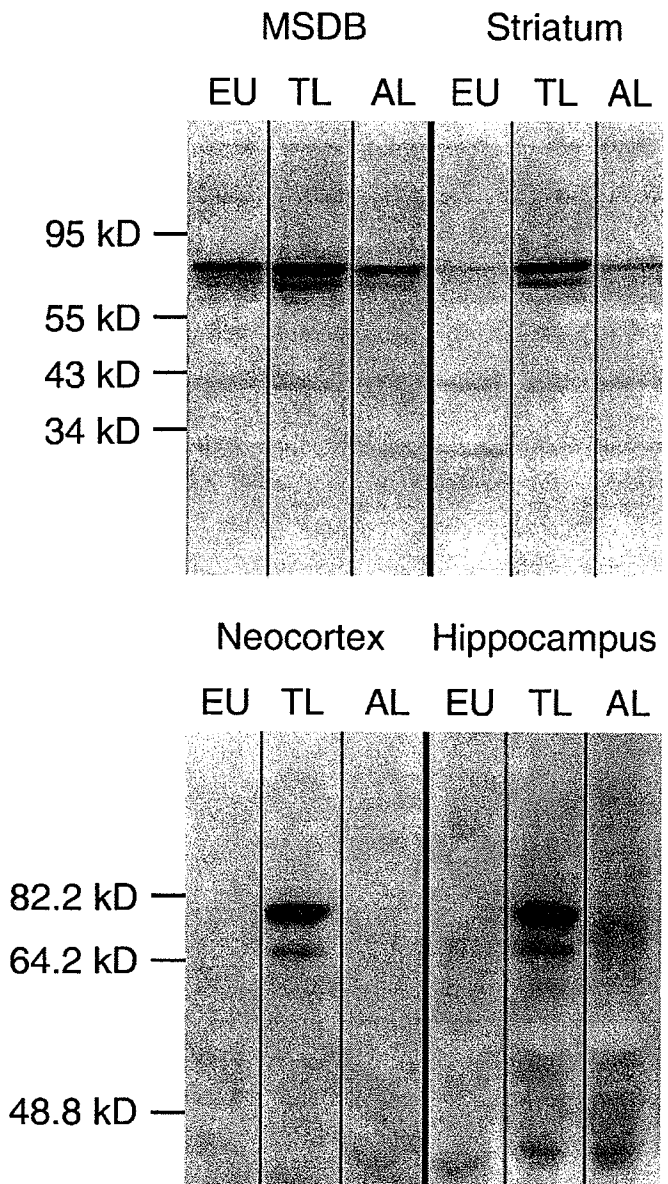


FIG. 1. Western blot analysis of PHF-like protein tau with the monoclonal mouse antibody AT8 in the medial septum/diagonal band (MSDB) complex, striatum, neocortex and hippocampus during different stages of hibernation. Comparison of representative samples obtained from euthermic animals (EU) and hamsters in torpor late (TL) and arousal late (AL) applied to SDS-PAGE and blotted to PVDF membranes. Immunodetection with peroxidase-conjugated goat anti-swine IgG and a chemiluminescence detection system. Notice the double band with apparent molecular weights between 50 and 70 kDa predominantly in torpor, largely disappearing during arousal and hardly visible in EU, except in the MSDB.



FIG. 2. Detection of reversible tau phosphorylation during hibernation of hamsters in the MSDB complex. AT8-staining with a streptavidin/biotin immunoperoxidase method and nickel-enhanced diaminobenzidine. (A) Euthermia. (B) Torpor late. (C) Arousal early. Already visible at lower magnification, AT8-immunoreactivity is apparently absent under euthermic conditions, strong in torpor and diminished during arousal. Scale bar: 400 μ m.

Immunohistochemical preparations with AT8 of the basal forebrain, hippocampus, cerebral cortex and ventral striatum (Figs 2 and 3) also displayed a strong immunoreactivity during torpor, which declined again after arousal confirming the reversible tau phosphorylation obtained on Western blots. These data exemplify similar findings, e.g. in the dorsal striatum as well as in the motor and entorhinal cortex (not shown).

Most cells containing PHF-like phosphorylated tau in the medial septum and diagonal band area were identified as cholinergic neurons, based on double-immunofluorescence for AT8 with cholinergic markers such as VAcHT or the neurotransmitter-synthesizing enzyme ChAT (Fig. 4). As shown in Fig. 4, both neuronal somata and axon terminals of cholinergic neurons, immunoreactive for VAcHT, contained PHF-like phosphorylated tau. The specific involvement of cholinergic neurons in the MSDB area was further verified by triple-immunofluorescence for the simultaneous detection of PHF-like tau (AT8), ChAT and p75^{NTR}. The majority of AT8-immunopositive structures were found to co-express ChAT in conjunction with p75^{NTR}. In addition, numerous ChAT-expressing cells of the striatum displayed immunopositivity for AT8, as exemplified in Fig. 5.

Despite the formation of PHF-like phosphorylated tau in cholinergic neurons of the MSDB, no obvious alterations in the expression of ChAT and VAcHT were observed in Western blots of samples from the MSDB and the striatum during the hibernation cycle (Fig. 6).

While cholinergic basal projection neurons were constantly affected by reversible tau phosphorylation during hibernation, non-cholinergic components of the basal forebrain corticopetal projection system were either not involved at all or at least less frequently affected. It is noteworthy that glutamatergic and GABAergic axon terminals could be identified by applying antibodies raised against peptide sequences corresponding to amino acid sequences of rat VGLUT2 and VGAT, respectively. Contrary to cholinergic axon terminals (see Fig. 4), none of the glutamatergic or GABAergic terminals contained PHF-like phosphorylated tau (Fig. 7A and B). Furthermore, parvalbumin-containing neurons, which in the basal forebrain basically represent GABAergic neurons (Freund & Antal, 1988; Freund, 1989; Brauer *et al.*, 1991), were devoid of PHF-like tau (Fig. 7C).

Neurons of the MSDB area immunoreactive for calbindin (Fig. 8A) or calretinin (Fig. 8B), which most likely represent the populations of glutamatergic neurons (Gritti *et al.*, 2003), only occasionally contained PHF-like tau (Fig. 8A' and B').

In control experiments, the omission of primary antibodies resulted in the expected absence of any staining. The switch of the fluorophores related to the relevant markers as additional control led to unaltered staining patterns. The treatment of all fluorescently

labelled sections with Sudan Black B quenching the fluorescence of age-dependently occurring lipofuscin was essential due to some autofluorescence in untreated tissues interfering with the specific immunosignals in parallel experiments (not shown).

Discussion

The present study demonstrates reversible PHF-like phosphorylation of the microtubule-associated protein tau during the hibernation cycle of Syrian hamsters, facultative hibernators forced into hibernation. Formation of PHF-like phosphorylated tau was found both at cortical and subcortical areas such as the basal forebrain.

Selective neuronal vulnerability against PHF-like phosphorylation of tau

To define why neurofibrillar degeneration selectively affects special types of neurons and brain areas while others are spared, i.e. to unravel the mechanism behind selective neuronal vulnerability, is a key issue to understand the process of neurodegeneration. More than 100 years ago, Paul Flechsig (1896) had advanced the idea that variations in vulnerability of different groups of neurons are to be traced back in large part to developmental conditions, a concept, later defined by Cecile and Oscar Vogt as the 'principle of pathoclosis' (Vogt & Vogt, 1951). Brain areas and neuronal types highly vulnerable against neurofibrillary degeneration in AD are indeed different to the rest of the brain at least with respect to two other aspects, which might be the key to understanding underlying mechanisms: they mature rather late during ontogenic development (Braak & Braak, 1996); and they exhibit a particularly high degree of synaptic plasticity and probably synaptic turnover (for review, see Arendt, 2003).

The present study shows within the MSDB complex a rather selective neuronal vulnerability with respect to formation of highly phosphorylated tau. Cholinergic neurons were constantly affected. Almost all neurons, expressing ChAT and VAcHT, also contained PHF-like phosphorylated tau. Moreover, axon terminals of cholinergic neurons, identified by VAcHT-immunolabelling, were typically filled with phosphorylated tau. This indicates that PHF-like phosphorylated tau is highly abundant not only in the soma but also in the presynaptic compartment of cholinergic neurons.

Numerous AT8-positive neurons were shown to be co-immunopositive for p75^{NTR} that in the basal forebrain of various mammalian species is exclusively expressed by cholinergic projection neurons (Springer *et al.*, 1987; Tremere *et al.*, 2000). The susceptibility of

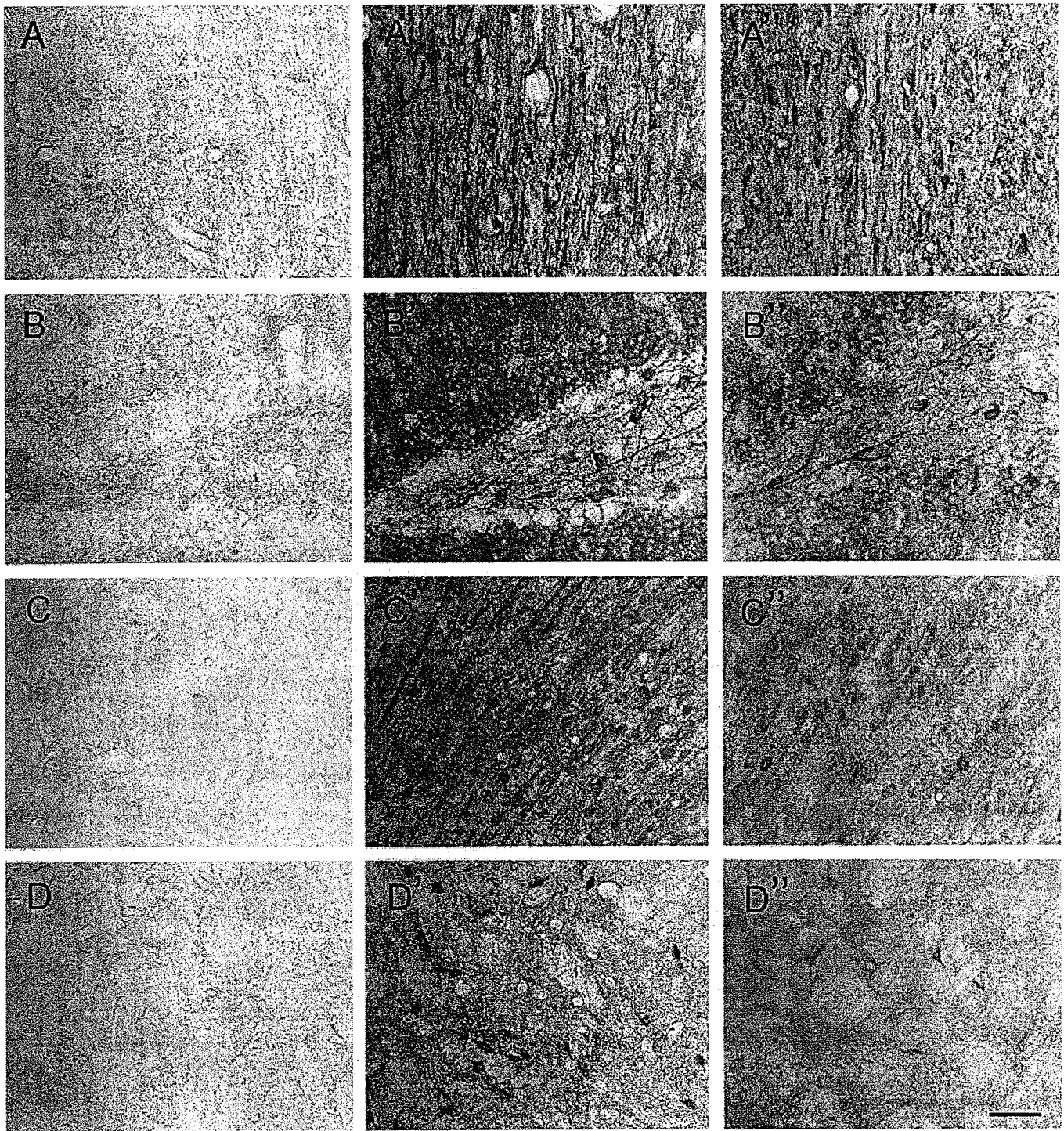


FIG. 3. Reversible tau phosphorylation during hibernation of hamsters in representative regions of the forebrain at a cellular level in (A, A', A'') the medial septum, (B, B', B'') the hippocampal gyrus dentatus, (C, C', C'') the cingulate cortex and (D, D', D'') the ventral striatum. AT8-staining with a streptavidin/biotin immunoperoxidase method and nickel-enhanced diaminobenzidine. (A–D) Euthermia. (A'–D') Torpor late. (A''–D'') Arousal early. AT8-immunoreactivity is apparently absent under euthermic conditions, strong in torpor and considerably diminished during arousal. Scale bar: 50 μ m (in D'', valid for all parts of the plate).

cholinergic neurons to tau hyperphosphorylation, however, was not restricted to the basal forebrain projection nuclei affected by neurofibrillar degeneration early in the course of AD (Morrison & Hof, 1997), but also found in cholinergic neurons of the ventral striatum that are similarly known to be involved in AD (Lehéricy *et al.*, 1989).

PHF-like phosphorylation of tau in hamsters was fully reversible, very quickly after arousing from torpor. Moreover, no quantitative changes in the expression of ChAT or VAcHT were observed in the MSDB area during the hibernation cycle. This indicates at least that formation of PHF-like phosphorylated tau in these neurons does not have any major effect on protein synthesis, and very

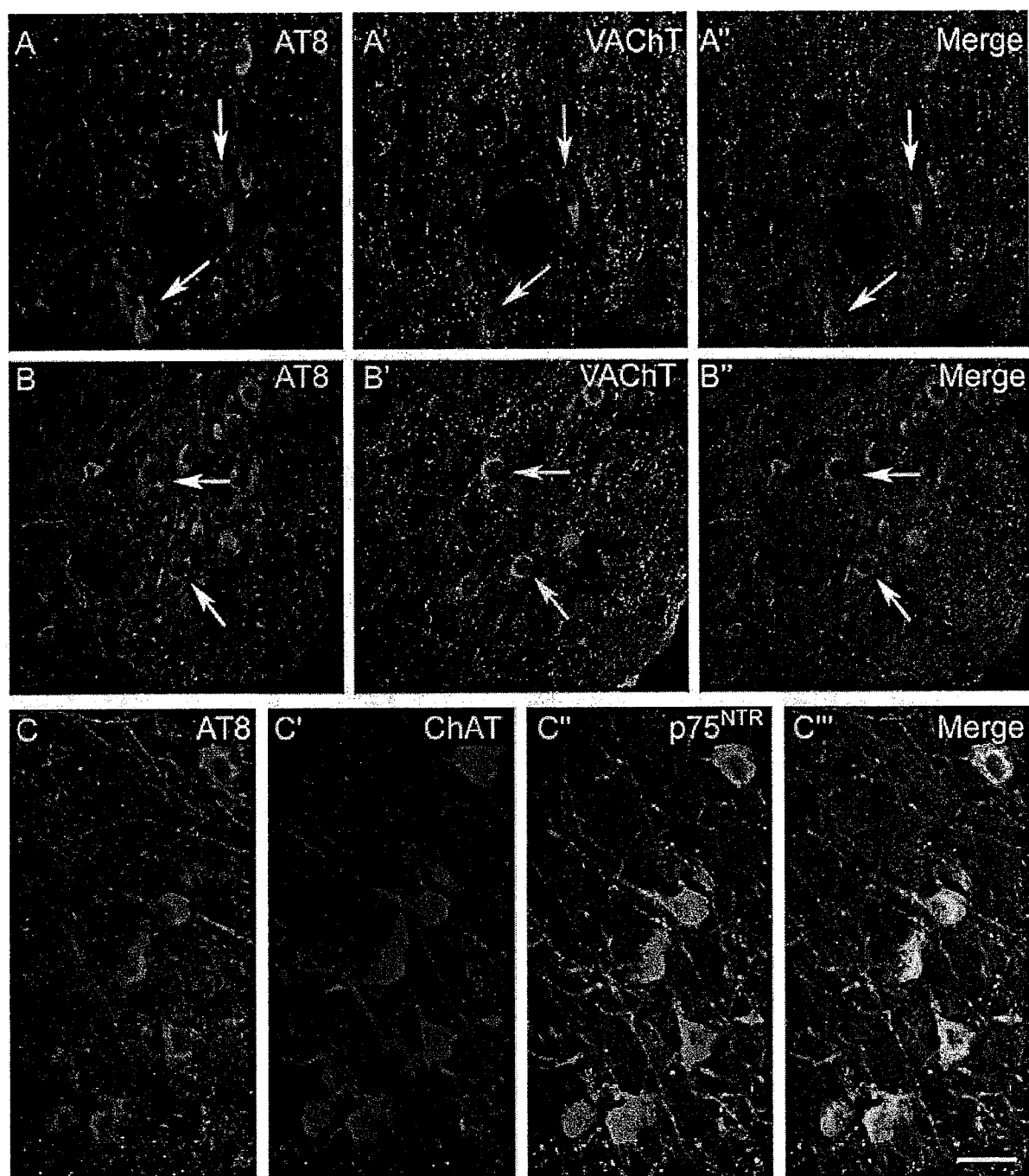


FIG. 4. PHF-like protein tau in cholinergic neurons in the basal forebrain of torpid hamsters revealed by multiple indirect immunofluorescence labelling and confocal laser-scanning microscopy. Combined immunodetection of AT8 and the vesicular acetylcholine transporter (VACHT) in the medial septum (A, A', A'') and in the diagonal band (B, B', B''). (A and B) Cy3-staining of AT8. (A' and B') Cy2-immunodecoration of VACHT. (A'' and B'') Merge. (C–C'') Multiple immunofluorescence labelling of AT8, choline acetyltransferase (ChAT) and the low-affinity neurotrophin receptor p75 (p75^{NTR}) in the diagonal band. (C) Cy3-staining of AT8. (C') ChAT-detection with Cy5. (C'') p75^{NTR}-labelling with Cy2. (C''') Merge. Co-expression of AT8 and ChAT-ir resulted in purple staining, whereas structures containing all three stained markers appeared white. Arrows indicate AT8-ir neurons co-expressing the cholinergic markers. Scale bar: 100 μ m.

unlikely affects neurotransmitter synthesis or even viability of neurons.

A major finding of this study is the absence of PHF-like phosphorylated tau in GABAergic basal forebrain neurons, identified by co-expression with parvalbumin (Freund, 1989; Brauer *et al.*, 1990). These neurons are also spared in human disorders associated

with neurofibrillar degeneration, such as AD (Rossor *et al.*, 1982; Sarter & Bruno, 2002). Quite similar, parvalbumin-containing basal forebrain neurons are less vulnerable than cholinergic septo-hippocampal projection neurons after experimental insults in rat such as intraseptal injection of β -amyloid peptide_{1–42} (Harkany *et al.*, 1995).

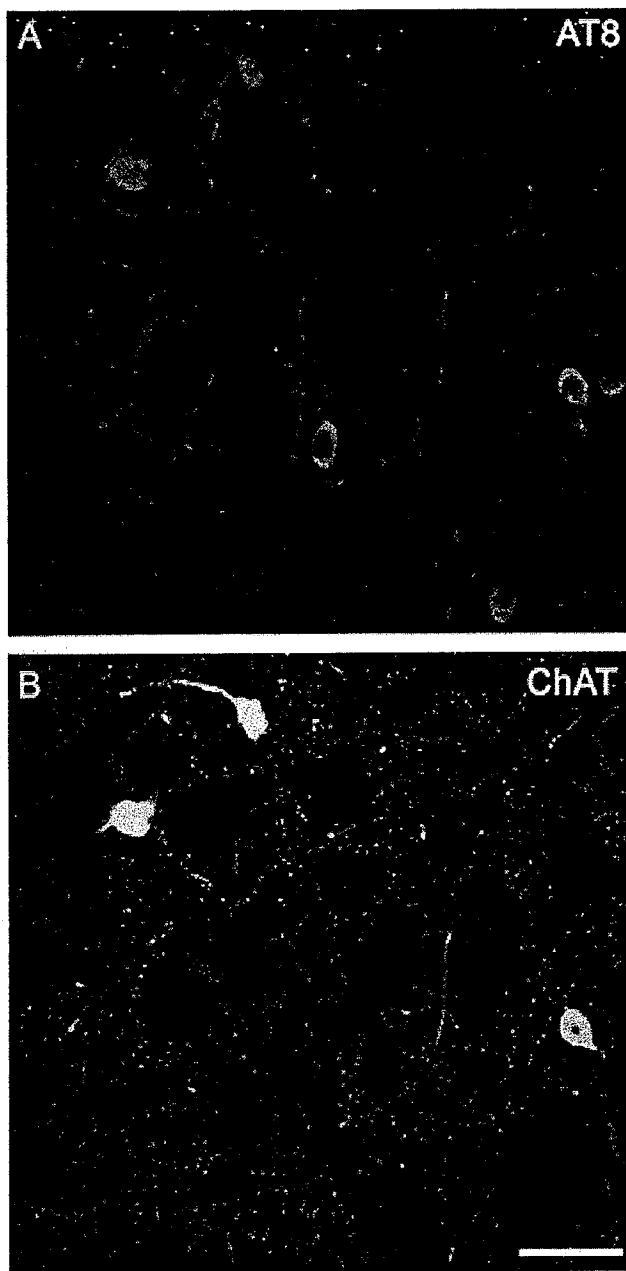


FIG. 5. PHF-like protein tau in cholinergic striatal neurons of torpid hamsters revealed by double-fluorescence labelling and confocal laser-scanning microscopy. (A) Cy3-staining of phospho-tau with AT8. (B) Cy2-immunolabelling of choline acetyltransferase (ChAT)-ir. Notice the co-expression of both markers in several neurons. Scale bar: 100 μ m.

Neurons expressing calbindin or calretinin were also affected to some extent by formation of PHF-like phosphorylated tau, but much less frequent than cholinergic neurons. Gritti *et al.* (2003) suggested that significant portions of both calbindin- and calretinin-containing neurons are likely to be glutamatergic.

Calretinin-immunopositive cells might predominantly comprise caudally or locally projecting glutamatergic neurons, while calbindin-containing neurons might represent cortically projecting glutamatergic basal forebrain neurons (Gritti *et al.*, 2003). Still, their neurotransmitter remains to be elucidated, and a GABAergic phenotype can not be ruled out (Manns *et al.*, 2001).

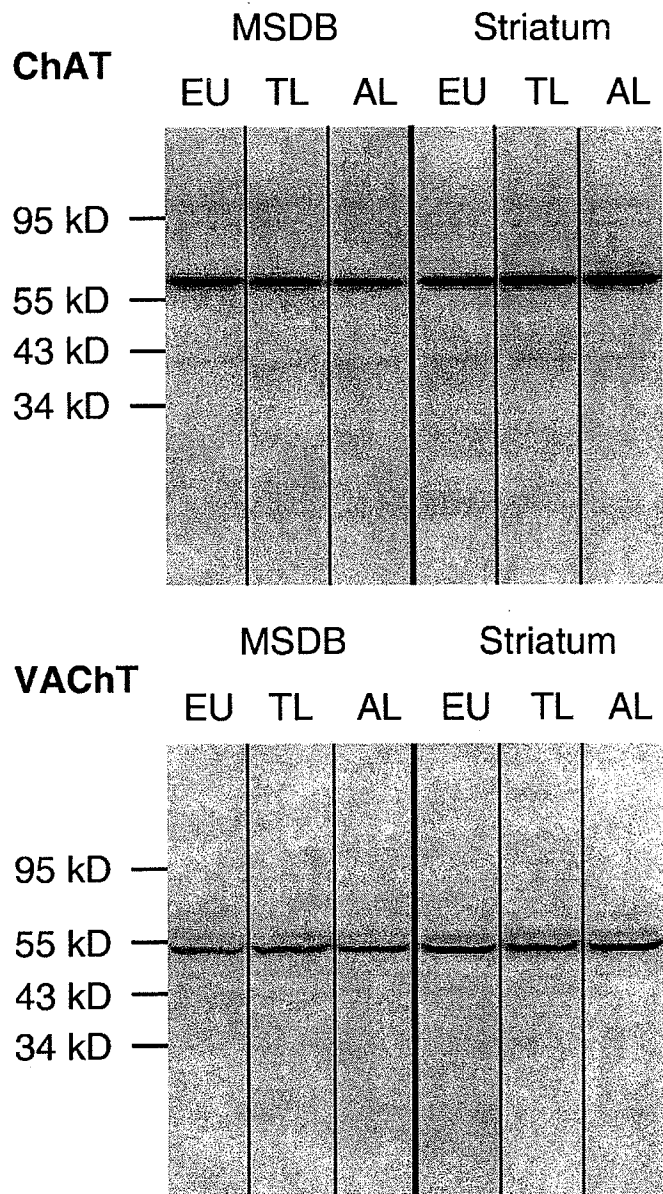


FIG. 6. Western blot analysis of the cholinergic markers choline acetyltransferase (ChAT) and vesicular acetylcholine transporter (VACHT) in the medial septum/diagonal band (MSDB) complex and the striatum during different stages of hibernation. No alterations of these proteins were revealed. Comparison of representative samples obtained from euthermic animals (EU), hamsters in torpor late (TL) and arousal late (AL), and applied to SDS-PAGE and blotting to PVDF membranes. Immunolabelling with rabbit anti-VACHT and goat anti-VACHT followed by the peroxidase-conjugates of swine anti-rabbit or donkey anti-goat and a chemiluminescence detection system.

Basal forebrain projection neurons and the control of cortical activity

Cholinergic projection neurons of the mammalian basal forebrain have been shown to control the excitability of neurons in large portions of the CNS including the cerebral cortex, hippocampus and thalamus (McCormick, 1990; Xiang *et al.*, 1998; Rasmussen, 2000). Anatomical, electrophysiological and pharmacological properties of these neurons and their effects on cortical neuronal excitability indicate that

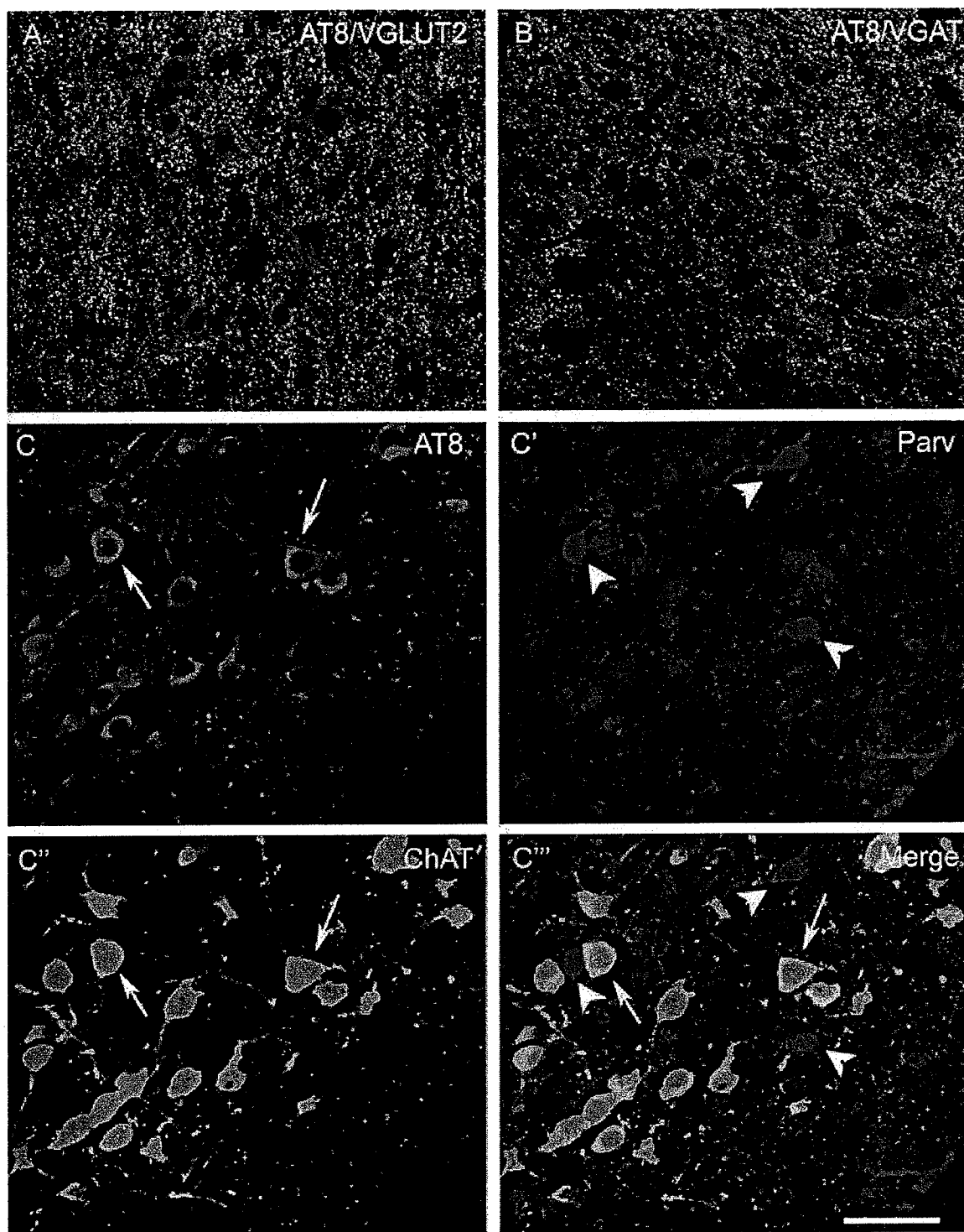


FIG. 7. Absent co-expression of PHF-like tau in vesicular glutamate transporter (VGLUT)2- and vesicular GABA transporter (VGAT)-immunopositive axonal endings and parvalbumin (Parv)-expressing somata in the diagonal band of torpid hamsters in contrast to cholinergic neurons containing phospho-tau. (A) Concomitant indirect immunofluorescence labelling of AT8 (Cy3, red) and VGLUT2 (Cy2, green). (B) Simultaneous indirect immunodetection of AT8 (Cy3, red) and VGAT (Cy2, green). (C–C'') Multiple immunofluorescence labelling of PHF-like protein tau, Parv and choline acetyltransferase (ChAT). (C) Cy3-staining of AT8. (C') ChAT-detection with Cy2. (C'') Parv-labelling with Cy2. (C''') Merge. Arrows in (C, C'', C''') indicate cholinergic neurons containing phospho-tau, whereas arrowheads in (C', C'') depict parvalbumin-containing neurons devoid of AT8-immunoreactivity. Scale bar: 100 μ m.

this system is utilized for setting the tone of cortical processing (Steriade & Buzsáki, 1990) and, thus, can be viewed as the most rostral extension of the ascending activation system.

Degeneration of these ascending cholinergic projections in AD might result in disturbances of cortical activation mechanisms as a prerequisite for efficient processing and transformation of afferent

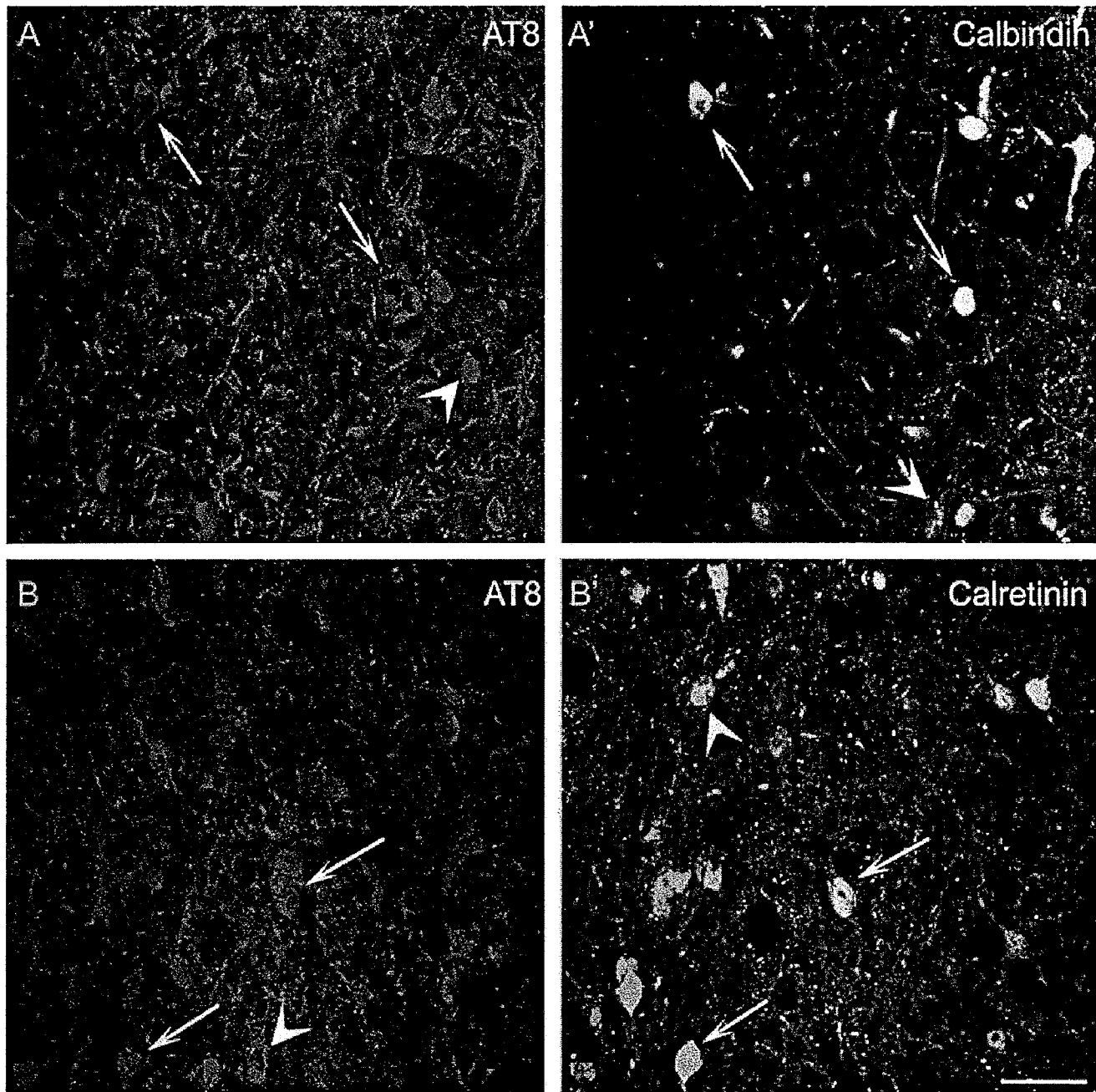


FIG. 8. AT8-immunopositive, highly phosphorylated tau in a subset of calbindin- and calretinin-ir neurons in the medial septum of torpid hamsters. (A and B) Red fluorescent Cy3-immunolabelling of highly phosphorylated tau using AT8 combined with green fluorescent Cy2-immunolabelling of calbindin (A') and calretinin (B'). Arrows exemplify cells co-expressing two stained markers, whereas the arrowheads indicate AT8-ir cells devoid of calcium-binding proteins (in A and B) or neurons containing calcium-binding proteins, but no AT8-ir (in A' and B'). Scale bar: 100 μ m.

information, which clinically appears as cognitive dysfunction. To some extent, this situation of depressed cortical activation is mimicked by the process of hibernation, which presumably begins with a reduction of the excitatory influence of the ascending activation system (Heller, 1979).

In particular, it had been the septo-hippocampal projection that was proposed to act as a 'sentry post' controlling depression of brain activity during torpor and triggering activation of the forebrain, which leads to arousal of hibernating animals (Belousov, 1993; Popova & Kokoz, 2004). As this pacemaker function that controls termination of torpor is

essential for the survival of hibernating animals, it requires protective mechanisms that guarantee their functional integrity even under conditions of metabolic suppression. It is therefore unlikely that formation of PHF-like phosphorylated tau in these neurons impairs their viability, and might rather reflect the induction of an active neuroprotective program against effects of reduced energy supply. This assumption is in agreement with a previous study, where after inhibition of protein phosphatase 2A *in vivo* through intrathecal application of okadaic acid, we observed a reduced rate of apoptosis in neurons containing hyperphosphorylated tau (Arendt *et al.*, 1998).

Hibernation as a model for hypometabolism, an early feature of neurodegenerative disorders

Neurodegeneration in AD and related disorders is associated with a slowly progressing deterioration of cell function, which for an unknown period of time represents a cellular 'vita minima' before cell death occurs. It might be assumed that this transient condition results in a hypometabolic state of the cell that confines their energy expenditure to functions essential for survival. Hypometabolic states and deficiencies in brain energy metabolism, however, have alternatively been proposed to be primary events in a pathogenetic chain eventually leading also to a hyperphosphorylated form of tau (Schubert *et al.*, 2003, 2004) and the whole spectrum of AD pathology (Frölich *et al.*, 1998; Hoyer, 1998; Gasparini & Xu, 2003; Haley *et al.*, 2006). As shown by functional brain imaging, this hypometabolic state occurs very early during the course of AD, even in presymptomatic stages, is a predictor of cognitive decline (Devous, 2002; de Leon *et al.*, 2001; Kim *et al.*, 2005) and might, thus, be an attractive therapeutic target (Swaab *et al.*, 2003). A potential pathogenetic role of hypometabolic conditions for AD is supported by recent data on thyroid disease as a potential risk factor for AD (Kalmijn *et al.*, 2000) as well as by the promoting effects of starvation on tau phosphorylation (Yanagisawa *et al.*, 1999; Planel *et al.*, 2001). However, the link between hypometabolic states and tau phosphorylation and the question whether tau phosphorylation might be cause or consequence of a reduced cell metabolism has not been analysed *in vivo*, as appropriate models have been lacking so far.

PHF-like phosphorylation of tau during obligatory and facultative hibernation

Hibernation is known as a hypometabolic state of lethargy with torpor, e.g. a subeuthermic temperature, shown by various mammalian species during winter time (Carey *et al.*, 2003; Storey, 2003; Storey & Storey, 2004), and may serve as a model for neuroprotection (Zhou *et al.*, 2001). Daily torpor and hibernation are considered as the most powerful measures of endotherms to reduce their energy expenditure. Small mammals use these strategies not only in a cold environment, but also under tropical conditions during timely limited 'bottlenecks of energy supply' (Heldmaier *et al.*, 2004). Characteristics of torpid animals are the suppression of protein synthesis (Frerichs *et al.*, 1998), controlled by protein phosphorylation and prolonged protein life time favouring adjusted metabolism and the protection of cell functions for long-term survival (Storey, 2003; Storey & Storey, 2004). We showed previously that reversible PHF-like phosphorylation of tau occurs in European ground squirrels, which are obligate hibernators (Arendt *et al.*, 2003). Here we confirm and extend these findings, and demonstrate that similar changes can be induced in facultative hibernators such as Syrian hamsters forced into hibernation. These results point towards the following. (i) A more general link between PHF-like phosphorylation of tau and the adaptation of neurons under conditions of a 'vita minima'. They indicate, furthermore, that (ii) formation of PHF-like phosphorylated tau in mammalian brain follows a certain hierarchy, affecting some neuronal types more frequently than others. Moreover, (iii) formation of PHF-like phosphorylated tau is not necessarily associated with impaired neuronal function and viability.

Syrian hamsters can much more easily be kept under animal house conditions than European ground squirrels and, thus, provide a comfortable physiological animal model suitable to analyse the mechanisms of PHF-like phosphorylation of tau and its cellular sequelae.

Acknowledgements

This study was supported by the Bundesministerium für Bildung und Forschung (BMBF, project 03 DU03LE) and the Interdisziplinäres Zentrum für Klinische Forschung (IZKF) at the University of Leipzig (01KS9504, project C1).

We thank Mrs Ute Bauer for excellent technical assistance and Dr Frank Nürnberger for support of the animal breeding. The work with the confocal laser-scanning microscope was kindly supported by Drs Jens Grosche, Bernd Biedermann and Markus Morawski.

Abbreviations

AD, Alzheimer's disease; AE, arousal early; AL, arousal late; ChAT, choline acetyltransferase; Cy, carbocyanine; EU, eutherm; GABA, γ -aminobutyric acid; MSDB, medial septum/diagonal band; p75^{NTR}, low-affinity neurotrophin receptor p75; PBS, phosphate-buffered saline; PHF, paired helical filament; PVDF, polyvinylidene fluoride; SDS-PAGE, sodium dodecyl sulphate-polyacrylamide gel electrophoresis; TBS, Tris-buffered saline; TE, torpor early; TL, torpor late; VACHT, vesicular acetylcholine transporter; VGAT, vesicular GABA transporter; VGLUT, vesicular glutamate transporter.

References

- Arendt, T. (2003) Synaptic plasticity and cell cycle activation in neurons are alternative effector pathways: the 'Dr. Jekyll and Mr. Hyde concept' of Alzheimer's disease or the yin and yang of neuroplasticity. *Prog. Neurobiol.*, **71**, 83–248.
- Arendt, T., Bigl, V., Arendt, A. & Tennstedt, A. (1983) Loss of neurons in the nucleus basalis of Meynert in Alzheimer's disease, paralysis agitans and Korsakoff's disease. *Acta Neuropathol.*, **61**, 101–108.
- Arendt, T., Holzer, M., Fruth, R., Brückner, M.K. & Gärtner, U. (1998) Phosphorylation of tau, A β -formation, and apoptosis after *in vivo* inhibition of PP-1 and PP-2A. *Neurobiol. Aging*, **19**, 3–13.
- Arendt, T., Stiel, J., Strijkstra, A.M., Hut, R.A., Rüdiger, J., Van der Zee, E.A., Harkany, T., Holzer, M. & Härtig, W. (2003) Reversible paired helical filament-like phosphorylation of tau is an adaptive process associated with neuronal plasticity in hibernating animals. *J. Neurosci.*, **23**, 6972–6981.
- Belousov, A.B. (1993) Role of the central nervous system in controlling hibernation. *Usp. Fiziol. Nauk*, **24**, 109–127.
- Bigl, V., Woolf, N.J. & Butcher, L.L. (1982) Cholinergic projections from the basal forebrain to frontal, parietal, temporal, occipital, and cingulate cortices: a combined fluorescent tracer and acetylcholinesterase analysis. *Brain Res. Bull.*, **8**, 727–749.
- Braak, H. & Braak, E. (1991) Neuropathological staging of Alzheimer-related changes. *Acta Neuropathol.*, **82**, 239–259.
- Braak, H. & Braak, E. (1996) Development of Alzheimer-related neurofibrillary changes in the neocortex inversely recapitulates cortical myelogenesis. *Acta Neuropathol.*, **92**, 197–201.
- Brauer, K., Schober, A., Wolff, J.R., Winkelmann, E., Lippa, H., Lüth, H.J. & Böttcher, H. (1991) Morphology of neurons in the rat basal forebrain nuclei: comparison between NADPH-diaphorase histochemistry and immunohistochemistry of glutamic acid decarboxylase, choline acetyltransferase, somatostatin and parvalbumin. *J. Hirnforsch.*, **32**, 1–17.
- Butcher, L.L. & Woolf, N.J. (2004) Cholinergic neurons and networks revisited. In Paxinos, G. (Ed.), *The Rat Nervous System*, 3rd Edn. Elsevier Academic Press, San Diego, pp. 1257–1268.
- Carey, H.V., Andrews, M.T. & Martin, S.L. (2003) Mammalian hibernation: cellular and molecular responses to depressed metabolism and low temperature. *Phys. Rev.*, **83**, 1153–1181.
- Colom, L.V. (2006) Septal networks: relevance to theta rhythm, epilepsy and Alzheimer's disease. *J. Neurochem.*, **96**, 609–623.
- Davies, P. & Maloney, A.J.F. (1976) Selective loss of central cholinergic neurons in Alzheimer's disease. *Lancet*, **2**, 1403.
- de Leon, M.J., Convit, A., Wolf, O.T., Tarshish, C.Y., DeSanti, S., Rusinek, H., Tsui, W., Kandil, E., Scherer, A.J., Roche, A., Imossi, A., Thom, E., Bobinski, M., Caraos, C., Lesbre, P., Schlyer, D., Poirier, J., Reisberg, B. & Fowler, J. (2001) Prediction of cognitive decline in normal elderly subjects with 2-[¹⁸F]fluoro-2-deoxy-D-glucose/positron-emission tomography (FDG/PET). *Proc. Natl Acad. Sci. USA*, **98**, 10966–10971.
- Devous, M.D.Sr (2002) Functional brain imaging in the dementia: role in early detection, differential diagnosis, and longitudinal studies. *Eur. J. Nucl. Med. Imaging*, **29**, 1685–1696.

- Fisher, R.S., Buchwald, N.A., Hull, C.D. & Levine, M.S. (1988) GABAergic basal forebrain neurons project to the neocortex: the localization of glutamic acid decarboxylase and choline acetyltransferase in feline corticopetal neurons. *J. Comp. Neurol.*, **272**, 489–502.
- Flechsig, P. (1896) *Gehirn und Seele*. Druck von Alexander Edelmann, Leipzig.
- Frerichs, K.U., Smith, C.B., Brenner, M., DeGracia, D.J., Krause, G.S., Marrone, L., Dever, T.E. & Hallenbeck, J.M. (1998) Suppression of protein synthesis in brain during hibernation involves inhibition of protein initiation and elongation. *Proc. Natl Acad. Sci. USA*, **95**, 14511–14516.
- Freund, T.F. (1989) GABAergic septohippocampal neurons contain parvalbumin. *Brain Res.*, **478**, 375–381.
- Freund, T.F. & Antal, M. (1988) GABA-containing neurons in the septum control inhibitory interneurons in the hippocampus. *Nature*, **336**, 170–173.
- Fröhlich, L., Blum-Degen, D., Bernstein, H.-G., Engelsberger, S., Humrich, J., Laufer, S., Muschner, D., Thalheimer, A., Türk, A., Hoyer, S., Zöchling, R., Boissl, K.W., Jellinger, K. & Riederer, P. (1998) Brain insulin and insulin receptors in aging and sporadic Alzheimer's disease. *J. Neural Transm.*, **105**, 423–438.
- Gasparini, L. & Xu, H. (2003) Potential roles of insulin and IGF-1 in Alzheimer's. *Dis. Trends Neurosci.*, **26**, 404–406.
- Geula, C. & Mesulam, M.-M. (1999) Cholinergic systems in Alzheimer disease. In Terry, R.D., Katzman, R., Bick, K.I. & Sisodia, S.S. (Eds), *Alzheimer Disease*, 2nd Edn. Lippincott, Williams & Wilkins, Philadelphia, pp. 269–292.
- Geula, C., Mesulam, M.-M., Saroff, D.M. & Wu, C.-K. (1998) Relationship between plaques, tangles, and loss of cortical cholinergic fibers in Alzheimer disease. *J. Neuropathol. Exp. Neurol.*, **57**, 63–75.
- Goedert, M., Jakes, R. & Vanmechelen, E. (1995) Monoclonal antibody AT8 recognises tau protein phosphorylated at both serine 202 and threonine 205. *Neurosci. Lett.*, **189**, 167–170.
- Goedert, M., Spillantini, G.M., Jakes, R., Rutherford, D. & Crowther, R.A. (1989) Multiple isoforms of human microtubule-associated protein tau: sequences and localization in neurofibrillary tangles of Alzheimer's disease. *Neuron*, **3**, 519–526.
- Gritti, I., Manns, I.D., Mainville, L. & Jones, B.E. (2003) Parvalbumin, calbindin, or calretinin in cortically projecting and GABAergic, cholinergic, or glutamatergic basal forebrain neurons of the rat. *J. Comp. Neurol.*, **458**, 11–31.
- Haley, A.P., Knight-Scott, J., Simnad, V.I. & Manning, C.A. (2006) Increased glucose concentration in the hippocampus in early Alzheimer's disease following oral glucose ingestion. *Magn. Reson. Imaging*, **24**, 715–720.
- Harkany, T., De Jong, G.I., Soos, K., Penke, B., Luiten, P.G. & Gulya, K. (1995) Beta-amyloid (1–42) affects cholinergic but not parvalbumin-containing neurons in the septal complex of the rat. *Brain Res.*, **698**, 270–274.
- Härtig, W., Bauer, A., Brauer, K., Grosche, J., Hortobágyi, T., Penke, B., Schliebs, R. & Harkany, T. (2002) Functional recovery of cholinergic basal forebrain neurons under disease conditions: old problems, new solutions? *Rev. Neurosci.*, **13**, 95–165.
- Härtig, W., Brückner, G., Holzer, M., Brauer, K. & Bigl, V. (1995) Digoxigenylated primary antibodies for sensitive dual-peroxidase labelling of neuronal markers. *Histochem. Cell Biol.*, **104**, 467–472.
- Härtig, W., Oklejewicz, M., Strijkstra, A.M., Boerema, A.S., Stieler, J. & Arendt, T. (2005) Phosphorylation of the tau protein sequence 199–205 in the hippocampal CA3 region of Syrian hamsters in adulthood and during aging. *Brain Res.*, **1056**, 100–104.
- Heldmaier, G., Ortmann, S. & Elvert, R. (2004) Natural hypometabolism during hibernation and daily torpor in mammals. *Respir. Physiol. Neurobiol.*, **141**, 317–329.
- Heller, H.C. (1979) Hibernation: neural aspects. *Annu. Rev. Physiol.*, **41**, 305–321.
- Hoyer, S. (1998) Is sporadic Alzheimer disease the brain type of non-insulin-dependent diabetes mellitus? A challenging hypothesis. *J. Neural Transm.*, **105**, 415–422.
- Iraizoz, I., Guíjarro, J.L., Gonzalo, L.M. & de Lacalle, S. (1999) Neuropathological changes in the nucleus basalis correlate with clinical measures of dementia. *Acta Neuropathol.*, **98**, 186–196.
- Janke, C., Beck, M., Stahl, T., Holzer, M., Brauer, K., Bigl, V. & Arendt, T. (1999) Phylogenetic diversity of the expression of the microtubule-associated protein tau: implications for neurodegenerative disorders. *Mol. Brain Res.*, **68**, 119–128.
- Kalmijn, S., Mehta, K.M., Pols, H.A., Hofman, A., Drexhage, H.A. & Breteler, M.M. (2000) Subclinical hyperthyroidism and the risk of dementia. The Rotterdam study. *Clin. Endocrinol.*, **53**, 733–737.
- Kása, P., Rakonczay, Z. & Gulya, K. (1997) The cholinergic system in Alzheimer's disease. *Prog. Neurobiol.*, **52**, 511–535.
- Kim, E.J., Cho, S.S., Jeong, Y., Park, K.C., Kang, S.J., Kim, S.E., Lee, K.H. & Na, D.L. (2005) Glucose metabolism in early onset versus late onset Alzheimer's disease: an SPM analysis of 120 patients. *Brain*, **128**, 1790–1801.
- Köhler, C., Chan-Palay, V. & Wu, J.Y. (1984) Septal neurons containing glutamic acid decarboxylase immunoreactivity project to the hippocampal region in the rat brain. *Anat. Embryol.*, **169**, 41–44.
- Lee, V.M.-Y., Goedert, M. & Trojanowski, J.Q. (2001) Neurodegenerative tauopathies. *Annu. Rev. Neurosci.*, **24**, 1121–1159.
- Lehéricy, S., Hirsch, E.C., Cervera, P., Hersch, L.B., Hauw, J.-L., Ruberg, M. & Agid, Y. (1989) Selective loss of cholinergic neurons in the ventral striatum of patients with Alzheimer disease. *Proc. Natl Acad. Sci. USA*, **86**, 8580–8584.
- Manns, I.D., Mainville, L. & Jones, B.E. (2001) Evidence for glutamate, in addition to acetylcholine and GABA, neurotransmitter synthesis in basal forebrain neurons projecting to the entorhinal cortex. *Neuroscience*, **107**, 249–263.
- McCormick, D.A. (1990) Cellular mechanisms of cholinergic control of neocortical and thalamic neuronal excitability. In Steriade, M. & Biesold, D. (Eds), *Brain Cholinergic Systems*. Oxford University Press, Oxford, pp. 236–264.
- McGeer, P.L., McGeer, E.G., Suzuki, J., Dolman, C.E. & Nagai, T. (1984) Aging, Alzheimer's disease, and the cholinergic system of the basal forebrain. *Neurology*, **34**, 741–745.
- Mesulam, M.M., Mufson, E.J., Wainer, B.J. & Levey, A.I. (1983) Central cholinergic pathways in the rat: an overview based on an alternative nomenclature (Ch1–Ch6). *Neuroscience*, **10**, 1185–1201.
- Morin, L.P. & Wood, R.I. (2001) *A Stereotaxic Atlas of the Golden Hamster Brain*. Academic Press, San Diego.
- Morrison, J.H. & Hof, P.R. (1997) Life and death of neurons in the aging brain. *Science*, **278**, 412–419.
- Oklejewicz, M., Daan, S. & Strijkstra, A.M. (2001) Temporal organization of hibernation in wild-type and tau mutant Syrian hamsters. *J. Comp. Physiol. B*, **171**, 431–439.
- Planel, E., Yasutake, K., Fujita, S.C. & Ishiguro, K. (2001) Inhibition of protein phosphatase 2A overrides tau protein kinase/glycogen synthase 3 β and cyclin-dependent kinase 5 inhibition and results in tau hyperphosphorylation in the hippocampus of starved mouse. *J. Biol. Chem.*, **276**, 34298–34306.
- Popov, V.I. & Bocharova, L.S. (1992) Hibernation-induced structural changes in synaptic contacts between mossy fibres and hippocampal neurons. *Neuroscience*, **48**, 53–62.
- Popov, V.I., Bocharova, L.S. & Bragin, A.G. (1992) Repeated changes of dendritic morphology in the hippocampus of ground squirrels in the course of hibernation. *Neuroscience*, **48**, 45–51.
- Popova, I.Y. & Kokoz, Y.M. (2004) The role of the medial septum in the control of hibernation. In Barnes, B.M. & Carey, H.V. (Eds), *Life in the Cold: Evolution, Mechanisms, Adaptation and Application*. Twelfth International Hibernation Symposium. Biological Papers of the University of Alaska, no. 27, pp. 451–465.
- Rasmusson, D.D. (2000) The role of acetylcholine in cortical synaptic plasticity. *Behav. Brain Res.*, **115**, 205–218.
- Rossor, M.N., Emson, P.C., Mountjoy, C.Q., Roth, M. & Iversen, L.L. (1982) Neurotransmitters of the cerebral cortex in senile dementia of Alzheimer type. *Exp. Brain Res. Suppl.*, **5**, 153–157.
- Samuel, W., Terry, R.D., DeTeresa, R., Butters, N. & Masliah, E. (1994) Clinical correlates of cortical and nucleus basalis pathology in Alzheimer dementia. *Arch. Neurol.*, **51**, 772–778.
- Sarter, M. & Bruno, J.P. (2002) The neglected constituent of the basal forebrain corticopetal projection system: GABAergic projections. *Eur. J. Neurosci.*, **15**, 1867–1873.
- Schnell, S.A., Staines, W.A. & Wessendorf, M.W. (1999) Reduction of lipofuscin-like autofluorescence in fluorescently labeled tissue. *J. Histochem. Cytochem.*, **47**, 719–730.
- Schober, A., Brauer, K. & Lippa, H. (1989) The cholinergic nuclei of the basal forebrain of the hamster (*Mesocricetus auratus*): a combined Golgi- and AChE-topochemical investigation. *J. Hirnforsch.*, **30**, 113–123.
- Schubert, M., Brazil, D.P., Burks, D.J., Kushner, J.A., Ye, J., Flint, C.L., Farhang-Fallah, J., Dikkes, P., Warot, X.M., Rio, C., Corfas, G. & White, M.F. (2003) Insulin receptor substrate-2 deficiency impairs brain growth and promotes tau phosphorylation. *J. Neurosci.*, **23**, 7084–7092.
- Schubert, M., Gautam, D., Surjo, D., Ueki, K., Baudier, S., Schubert, D., Kondo, T., Alber, J., Galldiks, N., Küstermann, E., Arndt, S., Jacobs, A.H., Krone, W., Kahn, C.R. & Brüning, J.C. (2004) Role for neuronal insulin resistance in neurodegenerative diseases. *Proc. Natl Acad. Sci. USA*, **101**, 3100–3105.

- Selkoe, D.J. (2001) Alzheimer's disease: genes, proteins and therapy. *Phys. Rev.*, **81**, 741–766.
- Semba, K. (2004) Phylogenetic and ontogenetic aspects of the basal forebrain cholinergic neurons and their innervation of the cerebral cortex. *Prog. Brain Res.*, **145**, 3–43.
- Springer, J.E., Koh, S., Tayrien, M.W. & Loy, R. (1987) Basal forebrain magnocellular neurons stain for nerve growth factor receptor: correlation with cholinergic cell bodies and effects of axotomy. *J. Neurosci. Res.*, **17**, 111–118.
- Steriade, M. & Buzsáki, G. (1990) Parallel activation of thalamic and cortical neurons by brainstem and basal forebrain cholinergic systems. In Steriade, M. & Biesold, D. (Eds), *Brain Cholinergic Systems*. Oxford University Press, Oxford, pp. 3–63.
- Storey, K.B. (2003) Mammalian hibernation. Transcriptional and translational controls. *Adv. Exp. Med. Biol.*, **543**, 21–38.
- Storey, K.B. & Storey, J.M. (2004) Metabolic rate depression in animals: transcriptional and translational controls. *Biol. Rev. Camb. Philos. Soc.*, **79**, 207–233.
- Swaab, D.F., Dubelaar, E.J., Scherder, E.J. & van Someren, E.J. & Verwer, R.W. (2003) Therapeutic strategies for Alzheimer disease: focus on neuronal reactivation of metabolically impaired neurons. *Alzheimer Dis. Assoc. Disord. Suppl.*, **4**, S114–S122.
- Tremere, L.A., Pinaud, R., Grosche, J., Härtig, W. & Rasmusson, D.D. (2000) Antibody for human p75 LNTR identifies cholinergic basal forebrain in cholinergic basal forebrain of non-primate species. *NeuroReport*, **11**, 2177–2183.
- Vogt, C. & Vogt, O. (1951) Importance of neuroanatomy in the field of neuropathology. *Neurology*, **1**, 205–218.
- Wenk, H., Bigl, V. & Meyer, U. (1980) Cholinergic projections from magnocellular nuclei of the basal forebrain to cortical areas in rats. *Brain Res. Rev.*, **2**, 295–316.
- Whitehouse, P.J., Price, D.L., Clark, A.W., Coyle, J.T. & DeLong, M.R. (1981) Alzheimer disease: evidence for selective loss of cholinergic neurons in the nucleus basalis. *Ann. Neurol.*, **10**, 122–126.
- Xiang, Z., Huguenard, J.R. & Prince, D.A. (1998) Cholinergic switching within neocortical inhibitory networks. *Science*, **281**, 985–988.
- Yanagisawa, M., Planel, E., Ishiguro, K. & Fujita, S.C. (1999) Starvation induces tau hyperphosphorylation in mouse brain: implications for Alzheimer's disease. *FEBS Lett.*, **461**, 329–333.
- Záborszky, L., Pang, K., Somogyi, J., Nadasdy, Z. & Kallo, I. (1999) The basal forebrain corticopetal system revisited. *Ann. N.Y. Acad. Sci.*, **877**, 339–367.
- Zhou, F., Zhu, X., Castellani, R.J., Stimmelmayer, R., Perry, G., Smith, M.A. & Drew, K.L. (2001) Hibernation, a model of neuroprotection. *Am. J. Pathol.*, **158**, 2145–2151.

EXHIBIT 12



Research report

Neurofibrillary lesions in experimental aluminum-induced encephalopathy and Alzheimer's disease share immunoreactivity for amyloid precursor protein, A β , α_1 -antichymotrypsin and ubiquitin-protein conjugates

Yue Huang ^a, Mary M. Herman ^c, Jia Liu ^a, Christos D. Katsetos ^d, Michael R. Wills ^{a,c},
John Savory ^{a,b,*}

^a Department of Pathology, University of Virginia Health Sciences Center, Box 168, Charlottesville, VA 22908, USA

^b Department of Biochemistry, University of Virginia Health Sciences Center, Box 168, Charlottesville, VA 22908, USA

^c Department of Internal Medicine, University of Virginia Health Sciences Center, Charlottesville, VA 22908, USA

^d Department of Microbiology and Immunology, Temple University School of Medicine, Philadelphia, PA 19140, USA

^e Clinical Brain Disorders Branch, NIMH Neuroscience Center at St. Elizabeths, IRP, NIH, Washington, DC 20032, USA

Accepted 10 June 1997

Abstract

Neurofibrillary tangles of Alzheimer's disease contain predominantly tau protein and to a lesser degree amyloid precursor protein (APP), A β protein, α_1 -antichymotrypsin (ACT) and ubiquitin. Previously we have demonstrated the presence of phosphorylated tau and neurofilament proteins in neurofibrillary degeneration (NFD) induced by aluminum (Al) maltolate in rabbits [Savory et al., Brain Res. 669 (1995) 325–329; Savory et al., Brain Res. 707 (1996) 272–281]. Using the same animal system we have now detected APP, A β , ACT and ubiquitin-like immunoreactivities in NFD-bearing neurons, often colocalizing in the NFD. Diffuse cytoplasmic staining for APP, A β and ubiquitin was also present in neurons without NFD from Al maltolate-treated rabbits. This study provides additional support for immunochemical similarities between Al-induced NFD in rabbits and the neurofibrillary tangles in human subjects with Alzheimer's disease. © 1997 Elsevier Science B.V.

Keywords: Neurofibrillary degeneration; Aluminum; Amyloid precursor protein; A β ; α_1 -Antichymotrypsin; Ubiquitin; Rabbit

1. Introduction

Hallmark neuropathological features of Alzheimer's disease are neuronal cell loss with neurofibrillary tangles, neuritic plaques with amyloid deposits, and neuropil threads [18]. Among the major components of these neurodegenerative lesions are the microtubule-associated protein tau (tau), the A β protein, and, to a lesser degree, altered, mostly hyperphosphorylated neurofilament proteins [18]. The serine protease inhibitor α_1 -antichymotrypsin (ACT), ubiquitin, and some complement components [18] are also present, thus leading to speculation that proteolytic dysfunction and ubiquitin-mediated proteolytic pathways are integral features involved in the pathogenesis of Alzheimer's disease. Recently ACT has been recognized as being closely related to A β [1]. Stable ubiquitin conjugates exist in the neurofibrillary tangles of Alzheimer's

disease and progressive supranuclear palsy, in Pick bodies of Pick's disease, and in Lewy bodies of Parkinson's disease [25]. The ubiquitin system and ACT may be involved in abnormal neuronal protein processing in Alzheimer's disease and perhaps in other neurodegenerative diseases [1,26]. Neuritic plaques consist principally of an approx. 40 amino acid A β fragment derived from four amyloid precursor protein (APP) isoforms encoded by a single gene localized on chromosome 21 [9,20,39]. Deposition of A β in Alzheimer's disease is observed not only in plaques, but also in neurofibrillary tangles, blood vessel walls, neuropil, subpial layer of the cerebral cortex, cerebral white matter, basal ganglia, and in the cerebellar Purkinje cells and molecular layer [3,28,29,43]. Recent genetic studies provide evidence that A β and APP may play a central role in the pathogenesis of Alzheimer's disease (for a review see Ref. [30]); however, the mechanism of the neuronal degeneration in Alzheimer's disease is still unknown.

* Corresponding author, at address 'a' or 'b'. Fax: +1 (804) 924-2574.

Investigations into these fundamental mechanisms will be aided greatly by the availability of experimental animal models. Rabbits have been reported recently to have many proteins with a molecular structure which closely resembles that of primates [10], thus making such an animal system of relevance to human neurodegenerative disease. We have demonstrated previously that administration of aluminum (Al) maltolate, by intraventricular [21] and intracisternal routes [33,34], is effective in inducing neurofibrillary degeneration (NFD) in rabbits. Moreover, this effect can be significantly reversed by initiating intramuscular desferrioxamine treatment [17,32]. Our previous experiments have shown that Al maltolate-induced NFD in rabbits contains phosphorylated and non-phosphorylated neurofilament proteins and also normal and abnormal forms of tau [21,33,34], all of which are seen in the neurofibrillary tangles of Alzheimer's disease. We now report abnormal accumulations of APP, A β , ACT and ubiquitin associated with the Al maltolate-induced neurofibrillary lesions.

2. Materials and methods

2.1. Animal experiments

Forty-nine male New Zealand white rabbits (aged 5–6 months) were used in this study. Thirty-eight rabbits received 100 μ l of 25 mM Al maltolate (2.5 μ M) via the intracisternal route of administration, and 11 control rabbits were injected in the same manner with 100 μ l of saline. The synthesis of Al maltolate and treatment of the animals was performed as described previously [4].

2.2. Immunohistochemistry

For immunohistochemical staining, all central nervous system specimens were fixed in one of the following two fixatives with several changes: 10% phosphate-buffered formalin, pH 7.0, at room temperature (RT) for 48 h (for A β and ACT) or 70% ethanol with 150 mM sodium chloride at 4°C for 24 h (for APP and ubiquitin) which are fixation conditions recommended by the providers of the monoclonal antibodies (mAb). After fixation, transverse sections were made of the medulla and cervical spinal cord and the specimens were progressively dehydrated in ethanol and embedded in paraffin. Sections were stained with H&E and with Bielschowsky's silver impregnation method for axons adapted for paraffin-embedded tissues, as employed in our earlier studies [4].

The 5 μ m deparaffinized sections were immunostained with the avidin-biotin complex technique [16]. Sections were incubated overnight at 4°C with one of four primary mouse mAb: (i) mAb recognizing APP that has a predicted amino acid sequence length of 695 [2], anti- β APP_{695aa} (clone LN27, Zymed Lab., San Francisco, CA), 1:200; (ii)

mAb against A β , the immunogen being a synthetic peptide consisting of residues 8–17 of A β (clone 6F/3D, DAKO, Denmark), 1:100; (iii) mAb recognizing conjugated and unconjugated ubiquitin, clone Ubi-1, Zymed Lab., San Francisco, CA, 1:1500; and (iv) mAb against ACT (Cat. No. 13803, a gift from QED, San Diego, CA), 1:1500. Sections were incubated for 30 min at RT with biotinylated secondary antibody and avidin, and biotinylated horseradish peroxidase (Vectastain Elite ABC Reagent, Vector Lab., Burlingame, CA). All slides were washed with 10 mM sodium phosphate in 0.9% saline, pH 7.5, after incubation with primary and secondary antibody, and with ABC reagent (Vectastain). Cerebral tissue with neuropathological changes consistent with Alzheimer's disease was included as a positive control for the immunostaining, and replacement of primary antibody by non-immune serum was used as a negative control. After development with diaminobenzidine tetrahydrochloride/hydrogen peroxide (Sigma, St. Louis, MO) at RT, the sections were lightly counterstained with hematoxylin.

Preabsorption of the A β was carried out with a synthetic peptide homologous to A β amino acid sequences 1–28 (Sigma) at RT for 8 h, followed by centrifugation at 10 000 rpm for 10 min and use of the supernatant for immunostaining. This A β mAb is an IgG₁ and molar ratios of IgG₁:A β 1–28 peptide of 1:5, 1:12.5, 1:25, and 1:50 were used for preabsorption. Tissue from the medulla of a male Al-treated rabbit which had been sacrificed 6 days following treatment and which demonstrated considerable NFD, was immunostained both with untreated and preabsorbed A β mAb.

2.3. Immunoblot analysis

Tissue for immunoblot analysis was obtained from five Al maltolate-treated and two control rabbits which at necropsy were gravity-perfused from a height of 1 m with 500 ml of buffer (RT), containing 16 mM Tris-HCl, pH 7.2, 6 mM ethylenediaminetetraacetic acid (EDTA), 6 mM ethylene glycol-bis(β -aminoethyl ether) *N,N,N,N*-tetraacetic acid (EGTA), 10 mM benzamidine, 10 mM sodium pyrophosphate and 0.1 mM phenylmethylsulfonyl fluoride (PMSF). Approx. 400 mg of tissue from the medulla was homogenized in 2 vols. of buffer (125 mM Tris-HCl, pH 6.8, 2% SDS, 10% glycerol, 5 mM EDTA, 5 mM EGTA, 0.1 M dithiothreitol). The protein content was determined by the bicinchoninic acid (BCA) method using bovine albumin as a standard [15]. Western blotting was performed using samples containing 30 μ g of total protein (both Al maltolate-treated and control rabbits), run on 4–15% ready gel SDS-PAGE, Tris-HCl (Bio-Rad, Hercules, CA), and transferred to nitrocellulose membranes [41]. The blot membrane was probed using the technique of enhanced chemiluminescence [40] with mAb β APP_{695aa} (1:1000), A β (1:200), ubiquitin (1:1500), and ACT (1:1500). The membrane was blocked for 1.5 h (RT) in

10% dried milk in Tris buffered saline-Tween (TBS-T), pH 7.6 (20 mM Tris, 137 mM sodium chloride, 0.1% Tween-20, and 3.8 mM HCl, per liter of distilled water). The membrane was incubated first for 1 h (RT) with the primary mAb and secondary antibody anti mouse Ig-horseradish peroxidase, 1:2000 (NA931, Amersham, Arlington Heights, IL), followed by a 1 min incubation with mixed equal volumes of enhanced chemiluminescence detection reagents 1 and 2, 0.125 ml/cm² (RPN2106, Amersham), and immediately exposed to film (Hyperfilm ECL, RPN2103, Amersham) for 15 s–10 min. Before each of

the above incubations, the membrane was washed 3 × 5 min (RT) with TBS-T buffer.

3. Results

3.1. Clinical and histologic findings

Starting on day 2 following the intracisternal administration of A1 maltolate which was injected on day 0, 30 of the 38 rabbits developed neurological symptoms character-

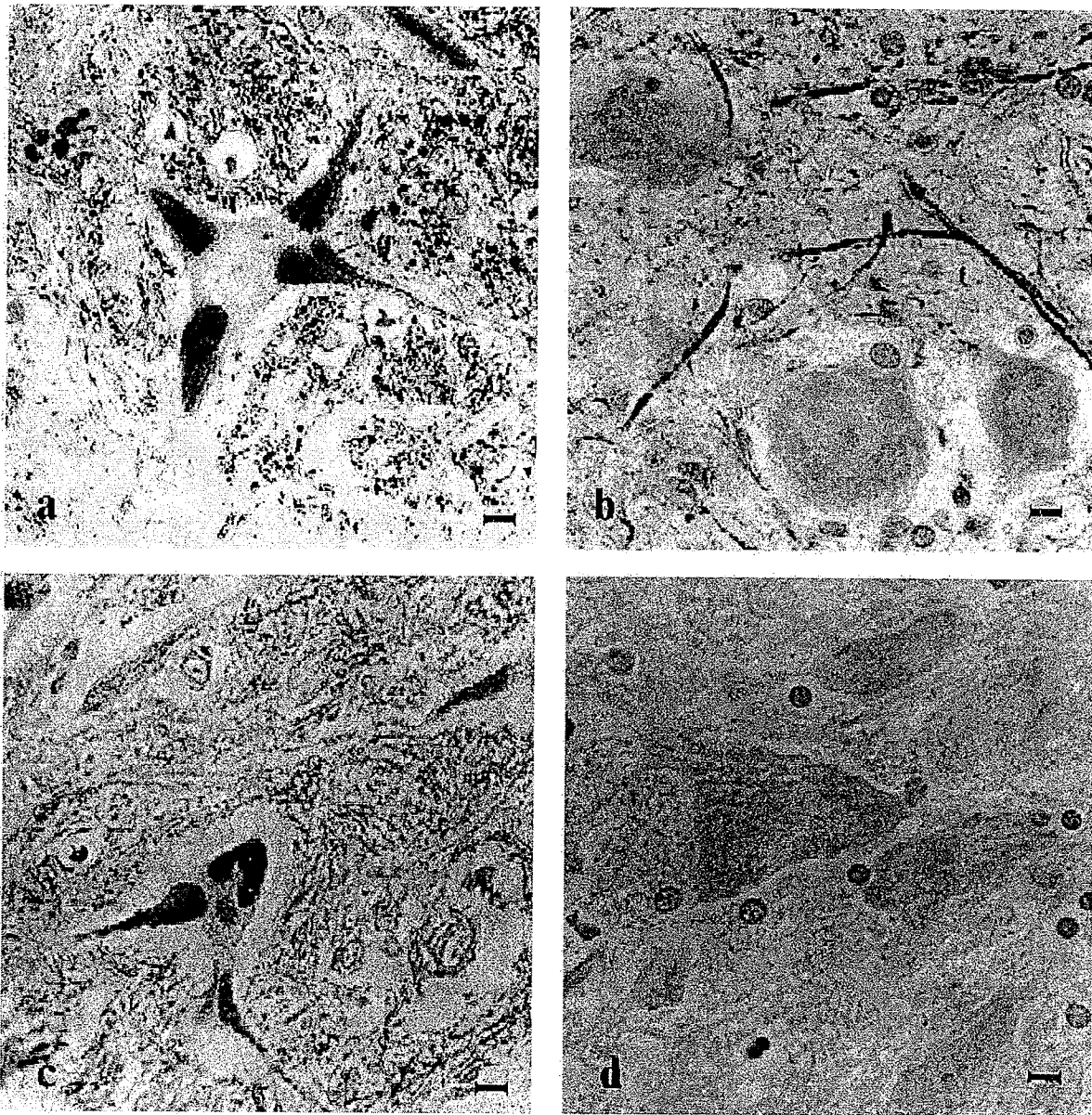


Fig. 1. a: pyramidal neuron in medulla containing NFD in several proximal neurites. The areas of NFD are strongly stained with a mAb against β -APP_{695aa}. Rabbit treated with A1 maltolate on day 0 and sacrificed on day 7. b: pyramidal neurons in medulla which are negative for mAb anti- β -APP_{695aa}. Neurites are positive with this mAb in both A1-treated and control rabbits. Control treated with saline on day 0, sacrificed on day 8. c: neurons in the medulla with marked staining of NFD by mAb anti- β -amyloid. A1 maltolate given on day 0, sacrificed on day 7. d: negative staining of neurons in medulla with mAb anti- β -amyloid. Control treated with saline on day 0, sacrificed on day 8. All sections counterstained lightly with hematoxylin. Bar = 10 μ m.

ized by forward head tilt, hemiplegic gait, loss of appetite, splaying of extremities, and paralysis. Most of the Al-treated rabbits demonstrated neurofibrillary pathology (NFD) throughout the spinal gray matter as described in our previous report [21]. The 11 control rabbits receiving saline remained asymptomatic, and no NFD was detected.

3.2. Immunohistochemistry and immunoblot analysis

Both the medulla and upper cervical spinal cord were evaluated in the following immunohistochemical analyses; immunoblot was performed on the medulla.

3.2.1. Amyloid precursor protein

The most striking observation was that neuronal cell bodies and particularly the perikaryal NFD of Al-treated rabbits were positive in 40% of the animals, whereas neurons of the saline-treated controls were not stained (Fig. 1a,b). In those animals with APP immunopositivity approx. 20–30% of the neurons with perikaryal NFD actually demonstrated this APP labeling. In Al-treated rabbits, APP had a diffuse granular distribution in the perikaryal cytoplasm of neurons (not related to NFD) or was colocalized in the NFD (Fig. 1a). Some APP-like staining was also present in proximal neurites of NFD-bearing neurons. In both groups of animals nerve cell processes in the white matter were also weakly labeled. Immunoblot analysis carried out on the caudal part of the medulla from five Al-treated rabbits demonstrated strong bands as compared to weak bands of two control animals. Typical results in one Al-treated and one control rabbit are

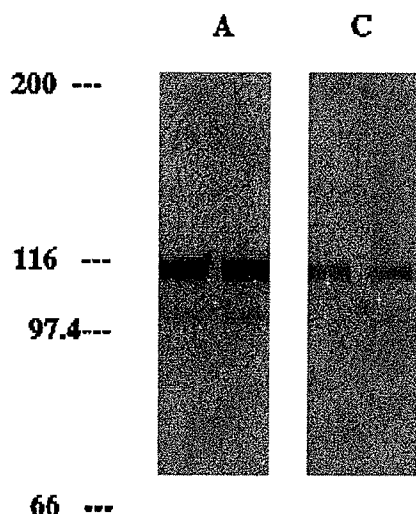


Fig. 2. Detection of APP in the upper cervical cord by immunoblot analysis with mAb anti- β -APP_{695aa}. The Al maltolate-treated rabbit (A, injected on day 0 and sacrificed on day 8) exhibits much greater binding intensity than the saline treated control (C, injected on day 0, sacrificed on day 8). Bands detected are approx. 115 and 110 kDa and correspond to amyloid precursor proteins. mAb anti- β -APP_{695aa} (clone LN27) reacts with an APP with a predicted amino acid sequence length of 695; this clone recognizes an epitope within the first 200 amino acids in the APP amino-terminus.

shown in Fig. 2. No bands were present in the 40–70 kDa range, indicating the lack of cross-reactivity of the APP mAb with tau.

3.2.2. A β

In all Al-treated rabbits in which NFD were present, positive staining was also found predominantly in the neurons of medulla which contained NFD (Fig. 1c). Staining for A β was similar to APP in that there was weak fine granular staining of neurites in all Al-treated and control rabbits. Only a few of the neurons containing NFD demonstrated this A β immunopositivity. The proximal neurites also showed positive reactivity with A β mAb. No A β staining was observed in neurons of five control rabbits (Fig. 1d). Despite immunohistochemical staining of tissue from Al-treated rabbits, there were no bands in the expected molecular weight range on immunoblot analysis for this peptide. However, no cross-reactivity was detected with APP which is the obvious candidate for interference in the detection of A β (data not shown). Preabsorption of the A β with increasing concentrations of synthetic A β having homologous amino acid sequences 1–28 demonstrated increasing diminution of the staining intensity of NFD in medulla of an Al-treated rabbit exhibiting extensive NFD in this region. Staining intensities at the following IgG:A β peptide molar ratios were as follows: 1:5, 4+; 1:12.5, 3+; 1:25, 2+; 1:50, negative. Staining intensity of this same tissue using A β mAb that had not been preabsorbed was 5+. Our evaluation in the present series of animals was performed at a 1:50 dilution of A β mAb. Therefore these preabsorption studies demonstrate at least partial specificity of the mAb for A β , thereby indicating that this peptide may also colocalize with Al-induced NFD. The lack of any bands in the 40–70 kDa range again indicates no cross-reactivity of the A β mAb with tau.

3.2.3. α_1 -Antichymotrypsin

Positive ACT immunostaining was observed in NFD of neurons in the medulla (Fig. 3a) and upper cervical cord, beginning on day 3 following Al administration. In Al-treated animals, ACT positivity was detected in a much higher percentage (14 of 20 rabbits, 70%) in the medulla than in the upper cervical spinal cord (four of 20 rabbits, 20%). In the latter area, only a few neurons in the four animals were positive. In the 30% (six of 20 rabbits) of rabbits that demonstrated ACT immunonegativity in neurons of the medulla, silver staining also failed to show the presence of NFD. In those animals with ACT immunopositivity approx. 40% of neurons with perikaryal NFD exhibited these staining characteristics. Neurons of control rabbits were negative for ACT staining (Fig. 3b). Immunostaining of NFD for ACT correlated well with silver staining of these foci of neurofibrillary degeneration, in that the mAb against ACT intensely labeled NFD in neurons containing abundant NFD, while it only faintly stained the

adjacent cytoplasm of NFD-bearing neurons. Immunoblot analysis revealed positive staining for ACT in the form of prominent bands spanning the molecular mass range of 45–60 kDa for both Al-treated and control rabbits. There were no apparent differences in band intensity between these two groups.

3.2.4. Ubiquitin

Positive immunostaining of neurons was observed in Al maltolate-treated rabbits starting on day 3, following intracisternal injection on day 0. There were three patterns of

ubiquitin staining in these Al-treated animals, i.e., localization in the NFD, and/or localization in the neuronal nucleus and perikaryon. In the medulla, ubiquitin immunoreactivity was most intense in neurons exhibiting argyrophilic NFD; the localization pattern of ubiquitin in NFD was granular or particulate rather than fibrillar (Fig. 3c). In sections of medulla, 60% (12 of 20 rabbits) of Al-treated animals possessed only cytoplasmic immunopositivity, whereas 20% (four of 20 rabbits) also showed staining of nuclei (Fig. 3c). This combined staining was not always present in the same cell as evaluated at the level of the

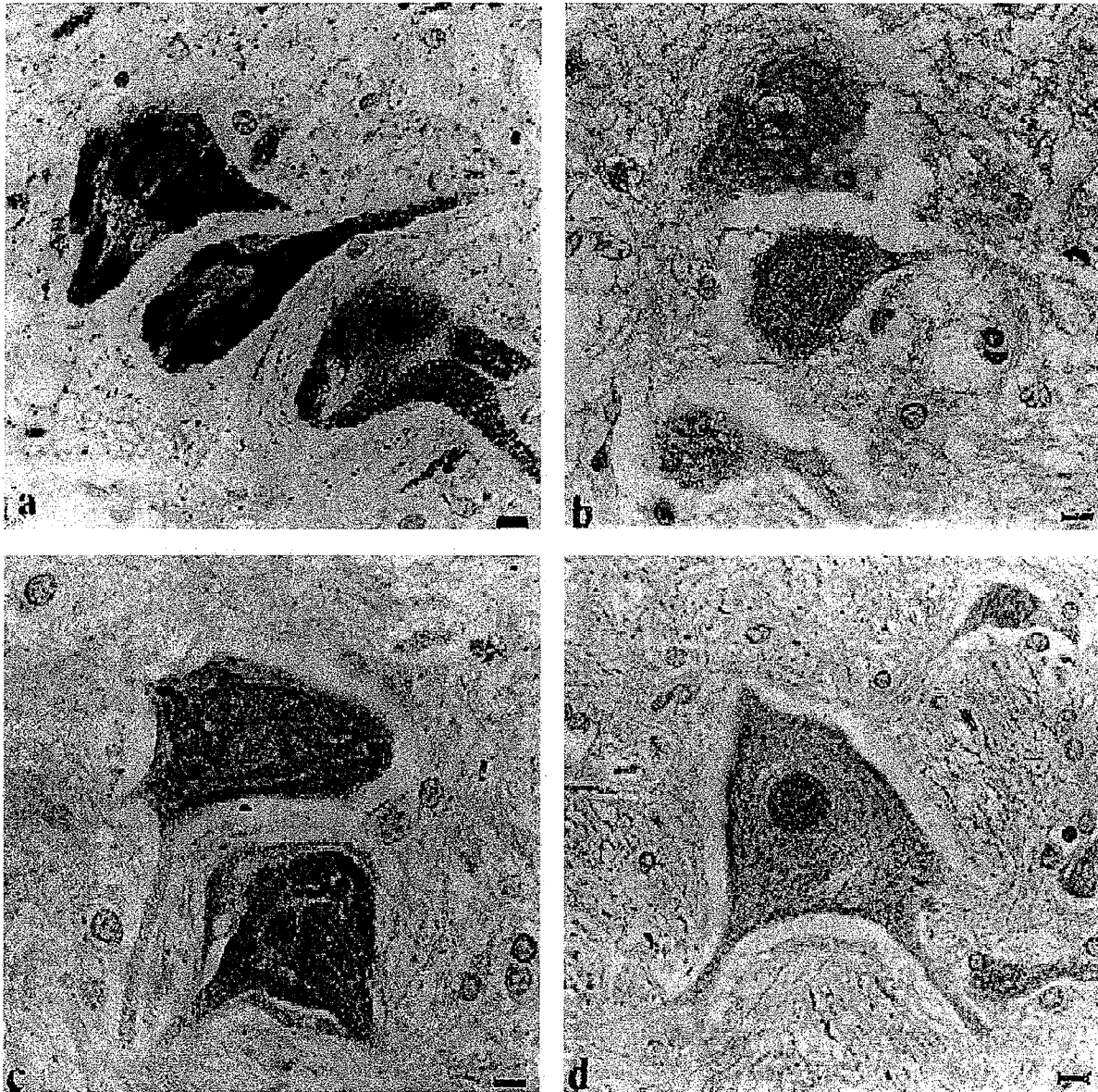


Fig. 3. a: NFD-bearing neurons in the medulla showing marked staining of the regions of NFD against α_1 -antichymotrypsin. Treated with Al maltolate on day 0, sacrificed on day 7. b: neurons in the medulla demonstrate a lack of staining with α_1 -antichymotrypsin. Control, treated with saline on day 0, sacrificed on day 8. c: two NFD-bearing neurons in the medulla showing marked staining of cytoplasm (both neurons) and nucleus (lower neuron only) with mAb anti-ubiquitin. Treated with Al maltolate on day 0, sacrificed on day 7. d: large neuron in medulla with less intense nuclear staining and negative cytoplasm using mAb anti-ubiquitin. Control treated with saline on day 0, sacrificed on day 8. Sections lightly counterstained with hematoxylin. Bar = 10 μ m.

section. Twenty percent (four of 20 rabbits) of the treated rabbits were negative for ubiquitin immunostaining, both in apparently normal neurons and in neurons with NFD. In the treated rabbits, some regions of NFD were not labeled by the ubiquitin mAb. The cervical spinal cord demonstrated positive ubiquitin immunostaining only in neuronal cell nuclei; this staining pattern was observed both in Al-treated and normal control rabbits. Control rabbits showed staining of most nuclei in both medulla and cervical spinal cord (six of six rabbits), with no staining of the cell bodies (Fig. 3d). In summary, a particulate pattern of ubiquitin localization was usually seen in Al-induced NFD, and Al treatment was associated with the elimination of nuclear staining. By contrast, ubiquitin-like nuclear staining was uniformly present in neurons from control animals.

4. Discussion

Although Al-induced NFD in rabbits do not share all morphologic and biochemical features with the neurofibrillary tangles of Alzheimer's disease, they nevertheless exhibit noteworthy similarities. As is developed below there are even greater similarities than originally believed. We describe the localization in Al-induced NFD lesions of four antigens that are abnormally expressed or processed in Alzheimer's disease, notably APP, A β , ACT and ubiquitin. The immunoreactivities observed for mAb β -APP_{695aa}, and mAb β -amyloid in neuronal perikarya, NFD, and proximal neurites in Al-induced rabbit lesions indicate that APP and A β are probable participants in the neurodegenerative process. The mAb (LN27) used to detect APP has been shown to label β -APP-positive neurites seen around plaques in the cortex of human brain tissue from aged patients [35]. The A β mAb (clone 6F/3D) recognizes the same epitope as clone IG10/2/3 which has been reported to stain human neuritic plaques [2].

The origins of abnormal deposits of APP and A β in Alzheimer's disease are still unknown, although multiple sources have been proposed, including neurons, astrocytes, microglia, endothelial cells, and elements of the circulatory system [36,39]. Ultrastructural studies have demonstrated that microglial cells can manufacture amyloid fibers which are produced in distended cisternae of smooth endoplasmic reticulum and then transported to cell membranes through a complex labyrinth of channels formed by altered endoplasmic reticulum [44]. APP and A β can be detected in neuronal perikarya and/or axons after loss of subcortical innervation, after axonal blockage by nerve ligation, or following dietary intake of cholesterol in some animals [23,37,42]. We have demonstrated previously that perikaryal accumulations of neurofilament proteins are observed as early as 24 h following Al administration to rabbits [34] which precedes signs of APP and A β immunostaining. This suggests that increases in expression

of APP and resultant elevations of A β may represent secondary effects resulting from Al toxicity. Whether such changes in APP and A β in Alzheimer's disease are also secondary effects or are primary events directly causing the disease, remains to be elucidated.

The role of proteases and protease inhibitors in the pathogenesis of Alzheimer's disease has been recognized. Lysosomal hydrolases of different classes have an abnormal distribution in Alzheimer's disease patients [6]. Immunoreactivity for α_2 -macroglobulin, the most potent of the known human protease inhibitors, has displayed intracellular localization in large hippocampal neurons in Alzheimer's disease brains [38]. Also, ACT demonstrates extracellular staining of amyloid deposits in normal aging, Alzheimer's disease, and Down's syndrome [1,31]. Neurons which are immunoreactive for ACT tend to be sparse and of larger size; these include large pyramidal neurons in the hippocampus, melanin-bearing neurons in the substantia nigra, and Purkinje cells in the cerebellum [1].

Ubiquitin is a 76-residue protein found in all eukaryotes. Levels of ubiquitin and ubiquitin-protein conjugates are altered in response to heat shock and in the process of cell development, differentiation and aging [5,12,14,19,27]. Neurofibrillary tangles and other abnormal filamentous inclusions in diverse diseases are associated with ubiquitin, as are several other tau-containing inclusions in both neurons and glia [7,24–27]. In the present study, ubiquitin immunoreactivity was found in nuclei of neurons in all normal control rabbits and in most Al-treated rabbits. In the Al maltolate-treated rabbits, the following finding was noted: ubiquitin staining in the cytoplasm gradually appeared as the number of neurons demonstrating NFD increased. As the process of NFD formation became evident, ubiquitin was detected in the cytoplasm as well as in nuclei; as NFD formation progressed to involve the majority of large, projection-type neurons, intense particulate ubiquitin staining was observed chiefly in the cytoplasm. This is in contrast to immunoprobe markers of NFD [21] and suggests that targets for ubiquitin conjugates may include proteins other than the cytoskeletal constituents of NFD. One presumed role of ubiquitin is to serve as a signal for attack by proteases specific for ubiquitin-protein complexes [8,11,13]. Conjugated ubiquitin-like staining has been found in an array of non-lysosomal filamentous inclusions, including those seen in pathological neurofibrillary lesions such as in Lewy and Pick's bodies, as well as in the neurofibrillary tangles of Alzheimer's disease [25]. Also, modified forms of ACT in the Al-induced NFD may be potential targets for ubiquitin conjugation. One likely modification may involve amino acid substitution of glutamate for lysine, thus rendering the actual serine protease inhibitor ubiquitinated [22]. A pattern of co-distribution of ACT and conjugated ubiquitin has been previously detected in astrocytic degenerative structures found in pilocytic astrocytomas referred to as eosinophilic granular bodies [22]. However, the present study does not ascertain

the functional state of ACT in Al-induced NFD, notably whether it exists in a native form complexed with proteases such as one of the cathepsins, or is in fact proteolytically inactivated.

Our studies suggest that the concept of animal models in the study of human disease may be applicable to Alzheimer's disease. Using the technique of intracisternal injections of Al maltolate, we have been able to induce widespread NFD in the central nervous system of the rabbit [33]. We have demonstrated that these NFD contain phosphorylated and non-phosphorylated epitopes of neurofilament proteins [21], as well as normal and hyperphosphorylated tau [33]. Now we report that APP, A β , ACT, and ubiquitin are also present in these NFD. Collectively, our results suggest that the formation of Al-induced NFD may share common fundamental mechanisms with the neurofibrillary tangles of Alzheimer's disease and related disorders, since tau, neurofilament proteins, APP, A β , ACT, and ubiquitin are identified in the neurofibrillary tangles of Alzheimer's disease and other neurodegenerative diseases [1,18,26]. Thus this rabbit experimental system appears to offer opportunities for exploring mechanisms of neurofibrillary pathology that may have relevance to Alzheimer's disease and perhaps some of the other neurodegenerative disorders.

Acknowledgements

We gratefully acknowledge the review and constructive critique provided by Dr. Ludwig A. Sternberger, and the photographic assistance of Mr. LeRoy Sundberg. Supported by the Virginia Center on Aging.

References

- [1] C.R. Abraham, T. Shirahama, H. Potter, α 1-Antichymotrypsin is associated solely with amyloid deposits containing the β -protein. Amyloid and cell localization of α 1-antichymotrypsin, *Neurobiol. Aging* 11 (1990) 123–129.
- [2] D. Allsop, M. Landon, M. Kidd, J.S. Lowe, G.P. Reynolds, A. Gardner, Monoclonal antibodies raised against a subsequence of senile plaque core protein react with plaque cores, plaque periphery and cerebrovascular amyloid in Alzheimer's disease, *Neurosci. Lett.* 68 (1986) 252–256.
- [3] H. Arai, V.M. Lee, M.L. Messinger, B.D. Greenberg, D.E. Lowery, J.Q. Trojanowski, Expression patterns of β -amyloid precursor protein (β -APP) in neural and nonneural human tissue from Alzheimer's disease and control subjects, *Ann. Neurol.* 30 (1991) 686–693.
- [4] R.L. Bertholf, M.M. Herman, J. Savory, R.M. Carpenter, B.C. Sturgill, C.D. Katsetos, S.R. VandenBerg, M.R. Wills, A long-term intravenous model of aluminum maltol toxicity in rabbits: tissue distribution, hepatic, renal, and neuronal cytoskeletal changes associated with systemic exposure, *Toxicol. Appl. Pharmacol.* 98 (1989) 58–74.
- [5] N. Carlson, S. Rogers, M. Rechsteiner, Microinjection of ubiquitin: changes in protein degradation in HeLa cells subjected to heat-shock, *J. Cell Biol.* 104 (1987) 547–555.
- [6] A.M. Cataldo, P.A. Paskevich, E. Kominami, R.A. Nixon, Lysosomal hydrolases of different classes are abnormally distributed in brains of patients with Alzheimer disease, *Proc. Natl. Acad. Sci. USA* 88 (1991) 10998–11002.
- [7] G.M. Cole, P.S. Timiras, Ubiquitin-protein conjugates in Alzheimer's lesions, *Neurosci. Lett.* 79 (1987) 207–212.
- [8] D. Finley, V. Chau, Ubiquitination (Review), *Annu. Rev. Cell Biol.* 7 (1991) 25–69.
- [9] T.E. Golde, S. Estus, M. Usiak, L.H. Younkin, S.G. Younkin, Expression of β -amyloid protein precursor mRNAs: recognition of a novel alternatively spliced form and quantitation in Alzheimer's disease using PCR, *Neuron* 4 (1990) 253–267.
- [10] D. Graur, L. Duret, M. Gouy, Phylogenetic position of the order Lagomorpha (rabbits, hares and allies), *Nature* 379 (1996) 333–335.
- [11] A.L. Haas, P.M. Bright, The immunochemical detection and quantitation of intracellular ubiquitin-protein conjugates, *J. Biol. Chem.* 260 (1985) 12464–12473.
- [12] A. Hershko, A. Ciechanover, Mechanisms of intracellular protein breakdown, *Annu. Rev. Biochem.* 51 (1982) 335–364.
- [13] A. Hershko, Ubiquitin-mediated protein degradation, *J. Biol. Chem.* 263 (1988) 15237–15240.
- [14] A. Hershko, A. Ciechanover, The ubiquitin system for protein degradation, *Annu. Rev. Biochem.* 61 (1992) 761–807.
- [15] H.D. Hill, J.G. Straka, Protein determination using bicinchoninic acid in the presence of sulfhydryl reagents, *Anal. Biochem.* 170 (1988) 203–208.
- [16] S.M. Hsu, L. Raine, H. Fanger, A comparative study of the peroxidase-antiperoxidase method and an avidin-biotin complex method for studying polypeptide hormones with radioimmunoassay antibodies, *Am. J. Clin. Pathol.* 75 (1981) 734–738.
- [17] Y. Huang, J. Savory, M.M. Herman, J.R. Nicholson, M.R. Reyes, J.C. Boyd, M.R. Wills, Quantitative evaluation of Al maltolate-induced neurodegeneration with subsequent Al removal by desferrioxamine treatment, *Neurotoxicology* 16 (1995) 291–296.
- [18] K. Iqbal, I. Grundke-Iqbal, Neurofibrillary tangles; β -protein fibrillogenesis and neuritic plaques, in: D.B. Calne (Ed.), *Neurodegenerative Disease*, W.B. Saunders, Philadelphia, PA, 1994, pp. 71–95.
- [19] J.H. Jahngen, R.D. Lipman, D.A. Eisenhauer, E.G. Jahngen Jr., A. Taylor, Aging and cellular maturation cause changes in ubiquitin-eye lens protein conjugates, *Arch. Biochem. Biophys.* 276 (1990) 32–37.
- [20] J. Kang, H.G. Lemaire, A. Unterbeck, J.M. Salbaum, C.L. Masters, K.H. Grzeschik, G. Multhaup, K. Beyreuther, B. Muller-Hill, The precursor of Alzheimer's disease amyloid A4 protein resembles a cell-surface receptor, *Nature* 325 (1987) 733–736.
- [21] C.D. Katsetos, J. Savory, M.M. Herman, R.M. Carpenter, A. Frankfurter, C.D. Hewitt, M.R. Wills, Neuronal cytoskeletal lesions induced in the CNS by intraventricular and intravenous aluminum maltol in rabbits, *Neuropathol. Appl. Neurobiol.* 16 (1990) 511–528.
- [22] C.D. Katsetos, L. Krishna, E. Friedberg, J. Reidy, G. Karkavelos, J. Savory, Lobar pilocytic astrocytomas of the cerebral hemispheres II. Pathobiology-morphogenesis of eosinophilic granular bodies, *Clin. Neuropathol.* 13 (1994) 306–314.
- [23] E.H. Koo, S.S. Sisodia, D.R. Archer, L.J. Martin, A. Weidemann, K. Beyreuther, P. Fischer, C.L. Masters, D.L. Price, Precursor of amyloid protein in Alzheimer disease undergoes fast anterograde axonal transport, *Proc. Natl. Acad. Sci. USA* 87 (1990) 1561–1565.
- [24] G. Lennox, J. Lowe, K. Morrell, M. Landon, R.J. Mayer, Ubiquitin is a component of neurofibrillary tangles in a variety of neurodegenerative diseases, *Neurosci. Lett.* 94 (1988) 211–217.
- [25] J. Lowe, A. Blanchard, K. Morrell, G. Lennox, L. Reynolds, M. Billett, M. Landon, R.J. Mayer, Ubiquitin is a common factor in intermediate filament inclusion bodies of diverse type in man, including those of Parkinson's disease, Pick's disease, and Alzheimer's disease, as well as Rosenthal fibers of cerebellar astrocytomas, cytoplasmic bodies in muscle, and Mallory bodies in alcoholic liver disease, *J. Pathol.* 155 (1988) 9–15.

- [26] J. Lowe, R.J. Mayer, M. Landon, Ubiquitin in neurodegenerative diseases, *Brain Pathol.* 3 (1993) 55–65.
- [27] R.J. Mayer, J. Lowe, M. Landon, Ubiquitin and the molecular pathology of chronic degenerative diseases (Editorial), *J. Pathol.* 163 (1991) 279–281.
- [28] K. Ogomori, T. Kitamoto, J. Tateishi, Y. Sato, M. Suetsugu, M. Abe, β -Protein amyloid is widely distributed in the central nervous system of patients with Alzheimer's disease, *Am. J. Pathol.* 134 (1989) 243–251.
- [29] G. Perry, P. Cras, S.L. Siedlak, M. Tabaton, M. Kawai, Beta protein immunoreactivity is found in the majority of neurofibrillary tangles of Alzheimer's disease, *Am. J. Pathol.* 140 (1992) 283–290.
- [30] D.L. Price, M.W. Becher, P.C. Wong, D.R. Borchelt, M.K. Lee, S.S. Sisodia, Inherited neurodegenerative diseases and transgenic models, *Brain Pathol.* 6 (1996) 467–480.
- [31] J.M. Rozemuller, J.J. Abbink, A.M. Kamp, F.C. Stam, C.E. Hack, P. Eikelenboom, Distribution pattern and functional state of α 1-antichymotrypsin in plaques and vascular amyloid in Alzheimer's disease, *Acta Neuropathol.* 82 (1991) 200–207.
- [32] J. Savory, M.M. Herman, R.T. Erasmus, J.C. Boyd, M.R. Wills, Partial reversal of aluminum-induced neurofibrillary degeneration by desferrioxamine in adult male rabbits, *Neuropathol. Appl. Neurobiol.* 20 (1994) 31–37.
- [33] J. Savory, Y. Huang, M.M. Herman, M.R. Reyes, M.R. Wills, Tau immunoreactivity associated with aluminum maltolate-induced neurofibrillary degeneration in rabbits, *Brain Res.* 669 (1995) 325–329.
- [34] J. Savory, Y. Huang, M.M. Herman, M.R. Wills, Quantitative image analysis of temporal changes in tau and neurofilament proteins during the course of acute experimental neurofibrillary degeneration; non-phosphorylated epitopes precede phosphorylation, *Brain Res.* 707 (1996) 272–281.
- [35] F.E. Sherriff, L.R. Bridges, S.M. Gentleman, S. Sivaloganathan, S. Wilson, Markers of axonal injury in post mortem human brain, *Acta Neuropathol.* 88 (1994) 433–439.
- [36] R. Siman, J.P. Card, R.B. Nelson, L.G. Davis, Expression of β -amyloid precursor protein in reactive astrocytes following neuronal damage, *Neuron* 3 (1989) 275–285.
- [37] D.L. Sparks, S.W. Scheff, J.C. Hunsaker III, H. Liu, T. Landers, D.R. Gross, Induction of Alzheimer-like β -amyloid immunoreactivity in the brains of rabbits with dietary cholesterol, *Exp. Neurol.* 126 (1994) 88–94.
- [38] S. Strauss, J. Bauer, U. Ganter, U. Jonas, M. Berger, B. Volk, Detection of interleukin-6 and α 2-macroglobulin immunoreactivity in cortex and hippocampus of Alzheimer's disease patients, *Lab. Invest.* 66 (1992) 223–230.
- [39] R.E. Tanzi, A.I. McClatchey, E.D. Lamperti, L. Villa-Komaroff, J.F. Gusella, R.L. Neve, Protease inhibitor domain encoded by an amyloid protein precursor mRNA associated with Alzheimer's disease, *Nature* 331 (1988) 528–530.
- [40] G.H.G. Thorpe, L.J. Kricka, Enhanced chemiluminescence assays for horseradish peroxidase: characteristics and applications, in: J. Scholmerich, R. Andreessen, A. Kapp, M. Ernst, W.G. Wood (Eds.), *Bioluminescence and Chemiluminescence*, Wiley and Sons, New York, 1987, pp. 199–210.
- [41] H. Towbin, T. Staehelin, J. Gordon, Electrophoretic transfer of proteins from polyacrylamide gels to nitrocellulose sheets: procedure and some applications, *Proc. Natl. Acad. Sci. USA* 76 (1979) 4350–4354.
- [42] W. Wallace, S.T. Ahlers, J. Gotlib, V. Bragin, J. Sugar, R. Gluck, P.A. Shea, K.L. Davis, V. Haroutunian, Amyloid precursor protein in the cerebral cortex is rapidly and persistently induced by loss of subcortical innervation, *Proc. Natl. Acad. Sci. USA* 90 (1993) 8712–8716.
- [43] H.M. Wisniewski, C. Bancher, M. Barcikowska, G.Y. Wen, J. Currie, Spectrum of morphological appearance of amyloid deposits in Alzheimer's disease, *Acta Neuropathol.* 78 (1989) 337–347.
- [44] H.M. Wisniewski, J. Wegiel, K.C. Wang, M. Kujawa, B. Lach, Ultrastructural studies of the cells forming amyloid fibers in classical plaques, *Can. J. Neurol. Sci.* 16 (1989) 535–542.

EXHIBIT 13



Review

Tau and transgenic animal models

Jürgen Götz*

Division of Psychiatry Research, University of Zürich, August Forel Strasse 1, 8008 Zürich, Switzerland

Accepted 21 March 2001

Abstract

Advances in genetics and transgenic approaches have a continuous impact on our understanding of Alzheimer's disease (AD) and related disorders, especially as aspects of the histopathology and neurodegeneration can be reproduced in animal models. AD is characterized by extracellular A β peptide-containing plaques and neurofibrillary aggregates of hyperphosphorylated isoforms of microtubule-associated protein tau. A causal link between A β production, neurodegeneration and dementia has been established with the identification of familial forms of AD which are linked to mutations in the amyloid precursor protein APP, from which the A β peptide is derived by proteolysis. No mutations have been identified in the tau gene in AD until today. Tau filament formation, in the absence of A β production, is also a feature of several additional neurodegenerative diseases including progressive supranuclear palsy, corticobasal degeneration, Pick's disease, and frontotemporal dementia with parkinsonism linked to chromosome 17 (FTDP-17). The identification of mutations in the tau gene which are linked to FTDP-17 established that dysfunction of tau can, as well as A β formation, lead to neurodegeneration and dementia. In this review, newly recognized cellular functions of tau, and the neuropathology and clinical syndrome of FTDP-17 will be presented, as well as recent advances that have been achieved in studies of transgenic mice expressing tau and AD-related kinases and phosphatases. These models link neurofibrillary lesion formation to neuronal loss, provide an *in vivo* model in which therapies can be assessed, and may contribute to determine the relationship between A β production and tau pathology. © 2001 Elsevier Science B.V. All rights reserved.

Theme: Disorders of the nervous system*Topic:* Degenerative disease: Alzheimer's — other*Keywords:* Tau; Frontotemporal dementia; Tauopathy; Neurofibrillary tangle; Phosphorylation; Transgenic mice**Contents**

1. Introduction	267
2. Role of microtubules and tau	267
3. Tauopathies	269
3.1. Tau mutations	269
3.2. Neuropathology and clinical syndromes	269
4. Animal models	271
4.1. Human wild-type tau transgenic lampreys	271
4.2. Human wild-type tau transgenic mice	272
4.3. Human FTDP-17 mutant tau transgenic mice	275
4.4. Limitations of tau transgenic approaches	277
4.5. Tau and MAP1B knock-out mice	277
4.6. Transgenic mouse models of AD-related phosphatases and kinases	278
5. The amyloid cascade hypothesis: relation between amyloid deposition and neurofibrillary tangle formation	279
Acknowledgements	280
References	280

*Tel. +41-1-634-8873; fax: +41-1-634-8874.

E-mail address: goetz@bli.unizh.ch (J. Götz).

1. Introduction

Alzheimer's disease (AD), the most frequent cause of senile dementia, is characterized by a well-defined neuropathological profile which includes extracellular β -amyloid-containing plaques (consisting mainly of aggregated A β peptide derived by proteolysis of the amyloid precursor protein APP), intracellular neurofibrillary tangles (NFTs), reduced synaptic density, and neuronal loss in selected brain areas. NFTs are composed of hyperphosphorylated microtubule-associated protein tau. They are, in the absence of amyloid plaques, also abundant in additional neurodegenerative diseases including Pick's disease, progressive supranuclear palsy, corticobasal degeneration, argyrophilic grain disease, and frontotemporal dementia with Parkinsonism linked to chromosome 17 (FTDP-17).

In nerve cells affected in these tauopathies, tau is abnormally phosphorylated and relocated from axonal to somatodendritic compartments where it accumulates in pretangle, filamentous aggregates (PHFs or paired helical filaments in AD) that eventually assemble into NFTs (Fig. 1) [22,74]. In contrast to AD, where hyperphosphorylated tau forms filaments only in neurons, numerous tau filament-containing glial cells are present in a variety of tauopathies including progressive supranuclear palsy and corticobasal degeneration. At present, it is unknown, whether the glial pathology affects neuronal degeneration and whether it is required for progression of disease [41,116].

The recent discovery of mutations in the tau gene in

FTDP-17 has established that dysfunction of tau in itself can cause neurodegeneration, and lead to dementia [102,152,179].

The main aim of the present article is to review newly identified cellular functions of tau, the role of tau mutations, the neuropathology and clinical syndromes of FTDP-17, and, in particular, recent advances that have been made in studies of various transgenic models. Treatment of AD and related tauopathies has remained a major challenge of modern medicine [165], and there is hope that the newly established transgenic models will contribute to therapeutic strategies aimed at halting or slowing down disease progression in affected individuals.

2. Role of microtubules and tau

Microtubules are hollow, 25-nm wide cylindrical polymers, assembled primarily from heterodimers of α - and β -tubulin and a collection of microtubule-associated proteins (MAPs). Microtubules have two general functions, as the primary structural component of the mitotic spindle, and in organizing the cytoplasm. The latter is important in neurons, which are postmitotic. In concert with actin and intermediate filaments, cytoskeletal microtubules establish and maintain the overall internal architecture of the cytoplasm and thereby comprise a major determinant of overall cell shape. A direct role for cytoplasmic microtubules in the distribution of organelles was first demonstrated in neurons, where the use of video-enhanced microscopy showed that the oriented microtubule arrays in axons serve as the tracks along which vesicles and cell organelles such as mitochondria are translocated from the cell center to the periphery and back again by members of the kinesin and cytoplasmic dynein families of motor proteins [2,144,190,192]. Microtubules isolated from cell extracts by multiple cycles of assembly/disassembly and differential centrifugation yield a final microtubule preparation of which about 80% is tubulin, while the remaining 20% are MAPs. Initially isolated from mammalian neurons, MAPs were named according to the three major size classes of polypeptides: MAP1 (>250 kDa), MAP2 (~200 kDa), and tau protein (50–70 kDa). MAP2 and tau are expressed together in most neurons, where they localize to separate subcellular compartments. MAP2 is largely found in dendrites, whereas tau is concentrated in axons. Tau has also been found in astrocytes and oligodendrocytes, although, under physiological conditions, levels are relatively low [186].

In the human central nervous system the tau gene (located on chromosome 17q21) contains 15 exons with the major tau protein isoform being encoded by 11 exons [4]. By alternative mRNA splicing of exons 2, 3, and 10, six tau isoforms are produced in adult human brain. They differ by the presence or absence of one or two short inserts in the amino-terminal half (0N, 1N, and 2N,

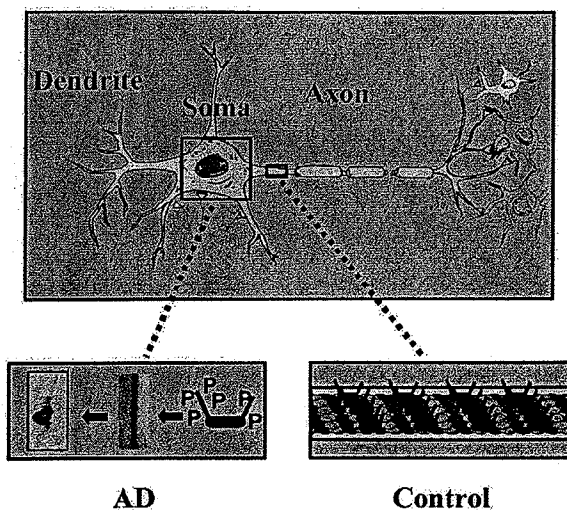


Fig. 1. Under physiological conditions, tau is localized to the axon where it binds to microtubules and polymerizes tubulin by establishing short crossbridges between axonal microtubules. Under pathological conditions such as AD, tau is hyperphosphorylated (P) and relocalized from axonal to somatodendritic compartments where it assembles into filamentous aggregates (PHFs, paired helical filaments). In advanced stages of disease, these filaments fill up the entire neuronal soma (NFTs, neurofibrillary tangles).

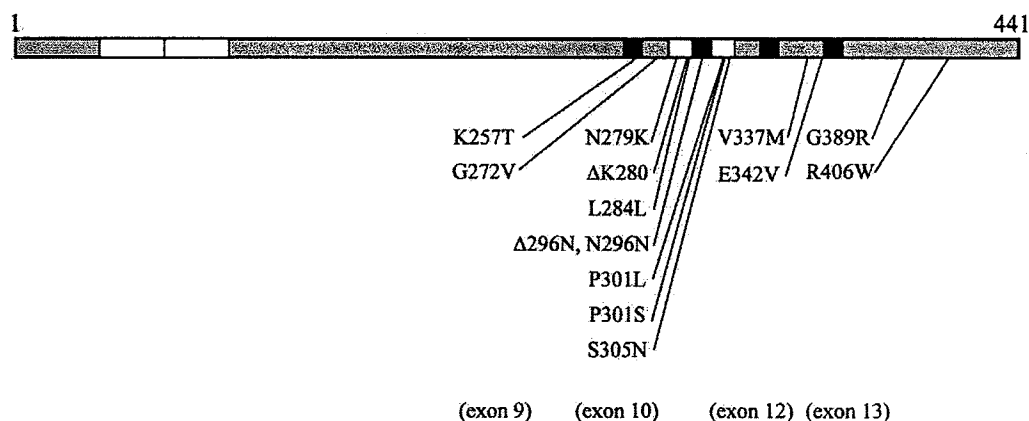


Fig. 2. The longest human tau isoform contains two amino-terminal inserts and four instead of three microtubule-binding repeats (alternatively spliced exon 10 shown in white). All FTDP-17-associated tau mutations identified so far are in the carboxy-terminal half of the tau protein suggesting that it is a hot spot of disease-causing mutations.

respectively), and have either three or four microtubule-binding repeat motifs in the carboxy-terminal half (3R and 4R) (Fig. 2). In contrast to humans, mice express only four-repeat tau isoforms (4R0N, 4R1N, and 4R2N) [66]. A 'big tau'-isoform containing approximately 300 additional residues (encoded by exon 4a) is expressed by peripheral nerves [33,71].

Besides stabilizing microtubules [119], recent data establish additional functions of MAPs [58]. The emergence of processes from cells often involves interactions between microtubules and actin filaments. Interactions between these two cytoskeletal systems are particularly apparent in neuronal growth cones. MAP2c is present in growth cones, where it mediates interactions between actin filaments and microtubules, and is an efficient actin gelation protein capable of organizing actin filaments at very low concentrations. Cells lacking the actin-binding protein-280 show a blebbing phenotype which can be rescued by microinjection of tau or MAP2 [34]. It is becoming increasingly apparent that the amino-terminal region of tau, which is not involved in microtubule interactions, has important functions. A proline-rich sequence in the amino-terminus interacts with the SH3 domains of fyn and src non-receptor tyrosine kinases [118]. This interaction may serve as a mechanism by which extracellular signals influence the spatial distribution of microtubules. The tyrosine phosphorylation of tau by fyn may also have a role in neurodegeneration, as fyn is upregulated in Alzheimer's disease [118], and activated by the cellular prion protein PrP^{Sc} [141]. A role for tau in conveying extracellular signals is supported by the finding that tau interacts with the plasma membrane during neuronal development, and that this membrane interaction is abolished when mutations simulating an AD-like hyperphosphorylation of tau were produced by site-directed mutagenesis of serine/threonine residues to negatively charged amino acids [130]. Co-immunoprecipitation of active phospholipase C-

γ (PLC-γ) with tau in a human neuroblastoma cell line suggests a role for tau in the PLC-γ signaling pathway. Tau also acts as a PIP2 (phosphatidylinositol bisphosphate) binding protein that serves as a precursor for diacylglycerol and inositol trisphosphate in signal transduction cascades and regulates the activities of several actin binding proteins that influence the organization of the actin cytoskeleton [3,37,55,108]. Upon overexpression of tau in cell lines, mitochondria were no longer transported to peripheral cell compartments suggesting that tau regulates intracellular vesicle transport [50]. In addition, tau is anchoring phosphatases [122,174,175] and kinases [140,156].

Under physiological conditions, tau is a phosphoprotein, and phosphorylation is developmentally regulated in that tau from immature brain is phosphorylated at more sites than tau from adult brain [69]. In AD and several AD-related tauopathies, tau is hyperphosphorylated [22]. Hyperphosphorylation means that tau is phosphorylated to a higher degree at physiological sites and at additional sites. Phosphorylation tends to dissociate tau from its natural partner, the microtubule. Since this increases the soluble pool of tau it might be an important first step in generating protein for the assembly of tau filaments. It is generally assumed, that soluble tau protein adopts a natively unfolded conformation [164].

In disease, tau undergoes conformational changes. Reactivity of the AD-diagnostic monoclonal antibodies Alz-50 and MC-1 is dependent on both the extreme amino-terminus of tau and a 30-amino acid sequence of tau in the third microtubule binding domain, suggesting that the specificity of the Alz-50 and MC-1 antibodies for pathological tau lies in their ability to recognize a specific conformation of the tau molecule in AD [109]. That tau can indeed adopt distinct conformations has been observed in sequential phosphorylation reactions where the AD-specific phospho-epitope of antibody AT100 can only be

generated by a sequential phosphorylation of tau first by GSK-3 β (glycogen synthase kinase-3 β) and then by PKA (protein kinase A), indicating that pre-phosphorylation at certain sites can alter the conformation such that other phosphorylation reactions are no longer possible [208].

3. Tauopathies

3.1. Tau mutations

In 1994, linkage of a familial disease called disinhibition–dementia–parkinsonism–amyotrophy complex (DDPAC) to chromosome 17q21–22 was reported [200]. It was followed by publications showing linkage of a number of inherited dementias with preceding personality changes to the same region of chromosome 17. A consensus conference grouped these diseases under the heading of ‘frontotemporal dementia and parkinsonism linked to chromosome 17’ (FTDP-17) [57]. As tau is located on chromosomal region 17q21–22, and as FTDP-17 is characterized by tau filament formation, the tau gene was sequenced in these families. Three missense mutations in exons 9, 10, and 13 (G272V, P301L and R406W) and three mutations in the 5' splice site of the alternatively spliced exon 10 were identified [102] (Fig. 2). In the same year, the V279M change was identified as an FTDP-17 causative mutation [152], and a G to A transition in the intron following exon 10 of the tau gene was linked to familial multiple system tauopathy with presenile dementia (MSTD) [179]. The splice-site mutations all destabilize a potential stem-loop structure which is probably involved in regulating the alternative splicing of exon 10. This causes more frequent usage of the 5' splice site and an increased proportion of tau transcripts that include exon 10. The increase in exon 10-containing mRNA is thought to increase the proportion of tau containing four microtubule-binding repeats (4R>3R), which is consistent with the neuropathology described in several families with FTDP-17. Together, these findings indicate that either an altered ratio of four-repeat to three-repeat tau isoforms (4R>3R) or a missense mutation can lead to the formation of abnormal tau filaments. All tau mutations identified so far are in the carboxy-terminal half of the tau protein suggesting that it is a hot spot of disease-causing mutations. Mutations in exon 9 (K257T and G272V), exon 12 (V337M and E342V) and exon 13 (G389R and R406W) affect all six tau isoforms. By contrast, mutations in the alternatively spliced exon 10 (N279K, Δ K280, Δ N296, P301L, P301S and S305N) only affect tau isoforms with four microtubule-binding repeats (Fig. 2). Silent mutations L284L (CTT to CTC) and N296N (AAT to AAC) in exon 10 are believed to disrupt an exon 10 splicing silencer sequence [8,30,41,42,47,49,72,125,136,148,160,176,177,189].

Analysis of sarcosyl-extracted frontal and temporal

cortical material from P301L patients, using polyclonal antibodies specific for P301L tau, provided the first direct evidence of a selective aggregation of mutant tau protein resulting in sarcosyl-insoluble deposits and the specific depletion of mutated tau protein in the soluble fraction [159]. Tau with FTDP-17-associated missense mutations is reported to exhibit altered physical and structural characteristics as determined by reversed-phase high-performance liquid chromatography and circular dichroism spectroscopy. These data suggest that these mutations are not merely benign polymorphisms, but may have functional consequences for microtubule binding, microtubule polymerization, rapid axonal transport, and the abnormal aggregation of tau as seen in a variety of neurodegenerative diseases [110]. On the other hand, based on studies of neuroblastoma and CHO cells transfected with green fluorescent protein (GFP)-tagged tau DNA constructs, both mutant (V337M and R406W) and wild-type tau transfectants were indistinguishable in the distribution pattern of tau in terms of co-localization with MT and generation of MT bundles. These results suggest that missense mutations of tau may not have an immediate impact on the integrity of the microtubule system, and that exposure of affected neurons to additional insults or factors (e.g., aging) may be needed to initiate the formation of tau inclusions in FTDP-17 [43].

Intronic mutations in the tau gene disrupt the normal balance between three-repeat and four-repeat tau isoform expression (4R>3R), and, as 4R tau can displace 3R tau from microtubules [128], altered kinetic competition among the isoforms for microtubule binding could be a disease precipitant. This raises the possibility that these isoforms may possess some distinct functional capabilities. In vitro mutagenesis studies revealed that 3R tau possesses a core microtubule binding domain composed of its first two repeats and the intervening inter-repeat. This observation is in marked contrast to the widely held notion that tau possesses multiple independent tubulin binding sites aligned in sequence along the length of the protein. In addition, the carboxyl-terminal sequences downstream of the repeat region make a strong but indirect contribution to microtubule binding activity in 3R, but not 4R tau [77,78].

3.2. Neuropathology and clinical syndromes

The term FTDP-17 is now widely used for a number of inherited dementias with initial personality changes linked to the same region of chromosome 17, although the wide range of clinical and pathological phenotypes associated with mutations in tau limits the utility of any descriptive term to encompass the entire syndrome. In addition to frontotemporal dementia, tau mutations can cause disease entities as diverse as subcortical gliosis [72], cortico-basal degeneration (CBD) [26], and pallido-ponto-nigral degeneration [205]. Common to all of the diseases associated with tau mutations is aberrant tau immunoreactivity in neurons

and/or glial cells, and in some cases the aberrant tau immunoreactivity contains tau aggregates that are indistinguishable from AD. Filamentous inclusions made of tau protein, in the absence of amyloid plaques, are also a defining characteristic of additional neurodegenerative diseases, such as progressive supranuclear palsy (PSP), and Pick's disease [23].

Frontotemporal dementia and parkinsonism linked to chromosome 17 (FTDP-17) has been related to mutations in the tau gene. Disinhibition and loss of initiative or apathy are the most-common symptoms. Patients lose interest in their environment, neglect their personal hygiene, and show a severe loss in judgement and insight. Other characteristic features of this syndrome are personality changes and psychiatric manifestations, such as verbal and physical aggressiveness, alcohol abuse, roaming, restlessness, and hyperorality, as well as deterioration of memory and executive functions and stereotypical behavior [146]. Psychiatric symptoms, such as hallucinations, delusions, persecution mania, and psychosis have been reported in some patients [129,183,193].

Neuropsychological changes include short-term memory, executive functions, attention and concentration [14,136,155,183,193]. Comprehension of spoken language is impaired in some patients. Mutism develops within 5–6 years from disease onset in most families [14,193]. The clinical diagnosis of frontotemporal dementia is often supported by neuroradiological evidence of a usually symmetrical, but occasionally asymmetrical atrophy of the frontal and temporal lobes [14,142,193]. In many cases, additional degenerative changes are observed in subcortical brain regions, such as the substantia nigra. Patients with early signs of parkinsonism have shown reduced striatal uptake of L-dopa [202]. These patients showed hypomimia, bradykinesia, postural instability and rigidity without resting tremor [129,178,202]. One family was even characterized by an early onset of rapidly progressive frontotemporal dementia and parkinsonism in combination with epileptic seizures [176]. In support of the high degree of variability of frontotemporal dementias, a family was identified with clinical and pathological features similar to those of several of the families included in descriptions of FTDP-17, but a linkage to tau has been excluded. Neuropathology showed frontotemporal atrophy, and microscopically tau- and α -synuclein-negative and ubiquitin-positive neuronal inclusions, in the background of superficial cortical spongiosis, neuronal loss, and gliosis, and tau expression was restricted to oligodendroglia [114].

All frontotemporal dementias with tau mutations that have been examined to date have a filamentous pathology made of hyperphosphorylated tau protein. The morphology of tau filaments and their isoform composition appears to be determined by whether tau mutations affect mRNA splicing of exon 10, or whether they are missense mutations located inside or outside of exon 10 [65]. As for PSP and CBD, hyperphosphorylated tau forms filaments not only in neurons, but also glial cells. A recent analysis of

two patients with the disease-causing FTDP-17-linked mutation N279K showed widespread neuronal and glial tau accumulation in the cortex, basal ganglia, brain stem nuclei as well as in the white matter. In neocortex, tau-immunoreactive glial cells outnumbered immunoreactive neurons [41].

Most patients with tau mutations develop frontotemporal dementia between 40 and 60 years of age, although several patients with the P301L, the R406W and some of the intronic mutations have an age of onset of more than 60 years [14,183,193]. In contrast, patients with the P301S mutation develop disease at less than 35 years of age [26]. Disease duration is usually between 6 and 12 years.

Pick's disease is a rare neurodegenerative disorder characterized by a progressive dementia and personality deterioration, associated with verbal and behavioural stereotypies. When Arnold Pick presented the case of an elderly demented patient with severe aphasia and global brain atrophy most accentuated at the left temporal lobe in 1892, he made no effort to describe a new form of dementia. His main interest was the relationship between focally accentuated brain degeneration and focally accentuated neuropsychological deficits. The term 'Pick's disease' was only introduced 30 years later [56] to describe a disease that is an extreme form of frontotemporal dementia, but difficult to differentiate clinically. It is characterized morphologically by a severe atrophy of the frontal and temporal lobes, gliosis, severe neuronal loss, ballooned neurons, and the presence of degenerative neuronal lesions referred to as Pick bodies. High densities of Pick bodies are observed in Ammon's horn, subiculum, entorhinal cortex, and in the granule cell layer of the dentate gyrus. In the frontal and temporal neocortex, they are preferentially distributed in layers II and VI [20,98]. The laminar distribution of Pick bodies is clearly different from that of neurofibrillary tangles in AD, CBD, and PSP [98]. Ultrastructurally, Pick bodies consist of random coiled and straight tau filaments. Interestingly, only 3R tau isoforms aggregate into Pick bodies [40]. Moreover, aggregated tau proteins in Pick's disease cannot be detected by the monoclonal antibody 12E8 directed against the phosphorylated tau epitope Ser262/Ser356. In contrast, this phosphorylation site is readily detected in other neurodegenerative disorders [40].

PSP is characterized by early signs of vertical gaze paresis and progression to total external ophthalmoplegia. Additional features are dysarthria, dysphagia, and parkinsonian symptoms. Dementia is progressive and is a dominant feature of the terminal stages of the disease [126,127]. Although most cases of PSP are considered to be sporadic, familial cases have been reported [38]. In particular, an intronic dinucleotide polymorphism has been associated with PSP [12,31]. Neuropathologically, PSP is characterized by neuronal loss, gliosis and tangle formation in basal ganglia, brain stem, and cerebellum, but also in the perirhinal, inferior temporal and prefrontal cortex [13,94,98].

In AD, for comparison, the most severe neuropathological changes occur in the hippocampal formation, the association cortices and subcortical structures including the amygdala and the nucleus basalis of Meynert [10]. In contrast to AD, where hyperphosphorylated tau forms filaments only in neurons, numerous tau filament-containing glial cells are also present in a variety of tauopathies including PSP and CBD [29,116]. In PSP, the neuritic and glial changes are composed of straight filaments and tubules, that are different from the paired helical filaments found in AD [27,39]. Remarkably, only 4R tau isoforms aggregate into filaments in PSP [131,167].

CBD is a rare, sporadic and slowly progressive late-onset neurodegenerative disease that is clinically characterized by cognitive disturbances, cortical sensory loss, extrapyramidal motor dysfunction, and unilateral rigidity [154]. The most common initial complaint of patients is a unilateral clumsy, stiff or jerky arm, which is often held in a striking and characteristic fixed dystonic posture. The next most common presentation is difficulty of walking due to clumsiness and loss of fine motor control of one leg due to apraxia or dysequilibrium, or a combination of both. The symptoms progress slowly. Higher mental function is relatively preserved in most patients and a cortical sensory loss is evident only in a subset of cases [158]. Histopathologically, CBD is characterized by glial and neuronal abnormalities. The glial pathology includes astrocytic plaques and numerous tau-immunoreactive inclusions in the white matter. Achromatic ballooned neurons are present in cortex, brain stem and subcortical structures, as are neuritic changes and neurofibrillary tangles [24,52,53,116,150]. Ultrastructural analysis indicates that tau aggregates in CBD form twisted filaments that differ from paired helical filaments of AD in length, width, and periodicity [117]. As for PSP, only 4R tau isoforms aggregate into filaments [167]. There is increasing evidence that CBD overlaps significantly with primary progressive aphasia and frontotemporal dementia, and that CBD is part of the Pick complex [115].

For a pre-mortem differential diagnosis of AD and other dementias, assays that measure levels of such histopathologically relevant molecules as apolipoprotein E, β -amyloid and tau in cerebrospinal fluid (CSF) are extremely important [96,101]. The lumbar puncture itself is usually well tolerated, and earlier studies have shown elevated levels of tau protein and decreased levels of A β 42 amyloid peptide in CSF from AD patients [15,97,112]. Compared to AD patients, several groups reported a significant decrease of CSF tau in patients with frontotemporal dementia [139,172]. Quantification of tau in CSF using a panel of different phosphorylation-dependent anti-tau antibodies may even improve the sensitivity and specificity of the diagnosis [194].

Currently, it is not known whether the presence of tau filaments causes neuronal degeneration or whether filament formation is only a consequence of a more general degenerative process. A causative role for filaments in

neurodegeneration is suggested by analogy to α 1-antitrypsin-associated liver disease, where hepatocyte loss and cirrhosis is clearly a consequence of abnormal deposits and not of a loss of function, because cirrhosis develops only with a conformationally unstable variant, but not with mutations that cause 'null' suppressions of synthesis [36]. Also, it is unlikely, that filament morphology per se contributes significantly to the clinical phenotype. Depending on the tau mutation filaments may tend to form faster allowing for a more rapid disease progression. Most importantly, the clinical phenotype will depend on where in the brain tau pathology is initiated, and how this brain region is connected to other regions.

Tauopathies and α -synucleinopathies account for most late-onset neurodegenerative diseases in man [63], and there is accumulating evidence that tauopathies may be associated with the hallmark lesion of α -synucleinopathies, i.e., the accumulation of filamentous α -synuclein. α -Synuclein is a major component of Lewy bodies (LBs) in sporadic Parkinson's disease, dementia with LBs, and the LB variant of AD [89]. Although it is possible that LBs are a nonspecific outcome of end-stage AD, LBs may reflect the co-occurrence of Parkinson's disease in a subset of AD patients. Alternatively, the accumulation of LBs in the AD brain may result from the pathogenic mechanisms that underlie AD and related tauopathies. Thus, although neurofibrillary tangles and amyloid plaques are the hallmark lesions of AD, unknown genetic or epigenetic factors may predispose neurons to accumulate LBs during the progression of AD in a subset of affected patients [123]. With α -synuclein-specific antibodies available as new tools, several groups demonstrated the presence of LBs in brains from cases of sporadic and familial AD, Down's syndrome, and the parkinsonism-dementia complex of Guam [6,123,124,204]. For example, in one study, LBs were detected in more than half of all familial AD amygdala samples, and some LBs colocalized with tau-positive neurofibrillary tangles [123]. LBs have not been reported in FTDP-17 cases so far. Studies of the sequence of events that underlie the formation of Lewy bodies, neurofibrillary tangles, and amyloid plaques may clarify the role of genetic and epigenetic factors in the pathogenesis of these lesions.

More specifically, an understanding of the pathogenesis of tauopathies requires the development of experimental animal models which reproduce the neuropathological characteristics of these diseases.

4. Animal models

4.1. Human wild-type tau transgenic lampreys

The sea lamprey (*Petromyzon marinus*) is a parasitic fish native to the North Atlantic Ocean and many of its tributaries. The central nervous system of this lower vertebrate is characterized by a set of six giant identified

neurons, so-called anterior bulbar cells or ABCs, in the hindbrain which are readily accessible for manipulation. ABCs have been morphologically characterized and studied in detail on a single-cell level [86]. They resemble most large vertebrate neurons in having extensively branched, tapered dendrites which receive large numbers of synaptic inputs, and have a cytoskeleton dominated by longitudinally oriented microtubules [85]. In a first study, individual ABCs were microinjected with vectors expressing full-length human tau isoforms and deletion mutants, and examined until 76 days post-injection. In contrast to ABCs expressing full-length tau, expression of amino- and carboxyl-terminal human tau fragments was never associated with the formation of dense tau deposits. Immunostaining for full-length human tau protein extended to the dendritic tip and up to 1 cm or more along the axon in all expressing cells examined. Tau was most heavily phosphorylated in dendrites as shown with antibody PHF-1 directed against the phosphorylated Ser396/Ser404 epitope of tau. A marked increase in the occurrence of 10–15-nm filaments was seen throughout the soma of injected compared to uninjected ABCs [88]. By 70 days post-injection, the largest cohort of tau filaments (those 10–18 nm in diameter) had become the only form of filaments in small dendrites, and resembled the straight filaments seen in neurofibrillary tangles in the brains of AD patients. A small number of filaments even exhibited periodic expansions and constrictions reminiscent of paired helical filaments [85]. Filament formation was associated with dendritic beading, the localized aggregation and lysis of membrane-bound organelles, and progressive dendritic microtubule and synapse loss [85]. As tau has been shown to interact with membrane in a phosphorylation-dependent manner [130], this raises the possibility that membranous structures might even become bound to tau filaments and/or to each other during neurofibrillary degeneration.

Studies of the early stages of neurofibrillary degeneration in human AD autopsy material suggest that abnormal tau deposits develop in a stereotyped spatiotemporal sequence [17]. To address the staging of neurofibrillary degeneration in lamprey, self-replicating mRNAs derived from Semliki Forest Virus (SFV) were used that resulted in chronic overexpression of tau in ABCs. The same stereotyped sequence of cytodegenerative changes throughout time was induced, with the earliest and most severe changes occurring in the distal-most dendrites. Moreover, this sequence of degenerative changes was spatiotemporally correlated with the appearance of some AD-related phospho-epitopes [87]. However, in contrast to AD [17], the AT8 phospho-epitope (Ser202/Thr205) appeared in tau-expressing ABCs only at a time when morphological degeneration was widespread in the distal dendrites, and did not precede overt morphological changes. Furthermore, Gallyas silver impregnation and Thioflavin-S labeling were negative in all tau-expressing ABCs examined, whereas most fibrillar tau deposits appeared to be argyrophilic in

humans [17]. This may be due to different time scales in humans versus lamprey (decades versus weeks or months), although, in transgenic mice, formation of Gallyas-positive tangles has been reproduced at an age comparable to that in the lamprey study (see below). Therefore, it is likely that species differences contribute to the formation of Gallyas-positive structures [92].

4.2. Human wild-type tau transgenic mice

As APP transgenic models failed to develop tau filaments [59], and FTDP-17 associated tau mutations were not identified at that time, several research groups generated human wild-type tau transgenic mice. The first tau model expressed the longest human four-repeat (4R) tau isoform, htau40, under control of the human Thy1 promoter [83]. Levels of human relative to endogenous murine tau were approximately 10%, as determined by immunoblot analysis of perchloric acid-extracted whole brain tissue (Table 1). Strongly labeled neurons were observed in most brain regions. Their numbers were relatively small, accounting for only a few percent of the total nerve cell population. However, as in AD, transgenic human tau protein was present in nerve cell bodies, axons and dendrites; moreover, it was phosphorylated at sites that are hyperphosphorylated in PHFs including Ser202/Thr205 and Ser396/Ser404, as determined by phosphorylation-dependent antibodies AT8 and PHF1 [70,84], respectively. Tau filament formation was not observed, and tau staining appeared homogeneous or granular, but not fibrillar [83]. A very similar phenotype was reported in mice with neuronal expression of the shortest human tau isoform, htau44, using the murine 3-hydroxy-methyl-glutaryl CoA reductase promoter. Transgenic human tau protein had a widespread brain distribution, and was also expressed in peripheral organs including heart, thymus, lung, and stomach. Transgenic brain phosphorylated tau at the phosphoepitopes AT180, AT270, AD2, 12E8 [25,68,168], but not at the AT8 epitope [70], a common phospho-epitope in AD. Tau was reactive also with Alz50, a conformation-dependent antibody diagnostic for AD [19]. In summary, both mouse strains showed early changes associated with the development of neurofibrillary lesions in AD and related disorders, but they failed to produce NFTs and lacked obvious neurological symptoms (Table 2).

A comparative analysis of APP transgenic mice showed that higher expression levels resulted in a more advanced phenotype [28,59,99,111,138,182]. Therefore, stronger promoters were chosen by several groups for expression of human tau in transgenic mice.

The murine PrP promoter was used, together with 5' intronic and 3' untranslated sequences, to express the shortest human tau isoform, htau44 [105]. Levels of transgenic tau were significantly higher as compared to previous models and were, for one particular line, up to 15-fold above endogenous mouse tau (Table 1). These

Table 1
Genetic parameters of human tau transgenic mice

Transgenic	Tau cDNA	Mutation	Transgene promoter	Strain background	Tau overexpression
ALZ7 [83]	htau40 (2+3+4R)	Wild-type	Human Thy1/ β -globin pA/splice cassette	B6D2F1×BGD2F1	10% of endogenous
TG23 [19]	htau44 (2–3–3R)	Wild-type	Murine HMG CoA reductase	C57BL/6×CBAF2	14% of endogenous
7, 43, and 27 [105,106]	htau44 (2–3–3R)	Wild-type	Murine PrP	B6D2F1×B6D2F1	5×, 10×, and 15× resp. (in spinal cord 60% of levels of cortex and hippocampus)
htau40-1, -2, -5 [180]	htau40 (2+3+4R)	Wild-type	Murine Thy1.2 genomic	FVB/N	4×, 4× and 1.5×, resp. (both in brain and spinal cord)
ALZ17 [153]	htau40 (2+3+4R)	Wild-type	Murine Thy1.2 genomic	B6D2F1×B6D2F1	Homozygous lines: 1.5× in brain, more than 10× in spinal cord)
JNPL3 [121]	htau43 (2–3–4R)	P301L	Murine PrP	B6D2SW	similar to endogenous (hemizygous mice)
pR5-183 [80]	htau40 (2+3+4R)	P301L	Murine Thy1.2 genomic	B6D2F1×B6D2F1	70% of endogenous (hemizygous mice)
Tg214 (Takashima et al., submitted)	htau40 (2+3+4R)	V337M	Murine PDGF	C57BL/6	10% of endogenous
pR3 (Götz et al., in press)	htau40 (2+3+4R)	G272V	Murine PrP with auto-regulatory transactivator loop	B6D2F1×B6D2F1	2–3× in spinal cord

mice were not viable beyond 3 months of age, and subsequent experiments were conducted with mice with 5- and 10-fold overexpression. When brain and spinal cord sections were stained with phosphorylation-dependent and -independent anti-neurofilament and anti-tau antibodies, multiple spheroids were evident which consisted of focal dilatations of axons (Table 2). Neurofilament-positive axonal spheroids are a neuropathological characteristic of the majority of cases of sporadic and familial amyotrophic lateral sclerosis (ALS), where they are believed to impair slow axonal transport [161]. In ALS, axonal spheroids form in the absence of tau pathology in spinal cord. By contrast, in patients with Guamanian ALS and parkinsonism–dementia complex, tau deposits in spinal cord are an essential feature of the pathology [132,162]. Also, in DDPAC (disinhibition–dementia–parkinsonism–amyotrophy complex), similar axonal spheroids and amyotrophy have been reported [169]. It has been suggested that the dephosphorylated carboxy-terminal region of neurofilament-H (NF-H) interacts with microtubules, and that tau and the NF-H tail compete for common binding sites on the carboxy-terminus of tubulin [137]. Like neurofilaments, tau is largely transported in the slow component a (SCa) of axonal transport [187]. Overexpression of tau may prevent the binding of neurofilaments to microtubules, thereby segregating microtubules from neurofilaments, and causing the accumulation of neurofilaments in the proximal axonal segment, further emphasizing that neurofilaments and microtubules are highly interdependent structures. Consistent with this finding, orthograde fast axonal transport was reduced in the ventral root axons of htau44

transgenic mice, and axons were degenerated [105]. The transgenic mice also developed progressive motor weakness, as demonstrated by their inability to stand on a slanted surface and by retraction of their hindlimbs when lifted by their tails [105].

Tau protein extracted from PrP-htau44 transgenic brain and spinal cord became increasingly insoluble as mice became older. In wild-type mice, about 90% of endogenous mouse tau was largely RAB (high-salt buffer)-soluble and no immunoreactivity was detected in the formic acid (FA)-soluble fraction. In transgenic mice, although the RAB-soluble tau remained constant at around 75–80% with increasing age, RAB-insoluble tau represented by the RIPA and FA fractions progressively accumulated in both the brain and spinal cord, reaching 25% in the RIPA- and 2% in the FA-fraction, respectively, at 9 months of age. As in the older models, tau was phosphorylated at several PHF-tau epitopes.

The murine Thy1.2 expression vector was used by two groups to achieve high expression levels of the longest human tau isoform, htau40 [153,180]. Two different genetic backgrounds (FVB and B6D2F1) were used to generate the transgenic strains. This, together with copy number and integration site of the transgene, may account for phenotypic differences. Whereas the FVB transgenic mice expressed between 1.5× and 4× of transgenic tau as compared to endogenous tau in both brain and spinal cord, expression levels in the B6D2F1 transgenic mice were 1.5× in brain and more than 10× in spinal cord. Tau hyperphosphorylation (Fig. 3), somatodendritic localization (Fig. 4), and the presence of axonal spheroids with

Table 2
Neuropathology in human tau transgenic mice

Transgenic line	Tau hyperphosphorylation and conformational changes	Spinal cord pathology	Astrocytosis	NFTs, neuronal loss
ALZ7 [83]	AT8, PHF1 pos	No	No	No
TG23 [19]	AT180, AT270, AD2, 12E8 pos.; AT8 neg.; Alz50 pos.	No	No	No
7, 43, and 27 [105,106]	PHF1, PHF6, T3P, AT8, AT270, 12E8 pos.; Alz50 pos.	Axonal degeneration, axonal spheroids	In brain and spinal cord	No, but Bodian-pos. Inclusions at 18–24 months of age; Gallyas+, Thioflavin S+ Congo red+; PHF1-Immuno EM on sections
htau40-1, -2, -5 [180]	AT8, AT180, AT270 PHF1 pos.; Alz50, MC1 pos.	Axonal degeneration axonal spheroids	Correlation with expression levels in brain and spinal cord	No, but Bielschowsky-pos. axonal dilations
ALZ17 [153]	AT8, AT180, PHF1, AD2 12E8 (AP422) pos.	Axonal degeneration axonal spheroids	N.D.*	No
JNPL3 [121]	AT8, CP3, TG3, CP9, CP13 PG5, PHF1 pos.; Ab39, Ab69, Alz50, MC1 pos.	Axonal degeneration axonal spheroids	In spinal cord, brain stem, diencephalon and telencephalon	CP3-Immuno EM on sections; Gallyas+, Thioflavin S+, Congo red+, Bielschowsky+, Bodian+; 48% reduction of motor neurons in spinal cord
pR5-183 [80]	TG3, AT180, S199P pos., AT8 weak, AD2/PHF1 neg.; MC1 pos.	No obvious degeneration	Pos. correlation of activated astrocytes and htau expression in cortex	Immuno EM on Sarcosyl-extracted filaments; AT8, TG3, AT100, S199P-pos.; Gallyas+, Thioflavin S+; TUNEL-pos. neurons in cortical areas
Tg214 (Takashima et al., submitted)	PS199, AT8 pos.; Alz50 pos.	No obvious degeneration	No	PS199-Immuno EM on sections; Tau-Immuno EM on RIPA-extracted filaments; Gallyas+, Thioflavin S+, Congo red+
pR3 (Götz et al., in press)	AT8, TG3, AD2, 12E8 pos., AT270, AT100 neg.; MC1 neg.	No obvious degeneration	N.D.*	EM on sections and Sarcosyl-extracted filaments; Thioflavin S+

* N.D., not done.

accumulations of neurofilaments, mitochondria, and vesicles were reported for both models [153,181].

Evidence for axonal Wallerian degeneration, including axonal breakdown and segmentation of myelin into ellipsoids (so-called 'digestion chambers') was obtained in anterior spinal roots of B6D2F1 transgenic mice. Clear evidence of neurogenic muscle atrophy, with groups of small angular muscle fibers, was present in the hindleg musculature of transgenic, but not control, mice [153]. In FVB transgenic mice, occasionally, microglia with phagocytosed myelin debris and myelin ovoids were present, indicating Wallerian degeneration [180].

The FVB transgenic mice were further subjected to a detailed sensorimotor analysis at the age of 2–4 months. Already at 3 weeks of age, homozygous transgenic mice flexed their hindlimbs when lifted by the tail. Motor abilities were determined in a forced swimming test. The swimming speed was about 70% of that of wild-type mice.

Also, transgenic mice were up to 90 times more likely to fall off a rod. Likewise, significantly more transgenic mice lost hold of the inverted wire mesh grid [180]. Together, these observations proved that these mice displayed a reduced endurance, a postural instability, a loss of motor coordination and of maintenance of equilibrium, and a muscular weakness. However, this motor disturbance prevented the mice from being tested in the Morris swimming navigation test (Morris water maze) [201], one of the most widely used paradigms to assess memory and hippocampal function [180]. The B6D2F1 transgenic mice progressively showed signs of neurological malfunction. When lifted by the tail, normal mice extend their hindlimbs and spread their toes. At 1–3 months of age, homozygous transgenic mice extended their legs, but retracted their paws, in marked contrast to control mice. When aged 8–16 months, the same mice were unable to extend their hindlimbs when lifted by the tail. When tested



Fig. 3. The murine Thy1.2 expression vector was used by two groups to achieve high expression levels of the longest human wild-type tau isoform, htau40 [153,180]. Two different genetic backgrounds (FVB and B6D2F1) were used to generate the transgenic strains. In B6D2F1 transgenic mice, tau was overexpressed and hyperphosphorylated in many cortical and hippocampal neurons as demonstrated with the phosphorylation-dependent diagnostic antibody AT8.

on the rotarod, control mice stayed on the rotarod twice as long as homozygous transgenic mice [153]. Again, no Morris water maze test was performed. Progressive loss of motor coordination and signs of neurogenic muscle atrophy, likely a consequence of large accumulations of closely packed neurofilaments in both distended motor neuron cell bodies and proximal axonal swellings, have been reported also in mice overexpressing wild-type murine neurofilament NFL or human NFH subunits [32,203].

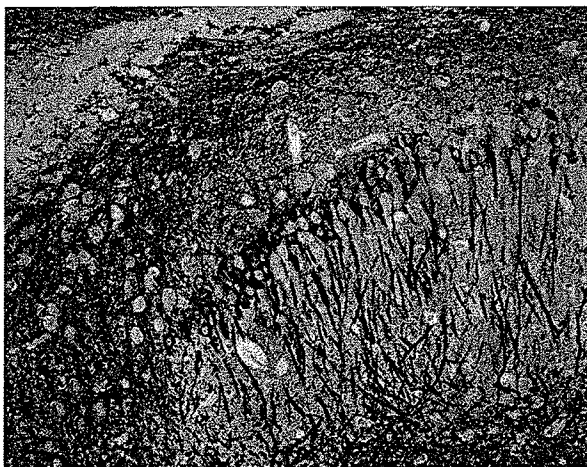


Fig. 4. In human wild-type tau transgenic mice, in addition to hyperphosphorylation of tau, another characteristic feature of AD and related tauopathies has been recapitulated. Tau was translocated from the axonal to the somatodendritic compartment. Staining of a parasagittal section of the CA1 region of the hippocampus with antibody AT8 revealed hyperphosphorylation of tau in cell bodies and apical dendrites.

To determine filament formation in the tau models, silver impregnation techniques were applied. In one model [105], brain and spinal cord inclusions were positively stained by the Bodian silver method, and they were not stained by an antibody to ubiquitin; in a second (FVB) model [180], Bielschowsky's stain revealed grossly dilated axons in brain and spinal cord, and immunohistochemical staining for ubiquitin labeled some of the dilated axons in cortex and spinal cord (Table 2). None of the transgenic models were thioflavine S- or Gallyas-positive, and none developed tau filaments.

The first report of tau filament formation in mice that express FTDP-17 mutant forms of tau (next section) firmly proved that filament formation can be achieved in mice. Therefore, htau44 transgenic mice were analyzed again at high age [106]. Congo red stainings and Gallyas silver impregnations demonstrated filamentous lesions in perikarya of cortical neurons in brains of 18–24-month-old mice. Ubiquitin immunoreactivity colocalized with tau staining in double immunofluorescence studies. Filaments were 10–20 nm wide, and labeled by phosphorylation-dependent antibody PHF1. Semiquantitative analyses showed that the frequency of occurrence of mouse tangle-like structures was about one to two per mouse brain section at 24 months of age [106].

Collectively, the neuropathology in the new series of tau overexpressing models partly mimics AD-like and partly ALS-like syndromes. The data establish that overexpression of wild-type human tau isoforms is sufficient to cause nerve cell dysfunction.

4.3. Human FTDP-17 mutant tau transgenic mice

As for presenilin mutations in familial AD, presence of particular mutations in tau seems to be correlated with disease onset [26,176]. Support for this notion comes from *in vitro* studies in which the differential effect of tau mutations on filament formation and microtubule assembly was determined [67,143,207]. These studies favored, at that time, expression of P301L tau in transgenic mice. Therefore, the human 4R tau isoform lacking the two amino-terminal inserts, htau43, was expressed together with tau mutation P301L under control of the murine PrP promoter [121]. Line JNPL3 expressed mutant tau at levels comparable to endogenous tau (Table 1). By 10 months of age, 90% of the mice developed motor and behavioural disturbances that were more pronounced than reported for previously published mouse models [105,153,180]. JNPL3 mice showed a delayed righting response and eventually became unable to go into the upright position [121]. In hang tests, they fell after grasping the rope briefly, whereas wild-type human tau transgenic mice with similar transgenic tau expression levels held with three limbs and tail without falling. Within 2 weeks of phenotype onset, JNPL3 animals could not ambulate. Weakness spread to all limbs and dystonic posturing developed. Affected animals

showed a reduction in weight, grooming and vocalization, and an increase in docility. JNPL3 mice developed eye irritations and had difficulty in opening their eyes. Within 3–4 weeks of initial signs, mice became moribund. Again, as for human wild-type tau transgenic mice, this motor disturbance prevented the mice from being tested in the Morris swimming navigation test (Morris water maze) [201].

Gliosis was found in brainstem, diencephalon and basal telencephalon. There was a reduction of 48% of motor neurons in spinal cord. NFTs were identified in the diencephalon, brainstem, cerebellum and spinal cord by Congo red, thioflavin S fluorescent microscopy, and Gallyas, Bielschowsky and Bodian silver stains (Table 2) [121].

In a second model (pR5 line, Table 1) the same mutation was expressed, but the longest tau isoform, htau40, was used. In addition, the mThy1.2 promoter was chosen instead of the mPrP promoter which may account for different expression patterns in these pR5 mice (Table 1) [80]. Expression of P301L tau was high in hippocampus, cortex, spinal cord, and amygdala, and weaker in brain stem and striatum (Table 2). Activated astrocytes were found in the amygdala and several cortical areas where astrogliosis was positively correlated with the number of tau expressing neurons. TUNEL (TdT-mediated dUTP nick end labeling)-positive neurons were identified in the cortex, but neuronal loss was not determined. NFTs were identified by Gallyas silver stain (Fig. 5) and thioflavin S-fluorescent microscopy, and sarcosyl-extracted tau filaments expressed the phosphoepitopes AT8, AT100, and S199P and the conformational epitope TG3 (Fig. 6) [40,44,68,70,167]. The abundance of shorter filaments in pR5 transgenic mice may be related to the presence of two amino-terminal inserts within the longest human tau isoform, with calpain recognition motifs that may subject tau to rapid proteolysis, thus favoring the formation of shorter over longer filaments [199] compared to JNPL3 mice which do not contain these inserts. Stability of tau is known to be involved in filament formation as FTDP-17 mutations tend to make tau more resistant to proteolysis compared to wild-type tau [206]. The presence of the two amino-terminal inserts on the construct and the use of a different promoter may explain why there is no overt neurological phenotype in the pR5 compared to the JNPL3 mice. Expression levels of human tau as determined by immunoblot analysis are comparable, yet, expression levels in particular cell types may vary. Also, immunohistochemistry with phosphorylation-dependent antibodies revealed differences between the two models with possible consequences for the observed phenotypes (Table 2). It remains to be determined which phosphoepitopes (if at all) are necessary and sufficient for filament formation *in vivo*.

FTDP-17 mutations V337M (A. Takashima, personal communication) and G272V (J. Götz, M. Tolnay, R. Barmettler, F. Chen, A. Probst and R.M. Nitsch, Eur. J.

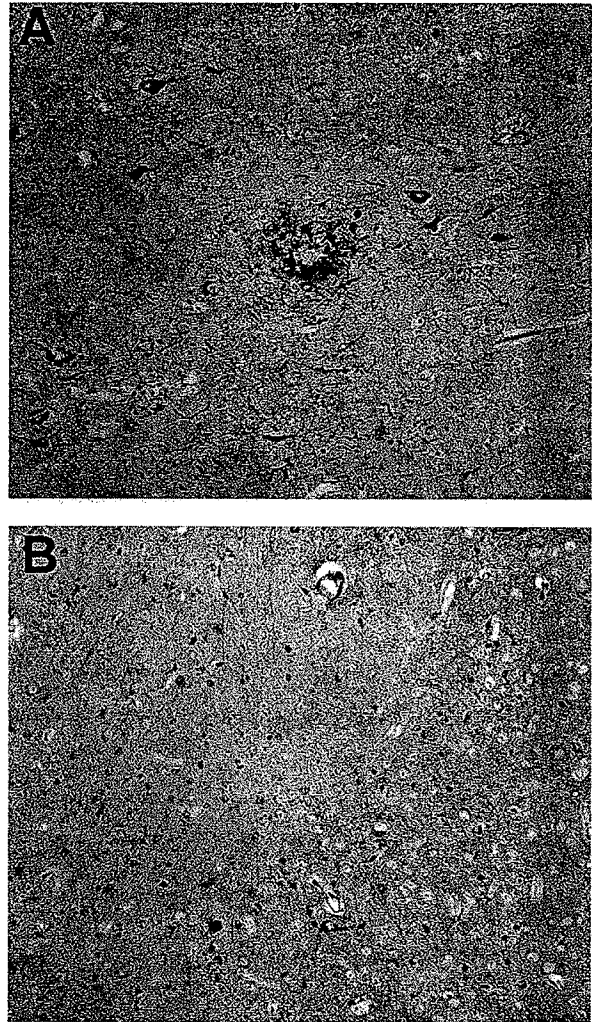


Fig. 5. The Gallyas silver impregnation technique revealed numerous neurofibrillary tangles, neuropil threads, and a neuritic plaque in the brain of an AD patient (A). Neurofibrillary tangles, although at a lower frequency, were also found in brains of P301L tau transgenic mice (B).

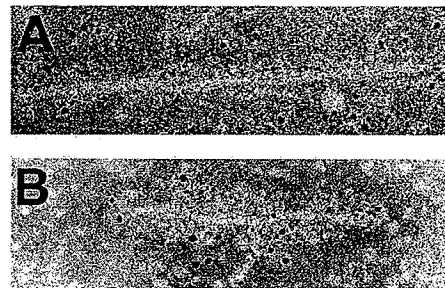


Fig. 6. Immunogold electron microscopy of extracts obtained from AD (A) and P301L tau transgenic (B) brain using phosphorylation- and conformation-dependent antibody TG3 identified 6-nm gold-decorated filaments.

Neurosci.) also were expressed in transgenic mice. V337M mutant mice formed neurofibrillary lesions in the hippocampus and neocortex, and showed progressive behavioral changes in the elevated plus maze (A. Takashima, personal communication). The G272V mutation was expressed in mouse brains by combining a prion protein promoter-driven expression system with an autoregulatory transactivator loop that resulted in high expression in a subset of neurons and oligodendrocytes. Electron microscopy established filament formation associated with phosphorylation at epitopes Ser202/Thr205, Thr231/Ser235 and Ser396/Ser404. Thioflavin S-positive fibrillary inclusions were identified in oligodendrocytes and motor neurons in spinal cord (Götz et al., submitted).

Findings similar to those obtained in transgenic mice were achieved in transfected cell lines which, in contrast to mice, can be rapidly screened for the role of distinct mutations in pathogenesis [195]. For example, Δ 280K, but not several other FTDP-17-linked mutations (e.g., V337M, P301L, R406W), developed amorphous and fibrillar aggregates in transfected Chinese hamster ovary (CHO) cell lines, whereas a triple tau mutant (VPR) containing V337M, P301L, and R406W substitutions also formed similar aggregates. Remarkably, the aggregates increased in size over time in culture. The formation of aggregated Δ 280K and VPR tau protein correlated with reduced affinity of these mutants to microtubules. Reduced phosphorylation at the PHF1-epitope Ser396/Ser404 was observed in R406W and Δ 280K tau mutants. As the PHF-1 epitope is the only phosphorylation site affected in the R406W mutant the observed reduction is most likely a consequence of altered secondary structure. This implies that a change in local secondary structure can impede phosphorylation by specific kinases. Together, these studies also imply that these missense mutations cause diverse neurodegenerative FTDP-17 syndromes by multiple mechanisms, including reduced microtubule binding and/or induction of filament formation [195].

In summary, the currently available FTDP-17 tau transgenic mouse models provide an *in vivo* model in which therapies can be assessed, and allow to determine the relationship between A β production and neurofibrillary lesion formation, by intercrossing tau transgenic mice with APP transgenic mice.

4.4. Limitations of tau transgenic approaches

Selective and massive neuronal losses are a hallmark of AD and related tauopathies. This key pathology, however, has not been recapitulated in any of the tau transgenic models published so far, with the exception of motor neuron losses in spinal cord [121]. Neurodegeneration may be reproduced by combining transgenic strains that express in brain different disease-associated genes. Alternatively, as murine neurons may be less susceptible to degeneration compared to human cells, neurodegeneration may be

reproduced in mice by transplanting into mouse brain human, neuron-like cells that express disease-associated genes [5,54,191].

A major drawback of the present models is that tau mutations are not expressed under control of the endogenous tau promoter. Axonal targeting signals and sequences governing mRNA stability [11] are not present on the transgenic constructs. The expression pattern is dependent on promoter choice, copy number, and integration site of the transgene. It is not possible in the current models to determine the relationship between tau mutation and neuropathology, i.e., why particular regions are affected in the presence of a particular mutation. Also, as only single tau isoforms have been expressed until now, it is not possible to model in mice the accumulation of 3R tau in Pick's disease versus accumulation of 4R tau in PSP and CBD. Transgenic technology suggests two basic approaches to address this question, either a knock-in approach (homologous recombination introducing an FTDP-17 linked tau mutation into the mouse tau genomic locus) or a human BAC transgenic model (transgenic expression of the entire human FTDP-17 mutant tau gene; BAC, bacterial artificial chromosome). As mice express only 4R tau isoforms, a knock-in approach will not allow expression of 3R tau mutant isoforms. Therefore, a knock-in approach seems suitable for the expression of FTDP-17 associated mutations that only affect 4R tau, such as P301L. It remains to be determined whether expression levels will be high enough to develop a phenotype within the life span of a mouse. The BAC/PAC approach seems generally more promising and has been used to over-express the entire wild-type human tau gene at levels that were 2–3-fold higher than those in ALZ17 mice (Table 1) but, in the absence of a tau mutation, these mice did not develop an obvious histopathological or neurological phenotype [48].

4.5. Tau and MAP1B knock-out mice

The question may be asked whether presence of tau mutations results in a loss of physiological function, or in a gain of toxic function? Mice lacking tau appeared to be immunohistologically normal, and, in large-calibre axons, the observed increase in MAP-1A levels seemed to compensate for the loss of tau. But in some small-calibre axons, microtubule stability was decreased and microtubule organization was significantly changed [90]. Interestingly, mice lacking tau showed a phenotype that paralleled some signs and symptoms of FTDP-17 patients. They developed muscle weakness in the wire-hanging test, hyperactivity in a novel environment, and impairment in the contextual fear conditioning experiment. They also had a tendency to fall off the rod more easily in the rod-walking test [103]. This suggests that the loss of tau protein may itself lead to some of the neurological characteristics observed in FTDP-17, and that a loss of

physiological function of tau in the presence of FTDP-17 mutations may contribute to the disease in FTDP-17 mutation carriers. Reduced levels of tau proteins, but not of tau mRNA, have been reported in cases of sporadic and familial forms of frontotemporal dementia, which could result in a tauopathy due to a loss of tau functions caused by losses of tau proteins. Remarkably, loss of tau protein was found in brain regions both with and without neuronal degeneration suggesting that tau dysfunction precedes neurodegeneration [9,209].

A gain of toxic function has been reported in MAP1B knockout mice where gene targeting produced a gene encoding a truncated product of MAP1B, which is likely to act in a dominant-negative fashion. Homozygotes died before reaching embryonic day 8, while heterozygotes showed severely abnormal phenotypes in their nervous systems, such as gait ataxia, spastic tremor, and limb paralysis [51]. This phenotype was different from a complete knockout of MAP1B that resulted only in a slightly decreased brain weight and delayed nervous system development. Other MAPs including tau, MAP1A, MAP2a, and MAP2b were not upregulated to compensate for the loss of functions of MAP1B, and no significant reduction of microtubule number and density was observed in MAP1B knockout axons [184].

The neurological symptoms in the above MAP1B dominant negative mutant mice [51] resemble those in P301L tau transgenic mice [121] suggesting — by analogy — that FTDP-17-associated tau mutations result in a gain of toxic function.

4.6. Transgenic mouse models of AD-related phosphatases and kinases

Careful staging of brains has shown, that tau phosphorylation precedes filament formation although the formal proof of a causal relationship is missing [18]. In vitro, phosphorylated tau fails to assemble into AD-like tau filaments. On the other hand, sulfated glycosaminoglycans stimulate tau phosphorylation at much lower concentrations than those required for filament formation [93]. At present, it is not known whether phosphorylation is necessary for filament formation, which phosphoepitopes are important for filament formation, and which kinase or phosphatase is involved in the regulation of these pathogenic sites in vivo, as the phosphorylation state of a phosphoprotein — such as tau — is the consequence of the relative activities of the protein kinases and phosphatases towards it.

Among the protein kinases that have been implicated in the phosphorylation of tau are glycogen synthase kinase-3 β (GSK-3 β) [104], neuronal cyclin-dependent kinase 5 (Cdk5) [133,135], mitogen-activated protein kinase [45], Ca²⁺/calmodulin-dependent kinase II [171], casein kinase I [170], MARK kinase [163], JNK (c-jun NH2-terminal kinase) [157], and protein kinase A (PKA) [163]. Interest-

ingly, APP is also a phosphoprotein and several kinases including PKC and casein kinases have been implicated in the regulation of APP metabolism [196,197].

The role of Cdk5 has been addressed in transgenic mice following reports of its neuronal accumulation in AD [149,151]. Cyclin-dependent kinase 5 (Cdk5) is required for proper development of the mammalian central nervous system. To be activated, Cdk5 has to associate with its regulatory subunit, p35. A truncated form of p35, p25, accumulates in neurons in the brains of patients with AD, and this accumulation correlates with an increase in Cdk5 activity. Unlike p35, p25 is not rapidly degraded, and binding of p25 to Cdk5 constitutively activates Cdk5, changes its cellular location and alters its substrate specificity. In vivo, the p25/Cdk5 complex hyperphosphorylates tau, which reduces the ability of tau to associate with microtubules. Moreover, expression of the p25/Cdk5 complex in cultured primary neurons induces cytoskeletal disruption, morphological degeneration and apoptosis. These findings indicate that cleavage of p35, followed by accumulation of p25, may be involved in the pathogenesis of cytoskeletal abnormalities and neuronal death in neurodegenerative diseases [149].

Mice lacking Cdk5 are not viable beyond postnatal day 0, and have extensive abnormalities in the CNS including cortical and hippocampal lamination defects and cerebellar hypoplasia [62,147]. Overexpression of human p25 in transgenic mice resulted in a hyperphosphorylation of tau and neurofilament chains. Neurons were silver-positive using the Bielschowsky stain but tau filament formation was not reported. Disturbances in neuronal cytoskeletal organization were apparent at the ultrastructural level, predominantly in the amygdala, thalamus, hypothalamus, and cortex. The p25 transgenic mice displayed increased spontaneous locomotor activity and differences from control in the elevated plus-maze test [1].

Initial reports of low-expressing GSK-3 β transgenic mice mainly revealed that the phosphorylation status of tau was elevated at the AT8 epitope suggesting that GSK-3 β is an in vivo tau kinase in brain [21]. Subsequently, transgenic mice were generated that expressed a constitutively active GSK-3 β mutant (Ser9Ala), and were intercrossed with wild-type tau transgenic mice (Table 1) [180]. A 2-fold increase in GSK-3 β activity, relative to the endogenous enzymatic activity, rescued nearly all neuropathological symptoms of single tau transgenic mice [181]. This restoration comprised the reduction by about an order of magnitude of the number of axonal dilations in brain and spinal cord, the reduction in axonal degeneration and muscular atrophy, and the alleviation of practically all the motor problems. The amount of tau associated with microtubules was reduced by 50% in preparations from brain and spinal cord of double transgenic compared to single htau40 transgenic animals. Moreover, unbound tau was hyperphosphorylated. This would suggest that an increase in tau protein, and not hyperphosphorylation, is

responsible for the neurological phenotype observed in tau transgenic mice. However, although more hyperphosphorylated tau was available, PHF formation was not observed [181]. Inhibition of GSK-3 β and Cdk5 in FTDP-17 tau filament-forming mice may tell whether these kinases play a causal role in filament formation and neurodegeneration.

Less is known about the role of protein phosphatases participating in the regulation of tau phosphorylation. To date, all of the 21 phosphorylation sites that have been identified in hyperphosphorylated tau in AD are either serine or threonine residues. Thus, serine/threonine-specific protein phosphatases are expected to be involved in the regulation of tau hyperphosphorylation in AD. These phosphatases with cytoplasmic localization are classified into four types, namely PP1 (protein phosphatase 1), PP2A, PP2B, and PP2C. By using the abnormally hyperphosphorylated tau isolated from AD brain as a substrate, PP2A, PP2B, and to a lesser extent, PP1 have been shown to efficiently dephosphorylate tau in vitro [75,198]. Similar findings have been reported by using 32 P-labeled tau with various kinases as a substrate in vitro. For example, mitogen-activated protein kinase phosphorylated recombinant tau and converted it to a form which was similar to PHF-tau. Of the major serine/threonine-specific protein phosphatases found in mammalian tissues only PP2A could dephosphorylate tau phosphorylated in this manner [46,64]. Among the phosphatases that dephosphorylate tau in vitro, PP2A is very abundant in brain and has been shown to be associated with microtubules [173]. However, to date it is not known which of these phosphatases regulates tau phosphorylation in vivo and by what mechanism tau is abnormally hyperphosphorylated in AD brain. Attempts to study the regulation of tau phosphorylation by protein phosphatases have been carried out in cultured cells, in the presence of inhibitors such as okadaic acid or calyculin A, which may not be entirely specific and this regulation in cultured cells is most likely different from that in mature mammalian brain. This is because all commonly used neuronal cell lines only express fetal type tau that is highly phosphorylated and composed of the shortest isoform. Tau in normal mature brain is less phosphorylated and composed of six isoforms due to alternative splicing of a single gene [134]. In addition, expression of protein phosphatases in cultured cell lines is different from that in brain [185]. An alternative approach to study the role of phosphatases in tau phosphorylation are chronic infusion into rodent brains of phosphatase inhibitors [7,107], or incubation of brain slices with these inhibitors [60,91]. By using metabolically competent rat brain slices as a model, selective inhibition of PP2A by okadaic acid induced an AD-like hyperphosphorylation and accumulation of tau. The hyperphosphorylated tau had a reduced ability to bind to microtubules and to promote microtubule assembly in vitro. Immunocytochemical staining revealed hyperphosphorylated tau accumulation in

pyramidal neurons in the CA1 and CA3 sectors of the cornu ammonis, and in neocortical neurons. The topography of these changes was similar to that of neurofibrillary tangles in AD brain [76]. In brains of transgenic mice lacking the catalytic subunit α c of PP2B, hyperphosphorylation of tau was restricted to the mossy fiber projection of the hippocampus [113]. Similar attempts to investigate PP2A have been unsuccessful since the selective knockout of PP2A expression was embryonically lethal and phosphatase activities in heterozygous knockout mice were not different from wild-type controls [81,82]. These limitations will be overcome by expressing dominant negative mutant forms of PP2A in neurons of transgenic mice [79].

5. The amyloid cascade hypothesis: relation between amyloid deposition and neurofibrillary tangle formation

The expression of FTDP-17 mutant (P301L) tau appears to accelerate tau filament formation in mice [80,121], as wild-type tau transgenic mice develop tau-containing filaments only at 18 months to 2 years of age [106]. P301L mutant mice are therefore suitable models to test the 'amyloid cascade' hypothesis that proposes a central role of β -amyloid in the pathogenesis of AD. The precise relation between β -amyloid deposition and neurofibrillary tangle formation is unknown. In rhesus monkeys, synthetic A β_{42} fibrils can induce tau-containing neurofibrillary lesions, but this toxicity is highly dependent on species and age: It is more pronounced than in marmoset monkey, and not significant at all in rats or mice, and the toxicity increases with advancing age [61]. Currently available transgenic mouse models that co-express human APP and FAD mutations are only partially suited to test this hypothesis, because the development of amyloid plaques in these mice is associated with only marginal neuronal damage, and no neurofibrillary lesion formation [59,100,182]. Interbreeding of APP transgenic A β -producing mice with tau filament-forming mice will determine whether A β induces faster and more pronounced filament formation and whether A β enhances the susceptibility for neurodegeneration in FTDP-17 tau expressing mice.

In the past years, proteins and genes have been identified which may link A β production and neurofibrillary lesion formation in AD. Several of these proteins and genes associated with AD have been found recently to play central roles in early neural development, particularly neuronal migration and axon extension. Intracellular signaling pathways including the Reelin pathway [35,95,166] have been identified that may link many of the proteins implicated genetically in AD [16]. Binding of Reelin causes the ApoE and VLDL receptors to recruit an intracellular adaptor protein, Disabled, that becomes phosphorylated on tyrosine residues. The Abl protein tyrosine

kinase, which acts in concert with the intracellular adaptor protein Disabled, phosphorylates and activates the kinase activity of Cdk5 [210]. ApoE is an alternative ligand for the ApoE and VLDL receptors, and neuronal expression of the human $\epsilon 4$ allele of ApoE in transgenic mice causes hyperphosphorylation of tau [188]. Cdk5 induces hyperphosphorylation of tau, and the proteolytic fragment p25 of its activating subunit p35 accumulates in brains of AD patients [120,145,149]; in addition, inactivation of Cdk5 by a gene-targeting approach, or overexpression of p25, leads to a neuronal pathology [1,147]. APP/P301L tau double transgenic mice may provide an *in vivo* assay to determine the role of the individual components of the Reelin signaling cascade in neurofibrillary tangle formation.

In summary, the currently available and newly established FTDP-17 mutant transgenic models will be suitable to determine which phosphoepitopes of tau are important for filament formation *in vivo*, which cells are susceptible to filament formation, which subcellular compartments are capable of making tau filaments, how filaments interfere with neuronal functions including axonal transport, and whether glial cells with tau filaments can influence neuronal functions. They will provide insight into the physiological role of tau. Eventually, the components of the pathocascade in AD and frontotemporal dementia will be identified. Finally, these mice will be available for drug testing aiming to halt or prevent AD and related tauopathies.

Acknowledgements

I thank Drs Roger M. Nitsch, Charo Gonzalez-Agosti, Stefan Kins, Johannes Streffer, and Markus Tolnay for helpful discussions and critical input on the manuscript; and Dr. Akihiko Takashima for sharing unpublished results.

References

- [1] M.K. Ahljianian, N.X. Barrezueta, R.D. Williams, A. Jakowski, K.P. Kowsz, S. McCarthy, T. Coskran, A. Carlo, P.A. Seymour, J.E. Burkhardt, R.B. Nelson, J.D. McNeish, Hyperphosphorylated tau and neurofilament and cytoskeletal disruptions in mice overexpressing human p25, an activator of cdk5, *Proc. Natl. Acad. Sci. USA* 97 (2000) 2910–2915.
- [2] R.D. Allen, D.G. Weiss, J.H. Hayden, D.T. Brown, H. Fujiwake, M. Simpson, Gliding movement of and bidirectional transport along single native microtubules from squid axoplasm: evidence for an active role of microtubules in cytoplasmic transport, *J. Cell. Biol.* 100 (1985) 1736–1752.
- [3] B.H. Anderton, R. Dayanandan, R. Killick, S. Lovestone, Does dysregulation of the Notch and wingless/Wnt pathways underlie the pathogenesis of Alzheimer's disease? *Mol. Med. Today* 6 (2000) 54–59.
- [4] A. Andreadis, W.M. Brown, K.S. Kosik, Structure and novel exons of the human tau gene, *Biochemistry* 31 (1992) 10626–10633.
- [5] P.W. Andrews, Teratocarcinomas and human embryology: pluripotent human EC cell lines. Review article, *APMIS* 106 (1998) 158–167, Discussion pp. 167–158.
- [6] Y. Arai, M. Yamazaki, O. Mori, H. Muramatsu, G. Asano, Y. Katayama, Alpha-synuclein-positive structures in cases with sporadic Alzheimer's disease: morphology and its relationship to tau aggregation, *Brain Res.* 888 (2001) 287–296.
- [7] T. Arendt, M. Holzer, R. Fruth, M.K. Bruckner, U. Gartner, Paired helical filament-like phosphorylation of tau, deposition of beta/A4-amyloid and memory impairment in rat induced by chronic inhibition of phosphatase 1 and 2A, *Neuroscience* 69 (1995) 691–698.
- [8] K. Arima, A. Kowalska, M. Hasegawa, M. Mukoyama, R. Watanabe, M. Kawai, K. Takahashi, T. Iwatsubo, T. Tabira, N. Sunohara, Two brothers with frontotemporal dementia and parkinsonism with an N279K mutation of the tau gene, *Neurology* 54 (2000) 1787–1795.
- [9] S.E. Arnold, L.Y. Han, C.M. Clark, M. Grossman, J.Q. Trojanowski, Quantitative neurohistological features of frontotemporal degeneration, *Neurobiol. Aging* 21 (2000) 913–919.
- [10] S.E. Arnold, B.T. Hyman, J. Flory, A.R. Damasio, G.W. Van Hoesen, The topographical and neuroanatomical distribution of neurofibrillary tangles and neuritic plaques in the cerebral cortex of patients with Alzheimer's disease, *Cereb. Cortex* 1 (1991) 103–116.
- [11] S. Aronov, R. Marx, I. Ginzburg, Identification of 3'UTR region implicated in tau mRNA stabilization in neuronal cells, *J. Mol. Neurosci.* 12 (1999) 131–145.
- [12] M. Baker, I. Litvan, H. Houlden, J. Adamson, D. Dickson, J. Perez-Tur, J. Hardy, T. Lynch, E. Bigio, M. Hutton, Association of an extended haplotype in the tau gene with progressive supranuclear palsy, *Hum. Mol. Genet.* 8 (1999) 711–715.
- [13] C. Bergeron, M.S. Pollanen, L. Weyer, A.E. Lang, Cortical degeneration in progressive supranuclear palsy. A comparison with cortical-basal ganglionic degeneration, *J. Neuropathol. Exp. Neurol.* 56 (1997) 726–734.
- [14] T.D. Bird, D. Nochlin, P. Poorkaj, M. Cherrier, J. Kaye, H. Payami, E. Peskind, T.H. Lampe, E. Nemens, P.J. Boyer, G.D. Schellenberg, A clinical pathological comparison of three families with frontotemporal dementia and identical mutations in the tau gene (P301L), *Brain* 122 (1999) 741–756.
- [15] M.A. Boss, Diagnostic approaches to Alzheimer's disease, *Biochim. Biophys. Acta* 1502 (2000) 188–200.
- [16] M. Bothwell, E. Giniger, Alzheimer's disease: neurodevelopment converges with neurodegeneration, *Cell* 102 (2000) 271–273.
- [17] E. Braak, H. Braak, E.M. Mandelkow, A sequence of cytoskeleton changes related to the formation of neurofibrillary tangles and neurofibrillary threads, *Acta Neuropathol.* 87 (1994) 554–567.
- [18] H. Braak, E. Braak, Staging of Alzheimer's disease-related neurofibrillary changes, *Neurobiol. Aging* 16 (1995) 271–278, discussion 278–284.
- [19] J.P. Brion, G. Tremp, J.N. Octave, Transgenic expression of the shortest human tau affects its compartmentalization and its phosphorylation as in the pretangle stage of Alzheimer's disease, *Am. J. Pathol.* 154 (1999) 255–270.
- [20] S. Brion, J. Plas, A. Jeanneau, [Pick's disease. Anatomical point of view], *Rev. Neurol.* 147 (1991) 693–704.
- [21] J. Brownlee, N.G. Irving, J.P. Brion, B.J. Gibb, U. Wagner, J. Woodgett, C.C. Miller, Tau phosphorylation in transgenic mice expressing glycogen synthase kinase-3 β transgenes, *Neuroreport* 8 (1997) 3251–3255.
- [22] L. Buee, T. Bussiere, V. Buee-Scherrer, A. Delacourte, P.R. Hof, Tau protein isoforms, phosphorylation and role in neurodegenerative disorders, *Brain Res. Brain Res. Rev.* 33 (2000) 95–130.
- [23] L. Buee, A. Delacourte, Comparative biochemistry of tau in progressive supranuclear palsy, corticobasal degeneration, FTDP-17 and Pick's disease, *Brain Pathol.* 9 (1999) 681–693.

- [24] V. Buee Scherrer, P.R. Hof, L. Buee, B. Leveugle, P. Vermersch, D.P. Perl, C.W. Olanow, A. Delacourte, Hyperphosphorylated tau proteins differentiate corticobasal degeneration and Pick's disease, *Acta Neuropathol.* 91 (1996) 351–359.
- [25] V. Buee-Scherrer, O. Condamines, C. Mourtou-Gilles, R. Jakes, M. Goedert, B. Pau, A. Delacourte, AD2, a phosphorylation-dependent monoclonal antibody directed against tau proteins found in Alzheimer's disease, *Brain Res. Mol. Brain Res.* 39 (1996) 79–88.
- [26] O. Bugiani, J.R. Murrell, G. Giaccone, M. Hasegawa, G. Ghigo, M. Tabaton, M. Morbin, A. Primavera, F. Carella, C. Solaro, M. Grisoli, M. Savoiardo, M.G. Spillantini, F. Tagliavini, M. Goedert, B. Ghetti, Frontotemporal dementia and corticobasal degeneration in a family with a P301S mutation in tau, *J. Neuropathol. Exp. Neurol.* 58 (1999) 667–677.
- [27] J. Cervos-Navarro, K. Schumacher, Neurofibrillary pathology in progressive supranuclear palsy (PSP), *J. Neural. Transm. Suppl.* 42 (1994) 153–164.
- [28] P.F. Chapman, G.L. White, M.W. Jones, D. Cooper-Blacketer, V.J. Marshall, M. Irizarry, L. Younkin, M.A. Good, T.V. Bliss, B.T. Hyman, S.G. Younkin, K.K. Hsiao, Impaired synaptic plasticity and learning in aged amyloid precursor protein transgenic mice, *Nat. Neurosci.* 2 (1999) 271–276.
- [29] S.S. Chin, J.E. Goldman, Glial inclusions in CNS degenerative diseases, *J. Neuropathol. Exp. Neurol.* 55 (1996) 499–508.
- [30] L.N. Clark, P. Poorkaj, Z. Wszolek, D.H. Geschwind, Z.S. Nasredine, B. Miller, D. Li, H. Payami, F. Awert, K. Markopoulou, A. Andreadis, I. D'Souza, V.M. Lee, L. Reed, J.Q. Trojanowski, V. Zhukareva, T. Bird, G. Schellenberg, K.C. Wilhelmsen, Pathogenic implications of mutations in the tau gene in pallido-ponto-nigral degeneration and related neurodegenerative disorders linked to chromosome 17, *Proc. Natl. Acad. Sci. USA* 95 (1998) 13103–13107.
- [31] C. Conrad, A. Andreadis, J.Q. Trojanowski, D.W. Dickson, D. Kang, X. Chen, W. Wiederholt, L. Hansen, E. Masliah, L.J. Thal, R. Katzman, Y. Xia, T. Saitoh, Genetic evidence for the involvement of tau in progressive supranuclear palsy, *Ann. Neurol.* 41 (1997) 277–281.
- [32] F. Cote, J.F. Collard, J.P. Julien, Progressive neuronopathy in transgenic mice expressing the human neurofilament heavy gene: a mouse model of amyotrophic lateral sclerosis, *Cell* 73 (1993) 35–46.
- [33] D. Couchie, C. Mavilia, I.S. Georgieff, R.K. Liem, M.L. Shelanski, J. Nunez, Primary structure of high molecular weight tau present in the peripheral nervous system, *Proc. Natl. Acad. Sci. USA* 89 (1992) 4378–4381.
- [34] C.C. Cunningham, N. Leclerc, L.A. Flanagan, M. Lu, P.A. Janmey, K.S. Kosik, Microtubule-associated protein 2c reorganizes both microtubules and microfilaments into distinct cytological structures in an actin-binding protein-280-deficient melanoma cell line, *J. Cell Biol.* 136 (1997) 845–857.
- [35] G. D'Arcangelo, R. Homayouni, L. Keshvara, D.S. Rice, M. Sheldon, T. Curran, Reelin is a ligand for lipoprotein receptors, *Neuron* 24 (1999) 471–479.
- [36] R.L. Davis, A.E. Shrimpton, P.D. Holohan, C. Bradshaw, D. Feiglin, G.H. Collins, P. Sonderegger, J. Kinter, L.M. Becker, F. Laebawan, D. Krasnewich, M. Muenke, D.A. Lawrence, M.S. Yerby, C.M. Shaw, B. Gooptu, P.R. Elliott, J.T. Finch, R.W. Carrell, D.A. Lomas, Familial dementia caused by polymerization of mutant neuroserpin, *Nature* 401 (1999) 376–379.
- [37] F. De Gv, N.C. Inestrosa, Wnt signaling function in Alzheimer's disease, *Brain Res. Brain Res. Rev.* 33 (2000) 1–12.
- [38] J.G. de Yebenes, J.L. Sarasa, S.E. Daniel, A.J. Lees, Familial progressive supranuclear palsy. Description of a pedigree and review of the literature, *Brain* 118 (1995) 1095–1103.
- [39] A. Delacourte, Pathological Tau proteins of Alzheimer's disease as a biochemical marker of neurofibrillary degeneration, *Biomed. Pharmacother.* 48 (1994) 287–295.
- [40] A. Delacourte, N. Sergeant, A. Wattez, D. Gauvreau, Y. Robitaille, Vulnerable neuronal subsets in Alzheimer's and Pick's disease are distinguished by their tau isoform distribution and phosphorylation, *Ann. Neurol.* 43 (1998) 193–204.
- [41] M.B. Delisle, J.R. Murrell, R. Richardson, J.A. Trofatter, O. Rascol, X. Soulages, M. Mohr, P. Calvas, B. Ghetti, A mutation at codon 279 (N279K) in exon 10 of the Tau gene causes a tauopathy with dementia and supranuclear palsy, *Acta Neuropathol. (Berlin)* 98 (1999) 62–77.
- [42] M.B. Delisle, E. Uro-Coste, J.R. Murrell, O. Rascol, B. Ghetti, *Bull. Acad. Natl. Med.* 184 (2000) 799–809.
- [43] M. DeTure, L.W. Ko, S. Yen, P. Nacharaju, C. Easson, J. Lewis, M. van Slegtenhorst, M. Hutton, S.H. Yen, Missense tau mutations identified in FTDP-17 have a small effect on tau-microtubule interactions, *Brain Res.* 853 (2000) 5–14.
- [44] D.W. Dickson, H.A. Crystal, C. Bevana, W. Honer, I. Vincent, P. Davies, Correlations of synaptic and pathological markers with cognition of the elderly, *Neurobiol. Aging* 16 (1995) 285–298, Discussion pp. 298–304.
- [45] G. Drewes, B. Lichtenberg-Kraag, F. Doring, E.M. Mandelkow, J. Biernat, J. Goris, M. Doree, E. Mandelkow, Mitogen activated protein (MAP) kinase transforms tau protein into an Alzheimer-like state, *EMBO J.* 11 (1992) 2131–2138.
- [46] G. Drewes, E.M. Mandelkow, K. Baumann, J. Goris, W. Merlevede, E. Mandelkow, Dephosphorylation of tau protein and Alzheimer paired helical filaments by calceurin and phosphatase-2A, *FEBS Lett.* 336 (1993) 425–432.
- [47] I. D'Souza, P. Poorkaj, M. Hong, D. Nochlin, V.M. Lee, T.D. Bird, G.D. Schellenberg, Missense and silent tau gene mutations cause frontotemporal dementia with parkinsonism-chromosome 17 type, by affecting multiple alternative RNA splicing regulatory elements, *Proc. Natl. Acad. Sci. USA* 96 (1999) 5598–5603.
- [48] K. Duff, H. Knight, L.M. Refolo, S. Sanders, X. Yu, M. Picciano, B. Malester, M. Hutton, J. Adamson, M. Goedert, K. Burki, P. Davies, Characterization of pathology in transgenic mice over-expressing human genomic and cDNA tau transgenes, *Neurobiol. Dis.* 7 (2000) 87–98.
- [49] C. Dumanchin, A. Camuzat, D. Campion, P. Verpillat, D. Hannequin, B. Dubois, P. Saugier-Verber, C. Martin, C. Penet, F. Charbonnier, Y. Agid, T. Frebourg, A. Brice, Segregation of a missense mutation in the microtubule-associated protein tau gene with familial frontotemporal dementia and parkinsonism, *Hum. Mol. Genet.* 7 (1998) 1825–1829.
- [50] A. Ebner, R. Godemann, K. Stamer, S. Illenberger, B. Trinczek, E. Mandelkow, Overexpression of tau protein inhibits kinesin-dependent trafficking of vesicles, mitochondria, and endoplasmic reticulum: implications for Alzheimer's disease, *J. Cell Biol.* 143 (1998) 777–794.
- [51] W. Edelmann, M. Zervas, P. Costello, L. Roback, I. Fischer, J.A. Hammarback, N. Cowan, P. Davies, B. Wainer, R. Kucherlapati, Neuronal abnormalities in microtubule-associated protein 1B mutant mice, *Proc. Natl. Acad. Sci. USA* 93 (1996) 1270–1275.
- [52] M.B. Feany, H. Ksiezak-Reding, W.K. Liu, I. Vincent, S.H. Yen, D.W. Dickson, Epitope expression and hyperphosphorylation of tau protein in corticobasal degeneration: differentiation from progressive supranuclear palsy, *Acta Neuropathol.* 90 (1995) 37–43.
- [53] M.B. Feany, L.A. Mattiace, D.W. Dickson, Neuropathologic overlap of progressive supranuclear palsy, Pick's disease and corticobasal degeneration, *J. Neuropathol. Exp. Neurol.* 55 (1996) 53–67.
- [54] A. Ferrari, E. Ehler, R.M. Nitsch, J. Götz, Immature human NT2 cells grafted into mouse brain differentiate into neuronal and glial cell types, *FEBS Lett.* 486 (2000) 121–125.
- [55] L.A. Flanagan, C.C. Cunningham, J. Chen, G.D. Prestwich, K.S. Kosik, P.A. Janmey, The structure of divalent cation-induced aggregates of PIP2 and their alteration by gelsolin and tau, *Biophys. J.* 73 (1997) 1440–1447.
- [56] H. Forstl, B. Baldwin, [Pick and focal brain atrophy], *Fortschr. Neurol. Psychiatr.* 62 (1994) 345–355.

- [57] N.L. Foster, K. Wilhelmsen, A.A. Sima, M.Z. Jones, C.J. D'Amato, S. Gilman, Frontotemporal dementia and parkinsonism linked to chromosome 17: a consensus conference. Conference Participants, *Ann. Neurol.* 41 (1997) 706–715.
- [58] P. Friedhoff, M. von Bergen, E.M. Mandelkow, E. Mandelkow, Structure of tau protein and assembly into paired helical filaments, *Biochim. Biophys. Acta* 1502 (2000) 122–132.
- [59] D. Games, D. Adams, R. Alessandrini, R. Barbour, P. Berthelette, C. Blackwell, T. Carr, J. Clemens, T. Donaldson, F. Gillespie et al., Alzheimer-type neuropathology in transgenic mice overexpressing V717F beta-amyloid precursor protein, *Nature* 373 (1995) 523–527.
- [60] T.D. Garver, G.A. Oyler, K.A. Harris, R. Polavarapu, Z. Damuni, R.A. Lehman, M.L. Billingsley, Tau phosphorylation in brain slices: pharmacological evidence for convergent effects of protein phosphatases on tau and mitogen-activated protein kinase, *Mol. Pharmacol.* 47 (1995) 745–756.
- [61] C. Geula, C.K. Wu, D. Saroff, A. Lorenzo, M. Yuan, B.A. Yankner, Aging renders the brain vulnerable to amyloid beta-protein neurotoxicity, *Nat. Med.* 4 (1998) 827–831.
- [62] E.C. Gilmore, T. Ohshima, A.M. Goffinet, A.B. Kulkarni, K. Herrup, Cyclin-dependent kinase 5-deficient mice demonstrate novel developmental arrest in cerebral cortex, *J. Neurosci.* 18 (1998) 6370–6377.
- [63] M. Goedert, Filamentous nerve cell inclusions in neurodegenerative diseases: tauopathies and alpha-synucleinopathies, *Phil. Trans. R. Soc. London B. Biol. Sci.* 354 (1999) 1101–1118.
- [64] M. Goedert, E.S. Cohen, R. Jakes, P. Cohen, p42 MAP kinase phosphorylation sites in microtubule-associated protein tau are dephosphorylated by protein phosphatase 2A1. Implications for Alzheimer's disease, *FEBS Lett.* 312 (1992) 95–99.
- [65] M. Goedert, R.A. Crowther, M.G. Spillantini, Tau mutations cause frontotemporal dementias, *Neuron* 21 (1998) 955–958.
- [66] M. Goedert, R. Jakes, Expression of separate isoforms of human tau protein: correlation with the tau pattern in brain and effects on tubulin polymerization, *EMBO J.* 9 (1990) 4225–4230.
- [67] M. Goedert, R. Jakes, R.A. Crowther, Effects of frontotemporal dementia FTDP-17 mutations on heparin-induced assembly of tau filaments, *FEBS Lett.* 450 (1999) 306–311.
- [68] M. Goedert, R. Jakes, R.A. Crowther, P. Cohen, E. Vanmechelen, M. Vandermeeren, P. Cras, Epitope mapping of monoclonal antibodies to the paired helical filaments of Alzheimer's disease: identification of phosphorylation sites in tau protein, *Biochem. J.* 301 (1994) 871–877.
- [69] M. Goedert, R. Jakes, R.A. Crowther, J. Six, U. Lubke, M. Vandermeeren, P. Cras, J.Q. Trojanowski, V.M. Lee, The abnormal phosphorylation of tau protein at Ser-202 in Alzheimer disease recapitulates phosphorylation during development, *Proc. Natl. Acad. Sci. USA* 90 (1993) 5066–5070.
- [70] M. Goedert, R. Jakes, E. Vanmechelen, Monoclonal antibody AT8 recognises tau protein phosphorylated at both serine 202 and threonine 205, *Neurosci. Lett.* 189 (1995) 167–169.
- [71] M. Goedert, M.G. Spillantini, R.A. Crowther, Cloning of a big tau microtubule-associated protein characteristic of the peripheral nervous system, *Proc. Natl. Acad. Sci. USA* 89 (1992) 1983–1987.
- [72] M. Goedert, M.G. Spillantini, R.A. Crowther, S.G. Chen, P. Parchi, M. Tabaton, D.J. Lanska, W.R. Markesbery, K.C. Wilhelmsen, D.W. Dickson, R.B. Petersen, P. Gambetti, Tau gene mutation in familial progressive subcortical gliosis, *Nat. Med.* 5 (1999) 454–457.
- [73] M. Goedert, M.G. Spillantini, R. Jakes, R.A. Crowther, E. Vanmechelen, A. Probst, J. Götz, K. Burki, P. Cohen, Molecular dissection of the paired helical filament, *Neurobiol. Aging* 16 (1995) 325–334.
- [74] C.X. Gong, I. Grundke-Iqbal, Z. Damuni, K. Iqbal, Dephosphorylation of microtubule-associated protein tau by protein phosphatase-1 and -2C and its implication in Alzheimer disease, *FEBS Lett.* 341 (1994) 94–98.
- [75] C.X. Gong, T. Lidsky, J. Wegiel, L. Zuck, I. Grundke-Iqbal, K. Iqbal, Phosphorylation of microtubule-associated protein tau is regulated by protein phosphatase 2A in mammalian brain. Implications for neurofibrillary degeneration in Alzheimer's disease, *J. Biol. Chem.* 275 (2000) 5535–5544.
- [76] B.L. Goode, M. Chau, P.E. Denis, S.C. Feinstein, Structural and functional differences between 3-repeat and 4-repeat tau isoforms. Implications for normal tau function and the onset of neurodegenerative disease, *J. Biol. Chem.* 275 (2000) 38182–38189.
- [77] B.L. Goode, S.C. Feinstein, Identification of a novel microtubule binding and assembly domain in the developmentally regulated inter-repeat region of tau, *J. Cell Biol.* 124 (1994) 769–782.
- [78] J. Götz, R. Barmettler, A. Ferrari, M. Goedert, A. Probst, R.M. Nitsch, In vivo analysis of wild-type and FTDP-17 tau transgenic mice, *Ann. NY Acad. Sci.* 920 (2000) 126–133.
- [79] J. Götz, F. Chen, R. Barmettler, R.M. Nitsch, Tau filament formation in transgenic mice expressing p301 tau, *J. Biol. Chem.* 276 (2001) 529–534.
- [80] J. Götz, A. Probst, E. Ehler, B. Hemmings, W. Kues, Delayed embryonic lethality in mice lacking protein phosphatase 2A catalytic subunit C α , *Proc. Natl. Acad. Sci. USA* 95 (1998) 12370–12375.
- [81] J. Götz, A. Probst, C. Mistl, R.M. Nitsch, E. Ehler, Distinct role of protein phosphatase 2A subunit c-alpha in the regulation of E-cadherin and beta-catenin during development, *Mech. Dev.* 93 (2000) 83–93.
- [82] J. Götz, A. Probst, M.G. Spillantini, T. Schafer, R. Jakes, K. Burki, M. Goedert, Somatodendritic localization and hyperphosphorylation of tau protein in transgenic mice expressing the longest human brain tau isoform, *EMBO J.* 14 (1995) 1304–1313.
- [83] S.G. Greenberg, P. Davies, J.D. Schein, L.I. Binder, Hydrofluoric acid-treated tau PHF proteins display the same biochemical properties as normal tau, *J. Biol. Chem.* 267 (1992) 564–569.
- [84] G.F. Hall, B. Chu, G. Lee, J. Yao, Human tau filaments induce microtubule and synapse loss in an in vivo model of neurofibrillary degenerative disease, *J. Cell Sci.* 113 (2000) 1373–1387.
- [85] G.F. Hall, M.J. Cohen, Extensive dendritic sprouting induced by close axotomy of central neurons in the lamprey, *Science* 222 (1983) 518–521.
- [86] G.F. Hall, V.M. Lee, G. Lee, J. Yao, Staging of neurofibrillary degeneration caused by human tau overexpression in a unique cellular model of human tauopathy, *Am. J. Pathol.* 158 (2001) 235–246.
- [87] G.F. Hall, J. Yao, G. Lee, Human tau becomes phosphorylated and forms filamentous deposits when overexpressed in lamprey central neurons in situ, *Proc. Natl. Acad. Sci. USA* 94 (1997) 4733–4738.
- [88] L. Hansen, D. Salmon, D. Galasko, E. Masliah, R. Katzman, R. DeTeresa, L. Thal, M.M. Pay, R. Hofstetter, M. Klauber et al., The Lewy body variant of Alzheimer's disease: a clinical and pathologic entity, *Neurology* 40 (1990) 1–8.
- [89] A. Harada, K. Oguchi, S. Okabe, J. Kuno, S. Terada, T. Ohshima, R. Sato-Yoshitake, Y. Takei, T. Noda, N. Hirokawa, Altered microtubule organization in small-calibre axons of mice lacking tau protein, *Nature* 369 (1994) 488–491.
- [90] K.A. Harris, G.A. Oyler, G.M. Doolittle, I. Vincent, R.A. Lehman, R.L. Kincaid, M.L. Billingsley, Okadaic acid induces hyperphosphorylated forms of tau protein in human brain slices, *Ann. Neurol.* 33 (1993) 77–87.
- [91] W. Hartig, C. Klein, K. Brauer, K.F. Schuppel, T. Arendt, G. Bruckner, V. Bigl, Abnormally phosphorylated protein tau in the cortex of aged individuals of various mammalian orders, *Acta Neuropathol. (Berlin)* 100 (2000) 305–312.
- [92] M. Hasegawa, R.A. Crowther, R. Jakes, M. Goedert, Alzheimer-like changes in microtubule-associated protein Tau induced by sulfated glycosaminoglycans. Inhibition of microtubule binding, stimulation of phosphorylation, and filament assembly depend on the degree of sulfation, *J. Biol. Chem.* 272 (1997) 33118–33124.
- [93] J.J. Hauw, M. Verny, P. Delaere, P. Cervera, Y. He, C. Duyckaerts, Constant neurofibrillary changes in the neocortex in progressive supranuclear palsy. Basic differences with Alzheimer's disease and aging, *Neurosci. Lett.* 119 (1990) 182–186.

- [95] T. Hiesberger, M. Trommsdorff, B.W. Howell, A. Goffinet, M.C. Mumby, J.A. Cooper, J. Herz, Direct binding of Reelin to VLDL receptor and ApoE receptor 2 induces tyrosine phosphorylation of disabled-1 and modulates tau phosphorylation, *Neuron* 24 (1999) 481–489.
- [96] C. Hock, S. Golombowski, F. Muller-Spahn, W. Naser, K. Beyreuther, U. Monning, D. Schenk, C. Vigo-Pelfrey, A.M. Bush, R. Moir, R.E. Tanzi, J.H. Growdon, R.M. Nitsch, Cerebrospinal fluid levels of amyloid precursor protein and amyloid beta-peptide in Alzheimer's disease and major depression — inverse correlation with dementia severity, *Eur. Neurol.* 39 (1998) 111–118.
- [97] C. Hock, S. Golombowski, W. Naser, F. Muller-Spahn, Increased levels of tau protein in cerebrospinal fluid of patients with Alzheimer's disease — correlation with degree of cognitive impairment, *Ann. Neurol.* 37 (1995) 414–415.
- [98] P.R. Hof, C. Bouras, D.P. Perl, J.H. Morrison, Quantitative neuropathologic analysis of Pick's disease cases: cortical distribution of Pick bodies and coexistence with Alzheimer's disease, *Acta Neuropathol.* 87 (1994) 115–124.
- [99] K. Hsiao, P. Chapman, S. Nilsen, C. Eckman, Y. Harigaya, S. Younkin, F. Yang, G. Cole, Correlative memory deficits, A-beta elevation, and amyloid plaques in transgenic mice, *Science* 274 (1996) 99–102.
- [100] K.K. Hsiao, D.R. Borchelt, K. Olson, R. Johannsdottir, C. Kitt, W. Yunis, S. Xu, C. Eckman, S. Younkin, D. Price et al., Age-related CNS disorder and early death in transgenic FVB/N mice overexpressing Alzheimer amyloid precursor proteins, *Neuron* 15 (1995) 1203–1218.
- [101] F. Hulstaert, K. Blennow, A. Ivanoiu, H.C. Schoonderwaldt, M. Riemenschneider, P.P. De Deyn, C. Bancher, P. Cras, J. Wiltfang, P.D. Mehta, K. Iqbal, H. Pöttel, E. Vanmechelen, H. Vanderstichele, Improved discrimination of AD patients using beta-amyloid(1-42) and tau levels in CSF, *Neurology* 52 (1999) 1555–1562.
- [102] M. Hutton, C.L. Lendon, P. Rizzu, M. Baker, S. Froelich, H. Houlden, S. Pickering-Brown, S. Chakraverty, A. Isaacs, A. Grover, J. Hackett, J. Adamson, S. Lincoln, D. Dickson, P. Davies, R.C. Petersen, M. Stevens, E. de Graaff, E. Wauters, J. van Baren, M. Hillebrand, M. Joosse, J.M. Kwon, P. Nowotny, P. Heutink et al., Association of missense and 5'-splice-site mutations in tau with the inherited dementia FTDP-17, *Nature* 393 (1998) 702–705.
- [103] S. Ikegami, A. Harada, N. Hirokawa, Muscle weakness, hyperactivity, and impairment in fear conditioning in tau-deficient mice, *Neurosci. Lett.* 279 (2000) 129–132.
- [104] K. Ishiguro, A. Shiratsuchi, S. Sato, A. Omori, M. Arioka, S. Kobayashi, T. Uchida, K. Imahori, Glycogen synthase kinase 3 beta is identical to tau protein kinase I generating several epitopes of paired helical filaments, *FEBS Lett.* 325 (1993) 167–172.
- [105] T. Ishihara, M. Hong, B. Zhang, Y. Nakagawa, M.K. Lee, J.Q. Trojanowski, V.M. Lee, Age-dependent emergence and progression of a tauopathy in transgenic mice overexpressing the shortest human tau isoform, *Neuron* 24 (1999) 751–762.
- [106] T. Ishihara, B. Zhang, M. Higuchi, Y. Yoshiyama, J.Q. Trojanowski, V.M. Lee, Age-dependent induction of congophilic neurofibrillary tau inclusions in tau transgenic mice, *Am. J. Pathol.* 158 (2001) 555–562.
- [107] C. Janke, U. Gartner, M. Holzer, T. Arendt, Reversible in vivo phosphorylation of tau induced by okadaic acid and by unspecific brain lesion in rat, *J. Hirnforsch.* 39 (1998) 143–153.
- [108] S.M. Jenkins, G.V. Johnson, Tau complexes with phospholipase C-gamma in situ, *Neuroreport* 9 (1998) 67–71.
- [109] G.A. Jicha, B. Berenfeld, P. Davies, Sequence requirements for formation of conformational variants of tau similar to those found in Alzheimer's disease, *J. Neurosci. Res.* 55 (1999) 713–723.
- [110] G.A. Jicha, J.M. Rockwood, B. Berenfeld, M. Hutton, P. Davies, Altered conformation of recombinant frontotemporal dementia-17 mutant tau proteins, *Neurosci. Lett.* 260 (1999) 153–156.
- [111] K. Johnson-Wood, M. Lee, R. Motter, K. Hu, G. Gordon, R. Barbour, K. Khan, M. Gordon, H. Tan, D. Games, I. Lieberburg, D. Schenk, P. Seubert, L. McConlogue, Amyloid precursor protein processing and A beta42 deposition in a transgenic mouse model of Alzheimer disease, *Proc. Natl. Acad. Sci. USA* 94 (1997) 1550–1555.
- [112] M. Kanai, E. Matsubara, K. Isoc, K. Urakami, K. Nakashima, H. Arai, H. Sasaki, K. Abe, T. Iwatsubo, T. Kosaka, M. Watanabe, Y. Tomidokoro, M. Shizuka, K. Mizushima, T. Nakamura, Y. Igeta, Y. Ikeda, M. Amari, T. Kawarabayashi, K. Ishiguro, Y. Harigaya, K. Wakabayashi, K. Okamoto, S. Hirai, M. Shoji, Longitudinal study of cerebrospinal fluid levels of tau, A beta1-40, and A beta1-42(43) in Alzheimer's disease: a study in Japan, *Ann. Neurol.* 44 (1998) 17–26.
- [113] U.S. Kayyali, W. Zhang, A.G. Yee, J.G. Seidman, H. Potter, Cytoskeletal changes in the brains of mice lacking calcineurin A alpha, *J. Neurochem.* 68 (1997) 1668–1678.
- [114] A. Kertesz, T. Kawarai, E. Rogacva, P.St. George-Hyslop, P. Poorkaj, T.D. Bird, D.G. Munoz, Familial frontotemporal dementia with ubiquitin-positive, tau-negative inclusions, *Neurology* 54 (2000) 818–827.
- [115] A. Kertesz, P. Martinez-Lage, W. Davidson, D.G. Munoz, The corticobasal degeneration syndrome overlaps progressive aphasia and frontotemporal dementia, *Neurology* 55 (2000) 1368–1375.
- [116] T. Komori, Tau-positive glial inclusions in progressive supranuclear palsy, corticobasal degeneration and Pick's disease, *Brain Pathol.* 9 (1999) 663–679.
- [117] H. Ksiezak-Reding, K. Morgan, L.A. Mattiace, P. Davies, W.K. Liu, S.H. Yen, K. Weidenheim, D.W. Dickson, Ultrastructure and biochemical composition of paired helical filaments in corticobasal degeneration, *Am. J. Pathol.* 145 (1994) 1496–1508.
- [118] G. Lee, S.T. Newman, D.L. Gard, H. Band, G. Panchamoorthy, Tau interacts with src-family non-receptor tyrosine kinases, *J. Cell Sci.* 111 (1998) 3167–3177.
- [119] G. Lee, S.L. Rook, Expression of tau protein in non-neuronal cells: microtubule binding and stabilization, *J. Cell Sci.* 102 (1992) 227–237.
- [120] M.S. Lee, Y.T. Kwon, M. Li, J. Peng, R.M. Friedlander, L.H. Tsai, Neurotoxicity induces cleavage of p35 to p25 by calpain, *Nature* 405 (2000) 360–364.
- [121] J. Lewis, E. McGowan, J. Rockwood, H. Melrose, P. Nacharaju, M. Van Slegtenhorst, K. Gwinn-Hardy, M. Paul Murphy, M. Baker, X. Yu, K. Duff, J. Hardy, A. Corral, W.L. Lin, S.H. Yen, D.W. Dickson, P. Davies, M. Hutton, Neurofibrillary tangles, amyotrophy and progressive motor disturbance in mice expressing mutant (P301L) tau protein, *Nat. Genet.* 25 (2000) 402–405.
- [122] H. Liao, Y. Li, D.L. Brautigan, G.G. Gundersen, Protein phosphatase 1 is targeted to microtubules by the microtubule-associated protein Tau, *J. Biol. Chem.* 273 (1998) 21901–21908.
- [123] C.F. Lippa, H. Fujiwara, D.M. Mann, B. Giasson, M. Baba, M.L. Schmidt, L.E. Nee, B. O'Connell, D.A. Pollen, P. St George-Hyslop, B. Ghetti, D. Nochlin, T.D. Bird, N.J. Cairns, V.M. Lee, T. Iwatsubo, J.Q. Trojanowski, Lewy bodies contain altered alpha-synuclein in brains of many familial Alzheimer's disease patients with mutations in presenilin and amyloid precursor protein genes, *Am. J. Pathol.* 153 (1998) 1365–1370.
- [124] C.F. Lippa, M.L. Schmidt, V.M. Lee, J.Q. Trojanowski, Antibodies to alpha-synuclein detect Lewy bodies in many Down's syndrome brains with Alzheimer's disease, *Ann. Neurol.* 45 (1999) 353–357.
- [125] C.F. Lippa, V. Zhukareva, T. Kawarai, K. Uryu, M. Shafiq, L.E. Nee, J. Grafman, Y. Liang, P.H. St George-Hyslop, J.Q. Trojanowski, V.M. Lee, Frontotemporal dementia with novel tau pathology and a Glu342Val tau mutation, *Ann. Neurol.* 48 (2000) 850–858.
- [126] I. Litvan, Y. Agid, J. Jankovic, C. Goetz, J.P. Brandel, E.C. Lai, G. Wenning, L. D'Olhaberriague, M. Verna, K.R. Chaudhuri, A. McKee, K. Jellinger, J.J. Bartko, C.A. Mangone, R.K. Pearce, Accuracy of clinical criteria for the diagnosis of progressive

- supranuclear palsy (Steele-Richardson-Olszewski syndrome), *Neurology* 46 (1996) 922–930.
- [127] I. Litvan, J.J. Hauw, J.J. Bartko, P.L. Lantos, S.E. Daniel, D.S. Horoupian, A. McKee, D. Dickson, C. Bancher, M. Tabaton, K. Jellinger, D.W. Anderson, Validity and reliability of the preliminary NINDS neuropathologic criteria for progressive supranuclear palsy and related disorders, *J. Neuropathol. Exp. Neurol.* 55 (1996) 97–105.
- [128] M. Lu, K.S. Kosik, Competition for microtubule-binding with dual expression of tau missense and splice isoforms, *Mol. Biol. Cell* 12 (2001) 171–184.
- [129] T. Lynch, M. Sano, K.S. Marder, K.L. Bell, N.L. Foster, R.F. Defendini, A.A. Sima, C. Keohane, T.G. Nygaard, S. Fahn et al., Clinical characteristics of a family with chromosome 17-linked disinhibition-dementia-parkinsonism-amyotrophy complex [see comments], *Neurology* 44 (1994) 1878–1884.
- [130] T. Maas, J. Eidenmuller, R. Brandt, Interaction of tau with the neural membrane cortex is regulated by phosphorylation at sites that are modified in paired helical filaments, *J. Biol. Chem.* 275 (2000) 15733–15740.
- [131] C. Mailliot, N. Sergeant, T. Bussiere, M.L. Caillet-Boudin, A. Delacourte, L. Buee, Phosphorylation of specific sets of tau isoforms reflects different neurofibrillary degeneration processes, *FEBS Lett.* 433 (1998) 201–204.
- [132] S. Matsumoto, A. Hirano, S. Goto, Spinal cord neurofibrillary tangles of Guamanian amyotrophic lateral sclerosis and parkinsonism-dementia complex: an immunohistochemical study, *Neurology* 40 (1990) 975–979.
- [133] M. Matsushita, H. Matsui, T. Itano, K. Tomizawa, M. Tokuda, H. Suwaki, J.H. Wang, O. Hatase, Developmental changes of cyclin dependent kinase 5 subcellular localization in the rat cerebellum, *Neuroreport* 6 (1995) 1267–1270.
- [134] M. Mawal-Dewan, J. Henley, A. Van de Voorde, J.Q. Trojanowski, V.M. Lee, The phosphorylation state of tau in the developing rat brain is regulated by phosphoprotein phosphatases, *J. Biol. Chem.* 269 (1994) 30981–30987.
- [135] G. Michel, M. Mercken, M. Murayama, K. Noguchi, K. Ishiguro, K. Imahori, A. Takashima, Characterization of tau phosphorylation in glycogen synthase kinase-3 β and cyclin dependent kinase-5 activator (p23) transfected cells, *Biochim. Biophys. Acta* 1380 (1998) 177–182.
- [136] S.S. Mirra, J.R. Murrell, M. Gearing, M.G. Spillantini, M. Goedert, R.A. Crowther, A.I. Levey, R. Jones, J. Green, J.M. Shoffner, B.H. Wainer, M.L. Schmidt, J.Q. Trojanowski, B. Ghetti, Tau pathology in a family with dementia and a P301L mutation in tau, *J. Neuropathol. Exp. Neurol.* 58 (1999) 335–345.
- [137] H. Miyasaka, S. Okabe, K. Ishiguro, T. Uchida, N. Hirokawa, Interaction of the tail domain of high molecular weight subunits of neurofilaments with the COOH-terminal region of tubulin and its regulation by tau protein kinase II, *J. Biol. Chem.* 268 (1993) 22695–22702.
- [138] D. Moechars, I. Dewachter, K. Lorent, D. Reverse, V. Baekelandt, A. Naidu, I. Tessier, K. Spittaels, C.V. Haute, F. Checler, E. Godaux, B. Cordell, F. Van Leuven, Early phenotypic changes in transgenic mice that overexpress different mutants of amyloid precursor protein in brain, *J. Biol. Chem.* 274 (1999) 6483–6492.
- [139] L. Molina, J. Touchon, M. Herpe, D. Lefranc, L. Duplan, J.P. Cristol, R. Sabatier, P. Vermersch, B. Pau, C. Mourton-Gilles, Tau and apo E in CSF: potential aid for discriminating Alzheimer's disease from other dementias, *Neuroreport* 10 (1999) 3491–3495.
- [140] M. Morishima-Kawashima, K.S. Kosik, The pool of map kinase associated with microtubules is small but constitutively active, *Mol. Biol. Cell* 7 (1996) 893–905.
- [141] S. Mouillet-Richard, M. Ermonval, C. Chebassier, J.L. Laplanche, S. Lehmann, J.M. Launay, O. Kellermann, Signal transduction through prion protein, *Science* 289 (2000) 1925–1928.
- [142] J.R. Murrell, M.G. Spillantini, P. Zolo, M. Guazzelli, M.J. Smith, M. Hasegawa, F. Redi, R.A. Crowther, P. Pietrini, B. Ghetti, M. Goedert, Tau gene mutation G389R causes a tauopathy with abundant pick body-like inclusions and axonal deposits, *J. Neuropathol. Exp. Neurol.* 58 (1999) 1207–1226.
- [143] P. Nacharaju, J. Lewis, C. Easson, S. Yen, J. Hackett, M. Hutton, S.H. Yen, Accelerated filament formation from tau protein with specific FTDP-17 missense mutations, *FEBS Lett.* 447 (1999) 195–199.
- [144] M. Nangaku, R. Sato-Yoshitake, Y. Okada, Y. Noda, R. Takemura, H. Yamazaki, N. Hirokawa, KIF1B, a novel microtubule plus end-directed monomeric motor protein for transport of mitochondria, *Cell* 79 (1994) 1209–1220.
- [145] R. Nath, M. Davis, A.W. Probert, N.C. Kupina, X. Ren, G.P. Schielke, K.K. Wang, Processing of cdk5 activator p35 to its truncated form (p25) by calpain in acutely injured neuronal cells, *Biochem. Biophys. Res. Commun.* 274 (2000) 16–21.
- [146] D. Neary, J.S. Snowden, L. Gustafson, U. Passant, D. Stuss, S. Black, M. Freedman, A. Kertesz, P.H. Robert, M. Albert, K. Boone, B.L. Miller, J. Cummings, D.F. Benson, Frontotemporal lobar degeneration: a consensus on clinical diagnostic criteria, *Neurology* 51 (1998) 1546–1554.
- [147] T. Ohshima, J.M. Ward, C.G. Huh, G. Longenecker, Veeranna, H.C. Pant, R.O. Brady, L.J. Martin, A.B. Kulkarni, Targeted disruption of the cyclin-dependent kinase 5 gene results in abnormal corticogenesis, neuronal pathology and perinatal death, *Proc. Natl. Acad. Sci. USA* 93 (1996) 11173–11178.
- [148] P. Pastor, E. Pastor, C. Carnero, R. Vela, T. Garcia, G. Amer, E. Tolosa, R. Oliva, Familial atypical progressive supranuclear palsy associated with homozygosity for the delN296 mutation in the tau gene, *Ann. Neurol.* 49 (2001) 263–267.
- [149] G.N. Patrick, L. Zukerberg, M. Nikolic, S. de la Monte, P. Dikkes, L.H. Tsai, Conversion of p35 to p25 deregulates Cdk5 activity and promotes neurodegeneration, *Nature* 402 (1999) 615–622.
- [150] W. Paulus, M. Selim, Corticospinal degeneration with neuronal achromasia and basal neurofibrillary tangles, *Acta Neuropathol.* 81 (1990) 89–94.
- [151] J.J. Pei, I. Grundke-Iqbal, K. Iqbal, N. Bogdanovic, B. Winblad, R.F. Cowburn, Accumulation of cyclin-dependent kinase 5 (cdk5) in neurons with early stages of Alzheimer's disease neurofibrillary degeneration, *Brain Res.* 797 (1998) 267–277.
- [152] P. Poorkaj, T.D. Bird, E. Wijsman, E. Nemens, R.M. Garruto, L. Anderson, A. Andreadis, W.C. Wiederholt, M. Raskind, G.D. Schellenberg, Tau is a candidate gene for chromosome 17 frontotemporal dementia, *Ann. Neurol.* 43 (1998) 815–825.
- [153] A. Probst, J. Gotz, K.H. Wiederhold, M. Tolnay, C. Mistl, A.L. Jaton, M. Hong, T. Ishihara, V.M. Lee, J.Q. Trojanowski, R. Jakes, R.A. Crowther, M.G. Spillantini, K. Burki, M. Goedert, Axonopathy and amyotrophy in mice transgenic for human four-repeat tau protein, *Acta Neuropathol. (Berlin)* 99 (2000) 469–481.
- [154] J.J. Rebeiz, E.H. Kolodny, E.P. Richardson, Corticodentatonigral degeneration with neuronal achromasia, *Arch. Neurol.* 18 (1968) 20–33.
- [155] L.A. Reed, T.J. Grabowski, M.L. Schmidt, J.C. Morris, A. Goate, A. Solodkin, G.W. Van Hoesen, R.L. Schelper, C.J. Talbot, M.A. Wragg, J.Q. Trojanowski, Autosomal dominant dementia with widespread neurofibrillary tangles, *Ann. Neurol.* 42 (1997) 564–572.
- [156] A.A. Reszka, R. Seger, C.D. Diltz, E.G. Krebs, E.H. Fischer, Association of mitogen-activated protein kinase with the microtubule cytoskeleton, *Proc. Natl. Acad. Sci. USA* 92 (1995) 8881–8885.
- [157] C.H. Reynolds, J.C. Betts, W.P. Blackstock, A.R. Nebreda, B.H. Anderton, Phosphorylation sites on tau identified by nanoelectrospray mass spectrometry: differences in vitro between the mitogen-activated protein kinases ERK2, c-Jun N-terminal kinase and P38, and glycogen synthase kinase-3 β , *J. Neurochem.* 74 (2000) 1587–1595.

- [158] J.O. Rinne, M.S. Lee, P.D. Thompson, C.D. Marsden, Corticobasal degeneration. A clinical study of 36 cases, *Brain* 117 (1994) 1183–1196.
- [159] P. Rizzu, M. Joosse, R. Ravid, A. Hoogeveen, W. Kamphorst, J.C. van Swieten, R. Willemsen, P. Heutink, Mutation-dependent aggregation of tau protein and its selective depletion from the soluble fraction in brain of P301L FTDP-17 patients, *Hum. Mol. Genet.* 9 (2000) 3075–3082.
- [160] P. Rizzu, J.C. Van Swieten, M. Joosse, M. Hasegawa, M. Stevens, A. Tibben, M.F. Niermeijer, M. Hillebrand, R. Ravid, B.A. Oostra, M. Goedert, C.M. van Duijn, P. Heutink, High prevalence of mutations in the microtubule-associated protein tau in a population study of frontotemporal dementia in the Netherlands, *Am. J. Hum. Genet.* 64 (1999) 414–421.
- [161] G.A. Rouleau, A.W. Clark, K. Rooke, A. Pramatarova, A. Krizus, O. Suchowersky, J.P. Julien, D. Figlewicz, SOD1 mutation is associated with accumulation of neurofilaments in amyotrophic lateral sclerosis, *Ann. Neurol.* 39 (1996) 128–131.
- [162] M.L. Schmidt, R. Garruto, J. Chen, V.M. Lee, J.Q. Trojanowski, Tau epitopes in spinal cord neurofibrillary lesions in Chamorros of Guam, *Neuroreport* 11 (2000) 3427–3430.
- [163] A. Schneider, J. Biernat, M. von Bergen, E. Mandelkow, E.M. Mandelkow, Phosphorylation that detaches tau protein from microtubules (Ser262, Ser214) also protects it against aggregation into Alzheimer paired helical filaments, *Biochemistry* 38 (1999) 3549–3558.
- [164] O. Schweers, E. Schonbrunn-Hanebeck, A. Marx, E. Mandelkow, Structural studies of tau protein and Alzheimer paired helical filaments show no evidence for beta-structure, *J. Biol. Chem.* 269 (1994) 24290–24297.
- [165] D.J. Selkoe, Alzheimer's disease: genotypes, phenotypes, and treatments, *Science* 275 (1997) 630–631.
- [166] K. Senzaki, M. Ogawa, T. Yagi, Proteins of the CNR family are multiple receptors for Reelin, *Cell* 99 (1999) 635–647.
- [167] N. Sergeant, A. Wattez, A. Delacourte, Neurofibrillary degeneration in progressive supranuclear palsy and corticobasal degeneration: tau pathologies with exclusively exon 10 isoforms, *J. Neurochem.* 72 (1999) 1243–1249.
- [168] P. Seubert, M. Mawal-Dewan, R. Barbour, R. Jakes, M. Goedert, G.V. Johnson, J.M. Litersky, D. Schenk, I. Lieberburg, J.Q. Trojanowski et al., Detection of phosphorylated Ser262 in fetal tau, adult tau, and paired helical filament tau, *J. Biol. Chem.* 270 (1995) 18917–18922.
- [169] A.A. Sima, R. Defendini, C. Keohane, C. D'Amato, N.L. Foster, P. Parchi, P. Gambetti, T. Lynch, K.C. Wilhelmsen, The neuropathology of chromosome 17-linked dementia, *Ann. Neurol.* 39 (1996) 734–743.
- [170] T.J. Singh, I. Grundke-Iqbal, K. Iqbal, Phosphorylation of tau protein by casein kinase-1 converts it to an abnormal Alzheimer-like state, *J. Neurochem.* 64 (1995) 1420–1423.
- [171] J.J. Sironi, S.H. Yen, J.A. Gondal, Q. Wu, I. Grundke-Iqbal, K. Iqbal, Ser-262 in human recombinant tau protein is a markedly more favorable site for phosphorylation by CaMKII than PKA or PhK, *FEBS Lett.* 436 (1998) 471–475.
- [172] M. Sjogren, L. Rosengren, L. Minthon, P. Davidsson, K. Blennow, A. Wallin, Cytoskeleton proteins in CSF distinguish frontotemporal dementia from AD, *Neurology* 54 (2000) 1960–1964.
- [173] E. Sontag, V. Nunbhakdi-Craig, G.S. Bloom, M.C. Mumby, A novel pool of protein phosphatase 2A is associated with microtubules and is regulated during the cell cycle, *J. Cell Biol.* 128 (1995) 1131–1144.
- [174] E. Sontag, V. Nunbhakdi-Craig, G. Lee, G.S. Bloom, M.C. Mumby, Regulation of the phosphorylation state and microtubule-binding activity of Tau by protein phosphatase 2A, *Neuron* 17 (1996) 1201–1207.
- [175] E. Sontag, V. Nunbhakdi-Craig, G. Lee, R. Brandt, C. Kamibayashi, J. Kuret, C.L. White 3rd, M.C. Mumby, G.S. Bloom, Molecular interactions among protein phosphatase 2A, tau, and microtubules. Implications for the regulation of tau phosphorylation and the development of tauopathies, *J. Biol. Chem.* 274 (1999) 25490–25498.
- [176] A.D. Sperfeld, M.B. Collatz, H. Baier, M. Palmbach, A. Storch, J. Schwarz, K. Tatsch, S. Reske, M. Joosse, P. Heutink, A.C. Ludolph, FTDP-17: an early-onset phenotype with parkinsonism and epileptic seizures caused by a novel mutation, *Ann. Neurol.* 46 (1999) 708–715.
- [177] M.G. Spillantini, R.A. Crowther, W. Kamphorst, P. Heutink, J.C. van Swieten, Tau pathology in two Dutch families with mutations in the microtubule-binding region of tau, *Am. J. Pathol.* 153 (1998) 1359–1363.
- [178] M.G. Spillantini, M. Goedert, R.A. Crowther, J.R. Murrell, M.R. Farlow, B. Ghetti, Familial multiple system tauopathy with presenile dementia: a disease with abundant neuronal and glial tau filaments, *Proc. Natl. Acad. Sci. USA* 94 (1997) 4113–4118.
- [179] M.G. Spillantini, J.R. Murrell, M. Goedert, M.R. Farlow, A. Klug, B. Ghetti, Mutation in the tau gene in familial multiple system tauopathy with presenile dementia, *Proc. Natl. Acad. Sci. USA* 95 (1998) 7737–7741.
- [180] K. Spittaels, C. Van den Haute, J. Van Dorpe, K. Bruynseels, K. Vandezande, I. Laenen, H. Geerts, M. Mercken, R. Sciot, A. Van Lommel, R. Loos, F. Van Leuven, Prominent axonopathy in the brain and spinal cord of transgenic mice overexpressing four-repeat human tau protein, *Am. J. Pathol.* 155 (1999) 2153–2165.
- [181] K. Spittaels, C. Van Den Haute, J. Van Dorpe, H. Geerts, M. Mercken, K. Bruynseels, R. Lasrado, K. Vandezande, I. Laenen, T. Boon, J. Van Lint, J. Vandenheede, D. Moechars, R. Loos, F. Van Leuven, Glycogen synthase kinase-3beta phosphorylates protein tau and rescues the axonopathy in the central nervous system of human four-repeat tau transgenic mice, *J. Biol. Chem.* 275 (2000) 41340–41349.
- [182] C. Sturchler-Pierrat, D. Abramowski, M. Duke, K.H. Wiederhold, C. Mistl, S. Rothacher, B. Ledermann, K. Burki, P. Frey, P.A. Paganetti, C. Waridel, M.E. Calhoun, M. Jucker, A. Probst, M. Staufenbiel, B. Sommer, Two amyloid precursor protein transgenic mouse models with Alzheimer disease-like pathology, *Proc. Natl. Acad. Sci. USA* 94 (1997) 13287–13292.
- [183] S.M. Sumi, T.D. Bird, D. Nochlin, M.A. Raskind, Familial presenile dementia with psychosis associated with cortical neurofibrillary tangles and degeneration of the amygdala, *Neurology* 42 (1992) 120–127.
- [184] Y. Takei, S. Kondo, A. Harada, S. Inomata, T. Noda, N. Hirokawa, Delayed development of nervous system in mice homozygous for disrupted microtubule-associated protein 1B (MAP1B) gene, *J. Cell Biol.* 137 (1997) 1615–1626.
- [185] T. Tanaka, J. Zhong, K. Iqbal, E. Trenkner, I. Grundke-Iqbal, The regulation of phosphorylation of tau in SY5Y neuroblastoma cells: the role of protein phosphatases, *FEBS Lett.* 426 (1998) 248–254.
- [186] K. Tashiro, M. Hasegawa, Y. Ihara, T. Iwatsubo, Somatodendritic localization of phosphorylated tau in neonatal and adult rat cerebral cortex, *Neuroreport* 8 (1997) 2797–2801.
- [187] T. Tashiro, X. Sun, M. Tsuda, Y. Komiya, Differential axonal transport of soluble and insoluble tau in the rat sciatic nerve, *J. Neurochem.* 67 (1996) 1566–1574.
- [188] I. Tesseur, J. Van Dorpe, K. Spittaels, C. Van den Haute, D. Moechars, F. Van Leuven, Expression of human apolipoprotein E4 in neurons causes hyperphosphorylation of protein tau in the brains of transgenic mice, *Am. J. Pathol.* 156 (2000) 951–964.
- [189] M. Tolnay, M. Grazia Spillantini, C. Rizzini, D. Eccles, J. Lowe, D. Ellison, A new case of frontotemporal dementia and parkinsonism resulting from an intron 10 +3-splice site mutation in the tau gene: clinical and pathological features, *Neuropathol. Appl. Neurobiol.* 26 (2000) 368–378.
- [190] B. Trinczek, A. Ebner, E.M. Mandelkow, E. Mandelkow, Tau regulates the attachment/detachment but not the speed of motors in

- microtubule-dependent transport of single vesicles and organelles, *J. Cell Sci.* 112 (1999) 2355–2367.
- [191] J.Q. Trojanowski, J.R. Manton, J.H. Lee, D.P. Seid, T. You, L.J. Inge, V.M. Lee, Neurons derived from a human teratocarcinoma cell line establish molecular and structural polarity following transplantation into the rodent brain, *Exp. Neurol.* 122 (1993) 283–294.
- [192] R.D. Vale, B.J. Schnapp, T.S. Reese, M.P. Sheetz, Organelle, bead, and microtubule translocations promoted by soluble factors from the squid giant axon, *Cell* 40 (1985) 559–569.
- [193] J.C. van Swieten, M. Stevens, S.M. Rosso, P. Rizzu, M. Joosse, I. de Koning, W. Kamphorst, R. Ravid, M.G. Spillantini, M.F. Niermeijer, P. Heutink, Phenotypic variation in hereditary frontotemporal dementia with tau mutations, *Ann. Neurol.* 46 (1999) 617–626.
- [194] E. Vanmechelen, H. Vanderstichele, P. Davidsson, E. Van Kerschaver, B. Van Der Perre, M. Sjogren, N. Andreasen, K. Blennow, Quantification of tau phosphorylated at threonine 181 in human cerebrospinal fluid: a sandwich ELISA with a synthetic phosphopeptide for standardization, *Neurosci. Lett.* 285 (2000) 49–52.
- [195] V. Vogelsberg-Ragaglia, J. Bruce, C. Richter-Landsberg, B. Zhang, M. Hong, J.Q. Trojanowski, V.M. Lee, Distinct FTDP-17 missense mutations in tau produce tau aggregates and other pathological phenotypes in transfected CHO cells, *Mol. Biol. Cell* 11 (2000) 4093–4104.
- [196] J. Walter, J. Grunberg, A. Capell, B. Pesold, A. Schindzielorz, M. Citron, K. Mendla, P.S. George-Hyslop, G. Multhaup, D.J. Selkoe, C. Haass, Proteolytic processing of the Alzheimer disease-associated presenilin-1 generates an in vivo substrate for protein kinase C, *Proc. Natl. Acad. Sci. USA* 94 (1997) 5349–5354.
- [197] J. Walter, A. Schindzielorz, B. Hartung, C. Haass, Phosphorylation of the beta-amyloid precursor protein at the cell surface by ectocasein kinases 1 and 2, *J. Biol. Chem.* 275 (2000) 23523–23529.
- [198] J.Z. Wang, C.X. Gong, T. Zaidi, I. Grundke-Iqbal, K. Iqbal, Dephosphorylation of Alzheimer paired helical filaments by protein phosphatase-2A and -2B, *J. Biol. Chem.* 270 (1995) 4854–4860.
- [199] K.K. Wang, Calpain and caspase: can you tell the difference? *Trends Neurosci.* 23 (2000) 20–26.
- [200] K.C. Wilhelmsen, T. Lynch, E. Pavlou, M. Higgins, T.G. Nygaard, Localization of disinhibition-dementia-parkinsonism-amyotrophy complex to 17q21-22, *Am. J. Hum. Genet.* 55 (1994) 1159–1165.
- [201] D.P. Wolfer, H.P. Lipp, Dissecting the behaviour of transgenic mice: is it the mutation, the genetic background, or the environment? *Exp. Physiol.* 85 (2000) 627–634.
- [202] Z.K. Wszolek, R.F. Pfeiffer, M.H. Bhatt, R.L. Schelper, M. Cordes, B.J. Snow, R.L. Rodnitzky, E.C. Wolters, F. Arwert, D.B. Calne, Rapidly progressive autosomal dominant parkinsonism and dementia with pallido-ponto-nigral degeneration, *Ann. Neurol.* 32 (1992) 312–320.
- [203] Z. Xu, L.C. Cork, J.W. Griffin, D.W. Cleveland, Increased expression of neurofilament subunit NF-L produces morphological alterations that resemble the pathology of human motor neuron disease, *Cell* 73 (1993) 23–33.
- [204] M. Yamazaki, Y. Arai, M. Baba, T. Iwatsubo, O. Mori, Y. Katayama, K. Oyanagi, Alpha-synuclein inclusions in amygdala in the brains of patients with the parkinsonism-dementia complex of Guam, *J. Neuropathol. Exp. Neurol.* 59 (2000) 585–591.
- [205] M. Yasuda, T. Kawamata, O. Komure, S. Kuno, I. D'Souza, P. Poorkaj, J. Kawai, S. Tanimukai, Y. Yamamoto, H. Hasegawa, M. Sasahara, F. Hazama, G.D. Schellenberg, C. Tanaka, A mutation in the microtubule-associated protein tau in pallido-nigro-lusian degeneration, *Neurology* 53 (1999) 864–868.
- [206] S. Yen, C. Easson, P. Nacharaju, M. Hutton, S.H. Yen, FTDP-17 tau mutations decrease the susceptibility of tau to calpain I digestion, *FEBS Lett.* 461 (1999) 91–95.
- [207] S.H. Yen, M. Hutton, M. DeTure, L.W. Ko, P. Nacharaju, Fibrillogenesis of tau: insights from tau missense mutations in FTDP-17, *Brain Pathol.* 9 (1999) 695–705.
- [208] Q. Zheng-Fischhofer, J. Biernat, E.M. Mandelkow, S. Illenberger, R. Godemann, E. Mandelkow, Sequential phosphorylation of Tau by glycogen synthase kinase-3 β and protein kinase A at Thr212 and Ser214 generates the Alzheimer-specific epitope of antibody AT100 and requires a paired-helical-filament-like conformation, *Eur. J. Biochem.* 252 (1998) 542–552.
- [209] V. Zhukareva, V. Vogelsberg-Ragaglia, V.M. Van Deerlin, J. Bruce, T. Shuck, M. Grossman, C.M. Clark, S.E. Arnold, E. Masliah, D. Galasko, J.Q. Trojanowski, V.M. Lee, Loss of brain tau defines novel sporadic and familial tauopathies with frontotemporal dementia, *Ann. Neurol.* 49 (2001) 165–175.
- [210] L.R. Zukerberg, G.N. Patrick, M. Nikolic, S. Humbert, C.L. Wu, L.M. Lanier, F.B. Gertler, M. Vidal, R.A. Van Etten, L.H. Tsai, Cables links Cdk5 and c-Abl and facilitates Cdk5 tyrosine phosphorylation, kinase upregulation, and neurite outgrowth, *Neuron* 26 (2000) 633–646.

EXHIBIT 14

Promoters and regulatory elements that improve adeno-associated virus transgene expression in the brain

Helen L. Fitzsimons,^{a,b} Ross J. Bland,^a and Matthew J. During^{a,b,*}

^a *CNS Gene Therapy Center, Department of Neurosurgery, Thomas Jefferson University, Philadelphia, PA 19107, USA*

^b *Department of Molecular Medicine and Pathology, University of Auckland School of Medicine, Auckland, New Zealand*

Accepted 15 July 2002

Abstract

Since the first demonstration of central nervous system (CNS) transduction with recombinant adeno-associated virus, improvements in vector production and promoter strength have lead to dramatic increases in the number of cells transduced and the level of expression within each cell. The improvements in promoter strength have resulted from a move away from the original cytomegalovirus (CMV) promoter toward the use of hybrid CMV-based promoters and constitutive cellular promoters. This review summarizes and compares different promoters and regulatory elements that have been used with rAAV as a reference toward achieving a high level of rAAV-mediated transgene expression in the CNS.

© 2002 Elsevier Science (USA). All rights reserved.

Keywords: Adeno-associated virus; Regulatory element; Promoter; NSE; CBA; Brain; CNS; Transgene; Glia; Neuron

1. Introduction

Recombinant adeno-associated virus (rAAV) has become an attractive vehicle for delivering transgenes to the central nervous system (CNS) due to its lack of toxicity and absence of inflammatory response. Constant improvements in rAAV vector technology have allowed high-titer, high-purity vectors that are free of wild-type AAV and adenovirus to be produced. These features, combined with the ability of rAAV to stably transduce a wide variety of neuronal cell types in many brain areas, have facilitated phenotypic correction in many rodent disease models.

The level of transgene expression within the rAAV-transduced cell can be critical. In some instances the expression cassette needs to be constantly regulated to maintain a therapeutic level of protein. This obstacle has been approached by using regulated gene expression systems that can tightly modulate the level of therapeutic protein by administration or removal of a drug. Conversely, disorders such as those caused by enzyme deficiencies may require a high level of sustained ex-

pression to approach normal protein levels in the brain. The aim of this review is to provide a summary and comparison of promoters and regulatory elements that have been used with rAAV in the brain as a guide to achieving optimal gene expression.

2. Viral-based promoters

2.1. Cytomegalovirus promoter

Early rAAV-based studies in the brain utilized the cytomegalovirus immediate early promoter and enhancer (CMV promoter) which had been previously demonstrated to drive strong expression in the brain [1]. The small size of 700 bp allowed transgenes of approximately 3.4 kb to be packaged into rAAV. A summary of studies using the CMV promoter is presented in Table 1.

In the first demonstration of rAAV-mediated transduction of brain cells, Kaplitt et al. [2] injected a rAAV vector containing tyrosine hydroxylase (TH) under control of the CMV promoter into the rat striatum. This resulted in the transduction of approximately 1000 TH-positive neurons at 3 weeks postinjection, although expression was somewhat diminished after 4 months.

* Corresponding author. Fax: +215-955-4878.

E-mail address: m.during@auckland.ac.nz (M.J. During).

Table 1
Use of viral or viral-derived promoters for rAAV-mediated transduction of the CNS

Promoter	Transgene	Virions injected	Brain area(s) targeted	Expression level and duration	Reference
CMV	TH	1×10^4 TU	Rat striatum	TH IHC revealed $>1 \times 10^3$ TH +ve cells after 1 week; expression was significantly decreased by 4 months (NQ)	[2]
CMV	<i>lacZ</i>	5×10^4 TU	Rat olfactory tubercle, inferior colliculus, hippocampus, piriform cortex and striatum	Olfactory tubercle, 10–20 <i>lacZ</i> +ve cells per 40- μ m section; inferior colliculus, 20–50 cells per section; expression in both brain areas was stable over 3-month experiment. Hippocampus and piriform cortex, >20 cells per section; striatum, <10 cells per section; expression in these three brain areas decreased after 3 weeks	[3]
CMV	GABA _A α -1 subunit	3×10^8 particles	Rat inferior colliculus	IHC with anti-GABA _A receptor α -1 subunit antibody revealed extensive expression in the inferior colliculus after 7 days (NQ)	[4]
CMV	GFP	3×10^5 TU	Rat parabrachial nucleus	340 GFP +ve cells when every fourth 40- μ m section was counted after 2 weeks. Expression was stable over 3-month experiment	[5]
CMV	TH-IRES-AADC	4.5×10^5 IU	Monkey striatum	IHC of FLAG-tagged AADC revealed expression in numerous striatal neurons (NQ). Expression decreased after 2 months but was still detectable after 4 months	[6]
CMV	<i>lacZ</i>	1×10^7 IU	BALB/c mouse striatum	Hundreds of <i>lacZ</i> +ve cells at 2 months. Expression decreased at 4–6 months although a few <i>lacZ</i> +ve cells still detected in some brains at 12 months (NQ)	[7]
CMV	GUSB	2×10^5 TU	MPSVII mouse striatum	GUSB activity 133% of heterozygous mice, enzyme activity spread from 2 mm at 6 weeks to 4 mm after 4 months	[8]
CMV	GUSB	4×10^8 particles	MPSVII mouse striatum/cortex, thalamus/hippocampus	GUSB activity was 8–12% of normal; expression stable over 5 months	[9]
CMV	GUSB	1.5×10^{11} particles	Delivery into CSF of neonatal MPSVII mice	GUSB activity in brain was $\sim 10\%$ of normal after 1 week and $\sim 25\%$ of normal after 4 months	[10]
CMV	GFP	2.5×10^5 TU	Rat striatum (anterior and posterior)	GFP +ve cells detected in the striatum, globus pallidus internal capsule (GPI), and stria terminalis. An average of 366 GFP +ve cells were detected in the striatum after 1 month. Expression decreased after 1 month but persisted at least 11 months. Expression in GPI was fivefold higher than in striatum	[11]
MD	GDNF	2×10^8 particles	Rat substantia nigra	$\sim 1 \times 10^3$ pg GDNF detected by GDNF ELISA which was ~ 10 -fold higher than that in control rats and stable over 3- to 10-week experiment	[14,15]
MD	TH, GTPCHI	1×10^8 particles	Rat striatum	TH IHC revealed $\sim 4 \times 10^3$ TH +ve cells at 3 weeks and 1×10^3 at 6 months. Expression persisted >1 year (NQ)	[16]
MD	AADC	3.6×10^8 particles	Rat striatum	AADC IHC revealed thousands of AADC +ve cells at 3, 6, and 12 months (NQ). AADC assay showed expression stable for >26 weeks	[17]
MD	GDNF	4×10^8 – 9×10^9 particles	Rat striatum and substantia nigra	GDNF IHC on striatally injected sections revealed widespread staining through striatum and through cortex and globus pallidus over 6-month experiment (NQ). GDNF ELISA after 4 weeks showed activity was 4- to 35-fold above baseline	[18]

CMV- β -globin intron	AADC	3.6×10^{11} particles	Monkey striatum	AADC IHC revealed $8\text{--}16 \times 10^6$ AADC +ve cells after 8 weeks. Positron emission tomography with an AADC tracer showed that expression was stable >12 months [19,20]
CMV- β -globin intron	AADC	4×10^9 particles	Rat striatum	AADC IHC revealed numerous AADC +ve neurons in the striatum after 3 weeks (NQ) [21]
CMV-hGH intron	TH, AADC	3×10^9 particles	Rat striatum	TH and AADC IHC revealed numerous TH and AADC +ve neurons in the striatum after 6 weeks (NQ) [22]
CMV-hGH intron	TH, GTP-CH1, AADC	1.5×10^8 particles	Rat striatum	TH IHC revealed $2\text{--}4 \times 10^4$ TH +ve neurons in striatum at 7 months and a similar level after 12 months (NQ) [23]
CBA	GFP	2.7×10^8 particles	Mouse cerebellum	Extensive GFP +ve in Purkinje cells of cerebellum after 1 week (NQ) [28]
CBA	GFP	3×10^8 IU	Rat hippocampus	Extensive GFP +ve cells in CA1 pyramidal neurons after 7 months (NQ) [29]
CBA	GUSB	1.5×10^{11} particles	Intravenous delivery into MPSVII mice	GUSB activity 25% of normal and stable from 1 week to >1 year [30]
CBA	GFP, α -synuclein-A30P-IRES-GFP	3×10^{10} particles	Rat substantia nigra	Extensive GFP +ve and α -synuclein+ve cells detected through a major fraction of the substantia nigra with expression remaining stable over 1 year experiment (NQ). GFP+ve and α -synuclein +ve nigrostriatal axons were present throughout striatum [31]
CBA	GFP, α -synuclein	1.6×10^9 IU	Rat substantia nigra	Extensive GFP +ve cells detected through substantia nigra with expression peaking at 8 weeks and remaining stable over 27-week experiment (NQ). GFP +ve fiber terminals filled striatum. Expression similar for α -synuclein with >90% of TH +ve neurons also expressing α -synuclein [32]
CBA	GFP	5×10^9 particles	Rat hippocampus	$\sim 2 \times 10^5$ GFP-expressing cells detected in hippocampus after 1 month with expression stable >18 months. Threefold more CBA-GFP-expressing cells detected than NSE-GFP-expressing cells with matched titers. [33]
MFG	NGF	3.4×10^9	Rat medial septum	87% cholinergic neuron survival after fimbria fornix lesion compared to 23% survival in control rats (NQ) [35]
RSV	<i>lacZ</i>	$2 \times 10^9\text{--}4 \times 10^9$ particles	Rat lateral ventricle and striatum	<10 <i>lacZ</i> +ve ependymal cells and <20 <i>lacZ</i> +ve striatal cells after 3 and 15 weeks [36]
RSV	bcl-2	1.7×10^{10} particles 2.4×10^{11} particles	Gerbil hippocampus	Extensive FLAG-tagged bcl-2 detected by IHC in CA1 pyramidal cells after 5 days (NQ) [37]

All times stated refer to the length of time after AAV administration. ELISA, enzyme-linked immunosorbent assay; +ve, positive; IHC, immunohistochemistry; IU, infectious units; TU, transducing units; NQ, transgene expression was not quantified; GDNF, glial-derived neurotrophic factor; GTPCH1, GTP cyclohydrolase 1; IRES, internal ribosome entry site; GUSB, β -glucuronidase. All other abbreviations are referred to in the text. The titer refers to the total amount of virus injected. Viruses titered by different methods are measured in different units. Virus titered using the infectious center assay is measured in IU; virus titered by a functional assay, such as counting immuno-positive cells after infection of a cell line with rAAV, is measured in TU; virus titered by dot blot or quantitative PCR to quantify number of genomes is measured in particles; virus titered by an ELISA using an antibody to the capsid is referred to as capsid titer. For further explanation see [38].

Transduction of various distinct brain areas was demonstrated by McCown et al. [3] who found that 3 weeks after injection of rAAV-CMV-*lacZ* into the olfactory tubercle, striatum, hippocampus, piriform cortex, and inferior colliculus of mice, *lacZ* expression was detected in each brain area, ranging from less than 10 cells per 40- μ m section in the striatum to over 50 cells per 40- μ m in the inferior colliculus. Three months postinjection, however, expression was substantially reduced in the hippocampus and piriform cortex and somewhat decreased in the striatum, suggesting that the level and duration of rAAV-mediated expression was specific to different brain areas.

There have since been many studies using the CMV promoter to drive transgene expression. Many studies where expression was monitored for a short time have demonstrated stable CMV-driven expression in many brain regions facilitating at least partial phenotypic recovery [8–10] or protecting from insult [4]. Studies monitoring expression over the long term, however, were plagued by declining expression over time [2,3,7]. This phenomenon has been ascribed to silencing of the viral-derived promoter by methylation based on a study by Prösch et al. [12] who showed that the CMV promoter was susceptible to transcriptional inactivation by methylation of cytosines in CpG dinucleotides. The observed promoter inactivation may also have been due, at least in part, to impurities in early vector preparations. It is also important to note that lentiviral vectors containing the CMV promoter have been demonstrated to sustain long-term expression in the rat brain [13]. The recent characterization of other promoters that drive a higher level of sustained AAV-mediated expression in the CNS has precipitated the phasing out of the original CMV promoter.

2.2. CMV-derived promoters

Modifications of the CMV promoter have been engineered in an effort to both enhance and stabilize gene expression. The (MD) promoter consists of the CMV promoter fused to β -globin exons two and three and an intervening intron. This promoter has been employed by the Mandel research group to transduce nigral and striatal neurons to test various transgenes for efficacy in a rat model of Parkinson's disease. Robust transduction of thousands of neurons was achieved and, furthermore, transgene expression was stable for greater than 1 year [14–18] (Table 1).

A similar promoter that contains the CMV promoter and a chimeric intron composed of a CMV splice donor and a human globin splice acceptor was employed by Bankiewicz et al. [19] and Sanchez-Pernaute et al. [21]. Injection of a rAAV vector containing aromatic L-amino-acid decarboxylase under control of this promoter resulted in transduction of approximately 8–16 million

neurons in the monkey striatum with expression persisting for at least 1 year [20].

Long-term expression was also observed when the CMV promoter was fused to the human growth hormone first intron. Approximately 20,000–40,000 striatal neurons were transduced when rAAV-TH was driven by this promoter with no attenuation of expression after 1 year [23].

Based on the similarities in results from all of these studies, it is likely that the increased expression levels and persistence of expression was due to stabilization of the CMV promoter by addition of an intron that may improve the efficiency of RNA processing [24].

2.3. CMV enhancer/chicken β -actin promoter

The CMV enhancer/chicken β -actin promoter (variously called CBA, CB, or CAG) was first described by Niwa et al. [25] as a strong constitutive promoter consisting of the chicken β -actin promoter fused downstream of the CMV enhancer. A 1.7-kb version of this promoter containing the CMV enhancer/chicken β -actin promoter fused to 90 nucleotides of exon one of the chicken β -actin gene, 917 nucleotides of a hybrid chicken β -actin/rabbit β -globin intron, and 55 nucleotides of rabbit β -globin exon three has been most commonly employed for gene therapy applications [26,27]. In the past few years, rAAV in conjunction with CBA has been shown to facilitate a high level of rAAV-mediated gene expression in various brain areas (Table 1).

In an initial study using CBA to promote rAAV-mediated gene expression in the brain, Kaemmerer et al. [28] demonstrated transduction of numerous Purkinje cells in the mouse cerebellum. By comparison, few green fluorescent protein (GFP) positive cells were observed after injection of a similar cassette driven by the CMV promoter. The authors hypothesize that this may have been due to transcriptional inactivation of the CMV promoter as coinjection with adenovirus serotype five did allow transduction of some Purkinje cells, possibly by activation of the CMV promoter by the adenovirus E1 protein.

The CBA promoter also facilitates stable, long-term gene expression. Extensive transduction of CA1 pyramidal cells in the rat hippocampus was observed 7 months after injection of rAAV [29] and therapeutic levels of β -glucuronidase (GUSB) persisted greater than one year after intravenous administration into MPSVII mice [30]. In two recent studies characterizing a new model of Parkinson's disease, AAV-CBA mediated overexpression of GFP led to transduction of the majority of the substantia nigra, filling the entire striatum with GFP positive terminals. GFP expression peaked by 1 [31] to 2 [32] months and remained at a constant level over the 6-month [32] or 1-year [31] duration of the study.

Klein et al. [33] directly compared the number of GFP-expressing cells in the rat hippocampus resulting from use of the CBA compared with the neuron-specific enolase (NSE) promoter (see Section 3) and found a 3.2-fold greater number of transduced cells when the CBA promoter was used. Our research group has qualitatively observed a 1.1-kb version of the CBA promoter with a shorter intron (derived from pBacMam3, Novagen, Madison, WI) to drive high levels of GFP in hippocampus, substantia nigra, and striatum (unpublished observations) at a level comparable with that of the NSE promoter. Furthermore, Björklund et al. [34] have found that the 1.7-kb CBA promoter in conjunction with the woodchuck post-transcriptional regulatory element (WPRE; see Section 4) provides a 7- to 50-fold higher transduction efficiency in striatum and substantia nigra than the MD promoter used in their previous studies.

2.4. Other viral promoters

In the context of rAAV, the Moloney murine leukemia virus long terminal repeat (MGF) and the Rous sarcoma virus long terminal repeat (RSV) promoters have been less well characterized. Injection of nerve growth factor under control of the MGF promoter into the medial septum has been shown to facilitate a 60% increase in survival of cholinergic neurons after fimbria-fornix lesion although the level of transgene expression was not measured directly in vivo [35].

The RSV promoter was found by Davidson et al. [36] to drive weak expression after injection into the rat lateral ventricle and striatum with only 10–20 *lacZ* positive cells detected; however, in another study the RSV promoter drove robust expression of *bcl-2* in numerous CA1 pyramidal cells of the gerbil hippocampus [37]. As AAV2 has been shown to readily transduce striatal neurons, whether the differences in expression levels in the two studies is a consequence of different titers or whether they reflect differences in tropism of the promoter for particular brain areas is not clear.

3. Cellular promoters

As a consequence of the decrease in expression associated with viral-derived promoters, cellular promoters were employed to assess their ability to promote sustained gene expression in the brain. A summary of cellular promoters that have been used with rAAV is presented in Table 2.

3.1. Other non cell-type-specific promoters

The elongation factor 1 α (EF1 α) gene is a ubiquitously expressed housekeeping gene that plays a pivotal role in protein synthesis and the human EF1 α promoter

has previously been shown to drive a high level of expression in mouse liver [39]. Lipshutz et al. [40] injected rAAV-EF1 α -luciferase intraperitoneally into mice in utero at day 15 of gestation, resulting in sustained expression in the brain for over 6 months. A decrease in luciferase activity after 1 month was attributed to the growth of the pups and an associated dilution of the episomal virus [40]. Xu et al. [41] measured rAAV-EF1 α -driven luciferase activity in various brain areas after 2 weeks and found expression comparable to that driven by the glial fibrillary acidic protein (GFAP) promoter, 8–18 times higher than that of the CMV promoter, and 2–8 times lower than that of the NSE promoter.

3.2. Neuron-specific promoters

The rat neuron-specific enolase promoter is probably the most well characterized neuronal promoter that has been used in the context of rAAV-mediated expression in the brain. This promoter was initially shown to drive a high level of neuronally restricted *lacZ* expression [42] in a transgenic mouse study. NSE was found to facilitate a very high level of rAAV-mediated expression in the CNS when utilized by Peel et al. [43] to transduce the rat spinal cord, facilitating GFP expression in thousands of spinal cord neurons. Subsequently, this promoter has also been demonstrated to promote a high level of sustained expression in the striatum [41,45], medial septum [44], substantia nigra [29,33,41,44], and hippocampus [33,41,44]. In a study comparing NSE to the CMV promoter, expression driven by CMV was 8.5-fold lower after 3 weeks and barely detectable at 3 months [44], whereas NSE-driven expression remained stable. Demonstration of the ability of the NSE promoter to drive long-term sustained expression was solidified by Klein et al. [29,33] who observed no attenuation of NSE-driven expression for over 1 year in the basal forebrain and for over 25 months in the substantia nigra.

Xu et al. [41] compared the ability of NSE and eight other promoters to generate luciferase expression 2 weeks postinjection in the rat cortex, hippocampus, substantia nigra, and striatum. NSE was significantly higher in all brain areas, being up to 69 times higher than CMV and up to 8 and 20 times higher than EF1 α and GFAP, respectively.

Another neuron-specific promoter that has been used in conjunction with rAAV is the human platelet-derived growth factor B chain (PDGF) promoter which was shown to specifically target gene expression to neurons in transgenic mouse studies [46].

A rAAV cassette with PDGF controlling GFP expression efficiently transduced spinal cord neurons with one GFP-expressing neuron per 45 infectious particles [43]. By comparison, NSE was three times more efficient than PDGF with one GFP-expressing neuron observed

Table 2
Use of cellular promoters for rAAV-mediated transduction of the CNS

Promoter	Transgene	Virions injected	Brain area(s) targeted	Expression level and duration	Reference
EF1 α	Luc	3×10^{11} particles	i.p. injection into day 15 mice in utero	Luc assay showed expression stable >6 months in brain although expression in brain lower than that in other organs	[40]
EF1 α	Luc	2.5×10^9 particles	Rat cortex, striatum, substantia nigra, hippocampus	EF1 α -Luc activity 8–18 times higher than CMV-Luc and, 2–8 times lower than NSE-Luc.	[41]
NSE	GFP	4×10^4 IU	Rat cervical spinal cord	857 GFP +ve cells counted (every third 40- μ m section counted); stable over 15-week experiment; 1 GFP +ve cell detected per 15 IU of virus	[43]
NSE	GFP	6×10^5 IU	Rat hippocampus, medial septum, substantia nigra	3×10^3 – 1.5×10^4 GFP +ve cells in medial septum and substantia nigra and stable over 19 months. 2×10^3 – 3×10^3 GFP +ve cells in hippocampus at 3 weeks; 8.5-fold higher than CMV-GFP	[44,29]
NSE	Luc	2.5×10^9 particles	Rat cortex, striatum, nigra, hippocampus	Expression stable over 15-month experiment as measured by luciferase assay. NSE-Luc activity 2- to 8- and 2- to 20-fold higher than those driven by GFAP and EF promoters, respectively.	[41]
NSE	GFP	1.4×10^{10} capsids	Rat striatum	415 GFP +ve cells per 35- μ m section transduced over 4-mm area after 3 weeks	[45]
NSE	GFP	5×10^9 particles	Rat hippocampus and substantia nigra	6×10^3 GFP-expressing cells detected in hippocampus after 1 month. 2.3×10^4 GFP +ve cells detected in substantia nigra after 25 months	[33]
PDGF	GFP	4×10^4 IU	Rat cervical spinal cord	309 GFP +ve cells counted (every third 40- μ m section counted); stable over 15-week experiment; 1 GFP +ve cell per 45 IU of virus	[43]
PDGF	GFP-2A- α -synuclein	1×10^5 IU	Rat substantia nigra	IHC revealed numerous α -synuclein and GFP +ve cells throughout the substantia nigra after 4 weeks (NQ)	[47]
MBP	GFP	6×10^9 particles	Mouse corpus callosum, striatum, thalamus, cortex	1×10^3 GFP +ve cells resembling oligodendrocytes in corpus callosum, expression stable over 3-month experiment; <50 GFP +ve cells detected in striatum, thalamus, and cortex	[53]
GFAP	Luc	2.5×10^9 particles	Rat hippocampus, striatum, cortex, substantia nigra	Luc activity 3–20 times higher than that of CMV-driven luc expression and 2–20 times lower than that of NSE-driven luc expression; 95% of expression appeared neuronal	[41]
GFAP	GFP	4×10^7 IU	Rat spinal cord	In normal spinal cord most cells transduced were neurons; however, in injured spinal cord, 15–30% of transduced cells were astrocytes	[29]

See note to Table 1 for details and abbreviations. Luc, luciferase.

for every 15 infectious particles injected; however, PDGF was still significantly more efficient at driving gene expression than CMV [43]. Interestingly, PDGF did transduce motoneurons in the cervical enlargement more efficiently than NSE [29]. rAAV-PDGF has also been shown to promote transgene expression throughout the rat substantia nigra for at least 1 month postinjection [47].

Improvements in rAAV expression could emerge from the utilization of multimeric repeats of *cis*-regulatory elements from endogenous promoters. Such an element has not yet been evaluated in an rAAV setting. However, a synthetic promoter containing eight copies of a noradrenergic-specific *cis*-regulatory element (PRS2) from the human dopamine β -hydroxylase (hDBH) promoter has been shown to direct >50 higher levels of transgene expression than the hDBH promoter *in vitro*, and, furthermore, drives high levels of adenovirus-mediated expression specifically in noradrenergic neurons in the rat locus coeruleus [48]. In addition to enhancing gene expression, at 300 bp the small size of this element is ideal for use with rAAV, where size is an important factor in expression cassette design.

3.3. Glia-specific promoters

In a transgenic mouse model, the human glial fibrillary acidic protein promoter was shown to direct expression specifically to astrocytes [49].

In the context of rAAV, however, very few transduced astrocytes were observed by Xu et al. [41] after injection of a reporter gene under control of the GFAP promoter into the hippocampus and less than 5% of striatal cells transduced with the same vectors were morphologically characteristic of astrocytes or colabeled with GFAP. Most GFP positive cells appeared neuronal and colabeled with neuronal marker NeuN. Peel and Klein [29] injected rAAV-GFAP-GFP into the spinal cord and detected expression primarily in neurons; however, in damaged spinal cord, the incidence of astrocytic expression increased to 15–30%. The expression of AAV-GFAP-driven cassettes in neurons was unexpected based on the exclusively astrocytic expression seen in transgenic mouse studies [49]. The AAV inverted terminal repeats contain promoter activity [50,51] which may have contributed to the observed expression.

An oligodendrocyte-specific promoter has also been used to drive rAAV expression. The myelin basic protein (MBP) promoter was originally demonstrated to restrict transgene expression specifically to myelin, forming oligodendrocytes in a transgenic mouse model [52]. Chen et al. [53] injected a rAAV-MBP cassette containing the GFP reporter gene into the mouse corpus callosum, resulting in transduction of oligodendrocytes with expression persisting for greater than 3 months. Injection into the gray matter yielded scarce GFP expression. All

GFP transduced cells were colabeled with the oligodendrocyte marker CNPase but not with the neuronal marker NeuN and were morphologically characteristic of type I oligodendrocytes [53].

4. The woodchuck posttranscriptional regulatory element

The woodchuck hepatitis virus posttranscriptional regulatory element is a posttranscriptional enhancer that facilitates cytoplasmic accumulation and translation of mRNA [54,55]. In the context of AAV, WPRE was first utilized *in vitro* to give up to a sixfold improvement in GFP expression. Paterna et al. [56] described the first use of WPRE *in vivo* by comparing GFP expression from constructs under control of either the PDGF or the CMV promoters with or without the WPRE element. Matched viruses were injected into the substantia nigra and the amount of GFP expression in tyrosine hydroxylase positive neurons was determined. The addition of WPRE to the PDGF-GFP cassette resulted in almost twofold more GFP expression, while addition of WPRE to CMV had no effect. High levels of expression were maintained long term with the WPRE vectors, with expression at 41 weeks similar to that found 4 weeks postinjection [56].

Xu et al. [41] confirmed the expression-enhancing properties of WPRE in other regions of the rat brain, showing that addition of WPRE to NSE-driven cassettes resulted in a 4- to 9-fold increase in luciferase expression in the rat striatum, hippocampus, cortex, and nigra. In agreement, Klein et al. [33] recently demonstrated by Western analysis that addition of WPRE to an AAV-CBA-GFP cassette increased expression 11-fold in the rat hippocampus.

5. Cell-type specific tropism of rAAV

Entry of rAAV into the cell is dependent on binding to the cell surface receptor heparan sulfate proteoglycan (HSPG) [57] and coreceptors fibroblast growth factor receptor-1 (FGFR-1) [58] or $\alpha V\beta 5$ [59]. Data gathered from numerous studies have provided overwhelming evidence of the strong tropism of the rAAV2 particle for neurons and this tropism appears, in most cases, to be independent of the promoter used. Most studies reported that approximately 5% or less of transduced cells appeared to be nonneuronal [2–4,16,18,41], and no glial cells were detected when using a neuron-specific promoter [43,44]. This neuronal specificity was demonstrated in an elegant study by Bartlett et al. [60] who distinguished uptake of virus from promoter activity by fluorescently labeling the AAV particle and observed that AAV was preferentially taken up into neurons in the rat brain.

The main exception to this finding in the literature is the oligodendrocyte-specific tropism of the MBP

promoter which was reported to almost exclusively transduce type II oligodendrocytes when injected into the white or gray matter [53]. This is a curious finding based on our knowledge of the strong neuronal tropism of AAV. Bartlett et al. [60] did not observe uptake of AAV particles into astrocytes or oligodendrocytes; however, some astrocytic expression has been observed [11,29], suggesting that glial uptake of AAV can occur under some circumstances. The MBP promoter appeared to be transcriptionally inactive in neurons; therefore, the oligodendrocyte transduction may reflect the 1–5% of glial transduction that other researchers have documented and/or altered tropism in response to needle injury.

Additional insight into transduction of nonneuronal cell types comes from a study by Tenenbaum et al. [11] who injected rAAV-CMV-GFP into the posterior striatum and observed transduction of cells with a glial-like morphology in the internal capsule, an area that lacks neurons. In addition, transduction of glial cultures with rAAV has been well documented [61]. The possibility exists that when there is a sparse neuronal population or when a brain area is enriched in reactive astrocytes, such as after an insult, the absence of neurons allows astrocytes the opportunity to take up the virus.

The HSPG receptor is distributed widely throughout the brain. The FGFR-1 coreceptor is expressed more highly in some brain areas than others and at a higher level in astrocytes than in neurons [62]. Additional coreceptor(s) that have yet to be identified may exist, allowing the possibility that differing levels of coreceptors in particular tissues and cell types may contribute to the ability of specific cell types in different brain areas to take up AAV.

Of the six described serotypes of AAV, only AAV2 gene transfer has been extensively characterized in the brain. Recently it was demonstrated by Davidson et al. [36] that AAV4 and AAV5 are also effective, with expression mediated by these two serotypes being significantly higher than that of rAAV2 in ependymal cells and in the striatum. Much of the AAV5-mediated expression was found in neurons; however, many transduced astrocytes were also evident in the striatum, cortex, and corpus callosum. This altered tropism is not surprising considering that AAV5 binds sialic acid which is not bound by AAV2 [63] and does not bind the AAV2 receptor HSPG [64]. The use of AAV serotypes that have an increased tropism for astrocytes may allow researchers to make more use of glial-specific promoters in driving a high level of expression to treat disease models where transduction of glia is favored.

6. Conclusion

The main limitation of using rAAV is a packaging size limit of around 4.7 kb which prohibits the packaging of expression cassettes over approximately 4.4 kb

(excluding the ITRs). To help overcome this obstacle, *trans*-splicing vectors that allow cassettes of twice wild-type AAV size to be packaged have been developed [65–68]. Although these vectors hold great promise for future rAAV studies, the current efficiency has been determined to be only 4–7% of that seen with a single vector containing a full-length gene [69]. Thus, decreasing the promoter size while maintaining promoter strength is essential.

To date there has been only one comprehensive study comparing AAV promoter strengths in the brain [38]. There is inherent difficulty in comparing results from different research groups due to different titering methods, brain areas targeted, routes of administration, and vector purity. To give a rough idea of the relative amounts of vector used in all studies presented here, titers and routes of administration were noted; however, due to the reasons stated above, the level of transgene expression resulting from injection of a particular virus titer cannot be directly compared from one study to the next.

The strongest promoters used with rAAV to date appear to be the NSE and CBA promoters. The NSE promoter has been better characterized in more brain areas and over a longer period of time than the CBA promoter, although it has been found in one study to drive threefold lower expression than CBA [33]. A disadvantage of using NSE is its relatively large size of 1.8–2.2 kb [41,44] which precludes the packaging of large transgenes. When targeting neuronal expression in the brain, the inherent neuronal tropism of rAAV allows advantage to be taken of smaller cell-specific promoters such as CBA. Our laboratory uses a 1.1-kb CBA promoter, allowing an additional 0.7–1.1 kb to be packaged over NSE which improves general utility. Other research groups [31,33] have used a 1.7-kb CBA promoter containing a larger intron which still allows 0.1–0.5 kb to be packaged over NSE. Whether the larger intron in the 1.7-kb CBA promoter provides increased expression levels over the 1.1-kb CBA promoter has not been tested.

The addition of WPRE will increase expression severalfold; however, it also adds an additional 600 bp to the cassette which, allowing for a polyadenylation signal of 300 bp, can accommodate a transgene of up to 1.6–2.0 kb.

Although the level of transgene expression has been greatly enhanced over that of early studies where modest levels of unstable expression directed by the CMV promoter were achieved, researchers remain constantly on the lookout for shorter, stronger promoters to further optimize AAV-mediated expression in the brain.

References

- [1] E.V. Schmidt, G. Christoph, R. Zeller, P. Leder, *Mol. Cell. Biol.* 10 (1990) 4406–4411.

- [2] M.G. Kaplitt, P. Leone, R.J. Samulski, X. Xiao, D.W. Pfaff, K.L. O'Malley, M.J. During, *Nat. Genet.* 8 (1994) 148–154.
- [3] T.J. McCown, X. Xiao, J. Li, G.R. Breese, R.J. Samulski, *Brain Res.* 713 (1996) 99–107.
- [4] X. Xiao, T.J. McCown, J. Li, G.R. Breese, A.L. Morrow, R.J. Samulski, *Brain Res.* 756 (1997) 76–83.
- [5] N.L. Chamberlin, B. Du, S. de Lacalle, C.B. Saper, *Brain Res.* 793 (1998) 169–175.
- [6] M.J. During, R.J. Samulski, J.D. Elsworth, M.G. Kaplitt, P. Leone, X. Xiao, J. Li, A. Freese, J.R. Taylor, R.H. Roth, J.R. Sladek Jr., K.L. O'Malley, D.E. Redmond Jr., *Gen. Ther.* 5 (1998) 820–827.
- [7] W.D. Lo, G. Qu, T.J. Sferra, R. Clark, R. Chen, P.R. Johnson, *Hum. Gen. Ther.* 10 (1999) 201–213.
- [8] A. Bosch, E. Perret, N. Desmaris, J.M. Heard, *Mol. Ther.* 1 (2000) 63–70.
- [9] A.F. Skorupa, K.J. Fisher, J.M. Wilson, M.K. Parente, J.H. Wolfe, *Exp. Neurol.* 160 (1999) 17–27.
- [10] S.S. Elliger, C.A. Elliger, C.P. Aguilar, N.R. Raju, G.L. Watson, *Gen. Ther.* 6 (1999) 1175–1178.
- [11] L. Tenenbaum, F. Jurysta, A. Stathopoulos, Z. Puschban, C. Melas, W.T.J.M.C. Hermens, J. Verhaagen, B. Pichon, T. Velu, M. Levivier, *Neuroreport* 11 (2000) 2277–2283.
- [12] S. Prösch, J. Stein, K. Staak, C. Liebenthal, H. Volk, D.H. Krüger, *Biol. Chem.* 377 (1996) 195–201.
- [13] L. Naldini, U. Blömer, F.H. Gage, D. Trono, I.M. Verma, *Proc. Natl. Acad. Sci. USA* 93 (1996) 11388–11482.
- [14] R.J. Mandel, S.K. Spratt, R.O. Snyder, S.E. Leff, *Proc. Natl. Acad. Sci. USA* 94 (1997) 14083–14088.
- [15] R.J. Mandel, R.O. Snyder, S.E. Leff, *Exp. Neurol.* 160 (1999) 205–214.
- [16] R.J. Mandel, K.G. Rendahl, S.K. Spratt, R.O. Snyder, L.K. Cohen, S.E. Leff, *J. Neurosci.* 18 (1998) 4271–4284.
- [17] S.E. Leff, S.K. Spratt, R.O. Snyder, R.J. Mandel, *Neuroscience* 92 (1999) 185–196.
- [18] D. Kirik, C. Rosenblad, A. Björklund, R.J. Mandel, *J. Neurosci.* 20 (2000) 4686–4700.
- [19] K.S. Bankiewicz, J.L. Eberling, M. Kohutnicka, W. Jagust, P. Pivrotto, J. Bringas, J. Cunningham, T.F. Budinger, J. Harvey-White, *Exp. Neurol.* 164 (2000) 2–14.
- [20] K.S. Bankiewicz, R. Sanchez-Pernaute, P. Pivrotto, P. Herscovitch, R. Carson, J. Cunningham, K. Eckelman, *Soc. Neurosci. Abstr.* 887.3, 2001.
- [21] R. Sanchez-Pernaute, J. Harvey-White, J. Cunningham, K.S. Bankiewicz, *Mol. Ther.* 4 (2001) 324–330.
- [22] D.-S. Fan, M. Ogawa, K. Fujimoto, K. Ikeguchi, Y. Ogasawara, M. Urabe, M. Nishizawa, I. Nakano, M. Yoshida, I. Nagatsu, H. Ichinose, T. Nagatsu, G.J. Kurtzman, K. Ozawa, *Hum. Gen. Ther.* 9 (1998) 2527–2535.
- [23] Y. Shen, S. Muramatsu, K. Ikeguchi, K. Fujimoto, D. Fan, M. Ogawa, H. Mizukami, M. Urabe, A. Kame, I. Nagatsu, F. Urano, T. Suzuki, H. Ichinose, T. Nagatsu, J. Monahan, I. Nakano, K. Ozawa, *Hum. Gen. Ther.* 11 (2000) 1509–1519.
- [24] M. Antoniou, F. Geraghty, J. Hurst, F. Grosfeld, *Nucleic Acids. Res.* 26 (1998) 721–729.
- [25] H. Niwa, K. Yamamura, J. Miyazaki, *Gene* 108 (1991) 193–200.
- [26] L. Xu, T. Daly, C. Gao, T.S. Flotte, S. Song, B.J. Byrne, M.S. Sands, K. Parker Ponder, *Hum. Gen. Ther.* 12 (2001) 563–573.
- [27] T.M. Daly, T. Okuyama, C. Vogler, M.E. Haskins, N. Muzyczka, M.S. Sands, *Hum. Gen. Ther.* 10 (1999) 85–94.
- [28] W.F. Kaemmerer, R.G. Reddy, C.A. Warlick, S.D. Hartung, R.S. McIvor, W.C. Low, *Mol. Ther.* 2 (2000) 446–457.
- [29] A.L. Peel, R.L. Klein, *J. Neurosci. Meth.* 98 (2000) 95–104.
- [30] T.M. Daly, K.K. Ohlemiller, M.S. Roberts, C.A. Vogler, M.S. Sands, *Gen. Ther.* 8 (2001) 1291–1298.
- [31] R.L. Klein, M.A. King, M.E. Hamby, E.M. Meyer, *Hum. Gene Ther.* 13 (2002) 605–612.
- [32] D. Kirik, C. Rosenblad, C. Burger, C. Lundberg, T.E. Johansen, N. Muzyczka, R.J. Mandel, A. Björklund, *J. Neurosci.* 22 (2002) 2780–2791.
- [33] R.L. Klein, M.E. Hamby, A.C. Hirko, Y. Gong, S. Wang, J.A. Hughes, M.A. King, E.M. Meyer, *Exp. Neurol.* 176 (2002) 66–74.
- [34] A. Björklund, D. Kirik, C. Rosenblad, B. Georgievskaya, C. Lundberg, R.J. Mandel, *Brain Res.* 886 (2000) 82–98.
- [35] R.J. Mandel, F.H. Gage, D.G. Clevenger, S.K. Spratt, R.O. Snyder, S.E. Leff, *Exp. Neurol.* 155 (1999) 59–64.
- [36] B.L. Davidson, C.S. Stein, J.A. Heth, I. Martins, R.M. Kotin, T.A. Derksen, J. Zabner, A. Ghodsi, J.A. Chiorini, *Proc. Natl. Acad. Sci. USA* 97 (2000) 3428–3432.
- [37] K. Shimazaki, M. Urabe, J. Monahan, K. Ozawa, N. Kawai, *Gen. Ther.* 7 (2000) 1244–1249.
- [38] X. Xiao, J. Li, T.J. McCown, R.J. Samulski, *Exp. Neurol.* 144 (1997) 113–124.
- [39] H. Nakai, R.W. Herzog, J.N. Hagstrom, J. Walter, S.H. Kung, E.Y. Yang, S.J. Tai, Y. Iwaki, G.J. Kurtzman, K.J. Fisher, P. Colsi, L.B. Couto, K.A. High, *Blood* 91 (1998) 4600–4607.
- [40] G.S. Lipshutz, C.A. Gruber, Y. Cao, J. Hardy, C.H. Contag, K.M.L. Gaensler, *Mol. Ther.* 3 (2001) 284–292.
- [41] R. Xu, C.G. Janson, M. Mastakov, P.A. Lawlor, D. Young, A.I. Mouraviev, H.L. Fitzsimons, K. Choi, H. Ma, M. Dragunow, P. Leone, Q. Chen, B. Dicker, M.J. During, *Gen. Ther.* 8 (2001) 1323–1332.
- [42] S. Forss-Petter, P.E. Danielson, S. Catsicas, E. Battenberg, J. Price, M. Nerenberg, J.G. Sutcliffe, *Neuron* 5 (1990) 187–197.
- [43] A.L. Peel, S. Zolotukhin, G.W. Schrimsher, N. Muzyczka, P.J. Reier, *Gen. Ther.* 4 (1997) 16–24.
- [44] R.L. Klein, E.M. Meyer, A.L. Peel, S. Zolotukhin, C. Meyers, N. Muzyczka, M.A. King, *Exp. Neurol.* 150 (1998) 183–194.
- [45] M.Y. Mastakov, K. Baer, R. Xu, H. Fitzsimons, M.J. During, *Mol. Ther.* 3 (2001) 225–232.
- [46] E. Masliah, E. Rockenstein, I. Veinbergs, M. Mallory, M. Hashimoto, A. Takeda, Y. Sagara, A. Sisk, L. Mucke, *Science* 287 (2000) 1265–1269.
- [47] S. Furler, J.-C. Paterna, M. Weibel, H. Bueler, *Gen. Ther.* 8 (2001) 864–873.
- [48] D. Hwang, W.A. Carlezon Jr., O. Isacson, K. Sim, *Hum. Gen. Ther.* 12 (2001) 1731–1740.
- [49] M. Brenner, W.C. Kisseberth, Y. Su, F. Besnard, A. Messing, *J. Neurosci.* 14 (1994) 1030–1037.
- [50] T.R. Flotte, S.A. Afione, C. Conrad, S.A. McGrath, R. Solow, H. Oka, P.L. Zeitlin, W.B. Guggino, B.J. Carter, *Proc. Natl. Acad. Sci. USA* 90 (1993) 10613–10617.
- [51] R.P. Haberman, T.J. McCown, R.J. Samulski, *J. Virol.* 74 (2000) 8732–8739.
- [52] A. Gow, V.L. Friedrich Jr., R.A. Lazzarini, *J. Cell Biol.* 119 (1992) 605–616.
- [53] H. Chen, D.D. McCarty, A.T. Bruce, K. Suzuki, K. Sukuji, *J. Neurosci. Res.* 55 (1998) 504–513.
- [54] J.E. Donello, A.A. Beeche, G.J. Smith, G.R. Lucero, T.J. Hope, *J. Virol.* 70 (1996) 4345–4351.
- [55] J.E. Loeb, W.S. Cordier, M.E. Harris, M.D. Weitzman, T.J. Hope, *Hum. Gen. Ther.* 10 (1999) 2295–2305.
- [56] J.-C. Paterna, T. Moccetti, A. Mura, J. Feldon, H. Bueler, *Gen. Ther.* 7 (2000) 1304–1311.
- [57] C. Summerford, R.J. Samulski, *J. Virol.* 72 (1998) 1438–1445.
- [58] K. Qing, C. Mah, J. Hansen, S. Zhou, V. Dwarki, A. Srivastava, *Nat. Med.* 5 (1999) 71–77.
- [59] C. Summerford, J.S. Bartlett, R.J. Samulski, *Nat. Med.* 5 (1999) 78–81.
- [60] J.S. Bartlett, R.J. Samulski, T.J. McCown, *Hum. Gen. Ther.* 9 (1998) 1181–1186.
- [61] S.D. Keir, J. Miller, G. Yu, R. Hamilton, R.J. Samulski, X. Xiao, C. Tornatore, *J. NeuroVirol.* 3 (1997) 322–330.

- [62] A.M. Gonzalez, M. Berry, P.A. Maher, A. Logan, A. Baird, *Brain Res.* 701 (1995) 201–226.
- [63] N. Kaludov, K. Brown, R. Walters, J. Zabner, J. Chorioni, *J. Virol.* 75 (2001) 6884–6893.
- [64] J.J. Rabinowitz, F. Rolling, C. Li, H. Conrath, W. Xiao, X. Xiao, R.J. Samulski, *J. Virol.* 76 (2002) 791–801.
- [65] D. Duan, Y. Yue, Z. Yan, J.F. Engelhardt, *Nat. Med.* 6 (2000) 595–598.
- [66] Z. Yan, Y. Zhang, D. Duan, J.F. Engelhardt, *Proc. Natl. Acad. Sci. USA* 97 (2000) 6716–6721.
- [67] L. Sun, J. Li, X. Xiao, *Nat. Med.* 6 (2000) 599–602.
- [68] H. Nakai, T.A. Storm, M.A. Kay, *Nat. Biotechnol.* 18 (2000) 527–532.
- [69] D. Duan, Y. Yue, J.F. Engelhardt, *Mol. Ther.* 4 (2001) 383–391.